Scopus Preview

This author profile is generated by Scopus. Learn more

Gopal Raj, Murugananth

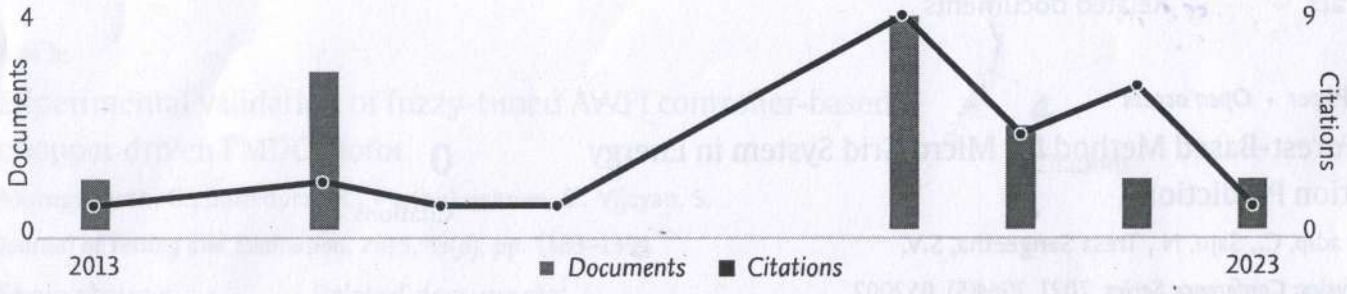
Ahalia School of Engineering and Technology, Palakkad, India 55764708100

https://orcid.org/0000-0003-1733-5248

25	12	4
Citations by **19** documents	Documents	*h*-index View *h*-graph

Set alert Edit profile ••• More

Document & citation trends



Scopus Preview

Scopus Preview users can only view a limited set of features. Check your institution's access to view all documents and features.

Check access

Beta

Documents 20 Co-Authors Topics 0 Awarded Grants

Documents (12) Cited by (19) Preprints (0)

Note:

Scopus Preview users can only view an author's last 10 documents, while most other features are disabled. Do have access through your institution? Check your institution's access to view all documents and features.

12 documents

Export all Add all to list

Sort by Date (...

Article • *Open access*

Development of Energy Management System for Micro Grid Operation

0 Citations

Jayaprakash, S., Gopi, B., Raj, M.G., ...Deepa, S., Swapna, S.

Computer Systems Science and Engineering, 2023, 45(3), pp. 2537–2551

Show abstract Related documents

Conference Paper

Residential Feeder Energy Audit Analysis and Recommendation with Aid of Software

0 Citations

Anitha, K., Shailesh, Ramesh, L., Raj, M.G.

Lecture Notes in Electrical Engineering, 2022, 881, pp. 1081–1090

Show abstract Related documents

Conference Paper • *Open access*

Random Forest-Based Method for Micro Grid System in Energy Consumption Prediction

0 Citations

Raj, M.G., Pradip, C., Saju, N., Tresa Sangeetha, S.V.

Journal of Physics: Conference Series, 2021, 1964(5), 052002

Show abstract Related documents

Conference Paper • *Open access*

Wind Energy Generation Based for Grid Connected System Using Zeta Converter and Terminal Sliding Mode Control

0 Citations

Pradip, C., Saju, N., Tresa Sangeetha, S.V., Raj, M.G.

Journal of Physics: Conference Series, 2021, 1964(5), 052011

Show abstract Related documents

Article

Analysis of artificial intelligence of things

2 Citations

Revathy, R., Raj, M.G., Selvi, M., Periasamy, J.K.

International Journal of Electrical Engineering and Technology, 2020, 11(4), pp. 275–280

Show abstract Related documents

.icle swarm optimization algorithm controlled chopper driven .MDC motor

2 Citations

Raj, M.G., Pradip, C., Saju, N.

Journal of Advanced Research in Dynamical and Control Systems, 2020, 12(7), pp. 511–516

Show abstract Related documents

Article

Antlion optimization algorithm controlled chopper driven PMDC motor

2 Citations

Raj, M.G., Samidurai, K., Muthuksirhsnan, S., Manickavasagam, A.

Journal of Advanced Research in Dynamical and Control Systems, 2020, 12(4 Special Issue), pp. 1180–1188

Show abstract Related documents

Review • *Open access*

Quality analysis of rice grains using ANN and SVM

5 Citations

Mohan, D., Gopal Raj, M.

Journal of Critical Reviews, 2020, 7(1), pp. 395–402

Show abstract Related documents

Article

Experimental validation of fuzzy-tuned AWPI controller-based chopper driven PMDC motor

4 Citations

Murugananth, G., Samidurai, K., Muthukrishnan, S., Vijayan, S.

Journal of Testing and Evaluation, 2015, 43(6), pp. 1383–1394

Show abstract Related documents

Article

Development of fuzzy controlled chopper drive for permanent magnet DC motor

4 Citations

Murugananth, G.R., Vijayan, S.

JVC/Journal of Vibration and Control, 2015, 21(3), pp. 555–562

Show abstract Related documents

Back to top

View list in search results format

View references

Set document alert

About Scopus

What is Scopus

Content coverage

Scopus blog

Scopus API

Privacy matters

Language

日本語版を表示する

查看简体中文版本

查看繁體中文版本

Просмотр версии на русском языке

Customer Service

Help

Tutorials

Contact us

ELSEVIER

Terms and conditions ↗ Privacy policy ↗

Copyright © Elsevier B.V ↗. All rights reserved. Scopus® is a registered trademark of Elsevier B.V.
We use cookies to help provide and enhance our service and tailor content. By continuing, you agree to the use of cookies ↗.

RELX

Scopus Preview

This author profile is generated by Scopus. Learn more

Kishor, Krishna Kumar

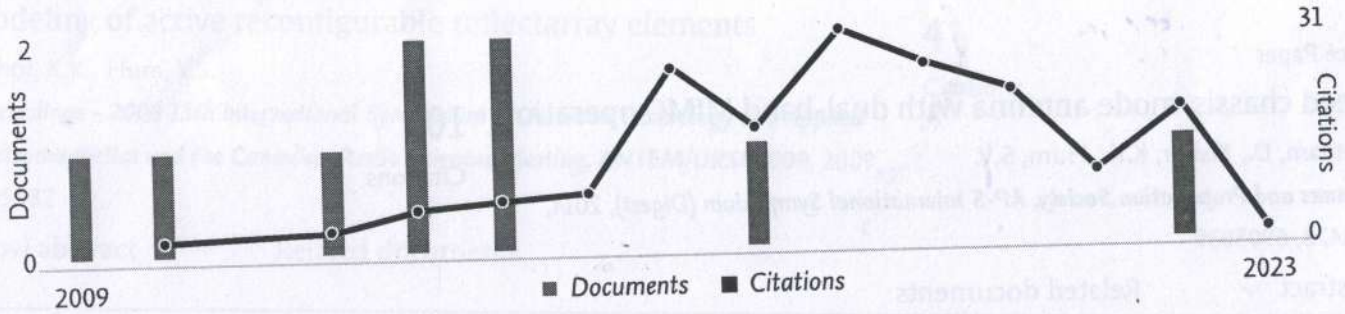
Ahalia School of Engineering and Technology, Palakkad, India 35100571900

https://orcid.org/0000-0002-9633-7374 Is this you? Connect to Mendeley account

178	9	6
Citations by **146** documents	Documents	*h*-index View *h*-graph

Set alert Edit profile ••• More

Document & citation trends



Scopus Preview

Scopus Preview users can only view a limited set of features. Check your institution's access to view all documents and features.

Check access

Beta

Documents 7 Co-Authors Topics 0 Awarded Grants

Documents (9) Cited by (146) Preprints (0)

Note:

Scopus Preview users can only view an author's last 10 documents, while most other features are disabled. Do you have access through your institution? Check your institution's access to view all documents and features.

9 documents

Export all Add all to list

Sort by Date (...

Conference Paper

A Compact Flexible Two-Port Textile Antenna

0 Citations

Hariprasad, S., Anusree, S., Sreedevi, R., ...Kishor, K.K., Balamurugan, V.

INDICON 2022 - 2022 IEEE 19th India Council International Conference, 2022

Show abstract Related documents

Article

Multiport Multiband Chassis-Mode Antenna Design Using Characteristic Modes

17 Citations

Kishor, K.K., Hum, S.V.

IEEE Antennas and Wireless Propagation Letters, 2017, 16, pp. 609–612, 7523241

Show abstract Related documents

Conference Paper

Multi-feed chassis-mode antenna with dual-band MIMO operation

10 Citations

Poopalaratnam, D., Kishor, K.K., Hum, S.V.

IEEE Antennas and Propagation Society, AP-S International Symposium (Digest), 2014, pp. 1427–1428, 6905039

Show abstract Related documents

Article

A pattern reconfigurable chassis-mode MIMO antenna

50 Citations

Kishor, K.K., Hum, S.V.

IEEE Transactions on Antennas and Propagation, 2014, 62(6), pp. 3290–3298, 6778018

Show abstract Related documents

Conference Paper

A reconfigurable chassis-mode MIMO antenna

6 Citations

Kishor, K.K., Hum, S.V.

2013 7th European Conference on Antennas and Propagation, EuCAP 2013, 2013, pp. 1992–1996, 6546639

Show abstract Related documents

.wo-port chassis-mode MIMO antenna

47 Citations

.ishor, K.K., Hum, S.V.

IEEE Antennas and Wireless Propagation Letters, 2013, 12, pp. 690–693, 6517887

Show abstract Related documents

Article

An amplifying reconfigurable reflectarray antenna

43 Citations

Kishor, K.K., Hum, S.V.

IEEE Transactions on Antennas and Propagation, 2012, 60(1), pp. 197–205, 6019001

Show abstract Related documents

Conference Paper

An amplifying reconfigurable reflectarray element

1 Citations

Kishor, K.K., Hum, S.V.

2010 IEEE International Symposium on Antennas and Propagation and CNC-USNC/URSI Radio Science Meeting - Leading the Wave, AP-S/URSI 2010, 2010, 5561002

Show abstract Related documents

Conference Paper

Modeling of active reconfigurable reflectarray elements

4 Citations

Kishor, K.K., Hum, V.S.

Proceedings - 2009 13th International Symposium on Antenna Technology and Applied Electromagnetics and the Canadian Radio Sciences Meeting, ANTEM/URSI 2009, 2009, 4805082

Show abstract Related documents

Back to top

View list in search results format

View references

Set document alert

About Scopus

What is Scopus

Content coverage

Scopus blog

Scopus API

Privacy matters

Language

日本語版を表示する

查看简体中文版本

查看繁體中文版本

Просмотр версии на русском языке

Customer Service

Help

Tutorials

Contact us

ELSEVIER

Terms and conditions ↗ Privacy policy ↗

Copyright © Elsevier B.V ↗. All rights reserved. Scopus® is a registered trademark of Elsevier B.V.
We use cookies to help provide and enhance our service and tailor content. By continuing, you agree to the use of cookies ↗.

RELX

Scopus Preview

2 author results

Refine results

Limit to Exclude

Source title

Affiliation

City

Country/territory

Limit to Exclude

Sort on: Document count (high-low)

All Request to merge authors

	Author	Documents	h-index	Affiliation	City	Country/Territor
1	Balamurugan, V.	1	0	Ahalia School of Engineering and Technology	Palakkad	Indi

Hide last title

Most recent document title:
Facial Expression and Genre-Based Musical Classification Using Deep Learning

2	Balamurugan, V.	1	0	Ahalia School of Engineering and Technology	Palakkad	Indi

Hide last title

Most recent document title:
A Compact Flexible Two-Port Textile Antenna

Display: 20 results per page

1

Top of pa

About Scopus

What is Scopus

Content coverage

Scopus blog

Scopus API

Privacy matters

Language

日本語版を表示する

查看简体中文版本

查看繁體中文版本

Просмотр версии на русском языке

Customer Service

Help

Tutorials

Contact us

ELSEVIER

Terms and conditions ↗ Privacy policy ↗

Copyright © Elsevier B.V ↗. All rights reserved. Scopus® is a registered trademark of Elsevier B.V.
We use cookies to help provide and enhance our service and tailor content. By continuing, you agree to the use of cookies ↗.

RELX

Scopus Preview

This author profile is generated by Scopus. Learn more

Alexis, S. John

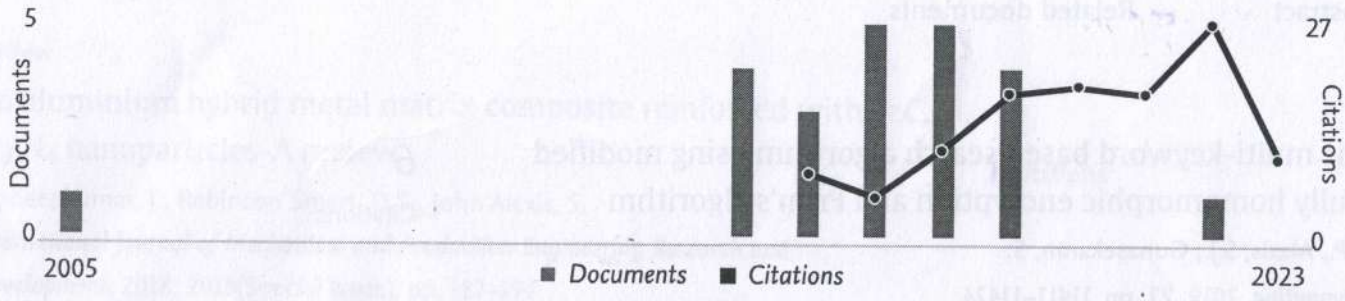
Ahalia School of Engineering and Technology, Palakkad, India 56771432700

https://orcid.org/0000-0002-0356-0121 Is this you? Connect to Mendeley account

116	23	6
Citations by ***102*** documents	Documents	*h*-index View *h*-graph

Set alert Edit profile ••• More

Document & citation trends



Scopus Preview

Scopus Preview users can only view a limited set of features. Check your institution's access to view all documents and features.

Check access

Beta

Documents 42 Co-Authors Topics 0 Awarded Grants

Documents (23) Cited by (102) Preprints (0)

Note:

Scopus Preview users can only view an author's last 10 documents, while most other features are disabled. Do y
have access through your institution? Check your institution's access to view all documents and features.

23 documents

Export all Add all to list

Sort by Date (...

Article

Experimental Investigation on Various Aluminium Composite Material for Aluminium-Air batteries

0 Citations

Thenmozhi, G., Samuel Ratnakumar, P.S., John Alexis, S., ...Siva, S., Hrithik, S.

International Journal of Vehicle Structures and Systems, 2022, 14(7), pp. 832–835

Show abstract Related documents

Article

Vibration Study on Aluminium Alloy 5083 Composite Reinforced with Montmorillonite

9 Citations

Samuel Ratna Kumar, P.S., Edwin Sudhagar, P., John Alexis, S., Subramani, M.

Transactions of the Indian Institute of Metals, 2019, 72(9), pp. 2449–2456

Show abstract Related documents

Article

Dynamic multi-keyword based search algorithm using modified based fully homomorphic encryption and Prim's algorithm

6 Citations

Rajan, D.P., Alexis, S.J., Gunasekaran, S.

Cluster Computing, 2019, 22, pp. 11411–11424

Show abstract Related documents

Conference Paper

Vibration-Impact study on AlMg4.5Mn reinforced nanoclay composites

4 Citations

Samuel Ratna Kumar, P.S., John Alexis, S., Saravana Mohan, M., Edwin Sudhagar, P., Madara, S.R.

Materials Today: Proceedings, 2019, 28, pp. 1140–1143

Show abstract Related documents

Article

Existence of solution of forest cross-diffusion model

0 Citations

Rajasingh, J., Murugesu, R., John Alexis, S.

International Journal of Recent Technology and Engineering, 2019, 7(4), pp. 162–167

Show abstract Related documents

Scopus Preview users can only view an author's last 10 documents, while most other features are disabled. Do y
have access through your institution? Check your institution's access to view all documents and features.

23 documents

Export all Add all to list

Sort by Date (...

Article

Experimental Investigation on Various Aluminium Composite Material for Aluminium-Air batteries

0 Citations

Thenmozhi, G., Samuel Ratnakumar, P.S., John Alexis, S., ...Siva, S., Hrithik, S.

International Journal of Vehicle Structures and Systems, 2022, 14(7), pp. 832–835

Show abstract Related documents

Article

Vibration Study on Aluminium Alloy 5083 Composite Reinforced with Montmorillonite

9 Citations

Samuel Ratna Kumar, P.S., Edwin Sudhagar, P., John Alexis, S., Subramani, M.

Transactions of the Indian Institute of Metals, 2019, 72(9), pp. 2449–2456

Show abstract Related documents

Article

Dynamic multi-keyword based search algorithm using modified based fully homomorphic encryption and Prim's algorithm

6 Citations

Rajan, D.P., Alexis, S.J., Gunasekaran, S.

Cluster Computing, 2019, 22, pp. 11411–11424

Show abstract Related documents

Conference Paper

Vibration-Impact study on AlMg4.5Mn reinforced nanoclay composites

4 Citations

Samuel Ratna Kumar, P.S., John Alexis, S., Saravana Mohan, M., Edwin Sudhagar, P., Madara, S.R.

Materials Today: Proceedings, 2019, 28, pp. 1140–1143

Show abstract Related documents

Article

Existence of solution of forest cross-diffusion model

0 Citations

Rajasingh, J., Murugesu, R., John Alexis, S.

International Journal of Recent Technology and Engineering, 2019, 7(4), pp. 162–167

Show abstract Related documents

...e • *Open access*

...n improved mechanical property of montmorillonite K10 reinforced AA5083 metal matrix composite

0 Citations

Ratna Kumar, P.S.S., Alexis, S.J., Siddharth, M.G., Smart, J.J.

International Journal of Mechanical and Production Engineering Research and Development, 2018, 8, pp. 783–789

Show abstract ∨ Related documents

Conference Paper • *Open access*

Evaluation of Mechanical Properties of MWCNT / Nanoclay Reinforced Aluminium alloy Metal Matrix Composite

9 Citations

Samuel Ratna Kumar, P.S., Robinson Smart, D.S., John Alexis, S.

IOP Conference Series: Materials Science and Engineering, 2018, 346(1), 012013

Show abstract ∨ Related documents

Conference Paper

Single pedal mechanism for leg amputated person and for the reduction of reaction time

0 Citations

Kishore, R., Arun, B., John Alexis, S., Hari Prasath, T., Mohnish Arya, P.

FISITA World Automotive Congress 2018, 2018, 2018-October, F2018-VCP-053

Show abstract ∨ Related documents

Review

An aluminium hybrid metal matrix composite reinforced with TaC, Ti, Si_3N_4 nanoparticles-A review

2 Citations

Pradeepkumar, J., Robinson Smart, D.S., John Alexis, S.

International Journal of Mechanical and Production Engineering Research and Development, 2018, 2018(Special Issue), pp. 187–194

Show abstract ∨ Related documents

Article

Improved mechanical properties of AA5083 reinforced with multiwall carbon nanotubes for automobile applications

2 Citations

Alexis, S.J., Kumar, P.S.S.R., Vinoth, K.R., Ragul, V.V., Kumar, N.S.

International Journal of Vehicle Structures and Systems, 2018, 10(4), pp. 278–281

Show abstract ∨ Related documents

Back to top

> View list in search results format

> View references

Set document alert

About Scopus

What is Scopus

Content coverage

Scopus blog

Scopus API

Privacy matters

Language

日本語版を表示する

查看简体中文版本

查看繁體中文版本

Просмотр версии на русском языке

Customer Service

Help

Tutorials

Contact us

ELSEVIER

Terms and conditions ↗ Privacy policy ↗

Copyright © Elsevier B.V ↗. All rights reserved. Scopus® is a registered trademark of Elsevier B.V.
We use cookies to help provide and enhance our service and tailor content. By continuing, you agree to the use of cookies ↗.

RELX

Scopus Preview

This author profile is generated by Scopus. Learn more

Gunasekaran, S.

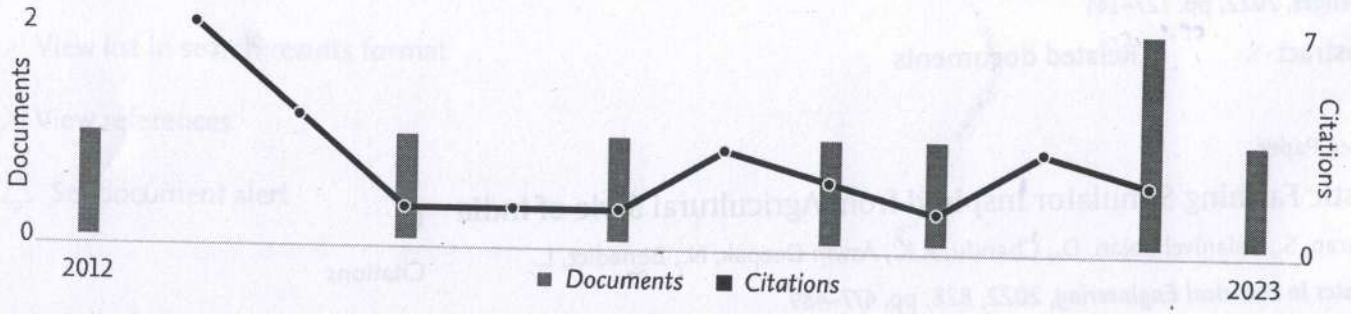
Ahalia School of Engineering and Technology, Palakkad, India 56594525200

https://orcid.org/0000-0001-9835-084X Is this you? Connect to Mendeley account

25	8	2
Citations by **25** documents	Documents	*h*-index View *h*-graph

Set alert Edit profile ••• More

Document & citation trends



Scopus Preview

Scopus Preview users can only view a limited set of features. Check your institution's access to view all documents and features.

Check access

Documents 13 Co-Authors Topics Beta 0 Awarded Grants

Documents (8) Cited by (25) Preprints (0)

Note:

Scopus Preview users can only view an author's last 10 documents, while most other features are disa
have access through your institution? Check your institution's access to view all documents and features.

8 documents

Export all Add all to list

Sort by Date (...

Book Chapter

Secure data communication using DNA computing adaptable to wireless sensor network

0 Citations

Gunasekaran, S., Kumar, M.

Advances in Computers, 2023, 129, pp. 317–361

Show abstract Related documents

Book Chapter

Blockchain Technology-Enabled Healthcare IoT to Increase Security and Privacy Using Fog Computing

0 Citations

Gunasekaran, S., Shanmugam, S., Rajan, D.P., Rontala, P.

Machine Learning, Blockchain, and Cyber Security in Smart Environments: Applications and Challenges, 2022, pp. 127–144

Show abstract Related documents

Conference Paper

A Realistic Farming Simulator Inspired from Agricultural Style of India

0 Citations

Gunasekaran, S., Palanivel Rajan, D., Chandu, R.K., Aswin Deepak, N., Benadict, L.

Lecture Notes in Electrical Engineering, 2022, 828, pp. 477–489

Show abstract Related documents

Article

H base repository design for sensor devices generated big data

0 Citations

Gunasekaran, S., Palanivel Rajan, D., Ravikumar, G.

International Journal of Advanced Science and Technology, 2020, 29(3), pp. 3989–4004

Show abstract Related documents

Article

Dynamic multi-keyword based search algorithm using modified based fully homomorphic encryption and Prim's algorithm

6 Citations

Rajan, D.P., Alexis, S.J., Gunasekaran, S.

Cluster Computing, 2019, 22, pp. 11411–11424

Show abstract Related documents

er

distributed transaction processing model using EJB and MTS

sekaran, S., Bargavi, V.

SQL: Database for Storage and Retrieval of Data in Cloud, 2017, pp. 23–46

0 Citations

Show abstract Related documents

Article

A survey on cloud metering service

Palanivel Rajan, D., Gunasekaran, S., Ranjith, G.

International Journal of Applied Engineering Research, 2015, 10(5), pp. 12693–12702

0 Citations

Show abstract Related documents

Conference Paper

Comparison of Network Intrusion Detection Systems in cloud computing environment

Vanathi, R., Gunasekaran, S.

2012 International Conference on Computer Communication and Informatics, ICCCI 2012, 2012, 6158820

19 Citations

Show abstract Related documents

Back to top

View list in search results format

View references

Set document alert

About Scopus

What is Scopus

Content coverage

Scopus blog

Scopus API

Privacy matters

Language

日本語版を表示する

查看简体中文版本

查看繁體中文版本

Просмотр версии на русском языке

Customer Service

Help

Tutorials

Contact us

ELSEVIER

Terms and conditions ↗ Privacy policy ↗

Copyright © Elsevier B.V ↗. All rights reserved. Scopus® is a registered trademark of Elsevier B.V.
We use cookies to help provide and enhance our service and tailor content. By continuing, you agree to the use of cookies ↗.

RELX

Scopus Preview

1 author results

Refine results

Limit to Exclude

Source title

Affiliation

City

Country/territory

Limit to Exclude

Sort on: Document count (high-low)

All Request to merge authors

	Author	Documents	h-index	Affiliation	City	Country/Territor
1	Khan, Vijitha	3	1	Ahalia School of Engineering and Technology	Kerala	Indi

Hide last title

Most recent document title:
Deep convolutional neural network-based cassava plant leaf disease classification

Display: 20 results per page

1

Top of pa

About Scopus

What is Scopus
Content coverage
Scopus blog
Scopus API
Privacy matters

Language

日本語版を表示する
查看简体中文版本
查看繁體中文版本
Просмотр версии на русском языке

Customer Service

Help
Tutorials
Contact us

ELSEVIER

Terms and conditions ↗ Privacy policy ↗

Copyright © Elsevier B.V ↗. All rights reserved. Scopus® is a registered trademark of Elsevier B.V.
We use cookies to help provide and enhance our service and tailor content. By continuing, you agree to the use of cookies ↗.

RELX



Turkish Journal of Computer and Mathematics Education Vol.12 No. 1S (2021), 631-639

Research Article

New form of generlized closed sets via neutrosophic topologicl spaces

BinoyBalan eK[1]*, C.Janaki[2] & Sandhya P.S[3]

[1] Department of Science & Humanities, Ahalia School of Engineering and Technology, Palakkad, Kerala, India
[2] Department of Mathematics, L.R.G. . College for Women, Tirupur-4, India
[3] Department of Applied Science & Humanities, Royal College of Engineering and Technology, Thrissur, Kerala, India
Email: binoypayyur@gmail.com[1], janakicsekar@yahoo.com[2] &

Article History: Received: 11 January 2021; Accepted: 27 February 2021; Published online: 5 April 2021

Abstract— Florentin eSmarandache egeneralized ethe eintuitionistic efuzzy esets eto eNeutrosophic eset etheory ein e1998 eas ea enew ebranch eof ephilosophy. eA.A. eSalama eintroduced ethe econcept eof eNeutrosophic etopological espaces eby eusing ethe eNeutrosophic ecrisp esets. eIn ethis epaper, ewe eintroduce eand estudy ea enew eclass eof eNeutrosophic egeneralized eset, enamely eNeutrsophic epre egeneralized eregular eα- eclosed eset ein eNeutrosophic etopological espaces. eSome einteresting epropositions ebased eon ethis eset eare eintroduced eand established ewith esuitable examples eand etheir eproperties eare ealso ediscussed.

Keywords— $\mathcal{N}$**pgrα**- closed set, $\mathcal{N}$**pgrα** - open set, $\mathcal{N}$**pgrα** -closure, $\mathcal{N}$**pgrα** - interior

1. INTRODUCTION AND PRELIMINARIES

L.A. Zadeh [20] introduced the concept of fuzzy sets in 1965. It shows the degree of membership of the lement in a set. Later, fuzzy topology was introduced by C.L.Chang [6] in 1968. Coker [7] introduced the notion of Intuitionistic fuzzy topological spaces by using Atanassov's [5] Intuitionistic fuzzy set. Neutrality the degree of indeterminacy, as an independent concept, was introduced by Smarandache [19] in 1998. He also defined the Neutrosophic set on three components, namely Truth (membership), Indeterminacy, Falsehood (non-membership) from the Fuzzy sets and Intuitionistic fuzzy sets. Smarandache's Neutrosophic concepts have wide range of real time applications for the fields of [[1]-[4],[10],[12],[15],[18]] Information systems, Computer science, Artificial Intelligence, Applied Mathematics and Decision making. A.A. Salama and S.A. Alblowi [16] introduced Neutrosophic topological spaces by using the Neutrosophic sets. Salama A. A. [17] introduced Neutrosophic closed set and Neutrosophic continuous functions in Neutrosophic topological spaces.R.Dhavaseelan and SaiedJafari [8] introduced Neutrosophic generalized closed sets. In this direction, we introduce and analyze a new class of Neutrosophic generalized closed set called Neutrsophic pre generalized regular α- closed set which is the weaker form of the above mentioned generalization and its properties are discussed in details.

Definition 1.[16]Let $\mathcal{I}$ be a non-empty fixed set. A Neutrosophic set [NS for short] $\mathcal{A}$ is an object having the form $\mathcal{A} = \{<a, \mu_{\mathcal{A}}(a), \sigma_{\mathcal{A}}(a), \nu_{v}(a)>: a\in \mathcal{I}\}$ where $\mu_{\mathcal{A}}(a)$, $\sigma_{\mathcal{A}}(a)$ and $\nu_{\mathcal{A}}(a)$ which represent the degree of membership function, degree of indeterminacy and the degree of non-membership respectively of each element $x \in A$ to the set $\mathcal{A}$.

Remark 1.2. [16] A Neutrosophic set $\mathcal{A} = \{<a, \mu_{\mathcal{A}}(a), \sigma_{\mathcal{A}}(a), \nu_{\mathcal{A}}(a)>: a\in \mathcal{I}\}$ can be identified to an ordered triple $\mathcal{A} = <a, \mu_{\mathcal{A}}(a), \sigma_{\mathcal{A}}(a), \nu_{\mathcal{A}}(a)>$ in non-standard unit interval $]\mathfrak{0}, 1^{+}[$ on $\mathcal{I}$.

For the sake of simplicity, we shall use the $\mathcal{A} = <\mu_{\mathcal{A}}(a), \sigma_{\mathcal{A}}(a), \nu_{\mathcal{A}}(a)>$ for the Neutrosophic set $\mathcal{A} = \{<a, \mu_{\mathcal{A}}(a), \sigma_{\mathcal{A}}(a), \nu_{v}(a)>: a\in \mathcal{I}\}$.

Definition 1.3. [16] Every Intuitionistic fuzzy set $\mathcal{A}$ is a nonempty set in $\mathcal{I}$ is obviously on Neutrosophic set having the form $\mathcal{A}=\{<a, \mu_{\mathcal{A}}(a),1-(\mu_{\mathcal{A}}(a)+\nu_{\mathcal{A}}(a)), \nu_{\mathcal{A}}(a)>: a\in \mathcal{I}\}$. Since our main purpose is to construct the tools for developing Neutrosophic set and Neutrosophic topology, we must introduce the Neutrosophic set $0_{\mathcal{N}}$ and $1_{\mathcal{N}}$ in $\mathcal{I}$ as follows:

$0_{\mathcal{N}}$ may be defined as:

$0_{\mathcal{N}}= \{<a, 0, 0, 1>: a\in \mathcal{I}\}$, $0_{\mathcal{N}}= \{<a, 0, 1, 1>: a\in \mathcal{I}\}$, $0_{\mathcal{N}}= \{<a, 0, 1, 0>: a\in \mathcal{I}\}$, $0_{\mathcal{N}}= \{<a, 0, 0, 0>: a\in \mathcal{I}\}$

$1_{\mathcal{N}}$ may be defined as:

$1_{\mathcal{N}}= \{<a, 1, 0, 0>: a\in \mathcal{I}\}$, $1_{\mathcal{N}}= \{<a, 1, 0, 1>: a\in \mathcal{I}\}$, $1_{\mathcal{N}}= \{<a, 1, 1, 0>: a\in \mathcal{I}\}$, $1_{\mathcal{N}}= \{<a, 1, 1, 1>: a\in \mathcal{I}\}$

Definition 1.4. [16] Let $\mathcal{A} =<\mu_{\mathcal{A}}(a), \sigma_{\mathcal{A}}(a), \nu_{\mathcal{A}}(a)>$ be an NS on $\mathcal{I}$ then the complement of the set $\mathcal{A}$ [$C(\mathcal{A})$ for short] may be defined as three kinds of complements:

(i) $C(\mathcal{A}) = \{ <a, 1-\mu_{\mathcal{A}}(a), 1-\sigma_{\mathcal{A}}(a), 1-\nu_{\mathcal{A}}(a)>:a\in \mathcal{I}\}$ (ii) $C(\mathcal{A}) = \{ <a,\nu_{\mathcal{A}}(a), \sigma_{\mathcal{A}}(a), \mu_{\mathcal{A}}(a)>: a\in \mathcal{I}\}$

(iii) $C(\mathcal{A}) = \{ <a,\nu_{\mathcal{A}}(a),1-\sigma_{\mathcal{A}}(a), \mu_{\mathcal{A}}(a)>:a\in \mathcal{I}\}$

Definition 1.5. [5] Let $\mathcal{I}$ be a nonempty set. Let $\mathcal{S}$ and $\mathcal{T}$ be any Neutrosophic sets on $\mathcal{I}$ in the form $\mathcal{S}$ ={<a, $\mu_{\mathcal{S}}$(a), $\sigma_{\mathcal{S}}$(a), $\nu_{\mathcal{S}}$(a) >: a∈ $\mathcal{I}$ } and $\mathcal{T}$ = {<a, $\mu_{\mathcal{T}}$(a), $\sigma_{\mathcal{T}}$(a), $\nu_{\mathcal{T}}$(a)>: a∈ $\mathcal{I}$ }. Then we may consider two possible definitions for subsets ($\mathcal{S} \subseteq \mathcal{T}$). $\mathcal{S} \subseteq \mathcal{T}$ may be defined as:

$\mathcal{S} \subseteq \mathcal{T} \Leftrightarrow \mu_{\mathcal{S}}(x) \leq \mu_{\mathcal{T}}(x)$, $\sigma_{\mathcal{S}}(x) \leq \sigma_{\mathcal{T}}(x)$, $\nu_{\mathcal{S}}(x) \geq \nu_{\mathcal{T}}(x)$ for all a∈ $\mathcal{I}$.

$\mathcal{S} \subseteq \mathcal{T} \Leftrightarrow \mu_{\mathcal{S}}(x) \leq \mu_{\mathcal{T}}(x)$, $\sigma_{\mathcal{S}}(x) \geq \sigma_{\mathcal{T}}(x)$, $\nu_{\mathcal{S}}(x) \geq \nu_{\mathcal{T}}(x)$ for all a $\in \mathcal{I}$.

Proposition 1.6. [5] For any Neutrosophic set $\mathcal{A}$ the following conditions hold:

$0_{\mathcal{N}} \subseteq \mathcal{A}$, $0_{\mathcal{N}} \subseteq 0_{\mathcal{N}}$, $\mathcal{A} \subseteq 1_{\mathcal{N}}$, $1_{\mathcal{N}} \subseteq 1_{\mathcal{N}}$

Definition 1.7.[16] Let $\mathcal{I}$ be a nonempty set. Let $\mathcal{S}$ = {<a, $\mu_{\mathcal{S}}$(a), $\sigma_{\mathcal{S}}$(a),$\nu_{\mathcal{S}}$(a)>}, $\mathcal{T}$ ={<a, $\mu_{\mathcal{T}}$(a), $\sigma_{\mathcal{T}}$(a),$\nu_{\mathcal{T}}$(a) >} are Neutrosophic sets. Then $\mathcal{S} \cap \mathcal{T}$ may be defined as:

(i) $\mathcal{S} \cap \mathcal{T}$=<a, $\mu_{\mathcal{S}}(a) \wedge \mu_{\mathcal{T}}(a)$, $\sigma_v(a) \wedge \sigma_{\mathcal{T}}(a)$,$\nu_{\mathcal{S}}(a) \vee \nu_{\mathcal{T}}(a)$>

(ii) $\mathcal{S} \cap \mathcal{T}$ = <a, $\mu_{\mathcal{S}}(a) \wedge \mu_{\mathcal{T}}(a)$, $\sigma_{\mathcal{S}}(a) \vee \sigma_{\mathcal{T}}(a)$, $\nu_{\mathcal{S}}(a)$ $\nu_{\mathcal{T}}(a)$>

$\mathcal{S} \cup \mathcal{T}$ may be defined as:

(i) $\mathcal{S} \cup \mathcal{T}$= <a, $\mu_{\mathcal{S}}(x) \vee \mu_{\mathcal{T}}(x)$, $\sigma_{\mathcal{S}}(x) \vee \sigma_{\mathcal{T}}(x)$, $\nu_{\mathcal{S}}(x) \wedge \nu_{\mathcal{T}}(x)$>

(ii) $\mathcal{S} \cup \mathcal{T}$ = <x, $\mu_{\mathcal{S}}(x) \vee \mu_{\mathcal{T}}(x)$, $\sigma_{\mathcal{S}}(x) \wedge \sigma_{\mathcal{T}}(x)$, $\nu_{\mathcal{S}}(x) \wedge \nu_{\mathcal{T}}(x)$>

We can easily generalize the operations of intersection and union to arbitrary family of Neutrosophic sets as follows:

Definition 1.8. [16] Let $\{\mathcal{A}_j: j \in J\}$ be a arbitrary family of Neutrosophic sets in A, then $\cap \mathcal{A}_j$ may be defined as

(i) $\cap \mathcal{A}_j$ = <a, $\wedge_{j\in J} \mu_{\mathcal{A}_j}(a)$, $\wedge_{j\in J} \sigma_{\mathcal{A}_j}(a)$,$\vee_{j\in J} \nu_{\mathcal{A}_j}(a)$>

(ii) $\cap \mathcal{A}_j$ = <a, $\wedge_{j\in J} \mu_{\mathcal{A}_j}(a)$, $\vee_{j\in J} \sigma_{\mathcal{A}_j}(a)$,$\vee_{j\in J} \nu_{\mathcal{A}_j}(a)$>

$\cup \mathcal{A}_j$ may be defined as

(i) $\cup \mathcal{A}_j$= <a, $\vee_{j\in J} \mu_{\mathcal{A}_j}(a)$, $\vee_{j\in J} \sigma_{\mathcal{A}_j}(a)$,$\wedge_{j\in J} \nu_{\mathcal{A}_j}(a)$>

(ii) $\cup \mathcal{A}_j$ = <a, $\vee_{j\in J} \mu_{\mathcal{A}_j}(a)$, $\wedge_{j\in J} \sigma_{\mathcal{A}_j}(a)$,$\wedge_{j\in J} \nu_{\mathcal{A}_j}(a)$>

Proposition 1.9. [16] For two Neutrosophic sets $\mathcal{S}$ and $\mathcal{T}$, the following conditions are true:

C ($\mathcal{S} \cap \mathcal{T}$)= C($\mathcal{S}$) ∪ C($\mathcal{T}$); C ($\mathcal{S} \cup \mathcal{T}$)= C($\mathcal{S}$)∩ C($\mathcal{T}$).

Definition 1.10 [16] A Neutrosophic topology [NT] on a nonempty set $\mathcal{I}$ is a family τ of Neutrosophic subsets in $\mathcal{I}$ satisfying the following axioms:

(i) $0_{\mathcal{N}}$, $1_{\mathcal{N}} \in \tau$

(ii) $\mathcal{G}_1 \cap \mathcal{G}_2 \in \tau$ for any $\mathcal{G}_1$, $\mathcal{G}_2 \in \tau$

(iii) $\cup \mathcal{G}_i \in \tau$ for every $\{\mathcal{G}_i: i \in J\} \subseteq \tau$

The pair of ($\mathcal{I}$, τ) is called Neutrosophic topological space [NTS for short]. The elements of τ are called Neutrosophic open set [NOS for short]. A Neutrosophic set $\mathcal{F}$ is Neutrosophic closed set [NCS for short] if and only if C($\mathcal{F}$) is Neutrosophic open set.

Example 1.11.[16]Let $\mathcal{I}$ ={a} and $\mathcal{A}_1$={< a, 0.6, 0.6, 0.5>: a ∈ $\mathcal{I}$}, $\mathcal{A}_2$={< a, 0.5, 0.7, 0.9>: a ∈ $\mathcal{I}$}, $\mathcal{A}_3$={<a, 0.6, 0.7, 0.5>: a ∈ $\mathcal{I}$}, $\mathcal{A}_4$ = {<a, 0.5, 0.6, 0.9>: a ∈ $\mathcal{I}$}.Then the family τ ={$0_{\mathcal{N}}$, $\mathcal{A}_1$, $\mathcal{A}_2$, $\mathcal{A}_3$, $\mathcal{A}_4$, 1_N} is called a Neutrosophic topological space on $\mathcal{I}$.

Definition 1.12[16] Let ($\mathcal{I}$,τ) be an NTS and $\mathcal{A}$= <a, $\mu_{\mathcal{S}}$(a), $\sigma_{\mathcal{S}}$(a), $\nu_{\mathcal{S}}$(a)> be an NS in $\mathcal{I}$. Then the Neutrosophic closure and Neutrosophic interior of $\mathcal{A}$ are defined by NCl($\mathcal{A}$) = ∩{$\mathcal{K}$: $\mathcal{K}$ is an NCS in $\mathcal{I}$ and $\mathcal{A} \subseteq \mathcal{K}$}, NInt($\mathcal{A}$) = ∪{$\mathcal{G}$: $\mathcal{G}$ is an NOS in $\mathcal{I}$ and $\mathcal{G} \subseteq \mathcal{A}$ }.

It can be also shown that NCl($\mathcal{A}$) is NCS and Nint($\mathcal{A}$) is a NOS in $\mathcal{I}$.

(i) $\mathcal{A}$ is NOS if and only if $\mathcal{A}$ = NInt($\mathcal{A}$)

(ii) $\mathcal{A}$ is NCS if and only if $\mathcal{A}$ = NCl($\mathcal{A}$)

Proposition 1.13.[16]For any Neutrosophic set $\mathcal{A}$ in ($\mathcal{I}$, τ) we have

(i) NCl(C($\mathcal{A}$))= C(NInt($\mathcal{A}$))

(ii) NInt(C($\mathcal{A}$))= C(NCl($\mathcal{A}$))

Proposition 1.14.[16] Let ($\mathcal{I}$,τ) be a NTS and $\mathcal{S}$, $\mathcal{T}$ be two Neutrosophic sets in $\mathcal{I}$. Then the following properties hold:

(i) NInt($\mathcal{S}$)⊆ $\mathcal{S}$ ⊆NCl($\mathcal{S}$)

(ii) $\mathcal{S} \subseteq \mathcal{T}$ ⇒NInt($\mathcal{S}$) ⊆NInt($\mathcal{T}$)and NCl($\mathcal{S}$) ⊆NCl($\mathcal{T}$)

(iii) NInt(NInt($\mathcal{S}$)) = NInt($\mathcal{S}$)

(iv) NCl(NCl($\mathcal{S}$))= NCl($\mathcal{S}$)

(v) NInt($\mathcal{S} \cap \mathcal{T}$)= NInt($\mathcal{S}$)∩NInt($\mathcal{T}$)

(vi) $NCl(\mathcal{S} \cup \mathcal{T}) = NCl(\mathcal{S}) \cup NCl(\mathcal{T})$

(vii) $NInt(0_{\mathcal{N}}) = 0_{\mathcal{N}}$, $NInt(1_{\mathcal{N}}) = 1_{\mathcal{N}}$

(viii) $NCl(0_{\mathcal{N}}) = 0_{\mathcal{N}}$, $NCl(1_{\mathcal{N}}) = 1_{\mathcal{N}}$

(ix) $\mathcal{S} \subseteq \mathcal{T} \Rightarrow C(\mathcal{S}) \subseteq C(\mathcal{T})$

(x) $NCl(\mathcal{S} \cap \mathcal{T}) \subseteq NCl(\mathcal{S}) \cap NCl(\mathcal{T})$

(xi) $NInt(\mathcal{S} \cup \mathcal{T}) \subseteq NInt(\mathcal{S}) \cup NInt(\mathcal{T})$

Definition 1.15. Let $\mathcal{A} = \{<a, \mu_{\mathcal{A}}(a), \sigma_{\mathcal{A}}(a), \nu_{\mathcal{A}}(a)>: a \in \mathcal{I}\}$ be a Neutrosophic set on a Neutrosophic topological space $(\mathcal{I},\tau)$ then $\mathcal{A}$ is called

(i) Neutrosophic regular open set (NROS for short)[12] if $\mathcal{A} = NInt(NCl(\mathcal{A}))$.

(ii) Neutrosophic pre-open set (NPOS for short)[14] if $\mathcal{A} \subseteq NInt(NCl(\mathcal{A}))$.

(iii) Neutrosophic α-open set (NαOS for short)[14] if $\mathcal{A} \subseteq NInt(NCl(NInt(\mathcal{A})))$.

An NS $\mathcal{A}$ is called Neutrosophic regular closed set, Neutrosophic pre closed set and Neutrosophic α-closed (NRCS, NPCS and NαCS for short) if the complement of $\mathcal{A}$ is NROS, NPOS and NαOS respectively.

Definition 1.16.[13] Let $\mathcal{A}=\{<a, \mu_{\mathcal{A}}(a), \sigma_{\mathcal{A}}(a), \nu_{\mathcal{A}}(a)>: a \in \mathcal{I}\}$ be a Neutrosophic set on Neutrosophic topological space $(\mathcal{I},\tau)$. Then the Neutrosophic pre-closure and Neutrosophic pre interior of $\mathcal{A}$ are defined by $NPCl(\mathcal{A}) = \{\mathcal{K}: K \text{ is a NPCS in } \mathcal{I} \text{ and } \mathcal{A} \subseteq \mathcal{K}\}$, $NPInt(\mathcal{A}) = \{\mathcal{G}: \text{ is a NPOS in } \mathcal{I} \text{ and } \subseteq \mathcal{A}\}$

Definition 1.17.[12] Let $\mathcal{A} = \{<a, \mu_{\mathcal{A}}(a), \sigma_{\mathcal{A}}(a), \nu_{\mathcal{A}}(a)>: a \in \mathcal{I}\}$ be a Neutrosophic set on a Neutrosophic topological space $(\mathcal{I},\tau)$. Then the Neutrosophic α-closure and Neutrosophic α-interior of $\mathcal{A}$ are defined by $N\alpha Cl(\mathcal{A}) = \{\mathcal{K}: \mathcal{K} \text{ is a N}\alpha\text{CS in } \mathcal{I} \text{ and } \mathcal{A} \subseteq \mathcal{K}\}$, $N\alpha Int(\mathcal{A}) = \{\mathcal{G}: \mathcal{G} \text{ is a N}\alpha\text{OS in } \mathcal{I} \text{ and } \mathcal{G} \subseteq \mathcal{A}\}$

Definition 1.18. Let $\mathcal{A}=\{<a, \mu_{\mathcal{A}}(a), \sigma_{\mathcal{A}}(a), \nu_{\mathcal{A}}(a)>: a \in \mathcal{I}\}$ be a Neutrosophic set on a Neutrosophic topological space $(\mathcal{I}, \tau)$. Then $\mathcal{A}$ is called

(i) Neutrosophic regular generalized closed set (NRGCS for short)[9], if $NCl(\mathcal{A}) \subseteq U$, whenever $\mathcal{A} \subseteq \mathcal{U}$ and $\mathcal{U}$ is a Neutrosophic regular open set in $\mathcal{I}$.

(ii) Neutrosophic regular α-generalized closed set (NRαGCS for short)[9], if $N\alpha Cl(\mathcal{A}) \subseteq \mathcal{U}$, whenever $\mathcal{A} \subseteq \mathcal{U}$ and $\mathcal{U}$ is a Neutrosophic regular open set in $\mathcal{I}$.

(iii) Neutrosophic generalized pre closed set (NGPCS for short)[13] if $NPCl(\mathcal{A}) \subseteq \mathcal{U}$ whenever $\mathcal{A} \subseteq \mathcal{U}$ and $\mathcal{U}$ is a Neutrosophic open set in $\mathcal{I}$.

(iv) Neutrosophic generalized pre regular closed set (NGPRCS for short)[11] if $NPCl(\mathcal{A}) \subseteq \mathcal{U}$ whenever $\mathcal{A} \subseteq \mathcal{U}$ and $\mathcal{U}$ is a Neutrosophic regular open set in $\mathcal{I}$.

An NS $\mathcal{A}$ is called Neutrosophic regular generalized open set, Neutrosophic regular α -generalized open set, Neutrosophic generalized pre-open set and Neutrosophic generalized pre regular open set (NRGOS,NRαGOS, NGPOS and NGPROS for short) if the complement of $\mathcal{A}$ is NRGCS,NRαGCS, NGPCS and NGPRCS respectively.

2. NEUTROSOPHIC PRE GENERALIZED REGULAR α-CLOSED SET

In this section, we introduce Neutrosophic pre generalized regular α- closed set and analyze some of their properties.

Definition 2.1. Let $\mathcal{A}= \{<a, \mu_{\mathcal{A}}(a), \sigma_{\mathcal{A}}(a), \nu_{\mathcal{A}}(a)>: a \in \mathcal{I}\}$ be a Neutrosophic set on a Neutrosophic topological space $(\mathcal{I}, \tau)$.Then $\mathcal{A}$ is called Neutrosophic regular α-open set (NRαOS for short) if there is a Neutrosophic regular open set $\mathcal{U}$ such that $\mathcal{U} \subset \mathcal{A} \subset N\alpha Cl(\mathcal{U})$.A Neutrosophic set $\mathcal{A}$ of a Neutrosophic space $(\mathcal{I}, \tau)$ is called a Neutrosophic regular α -closed set (NRαCS for short) if $C(\mathcal{A})$ is a NRαOS in $(\mathcal{I}, \tau)$.

Definition 2.2. Let $\mathcal{A}= \{<a, \mu_{\mathcal{A}}(a), \sigma_{\mathcal{A}}(a), \nu_{\mathcal{A}}(a)>: a \in \mathcal{I}\}$ be a Neutrosophic set on a Neutrosophic topological space $(\mathcal{I}, \tau)$. Then $\mathcal{A}$ is called Neutrosophic pre generalized regular α- closed set ($\mathcal{NPGR}\alpha$CS for short), if $NPCl(\mathcal{A}) \subseteq \mathcal{U}$ whenever $\mathcal{A} \subseteq \mathcal{U}$ and $\mathcal{U}$ is a NRαOS in $(\mathcal{I}, \tau)$.

Alternatively, a Neutrosophic set $\mathcal{A}$ is said to be a Neutrosophic pre generalized regular α-open set ($\mathcal{NPGR}\alpha$OS for short) if $C(\mathcal{A})$ is a $\mathcal{NPGR}\alpha$CS in $(\mathcal{I}, \tau)$.

The family of all $\mathcal{NPGR}\alpha$CSs [$\mathcal{NPGR}\alpha$OSs] of an NTS $(\mathcal{I}, \tau)$ is denoted by $\mathcal{NPGR}\alpha C(\mathcal{I})$ [$\mathcal{NPGR}\alpha O(\mathcal{I})$].

Example 2.3. Let $\mathcal{I} = \{a, b\}$ and $\tau = \{0_{\mathcal{N}}, U, V, 1_{\mathcal{N}}\}$ where $\mathcal{U}= \{<0.5, 0.3, 0.6>, <0.4, 0.4, 0.7>\}$ and $\mathcal{V} = \{<0.7, 0.5, 0.3>, <0.7, 0.5, 0.2>\}$. Then $(\mathcal{I}, \tau)$ is a Neutrosophic topological space. Here the

Neutrosophic set $\mathcal{A}$= {<0.5, 0.3, 0.4>, <0.6, 0.6, 0.3>} is a $\mathcal{NPGR}\alpha$CS in ($\mathcal{I}$, τ). Since $\mathcal{A} \subseteq \mathcal{U}$ and $\mathcal{U}$ is a NRαOS, we have NPCl($\mathcal{A}$) = $\mathcal{A} \subseteq \mathcal{U}$.

Theorem 2.4.

(i) Every Neutrosophic closed set is $\mathcal{NPGR}\alpha$- closed set in $\mathcal{I}$.
(ii) Every Neutrosophic regular closed set is $\mathcal{NPGR}\alpha$-closed set in $\mathcal{I}$.
(iii) Every Neutrosophic pre closed set is $\mathcal{NPGR}\alpha$-closed set in $\mathcal{I}$.
(iv) Every Neutrosophic α-closed set is $\mathcal{NPGR}\alpha$-closed set in $\mathcal{I}$.
(v) Every $\mathcal{NPGR}\alpha$-closed set is Neutrosophic generalized pre regular closed set in $\mathcal{I}$.
(vi) Every Neutrosophic regular α-generalized closed set in X is a $\mathcal{NPGR}\alpha$-closed set in $\mathcal{I}$.
(vii) Every Neutrosophic generalized pre closed set in X is a $\mathcal{NPGR}$ α-closed set in $\mathcal{I}$.
(viii) Every Neutrosophic regular generalized closed set in X is a $\mathcal{NPGR}$ α-closed set in $\mathcal{I}$.

Proof: Straight forward. Converse of the above need not be true as in the following examples.

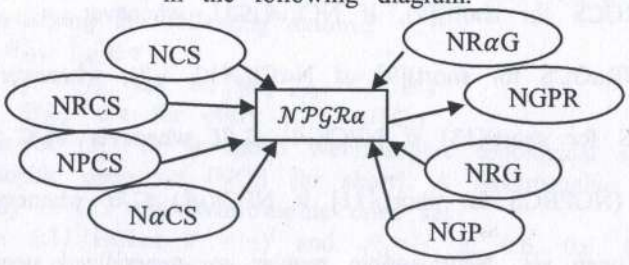
Example 2.5.

(i) Let $\mathcal{I}$ ={a, b} and $\mathcal{A}_1$ = {<0.4, 0.6, 0.5>,<0.7, 0.3, 0.6 >},$\mathcal{A}_2$ = {<0.3, 0.7, 0.8>,<0.6, 0.4, 0.2 >}, $\mathcal{A}_3$ = {<0.4, 0.7, 0.5>,<0.7, 0.4, 0.2 >} and $\mathcal{A}_4$ = {<0.3, 0.6, 0.8>,<0.6, 0.3, 0.6>} be an NSs on $\mathcal{I}$. Now τ ={$0_{\mathcal{N}}$ $\mathcal{A}_1$, $\mathcal{A}_2$, $\mathcal{A}_3$, $\mathcal{A}_4$, $1_{\mathcal{N}}$} is a Neutrosophic topological spaces on $\mathcal{I}$.Then $\mathcal{A}$ = {<0.3, 0.6, 0.8>, <0.5, 0.3, 0.7>} is $\mathcal{NPGR}\alpha$CS in $\mathcal{I}$. But $\mathcal{A}$ is not NCS, NRCS, NPCS, NαCS in $\mathcal{I}$.

(ii) Let $\mathcal{I}$ = {a, b} and $\mathcal{U}$ = {<0.6, 0.5, 0.2>,<0.7, 0.5, 0.1 >} and $\mathcal{V}$= {<0.5, 0.4, 0.7>,<0.4, 0.5, 0.6 >}, be an NSs on $\mathcal{I}$. Now τ = {$0_{\mathcal{N}}$, $1_{\mathcal{N}}$, $\mathcal{U}$, $\mathcal{V}$} is a Neutrosophic topological spaces on $\mathcal{I}$. Here the Neutrosophic set $\mathcal{A}$ = {<0.8, 0.6, 0.1>, <0.8, 0.6, 0>} is a Neutrosophic generalized pre regular closed set in $\mathcal{I}$. But $\mathcal{A} \subseteq \mathcal{W}$ and $\mathcal{W}$={<0.5, 0.5, 0.8>, <0.4, 0.3, 0.6>} is NRαOS and NPCl(A) = $1_{\mathcal{N}} \not\subseteq \mathcal{W}$, $\mathcal{A}$ is not a $\mathcal{NPGR}\alpha$-closed set in $\mathcal{I}$. .

(iii) Let $\mathcal{I}$ = {a, b} and $\mathcal{U}$ = {<0.6, 0.5, 0.2>, <0.7, 0.5, 0.1 >} and $\mathcal{V}$ = {<0.5, 0.4, 0.7>,<0.4, 0.5, 0.6 >}, be an NSs on $\mathcal{I}$. Now τ = {0_N, 1_N, $\mathcal{U}$, $\mathcal{V}$ } is a Neutrosophic topological spaces on $\mathcal{I}$. Here the Neutrosophic set $\mathcal{A}$ = {<0.4, 0.3, 0.7>, <0.3, 0.2, 0.6>} is a $\mathcal{NPGR}\alpha$CS in $\mathcal{I}$. But $\mathcal{A}$ is not NRαGCS, NGPCS and NRGCS in $\mathcal{I}$. Here $\mathcal{A} \subseteq \mathcal{W}$ and $\mathcal{W}$={<0.5, 0.5, 0.8>, <0.4, 0.3, 0.6>} is NRαOS, but not NOS and NROS in $\mathcal{I}$.

Remark 2.6. The above discussions are summarized in the following diagram.



Remark 2.7. The union of any two $\mathcal{NPGR}\alpha$CSs in ($\mathcal{I}$, τ) is not an $\mathcal{NPGR}\alpha$CS in ($\mathcal{I}$, τ) in general as seen from the following example.

Example 2.8. Let $\mathcal{I}$ = {a, b} and τ = {$0_{\mathcal{N}}$, $1_{\mathcal{N}}$, $\mathcal{U}$, $\mathcal{V}$} where $\mathcal{U}$ ={<0.5, 0.3, 0.6>, <0.4, 0.4, 0.7>} and $\mathcal{V}$ = {<0.7, 0.5, 0.3>, <0.7, 0.5, 0.2>}. Then the NSs $\mathcal{A}$ = {<0.2, 0.1, 0.7>, <0.4, 0.4, 0.7>} and $\mathcal{B}$= {<0.5, 0.3, 0.6>, <0.2, 0.2, 0.8>} are $\mathcal{NPGR}\alpha$CSs in ($\mathcal{I}$, τ). But $\mathcal{A} \cup \mathcal{B}$={<0.5,0.3,0.6>, <0.4,0.4,0.7>} is not an $\mathcal{NPGR}\alpha$CS in ($\mathcal{I}$, τ).

Since ($\mathcal{A} \cup \mathcal{B}$)$\subseteq$ $\mathcal{U}$ and NPCl($\mathcal{A} \cup \mathcal{B}$) ={<0.6,0.7,0.5), (0.7,0.6,0.4>}= C($\mathcal{U}$)$\not\subseteq$ $\mathcal{U}$.

Remark 2.9.: The intersection of any two $\mathcal{NPGR}\alpha$CSs in ($\mathcal{I}$, τ) is not an $\mathcal{NPGR}\alpha$CS in ($\mathcal{I}$, τ) in general as seen from the following example.

Example 2.10. Let $\mathcal{I}$ = {a, b} and τ = {$0_{\mathcal{N}}$, $1_{\mathcal{N}}$, $\mathcal{U}$, $\mathcal{V}$} where $\mathcal{U}$ = [<0.5, 0.3, 0.6>, <0.4, 0.4, 0.7>} and $\mathcal{V}$ = {<0.7, 0.5, 0.3>, <0.7, 0.5, 0.2>}. Then the NSs $\mathcal{A}$ = {<0.5, 0.5, 0.4>, <0.7, 0.6, 0.7>} and $\mathcal{B}$ = {<0.6, 0.3, 0.6>, <0.4, 0.4, 0.3>} are $\mathcal{NPGR}\alpha$CSs in ($\mathcal{I}$, τ). But $\mathcal{A} \cap \mathcal{B}$ = {<0.5, 0.3, 0.6>, <0.4, 0.4, 0.7>} is not a $\mathcal{NPGR}\alpha$CS in ($\mathcal{I}$, τ). Since ($\mathcal{A} \cap \mathcal{B}$)$\subseteq$ $\mathcal{U}$ but NPCl($\mathcal{A} \cap \mathcal{B}$) = {<0.6, 0.7, 0.4>, <0.7, 0.6, 0.4>}$\not\subseteq$ $\mathcal{U}$.

Theorem 2.11. Let ($\mathcal{I}$, τ) be an NTS. Then for every $\mathcal{A}$ $\in$NPGRαC($\mathcal{I}$) and for every Neutrosophic set $\mathcal{B}$ $\in$NS($\mathcal{I}$),$\mathcal{A} \subseteq \mathcal{B} \subseteq$NPCl($\mathcal{A}$) implies $\mathcal{B}$ $\in$NPGRαC($\mathcal{I}$).

Proof: Let $\mathcal{B} \subseteq \mathcal{U}$ and $\mathcal{U}$ is a Neutrosophic regular α-open set in $(\mathcal{I}, \tau)$. Since $\subseteq \mathcal{B}$, then $\mathcal{A} \subseteq \mathcal{U}$.Given $\mathcal{A}$ is a NPGRαCS, it follows that NPCl($\mathcal{A}$) $\subseteq \mathcal{U}$. Now $\mathcal{B} \subseteq$NPCl($\mathcal{A}$) implies NPCl($\mathcal{B}$) $\subseteq$NPCl(NPCl($\mathcal{A}$)) = NPCl($\mathcal{A}$). Thus, NPCl($\mathcal{B}$)$\subseteq \mathcal{U}$. This proves that $\mathcal{B} \in$ NPGRαC($\mathcal{I}$).

Theorem 2.12. If $\mathcal{A}$ is a Neutrosophic regular α-open set and $\mathcal{NPGR}\alpha$CS in $(\mathcal{I}, \tau)$, then $\mathcal{A}$ is a Neutrosophic pre closed set in $(\mathcal{I}, \tau)$.

Proof: Since $\mathcal{A} \subseteq \mathcal{A}$ and $\mathcal{A}$ is a Neutrosophic regular α-open set in $(\mathcal{I}, \tau)$, by hypothesis, NPCl($\mathcal{A}$) $\subseteq \mathcal{A}$. But since $\mathcal{A} \subseteq$NPCl($\mathcal{A}$). Therefore NPCl($\mathcal{A}$)= $\mathcal{A}$. Hence $\mathcal{A}$ is a Neutrosophic pre closed set in $(\mathcal{I}, \tau)$.

2.NEUTROSOPHIC PRE GENERALIZED REGULAR α-CLOSURE IN NEUTROSOPHIC TOPOLOGICAL SPACES

In this section, we introduce the concept of Neutrosophic pre generalized regular α-closure operators in a Neutrosophic topological spaces.

Definition 3.1. Let $(\mathcal{I}, \tau)$ be a Neutrosophic topological space. Then for a Neutrosophic subset $\mathcal{A}$ of $\mathcal{I}$,

(i) Neutrosophic pre generalized regular α-interior of $\mathcal{A}$ is the union of all Neutrosophic pre generalized regular α-open sets of $\mathcal{I}$ contained in $\mathcal{A}$. i.e., $\mathcal{NPGR}\alpha$ -Int($\mathcal{A}$)=$\cup\{\mathcal{G} : \mathcal{G}$ is a $\mathcal{NPGR}\alpha$-open set in $\mathcal{I}$ and $\mathcal{G} \subseteq \mathcal{A}\}$.

(ii) Neutrosophic pre generalized regular α-closure of $\mathcal{A}$ is the intersection of all Neutrosophic pre generalized regular α-closed sets of $\mathcal{I}$ containing in $\mathcal{A}$. i.e., $\mathcal{NPGR}\alpha$-Cl($\mathcal{A}$) =$\cap\{ \mathcal{K} : \mathcal{K}$ is a $\mathcal{NPGR}\alpha$-closed set in $\mathcal{I}$ and $\mathcal{K} \supseteq \mathcal{A}\}$.

Theorem 3.2. Let $(\mathcal{I}, \tau)$ be a Neutrosophic topological space. Then for a Neutrosophic subsets $\mathcal{A}$ and $\mathcal{B}$ of $\mathcal{I}$, we have

(i) $\mathcal{NPGR}\alpha$-Int($\mathcal{A}$) $\subseteq \mathcal{A}$

(ii) $\mathcal{A}$ *is* $\mathcal{NPGR}\alpha$ -open set in A $\Leftrightarrow$ $\mathcal{NPGR}\alpha$ -Int($\mathcal{A}$)= $\mathcal{A}$

(iii) $\mathcal{NPGR}\alpha$ -Int($\mathcal{NPGR}\alpha$ -Int($\mathcal{A}$))= $\mathcal{NPGR}\alpha$ -Int($\mathcal{A}$)

(iv) If $\mathcal{A} \subseteq \mathcal{B}$ then $\mathcal{NPGR}\alpha$ -Int($\mathcal{A}$)$\subseteq$ $\mathcal{NPGR}\alpha$ -Int($\mathcal{B}$)

(v) $\mathcal{NPGR}\alpha$ -Int($\mathcal{A} \cap \mathcal{B}$)= $\mathcal{NPGR}\alpha$ -Int($\mathcal{A}$) $\cap$ $\mathcal{NPGR}\alpha$ -Int($\mathcal{B}$)

(vi) $\mathcal{NPGR}\alpha$ -Int($\mathcal{A} \cup \mathcal{B}$)$\supseteq$ $\mathcal{NPGR}\alpha$ Int($\mathcal{A}$)$\cup$ $\mathcal{NPGR}\alpha$ -Int($\mathcal{B}$).

Proof: Follows from Definition 3.1.(i).This proves (i).

Let $\mathcal{A}$ be an $\mathcal{NPGR}\alpha$-open set in $\mathcal{I}$. Then $\mathcal{A} \subseteq \mathcal{NPGR}\alpha$-Int($\mathcal{A}$). By using Theorem 3.2 (i) we get $\mathcal{A}$ = $\mathcal{NPGR}\alpha$-Int($\mathcal{A}$). Conversely assume that $\mathcal{A}$ = $\mathcal{NPGR}\alpha$-Int($\mathcal{A}$). By using Definition 3.1(i), $\mathcal{A}$ is $\mathcal{NPGR}\alpha$-open set in $\mathcal{I}$. Thus (ii) is proved.

By using Theorem 3.2 (ii), $\mathcal{NPGR}\alpha$-Int($\mathcal{NPGR}\alpha$-Int($\mathcal{A}$)) = $\mathcal{NPGR}\alpha$-Int($\mathcal{A}$). This proves (iii).

Since $\mathcal{A} \subseteq \mathcal{B}$, by using Theorem 3.2 (i), $\mathcal{NPGR}\alpha$-Int($\mathcal{A}$)$\subseteq$ $\mathcal{A} \subseteq \mathcal{B}$. That is $\mathcal{NPGR}\alpha$-Int ($\mathcal{A}$)$\subseteq$ $\mathcal{B}$.

By Theorem 3.2 (iii), $\mathcal{NPGR}\alpha$-Int($\mathcal{NPGR}\alpha$-Int($\mathcal{A}$))$\subseteq\mathcal{NPGR}\alpha$-Int($\mathcal{B}$).This proves (iv).

Since $\mathcal{A} \cap \mathcal{B} \subseteq \mathcal{A}$ and $\mathcal{A} \cap \mathcal{B} \subseteq \mathcal{B}$, by using Theorem 3.2(iv), $\mathcal{NPGR}\alpha$-Int($\mathcal{A} \cap \mathcal{B}$) $\subseteq$ $\mathcal{NPGR}\alpha$-Int($\mathcal{A}$) and $\mathcal{NPGR}\alpha$-Int($\mathcal{A} \cap \mathcal{B}$) $\subseteq$ $\mathcal{NPGR}\alpha$-Int($\mathcal{B}$).This implies that $\mathcal{NPGR}\alpha$-Int($\mathcal{A} \cap \mathcal{B}$) $\subseteq$ $\mathcal{NPGR}\alpha$-Int($\mathcal{A}$) $\cap$ $\mathcal{NPGR}\alpha$-Int($\mathcal{B}$) (1)

By using Theorem 3.2(i), $\mathcal{NPGR}\alpha$-Int($\mathcal{A}$) $\subseteq \mathcal{A}$ and $\mathcal{NPGR}\alpha$-Int($\mathcal{B}$) $\subseteq \mathcal{B}$. This implies that $\mathcal{NPGR}\alpha$-Int($\mathcal{A}$) $\cap$ $\mathcal{NPGR}\alpha$-Int($\mathcal{B}$) $\subseteq$ ($\mathcal{A} \cap \mathcal{B}$) . Now applying Theorem 3.2(iv), $\mathcal{NPGR}\alpha$-Int(($\mathcal{NPGR}\alpha$-Int($\mathcal{A}$) $\cap$ $\mathcal{NPGR}\alpha$-Int($\mathcal{B}$)) $\subseteq$ $\mathcal{NPGR}\alpha$-Int($\mathcal{A} \cap \mathcal{B}$). By Theorem 3.2(iii), $\mathcal{NPGR}\alpha$-Int($\mathcal{A}$) $\cap$ $\mathcal{NPGR}\alpha$-Int($\mathcal{B}$) $\subseteq\mathcal{NPGR}\alpha$-Int($\mathcal{A} \cap \mathcal{B}$) (2)

From equations (1) and (2), $\mathcal{NPGR}\alpha$-Int($\mathcal{A} \cap \mathcal{B}$) = $\mathcal{NPGR}\alpha$-Int($\mathcal{A}$) $\cap$ $\mathcal{NPGR}\alpha$-Int($\mathcal{B}$). This proves (v).

Since $\mathcal{A} \subseteq \mathcal{A} \cup \mathcal{B}$ and B $\subseteq \mathcal{A} \cup \mathcal{B}$, by using Theorem 3.2(iv), $\mathcal{NPGR}\alpha$-Int($\mathcal{A}$) $\subseteq$ $\mathcal{NPGR}\alpha$-Int($\mathcal{A} \cup \mathcal{B}$) and $\mathcal{NPGR}\alpha$-Int($\mathcal{B}$) $\subseteq$ $\mathcal{NPGR}\alpha$-Int($\mathcal{A} \cup \mathcal{B}$).This implies that $\mathcal{NPGR}\alpha$-Int($\mathcal{A}$) $\cup\cap$ $\mathcal{NPGR}\alpha$-Int($\mathcal{B}$) $\subseteq$ $\mathcal{NPGR}\alpha$-Int($\mathcal{A} \cup \mathcal{B}$). This proves (vi).

Remark 3.3. The following example shows that the equality need not hold in Theorem 3.3(vi).

Example 3.4. Let $\mathcal{I}$ = {a, b} and τ = {$0_{\mathcal{N}}$, $1_{\mathcal{N}}$, $\mathcal{U}$, $\mathcal{V}$} where $\mathcal{U}$ = {<0.5, 0.3, 0.6>, <0.4, 0.4, 0.7>} and $\mathcal{V}$ ={<0.7, 0.5, 0.3>, <0.7, 0.5, 0.2>]. Then $(\mathcal{I}, \tau)$ is a Neutrosophic topological spaces. Consider the NSs $\mathcal{A}$ ={<0.8, 0.9, 0.2>, <0.7, 0.6, 0.4>} and $\mathcal{B}$ ={<0.6, 0.7, 0.5>,<0.9, 0.8, 0.2>} in $(\mathcal{I},\tau)$.

Then $\mathcal{NPGR}\alpha$ -Int($\mathcal{A}$)={<0.7, 0.9, 0.2.>), <0.7, 0.6,

0.4>}and $\mathcal{NPGR}\alpha$ -Int($\mathcal{B}$)={<0.6, 0.7, 0.5), <0.8, 0.8, 0.2>}, this implies $\mathcal{NPGR}\alpha$ -Int($\mathcal{A}$)∪ $\mathcal{NPGR}\alpha$ – Int($\mathcal{B}$)= {<0.7, 0.9, 0.2>, <0.8, 0.8, 0.2>]. But $\mathcal{NPGR}\alpha$ -Int($\mathcal{A}$ ∪ $\mathcal{B}$)={<0.8,0.9,0.2>, <0.9,0.8,0.2>}.

Then $\mathcal{NPGR}\alpha$ -Int($\mathcal{A}$ ∪ $\mathcal{B}$)⊄ $\mathcal{NPGR}\alpha$ -Int($\mathcal{A}$ ∪ $\mathcal{B}$).

Proposition 3.5. Let ($\mathcal{I}$, τ) be a Neutrosophic topological space. Then for any Neutrosophic subsets $\mathcal{A}$ of $\mathcal{I}$,

(i) C($\mathcal{NPGR}\alpha$-Int($\mathcal{A}$))=$\mathcal{NPGR}\alpha$-Cl(C($\mathcal{A}$)),

(ii) C($\mathcal{NPGR}\alpha$-Cl($\mathcal{A}$))=$\mathcal{NPGR}\alpha$-Int(C($\mathcal{A}$)).

Proof : By using Definition 3.1(i), $\mathcal{NPGR}\alpha$-Int($\mathcal{A}$) = ∪{$\mathcal{G}$: $\mathcal{G}$ is a $\mathcal{NPGR}\alpha$-open set in A and $\mathcal{G}$ ⊆ $\mathcal{A}$ }.

Taking complement on both sides, C($\mathcal{NPGR}\alpha$-Int($\mathcal{A}$))=C(∪{$\mathcal{G}$: $\mathcal{G}$ is a $\mathcal{NPGR}\alpha$-open set in $\mathcal{I}$ and $\mathcal{G}$ ⊆ $\mathcal{A}$ }) =∩{C($\mathcal{G}$):C($\mathcal{G}$) is a $\mathcal{NPGR}\alpha$-closed set in $\mathcal{I}$ and C($\mathcal{A}$) ⊆ C(G)}. Replacing C(G) by $\mathcal{K}$, we get C($\mathcal{NPGR}\alpha$-Int($\mathcal{A}$))=∩{ $\mathcal{K}$: $\mathcal{K}$ is a $\mathcal{NPGR}\alpha$-closed set in $\mathcal{I}$ and $\mathcal{K}$ ⊇ C($\mathcal{A}$)}. By Definition 3.1(ii), C($\mathcal{NPGR}\alpha$-Int($\mathcal{A}$)) = $\mathcal{NPGR}\alpha$-Cl(C($\mathcal{A}$)). This proves (i).

By using Proposition 3.5 (i), C($\mathcal{NPGR}\alpha$-Int(C($\mathcal{A}$)))=$\mathcal{NPGR}\alpha$-Cl(C(C($\mathcal{A}$)))=$\mathcal{NPGR}\alpha$-Cl($\mathcal{A}$). Taking complement on both sides, we get $\mathcal{NPGR}\alpha$-Int(C($\mathcal{A}$))=C($\mathcal{NPGR}\alpha$-Cl($\mathcal{A}$)). Thus (ii) is proved.

Proposition 3.6. Let ($\mathcal{I}$, τ) be a Neutrosophic topological spaces .Then for any Neutrosophic subsets $\mathcal{A}$ and $\mathcal{B}$ of $\mathcal{I}$ we have

(i) $\mathcal{A}$ ⊆ $\mathcal{NPGR}\alpha$-Cl($\mathcal{A}$).

(ii) $\mathcal{A}$ is $\mathcal{NPGR}\alpha$-closed set in $\mathcal{I}$ ⇔$\mathcal{NPGR}\alpha$-Cl($\mathcal{A}$)= $\mathcal{A}$.

(iii) $\mathcal{NPGR}\alpha$-Cl($\mathcal{NPGR}\alpha$-Cl($\mathcal{A}$))=$\mathcal{NPGR}\alpha$-Cl($\mathcal{A}$).

(iv) If $\mathcal{A}$ ⊆ $\mathcal{B}$ then $\mathcal{NPGR}\alpha$-Cl($\mathcal{A}$)⊆$\mathcal{NPGR}\alpha$-Cl($\mathcal{B}$)

Proof: Follows from the Definition 3.1(ii). This proves (i).

Let $\mathcal{A}$ be $\mathcal{NPGR}\alpha$-closed set in $\mathcal{I}$. Then C($\mathcal{A}$) is $\mathcal{NPGR}\alpha$-open set in $\mathcal{I}$. By theorem 3.2(ii), $\mathcal{NPGR}\alpha$-Int(C($\mathcal{A}$))=C($\mathcal{A}$)

⇔C($\mathcal{NPGR}\alpha$-Cl($\mathcal{A}$))=C($\mathcal{A}$)⇔

$\mathcal{NPGR}\alpha$-Cl($\mathcal{A}$)= $\mathcal{A}$.Thus (ii) is proved.

By using Proposition 3.6 (ii), $\mathcal{NPGR}\alpha$-Cl($\mathcal{NPGR}\alpha$-Cl($\mathcal{A}$))=$\mathcal{NPGR}\alpha$-Cl($\mathcal{A}$) .This proves(iii).

Since $\mathcal{A}$ ⊆ $\mathcal{B}$, C($\mathcal{B}$)⊆C($\mathcal{A}$). By using Theorem 3.2(iv), $\mathcal{NPGR}\alpha$-Int(C($\mathcal{B}$))⊆$\mathcal{NPGR}\alpha$-Int(C($\mathcal{A}$)). Taking complement on both sides, C($\mathcal{NPGR}\alpha$-Int(C($\mathcal{B}$)))⊇C($\mathcal{NPGR}\alpha$-Int(C($\mathcal{A}$))). By Proposition 3.5(ii), $\mathcal{NPGR}\alpha$-Cl($\mathcal{A}$)⊆$\mathcal{NPGR}\alpha$-Cl($\mathcal{B}$).This proves(iv).

Proposition 3.7. Let ($\mathcal{I}$, τ) be a Neutrosophic topological spaces. Then for any Neutrosophic subset $\mathcal{A}$ and $\mathcal{B}$ of $\mathcal{I}$, we have

(i) $\mathcal{NPGR}\alpha$-Cl($\mathcal{A}$ ∪ $\mathcal{B}$) =$\mathcal{NPGR}\alpha$-Cl($\mathcal{A}$)∪$\mathcal{NPGR}\alpha$-Cl($\mathcal{B}$) and

(ii) $\mathcal{NPGR}\alpha$-Cl($\mathcal{A}$ ∩ $\mathcal{B}$)⊆$\mathcal{NPGR}\alpha$-Cl($\mathcal{A}$)∩$\mathcal{NPGR}\alpha$-Cl($\mathcal{B}$).

Proof: Since $\mathcal{NPGR}\alpha$-Cl($\mathcal{A}$ ∪ $\mathcal{B}$)= $\mathcal{NPGR}\alpha$-Cl(C(C($\mathcal{A}$ ∪ $\mathcal{B}$))), By using Proposition 3.5(i), $\mathcal{NPGR}\alpha$-Cl($\mathcal{A}$ ∪ $\mathcal{B}$)=C($\mathcal{NPGR}\alpha$-Int(C($\mathcal{A}$ ∪ $\mathcal{B}$))) =C($\mathcal{NPGR}\alpha$-Int(C($\mathcal{A}$)∩C($\mathcal{B}$))). Again using Proposition 3.2(v), $\mathcal{NPGR}\alpha$-Cl($\mathcal{A}$∪ $\mathcal{B}$)=C($\mathcal{NPGR}\alpha$-Int(C($\mathcal{A}$))∩$\mathcal{NPGR}\alpha$-Int(C($\mathcal{B}$)))=C($\mathcal{NPGR}\alpha$-Int(C($\mathcal{A}$))) ∪ C($\mathcal{NPGR}\alpha$-Int(C($\mathcal{B}$))).By using Proposition 3.5(i),

$\mathcal{NPGR}\alpha$-Cl($\mathcal{A}$ ∪ $\mathcal{B}$)=$\mathcal{NPGR}\alpha$-Cl (C(C($\mathcal{A}$)))∪ $\mathcal{NPGR}\alpha$-Cl(C(C($\mathcal{B}$)))= $\mathcal{NPGR}\alpha$-Cl ($\mathcal{A}$)∪ $\mathcal{NPGR}\alpha$-Cl($\mathcal{B}$).

Thus (i) is proved.

Since $\mathcal{A}$ ∩ $\mathcal{B}$ ⊆ $\mathcal{A}$ and $\mathcal{A}$ ∩ $\mathcal{B}$ ⊆ $\mathcal{B}$, by using Proposition 3.6(iv), $\mathcal{NPGR}\alpha$-Cl($\mathcal{A}$ ∩ $\mathcal{B}$)⊆$\mathcal{NPGR}\alpha$-Cl($\mathcal{A}$) and $\mathcal{NPGR}\alpha$-Cl ($\mathcal{A}$ ∩ $\mathcal{B}$) ⊆$\mathcal{NPGR}\alpha$-Cl($\mathcal{B}$).

This implies that $\mathcal{NPGR}\alpha$-Cl($\mathcal{A}$ ∩ $\mathcal{B}$)⊆$\mathcal{NPGR}\alpha$-Cl($\mathcal{A}$)∩ $\mathcal{NPGR}\alpha$-Cl($\mathcal{B}$).This proves (ii).

Remark 3.8. The following example shows that the equality need not hold in Proposition 3.7(ii).

Example 3.9. Let $\mathcal{I}$ = {a, b} and τ = {$0_{\mathcal{N}}$, $1_{\mathcal{N}}$, $\mathcal{U}$, $\mathcal{V}$} where $\mathcal{U}$ ={<0.5, 0.3, 0.6>, <0.4, 0.4, 0.7>} and $\mathcal{V}$ ={<0.7, 0.5, 0.3>, <0.7, 0.5, 0.2>}. Then ($\mathcal{I}$, τ) is a Neutrosophic topological space. Consider the NSs $\mathcal{A}$ ={<0.4, 0.5, 0.4>, <0.7, 0.6, 0.8>} and $\mathcal{B}$={<0.6, 0.3, 0.6>, <0.2, 0.4, 0.5>}in ($\mathcal{I}$, τ).

Then $\mathcal{NPGR}\alpha$-Cl($\mathcal{A}$)={<0.5, 0.5, 0.4>, <0.7, 0.6, 0.7>} and $\mathcal{NPGR}\alpha$-Cl($\mathcal{B}$)={<0.6, 0.3, 0.6>, <0.4, 0.4, 0.3>}, this implies $\mathcal{NPGR}\alpha$-Cl($\mathcal{A}$)∩ $\mathcal{NPGR}\alpha$-Cl($\mathcal{B}$) = {<0.5, 0.3, 0.6>, <0.4, 0.4, 0.7>}.

But $\mathcal{NPGR}\alpha$-Cl($\mathcal{A}$ ∩ $\mathcal{B}$)={<0.4,0.3,0.6>, <0.2,0.4,0.8>}.

Then $\mathcal{NPGR}\alpha$-Cl($\mathcal{A}$)∩$\mathcal{NPGR}\alpha$-Cl($\mathcal{B}$)⊄ $\mathcal{NPGR}\alpha$ -Cl($\mathcal{A}$ ∩$\mathcal{B}$).



0.4>}and $\mathcal{NPGR}\alpha$ -Int($\mathcal{B}$)={<0.6, 0.7, 0.5), <0.8, 0.8, 0.2>}, this implies $\mathcal{NPGR}\alpha$ -Int($\mathcal{A}$)∪ $\mathcal{NPGR}\alpha$ – Int($\mathcal{B}$)= {<0.7, 0.9, 0.2>, <0.8, 0.8, 0.2>]. But $\mathcal{NPGR}\alpha$ -Int($\mathcal{A}$ ∪ $\mathcal{B}$)={<0.8,0.9,0.2>, <0.9,0.8,0.2>}.

Then $\mathcal{NPGR}\alpha$ -Int($\mathcal{A}$ ∪ $\mathcal{B}$)⊄ $\mathcal{NPGR}\alpha$ -Int($\mathcal{A}$ ∪ $\mathcal{B}$).

Proposition 3.5. Let ($\mathcal{I}$, τ) be a Neutrosophic topological space. Then for any Neutrosophic subsets $\mathcal{A}$ of $\mathcal{I}$,

(i) C($\mathcal{NPGR}\alpha$-Int($\mathcal{A}$))=$\mathcal{NPGR}\alpha$-Cl(C($\mathcal{A}$)),

(ii) C($\mathcal{NPGR}\alpha$-Cl($\mathcal{A}$))=$\mathcal{NPGR}\alpha$-Int(C($\mathcal{A}$)).

Proof : By using Definition 3.1(i), $\mathcal{NPGR}\alpha$-Int($\mathcal{A}$) = ∪{$\mathcal{G}$: $\mathcal{G}$ is a $\mathcal{NPGR}\alpha$-open set in A and $\mathcal{G}$ ⊆ $\mathcal{A}$ }.

Taking complement on both sides, C($\mathcal{NPGR}\alpha$-Int($\mathcal{A}$))=C(∪{$\mathcal{G}$: $\mathcal{G}$ is a $\mathcal{NPGR}\alpha$-open set in $\mathcal{I}$ and $\mathcal{G}$ ⊆ $\mathcal{A}$ }) =∩{C($\mathcal{G}$):C($\mathcal{G}$) is a $\mathcal{NPGR}\alpha$-closed set in $\mathcal{I}$ and C($\mathcal{A}$) ⊆ C(G)}. Replacing C(G) by $\mathcal{K}$, we get C($\mathcal{NPGR}\alpha$-Int($\mathcal{A}$))=∩{ $\mathcal{K}$: $\mathcal{K}$ is a $\mathcal{NPGR}\alpha$-closed set in $\mathcal{I}$ and $\mathcal{K}$ ⊇ C($\mathcal{A}$)}. By Definition 3.1(ii), C($\mathcal{NPGR}\alpha$-Int($\mathcal{A}$)) = $\mathcal{NPGR}\alpha$-Cl(C($\mathcal{A}$)). This proves (i).

By using Proposition 3.5 (i), C($\mathcal{NPGR}\alpha$-Int(C($\mathcal{A}$)))=$\mathcal{NPGR}\alpha$-Cl(C(C($\mathcal{A}$)))=$\mathcal{NPGR}\alpha$-Cl($\mathcal{A}$). Taking complement on both sides, we get $\mathcal{NPGR}\alpha$-Int(C($\mathcal{A}$))=C($\mathcal{NPGR}\alpha$-Cl($\mathcal{A}$)). Thus (ii) is proved.

Proposition 3.6. Let ($\mathcal{I}$, τ) be a Neutrosophic topological spaces .Then for any Neutrosophic subsets $\mathcal{A}$ and $\mathcal{B}$ of $\mathcal{I}$ we have

(i) $\mathcal{A}$ ⊆ $\mathcal{NPGR}\alpha$-Cl($\mathcal{A}$).

(ii) $\mathcal{A}$ is $\mathcal{NPGR}\alpha$-closed set in $\mathcal{I}$ ⇔$\mathcal{NPGR}\alpha$-Cl($\mathcal{A}$)= $\mathcal{A}$.

(iii) $\mathcal{NPGR}\alpha$-Cl($\mathcal{NPGR}\alpha$-Cl($\mathcal{A}$))=$\mathcal{NPGR}\alpha$-Cl($\mathcal{A}$).

(iv) If $\mathcal{A}$ ⊆ $\mathcal{B}$ then $\mathcal{NPGR}\alpha$-Cl($\mathcal{A}$)⊆$\mathcal{NPGR}\alpha$-Cl($\mathcal{B}$)

Proof: Follows from the Definition 3.1(ii). This proves (i).

Let $\mathcal{A}$ be $\mathcal{NPGR}\alpha$-closed set in $\mathcal{I}$. Then C($\mathcal{A}$) is $\mathcal{NPGR}\alpha$-open set in $\mathcal{I}$. By theorem 3.2(ii), $\mathcal{NPGR}\alpha$-Int(C($\mathcal{A}$))=C($\mathcal{A}$)

⇔C($\mathcal{NPGR}\alpha$-Cl($\mathcal{A}$))=C($\mathcal{A}$)⇔

$\mathcal{NPGR}\alpha$-Cl($\mathcal{A}$)= $\mathcal{A}$.Thus (ii) is proved.

By using Proposition 3.6 (ii), $\mathcal{NPGR}\alpha$-Cl($\mathcal{NPGR}\alpha$-Cl($\mathcal{A}$))=$\mathcal{NPGR}\alpha$-Cl($\mathcal{A}$) .This proves(iii).

Since $\mathcal{A}$ ⊆ $\mathcal{B}$, C($\mathcal{B}$)⊆C($\mathcal{A}$). By using Theorem 3.2(iv), $\mathcal{NPGR}\alpha$-Int(C($\mathcal{B}$))⊆$\mathcal{NPGR}\alpha$-Int(C($\mathcal{A}$)). Taking complement on both sides, C($\mathcal{NPGR}\alpha$-Int(C($\mathcal{B}$)))⊇C($\mathcal{NPGR}\alpha$-Int(C($\mathcal{A}$))). By Proposition 3.5(ii), $\mathcal{NPGR}\alpha$-Cl($\mathcal{A}$)⊆$\mathcal{NPGR}\alpha$-Cl($\mathcal{B}$).This proves(iv).

Proposition 3.7. Let ($\mathcal{I}$, τ) be a Neutrosophic topological spaces. Then for any Neutrosophic subset $\mathcal{A}$ and $\mathcal{B}$ of $\mathcal{I}$, we have

(i) $\mathcal{NPGR}\alpha$-Cl($\mathcal{A}$ ∪ $\mathcal{B}$) =$\mathcal{NPGR}\alpha$-Cl($\mathcal{A}$)∪$\mathcal{NPGR}\alpha$-Cl($\mathcal{B}$) and

(ii) $\mathcal{NPGR}\alpha$-Cl($\mathcal{A}$ ∩ $\mathcal{B}$)⊆$\mathcal{NPGR}\alpha$-Cl($\mathcal{A}$)∩$\mathcal{NPGR}\alpha$-Cl($\mathcal{B}$).

Proof: Since $\mathcal{NPGR}\alpha$-Cl($\mathcal{A}$ ∪ $\mathcal{B}$)= $\mathcal{NPGR}\alpha$-Cl(C(C($\mathcal{A}$ ∪ $\mathcal{B}$))), By using Proposition 3.5(i), $\mathcal{NPGR}\alpha$-Cl($\mathcal{A}$ ∪ $\mathcal{B}$)=C($\mathcal{NPGR}\alpha$-Int(C($\mathcal{A}$ ∪ $\mathcal{B}$))) =C($\mathcal{NPGR}\alpha$-Int(C($\mathcal{A}$)∩C($\mathcal{B}$))). Again using Proposition 3.2(v), $\mathcal{NPGR}\alpha$-Cl($\mathcal{A}$∪ $\mathcal{B}$)=C($\mathcal{NPGR}\alpha$-Int(C($\mathcal{A}$))∩$\mathcal{NPGR}\alpha$-Int(C($\mathcal{B}$)))=C($\mathcal{NPGR}\alpha$-Int(C($\mathcal{A}$))) ∪ C($\mathcal{NPGR}\alpha$-Int(C($\mathcal{B}$))).By using Proposition 3.5(i),

$\mathcal{NPGR}\alpha$-Cl($\mathcal{A}$ ∪ $\mathcal{B}$)=$\mathcal{NPGR}\alpha$-Cl (C(C($\mathcal{A}$)))∪ $\mathcal{NPGR}\alpha$-Cl(C(C($\mathcal{B}$)))= $\mathcal{NPGR}\alpha$-Cl ($\mathcal{A}$)∪ $\mathcal{NPGR}\alpha$-Cl($\mathcal{B}$).

Thus (i) is proved.

Since $\mathcal{A}$ ∩ $\mathcal{B}$ ⊆ $\mathcal{A}$ and $\mathcal{A}$ ∩ $\mathcal{B}$ ⊆ $\mathcal{B}$, by using Proposition 3.6(iv), $\mathcal{NPGR}\alpha$-Cl($\mathcal{A}$ ∩ $\mathcal{B}$)⊆$\mathcal{NPGR}\alpha$-Cl($\mathcal{A}$) and $\mathcal{NPGR}\alpha$-Cl ($\mathcal{A}$ ∩ $\mathcal{B}$) ⊆$\mathcal{NPGR}\alpha$-Cl($\mathcal{B}$).

This implies that $\mathcal{NPGR}\alpha$-Cl($\mathcal{A}$ ∩ $\mathcal{B}$)⊆$\mathcal{NPGR}\alpha$-Cl($\mathcal{A}$)∩ $\mathcal{NPGR}\alpha$-Cl($\mathcal{B}$).This proves (ii).

Remark 3.8. The following example shows that the equality need not hold in Proposition 3.7(ii).

Example 3.9. Let $\mathcal{I}$ = {a, b} and τ = {$0_{\mathcal{N}}$, $1_{\mathcal{N}}$, $\mathcal{U}$, $\mathcal{V}$} where $\mathcal{U}$ ={<0.5, 0.3, 0.6>, <0.4, 0.4, 0.7>} and $\mathcal{V}$ ={<0.7, 0.5, 0.3>, <0.7, 0.5, 0.2>}. Then ($\mathcal{I}$, τ) is a Neutrosophic topological space. Consider the NSs $\mathcal{A}$ ={<0.4, 0.5, 0.4>, <0.7, 0.6, 0.8>} and $\mathcal{B}$={<0.6, 0.3, 0.6>, <0.2, 0.4, 0.5>}in ($\mathcal{I}$, τ).

Then $\mathcal{NPGR}\alpha$-Cl($\mathcal{A}$)={<0.5, 0.5, 0.4>, <0.7, 0.6, 0.7>} and $\mathcal{NPGR}\alpha$-Cl($\mathcal{B}$)={<0.6, 0.3, 0.6>, <0.4, 0.4, 0.3>}, this implies $\mathcal{NPGR}\alpha$-Cl($\mathcal{A}$)∩ $\mathcal{NPGR}\alpha$-Cl($\mathcal{B}$) = {<0.5, 0.3, 0.6>, <0.4, 0.4, 0.7>}.

But $\mathcal{NPGR}\alpha$-Cl($\mathcal{A}$ ∩ $\mathcal{B}$)={<0.4,0.3,0.6>, <0.2,0.4,0.8>}.

Then $\mathcal{NPGR}\alpha$-Cl($\mathcal{A}$)∩$\mathcal{NPGR}\alpha$-Cl($\mathcal{B}$)⊄ $\mathcal{NPGR}\alpha$ -Cl($\mathcal{A}$ ∩$\mathcal{B}$).



Remark 3.10. Let $\mathcal{A}$ be a Neutrosophic set in a Neutrosophic topological space on $\mathcal{I}$. Then $\text{NInt}(\mathcal{A}) \subseteq \mathcal{NPGR}\alpha\text{-Int}(\mathcal{A}) \subseteq \mathcal{A} \subseteq \mathcal{NPGR}\alpha\text{-Cl}(\mathcal{A}) \subseteq \text{NCl}(\mathcal{A})$.

Theorem 3.11. Let $(\mathcal{I}, \tau)$ be a NTS. Then for any Neutrosophic subsets $\mathcal{A}$ and $\mathcal{B}$ of A we have

(i) $\mathcal{NPGR}\alpha\text{-Cl}(\mathcal{A}) \supseteq \mathcal{A} \cup \mathcal{NPGR}\alpha\text{-Cl}(\mathcal{NPGR}\alpha\text{-Int}(\mathcal{A}))$.

(ii) $\mathcal{NPGR}\alpha\text{-Int}(\mathcal{A}) \subseteq \mathcal{A} \cap \mathcal{NPGR}\alpha\text{-Int}(\mathcal{NPGR}\alpha\text{-Cl}(\mathcal{A}))$.

(iii) $\text{NInt}(\mathcal{NPGR}\alpha\text{-Cl}(\mathcal{A})) \subseteq \text{NInt}(\text{NCl}(\mathcal{A}))$.

(iv) $\text{NInt}(\mathcal{NPGR}\alpha\text{-Cl}(\mathcal{A})) \supseteq \text{NInt}(\mathcal{NPGR}\alpha\text{-Cl}(\mathcal{NPGR}\alpha\text{-Int}(\mathcal{A})))$.

Proof:

By Proposition 3.6(i), $\mathcal{A} \subseteq \mathcal{NPGR}\alpha\text{-Cl}(\mathcal{A})$ (3).

Again using Theorem 3.2(i), $\mathcal{NPGR}\alpha\text{-Int}(\mathcal{A}) \subseteq \mathcal{A}$.

Then, $\mathcal{NPGR}\alpha\text{-Cl}(\mathcal{NPGR}\alpha\text{-Int}(\mathcal{A})) \subseteq \mathcal{NPGR}\alpha\text{-Cl}(\mathcal{A})$ (4).

By(3) and (4) we have, $\mathcal{A} \cup \mathcal{NPGR}\alpha\text{-Cl}(\mathcal{NPGR}\alpha\text{-Int}(\mathcal{A})) \subseteq \mathcal{NPGR}\alpha\text{-Cl}(\mathcal{A})$.

This proves (i).

Taking $\mathcal{NPGR}\alpha$-interior on both sides of equation (3)

$\mathcal{NPGR}\alpha\text{-Int}(\mathcal{A}) \subseteq \mathcal{NPGR}\alpha\text{-Int}(\mathcal{NPGR}\alpha\text{-Cl}(\mathcal{A}))$ (5).

From (4) and (5), $\mathcal{NPGR}\alpha\text{-Int}(\mathcal{A}) \subseteq (\mathcal{A} \cap \mathcal{NPGR}\alpha\text{-Int}(\mathcal{NPGR}\alpha\text{-Cl}(\mathcal{A})))$. This proves (ii).

By Remark 3.10, $\mathcal{NPGR}\alpha\text{-Cl}(\mathcal{A}) \subseteq \text{NCl}(\mathcal{A})$.We get

$\text{NInt}(\mathcal{NPGR}\alpha\text{-Cl}(\mathcal{A})) \subseteq \text{NInt}(\text{NCl}(\mathcal{A}))$.

This proves (iii).

By Theorem 3.11(i), $\mathcal{NPGR}\alpha\text{-Cl}(\mathcal{A}) \supseteq (\mathcal{A} \cup \mathcal{NPGR}\alpha\text{-Cl}(\mathcal{NPGR}\alpha\text{-Int}(\mathcal{A})))$. Taking Neutrosophic interior on both sides, $\text{NInt}(\mathcal{NPGR}\alpha\text{-Cl}(\mathcal{A}) \supseteq \text{NInt}(\mathcal{A} \cup \mathcal{NPGR}\alpha\text{-Cl}(\mathcal{NPGR}\alpha\text{-Int}(\mathcal{A})))$.

Since $\text{NInt}(\mathcal{A} \cup \mathcal{B}) \supseteq \text{NInt}(\mathcal{A}) \cup \text{NInt}(\mathcal{B})$, $\text{NInt}(\mathcal{NPGR}\alpha\text{-Cl}(\mathcal{A}) \supseteq \text{NInt}(\text{A}) \cup \text{NInt}(\mathcal{NPGR}\alpha\text{-Int}(\mathcal{NPGR}\alpha\text{-Int}(\mathcal{A}))) \supseteq \text{NInt}(\mathcal{NPGR}\alpha\text{-Cl}(\mathcal{NPGR}\alpha\text{-Int}(\mathcal{A})))$.Thus (iv) is proved.

Theorem 3.12. Let $(\mathcal{I}, \tau)$ be a Neutrosophic topological space. Then for any Neutrosophic subset $\mathcal{A}$ and $\mathcal{B}$ of $\mathcal{I}$,

(i) $\mathcal{NPGR}\alpha\text{-Cl}(\mathcal{A}) \supseteq \mathcal{A} \cup \mathcal{NPGR}\alpha\text{-Cl}(\mathcal{NPGR}\alpha\text{-Int}(\mathcal{A}))$.

(ii) $\mathcal{NPGR}\alpha\text{-Int}(\mathcal{A}) \subseteq \mathcal{A} \cap \mathcal{NPGR}\alpha\text{-Int}(\mathcal{NPGR}\alpha\text{-Cl}(\mathcal{A}))$.

(iii) $\text{NInt}(\mathcal{NPGR}\alpha\text{-Cl}(\mathcal{A})) \subseteq \text{NInt}(\text{NCl}(\mathcal{A}))$.

(iv) $\text{NInt}(\mathcal{NPGR}\alpha\text{-Cl}(\mathcal{A})) \supseteq \text{NInt}(\mathcal{NPGR}\alpha\text{-Cl}(\mathcal{NPGR}\alpha\text{-Int}(\mathcal{A})))$.

Proof: By Proposition 3.6(i), $\mathcal{A} \subseteq \mathcal{NPGR}\alpha\text{-Cl}(\mathcal{A})$ (6).

Again using Theorem 3.2(i),

$\mathcal{NPGR}\alpha\text{-Int}(\mathcal{A}) \subseteq \mathcal{A}$. (7).

Taking $\mathcal{NPGR}\alpha$-closure on both sides, $\mathcal{NPGR}\alpha\text{-Cl}(\mathcal{NPGR}\alpha\text{-Int}(\mathcal{A})) \subseteq \mathcal{NPGR}\alpha\text{-Cl}(\mathcal{A})$ (8).

By equation (6) and (8), $\mathcal{A} \cup \mathcal{NPGR}\alpha\text{-Cl}(\mathcal{NPGR}\alpha\text{-Int}(\mathcal{A})) \subseteq \mathcal{NPGR}\alpha\text{-Cl}(\mathcal{A})$.

This proves (i).

Again using Theorem 3.2(i), $\mathcal{A} \subseteq \mathcal{NPGR}\alpha\text{-Cl}(\mathcal{A})$. Taking $\mathcal{NPGR}\alpha$-interior on both sides,

$\mathcal{NPGR}\alpha\text{-Int}(\mathcal{A}) \subseteq \mathcal{NPGR}\alpha\text{-Int}(\mathcal{NPGR}\alpha\text{-Cl}(\mathcal{A}))$ (9).

From (7) and (9), we have $\mathcal{NPGR}\alpha\text{-Int}(\mathcal{A}) \subseteq (\mathcal{A} \cap \mathcal{NPGR}\alpha\text{-Int}(\mathcal{NPGR}\alpha\text{-Cl}(\mathcal{A})))$.This proves (ii).

By Theorem 3.11, $\mathcal{NPGR}\alpha\text{-Cl}(\mathcal{A}) \subseteq \text{NCl}(\mathcal{A})$.Then $\text{NInt}(\mathcal{NPGR}\alpha\text{-Cl}(\mathcal{A})) \subseteq \text{NInt}(\text{NCl}(\mathcal{A}))$.Thus (iii) is proved.

By Theorem 3.12(i),$\mathcal{NPGR}\alpha\text{-Cl}(\mathcal{A}) \supseteq (\mathcal{A} \cup \mathcal{NPGR}\alpha\text{-}(\mathcal{NPGR}\alpha\text{-Int}(\mathcal{A})))$.

This implies $\text{NInt}(\mathcal{NPGR}\alpha\text{-Cl}(\mathcal{A}) \supseteq \text{NInt}(\mathcal{A} \cup \mathcal{NPGR}\alpha\text{-Cl}(\mathcal{NPGR}\alpha\text{-Int}(\mathcal{A})))$.

Since $\text{NInt}(\mathcal{A} \cup \mathcal{A}) \supseteq \text{NInt}(\mathcal{A}) \cup \text{NInt}(\mathcal{B})$,$\mathcal{NPGR}\alpha\text{-Int}(\mathcal{NPGR}\alpha\text{-Cl}(\mathcal{A}) \supseteq \text{NInt}(\mathcal{A}) \cup \text{NInt}(\mathcal{NPGR}\alpha\text{-Cl}(\mathcal{NPGR}\alpha\text{-Int}(\mathcal{A}))) \supseteq \text{NInt}(\mathcal{NPGR}\alpha\text{-Cl}(\mathcal{NPGR}\alpha\text{-Int}(\mathcal{A})))$.Thus (iv) is proved.

REFERENCES

[1] M.Abdel-Baset, M., Chang V., and Gamal A., *Evaluation of the green supply chain management practices: A Novel neutrosophic approach, Computers in Industry*, Vol. *108, pp.*210-220, 2019.

[2] Abdel-Basset, M., El-hoseny, M., Gamal, A., &Smarandache, F. *A novel model for evaluation Hospital medical care systems based on plithogenic sets. Artificial intelligence in medicine*, Vol.100, pp.101-110, 2019.

[3] Abdel-Basset, M., Mohamed, R., Zaied, A. E. N. H., & marandache, F., *A hybrid plithogenic decision-making approach with quality function deployment for selecting supply chain sustainability metrics*, *Symmetry,Vol.11(7)*, pp.90, 2019.

[4] Abdel-Basset, M., Saleh, M., Gamal, A., &Smarandache, F. (2019). *An approach of TOPSIS technique for developing supplier selection with group decision making under type-2 neutrosophic number*, Applied Soft Computing, Vol.77, pp.438- 452, 2019.

[5] Atanassov K.T., *Intuitionistic fuzzy sets*, Fuzzy Sets and Systems, pp.87-96, 1986.

[6] Chang C. L., *Fuzzy topological spaces J.Math.Anal.Appl.* Vol.*24*,No.1, pp. 182- 190, 1968.

[7] D. Coker, *An Introduction to Intuitionistic fuzzy topological spaces*, Fuzzy Sets and Systems,Vol. 88, No.1,pp. 81-89, 1997.

[8] R.Dhavaseelan and S. Jafari, *Generalized Neutrosophic closed sets*, New trends in Neutrosophictheory and applications Vol. II, pp.261-273,2018.

[9] Harshitha A. and Jayanthi D., *Regular α-Generalized Closed Ses in Neutrosophic topological Spaces*, IOSR Journal of Mathematics, Vol.15,No. 02,pp.11-18, 2019.

[10] Ishwarya P.and K. Bageerathi, On *Neutrosophic semi-open sets in Neutrosophic topological spaces*,International Journal of math. Trends and Tech., pp.214-223, 2016.

[11] I.M.A. Jaffer and K. Ramesh, *Neutrosophic Generalized Pre Regular Closed Sets*, Neutrosophic Sets and Systems,Vol. 30, pp.171, 2019

[12] Jayanthi D., *On αGeneralized closed sets in Neutrosophic topological spaces*, International conference on Recent trends in mathematics and Information technology (ICRMIT 2018)

[13] W. Al-Omeri and S. Jafari, *On Generalized Closed Sets and Generalized pre-Closed sets in Neutrosophic Topological Spaces*, *Mathematics MDPI*,Vol.7, No.1,pp. 01-12, 2018.

[14] W. Al-omeri and F. Smarandache, *New Neutrosophic sets via Neutrosophic Topological spaces*, New Trends in Neutrosophic Theory and Applications, Vol(2), June 2016.

[15] A.Pushpalatha and T. Nandhini, *Generalized closed sets via neutrosophic topological spaces*, Malaya Journal of Matematik, Vol.7, No.1, pp.50-54, 2019

[16] Salama A.A. and Alblowi S.A., *Neutrosophic set and Neutrosophic topological space*, IOSR Journal of Mathematics, Vol.3, No.4, pp. 31-35,2012.

[17] Salama A. A., F.Smarandache and V. Kroumov, *Neutrosophic closed set and Neutrosophic continuous functions*, *Neutrosophic Sets and Systems*,Vol. 4,pp. 4–8,2014.

[18] Santhi R. and Udhayarani N.,et al., *Nω –Closed sets in Neutrosophic Topological Spaces*, *Neutrosophic Sets and Systems*, Vol.12,No.1, pp. 114-117, 2016.

. [19] F. Smarandache ,*Neutrosophic and Neutrosophic Logic*, First International Conference on Neutrosophic ,Neutrosophic Logic, Set, Probability, and Statistics, University of New Mexico, Gallup, NM, Vol. 87301, USA (2002).

[20]Zadeh, L.A., *Fuzzy sets*, Information and Control, Vol. 8, No.3, pp.338-353, 1965.

Silver nanoparticle - poly (n-isopropylacrylamide) conjugate preparation: biological and chemical characterization studies of the conjugates

Basil Baby[1] and Maya Devi S[2]

[1]Research scholar, Research and Development Center, Bharathiar University, Coimbatore-641046,E Mail :basilvattappillil@gmail.com

[2]Assistant Professor, Department of Chemistry, NSS College of Engineering, Palakkad- 678008, Kerala, E mail: mayadevi968@gmail.com, Ph: 9447217701



Abstract

Conjugation of nanoparticles with organic compounds are performed to enhance the activity and to increase their stability. This property would aid in developing different life saving biomedical products. Based on this objective, silver nanoparticle - poly (N-isopropylacrylamide) conjugate was developed with the aim of investigating its wound healing ability and biocompatibility in the present study. Chemical characterization of developed silver nanoparticles was also studied using FESEM and UV spectroscopic analysis.

Keywords: Silver nanoparticles, poly (N-isopropylacrylamide), Organic ligand, Wound healing, Biocompatibility.

1.0 Introduction

Silver nanoparticles exhibit unique optical properties in the visible spectrum produced by local surface plasmon resonance – SPR (1). Coupling of nearest neighbour nanoparticles within self-assembled arrays further results in new properties so-called collective SPR (2), which induces a shift of the plasmonic peaks or creates hot spots that depend on the interparticle distance (3). Early efforts were focused on synthesis of monodisperse nanoparticles with controlled organic chain length (4). Organic ligands on a nanoparticle surface play an important role in preventing nanoparticles from aggregating, which essentially enables control of interparticle spacing (5). The interparticle distance of the resulting nanoparticles are ill-defined, which limits the ability to tune the SPR. More complicated chemistry is involved during synthesis, which often also results in poor quality control of the monodispersity of the functionalized nanoparticles (6). One way to accomplish this is to use organic ligands that respond to external environmental stimuli (e.g., thermal or pH changes), in order to functionalize the nanoparticle surface (through chemical bonding) so that the interparticle spacing of the resulting functionalized nanoparticles varies in response to external temperature or pH changes (7).

In the recent past, there have been sincere efforts to prepare Ag-NPs–polymer composite materials for applications in the biomedical field. In a work by Li and co-workers [8], polyaniline/silver nanocomposite has been synthesized via in situ chemical oxidation polymerization of aniline in silver salt by some chemical method using H_2O_2 as an external medium. In a significant work by Shameli et al. [9], the antibacterial characteristics of silver/poly(lactic acid) (Ag/PLA-NC) nanocomposite film were investigated. Silver nanoparticles (Ag-NPs) were synthesized into biodegradable PLA via chemical reduction in a diphase solvent. Silver nitrate and sodium borohydride, respectively, were used as a silver precursor and reducing agent in the PLA, which acted as a polymer matrix and stabilizer. In an interesting work by Thomas et al. [10], silver nanoparticles were introduced into poly(acrylamide-co-N-vinyl-2-pyrrolidone) network using a unique strategy, called "Breathing-in–breathing-out" process, using water and acetone as a swelling and shrinking agent for hydrogels respectively [11].

Based on the concept of conjugating silver nanoparticles with an organic compound, we developed a simple and reliable method to synthesize poly (N-isopropyl acrylamide) (PNIPAM) derivative functionalized silver nanoparticle conjugates that are responsive and highly stable to external environmental changes. Thus the conjugate may be used in developing different wound healing materials that could be able to prevent the growth of infectious agents at wound site.

It has long been known that silver, in its ionic form (Ag+), is an environment friendly antimicrobial that is commonly used against many species of bacteria [12]. However, recent investigations of silver in the form of silver nanoparticles (Ag-NPs) have also demonstrated a similar effect at lower concentrations than with the ionic form; effective concentrations have been reported in the literature [13]. The possible use of silver nanoparticles (Ag-NPs) as antibacterial agent has, therefore, been investigated as a means of arresting increasing bacterial resistance to conventional bactericides and antibiotics [14]. The proposed mode of action of Ag-NPs is that they attach to the phosphate and sulfur groups that are part of the phospholipids cell membrane or to the membrane protein and severely damage the cell and its major functions such as permeability, regulation of enzymatic signalling activity and cellular oxidation and respiratory processes. Ag-NPs can penetrate the bacterial cell and accumulate to toxic levels that may cause death of the organism [15].

The objective of developing silver nanoparticle with poly (N-isopropyl acrylamide) compound with the aim of investigating its wound healing ability and biocompatibility was studied in the present study. Chemical characterization of developed silver nanoparticles was also studied using FESEM and UV spectroscopic analysis.

2.0 Materials and methods

2.1 Preparation of Ag nanoparticles (Maribel et al., 2009)

For the preparation of silver nanoparticles two stabilizing agents, Sodium Dodecyl Sulphate (SDS) and Citrate of sodium were used. For the synthesis of silver nanoparticles, silver nitrate solution (1mM) and 8% (w/w) Sodium Dodecyl

Sulphate (SDS) were used as a metal salt precursor and a stabilizing agent, respectively. Hydrazine hydrate solution with a concentrate (2mM) and Citrate of sodium solution (1mM) were used as a reducing agent. Citrate of sodium was also used as stabilizing agent at room temperature. The transparent colourless solution was converted to the characteristic pale yellow and pale red colour, when citrate of sodium was used as stabilizing agent. The occurrence of colour was indicated the formation of silver nanoparticles. The silver nanoparticles were purified by centrifugation. To remove excess silver ions, the silver colloids were washed at least three times with deionized water.

2.2 Preparation of Np-PNIPAM Composites (Ruben and Wolfgang, 2007)

Aqueous mixtures of 1mM silver nitrate and PNIPAM at indicated molar ratios of PNIPAM/Ag were prepared and stirred at room temperature. After 5 min of stirring, $NaBH_4$was added to achieve a 3:1 molar ratio of$NaBH_4$/Ag+. The solution was stirred for 5 min to react and then immediately diluted with water to 4 times the volume to stop the reaction. The diluted solution was then heated to 40°C during centrifugation at 16 600 g for 15 min to sequentially precipitate Ag-PNIPAM and then the polymer. The Ag-PNIPAM nanoparticles were recovered by centrifugation at 10000 rpm for 10 min and then resuspended in water. This process was performed twice, followed by freeze drying to recuperate the nanocomposite in a powder form for storage at-20°C.

2.3 Chemical characterization of Ag nanoparticles

Field emission scanning electron microscopy (FESEM)

The size and morphology of the synthesized silver nanoparticles using field emission scanning electron microscopy (JSM-7500F, JEOL, Japan) was analyzed. A minute drop of nanoparticle powder was cast on to a carbon-coated copper grid and subsequently transferred to the microscope. The high-resolution images of silver nanoparticles were recorded and the morphology of AgNPs was further studied.

UV-Vis spectrophotometer studies

The UV-Vis spectrophotometer (Elico–BL 198) was used to measure the wavelength between 300 and 800 nm to monitor the formation of silver nanoparticles at regular intervals. Dilutions of samples were made if the sample was too concentrated. The UV-visible reading was recorded and then analyzed using the Origin Pro or Microsoft Excel analysis tool.

2.34 Biological characterization of Ag-NIPAM conjugates

Development of wound healing materials coated with Ag-NIPAM composite

The functional coating of wound healing mesh material using the developed Ag-NIPAM composite was done by a standard two dip-coating technique (Gollwitzer et al., 2003). The technique started with the preparation of stable slurry with 500 mg of Ag-NIPAM composites in the molten polyethylene glycol (1000 mg) in a glass vial. The mixture was heated at the range of 60°C–70°C in a water bath to obtain homogeneous slurry. The resulting slurry was homogenized in a magnetic stirrer for 5–10 minutes. The wound healing mesh disk was cut (10mm) using sterile devices and dip-coated twice with intermittent drying (suspension coating method).

The dip-coating procedure was carried out in sterile glass beakers on a shaker (120 rpm) for 30 min, with a drying period of about 15 minutes between the two coating procedures, followed by drying at room temperature. All the coating steps were carried out under strict aseptic conditions. After the coating procedure, the materials were stored at 4°C for up to 15 minutes. In order to increase the composite load and prevent excessive increase in material thickness, the coating process were repeated for replicates of each sample. Subsequently, in order to slow down the release rate of composite from PEG coating and mitigate the friction effect between material surfaces, a second coating layer was formed using PVA (poly vinyl alcohol). PVA was dissolved in DMSO to acquire a 10% (w/w) solution. PEG coated materials were submerged into PVA solution three times for 1 minute each. The coated materials were left to dry on a clean bench for 24–48 hours at room temperature to remove residual DMSO. The wound healing mesh coated with Ag-NIPAM composite was subjected to determine its wound healing ability and biocompatibility property.

Determining the wound healing ability of composite – Wound scratch assay

L_{929} mouse fibroblast cells grown in 24 well plates at a density (1 X 10^5 cells per ml) with ~80 % confluence was taken for the analysis. A small linear scratch was created in the confluent monolayer by gently scraping with sterile cell scrapper as per the method of Liang et al. (2007). After creating a scratch on L_{929} mouse fibroblast cell lines, the cell migration, cell proliferation and wound closure was measured for the selected concentrate (100 µg) of Ag-NIPAM composite at different time periods (0^{th} hour, 12^{th} hour and 24^{th} hour). Migration of cells between the scratch site and the distance traversed by cells migrating into the denuded area which emphasize the self-healing was observed using phase contrast microscope for each time period.

***In vitro* biocompatibility studies of Ag-NIPAM composite using standard MTT assay methods (Ebtesam Saad Al-Sheddi *et al.*, 2014)**

Cytotoxicity assay is often used to evaluate the *in-vitro* cytotoxicity of polymeric components as it is a quick, effective method for testing mitochondrial impairment and correlates quite well with cell proliferation. It is based on the use of tetrazolium salt 3-[4,5-dimethylthiazolyl-2]-2,5-diphenyl tetrazolium bromide (MTT), which can be converted to an insoluble blue formazan product by mitochondrial enzymes in viable cells. L_{929} fibroblast cell line is often used to evaluate cytotoxicity of Ag-NIPAM composite.

The fibroblast cell lines were cultivated in 12-well-microtitre plates to reach confluence growth. The composite sample was applied directly to the developed fibroblast monolayer. Before cell seeding, the plates were pre-wetted in 70 % aqueous ethanol solution for 48 h, rinsed twice with ultrapure (deionized) water. The specimens were then seeded with L_{929} fibroblast cell line at 10,000 cells per well according to routine cell-culture methods. The plates were incubated at 37°C and 5 % CO_2 for fifteen days. The effect of composite on the biocompatibility of fibroblast was evaluated using the photometric MTT assay.

At each time point, samples were taken from the 24-well plates and transferred into new plates for the MTT study. The MTT solution was prepared by dissolving the powder in phosphate buffered saline at a concentration 1 mg/ml. After 1hr of incubation, the purple crystals were dissolved by adding sodium dodecylsulphate (SDS) in a 1:1 mixture of water and dimethyl formamide (DMF)

at a concentration of 20% w/v. After adding 1ml of MTT medium (0.0005mg/ml) to each well, the plates were incubated for 3h, rinsed and desorbed in 100 ul of 70 % isopropanol. After being agitated rapidly at 400 rpm /min for 40 min, the dyed medium was transferred to 96-well plate, and read at 550 nm. The biocompatibility or cell viability is expressed as a percentage of the control sample (100 %).

Evaluating the efficacy of developed wound healing materials coated with Ag-NIPAM composite against wound causing bacteria

An Ag-NIPAM composite coated mesh sample was subjected to evaluate its efficacy against the wound causing organisms. Standard Disc diffusion method was used to evaluate the activity. Briefly, Mueller-Hinton agar plates (Composition g/L: Acid hydrolysate of Casein: 17.5 g; Starch: 1.5 g, Sodium chloride: 5.0 g, Agar 17.0 g; Final pH - 7.0 ± 0.2) plates were prepared by pouring 15 ml of media into sterile Petri dishes. The plates were allowed to solidify for 5min and 0.1ml inoculum was swabbed uniformly and allowed to dry for 60 sec. Premeasured disc shaped (20 mm in diameter) Ag-NIPAM composite coated wound mesh were placed on the Mueller-Hinton agar plates plates (seeded with test bacterial inoculum). The disc was gently pressed to attach on the agar surface using sterile conditions. A plain mesh without composite was also kept in the plate as control. All the plates were incubated at 37 °C for 24 to 48 h. At the end of incubation, the zone of inhibition formed around each material was measured in millimeter. Experiments were carried out in triplicates and the activity was expressed in Standard deviation values using Statistical Package for Social Sciences (SPSS - 9 for Windows 7.0) software.

3.0 Results and discussion

The synthesis of AgNPs was performed with 0.01 M of silver nitrate solution with marine alga extract in Erlenmeyer flask in the ratio of 1:10, respectively, at the initial time point of the synthesis reaction, and 0.01 M of silver nitrate solution without marine alga extract was maintained as a control. The solution remains colorless and showed no color change even after 48 h upon heating as shown in Fig. 3a. The reduction of silver nitrate ($AgNO_3$) was visually confirmed by the change of color from yellowish-brown to reddish-brown after 30 min of reaction

as shown in Fig. 3b. The color of the marine alga extract became turbid after the addition of aqueous $AgNO_3$ solution signifying the initiation of the reaction. The intensity of brown color increased in direct proportion to the heating period of 24 h followed by 48 h as shown in Fig. 3c, d

3.1 Chemical characterization of Ag nanoparticles

Field emission scanning electron microscopy analysis

A field emission scanning electron microscope (FESEM) was employed to analyze the morphology structure, size, shape, and distribution of the nanoparticles formed. From Fig. 1, it is evident that the silver nanoparticles were coalesced to nano-clusters. When the reaction mixtures of the synthesis medium of silver nanoparticles were indirectly heated for 48h, most of the nanoparticles tend to be aggregated as shown in Fig.1. When silver nanoparticles aggregate, the metal particles become electronically coupled and this coupled system has a different surface plasmon resonance than the individual particles.

UV-Vis spectrophotometer studies

In order to confirm the formation of silver nanoparticles in the developed conjugate, UV-Vis absorption studies revealed a strong characteristic absorption peak around 405 nm for the silver nanoparticles due to the surface plasmon resonance effect (Fig. 2). However, the plain PNIPAM did not revealed any peaks indicating the absence of silver in the sample. Similar results have also been reported by Thomas et al (10) when poly (acrylamide-co-acrylic acid) hydrogel/silver nanocomposites demonstrated a sharp surface plasmon resonance peak at 406 nm.

3.2 Biological characterization of Ag-NIPAM conjugates

Determining the wound healing ability of composite – Wound scratch assay

In vitro wound healing assays have commonly been applied to measure cell migration, cell proliferation and wound closure in response to stimulation with specific agents. In this study, the Ag-NIPAM composite used for the cell adhesion

studies was determined for its ability to improve wound healing by acting directly on L_{929} mouse fibroblast cells.

After creating a scratch on L_{929} mouse fibroblast cell lines, the cell migration, cell proliferation and wound closure was measured for a known concentration (100 µg) of Ag-NIPAM composite at three different time periods (0^{th} hour, 12^{th} hour and 24^{th} hour). Fig. 3 corresponding to self-wound healing ability of the developed Ag-NIPAM composite showed that, at 0^{th} hour, no cell migration and proliferation was observed for the known concentrate (100 µg) including control (Distilled water). At 12^{th} hour, positive cell migration and cell proliferation was observed when compared to the control sample. After 24hours, more cell proliferation was evident and thus indicating the better wound healing ability of Ag-NIPAM composite.

In vitro scratch assay could be recorded as an appropriate and inexpensive method for the wound healing potential of herbal composite used in the present research. Similar *in vitro* wound scratch assay method was recorded from the literature survey. Srinivasa Rao Bolla et al. (2019) recently investigated the wound healing capacity of *Aristolochia saccata* leaf extract by using *In vitro* wound scratch assay, where proliferative and migratory capabilities of test compounds could be monitored through microscopy studies. L_{929} fibroblast cell line was used for the assay. Scratch assay showed 34.05 %, 70.00 %, 93.52 % wound closure at 12 hrs, 24 hrs and 48 hrs of incubation respectively. These results were similar compared to positive control which showed 37.60 %, 56.41% and 99.05 % of wound closure. As there was similar wound healing abilities were noted for many antimicrobial compounds from the literature survey on L_{929} mouse fibroblast cell lines, it was proved that the developed Ag-NIPAM composite could be used for the development of novel tissue engineered wound healing materials.

Biocompatibility of the developed organometallic conjugates – MTT assay

The biocompatibility test of any medical product / devices / wound dressing is essential to assure its safety to the patients. Biocompatibility of the device is normally investigated using analytical chemistry, *in-vitro* test, and animal models. Here, the biocompatibility of non-adhering wound mesh materials coated with Ag-NIPAM composite was evaluated by cytotoxicity assay (*in-vitro*

cell culture model). *In-vitro* methods of cytotoxicity can demonstrate the occurrence of changes within the cells, ranging from cell death to very subtle alterations of certain cellular functions. Non-adhering dressings are commonly used during granulation, tissue formation, and re-epithelialization. Dressings' effects were investigated by comprehensive *in vitro* approach- MTT assay measuring cell viability after direct contact. MTT assay is often used to evaluate the *in-vitro* cytotoxicity of polymeric components as it is a quick, effective method for testing mitochondrial impairment and correlates quite well with cell proliferation. It is based on the use of tetrazolium salt 3-[4,5-dimethylthiazolyl-2]-2,5-diphenyl tetrazolium bromide (MTT), which can be converted to an insoluble blue formazan product by mitochondrial enzymes in viable cells. L_{929} fibroblast cell line is often used to evaluate cytotoxicity of wound dressing mesh as tissue engineered skin containing different types of cells like keratinocytes, melanocytes, and fibroblasts.

The fibroblast cell lines were cultivated in 12-well-microtitre plates to reach confluence growth. The dressing samples (1.0 cm × 1.0 cm) were applied directly to the developed fibroblast monolayer. The effect of the different non-adhering dressings on fibroblast viability was evaluated using the photometric MTT assay. The wound dressing coated with Ag-NIPAM composite exhibited no effect on cell viability, indicating that they did not alter viable cell count over the respective study period (24 hours) compared to the untreated control samples. The results were described below separately for each selected concentration of synergistic drugs + carrier with the support of table values and graphical representations attributing for cell cytotoxicity and cell viability. The cytotoxic effect on cell viability and cell morphology was also depicted for each concentration of Ag-NIPAM composite in Fig. 4.

The biocompatibility of the synergistic drug concentrations (5, 10, 15, 20, 25 μg/ml) were tested. During the analysis, no significant cytotoxicity was observed for the selected drug concentrations; the cytotoxicity was ranging between 5.2 % and 14.7 %. Interestingly, higher cell viability for the drug concentrations was evident (85.3 % to 99 %). The cytotoxicity (%) of the drug combinations were 14.7 % for 5 μg, 7.1 % for 10 μg, 6.5 % for 15μg, 5.2 % for 20

μg and 0% for 25 μg. The cell viability (%) for the drug combinations were found to be 85.3% for 5 μg, 92.9 % for 10 μg, 93.5% for 15 μg, 94.8 % for 20 μg and > 99 % for 25 μg (Table-2).

In Fig. 4, the wound dressing mesh coated with selected concentrations (5, 10, 15, 20μg/ml) do not have much cytotoxic effect, as they show high cell viability in all extract concentrations. Further, there was no significant difference in the morphology of the L_{929} fibroblast cells after 24 hours of cell culturing in the cell culture media (DMEM). Even after 24 hours not much significant difference occurred on cell morphology of fibroblast cells even though some notable differences in cell morphology and appearance of few vacuoles have been found in 10, 15, 20, 25 μg concentrates. The appearance of these vacuoles may be due to the fusion of multiple membranes of fibroblast cells.

The results revealed that the drug concentration did not inhibit the growth of cells; thus indicating the biocompatibility of the synergistic drug combinations for the development of tissue engineered wound dressing materials.

Evaluating the efficacy of developed wound healing materials coated with Ag-NIPAM composite against wound causing bacteria

The efficacy of developed wound healing materials coated with Ag-NIPAM composite showed good inhibitory activity against wound causing bacteria. About 27.3 ± 0.56 mm and 27.1 ± 1.03 mm of inhibitory zone was observed for *Enterococcus faecium* and *Staphylococcus aureus*. Followed by, 27.8 ± 0.27 mm and 27.3 ± 0.56 mm of inhibitory zone was observed for *Klebsiella pneumonia* and *Acenitobacter baumanni. Proteus* sp. *Pseudomonas aeruginosa* exhibited 27.6 ± 1.03 mm and 27.9 ± 0.27 mm respectively (Table-1, Fig-5). The mechanism of action of the antibacterial activity of AgNPs is attacking the respiratory chain and cell division that ultimately leads to cell death. The silver nanoparticles have also been reported to release silver ions inside the bacterial cells, further enhancing their bactericidal activity (16). It has also been proposed that there can be release of silver ions by the nanoparticles, and these ions can interact with the thiol groups of many vital enzymes and inactivate them. The bacterial cells in contact with silver take in silver ions, which inhibit several functions in the cell and damage the cells. Then, there is the generation of reactive

μg and 0% for 25 μg. The cell viability (%) for the drug combinations were found to be 85.3% for 5 μg, 92.9 % for 10 μg, 93.5% for 15 μg, 94.8 % for 20 μg and > 99 % for 25 μg (Table-2).

In Fig. 4, the wound dressing mesh coated with selected concentrations (5, 10, 15, 20μg/ml) do not have much cytotoxic effect, as they show high cell viability in all extract concentrations. Further, there was no significant difference in the morphology of the L_{929} fibroblast cells after 24 hours of cell culturing in the cell culture media (DMEM). Even after 24 hours not much significant difference occurred on cell morphology of fibroblast cells even though some notable differences in cell morphology and appearance of few vacuoles have been found in 10, 15, 20, 25 μg concentrates. The appearance of these vacuoles may be due to the fusion of multiple membranes of fibroblast cells.

The results revealed that the drug concentration did not inhibit the growth of cells; thus indicating the biocompatibility of the synergistic drug combinations for the development of tissue engineered wound dressing materials.

Evaluating the efficacy of developed wound healing materials coated with Ag-NIPAM composite against wound causing bacteria

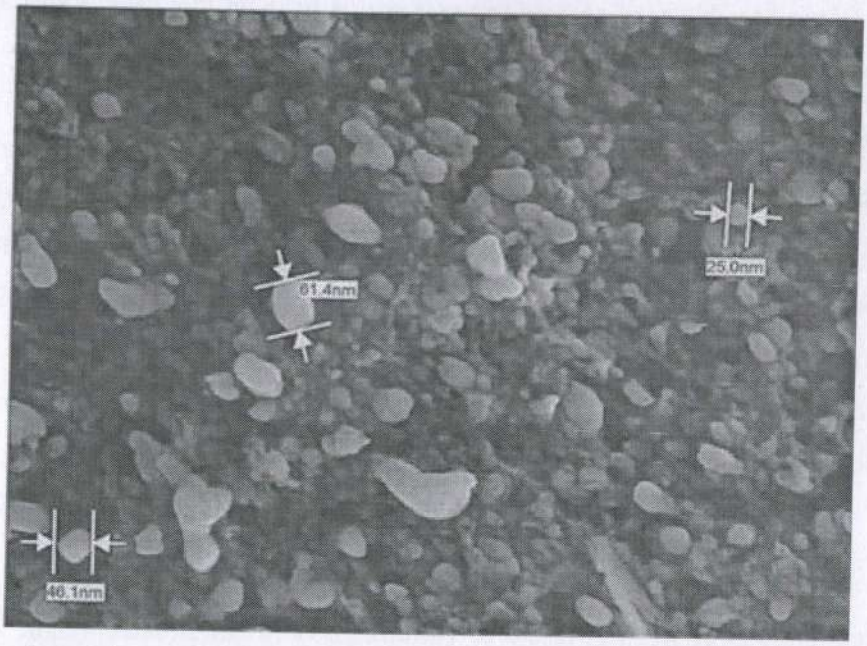
The efficacy of developed wound healing materials coated with Ag-NIPAM composite showed good inhibitory activity against wound causing bacteria. About 27.3 ± 0.56 mm and 27.1 ± 1.03 mm of inhibitory zone was observed for *Enterococcus faecium* and *Staphylococcus aureus*. Followed by, 27.8 ± 0.27 mm and 27.3 ± 0.56 mm of inhibitory zone was observed for *Klebsiella pneumonia* and *Acenitobacter baumanni*. *Proteus* sp. *Pseudomonas aeruginosa* exhibited 27.6 ± 1.03 mm and 27.9 ± 0.27 mm respectively (Table-1, Fig-5). The mechanism of action of the antibacterial activity of AgNPs is attacking the respiratory chain and cell division that ultimately leads to cell death. The silver nanoparticles have also been reported to release silver ions inside the bacterial cells, further enhancing their bactericidal activity (16). It has also been proposed that there can be release of silver ions by the nanoparticles, and these ions can interact with the thiol groups of many vital enzymes and inactivate them. The bacterial cells in contact with silver take in silver ions, which inhibit several functions in the cell and damage the cells. Then, there is the generation of reactive

oxygen species, which are produced possibly through the inhibition of a respiratory enzyme by silver ions and attack the cell itself. Silver is a soft acid, and there is a natural tendency of an acid to react with a base, in this case, a soft acid to react with a soft base (17).

Conflict of Interest

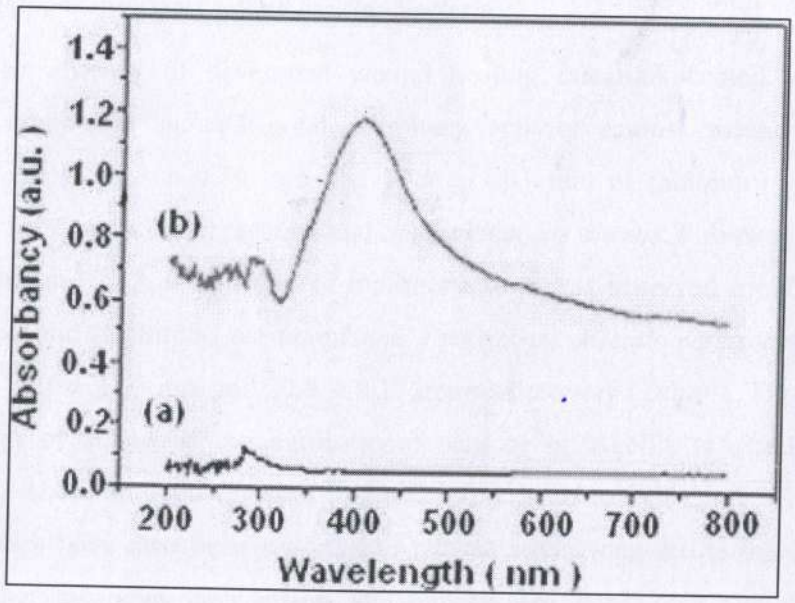
Authors declare no conflict of interest in the present research.

Fig-1: Field emission scanning electron microscopy analysis of silver nanoparticles



Coalesced nano-clusters of silver nanoparticles with varied size observed during FESEM analysis

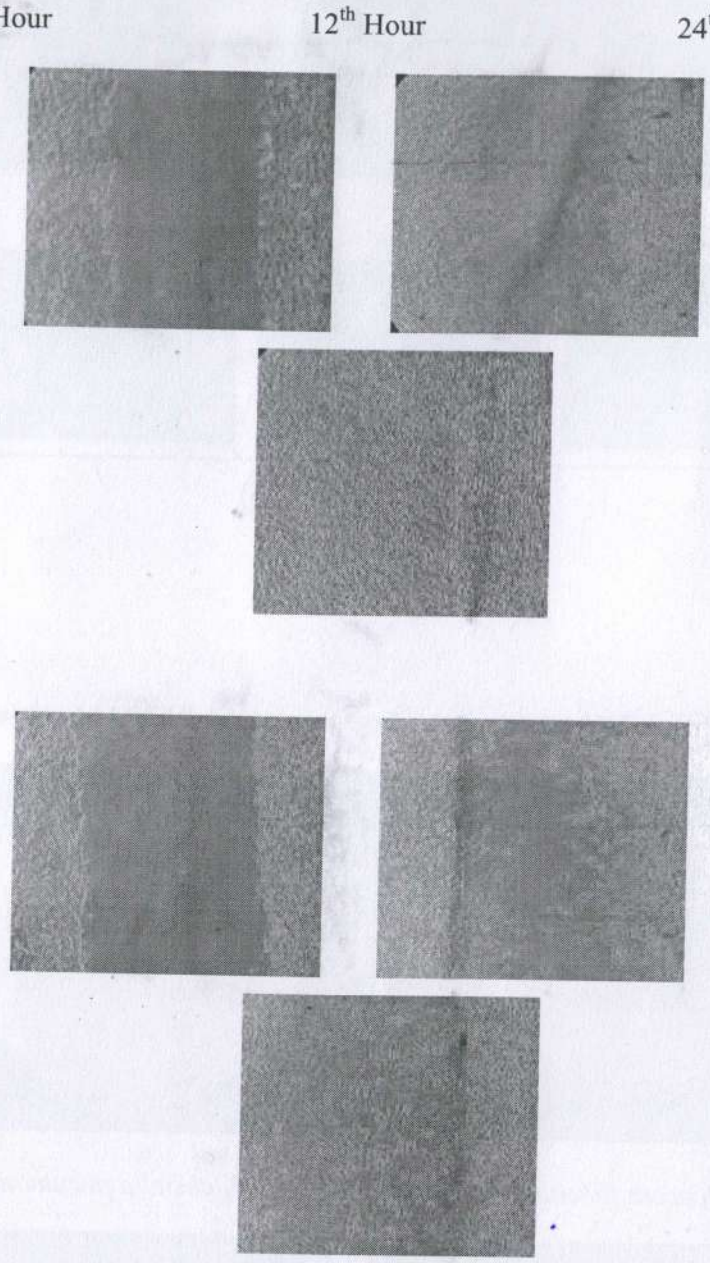
Fig-2: UV-Vis spectrophotometer studies



(a) UV-Vis spectrophotometer studies of Silver nanoparticles in conjugate

(b) UV-Vis spectrophotometer studies of plain PNIPAM without silver nanoparticles

Fig. 3: Self-wound healing scratch assay: *In vitro* Wound Scratch Assay



A: Control (Distilled water) [Top three pictures]

B: Herbal extract sample (100µg) [Bottom three pictures]

Fig. 4: Microscopic analysis of the Biocompatibility of Ag-NIPAM composite coated wound mesh

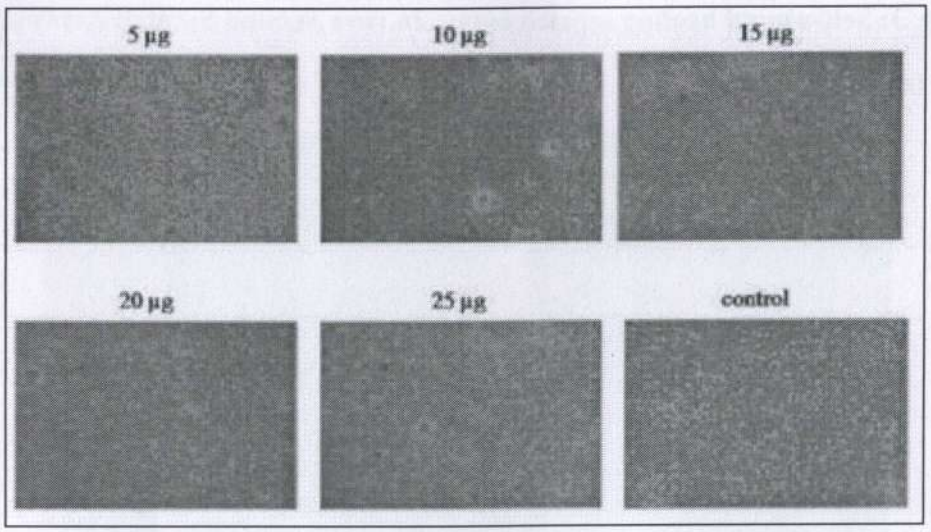
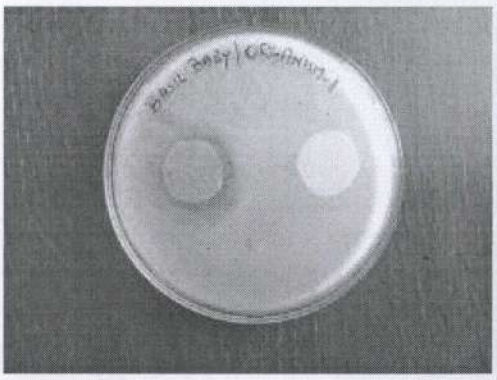
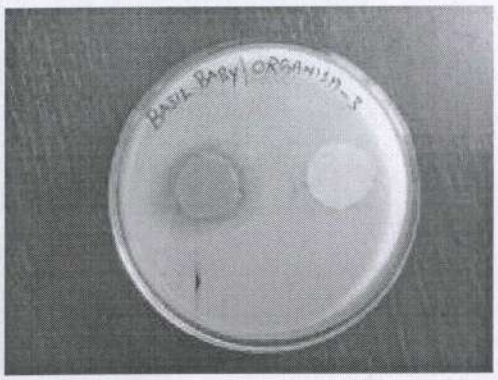


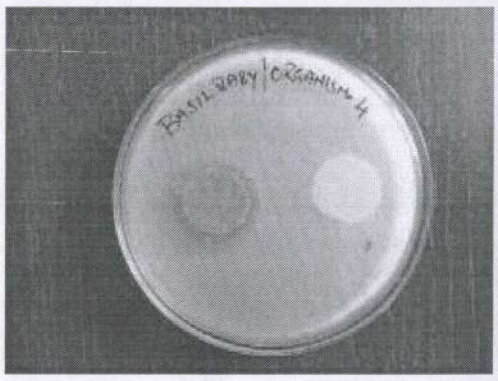
Fig-5: Antibacterial activity of the Ag Nps and Ag-PNIPAM conjugates



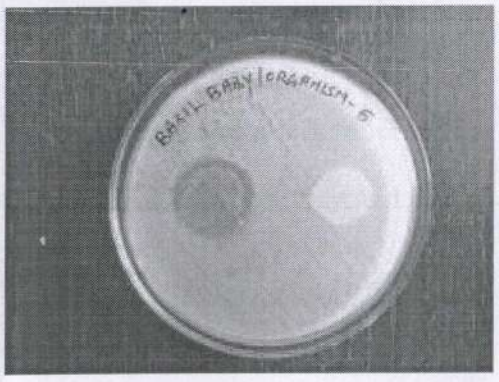
Enterococcus faecium



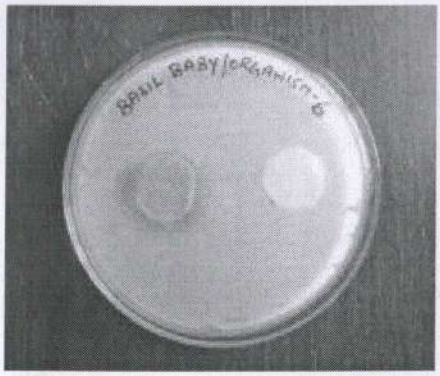
Klebsiella pneumonia



Acenitobacter baumannii



Proteus sp



Pseudomonas aeruginosa

Table-1: Antibacterial activity of the Ag Nps and Ag-PNIPAM composites

S. No	Test Organisms	Inhibitory zones (mm)	
		Ag Nps Coated	Ag-PNIPAM Coated
1	*Enterococcus faecium*	0	27.3 ± 0.56
2	*Staphylococcus aureus*	0	27.1 ± 1.03
3	*Klebsiella pneumoniae*	0	27.8 ± 0.27
4	*Acenitobacter baumannii*	0	27.3 ± 0.56
5	*Proteus* sp	0	27.6 ± 1.03
6	*Pseudomonas aeruginosa*	0	27.9 ± 0.27

Table-2: Cytotoxicity analysis of wound dressings

S. No.	Fibroblast cell lines – MTT Assay			Cytotoxic reactivity
	Concentration (µg)	Cytotoxicity (%)	Cell viability (%)	
1	5	14.7	85.3	Slight
2	10	7.1	92.9	Slight
3	15	6.5	93.5	Slight
4	20	5.2	94.8	Slight
5	25	0	>99	No cytotoxicity

References

1. Wu, T.; Ge, Z. S.; Liu, S. Y. Fabrication of Thermoresponsive Cross-Linked Poly(N-Isopropylacrylamide) Nanocapsules and Silver Nanoparticle-Embedded Hybrid Capsules with Controlled Shell Thickness. Chem. Mater. 2011, 23, 2370–2380.

2. Chiu, C. S.; Chen, H. Y.; Hsiao, C. F.; Lin, M. H.; Gwo, S. Ultrasensitive Surface Acoustic Wave Detection of Collective Plasmonic Heating by Close-Packed Colloidal Gold

Nanoparticles Arrays. J. Phys. Chem. C 2013, 117, 2442–2448.

3. Tian, L. M.; Chen, E.; Gandra, N.; Abbas, A.; Singamaneni, S. Gold Nanorods as Plasmonic Nanotransducers: Distance-Dependent Refractive Index Sensitivity. Langmuir 2012, 28, 17435–17442.

4. Choi, J. J.; Luria, J.; Hyun, B. R.; Bartnik, A. C.; Sun, L.; Lim, Y. F.; Marohn, J. A.; Wise, F. W.; Hanrath, T. Photogenerated Exciton Dissociation in Highly Coupled Lead Salt Nanocrystal Assemblies. Nano Lett. 2010, 10, 1805–1811.

5. Chen, C. F.; Tzeng, S. D.; Chen, H. Y.; Lin, K. J.; Gwo, S. Tunable Plasmonic Response from Alkanethiolate-Stabilized Gold Nanoparticle Superlattices: Evidence of Near-Field Coupling. J. Am. Chem. Soc. 2008, 130, 824–826.

6. Li, D. X.; He, Q.; Yang, Y.; Mohwald, H.; Li, J. B. Two-Stage pH Response of Poly(4-Vinylpyridine) Grafted Gold Nanoparticles. Macromolecules 2008, 41, 7254–7256.

7. Tang, F.; Ma, N.; Wang, X. Y.; He, F.; Li, L. D. Hybrid Conjugated Polymer-Ag@PNIPAM Fluorescent Nanoparticles with Metal-Enhanced Fluorescence. J. Mater. Chem. 2011, 21, 16943–16948.

8. Mahesh D. Bedre, Raghunandan Deshpande, Basavaraj Salimath, Venkataraman Abbaraju. Preparation and characterization of polyaniline-co_3o_4 nanocomposites via interfacial polymerization. Amer J Mat Sci. 2012; 2(3): 39-43.

9. Shameli, K, Ahmad, MB, Md Zin Wan Yunus, W, Ibrahim, NA, Rahman, RA, Jokar, M, and Darroudi M. Silver/poly (lactic acid) nanocomposites: Preparation, characterization, and antibacterial activity. Int J Nanomed. 2010; 5(1): 573-579.

10. Thomas V, Yallapu MM, Sreedhar B and Bajpai SK. Breathing-in/breathing-out approach to preparing nanosilver-loaded hydrogels: Highly efficient antibacterial nanocomposites. J. Appl. Polym. Sci. 2008; 111: 934-944.

11. Mohan YM, Vimala K, Thomas V, Varaprasad K, Sreedhar B and Bajpai SK. Controlling of silver nanoparticles structure by hydrogel networks. J. Colloid Interface Sci. 2010; 342(1): 73-82.

12. Kim JS, Antibacterial activity of Ag ion-containing silver nanoparticles prepared using the alcohol reduction method. J. Ind. Eng. Chem. 2007; 13(5): 718-72.

13. Dror-Ehre A, H. Mamane, T. Belenkova, G. Markovich and A. Adin, J. Silver nanoparticle – *Escherichia coli* colloidal interaction in water and effect on E. coli survival. Colloid Interface Sci.2009: 339: 521.

14. Saxena S and Bajpai SK, Is a Cationic-Resin-Loaded Polymeric Gel a Better Antibacterial Material than a Nanosilver-Loaded Gel. Designed Monomers Polymers. 2010: 13: 157-165.

15. P. Sanpui, A. Murugadoss, P. V. Durga-Prasad, S. S. Ghosh and A. Chatopadhyay, The antibacterial properties of a novel chitosan-Ag-nanoparticle composite. Int. J. Food Microbiol. 2008; 124: 142-146.

16. Sukumaran Prabhu and Eldho K Poulose. Silver nanoparticles: mechanism of antimicrobial action, synthesis, medical applications, and toxicity effects. Int Nano Lett. 2012; 32.

17. Yun'an Qing, Lin Cheng, Ruiyan Li, Guancong Liu, Yanbo Zhang, Xiongfeng Tang, Jincheng Wang, He Liu, and Yanguo Qin. Potential antibacterial mechanism of silver nanoparticles and the optimization of orthopedic implants by advanced modification technologies. Int J Nanomedicine. 2018; 13: 3311–3327.

Journal of Physics: Conference Series

PAPER • OPEN ACCESS

Fractional derivatives of some special functions using ABR and ABC derivatives

To cite this article: R. Prabha and S. Kiruthika 2021 *J. Phys.: Conf. Ser.* **1850** 012040

View the article online for updates and enhancements.

ECS

240th ECS Meeting

Digital Meeting, Oct 10-14, 2021

We are going fully digital!

Attendees register for free!

REGISTER NOW



This content was downloaded from IP address 27.61.23.66 on 23/09/2021 at 05:06

Fractional derivatives of some special functions using ABR and ABC derivatives

Prabha R.[1] **& Kiruthika S.**[2]

[1] Department of Science and Humanities, Ahalia School of Engineering and Technology, Palakkad, India.
[2]Department of Mathematics, Amrita School of Engineering, Amrita Vishwa Vidyapeetham, Coimbatore, India.

E-mail: s_kiruthika@cb.amrita.edu

Abstract

In this paper, we present the Atangana Baleanu fractional derivatives of some special functions such as trigonometric, exponential and hyperbolic functions. The AB fractional derivatives are calculated using the formula for RL derivatives and are calculated for all functions which belong to L^1 [a,b]. The importance of these derivatives comes from the fact that certain dissipative phenomena cannot be explained using classical fractional operators.

Keywords: Atangana Baleanu fractional derivatives, Mittag Leffler kernel, Normalisation function

1. Introduction

Fractional calculus is an emerging field of research in the past two decades with expeditious development and continuous extension which has its origin 3 centuries ago. The classical calculus gives prominence on finding the solutions of linear differential equations [25, 19]whereas the fractional calculus gives importance for finding the solutions of nonlinear differential equations which are used to solve differential equations of non-integer order and applied in the field of confined ground water modelling [2, 17, 18], optimization theory [1, 6] and so on. Fractional calculus is applied and practised in many research fields, especially in medicine where it is used for the control of diseases like dengue, tuberculosis, ebola, hepatitis, blood flow [24] and in physics for stability, image processing [23, 14, 16, 13]. The contributors in the field of fractional calculus include Riemann Liouville, Caputo, Abel, etc. Out of all, Niels Henrick Abel made a tremendous contribution to the field of fractional calculus

Content from this work may be used under the terms of the Creative Commons Attribution 3.0 licence. Any further distribution of this work must maintain attribution to the author(s) and the title of the work, journal citation and DOI.
Published under licence by IOP Publishing Ltd

in generalization of the tautochrone problem for finding the solution of curve along which a bead can move down with the least time of descent [4]. The nonlocal property of the fractional derivatives having memory effect attracted the interests of researchers to design various modelling problems which cannot be accomplished using derivatives of integer order [12, 9].

Several definitions for fractional derivatives are derived in a manner that the classical derivatives are substituted and used in different fields of research. During the initial stages, researchers used classical fractional operators defined using a singular kernel which is not capable of solving complicated problems of real dynamics. Thus, a new class of fractional derivatives using non-singular kernel is introduced for modelling problems [5, 6, 11, 8] which include Caputo Fabrizio derivatives having exponential kernel and Atangana Baleanu derivatives having Mittag Leffler kernel. These derivatives with non-singular kernels have captured the attention of many scientists not only in mathematics but also in economics, social sciences, data science and so on. Their importance is mainly focused in the AB model of fractional calculus [3, 21, 14], in mechanisms of biological systems for the treatment of cancer and so on. One such method is chemotherapy which has got many side effects such as vomiting, hair loss, and many serious health issues. Hence a mathematical model using these fractional derivatives with non-singular kernel has been employed to optimize the drug content so that the chemotherapy side effects are minimized. This motivated us to derive the derivatives of these special functions.

In this paper, we derive the ABR, ABC derivatives of some special functions using the Maclaurin's series expansion and these derivatives are obtained using the Riemann Liouville integral of the power function of various orders. The paper is structured as follows: In section 2, we have given the definitions, results and formulae used. We present the ABR and ABC derivatives of trigonometric, exponential and hyperbolic functions in sections 3, 4 and 5 respectively and the conclusion is given in section 6.

2. Preliminaries

Definition 2.1. [10] The Atangana Baleanu Riemann Liouville derivative of order α, $0 < \alpha < 1$, is given by

$$^{ABR}D^{\alpha}_{a+}f(t) = \frac{B(\alpha)}{1-\alpha}\frac{d}{dt}\int_a^t f(x)E_{\alpha}(\frac{-\alpha}{1-\alpha}(t-x)^{\alpha})dx.$$

Definition 2.2. [10] The Atangana Baleanu Caputo derivative of order $\alpha, 0 < \alpha < 1$, is given by

$$^{ABC}D^{\alpha}_{a+}f(t) = \frac{B(\alpha)}{1-\alpha}\int_a^t f'(x)E_{\alpha}(\frac{-\alpha}{1-\alpha}(t-x)^{\alpha})dx.$$

In the above definitions, the Mittag Leffler function in one parameter is given by

$$E_\alpha(z) = \sum_{k=0}^{\infty} \frac{(z)^k}{\Gamma(\alpha k + 1)}$$

We have used the definitions of ABR and ABC fractional derivatives of order α, $0 < \alpha < 1$, using Mittag Leffler kernel [15, 7] needed to establish our results and studied the existence of fractional derivatives for the trignometric, exponential and hyperbolic functions which are useful in solving the differential equations of the same kind. The normalisation function $B(\alpha)$ can be chosen according to our wish to satisfy certain properties [7, 10]. So, throughout this paper, in the derivation of ABR and ABC derivatives of the special functions, we take $a = 0$, $\alpha = \frac{1}{2}$, $B\left(\frac{1}{2}\right) = 1$ and the RL intergal [12, 20] of the power function of order $\frac{k}{2}+1$. Also the final results of ABR and ABC derivatives of special functions are obtained as a sum of Mittag-Leffler functions in two parameters [19] which plays a vital role in fractional calculus, as gamma function does in the ordinary calculus.

3. ABR and ABC derivatives of sine and cosine functions

3.1. ABR derivative of sine function

$$\begin{aligned}
{}^{ABR}D_{0+}^{\frac{1}{2}} \sin t &= \frac{B(\frac{1}{2})}{1-\frac{1}{2}} \frac{d}{dt} \int_0^t \sin x \; E_{\frac{1}{2}} \left(\frac{\frac{-1}{2}(t-x)^{\frac{1}{2}}}{1-\frac{1}{2}} \right) dx \\
&= 2B(\frac{1}{2}) \frac{d}{dt} \int_0^t \sin x \; E_{\frac{1}{2}} \left(-(t-x)^{\frac{1}{2}} \right) dx \\
&= 2 \frac{d}{dt} \int_0^t \sin x \; E_{\frac{1}{2}} \left(-(t-x)^{\frac{1}{2}} \right) dx \\
&= 2 \frac{1}{\Gamma(\frac{k}{2}+1)} \frac{d}{dt} \int_0^t \sin x \sum_{k=0}^{\infty} (-1)^k (t-x)^{\frac{k}{2}} dx \\
&= 2 \frac{1}{\Gamma(\frac{k}{2}+1)} \sum_{k=0}^{\infty} (-1)^k \frac{d}{dt} \int_0^t \sin x (t-x)^{\frac{k}{2}} dx \\
&= 2 \frac{1}{\Gamma(\frac{k}{2}+1)} \sum_{k=0}^{\infty} (-1)^k \frac{d}{dt} \int_0^t (x - \frac{x^3}{3!} + \frac{x^5}{5!} - \cdots)(t-x)^{\frac{k}{2}} \; dx \\
&= 2 \frac{1}{\Gamma(\frac{k}{2}+1)} \sum_{k=0}^{\infty} (-1)^k \frac{d}{dt} \left\{ \int_0^t x(t-x)^{\frac{k}{2}} - \int_0^t \frac{x^3}{3!}(t-x)^{\frac{k}{2}} + \int_0^t \frac{x^5}{5!}(t-x)^{\frac{k}{2}} - \cdots \right\} dx \\
&= 2 \sum_{k=1}^{\infty} (-1)^{(k-1)} (t)^{(2k-1)} E_{\frac{1}{2},2k}(-t)^{\frac{1}{2}}.
\end{aligned}$$



Fractional derivatives of some special functions using ABR and ABC derivatives

3.2. ABC derivative of sine function

$$
\begin{aligned}
{}^{ABC}D^{\frac{1}{2}}_{0+}\sin t &= \frac{B(\frac{1}{2})}{1-\frac{1}{2}}\int_0^t \cos x\; E_{\frac{1}{2}}\left(\frac{\frac{-1}{2}(t-x)^{\frac{1}{2}}}{1-\frac{1}{2}}\right)dx \\
&= 2B(\frac{1}{2})\int_0^t \cos x\; E_{\frac{1}{2}}\left(-(t-x)^{\frac{1}{2}}\right)dx \\
&= 2\int_0^t \cos x\; E_{\frac{1}{2}}\left(-(t-x)^{\frac{1}{2}}\right)dx \\
&= 2\frac{1}{\Gamma(\frac{k}{2}+1)}\int_0^t \cos x\sum_{k=0}^{\infty}(-1)^k(t-x)^{\frac{k}{2}}dx \\
&= 2\frac{1}{\Gamma(\frac{k}{2}+1)}\sum_{k=0}^{\infty}(-1)^k\int_0^t \cos x(t-x)^{\frac{k}{2}}dx \\
&= 2\frac{1}{\Gamma(\frac{k}{2}+1)}\sum_{k=0}^{\infty}(-1)^k\int_0^t (1-\frac{x^2}{2!}+\frac{x^4}{4!}-\cdots)(t-x)^{\frac{k}{2}}\;dx \\
&= 2\frac{1}{\Gamma(\frac{k}{2}+1)}\sum_{k=0}^{\infty}(-1)^k\left\{\int_0^t 1(t-x)^{\frac{k}{2}}-\int_0^t\frac{x^2}{2!}(t-x)^{\frac{k}{2}}+\int_0^t\frac{x^4}{4!}(t-x)^{\frac{k}{2}}-\cdots)\right\}dx \\
&= 2\sum_{k=1}^{\infty}(-1)^{(k-1)}(t)^{(2k-1)}E_{\frac{1}{2},2k}(-t)^{\frac{1}{2}}.
\end{aligned}
$$

3.3. ABR derivative of cosine function

$$
\begin{aligned}
{}^{ABR}D^{\frac{1}{2}}_{0+}\cos t &= \frac{B(\frac{1}{2})}{1-\frac{1}{2}}\frac{d}{dt}\int_0^t \cos x\; E_{\frac{1}{2}}\left(\frac{\frac{-1}{2}(t-x)^{\frac{1}{2}}}{1-\frac{1}{2}}\right)dx \\
&= 2B(\frac{1}{2})\frac{d}{dt}\int_0^t \cos x\; E_{\frac{1}{2}}\left(-(t-x)^{\frac{1}{2}}\right)dx \\
&= 2\frac{d}{dt}\int_a^t \cos x\; E_{\frac{1}{2}}\left(-(t-x)^{\frac{1}{2}}\right)dx \\
&= 2\frac{1}{\Gamma(\frac{k}{2}+1)}\frac{d}{dt}\int_0^t \cos x\sum_{k=0}^{\infty}(-1)^k(t-x)^{\frac{k}{2}}dx \\
&= 2\frac{1}{\Gamma(\frac{k}{2}+1)}\sum_{k=0}^{\infty}(-1)^k\frac{d}{dt}\int_0^t \cos x(t-x)^{\frac{k}{2}}dx \\
&= 2\frac{1}{\Gamma(\frac{k}{2}+1)}\sum_{k=0}^{\infty}(-1)^k\frac{d}{dt}\int_0^t (1-\frac{x^2}{2!}+\frac{x^4}{4!}-\cdots)(t-x)^{\frac{k}{2}}\;dx \\
&= 2\frac{1}{\Gamma(\frac{k}{2}+1)}\sum_{k=0}^{\infty}(-1)^k\frac{d}{dt}\left\{\int_0^t 1(t-x)^{\frac{k}{2}}-\int_0^t\frac{x^2}{2!}(t-x)^{\frac{k}{2}}+\int_0^t\frac{x^4}{4!}(t-x)^{\frac{k}{2}}-\cdots\right\}dx \\
&= 2\sum_{k=1}^{\infty}(-t^2)^{(k-1)}E_{\frac{1}{2},2k-1}(-t)^{\frac{1}{2}}.
\end{aligned}
$$

Fractional derivatives of some special functions using ABR and ABC derivatives

3.4. ABC derivative of cosine function

$$
\begin{aligned}
{}^{ABC}D^{\frac{1}{2}}_{0+}cost &= \frac{B(\frac{1}{2})}{1-\frac{1}{2}}\int_0^t -sinxE_{\frac{1}{2}}(\frac{-\frac{1}{2}}{1-\frac{1}{2}}(t-x)^{\frac{1}{2}}) \\
&= 2B(\frac{1}{2})\int_0^t -\sin x E_{\frac{1}{2}}(-(t-x)^{\frac{1}{2}})dx \\
&= 2\int_0^t -\sin x E_{\frac{1}{2}}(-(t-x)^{\frac{1}{2}})dx \\
&= 2\frac{1}{\Gamma(\frac{k}{2}+1)}\int_0^t -\sin x\sum_{k=0}^{\infty}(-1)^k(t-x)^{\frac{k}{2}}dx \\
&= 2\frac{1}{\Gamma(\frac{k}{2}+1)}\sum_{k=0}^{\infty}(-1)^k\int_0^t -\sin x(t-x)^{\frac{k}{2}}dx \\
&= 2\frac{1}{\Gamma(\frac{k}{2}+1)}\sum_{k=0}^{\infty}(-1)^k\int_0^t -(x-\frac{x^3}{3!}+\frac{x^5}{5!}-\cdots)(t-x)^{\frac{k}{2}}dx \\
&= 2\frac{1}{\Gamma(\frac{k}{2}+1)}\sum_{k=0}^{\infty}(-1)^k\left\{\int_0^t -x(t-x)^{\frac{k}{2}}+\int_0^t\frac{x^3}{3!}(t-x)^{\frac{k}{2}}-\int_0^t\frac{x^5}{5!}(t-x)^{\frac{k}{2}}+\cdots)\right\}dx \\
&= 2\sum_{k=1}^{\infty}(-1)^k(t)^{2k}E_{\frac{1}{2},2k+1}(-t)^{\frac{1}{2}}.
\end{aligned}
$$

4. ABR and ABC derivatives of Exponential function

4.1. ABR derivative of the Exponential function

$$
\begin{aligned}
{}^{ABR}D^{\frac{1}{2}}_{0+}e^t &= \frac{B(\frac{1}{2})}{1-\frac{1}{2}}\frac{d}{dt}\int_0^t e^x E_{\frac{1}{2}}\left(\frac{-\frac{1}{2}}{1-\frac{1}{2}}(t-x)^{\frac{1}{2}}\right)\,dx \\
&= 2\frac{d}{dt}\int_0^t e^x E_{\frac{1}{2}}(-(t-x)^{\frac{1}{2}})dx \\
&= 2\frac{1}{\Gamma(\frac{k}{2}+1)}\frac{d}{dt}\int_0^t e^x\sum_{k=0}^{\infty}(-1)^k(t-x)^{\frac{k}{2}}\,dx \\
&= 2\frac{1}{\Gamma(\frac{k}{2}+1)}\sum_{k=0}^{\infty}(-1)^k\frac{d}{dt}\int_0^t e^x(t-x)^{\frac{k}{2}}\,dx \\
&= 2\frac{1}{\Gamma(\frac{k}{2}+1)}\sum_{k=0}^{\infty}(-1)^k\frac{d}{dt}\int_0^t(1+\frac{x}{1!}+\frac{x^2}{2!}+\cdots)(t-x)^{\frac{k}{2}}\,dx \\
&= 2\sum_{k=1}^{\infty}t^{k-1}E_{\frac{1}{2},k}(-t)^{\frac{1}{2}}.
\end{aligned}
$$



Fractional derivatives of some special functions using ABR and ABC derivatives

4.2. ABC derivative of the Exponential function

$$
\begin{aligned}
{}^{ABC}D_{0+}^{\frac{1}{2}}e^t &= \frac{B(\frac{1}{2})}{1-\frac{1}{2}}\int_0^t e^x E_{\frac{1}{2}}\left(\frac{-\frac{1}{2}}{1-\frac{1}{2}}(t-x)^{\frac{1}{2}}\right)\,dx \\
&= 2B(\frac{1}{2})\int_0^t e^x E_{\frac{1}{2}}(-(t-x)^{\frac{1}{2}})\,dx \\
&= \int_0^t e^x E_{\frac{1}{2}}(-(t-x)^{\frac{1}{2}})dx \\
&= 2\frac{1}{\Gamma(\frac{k}{2}+1)}\int_0^t e^x \sum_{k=0}^{\infty}(-1)^k(t-x)^{\frac{k}{2}}\,dx \\
&= 2\frac{1}{\Gamma(\frac{k}{2}+1)}\sum_{k=0}^{\infty}(-1)^k\int_0^t e^x(t-x)^{\frac{k}{2}}\,dx \\
&= 2\frac{1}{\Gamma(\frac{k}{2}+1)}\sum_{k=0}^{\infty}(-1)^k\int_0^t (1+\frac{x}{1!}+\frac{x^2}{2!}+\cdots)(t-x)^{\frac{k}{2}}\,dx \\
&= 2\frac{1}{\Gamma(\frac{k}{2}+1)}\sum_{k=0}^{\infty}(-1)^k\left\{\int_0^t 1(t-x)^{\frac{k}{2}}+\int_0^t \frac{x}{1!}(t-x)^{\frac{k}{2}}+\int_0^t \frac{x^2}{2!}(t-x)^{\frac{k}{2}}-\cdots\right\}dx \\
&= 2\sum_{k=1}^{\infty}t^k E_{\frac{1}{2},k+1}(-t)^{\frac{1}{2}}.
\end{aligned}
$$

5. ABR and ABC derivatives of the Hyperbolic functions

5.1. ABR derivative of hyperbolic sine function

$$
\begin{aligned}
{}^{ABR}D_{0+}^{\frac{1}{2}}\sinh t &= \frac{B(\frac{1}{2})}{1-\frac{1}{2}}\frac{d}{dt}\int_0^t \sinh x\; E_{\frac{1}{2}}\left(\frac{\frac{-1}{2}(t-x)^{\frac{1}{2}}}{1-\frac{1}{2}}\right)dx \\
&= 2\int_0^t \sinh x\; E_{\frac{1}{2}}\left(-(t-x)^{\frac{1}{2}}\right)dx \\
&= 2\frac{1}{\Gamma(\frac{k}{2}+1)}\frac{d}{dt}\int_0^t \sinh x\sum_{k=0}^{\infty}(-1)^k(t-x)^{\frac{k}{2}}dx \\
&= 2\frac{1}{\Gamma(\frac{k}{2}+1)}\sum_{k=0}^{\infty}(-1)^k\frac{d}{dt}\int_0^t \sinh x(t-x)^{\frac{k}{2}}dx \\
&= 2\frac{1}{\Gamma(\frac{k}{2}+1)}\sum_{k=0}^{\infty}(-1)^k\frac{d}{dt}\int_0^t (x+\frac{x^3}{3!}+\frac{x^5}{5!}+\cdots)(t-x)^{\frac{k}{2}}\,dx \\
&= 2\sum_{k=1}^{\infty}(t)^{(2k-1)}E_{\frac{1}{2},2k}(-t)^{\frac{1}{2}}.
\end{aligned}
$$

Fractional derivatives of some special functions using ABR and ABC derivatives

5.2. ABR derivative of hyperbolic cosine function

$$
\begin{aligned}
{}^{ABR}D_{0+}^{\frac{1}{2}}\cosh t &= \frac{B(\frac{1}{2})}{1-\frac{1}{2}}\frac{d}{dt}\int_0^t \cosh x\; E_{\frac{1}{2}}\left(\frac{\frac{-1}{2}(t-x)^{\frac{1}{2}}}{1-\frac{1}{2}}\right)dx \\
&= 2\int_a^t \cosh x\; E_{\frac{1}{2}}\left(-(t-x)^{\frac{1}{2}}\right)dx \\
&= 2\frac{1}{\Gamma(\frac{k}{2}+1)}\frac{d}{dt}\int_0^t \cosh x\sum_{k=0}^{\infty}(-1)^k(t-x)^{\frac{k}{2}}dx \\
&= 2\frac{1}{\Gamma(\frac{k}{2}+1)}\sum_{k=0}^{\infty}(-1)^k\frac{d}{dt}\int_0^t \cosh x(t-x)^{\frac{k}{2}}dx \\
&= 2\frac{1}{\Gamma(\frac{k}{2}+1)}\sum_{k=0}^{\infty}(-1)^k\frac{d}{dt}\int_0^t (1++\frac{x^2}{2!}+\frac{x^4}{4!}+\cdots)(t-x)^{\frac{k}{2}}\;dx \\
&= 2\frac{1}{\Gamma(\frac{k}{2}+1)}\sum_{k=0}^{\infty}(-1)^k\frac{d}{dt}\left\{\int_0^t 1(t-x)^{\frac{k}{2}}+\int_0^t\frac{x^2}{2!}(t-x)^{\frac{k}{2}}+\int_0^t\frac{x^4}{4!}(t-x)^{\frac{k}{2}}-\cdots\right\}dx \\
&= 2\sum_{k=1}^{\infty}(t^2)^{(k-1)}E_{\frac{1}{2},2k-1}(-t)^{\frac{1}{2}}.
\end{aligned}
$$

5.3. ABC derivative of hyperbolic sine function

$$
\begin{aligned}
{}^{ABC}D_{0+}^{\frac{1}{2}}\sinh t &= \frac{B(\frac{1}{2})}{1-\frac{1}{2}}\int_0^t \cosh x\; E_{\frac{1}{2}}\left(\frac{\frac{-1}{2}(t-x)^{\frac{1}{2}}}{1-\frac{1}{2}}\right)dx \\
&= 2B(\frac{1}{2})\int_0^t \cosh x\; E_{\frac{1}{2}}\left(-(t-x)^{\frac{1}{2}}\right)dx \\
&= 2\int_0^t \cosh x\; E_{\frac{1}{2}}\left(-(t-x)^{\frac{1}{2}}\right)dx \\
&= 2\frac{1}{\Gamma(\frac{k}{2}+1)}\int_0^t \cosh x\sum_{k=0}^{\infty}(-1)^k(t-x)^{\frac{k}{2}}dx \\
&= 2\frac{1}{\Gamma(\frac{k}{2}+1)}\sum_{k=0}^{\infty}(-1)^k\int_0^t \cosh x(t-x)^{\frac{k}{2}}dx \\
&= 2\frac{1}{\Gamma(\frac{k}{2}+1)}\sum_{k=0}^{\infty}(-1)^k\int_0^t (1+\frac{x^2}{2!}+\frac{x^4}{4!}+\cdots)(t-x)^{\frac{k}{2}}\;dx \\
&= 2\frac{1}{\Gamma(\frac{k}{2}+1)}\sum_{k=0}^{\infty}(-1)^k\left\{\int_0^t 1(t-x)^{\frac{k}{2}}+\int_0^t\frac{x^2}{2!}(t-x)^{\frac{k}{2}}+\int_0^t\frac{x^4}{4!}(t-x)^{\frac{k}{2}}+\cdots\right\}dx \\
&= 2\sum_{k=1}^{\infty}t^{2k-1}E_{\frac{1}{2},2k}(-t)^{\frac{1}{2}}.
\end{aligned}
$$



Fractional derivatives of some special functions using ABR and ABC derivatives

5.4. ABC derivative of hyperbolic cosine function

$$
\begin{aligned}
{}^{ABC}D^{\frac{1}{2}}_{0+}cosht &= \frac{B(\frac{1}{2})}{1-\frac{1}{2}}\int_0^t sinhxE_{\frac{1}{2}}(\frac{-\frac{1}{2}}{1-\frac{1}{2}}(t-x)^{\frac{1}{2}}) \\
&= 2\int_0^t \sinh x E_{\frac{1}{2}}(-(t-x)^{\frac{1}{2}})dx \\
&= 2\frac{1}{\Gamma(\frac{k}{2}+1)}\int_0^t \sinh x \sum_{k=0}^{\infty}(-1)^k(t-x)^{\frac{k}{2}}dx \\
&= 2\frac{1}{\Gamma(\frac{k}{2}+1)}\sum_{k=0}^{\infty}(-1)^k\int_0^t \sinh x(t-x)^{\frac{k}{2}}dx \\
&= 2\frac{1}{\Gamma(\frac{k}{2}+1)}\sum_{k=0}^{\infty}(-1)^k\int_0^t (x+\frac{x^3}{3!}+\frac{x^5}{5!}+\cdots)(t-x)^{\frac{k}{2}}dx \\
&= 2\frac{1}{\Gamma(\frac{k}{2}+1)}\sum_{k=0}^{\infty}(-1)^k\left\{\int_0^t x(t-x)^{\frac{k}{2}}+\int_0^t \frac{x^3}{3!}(t-x)^{\frac{k}{2}}+\int_0^t \frac{x^5}{5!}(t-x)^{\frac{k}{2}}+\cdots)\right\}dx \\
&= 2\frac{1}{\Gamma(\frac{k}{2}+1)}\sum_{k=0}^{\infty}(-1)^k\left\{\int_0^t x(t-x)^{\frac{k}{2}}+\int_0^t \frac{x^3}{3!}(t-x)^{\frac{k}{2}}+\int_0^t \frac{x^5}{5!}(t-x)^{\frac{k}{2}}+\cdots)\right\}dx \\
&= 2\sum_{k=1}^{\infty}(t)^{2k}E_{\frac{1}{2},2k+1}(-t)^{\frac{1}{2}}.
\end{aligned}
$$

6. Conclusion

The ABR and ABC derivatives are used for solving differential equations using numerical methods and Laplace transforms which are applied in the modelling problems of physics, chaos theory and various other fields [17, 18]. The Atangana Baleanu derivatives are also evaluated for many other functions [1, 3, 22, 7] such as power function, product of two functions etc. in which these derivatives satisfy the product rule, chain rule, semigroup property and so on. The results established in this paper can be extended to different orders and these describe a foundation for the theory of AB differintegrals.

References

[1] Alqahtani.R.T 2016 Atangana Baleanu derivative with fractional order applied to the model of groundwater with an unconfined acquifier *J.Nonlinear Sci. Appl* **9** 3647-3654.

[2] Abdeljawad.T and Baleanu.D 2011 Fractional differences and integration by parts *J.Comput.Anal.Appl* **13** 574-582 .

[3] Abdeljawad.T and Baleanu.D 2016 Discrete fractional differences with non singular discrete Mittag Leffler Kernels *Advances in difference Equations* **232** 1-18.

[4] Abdeljawad.T and Baleanu.D 2017 Integration by parts and its applications of a new non local fractional derivative with Mittag Leffler nonsingular kernel *J.Nonlinear Sci. Appl* **10** 1098-1107.

[5] Abdeljawad.T and Baleanu.D 2017 On fractional derivatives with exponential kernel and their discrete versions *Rep.Math Phys* **80** 11-27.
[6] Abdeljawad.T and Baleanu.D 2018 *Advances in difference Equations* pp 468.
[7] Atangana.A and Baleanu.D 2016 New fractional derivatives with nonlocal and nonsingular kernel *Theory and Application to heat transfer model Therm Sci* **20** 763-769.
[8] Caputo.M and Fabrizio.M 2015 A new definition of fractional derivative without singular kernel *Progr Fract Differ Appl* **1** 73-85.
[9] Evans.L.C 2010 *Partial differrential equations* American Mathematical Society.
[10] Fernandez.A and Baleanu.D 2018 On some new properties of fractional derivatives with Mittag Leffler kernel *Common Nonlinear Sci Numer Simulat* **59** 444-462.
[11] Fernandez.A and Baleanu.D 2018 The mean value theorem and Taylors' theorem for fractional derivatives with Mittag Leffler Kernel, *Advances in difference Equations* **86**.
[12] Haubold.H.J, Mathai.A.M and Saxena.R.K 2011 Mittag Leffler Functions and their Applications *Journal Of Applied Mathematics* pp 51.
[13] Hilfer. R 2000 *Applications of Fractional Calculus in Physics* World Scientific, Singapore.
[14] Kilbas A.A 2005 *Fractional Calculus and Applied Analysis* **8** 113–126.
[15] Kilbas.A.A, Saigo.M, Saxena.K 2004 Generalized Mittag-Leffler function and generalized fractional calculus operators *Integral Transforms Spec.Funct.* **15** 31-49.
[16] Kilbas.A.A, Srivastava.H.M and Trujillo.J.J, *Theory and Applications of Fractional Differential Equations* Elsevier, Amsterdam, 2006.
[17] Mehdinejadiani.B, Jafari.H and Baleanu.D 2013 Derivation of a fractional Boussinesq equation for modelling unconfined groundwater *Eur.Phys.J.Spec.Top.* **222** 1805–1812.
[18] Mehdinejadiani.B, Naseri.A.A, Jafari.H, Ghanbarzadeh.A, Baleanu.D 2013 A Mathematical model for simulation of a water table profile between two parallel subsurface drains using fractional derivative *Comput.Math.Appl.* **66** 785–794.
[19] Miller.K.S and Ross.B 1993 *An Introduction to the Fractional Calculus and Fractional Differential Equations,* Wiley,New York.
[20] Podlubny.I 1999 *Fractional Differential Equations,* Academic Press, New York.
[21] Prabhakar T.R 1971 A singular integral equation with a generalized Mittag Leffler function in the kernel *Yokohama Math.J* **19** 7-15.
[22] Samko. S.G, Kilbas. A.A and Marichev. O.I 1993 *Fractional Integrals and Derivatives; Theory and Applications,* Gordon and Breach,Amsterdam.
[23] Vinodkumar.A, Senthilkumar.T, Li. X 2018 Robust exponential stability results for uncertain infinite delay differential systems with random impulsive moments, *Advances in Difference Equations.*
[24] Ali.F, Yousaf.S, Khan.I, Sheikh NA 2019 A new idea of Atangana Baleanu fractional derivatives to blood flow with magnetics particles in a circular cylinder, *Journal of Magnetism And Magnetic Materials* **486** 165282.
[25] Gao.W, Ghanbari.B, Boskunos.H.M 2019 New Numerical simulations for some real world problems with Atangana Baleanu fractional derivative *Chaos,solitons and fractals* **128** 34-43



Journal of Physics: Conference Series

PAPER • OPEN ACCESS

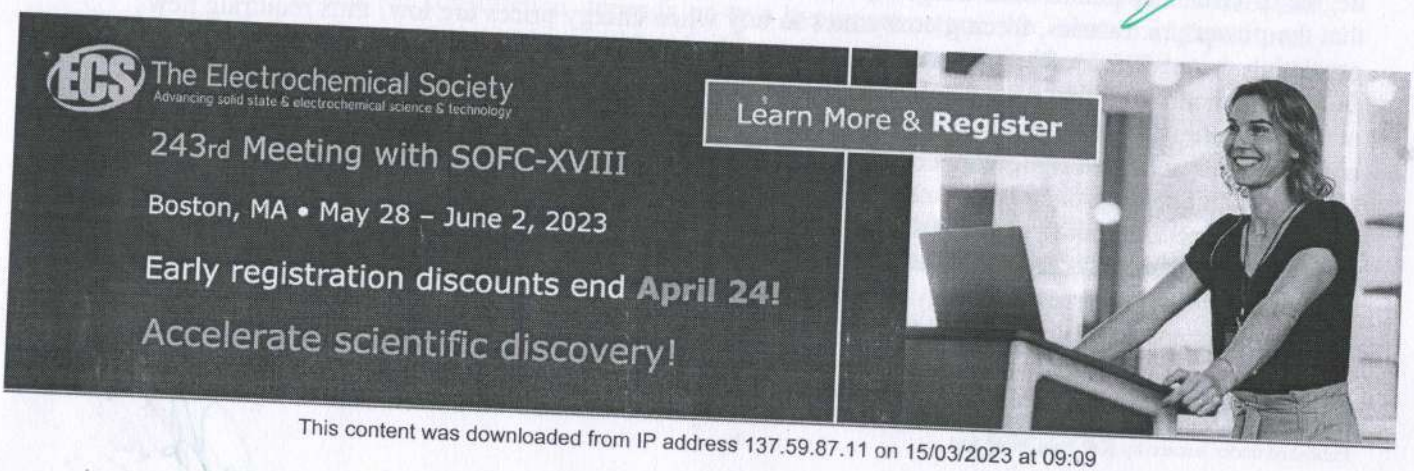
Random Forest-Based Method for Micro Grid System in Energy Consumption Prediction

To cite this article: Murugananth Gopal Raj *et al* 2021 *J. Phys.: Conf. Ser.* **1964** 052002

View the article online for updates and enhancements.

You may also like

- On-Line Optimization of Microgrid Operating Cost Based on Deep Reinforcement Learning
S H Lin, H H Yu and H W Chen
- Direct, Efficient, and Real-Time Simulation of Physics-Based Battery Models for Stand-Alone PV-Battery Microgrids
Seong Beom Lee, Chintan Pathak, Venkatasailanathan Ramadesigan et al.
- A review on optimization dispatching and control for microgrid
Jianmin Hou, Chengye Ji, Junjie Wang et al.



This content was downloaded from IP address 137.59.87.11 on 15/03/2023 at 09:09

Random Forest-Based Method for Micro Grid System in Energy Consumption Prediction

Murugananth Gopal Raj[1*], C Pradip[2], N Saju[2], S V Tresa Sangeetha[3#]
[1]Department of Electrical and Electronics Engineering, Ahalia School of Engineering and Technology, Kozhippara, Kerala, India
[2]Department of Electrical and Electronics Engineering, NSS College of Engineering, Palakkad, Kerala, India
[3]Department of Electrical and Electronics Engineering, University of Technology and Applied Science-Al Mudabah, Muladdah, Musanna, Sultanate of Oman
Email: *gmuruganantn@gmail.com, #tresa@act.edu.om

Abstract. As a solution to mitigating rising energy needs, microgrids (MG) have arisen. But instead of microgrids are focused mainly on unconventional sources of energy. In their service, there is significant variability. Energy users will not know if their estimated load is long or short related to historical records. This paper aims to formulate a robust energy prediction of consumption in the microgrid system that uses random forest (RF) method theory as the mathematical framework. Effective MG energy forecast plays an essential role in power improvement MG efficacy. Comparing RF models with various parameter configurations and examining the parameters setting affects the model's estimation efficiency.
Keywords: MG, prediction of energy consumption, RF method.

1. Introduction

Electricity consumption prediction is now one of the new phenomena thanks to improvement in energy, power and control systems. For power controllers, the estimation of load demand is a daunting task. It is an old trend of research which preceded the growth of power plants and computer techniques [1-4]. At the beginning of the 21st century, clean natural resources and smart grids are now evolving. It is increasingly relevant.

Due to two major factors, load forecasts become tougher than ever. Firstly, in many countries, privatization and restructuring of power markets ensure that energy users can select their supplier from different operators. The second is that the strong penetration of unreliable energy enhances the great degree of instability due to their irregular actions into the grid, wind and solar. Market reform ensures that the power price varies, forcing consumers to buy when energy prices are low, thus requiring new prediction systems [5-6]. Short-term energy load projections use the most relevant historical evidence, from a few hours to a few weeks before the predicted day. Lately, research experiments used advance machine learning in short-term prediction models. The clean energy of the economy's manufacturing and residential areas is a significant economic growth guideline [7].

The traditional approach is to categories the predicted benefit into low, medium, and high stages, which customers can interpret. This research suggests an alternate approach used when predicted levels are appropriate for a predictive control framework rather than real values. In recent years power sector reform and renewable energy introduction have made the electricity load forecast more and more relevant. Advanced intelligent methods are built to address the coming difficulties and ensure

Content from this work may be used under the terms of the Creative Commons Attribution 3.0 licence. Any further distribution of this work must maintain attribution to the author(s) and the title of the work, journal citation and DOI.
Published under licence by IOP Publishing Ltd

precise power predictions for various times [8-10]. The use of smart prediction algorithms is an effective method to deal with uncertainty and a core aspect of smart grids.

Load forecasts mean the projection of potential trends in a single apartment, local grid, an area, or even a whole country's electricity. This prediction is made over one or more time stages over duration called the forecast horizon. For load shipments, unit participation, and energy sharing decisions, a specific power forecast of one or multiple hours is of great significance [11-13]. For maintenance planning and energy efficiency strategies, forecasting loads for a prolonged period of time is beneficial [11-15].

This paper suggests a short-term forecast model based on the random forestry strategy to overcome the above challenges. This model is intended for a one-hour regular forecast in support of the Tunisian power system requirements such as a limited area, high humidity, no deregulation or irregular energy presence.

2. Methods

This section explains, discussed concepts and terminology which are used in every part of this paper. Throughout the area of computer engineering, energy use has been extensively researched for decades. Although energy is being used as a metric in machine education, most research still focuses on achieving high accuracy without any computational constraints. We present a review of the different approaches in general and machine learning applications to estimate energy consumption in this challenge. We also present state-of-the-art technical methods to approximate energy values along with two case studies that improve computer education energy usage.

The reliability improvement of the electricity is to be ensured from the consumer's viewpoint so that peak demand is compensated by the design of generation capacity. The reduction in the load profile of peak to average ratio is achieved through this design to reduce the more power plants requirement. This is obtained by two methods that smart pricing technique and optimal load control. Smart pricing technique is applied by utility side to manage the peak loads.

3. Random Forest

The Random Forest (RF) is a group method which combines several decision trees with prediction. The key theory is bagging; if a sample n is randomly picked from the training range, Sn is fitted to a backbone. This sample is known as bootstrap and is used to replace the sample.

A bootstrap analysis is collected by randomly choosing previous samples with Sn's substitution, and each measurement can pick 1=n. The independently dispersed random variable Hl represents this random collection. It selects multiple samples from the bagging process.

RF simple steps are approximately separated into four steps:

Step 1: Collecting n observations from a bootstrap sampling process;

Step 2: Choosing the c attributes of each entry feature by randomized selection and determining the optimal segmentation characteristics as a branch to create a regression tree;

Step 3: Repeated steps 1 and 2 for a maximum of m times to construct the m regress tree.

Step 4: Combining the outcomes of m trees for the final estimation function.

Random forest (RF) is a modified bagging that produces a large collection of independent trees and averages their results. RF construction depends on two hyperparameters: the number of forest trees and the number of characteristics to be considered when determining the right fraction. Figure 1 shows the tree structure in a random forest method.

A fresh bootstrapped DB dataset is created from training set D for each incremental tree. As the amount of tree in the forest grows, trees are more likely to collide. However, the benefit is that more ballots are cast in the training algorithm, minimizing the common error.

The number of trees has been shown to rise, and the theoretical threshold of the forest is reaching accuracy. The number of characteristics considered for each division influences the variety of trees. By taking into account all the characteristics at each break, each tree chooses its optimal global function, allowing similar trees. Reducing the number of features considered on each break raises the

probability that the best global function is omitted from the test subset of features. The goal is to build a combination of decision-making trees in different ways, contributing to various predictions. Figure 1 represents method of random forest.

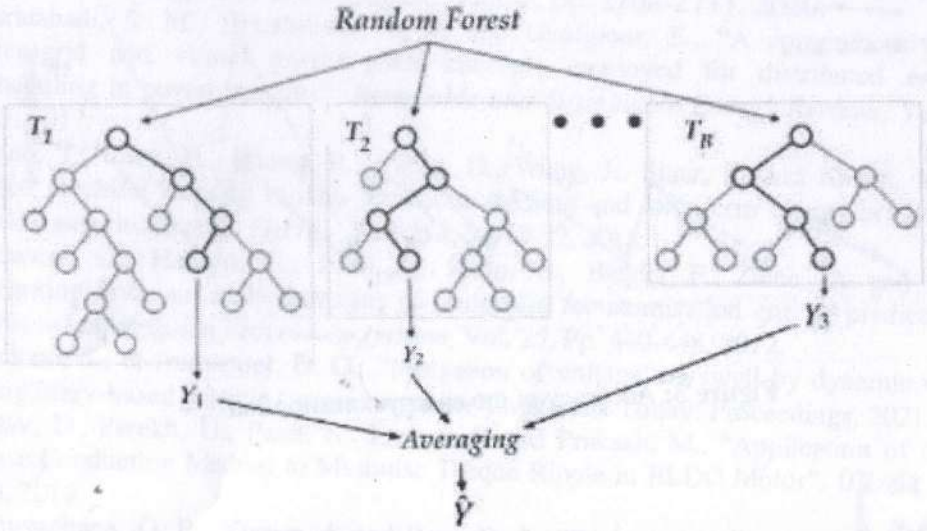


Figure 1: Random forest method

Each of the trees produced by bagging is distributed equally, making it impossible to change other than to minimize variances. RF conducts a tree developmental process by randomly choosing an input variable to improve bagging without undue variation by reducing the association between the trees. The model is built according to an online learner using the RF characterized by resistance to parameter changes and intrinsic cross-validation.

4. Results

This removed anomalies from the data in the pre-processing layer. The knowledge is considered noise based on the intrinsic nature of the data collection, which influences interpretation by various external aspects. The results of the RF-based load scheduling and the energy consumption is predicted. The obtained results are verified that shows the distribution of energy consumption based on the hour, as illustrated in the figure. 2. The figure. 3 One-month energy consumption of Actual method versus RF. The Actual versus RF predicted results for one-year energy consumption is shown in the figure. 4.

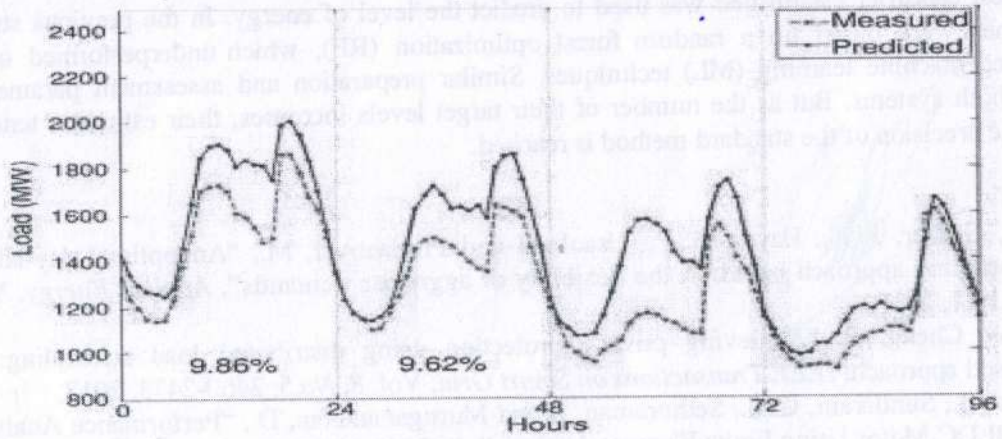


Figure 2: Actual vs RF predicted energy consumption

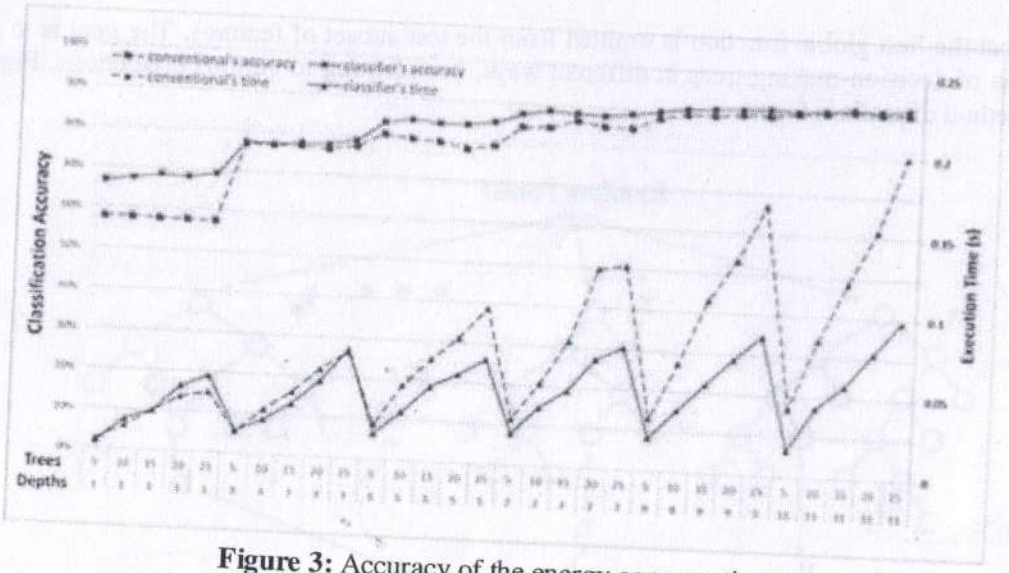


Figure 3: Accuracy of the energy consumption

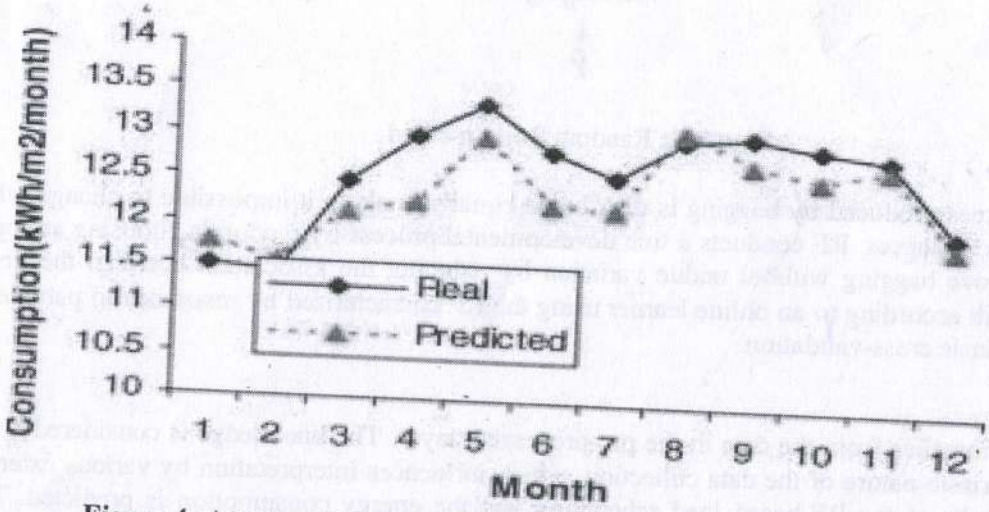


Figure 4: Actual vs RF predicted results for one-year energy consumption

5. Conclusion

A random forest classifier established was used to predict the level of energy. In the previous study, both approaches were based on a random forest optimization (RF), which underperformed other commonly used machine learning (ML) techniques. Similar preparation and assessment parameters were used in both systems. But as the number of their target levels increases, their estimates tend to decline, and the precision of the standard method is reached.

References

[1]. Ayón, X., Gruber, J. K., Hayes, B. P., Usaola, J and Prodanović, M., "An optimal day-ahead load scheduling approach based on the flexibility of aggregate demands", *Applied Energy*, Vol. *198*, Pp.1-11, 2017.

[2]. Liu, E., & Cheng, P. "Achieving privacy protection using distributed load scheduling: A randomised approach. *IEEE Transactions on Smart Grid*, Vol. *8, No.*5, 2460-2473, 2017.

[3]. Rajkumar, S., Sundaram, C. S., Sethuraman, K and Muruganandhan, D., "Performance Analysis of Hub BLDC Motor Using Finite Element Analysis", In *2019 ICSCAN*, pp. 1-5, 2019

[4]. Anvari-Moghaddam, A., Guerrero, J. M., Vasquez, J. C., Monsef, H., & Rahimi-Kian, A., "Efficient energy management for a grid-tied residential microgrid", *IET Generation, Transmission & Distribution*, Vol. *11, No.*11, Pp. 2752-2761, 2017.

[5]. Wang, S., Janabi, A., & Wang, B., "Generalised Optimal SVPWM for the Switched-Capacitor Voltage Boost Converter", ECCE, pp. 2708-2711, 2020.

[6]. Nosratabadi, S. M., Hooshmand, R. A and Gholipour, E., "A comprehensive review on microgrid and virtual power plant concepts employed for distributed energy resources scheduling in power systems", *Renewable and Sustainable Energy Reviews*, Vol. *67*, Pp. 341-363, 2017.

[7]. Ahmad, T., Chen, H., Huang, R., Yabin, G., Wang, J., Shair, J., and Kazim, M., "Supervised based machine learning models for short, medium and long-term energy prediction in distinct building environment", *Energy*, Vol. *158*, Pp.17-32, 2018.

[8]. Montavon, G., Hansen, K., Fazli, S., Rupp, M., Biegler, F., Ziehe, A and Müller, K. R., "Learning invariant representations of molecules for atomisation energy prediction", *Advances in neural information processing systems*, Vol. *25*, Pp. 440-448, 2012.

[9]. Sudharani, S., & Immanuel, D. G., "Mitigation of voltage sag/swell by dynamic voltage restorer using fuzzy-based particle swarm controller", Materials Today: Proceedings, 2021.

[10]. Yadav, D., Parekh, U., Patel, K., Parmar, R and Prakash, M., "Application of Modified Three Phase Conduction Method to Minimise Torque Ripple in BLDC Motor", IJRAR, vol. 6(1), 155-156, 2019.

[11]. Mahusudhana, G. R., Kumar, A and Ram, B. S., "Design of Neuro-fuzzy Inference distributed power flow controller for transient stability improvement. *Word Journal of Modeling and Simulation*, Vol. *10, No.*4, Pp. 252-260, 2014.

[12]. Suresh, G., Kumar, N. C. S., Murugesan, R and Mukunthan, P., "Multi-object and dynamic query-based CBIR system using DCT incorporated with HOG and HTF", *International Journal of Innovative Technology and Exploring Engineering (IJITEE)*, *9*(2S3), 2019.

[13]. de Ves, E., Benavent, X., Coma, I and Ayala, G., "A novel dynamic multi-model relevance feedback procedure for content-based image retrieval", Neurocomputing, Vol. 208, Pp.99-107, 2016.

[14]. Joseph, F and Subbiah, M., "Hybrid windowing adaptive FIR filter technique in underwater communication", *International Journal-of MC Square Scientific Research, Vol. 10, No.*2, Pp.17-21, 2018.

[15]. Memon, Li, J.P., Memon, I and Arain, Q.A., "GEO matching regions: multiple regions of interests using content-based image retrieval based on relative locations", Multimedia Tools and Applications, Vol. 76, No.14, pp.15377-15411, 2017.

Turkish Journal of Computer and Mathematics Education Vol.12 No. 1S (2021), 631-639

Research Article

New form of generlized closed sets via neutrosophic topologicl spaces

BinoyBalan eK[1]*, C.Janaki[2] & Sandhya P.S[3]

[1] Department of Science & Humanities, Ahalia School of Engineering and Technology, Palakkad, Kerala, India
[2] Department of Mathematics, L.R.G. . College for Women, Tirupur-4, India
[3] Department of Applied Science & Humanities, Royal College of Engineering and Technology, Thrissur, Kerala, India
Email: binoypayyur@gmail.com[1], janakicsekar@yahoo.com[2] &

Article History: Received: 11 January 2021; Accepted: 27 February 2021; Published online: 5 April 2021

Abstract— Florentin eSmarandache egeneralized ethe eintuitionistic efuzzy esets eto eNeutrosophic eset etheory ein e1998 eas ea enew ebranch eof ephilosophy. eA.A. eSalama eintroduced ethe econcept eof eNeutrosophic etopological espaces eby eusing ethe eNeutrosophic ecrisp esets. eIn ethis epaper, ewe eintroduce eand estudy ea enew eclass eof eNeutrosophic egeneralized eset, enamely eNeutrsophic epre egeneralized eregular eα- eclosed eset ein eNeutrosophic etopological espaces. eSome einteresting epropositions ebased eon ethis eset eare eintroduced eand established ewith esuitable examples eand etheir eproperties eare ealso ediscussed.

Keywords— $\mathcal{N}$pgrα- closed set, $\mathcal{N}$pgrα - open set, $\mathcal{N}$pgrα -closure, $\mathcal{N}$pgrα - interior

1. INTRODUCTION AND PRELIMINARIES

L.A. Zadeh [20] introduced the concept of fuzzy sets in 1965. It shows the degree of membership of the lement in a set. Later, fuzzy topology was introduced by C.L.Chang [6] in 1968. Coker [7] introduced the notion of Intuitionistic fuzzy topological spaces by using Atanassov's [5] Intuitionistic fuzzy set. Neutrality the degree of indeterminacy, as an independent concept, was introduced by Smarandache [19] in 1998. He also defined the Neutrosophic set on three components, namely Truth (membership), Indeterminacy, Falsehood (non-membership) from the Fuzzy sets and Intuitionistic fuzzy sets. Smarandache's Neutrosophic concepts have wide range of real time applications for the fields of [[1]-[4],[10],[12],[15],[18]] Information systems, Computer science, Artificial Intelligence, Applied Mathematics and Decision making. A.A. Salama and S.A. Alblowi [16] introduced Neutrosophic topological spaces by using the Neutrosophic sets. Salama A. A. [17] introduced Neutrosophic closed set and Neutrosophic continuous functions in Neutrosophic topological spaces.R.Dhavaseelan and SaiedJafari [8] introduced Neutrosophic generalized closed sets. In this direction, we introduce and analyze a new class of Neutrosophic generalized closed set called Neutrsophic pre generalized regular α- closed set which is the weaker form of the above mentioned generalization and its properties are discussed in details.

Definition 1.[16]Let $\mathcal{J}$ be a non-empty fixed set. A Neutrosophic set [NS for short] $\mathcal{A}$ is an object having the form $\mathcal{A} = \{\langle a, \mu_{\mathcal{A}}(a), \sigma_{\mathcal{A}}(a), \nu_{\mathcal{A}}(a)\rangle : a \in \mathcal{J}\}$ where $\mu_{\mathcal{A}}(a)$, $\sigma_{\mathcal{A}}(a)$ and $\nu_{\mathcal{A}}(a)$ which represent the degree of membership function, degree of indeterminacy and the degree of non-membership respectively of each element $x \in A$ to the set $\mathcal{A}$.

Remark 1.2. [16] A Neutrosophic set $\mathcal{A} = \{\langle a, \mu_{\mathcal{A}}(a), \sigma_{\mathcal{A}}(a), \nu_{\mathcal{A}}(a)\rangle : a \in \mathcal{J}\}$ can be identified to an ordered triple $\mathcal{A} = \langle a, \mu_{\mathcal{A}}(a), \sigma_{\mathcal{A}}(a), \nu_{\mathcal{A}}(a)\rangle$ in non-standard unit interval $]^-0, 1^+[$ on $\mathcal{J}$.

For the sake of simplicity, we shall use the $\mathcal{A} = \langle \mu_{\mathcal{A}}(a), \sigma_{\mathcal{A}}(a), \nu_{\mathcal{A}}(a)\rangle$ for the Neutrosophic set $\mathcal{A} = \{\langle a, \mu_{\mathcal{A}}(a), \sigma_{\mathcal{A}}(a), \nu_{\mathcal{A}}(a)\rangle : a \in \mathcal{J}\}$.

Definition 1.3. [16] Every Intuitionistic fuzzy set $\mathcal{A}$ is a nonempty set in $\mathcal{J}$ is obviously on Neutrosophic set having the form $\mathcal{A}=\{\langle a, \mu_{\mathcal{A}}(a), 1-(\mu_{\mathcal{A}}(a)+\nu_{\mathcal{A}}(a)), \nu_{\mathcal{A}}(a)\rangle : a \in \mathcal{J}\}$. Since our main purpose is to construct the tools for developing Neutrosophic set and Neutrosophic topology, we must introduce the Neutrosophic set $0_{\mathcal{N}}$ and $1_{\mathcal{N}}$ in $\mathcal{J}$ as follows:

$0_{\mathcal{N}}$ may be defined as:

$0_{\mathcal{N}} = \{\langle a, 0, 0, 1\rangle : a \in \mathcal{J}\}$, $0_{\mathcal{N}} = \{\langle a, 0, 1, 1\rangle : a \in \mathcal{J}\}$, $0_{\mathcal{N}} = \{\langle a, 0, 1, 0\rangle : a \in \mathcal{J}\}$, $0_{\mathcal{N}} = \{\langle a, 0, 0, 0\rangle : a \in \mathcal{J}\}$

$1_{\mathcal{N}}$ may be defined as:

$1_{\mathcal{N}} = \{\langle a, 1, 0, 0\rangle : a \in \mathcal{J}\}$, $1_{\mathcal{N}} = \{\langle a, 1, 0, 1\rangle : a \in \mathcal{J}\}$, $1_{\mathcal{N}} = \{\langle a, 1, 1, 0\rangle : a \in \mathcal{J}\}$, $1_{\mathcal{N}} = \{\langle a, 1, 1, 1\rangle : a \in \mathcal{J}\}$

Definition 1.4. [16] Let $\mathcal{A} = \langle \mu_{\mathcal{A}}(a), \sigma_{\mathcal{A}}(a), \nu_{\mathcal{A}}(a)\rangle$ be an NS on $\mathcal{J}$ then the complement of the set $\mathcal{A}$ [$C(\mathcal{A})$ for short] may be defined as three kinds of complements:

(i) $C(\mathcal{A}) = \{\langle a, 1-\mu_{\mathcal{A}}(a), 1-\sigma_{\mathcal{A}}(a), 1-\nu_{\mathcal{A}}(a)\rangle : a \in \mathcal{J}\}$ (ii) $C(\mathcal{A}) = \{\langle a, \nu_{\mathcal{A}}(a), \sigma_{\mathcal{A}}(a), \mu_{\mathcal{A}}(a)\rangle : a \in \mathcal{J}\}$

(iii) $C(\mathcal{A}) = \{\langle a, \nu_{\mathcal{A}}(a), 1-\sigma_{\mathcal{A}}(a), \mu_{\mathcal{A}}(a)\rangle : a \in \mathcal{J}\}$

Research Article

Definition 1.5. [5] Let $\mathcal{J}$ be a nonempty set. Let $\mathcal{S}$ and $\mathcal{T}$ be any Neutrosophic sets on $\mathcal{J}$ in the form $\mathcal{S}$ ={<a, $\mu_{\mathcal{S}}$(a), $\sigma_{\mathcal{S}}$(a), $\nu_{\mathcal{S}}$(a) >: a∈ $\mathcal{J}$ } and $\mathcal{T}$ = {<a, $\mu_{\mathcal{T}}$(a), $\sigma_{\mathcal{T}}$(a), $\nu_{\mathcal{T}}$(a)>: a∈ $\mathcal{J}$ }. Then we may consider two possible definitions for subsets ($\mathcal{S}\subseteq\ \mathcal{T}$). $\mathcal{S}\subseteq\ \mathcal{T}$ may be defined as:

$\mathcal{S}\subseteq\ \mathcal{T} \Leftrightarrow \mu_{\mathcal{S}}(x)\leq\ \mu_{\mathcal{T}}(x),\ \sigma_{\mathcal{S}}(x)\leq\ \sigma_{\mathcal{T}}(x),$

$\nu_{\mathcal{S}}(x) \geq \nu_{\mathcal{T}}(x\ )$ for all a∈ $\mathcal{J}$.

$\mathcal{S}\subseteq\ \mathcal{T} \Leftrightarrow \mu_{\mathcal{S}}(x)\leq\ \mu_{\mathcal{T}}(x),\ \sigma_{\mathcal{S}}(x)\geq\ \sigma_{\mathcal{T}}(x),\ \ \nu_{\mathcal{S}}(x\ )\geq \nu_{\mathcal{T}}(x\ )$ for all a ∈ $\mathcal{J}$.

Proposition 1.6. [5] For any Neutrosophic set $\mathcal{A}$ the following conditions hold:

$0_{\mathcal{N}}\subseteq\mathcal{A},\ 0_{\mathcal{N}}\subseteq 0_{\mathcal{N}}, \mathcal{A}\subseteq 1_{\mathcal{N}},\ 1_{\mathcal{N}}\subseteq\ 1_{\mathcal{N}}$

Definition 1.7.[16] Let $\mathcal{J}$ be a nonempty set. Let $\mathcal{S}$ = {<a, $\mu_{\mathcal{S}}$(a), $\sigma_{\mathcal{S}}$(a),$\nu_{\mathcal{S}}$(a)>}, $\mathcal{T}$ ={<a, $\mu_{\mathcal{T}}$(a), $\sigma_{\mathcal{T}}$(a),$\nu_{\mathcal{T}}$(a) >} are Neutrosophic sets. Then $\mathcal{S}\cap\mathcal{T}$ may be defined as:

(i) $\mathcal{S}\cap\mathcal{T}$=<a, $\mu_{\mathcal{S}}(a)\wedge\mu_{\mathcal{T}}(a)$, $\sigma_{\nu}(a)\wedge\sigma_{\mathcal{T}}(a)$,$\nu_{\mathcal{S}}(a)\vee\nu_{\mathcal{T}}(a)$>

(ii) $\mathcal{S}\cap\mathcal{T}$ = <a, $\mu_{\mathcal{S}}(a)\wedge\mu_{\mathcal{T}}(a)$, $\sigma_{\mathcal{S}}(a)\vee\sigma_{\mathcal{T}}(a)$, $\nu_{\mathcal{S}}(a)\ \nu_{\mathcal{T}}(a)$>

$\mathcal{S}\cup\ \mathcal{T}$ may be defined as:

(i) $\mathcal{S}\cup\ \mathcal{T}$= <a, $\mu_{\mathcal{S}}(x)\vee\mu_{\mathcal{T}}(x)$, $\sigma_{\mathcal{S}}(x)\vee\sigma_{\mathcal{T}}(x)$, $\nu_{\mathcal{S}}(x\ )\wedge\nu_{\mathcal{T}}(x\ )$>

(ii) $\mathcal{S}\cup\ \mathcal{T}$ = <x, $\mu_{\mathcal{S}}(x)\vee\mu_{\mathcal{T}}(x)$, $\sigma_{\mathcal{S}}(x)\wedge\sigma_{\mathcal{T}}(x)$, $\nu_{\mathcal{S}}(x\ )\wedge\nu_{\mathcal{T}}(x\ )$>

We can easily generalize the operations of intersection and union to arbitrary family of Neutrosophic sets as follows:

Definition 1.8. [16] Let $\{\mathcal{A}_j$: j∈J } be a arbitrary family of Neutrosophic sets in A, then $\cap\mathcal{A}_j$ may be defined as

(i) $\cap\mathcal{A}_j$ = <a, $\wedge_{j\in J}\mu_{\mathcal{A}_j}(a)$, $\wedge_{j\in J}\sigma_{\mathcal{A}_j}(a)$,$\vee_{j\in J}\nu_{\mathcal{A}_j}(a)$>

(ii) $\cap\mathcal{A}_j$ = <a, $\wedge_{j\in J}\mu_{\mathcal{A}_j}(a)$, $\vee_{j\in J}\sigma_{\mathcal{A}_j}(a)$,$\vee_{j\in J}\nu_{\mathcal{A}_j}(a)$>

$\cup\mathcal{A}_j$ may be defined as

(i) $\cup\mathcal{A}_j$= <a, $\vee_{j\in J}\mu_{\mathcal{A}_j}(a)$, $\vee_{j\in J}\sigma_{\mathcal{A}_j}(a)$,$\wedge_{j\in J}\nu_{\mathcal{A}_j}(a)$>

(ii) $\cup\mathcal{A}_j$ = <a, $\vee_{j\in J}\mu_{\mathcal{A}_j}(a)$, $\wedge_{j\in J}\sigma_{\mathcal{A}_j}(a)$,$\wedge_{j\in J}\nu_{\mathcal{A}_j}(a)$>

Proposition 1.9. [16] For two Neutrosophic sets $\mathcal{S}$ and $\mathcal{T}$, the following conditions are true:

C ($\mathcal{S}\cap\mathcal{T}$)= C($\mathcal{S}$) ∪ C($\mathcal{T}$); C ($\mathcal{S}\cup\ \mathcal{T}$)= C($\mathcal{S}$)∩ C($\mathcal{T}$).

Definition 1.10 [16] A Neutrosophic topology [NT] on a nonempty set $\mathcal{J}$ is a family τ of Neutrosophic subsets in $\mathcal{J}$ satisfying the following axioms:

(i) $0_{\mathcal{N}}$, $1_{\mathcal{N}}\in\tau$

(ii) $\mathcal{G}_1\ \cap\mathcal{G}_2\ \in\tau$ for any $\mathcal{G}_1$, $\mathcal{G}_2\ \in\tau$

(iii) $\cup\mathcal{G}_i\ \in\tau$ for every $\{\mathcal{G}_i$: i∈J}⊆ τ

The pair of ($\mathcal{J}$, τ) is called Neutrosophic topological space [NTS for short]. The elements of τ are called Neutrosophic open set [NOS for short]. A Neutrosophic set $\mathcal{F}$ is Neutrosophic closed set [NCS for short] if and only if C($\mathcal{F}$) is Neutrosophic open set.

Example 1.11.[16]Let $\mathcal{J}$ ={a} and $\mathcal{A}_1$={< a, 0.6, 0.6, 0.5>: a ∈ $\mathcal{J}$}, $\mathcal{A}_2$={< a, 0.5, 0.7, 0.9>: a ∈ $\mathcal{J}$}, $\mathcal{A}_3$={<a, 0.6, 0.7, 0.5>: a ∈ $\mathcal{J}$}, $\mathcal{A}_4$ = {<a, 0.5, 0.6, 0.9>: a ∈ $\mathcal{J}$}.Then the family τ ={$0_{\mathcal{N}}$, $\mathcal{A}_1$, $\mathcal{A}_2$, $\mathcal{A}_3$, $\mathcal{A}_4$, $1_{\mathcal{N}}$} is called a Neutrosophic topological space on $\mathcal{J}$.

Definition 1.12[16] Let ($\mathcal{J}$,τ) be an NTS and $\mathcal{A}$= <a, $\mu_{\mathcal{S}}$(a), $\sigma_{\mathcal{S}}$(a), $\nu_{\mathcal{S}}$(a)> be an NS in $\mathcal{J}$. Then the Neutrosophic closure and Neutrosophic interior of $\mathcal{A}$ are defined by NCl($\mathcal{A}$) = ∩{$\mathcal{K}$: $\mathcal{K}$ is an NCS in $\mathcal{J}$ and $\mathcal{A}\subseteq\mathcal{K}$}, NInt($\mathcal{A}$) = ∪{$\mathcal{G}$: $\mathcal{G}$ is an NOS in $\mathcal{J}$ and $\mathcal{G}\subseteq\mathcal{A}$ }.

It can be also shown that NCl($\mathcal{A}$) is NCS and NInt($\mathcal{A}$) is a NOS in $\mathcal{J}$.

(i) $\mathcal{A}$ is NOS if and only if $\mathcal{A}$ = NInt($\mathcal{A}$)

(ii) $\mathcal{A}$ is NCS if and only if $\mathcal{A}$ = NCl($\mathcal{A}$)

Proposition 1.13.[16]For any Neutrosophic set $\mathcal{A}$ in ($\mathcal{J}$, τ) we have

(i) NCl(C($\mathcal{A}$))= C(NInt($\mathcal{A}$))

(ii) NInt(C($\mathcal{A}$))= C(NCl($\mathcal{A}$))

Proposition 1.14.[16] Let ($\mathcal{J}$,τ) be a NTS and $\mathcal{S}$, $\mathcal{T}$ be two Neutrosophic sets in $\mathcal{J}$. Then the following properties hold:

(i) NInt($\mathcal{S}$)⊆ $\mathcal{S}\subseteq$NCl($\mathcal{S}$)

(ii) $\mathcal{S}\subseteq\mathcal{T}$ ⇒NInt($\mathcal{S}$) ⊆NInt($\mathcal{T}$)and NCl($\mathcal{S}$) ⊆NCl($\mathcal{T}$)

(iii) NInt(NInt($\mathcal{S}$)) = NInt($\mathcal{S}$)

(iv) NCl(NCl($\mathcal{S}$))= NCl($\mathcal{S}$)

(v) NInt($\mathcal{S}\cap\ \mathcal{T}$)= NInt($\mathcal{S}$)∩NInt($\mathcal{T}$)

(vi) $NCl(\mathcal{S} \cup \mathcal{T}) = NCl(\mathcal{S}) \cup NCl(\mathcal{T})$
(vii) $NInt(0_{\mathcal{N}}) = 0_{\mathcal{N}}$, $NInt(1_{\mathcal{N}}) = 1_{\mathcal{N}}$
(viii) $NCl(0_{\mathcal{N}}) = 0_{\mathcal{N}}$, $NCl(1_{\mathcal{N}}) = 1_{\mathcal{N}}$
(ix) $\mathcal{S} \subseteq \mathcal{T} \Rightarrow C(\mathcal{S}) \subseteq C(\mathcal{T})$
(x) $NCl(\mathcal{S} \cap \mathcal{T}) \subseteq NCl(\mathcal{S}) \cap NCl(\mathcal{T})$
(xi) $NInt(\mathcal{S} \cup \mathcal{T}) \subseteq NInt(\mathcal{S}) \cup NInt(\mathcal{T})$

Definition 1.15. Let $\mathcal{A} = \{\langle a, \mu_{\mathcal{A}}(a), \sigma_{\mathcal{A}}(a), \nu_{\mathcal{A}}(a)\rangle : a \in \mathcal{I}\}$ be a Neutrosophic set on a Neutrosophic topological space $(\mathcal{I}, \tau)$ then $\mathcal{A}$ is called

(i) Neutrosophic regular open set (NROS for short)[12] if $\mathcal{A} = NInt(NCl(\mathcal{A}))$.
(ii) Neutrosophic pre-open set (NPOS for short)[14] if $\mathcal{A} \subseteq NInt(NCl(\mathcal{A}))$.
(iii) Neutrosophic α-open set (NαOS for short)[14] if $\mathcal{A} \subseteq NInt(NCl(NInt(\mathcal{A})))$.

An NS $\mathcal{A}$ is called Neutrosophic regular closed set, Neutrosophic pre closed set and Neutrosophic α-closed (NRCS, NPCS and NαCS for short) if the complement of $\mathcal{A}$ is NROS, NPOS and NαOS respectively.

Definition 1.16.[13] Let $\mathcal{A} = \{\langle a, \mu_{\mathcal{A}}(a), \sigma_{\mathcal{A}}(a), \nu_{\mathcal{A}}(a)\rangle : a \in \mathcal{I}\}$ be a Neutrosophic set on Neutrosophic topological space $(\mathcal{I}, \tau)$. Then the Neutrosophic pre-closure and Neutrosophic pre interior of $\mathcal{A}$ are defined by $NPCl(\mathcal{A}) = \{\mathcal{K} : K \text{ is a NPCS in } \mathcal{I} \text{ and } \mathcal{A} \subseteq \mathcal{K}\}$,
$NPInt(\mathcal{A}) = \{\mathcal{G} : \mathcal{G} \text{ is a NPOS in } \mathcal{I} \text{ and } \subseteq \mathcal{A}\}$

Definition 1.17.[12] Let $\mathcal{A} = \{\langle a, \mu_{\mathcal{A}}(a), \sigma_{\mathcal{A}}(a), \nu_{\mathcal{A}}(a)\rangle : a \in \mathcal{I}\}$ be a Neutrosophic set on a Neutrosophic topological space $(\mathcal{I}, \tau)$. Then the Neutrosophic α-closure and Neutrosophic α-interior of $\mathcal{A}$ are defined by
$N\alpha Cl(\mathcal{A}) = \{\mathcal{K} : \mathcal{K} \text{ is a N}\alpha\text{CS in } \mathcal{I} \text{ and } \mathcal{A} \subseteq \mathcal{K}\}$,
$N\alpha Int(\mathcal{A}) = \{\mathcal{G} : \mathcal{G} \text{ is a N}\alpha\text{OS in } \mathcal{I} \text{ and } \mathcal{G} \subseteq \mathcal{A}\}$

Definition 1.18. Let $\mathcal{A} = \{\langle a, \mu_{\mathcal{A}}(a), \sigma_{\mathcal{A}}(a), \nu_{\mathcal{A}}(a)\rangle : a \in \mathcal{I}\}$ be a Neutrosophic set on a Neutrosophic topological space $(\mathcal{I}, \tau)$. Then $\mathcal{A}$ is called

(i) Neutrosophic regular generalized closed set (NRGCS for short)[9], if $NCl(\mathcal{A}) \subseteq U$, whenever $\mathcal{A} \subseteq \mathcal{U}$ and $\mathcal{U}$ is a Neutrosophic regular open set in $\mathcal{I}$.
(ii) Neutrosophic regular α-generalized closed set (NRαGCS for short)[9], if $N\alpha Cl(\mathcal{A}) \subseteq \mathcal{U}$, whenever $\mathcal{A} \subseteq \mathcal{U}$ and $\mathcal{U}$ is a Neutrosophic regular open set in $\mathcal{I}$.
(iii) Neutrosophic generalized pre closed set (NGPCS for short)[13] if $NPCl(\mathcal{A}) \subseteq \mathcal{U}$ whenever $\mathcal{A} \subseteq \mathcal{U}$ and $\mathcal{U}$ is a Neutrosophic open set in $\mathcal{I}$.
(iv) Neutrosophic generalized pre regular closed set (NGPRCS for short)[11] if $NPCl(\mathcal{A}) \subseteq \mathcal{U}$ whenever $\mathcal{A} \subseteq \mathcal{U}$ and $\mathcal{U}$ is a Neutrosophic regular open set in $\mathcal{I}$.

An NS $\mathcal{A}$ is called Neutrosophic regular generalized open set, Neutrosophic regular α -generalized open set, Neutrosophic generalized pre-open set and Neutrosophic generalized pre regular open set (NRGOS,NRαGOS, NGPOS and NGPROS for short) if the complement of $\mathcal{A}$ is NRGCS,NRαGCS, NGPCS and NGPRCS respectively.

2. NEUTROSOPHIC PRE GENERALIZED REGULAR α-CLOSED SET

In this section, we introduce Neutrosophic pre generalized regular α- closed set and analyze some of their properties.

Definition 2.1. Let $\mathcal{A} = \{\langle a, \mu_{\mathcal{A}}(a), \sigma_{\mathcal{A}}(a), \nu_{\mathcal{A}}(a)\rangle : a \in \mathcal{I}\}$ be a Neutrosophic set on a Neutrosophic topological space $(\mathcal{I}, \tau)$.Then $\mathcal{A}$ is called Neutrosophic regular α-open set (NRαOS for short) if there is a Neutrosophic regular open set $\mathcal{U}$ such that $\mathcal{U} \subset \mathcal{A} \subset N\alpha Cl(\mathcal{U})$.A Neutrosophic set $\mathcal{A}$ of a Neutrosophic space $(\mathcal{I}, \tau)$ is called a Neutrosophic regular α -closed set (NRαCS for short) if $C(\mathcal{A})$ is a NRαOS in $(\mathcal{I}, \tau)$.

Definition 2.2. Let $\mathcal{A} = \{\langle a, \mu_{\mathcal{A}}(a), \sigma_{\mathcal{A}}(a), \nu_{\mathcal{A}}(a)\rangle : a \in \mathcal{I}\}$ be a Neutrosophic set on a Neutrosophic topological space $(\mathcal{I}, \tau)$. Then $\mathcal{A}$ is called Neutrosophic pre generalized regular α- closed set ($\mathcal{NPGR}\alpha$CS for short), if $NPCl(\mathcal{A}) \subseteq \mathcal{U}$ whenever $\mathcal{A} \subseteq \mathcal{U}$ and $\mathcal{U}$ is a NRαOS in $(\mathcal{I}, \tau)$.

Alternatively, a Neutrosophic set $\mathcal{A}$ is said to be a Neutrosophic pre generalized regular α-open set ($\mathcal{NPGR}\alpha$OS for short) if $C(\mathcal{A})$ is a $\mathcal{NPGR}\alpha$CS in $(\mathcal{I}, \tau)$.

The family of all $\mathcal{NPGR}\alpha$CSs [$\mathcal{NPGR}\alpha$OSs] of an NTS $(\mathcal{I}, \tau)$ is denoted by $\mathcal{NPGR}\alpha C(\mathcal{I})$ [$\mathcal{NPGR}\alpha O(\mathcal{I})$].

Example 2.3. Let $\mathcal{I} = \{a, b\}$ and $\tau = \{0_{\mathcal{N}}, U, V, 1_{\mathcal{N}}\}$ where $\mathcal{U} = \{\langle 0.5, 0.3, 0.6\rangle, \langle 0.4, 0.4, 0.7\rangle\}$ and $\mathcal{V} = \{\langle 0.7, 0.5, 0.3\rangle, \langle 0.7, 0.5, 0.2\rangle\}$. Then $(\mathcal{I}, \tau)$ is a Neutrosophic topological space. Here the

Neutrosophic set $\mathcal{A}$= {<0.5, 0.3, 0.4>, <0.6, 0.6, 0.3>} is a $\mathcal{NPGR}\alpha$CS in ($\mathcal{I}$, τ). Since $\mathcal{A} \subseteq \mathcal{U}$ and $\mathcal{U}$ is a NRαOS, we have NPCl($\mathcal{A}$) = $\mathcal{A} \subseteq \mathcal{U}$.

Theorem 2.4.

(i) Every Neutrosophic closed set is $\mathcal{NPGR}\alpha$- closed set in $\mathcal{I}$.
(ii) Every Neutrosophic regular closed set is $\mathcal{NPGR}\alpha$-closed set in $\mathcal{I}$.
(iii) Every Neutrosophic pre closed set is $\mathcal{NPGR}\alpha$-closed set in $\mathcal{I}$.
(iv) Every Neutrosophic α-closed set is $\mathcal{NPGR}\alpha$-closed set in $\mathcal{I}$.
(v) Every $\mathcal{NPGR}\alpha$-closed set is Neutrosophic generalized pre regular closed set in $\mathcal{I}$.
(vi) Every Neutrosophic regular α-generalized closed set in X is a $\mathcal{NPGR}\alpha$-closed set in $\mathcal{I}$.
(vii) Every Neutrosophic generalized pre closed set in X is a $\mathcal{NPGR}$ α-closed set in $\mathcal{I}$.
(viii) Every Neutrosophic regular generalized closed set in X is a $\mathcal{NPGR}$ α-closed set in $\mathcal{I}$.

Proof: Straight forward. Converse of the above need not be true as in the following examples.

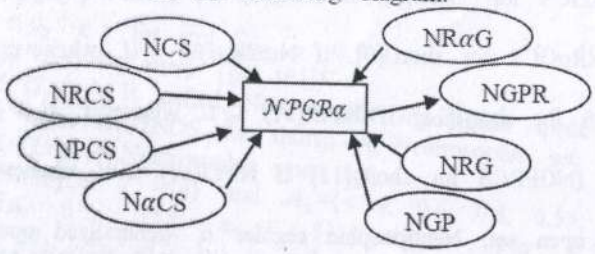
Example 2.5.

(i) Let $\mathcal{I}$ ={a, b} and $\mathcal{A}_1$ = {<0.4, 0.6, 0.5>,<0.7, 0.3, 0.6 >},$\mathcal{A}_2$ = {<0.3, 0.7, 0.8>,<0.6, 0.4, 0.2 >}, $\mathcal{A}_3$ = {<0.4, 0.7, 0.5>,<0.7, 0.4, 0.2 >} and $\mathcal{A}_4$ = {<0.3, 0.6, 0.8>,<0.6, 0.3, 0.6>} be an NSs on $\mathcal{I}$. Now τ ={$0_{\mathcal{N}}$ $\mathcal{A}_1$, $\mathcal{A}_2$, $\mathcal{A}_3$, $\mathcal{A}_4$, $1_{\mathcal{N}}$} is a Neutrosophic topological spaces on $\mathcal{I}$.Then $\mathcal{A}$ = {<0.3, 0.6, 0.8>, <0.5, 0.3, 0.7>} is $\mathcal{NPGR}\alpha$CS in $\mathcal{I}$. But $\mathcal{A}$ is not NCS, NRCS, NPCS, NαCS in $\mathcal{I}$.

(ii) Let $\mathcal{I}$ = {a, b} and $\mathcal{U}$ = {<0.6, 0.5, 0.2>,<0.7, 0.5, 0.1 >} and $\mathcal{V}$= {<0.5, 0.4, 0.7>,<0.4, 0.5, 0.6 >}, be an NSs on $\mathcal{I}$. Now τ = {$0_{\mathcal{N}}$, $1_{\mathcal{N}}$, $\mathcal{U}$, $\mathcal{V}$} is a Neutrosophic topological spaces on $\mathcal{I}$. Here the Neutrosophic set $\mathcal{A}$ = {<0.8, 0.6, 0.1>, <0.8, 0.6, 0>} is a Neutrosophic generalized pre regular closed set in $\mathcal{I}$. But $\mathcal{A} \subseteq \mathcal{W}$ and $\mathcal{W}$={<0.5, 0.5, 0.8>, <0.4, 0.3, 0.6>} is NRαOS and NPCl(A) = $1_{\mathcal{N}} \not\subseteq \mathcal{W}$, $\mathcal{A}$ is not a $\mathcal{NPGR}\alpha$-closed set in $\mathcal{I}$. .

(iii) Let $\mathcal{I}$ = {a, b} and $\mathcal{U}$ = {<0.6, 0.5, 0.2>, <0.7, 0.5, 0.1 >} and $\mathcal{V}$ = {<0.5, 0.4, 0.7>,<0.4, 0.5, 0.6 >}, be an NSs on $\mathcal{I}$. Now τ = {0_N, 1_N, $\mathcal{U}$, $\mathcal{V}$ } is a Neutrosophic topological spaces on $\mathcal{I}$. Here the Neutrosophic set $\mathcal{A}$ = {<0.4, 0.3, 0.7>, <0.3, 0.2, 0.6>} is a $\mathcal{NPGR}\alpha$CS in $\mathcal{I}$. But $\mathcal{A}$ is not NRαGCS, NGPCS and NRGCS in $\mathcal{I}$. Here $\mathcal{A} \subseteq \mathcal{W}$ and $\mathcal{W}$={<0.5, 0.5, 0.8>, <0.4, 0.3, 0.6>} is NRαOS, but not NOS and NROS in $\mathcal{I}$.

Remark 2.6. The above discussions are summarized in the following diagram.



Remark 2.7. The union of any two $\mathcal{NPGR}\alpha$CSs in ($\mathcal{I}$, τ) is not an $\mathcal{NPGR}\alpha$CS in ($\mathcal{I}$, τ) in general as seen from the following example.

Example 2.8. Let $\mathcal{I}$ = {a, b} and τ = {$0_{\mathcal{N}}$, $1_{\mathcal{N}}$, $\mathcal{U}$, $\mathcal{V}$} where $\mathcal{U}$ ={<0.5, 0.3, 0.6>, <0.4, 0.4, 0.7>} and $\mathcal{V}$ = {<0.7, 0.5, 0.3>, <0.7, 0.5, 0.2>}. Then the NSs $\mathcal{A}$ = {<0.2, 0.1, 0.7>, <0.4, 0.4, 0.7>} and $\mathcal{B}$= {<0.5, 0.3, 0.6>, <0.2, 0.2, 0.8>} are $\mathcal{NPGR}\alpha$CSs in ($\mathcal{I}$, τ). But $\mathcal{A} \cup \mathcal{B}$={<0.5,0.3,0.6>, <0.4,0.4,0.7>} is not an $\mathcal{NPGR}\alpha$CS in ($\mathcal{I}$, τ).

Since ($\mathcal{A} \cup \mathcal{B}$)$\subseteq$ $\mathcal{U}$ and NPCl($\mathcal{A} \cup \mathcal{B}$) ={<0.6,0.7,0.5), (0.7,0.6,0.4>}$\not=$ C($\mathcal{U}$)$\not\subseteq$ $\mathcal{U}$.

Remark 2.9. The intersection of any two $\mathcal{NPGR}\alpha$CSs in ($\mathcal{I}$, τ) is not an $\mathcal{NPGR}\alpha$CS in ($\mathcal{I}$, τ) in general as seen from the following example.

Example 2.10. Let $\mathcal{I}$ = {a, b} and τ = {$0_{\mathcal{N}}$, $1_{\mathcal{N}}$, $\mathcal{U}$, $\mathcal{V}$} where $\mathcal{U}$ = [<0.5, 0.3, 0.6>, <0.4, 0.4, 0.7>} and $\mathcal{V}$ = {<0.7, 0.5, 0.3>, <0.7, 0.5, 0.2>}. Then the NSs $\mathcal{A}$ = {<0.5, 0.5, 0.4>, <0.7, 0.6, 0.7>} and $\mathcal{B}$ = {<0.6, 0.3, 0.6>, <0.4, 0.4, 0.3>} are $\mathcal{NPGR}\alpha$CSs in ($\mathcal{I}$, τ). But $\mathcal{A} \cap \mathcal{B}$ = {<0.5, 0.3, 0.6>, <0.4, 0.4, 0.7>} is not a $\mathcal{NPGR}\alpha$CS in ($\mathcal{I}$, τ). Since ($\mathcal{A} \cap \mathcal{B}$)$\subseteq$ $\mathcal{U}$ but NPCl($\mathcal{A} \cap \mathcal{B}$) = {<0.6, 0.7, 0.4>, <0.7, 0.6, 0.4>}$\not\subseteq$ $\mathcal{U}$.

Theorem 2.11. Let ($\mathcal{I}$, τ) be an NTS. Then for every $\mathcal{A}$ $\in$NPGRαC($\mathcal{I}$) and for every Neutrosophic set $\mathcal{B}$ $\in$NS($\mathcal{I}$),$\mathcal{A} \subseteq \mathcal{B} \subseteq$NPCl($\mathcal{A}$) implies $\mathcal{B}$ $\in$NPGRαC($\mathcal{I}$).

Proof: Let $\mathcal{B} \subseteq \mathcal{U}$ and $\mathcal{U}$ is a Neutrosophic regular α-open set in $(\mathcal{I}, \tau)$. Since $\subseteq \mathcal{B}$, then $\mathcal{A} \subseteq \mathcal{U}$.Given $\mathcal{A}$ is a NPGRαCS, it follows that NPCl($\mathcal{A}$) $\subseteq \mathcal{U}$. Now $\mathcal{B} \subseteq$NPCl($\mathcal{A}$) implies NPCl($\mathcal{B}$) $\subseteq$NPCl(NPCl($\mathcal{A}$)) = NPCl($\mathcal{A}$). Thus, NPCl($\mathcal{B}$)$\subseteq \mathcal{U}$. This proves that $\mathcal{B} \in$ NPGRαC($\mathcal{I}$).

Theorem 2.12. If $\mathcal{A}$ is a Neutrosophic regular α-open set and $\mathcal{NPGR}\alpha$CS in $(\mathcal{I}, \tau)$, then $\mathcal{A}$ is a Neutrosophic pre closed set in $(\mathcal{I}, \tau)$.

Proof: Since $\mathcal{A} \subseteq \mathcal{A}$ and $\mathcal{A}$ is a Neutrosophic regular α-open set in $(\mathcal{I}, \tau)$, by hypothesis, NPCl($\mathcal{A}$) $\subseteq \mathcal{A}$. But since $\mathcal{A} \subseteq$NPCl($\mathcal{A}$). Therefore NPCl($\mathcal{A}$)= $\mathcal{A}$. Hence $\mathcal{A}$ is a Neutrosophic pre closed set in $(\mathcal{I}, \tau)$.

2.NEUTROSOPHIC PRE GENERALIZED REGULAR α-CLOSURE IN NEUTROSOPHIC TOPOLOGICAL SPACES

In this section, we introduce the concept of Neutrosophic pre generalized regular α-closure operators in a Neutrosophic topological spaces.

Definition 3.1. Let $(\mathcal{I}, \tau)$ be a Neutrosophic topological space. Then for a Neutrosophic subset $\mathcal{A}$ of $\mathcal{I}$,

(i) Neutrosophic pre generalized regular α-interior of $\mathcal{A}$ is the union of all Neutrosophic pre generalized regular α-open sets of $\mathcal{I}$ contained in $\mathcal{A}$. i.e., $\mathcal{NPGR}\alpha$ -Int($\mathcal{A}$)=$\cup\{\mathcal{G} : \mathcal{G}$ is a $\mathcal{NPGR}\alpha$-open set in $\mathcal{I}$ and $\mathcal{G} \subseteq \mathcal{A}\}$.

(ii) Neutrosophic pre generalized regular α-closure of $\mathcal{A}$ is the intersection of all Neutrosophic pre generalized regular α-closed sets of $\mathcal{I}$ containing in $\mathcal{A}$. i.e., $\mathcal{NPGR}\alpha$-Cl($\mathcal{A}$) =$\cap\{ \mathcal{K} : \mathcal{K}$ is a $\mathcal{NPGR}\alpha$-closed set in $\mathcal{I}$ and $\mathcal{K} \supseteq \mathcal{A}\}$.

Theorem 3.2. Let $(\mathcal{I}, \tau)$ be a Neutrosophic topological space. Then for a Neutrosophic subsets $\mathcal{A}$ and $\mathcal{B}$ of $\mathcal{I}$, we have

(i) $\mathcal{NPGR}\alpha$-Int($\mathcal{A}$) $\subseteq \mathcal{A}$

(ii) $\mathcal{A}$ *is* $\mathcal{NPGR}\alpha$ -open set in A $\Leftrightarrow$ $\mathcal{NPGR}\alpha$ -Int($\mathcal{A}$)= $\mathcal{A}$

(iii) $\mathcal{NPGR}\alpha$ -Int($\mathcal{NPGR}\alpha$ -Int($\mathcal{A}$))= $\mathcal{NPGR}\alpha$ -Int($\mathcal{A}$)

(iv) If $\mathcal{A} \subseteq \mathcal{B}$ then $\mathcal{NPGR}\alpha$ -Int($\mathcal{A}$)$\subseteq$ $\mathcal{NPGR}\alpha$ -Int($\mathcal{B}$)

(v) $\mathcal{NPGR}\alpha$ -Int($\mathcal{A} \cap \mathcal{B}$)= $\mathcal{NPGR}\alpha$ -Int($\mathcal{A}$) $\cap$ $\mathcal{NPGR}\alpha$ -Int($\mathcal{B}$)

(vi) $\mathcal{NPGR}\alpha$ -Int($\mathcal{A} \cup \mathcal{B}$)$\supseteq$ $\mathcal{NPGR}\alpha$ Int($\mathcal{A}$)$\cup$ $\mathcal{NPGR}\alpha$ -Int($\mathcal{B}$).

Proof: Follows from Definition 3.1.(i).This proves (i).

Let $\mathcal{A}$ be an $\mathcal{NPGR}\alpha$-open set in $\mathcal{I}$. Then $\mathcal{A} \subseteq \mathcal{NPGR}\alpha$-Int($\mathcal{A}$). By using Theorem 3.2 (i) we get $\mathcal{A}$ = $\mathcal{NPGR}\alpha$-Int($\mathcal{A}$). Conversely assume that $\mathcal{A}$ = $\mathcal{NPGR}\alpha$-Int($\mathcal{A}$). By using Definition 3.1(i), $\mathcal{A}$ is $\mathcal{NPGR}\alpha$-open set in $\mathcal{I}$. Thus (ii) is proved.

By using Theorem 3.2 (ii), $\mathcal{NPGR}\alpha$-Int($\mathcal{NPGR}\alpha$-Int($\mathcal{A}$)) = $\mathcal{NPGR}\alpha$-Int($\mathcal{A}$). This proves (iii).

Since $\mathcal{A} \subseteq \mathcal{B}$, by using Theorem 3.2 (i), $\mathcal{NPGR}\alpha$-Int($\mathcal{A}$)$\subseteq$ $\mathcal{A} \subseteq \mathcal{B}$. That is $\mathcal{NPGR}\alpha$-Int ($\mathcal{A}$)$\subseteq$ $\mathcal{B}$.

By Theorem 3.2 (iii), $\mathcal{NPGR}\alpha$-Int($\mathcal{NPGR}\alpha$-Int($\mathcal{A}$))$\subseteq\mathcal{NPGR}\alpha$-Int($\mathcal{B}$).This proves (iv).

Since $\mathcal{A} \cap \mathcal{B} \subseteq \mathcal{A}$ and $\mathcal{A} \cap \mathcal{B} \subseteq \mathcal{B}$, by using Theorem 3.2(iv), $\mathcal{NPGR}\alpha$-Int($\mathcal{A} \cap \mathcal{B}$) $\subseteq$ $\mathcal{NPGR}\alpha$-Int($\mathcal{A}$) and $\mathcal{NPGR}\alpha$-Int($\mathcal{A} \cap \mathcal{B}$) $\subseteq$ $\mathcal{NPGR}\alpha$-Int($\mathcal{B}$).This implies that

$\mathcal{NPGR}\alpha$-Int($\mathcal{A} \cap \mathcal{B}$) $\subseteq$ $\mathcal{NPGR}\alpha$-Int($\mathcal{A}$) $\cap$ $\mathcal{NPGR}\alpha$-Int($\mathcal{B}$)

(1)

By using Theorem 3.2(i), $\mathcal{NPGR}\alpha$-Int($\mathcal{A}$) $\subseteq \mathcal{A}$ and $\mathcal{NPGR}\alpha$-Int($\mathcal{B}$) $\subseteq \mathcal{B}$. This implies that $\mathcal{NPGR}\alpha$-Int($\mathcal{A}$) $\cap$ $\mathcal{NPGR}\alpha$-Int($\mathcal{B}$) $\subseteq (\mathcal{A} \cap \mathcal{B})$. Now applying Theorem 3.2(iv), $\mathcal{NPGR}\alpha$-Int(($\mathcal{NPGR}\alpha$-Int($\mathcal{A}$) $\cap$ $\mathcal{NPGR}\alpha$-Int($\mathcal{B}$)) $\subseteq$ $\mathcal{NPGR}\alpha$-Int($\mathcal{A} \cap \mathcal{B}$). By Theorem 3.2(iii),

$\mathcal{NPGR}\alpha$-Int($\mathcal{A}$) $\cap$ $\mathcal{NPGR}\alpha$-Int($\mathcal{B}$) $\subseteq\mathcal{NPGR}\alpha$-Int($\mathcal{A} \cap \mathcal{B}$)

(2)

From equations (1) and (2), $\mathcal{NPGR}\alpha$-Int($\mathcal{A} \cap \mathcal{B}$) = $\mathcal{NPGR}\alpha$-Int($\mathcal{A}$) $\cap$ $\mathcal{NPGR}\alpha$-Int($\mathcal{B}$). This proves (v).

Since $\mathcal{A} \subseteq \mathcal{A} \cup \mathcal{B}$ and B $\subseteq \mathcal{A} \cup \mathcal{B}$, by using Theorem 3.2(iv), $\mathcal{NPGR}\alpha$-Int($\mathcal{A}$) $\subseteq$ $\mathcal{NPGR}\alpha$-Int($\mathcal{A} \cup \mathcal{B}$) and $\mathcal{NPGR}\alpha$-Int($\mathcal{B}$) $\subseteq$ $\mathcal{NPGR}\alpha$-Int($\mathcal{A} \cup \mathcal{B}$).This implies that $\mathcal{NPGR}\alpha$-Int($\mathcal{A}$) $\cup\cap$ $\mathcal{NPGR}\alpha$-Int($\mathcal{B}$) $\subseteq$ $\mathcal{NPGR}\alpha$-Int($\mathcal{A} \cup \mathcal{B}$). This proves (vi).

Remark 3.3. The following example shows that the equality need not hold in Theorem 3.3(vi).

Example 3.4. Let $\mathcal{I}$ = {a, b} and τ = {$0_{\mathcal{N}}$, $1_{\mathcal{N}}$, $\mathcal{U}$, $\mathcal{V}$} where $\mathcal{U}$ = {<0.5, 0.3, 0.6>, <0.4, 0.4, 0.7>} and $\mathcal{V}$ ={<0.7, 0.5, 0.3>, <0.7, 0.5, 0.2>]. Then $(\mathcal{I}, \tau)$ is a Neutrosophic topological spaces. Consider the NSs $\mathcal{A}$ ={<0.8, 0.9, 0.2>, <0.7, 0.6, 0.4>} and $\mathcal{B}$ ={<0.6, 0.7, 0.5>,<0.9, 0.8, 0.2>} in $(\mathcal{I},\tau)$.

Then $\mathcal{NPGR}\alpha$ -Int($\mathcal{A}$)={<0.7, 0.9, 0.2.>), <0.7, 0.6,

0.4>}and $\mathcal{NPGR}\alpha$ -Int($\mathcal{B}$)={<0.6, 0.7, 0.5), <0.8, 0.8, 0.2>}, this implies $\mathcal{NPGR}\alpha$ -Int($\mathcal{A}$)∪ $\mathcal{NPGR}\alpha$ – Int($\mathcal{B}$)= {<0.7, 0.9, 0.2>, <0.8, 0.8, 0.2>]. But $\mathcal{NPGR}\alpha$ -Int($\mathcal{A}$ ∪ $\mathcal{B}$)={<0.8,0.9,0.2>, <0.9,0.8,0.2>}.

Then $\mathcal{NPGR}\alpha$ -Int($\mathcal{A}$ ∪ $\mathcal{B}$)⊄ $\mathcal{NPGR}\alpha$ -Int($\mathcal{A}$ ∪ $\mathcal{B}$).

Proposition 3.5. Let ($\mathcal{I}$, τ) be a Neutrosophic topological space. Then for any Neutrosophic subsets $\mathcal{A}$ of $\mathcal{I}$,

(i) C($\mathcal{NPGR}\alpha$-Int($\mathcal{A}$))=$\mathcal{NPGR}\alpha$-Cl(C($\mathcal{A}$)).

(ii) C($\mathcal{NPGR}\alpha$-Cl($\mathcal{A}$))=$\mathcal{NPGR}\alpha$-Int(C($\mathcal{A}$)).

Proof : By using Definition 3.1(i), $\mathcal{NPGR}\alpha$-Int($\mathcal{A}$) = ∪{$\mathcal{G}$: $\mathcal{G}$ is a $\mathcal{NPGR}\alpha$-open set in A and $\mathcal{G}$ ⊆ $\mathcal{A}$ }.

Taking complement on both sides, C($\mathcal{NPGR}\alpha$-Int($\mathcal{A}$))=C(∪{$\mathcal{G}$: $\mathcal{G}$ is a $\mathcal{NPGR}\alpha$-open set in $\mathcal{I}$ and $\mathcal{G}$ ⊆ $\mathcal{A}$ }) =∩{C($\mathcal{G}$):C($\mathcal{G}$) is a $\mathcal{NPGR}\alpha$-closed set in $\mathcal{I}$ and C($\mathcal{A}$) ⊆ C(G)}. Replacing C(G) by $\mathcal{K}$, we get C($\mathcal{NPGR}\alpha$-Int($\mathcal{A}$))=∩{ $\mathcal{K}$: $\mathcal{K}$ is a $\mathcal{NPGR}\alpha$-closed set in $\mathcal{I}$ and $\mathcal{K}$ ⊇ C($\mathcal{A}$)}. By Definition 3.1(ii), C($\mathcal{NPGR}\alpha$-Int($\mathcal{A}$)) = $\mathcal{NPGR}\alpha$-Cl(C($\mathcal{A}$)). This proves (i).

By using Proposition 3.5 (i), C($\mathcal{NPGR}\alpha$-Int(C($\mathcal{A}$)))=$\mathcal{NPGR}\alpha$-Cl(C(C($\mathcal{A}$)))=$\mathcal{NPGR}\alpha$-Cl($\mathcal{A}$). Taking complement on both sides, we get $\mathcal{NPGR}\alpha$-Int(C($\mathcal{A}$))=C($\mathcal{NPGR}\alpha$-Cl($\mathcal{A}$)). Thus (ii) is proved.

Proposition 3.6. Let ($\mathcal{I}$, τ) be a Neutrosophic topological spaces .Then for any Neutrosophic subsets $\mathcal{A}$ and $\mathcal{B}$ of $\mathcal{I}$ we have

(i) $\mathcal{A}$ ⊆ $\mathcal{NPGR}\alpha$-Cl($\mathcal{A}$).

(ii) $\mathcal{A}$ is $\mathcal{NPGR}\alpha$-closed set in $\mathcal{I}$ ⇔$\mathcal{NPGR}\alpha$-Cl($\mathcal{A}$)= $\mathcal{A}$.

(iii) $\mathcal{NPGR}\alpha$-Cl($\mathcal{NPGR}\alpha$-Cl($\mathcal{A}$))=$\mathcal{NPGR}\alpha$-Cl($\mathcal{A}$).

(iv) If $\mathcal{A}$ ⊆ $\mathcal{B}$ then $\mathcal{NPGR}\alpha$-Cl($\mathcal{A}$)⊆$\mathcal{NPGR}\alpha$-Cl($\mathcal{B}$)

Proof: Follows from the Definition 3.1(ii). This proves (i).

Let $\mathcal{A}$ be $\mathcal{NPGR}\alpha$-closed set in $\mathcal{I}$. Then C($\mathcal{A}$) is $\mathcal{NPGR}\alpha$-open set in $\mathcal{I}$. By theorem 3.2(ii), $\mathcal{NPGR}\alpha$-Int(C($\mathcal{A}$))=C($\mathcal{A}$) ⇔C($\mathcal{NPGR}\alpha$-Cl($\mathcal{A}$))=C($\mathcal{A}$)⇔ $\mathcal{NPGR}\alpha$-Cl($\mathcal{A}$)= $\mathcal{A}$.Thus (ii) is proved.

By using Proposition 3.6 (ii), $\mathcal{NPGR}\alpha$-Cl($\mathcal{NPGR}\alpha$-Cl($\mathcal{A}$))=$\mathcal{NPGR}\alpha$-Cl($\mathcal{A}$) .This proves(iii).

Since $\mathcal{A}$ ⊆ $\mathcal{B}$, C($\mathcal{B}$)⊆C($\mathcal{A}$). By using Theorem 3.2(iv), $\mathcal{NPGR}\alpha$-Int(C($\mathcal{B}$))⊆$\mathcal{NPGR}\alpha$-Int(C($\mathcal{A}$)). Taking complement on both sides, C($\mathcal{NPGR}\alpha$-Int(C($\mathcal{B}$)))⊇C($\mathcal{NPGR}\alpha$-Int(C($\mathcal{A}$))). By Proposition 3.5(ii), $\mathcal{NPGR}\alpha$-Cl($\mathcal{A}$)⊆$\mathcal{NPGR}\alpha$-Cl($\mathcal{B}$).This proves(iv).

Proposition 3.7. Let ($\mathcal{I}$, τ) be a Neutrosophic topological spaces. Then for any Neutrosophic subset $\mathcal{A}$ and $\mathcal{B}$ of $\mathcal{I}$, we have

(i) $\mathcal{NPGR}\alpha$-Cl($\mathcal{A}$ ∪ $\mathcal{B}$) =$\mathcal{NPGR}\alpha$-Cl($\mathcal{A}$)∪$\mathcal{NPGR}\alpha$-Cl($\mathcal{B}$) and

(ii) $\mathcal{NPGR}\alpha$-Cl($\mathcal{A}$ ∩ $\mathcal{B}$)⊆$\mathcal{NPGR}\alpha$-Cl($\mathcal{A}$)∩$\mathcal{NPGR}\alpha$-Cl($\mathcal{B}$).

Proof: Since $\mathcal{NPGR}\alpha$-Cl($\mathcal{A}$ ∪ $\mathcal{B}$)= $\mathcal{NPGR}\alpha$-Cl(C(C($\mathcal{A}$ ∪ $\mathcal{B}$))), By using Proposition 3.5(i), $\mathcal{NPGR}\alpha$-Cl($\mathcal{A}$ ∪ $\mathcal{B}$)=C($\mathcal{NPGR}\alpha$-Int(C($\mathcal{A}$ ∪ $\mathcal{B}$))) =C($\mathcal{NPGR}\alpha$-Int(C($\mathcal{A}$)∩C($\mathcal{B}$))). Again using Proposition 3.2(v), $\mathcal{NPGR}\alpha$-Cl($\mathcal{A}$∪ $\mathcal{B}$)=C($\mathcal{NPGR}\alpha$-Int(C($\mathcal{A}$))∩$\mathcal{NPGR}\alpha$-Int(C($\mathcal{B}$)))=C($\mathcal{NPGR}\alpha$-Int(C($\mathcal{A}$))) ∪ C($\mathcal{NPGR}\alpha$-Int(C($\mathcal{B}$))).By using Proposition 3.5(i),

$\mathcal{NPGR}\alpha$-Cl($\mathcal{A}$ ∪ $\mathcal{B}$)=$\mathcal{NPGR}\alpha$-Cl (C(C($\mathcal{A}$)))∪ $\mathcal{NPGR}\alpha$-Cl(C(C($\mathcal{B}$)))= $\mathcal{NPGR}\alpha$-Cl ($\mathcal{A}$)∪ $\mathcal{NPGR}\alpha$-Cl($\mathcal{B}$).

Thus (i) is proved.

Since $\mathcal{A}$ ∩ $\mathcal{B}$ ⊆ $\mathcal{A}$ and $\mathcal{A}$ ∩ $\mathcal{B}$ ⊆ $\mathcal{B}$, by using Proposition 3.6(iv), $\mathcal{NPGR}\alpha$-Cl($\mathcal{A}$ ∩ $\mathcal{B}$)⊆$\mathcal{NPGR}\alpha$-Cl($\mathcal{A}$) and $\mathcal{NPGR}\alpha$-Cl ($\mathcal{A}$ ∩ $\mathcal{B}$) ⊆$\mathcal{NPGR}\alpha$-Cl($\mathcal{B}$).

This implies that $\mathcal{NPGR}\alpha$-Cl($\mathcal{A}$ ∩ $\mathcal{B}$)⊆$\mathcal{NPGR}\alpha$-Cl($\mathcal{A}$)∩ $\mathcal{NPGR}\alpha$-Cl($\mathcal{B}$).This proves (ii).

Remark 3.8. The following example shows that the equality need not hold in Proposition 3.7(ii).

Example 3.9. Let $\mathcal{I}$ = {a, b} and τ = {$0_{\mathcal{N}}$, $1_{\mathcal{N}}$, $\mathcal{U}$, $\mathcal{V}$} where $\mathcal{U}$ ={<0.5, 0.3, 0.6>, <0.4, 0.4, 0.7>} and $\mathcal{V}$ ={<0.7, 0.5, 0.3>, <0.7, 0.5, 0.2>}. Then ($\mathcal{I}$, τ) is a Neutrosophic topological space. Consider the NSs $\mathcal{A}$ ={<0.4, 0.5, 0.4>, <0.7, 0.6, 0.8>} and $\mathcal{B}$={<0.6, 0.3, 0.6>, <0.2, 0.4, 0.5>}in ($\mathcal{I}$, τ).

Then $\mathcal{NPGR}\alpha$-Cl($\mathcal{A}$)={<0.5, 0.5, 0.4>, <0.7, 0.6, 0.7>} and $\mathcal{NPGR}\alpha$-Cl($\mathcal{B}$)={<0.6, 0.3, 0.6>, <0.4, 0.4, 0.3>}, this implies $\mathcal{NPGR}\alpha$-Cl($\mathcal{A}$)∩ $\mathcal{NPGR}\alpha$-Cl($\mathcal{B}$) = {<0.5, 0.3, 0.6>, <0.4, 0.4, 0.7>}.

But $\mathcal{NPGR}\alpha$-Cl($\mathcal{A}$ ∩ $\mathcal{B}$)={<0.4,0.3,0.6>, <0.2,0.4,0.8>}.

Then $\mathcal{NPGR}\alpha$-Cl($\mathcal{A}$)∩$\mathcal{NPGR}\alpha$-Cl($\mathcal{B}$)⊄ $\mathcal{NPGR}\alpha$ -Cl($\mathcal{A}$ ∩ $\mathcal{B}$).

Remark 3.10. Let $\mathcal{A}$ be a Neutrosophic set in a Neutrosophic topological space on $\mathcal{J}$. Then NInt($\mathcal{A}$)$\subseteq$$\mathcal{NPGR\alpha}$-Int($\mathcal{A}$)$\subseteq$ $\mathcal{A}$ $\subseteq$$\mathcal{NPGR\alpha}$-Cl($\mathcal{A}$) $\subseteq$NCl($\mathcal{A}$).

Theorem 3.11. Let ($\mathcal{J}$, τ) be a NTS. Then for any Neutrosophic subsets $\mathcal{A}$ and $\mathcal{B}$ of A we have

(i) $\mathcal{NPGR\alpha}$-Cl($\mathcal{A}$)$\supseteq$ $\mathcal{A}$ $\cup$ $\mathcal{NPGR\alpha}$-Cl($\mathcal{NPGR\alpha}$-Int($\mathcal{A}$)).

(ii) $\mathcal{NPGR\alpha}$-Int($\mathcal{A}$)$\subseteq$ $\mathcal{A}$ $\cap$$\mathcal{NPGR\alpha}$-Int($\mathcal{NPGR\alpha}$-Cl($\mathcal{A}$)).

(iii) NInt($\mathcal{NPGR\alpha}$-Cl($\mathcal{A}$)) $\subseteq$NInt(NCl($\mathcal{A}$)).

(iv) NInt($\mathcal{NPGR\alpha}$-Cl($\mathcal{A}$)) $\supseteq$NInt($\mathcal{NPGR\alpha}$-Cl($\mathcal{NPGR\alpha}$-Int($\mathcal{A}$))).

Proof:

By Proposition 3.6(i), $\mathcal{A}$ $\subseteq$ $\mathcal{NPGR\alpha}$-Cl($\mathcal{A}$) (3).

Again using Theorem 3.2(i), $\mathcal{NPGR\alpha}$-Int($\mathcal{A}$) $\subseteq$ $\mathcal{A}$.

Then, $\mathcal{NPGR\alpha}$-Cl($\mathcal{NPGR\alpha}$-Int($\mathcal{A}$))$\subseteq$$\mathcal{NPGR\alpha}$-Cl($\mathcal{A}$) (4).

By(3) and (4) we have, $\mathcal{A}$ $\cup$ $\mathcal{NPGR\alpha}$-Cl($\mathcal{NPGR\alpha}$-Int ($\mathcal{A}$)) $\subseteq$$\mathcal{NPGR\alpha}$-Cl($\mathcal{A}$).

This proves (i).

Taking $\mathcal{NPGR\alpha}$-interior on both sides of equation (3)

$\mathcal{NPGR\alpha}$-Int($\mathcal{A}$)$\subseteq$$\mathcal{NPGR\alpha}$-Int($\mathcal{NPGR\alpha}$-Cl($\mathcal{A}$))

(5).

From (4) and (5), $\mathcal{NPGR\alpha}$-Int($\mathcal{A}$) $\subseteq$ ($\mathcal{A}$ $\cap$ $\mathcal{NPGR\alpha}$-Int($\mathcal{NPGR\alpha}$-Cl($\mathcal{A}$))). This proves (ii).

By Remark 3.10, $\mathcal{NPGR\alpha}$-Cl($\mathcal{A}$) $\subseteq$ NCl($\mathcal{A}$).We get NInt($\mathcal{NPGR\alpha}$-Cl($\mathcal{A}$)) $\subseteq$ NInt(NCl($\mathcal{A}$)).

This proves (iii).

By Theorem 3.11(i), $\mathcal{NPGR\alpha}$-Cl($\mathcal{A}$) $\supseteq$ ($\mathcal{A}$ $\cup$ $\mathcal{NPGR\alpha}$-Cl ($\mathcal{NPGR\alpha}$-Int($\mathcal{A}$))). Taking Neutrosophic interior on both sides, NInt($\mathcal{NPGR\alpha}$-Cl($\mathcal{A}$) $\supseteq$NInt($\mathcal{A}$ $\cup$$\mathcal{NPGR\alpha}$-Cl($\mathcal{NPGR\alpha}$-Int($\mathcal{A}$))).

Since NInt($\mathcal{A}\cup$ $\mathcal{B}$)$\supseteq$NInt($\mathcal{A}$)$\cup$NInt($\mathcal{B}$), NInt($\mathcal{NPGR\alpha}$-Cl($\mathcal{A}$)$\supseteq$NInt(A)$\cup$NInt($\mathcal{NPGR\alpha}$-lnt($\mathcal{NPGR\alpha}$-Int($\mathcal{A}$)))$\supseteq$NInt($\mathcal{NPGR\alpha}$-Cl($\mathcal{NPGR\alpha}$-Int($\mathcal{A}$))).Thus (iv) is proved.

Theorem 3.12. Let ($\mathcal{J}$, τ) be a Neutrosophic topological space. Then for any Neutrosophic subset $\mathcal{A}$ and $\mathcal{B}$ of $\mathcal{J}$,

(i) $\mathcal{NPGR\alpha}$-Cl($\mathcal{A}$)$\supseteq$ $\mathcal{A}\cup\mathcal{NPGR\alpha}$-Cl($\mathcal{NPGR\alpha}$-Int($\mathcal{A}$)).

(ii) $\mathcal{NPGR\alpha}$-Int($\mathcal{A}$)$\subseteq$ $\mathcal{A}\cap$ $\mathcal{NPGR\alpha}$-Int($\mathcal{NPGR\alpha}$-Cl($\mathcal{A}$)).

(iii) NInt($\mathcal{NPGR\alpha}$-Cl($\mathcal{A}$))$\subseteq$NInt(NCl($\mathcal{A}$)).

(iv) NInt($\mathcal{NPGR\alpha}$-Cl($\mathcal{A}$))$\supseteq$NInt($\mathcal{NPGR\alpha}$-Cl ($\mathcal{NPGR\alpha}$-Int($\mathcal{A}$))).

Proof: By Proposition 3.6(i), $\mathcal{A}$ $\subseteq$$\mathcal{NPGR\alpha}$-Cl($\mathcal{A}$) (6).

Again using Theorem 3.2(i),

$\mathcal{NPGR\alpha}$-Int($\mathcal{A}$) $\subseteq$ $\mathcal{A}$. (7).

Taking $\mathcal{NPGR\alpha}$-closure on both sides, $\mathcal{NPGR\alpha}$-Cl($\mathcal{NPGR\alpha}$-Int($\mathcal{A}$))$\subseteq$$\mathcal{NPGR\alpha}$-Cl($\mathcal{A}$) (8).

By equation (6) and (8), $\mathcal{A}$ $\cup$$\mathcal{NPGR\alpha}$-Cl($\mathcal{NPGR\alpha}$-Int($\mathcal{A}$)) $\subseteq$$\mathcal{NPGR\alpha}$-Cl($\mathcal{A}$).

This proves (i).

Again using Theorem 3.2(i), $\mathcal{A}$ $\subseteq$$\mathcal{NPGR\alpha}$-Cl($\mathcal{A}$). Taking $\mathcal{NPGR\alpha}$-interior on both sides,

$\mathcal{NPGR\alpha}$-Int($\mathcal{A}$)$\subseteq$$\mathcal{NPGR\alpha}$-Int($\mathcal{NPGR\alpha}$-Cl($\mathcal{A}$))

(9).

From (7) and (9), we have $\mathcal{NPGR\alpha}$-Int($\mathcal{A}$)$\subseteq$($\mathcal{A}$ $\cap$ $\mathcal{NPGR\alpha}$-Int($\mathcal{NPGR\alpha}$-Cl($\mathcal{A}$))).This proves (ii).

By Theorem 3.11, $\mathcal{NPGR\alpha}$-Cl($\mathcal{A}$)$\subseteq$NCl($\mathcal{A}$).Then NInt($\mathcal{NPGR\alpha}$-Cl($\mathcal{A}$))$\subseteq$NInt(NCl($\mathcal{A}$)).Thus (iii) is proved.

By Theorem 3.12(i),$\mathcal{NPGR\alpha}$-Cl($\mathcal{A}$)$\supseteq$($\mathcal{A}\cup\mathcal{NPGR\alpha}$-($\mathcal{NPGR\alpha}$-Int($\mathcal{A}$))).

This implies NInt($\mathcal{NPGR\alpha}$-Cl($\mathcal{A}$)$\supseteq$NInt($\mathcal{A}$ $\cup$$\mathcal{NPGR\alpha}$-Cl($\mathcal{NPGR\alpha}$-Int($\mathcal{A}$))).

Since NInt($\mathcal{A}\cup$ $\mathcal{A}$)$\supseteq$NInt($\mathcal{A}$)$\cup$NInt($\mathcal{B}$),$\mathcal{NPGR\alpha}$-Int($\mathcal{NPGR\alpha}$-Cl($\mathcal{A}$)$\supseteq$NInt($\mathcal{A}$)$\cup$NInt($\mathcal{NPGR\alpha}$-Cl($\mathcal{NPGR\alpha}$-Int($\mathcal{A}$)))$\supseteq$NInt($\mathcal{NPGR\alpha}$-Cl($\mathcal{NPGR\alpha}$-Int($\mathcal{A}$))).Thus (iv) is proved.

REFERENCES

[1] M.Abdel-Baset, M., Chang V., and Gamal A., *Evaluation of the green supply chain management practices: A Novel neutrosophic approach, Computers in Industry*, Vol. *108, pp.*210-220, 2019.

[2] Abdel-Basset, M., El-hoseny, M., Gamal, A., &Smarandache, F. *A novel model for evaluation Hospital medical care systems based on plithogenic sets. Artificial intelligence in medicine*, Vol.100, pp.101-110, 2019.

[3] Abdel-Basset, M., Mohamed, R., Zaied, A. E. N. H., & marandache, F., *A hybrid plithogenic decision-making approach with quality function deployment for selecting supply chain sustainability metrics. Symmetry,Vol.11(7)*, pp.90, 2019.

[4] Abdel-Basset, M., Saleh, M., Gamal, A., &Smarandache, F. (2019). *An approach of TOPSIS technique for developing supplier selection with group decision making under type-2 neutrosophic number*. Applied Soft Computing, Vol.77, pp.438- 452, 2019.

[5] Atanassov K.T., *Intuitionistic fuzzy sets*, Fuzzy Sets and Systems, pp.87-96, 1986.

[6] Chang C. L., *Fuzzy topological spaces J.Math.Anal.Appl.* Vol.*24*,No.1, pp. 182- 190, 1968.

[7] D. Coker, *An Introduction to Intuitionistic fuzzy topological spaces*, Fuzzy Sets and Systems,Vol. 88, No.1,pp. 81-89, 1997.

[8] R.Dhavaseelan and S. Jafari, *Generalized Neutrosophic closed sets*, New trends in Neutrosophictheory and applications Vol. II, pp.261-273,2018.

[9] Harshitha A. and Jayanthi D., *Regular α-Generalized Closed Ses in Neutrosophic topological Spaces*, IOSR Journal of Mathematics, Vol.15,No. 02,pp.11-18, 2019.

[10] Ishwarya P.and K. Bageerathi, On *Neutrosophic semi-open sets in Neutrosophic topological spaces*,International Journal of math. Trends and Tech., pp.214-223, 2016.

[11] I.M.A. Jaffer and K. Ramesh, *Neutrosophic Generalized Pre Regular Closed Sets*, Neutrosophic Sets and Systems,Vol. 30, pp.171, 2019

[12] Jayanthi D., *On αGeneralized closed sets in Neutrosophic topological spaces*, International conference on Recent trends in mathematics and Information technology (ICRMIT 2018)

[13] W. Al-Omeri and S. Jafari, *On Generalized Closed Sets and Generalized pre-Closed sets in Neutrosophic Topological Spaces, Mathematics MDPI*,Vol.7, No.1,pp. 01-12, 2018.

[14] W. Al-omeri and F. Smarandache, *New Neutrosophic sets via Neutrosophic Topological spaces*, New Trends in Neutrosophic Theory and Applications, Vol(2), June 2016.

[15] A.Pushpalatha and T. Nandhini, *Generalized closed sets via neutrosophic topological spaces*, Malaya Journal of Matematik, Vol.7, No.1, pp.50-54, 2019

[16] Salama A.A. and Alblowi S.A., *Neutrosophic set and Neutrosophic topological space*, IOSR Journal of Mathematics, Vol.3, No.4, pp. 31-35,2012.

[17] Salama A. A., F.Smarandache and V. Kroumov, *Neutrosophic closed set and Neutrosophic continuous functions, Neutrosophic Sets and Systems*,Vol. 4,pp. 4–8,2014.

[18] Santhi R. and Udhayarani N.,et al., *Nω –Closed sets in Neutrosophic Topological Spaces. Neutrosophic Sets and Systems*, Vol.12,No.1, pp. 114-117, 2016.

[19] F. Smarandache ,*Neutrosophic and Neutrosophic Logic*, First International Conference on Neutrosophic ,Neutrosophic Logic, Set, Probability, and Statistics, University of New Mexico, Gallup, NM, Vol. 87301, USA (2002).

[20]Zadeh, L.A., *Fuzzy sets*, Information and Control, Vol. 8, No.3, pp.338-353, 1965.

e-ISSN: 2582-5208
International Research Journal of Modernization in Engineering Technology and Science
Volume:03/Issue:06/June-2021 Impact Factor- 5.354 www.irjmets.com

BLOCKCHAIN POWERED SUPPLY CHAIN MANAGEMENT IN SMALL AND MEDIUM SCALE INDUSTRIES

Anand Haridas*[1], Devaprasad V*[2], Diya S*[3], Fathima Nazrin S*[4], Thahseen Shadat*[5]

*[1]Assistant Professor, Ahalia School Of Engineering And Technology, Palakkad, Kerala, India.

*[2,3,4,5]Student, Ahalia School Of Engineering And Technology, Palakkad, Kerala, India.

ABSTRACT

Efficient supply chain management is an inevitable part of any progressive industry, and in a way it is the most convoluted component of any industry, especially the small and medium scale industries, as well. Since supply chain management is a tangled cycle that involves a whole lot of stake holders right from raw material, suppliers, manufacturers, distributors and finally the customers, trust among these stakeholders has been the only major factor on which organizations has relied on heavily when it came to the management of this supply chain, conventionally. But as with any other industry, of late, this lack of trust among the stake holders has seen a meteoric rise thereby leading to product delays, products getting tampered, commodities getting misplaced and eventually as a resultant of these mishaps, organization loses out on its credibility front. It is at this juncture that the block chain technology comes as the saviour of sorts by providing an efficient technological solution to make this entire supply chain cycle transparent by inducing an overall trust and accountability among the entire system that involves stakeholders who are not trust worthy.

Keywords: Block Chain, Supply Chain, Stakeholders.

I. INTRODUCTION

Block chain can be considered very well as a virtual ledger that precisely records each and every transaction on a real time basis and this virtual ledger is available at the end of all the stake holders .This virtual ledger is more or less a replicated copy that gets instantaneously updated, and this updation is reflected across all the other virtual ledgers that are present at the end of all other stake holders almost simultaneously, thereby inducing a much needed transparency and accountability in this whole cycle consisting of numerous and varied stake holders. This could be understood by a simple case study of an SME company say, ABC. Assuming ABC is a SME that exclusively transports food products based on block chain based supply chain system from India to the US, it will have to route its products through various transit points like the middle-east, the Europe before finally reaching the US. Now assuming an occurrence of an untoward incident somewhere in the transit path, as a result of which the product that had reached the US was found to be unfit for consumption due to some delay induced at some transit point, this predicament could very well be addressed by tracing and penalizing the exact stakeholder end that was responsible for inducing the delay, thereby increasing the overall accountability. This is done by simply examining each and every transaction that was recorded in a foolproof manner in the virtual ledgers enroute to the US.

II. METHODOLOGY

The ledger forms the major component of any block chain based implementations, the virtual ledger could very well be considered as a data structure that has the ability to record a number of data in the most secure way. This is possible by virtue of its inherent nature. It has a block structure where in each and every block is interconnected using a hash value and this hash value which is unique in every aspect provides a mode by which it can always be assured that the data contained in these ledgers never gets tampered. This is as represented in figure.1 and figure.2 which respectively shows the basic architecture and the block structure of block chain implementation. Moreover this architecture could be made even more robust with the usage of IOT in tandem. By the integration of IOT components with this block chain architecture the overall supply chain network could be made even more efficient, accountable and transparent. The blockchain architecture as depicted in figure.1 could be considered as a collection of records arranged in tandem so strongly with the help of various cryptographic techniques such that there is no possibility for any intruder nodes to get in between and tamper with the basic blockchain network. In this the head node is often called as the genesis block that is the node that comes at first place followed by each and every other nodes in order of the transaction that has taken place and could probably go upto 'n' number of records based on the volume of the transaction that takes

place. Each record, as showed in the figure.2, in turn could be considered as a combination of data and pointer. The data is very well the transactional data and the pointer is an address that simply keeps all these nodes chained together.

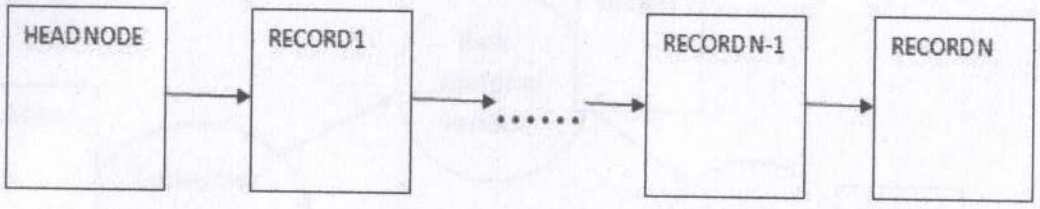


Figure:1 Basic Architecture

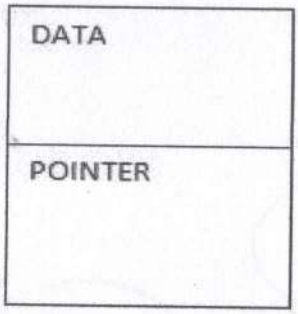


Figure:2 Block Structure

III. MODELING AND ANALYSIS

Supply chain management acts as the perfect application area of the block chain as it, conventionally has remained as the most difficult part as far as any industry is concerned. This is because there are innumerable stakeholders in a supply chain management system that may not be trustworthy. The supply chain cycle of a small and medium scale industry as showed in the figure.3, consists of innumerable stakeholders that might not be necessarily trustworthy as each and every stakeholder is a separate business entity operating for serving out their own business interests. In such a scenario an environment of trustworthiness is achieved by making each and every stake holder accountable by putting them under a zone of patrol .This is achieved by assigning a ledger to every stake holder that can in no way be altered with whatsoever means ensuring that whatever is being entered into this ledger remains permanently moreover this ledger is shared among all other users as well in the form of a copy at every stake holder end ensuring that this ledger entry remains very much transparent across entire network.

Here each ledger can be considered as a container holding the entire transactional chains, which keeps growing based on the number and frequency of transactions. And each and every ledger at the various stakeholders end is necessarily a mirror copy that operates in tandem and never ever this chain of transactions can be altered either by tampering the entries or by reordering the the chain as each and every block is linked cryptographically linked to one another thus ruling out even the slightest of possibility of data manipulation.

Whenever a new stakeholder gets physically added to the supply chain for example in figure.3, if a new stakeholder called logistic agency gets introduced, this new addition can easily be accommodated in block chain backbone as another new replica of existing ledger is created and assigned to the newly introduced stakeholder that is the logistics agency, thus allowing maximum flexibility without any inconvenience to others who are already a part of it.

This can be further illustrated with the help of a case study of a supply chain system managing transactions of meat based products across various geographies, it includes stakeholder such as supplier, manufacturer, transporters etc all of which has a local copy in the form of ledger that is a repository of transactions that happens at various point of time for example once the supplier supplies the consignment through logistic provider by paying the required fee this is added as a transaction in the ledger, similarly each and every such transactions are recorded and entered. If due to some delay by logistic provider the product reaches delayed at

e-ISSN: 2582-5208
International Research Journal of Modernization in Engineering Technology and Science
Volume:03/Issue:06/June-2021 Impact Factor- 5.354 www.irjmets.com

receiver end, then the cause of delay can be easily traced with the help of time recorded in ledger thus ascertaining the delay inducing stakeholder end and thereby penalizing this particular stakeholder.

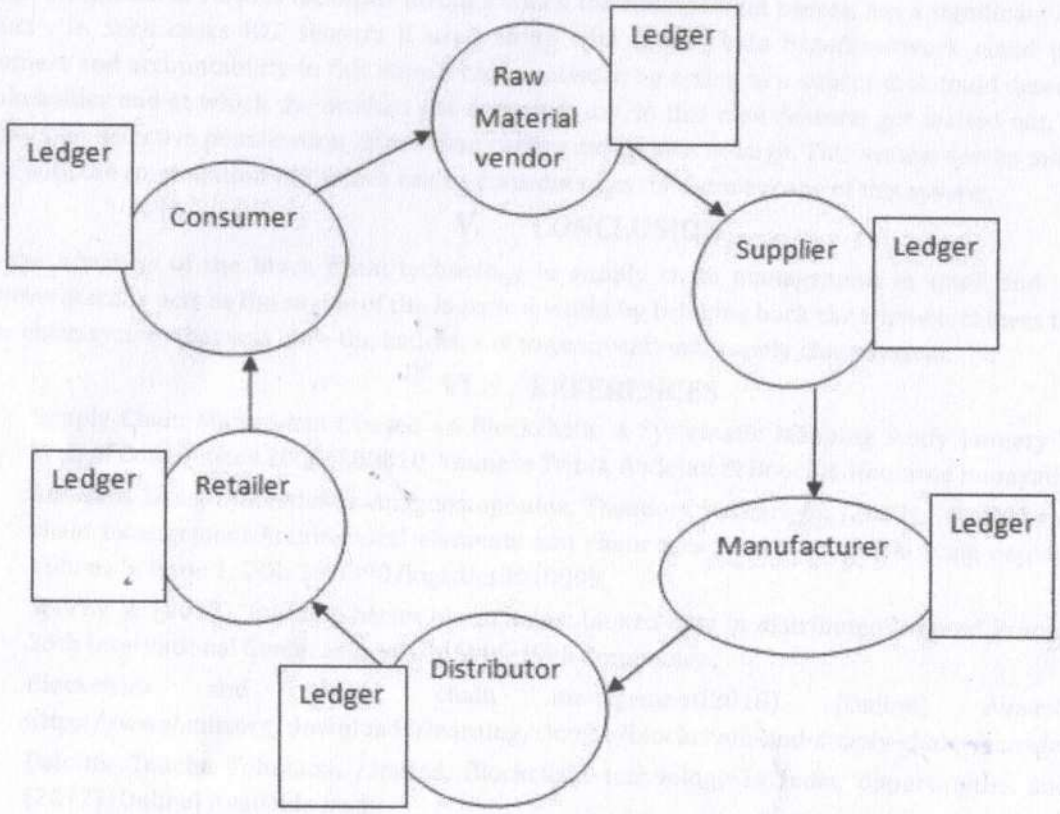


Figure:3 Supply Chain Cycle in a Small and Medium scale Industry

IV. RESULTS AND DISCUSSION

The block chain based supply management system when used and implemented properly could be the greatest game changer in the logistical arena where commodities are transported across far off geographical locations. This can be understood from the table below that shows the comparison of conventional and block chain based supply chain system.

Table 1. Comparison of conventional and block chain based supply chain system.

S.no	Factors	Block chain based supply chain	Conventional supply chain
1	Implementation Cost	High	Less
2	Ease of use	High	Less
3	Efficiency	High	Very less
4	Longevity	High	Less
5	Reliability	High	Very less
6	Operational cost	Less	High
7	Maintenance cost	Less	High

Going by the comparison as listed in Table 1. it can very well be inferred that block chain based system can bring in a revolutionary change in the way the supply chain management is carried out in small and medium scale industries. Except for the initial implementation cost that is comparatively bit high due to the cost associated with configuring a distributed system network which are autonomous in all respects, all the other factors are highly positive with the adoption of block chain based system. Once the block chain system is deployed the costs associated with transaction, maintenance etc. are comparatively less.

Considering a scenario where in the products that are being commuted as part of supply chain network are desserts/frozen desserts, the probability of the product getting melted out in transit are very high as the climatic conditions of various locations through which the consignment passes, has a significant effect over the product . In such cases IOT sensors if used along with block chain based network could provide added robustness and accountability to this supply chain network by acting as a source that could detect the location of stakeholder end at which the product got damaged, say, in this case desserts got melted out. Thus opening the doors for selective penalization rather than casting aspersions at large. This system can be made even more robust with the combination IOT which can be considered as the future scope of this system.

V. CONCLUSION

Thus the adoption of the block chain technology in supply chain management in small and medium scale industries literally acts as the savior of the logistical world by bringing back the trustworthiness to the modern supply chain system that was once the hallmark of the conventional supply chain system.

VI. REFERENCES

[1] Supply Chain Management based on Blockchain: A Systematic Mapping Study January 2018 MATEC Web of Conferences 200(2):00020, Youness Tribis, Abdelali El Bouchti, Houssine Bouayad.

[2] Antonios Litke, Dimosthenis Anagnostopoulos, Theodora Varvarigou (2019), "Blockchains for supply chain management:Architectural elements and challenges towards a global scale deployment, *MDPI*, Volume 3, Issue 1, DOI: 10.3390/logistics3010005.

[3] Sporny M. (2017),"Building better blockchains: Linked data in distributed ledgers",Proceedings of the 26th International Conference World Wide Web Companion.

[4] Blockchain and supply chain management(2018) [Online] Available from: https://www.mhi.org/downloads/learning/cicmhe/blockchain-and-supply-chain-management.pdf

[5] Deloitte Touche Tohmatsu Limited, Blockchain technology in India, opportunities and challenges (2017) [Online] Available from:

[6] https://www2.deloitte.com/content/dam/Deloitte/in/Documents/strategy/in-strategy-innovation-blockchain-technology-india-opportunities-challenges-noexp.pdf

[7] Diabat, A., Kannan, D., & Mathiyazhagan, K. (2014). Analysis of enablers for implementation of sustainable supply chain management–A textile case. Journal of Cleaner Production, 83, 391–403.

[8] Gopalakrishnan, K., Yusuf, Y. Y., Musa, A., Abubakar, T., & Ambursa, H. M. (2012). Sustainable supply chain management: A case study of British Aerospace (BAe) systems. International Journal of Production Economics, 140(1), 193–203.

IJE TRANSACTIONS A: Basics Vol. 33, No. 10, (October 2020) 1897-1903

International Journal of Engineering

Journal Homepage: www.ije.ir

Influence of Fiber on Shear Behavior of Concrete Exposed to Elevated Temperature

A. Varghese, N. Anand*, P. G. Arulraj

Department of Civil Engineering, Karunya Institute of Technology and Sciences (KITS), Coimbatore, India

PAPER INFO

Paper history:
Received 07 April 2020
Received in revised form 03 July 2020
Accepted 04 August 2020

Keywords:
Elevated Temperature
Fiber Reinforced Concrete
Shear Strength
Spalling

ABSTRACT

Fire accidents are inevitable and it is one of the significant hazards, which causes loss of life and valuables. The present investigation focused to study the influence of fibers on shear strength of concrete exposed to elevated temperature as per ISO 834. The fibers used in the study were Basalt, Carbon, Glass, Polypropylene and Poly vinyl alcohol. M20, M30, M40 and M50 grades of concrete were used for the investigation. The results revealed that the shear strength is declined with increase in temperature. The shear strength is enhanced by the addition of fiber in the reinforced concrete beams exposed to elevated temperature. Carbon fiber reinforced concrete specimens exhibited better residual shear strength than the other specimens. Addition of carbon fiber and basalt fiber in concrete reduced the micro cracks in the specimens exposed to elevated temperature. Addition of polypropylene fiber and poly vinyl alcohol fiber reduced the spalling but the crack propagation was not prevented in the specimens exposed to high temperatures.

***doi**: 10.5829/ije.2020.33.10a.08*

NOMENCLATURE

T	Furnace temperature at time t	PVAFRC	Poly vinyl alcohol FRC
T_0	Initial furnace temperature	t	Duration heat exposure (min)
°C/t	Rate of heating	°C/min.	Degree celcius per minute
°C/hr	Degree celcius per hour	RC	Reinforced Concrete
CC	Control Concrete (without fiber)	E	Young's modulus (GPa)
FRC	Fiber Reinforced Concrete	L	Length (mm)
CFRC	Carbon FRC	T_m	Melting point (°C)
BFRC	Basalt FRC	Vol/%	Dosage of fiber (%)
GFRC	Glass FRC	P	Load
PPFRC	Polypropelne FRC	ϕ	Diameter (mm)

1. INTRODUCTION

Fiber Reinforced Concrete (FRC) is known for many property enhancements in conventional concrete. There are numerous studies carried out during last three decades to overcome the weak tensile behavior of concrete. The performance of concrete is always associated with its compressive strength and tensile strength. These two properties are much important that decides the characteristics of concrete. The fibers added in concrete helps to reduce the brittleness of the concrete by bridging the micro cracks and thus prevented the macro crack development [1]. Only limited studies have been carried out on the effects of elevated temperature on the shear strength of FRC. Majority of the investigations focused on the effect of steel fibers and PolyPropylene Fiber (PPF) on the shear strength of the concrete. Considering FRC in terms of fire resistance, some tests have been conducted to identify the effect of fibers in resisting the fire related damages that occurs in concrete structures [1, 2]. Mainly, these are emphasized on the effect of fibers on the basis of its shape, type and the percentage of addition (quantity) on the strength parameters of concrete. Commonly the experiments are carried out in

*Corresponding Author E-mail: *davids1612@gmail.com* (N. Anand)

Please cite this article as: A. Varghese, N. Anand, P. G. Arulraj, Influence of Fiber on Shear Behavior of Concrete Exposed to Elevated Temperature, International Journal of Engineering (IJE), IJE TRANSACTIONS A: Basics Vol. 33, No. 10, (October 2020) 1897-1903

terms of compressive strength, tensile strength and modulus of elasticity [1–5]. Widely used fibers in the concrete industry are synthetic fibers such as PPF and Poly Vinyl Alcohol Fiber (PVAF), Steel Fibers (SF), and hybrid of SF and PPF. There are also a few examinations, which tested concrete with Carbon Fibers (CF), and Glass Fibers (GF) [4, 5].

Kurup and Senthil-Kumar [6] found that addition of PVC fibers improved the ductility behavior of concrete and reduced the brittle failure of concrete. Shear strength values were reduced in the case of fiber reinforced concrete with respect to the addition of PVC fibers and silica fibers (0.6 to 1%) [6]. Bae et al. [7] concluded that, an increase in shear strength according to inclusion of steel fiber was more effective than the four times volume fraction of shear reinforcement. Based on experimental results of the study conducted by Abdi Moghadam and Izadifard [8] it is found that although the inclusion of steel fibers decreased the compressive strength, it has improved the shear strength of plain concrete at 28 days of curing. Smith et al. [9] experimentally investigated the shear strength of fire affected (622°C) beam specimens. The rate of heating was 10°C/min. It was found that 30% reduction in shear strength occurred. Cai et al. [10] studied the residual shear strength of concrete beam specimens after exposure to ISO 834 time temperature curve and the reduction in shear strength was found. For the exposure time of 30 min., 60 min. and 90 min the shear strength reductions were 15, 23 and 26%, respectively. Yusuf [11] examined the residual shear strength of concrete push off specimens after exposure to 200°C, 350°C and 500°C with a rate of 17°C/h. heating. The residual strengths after the specimens exposure to 200°C, 350°C and 500°C, were 26%, 41% and 66%, respectively. Concrete with PP fibers showed the negative performance on improving the mechanical properties beyond the critical temperature (more than 500°C). It was due to the loss of bond between the fiber and cement matrix. It may be due to the development extra pores during melting of PPF [12–14]. Information are limited on the effect of fibers on shear strength of concrete exposed to elevated temperature.

The shear strength is a significant property, which enables concrete to withstand against the fatigue forces. It is considerably less than the compressive strength, because the micro cracks developed in concrete can spread and widen under bending loads. When exposed to fire, bending strength of concrete is reduced due to the spalling that occurs within concrete elements [15–17].

Information on the residual shear strength of FRC with CF, Basalt Fiber (BF), GF, PPF and PVAF exposed to standard fire curve (ISO 834) was found to be missing in the literature. Effect of elevated temperature on FRC with different strength grades are to be evaluated. Hence, it is necessary to understand the influence of different types of fibers on the strength and surface defects of concrete when exposed to elevated temperature. An attempt has been made to study the key factors such as type of fibers, grade of concrete and intensity of temperature, which affect the residual shear properties of concrete.

This paper investigates the shear response of FRC exposed to elevated temperature. The fibers used in the study are BF, CF, GF, PPF and PVAF. The study was conducted in M20, M30, M40 and M50 grades of concrete. Residual shear capacity of different grades of concrete with different fibers are presented in this work.

The main objective of the investigation is to examine the influence of fibers on the shear strength of concrete after exposure to elevated temperature.

2. EXPERIMENTAL INVESTIGATION

2. 1. Materials The ordinary Portland cement of grade 53 conforming to IS: 12269–2013 and Manufactured sand (M-sand) as fine aggregate (Zone II) as per IS: 383:2016 were used. Crushed granite stones of size 20mm confirming to IS 383:2016 were used as coarse aggregate. The quality of water was found to satisfy the requirements of IS 456:2000. Considering the properties of materials, the mix proportion of concrete was designed as per IS 10262:2019. A water reducing agent Master Glenium SKY 8233 was used to control the workability (slump cone test) of all concrete mixtures. The water reducing agent maintained the workability of the mix in between 75 and 100mm even after the addition of fibers into the mix without affecting the water cement ratio. Fe 500 steel bars were used as reinforcement. Table 1 shows the details of fibers.

2. 2. Preparation of Specimens and Test Procedure Singly reinforced FRC beams were cast and used for testing the shear behavior after exposure to elevated temperature. 700 x 150 x 150mm size beams were used for the investigation considering the limitation of the furnace size. Two numbers of 6mm diameter bars were used at top and bottom of the specimens. In order to ensure shear failure, two legged 6mm diameter stirrups are provided at supports and loading points only to hold the main bars (Figure 1). With respect to the proposed

TABLE 1. Details of fibers

Fibers	L (mm)	E (GPa)	σt (MPa)	T_m (°C)	Vol/%
PPF	12	165	317	165	0.25
PVA	12	220	396	220	0.25
GF	12	77	2050	1500	0.25
BF	12	100	3100	1400	0.25
CF	12	240	3500	1200	0.25

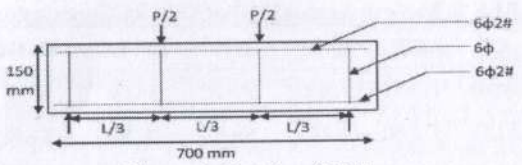


Figure 1. Details of RC beam

beam size molds were made with cast iron. The two-point loading arrangement was adopted from IS 516:1959.

After 24 hours of casting, the sides of the formwork were removed and the specimens were cured in water for 28 days. After curing, specimens were dried and heated following stranded fire curve.

A computer controlled electrical furnace with inner dimensions of 700 × 400 × 400 mm having the capacity power of 100kW was used to heat the specimens (Figure 2). The maximum operating temperature of the furnace is 1200°C, with a capability to set the standard fire temperature curve (Equation (1)). Type K thermocouples connected to a microprocessor based data acquisition unit were used to monitor the temperature inside the furnace.

$$T - T_0 = 345 \log_{10}(8t + 1) \quad (1)$$

Concrete specimens were exposed to heating durations of 30 min (821°C), 60 min (925°C) and 90 min (986°C) as per standard fire curve (Figure 3) following ISO 834. Heated specimens were cooled in ambient condition before the test. The furnace temperature of the heated specimens and its surface cooling rate are shown in Figure 3. The investigation was carried out for different grades of concrete such as M20, M30, M40 and M50. After cooling in air, the shear resistance of Reinforced Concrete (RC) beams were tested using a computerized Universal Testing Machine (UTM) of capacity 1000 kN. Two-point load was applied with appropriate test setup to ensure constant shear in the specimens. The loading gauge was connected with the digital testing machine that records the failure load of the specimens. After curing, cube specimens were exposed to 90 minutes of elevated temperature (986°C) to observe the surface defects. Figure 4 shows the methodology adopted.

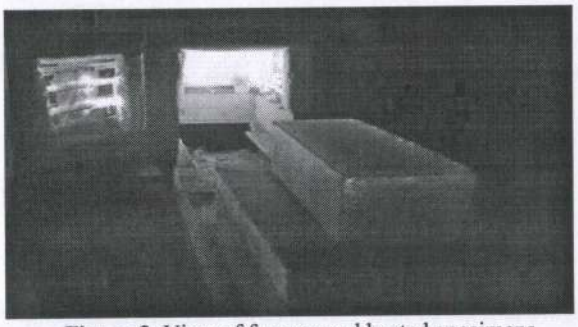


Figure 2. View of furnace and heated specimens

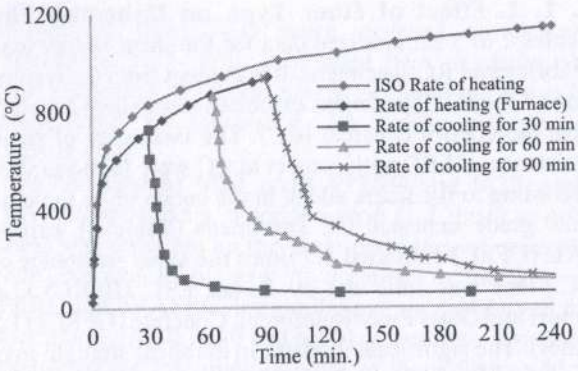


Figure 3. Heating and cooling regime of specimen

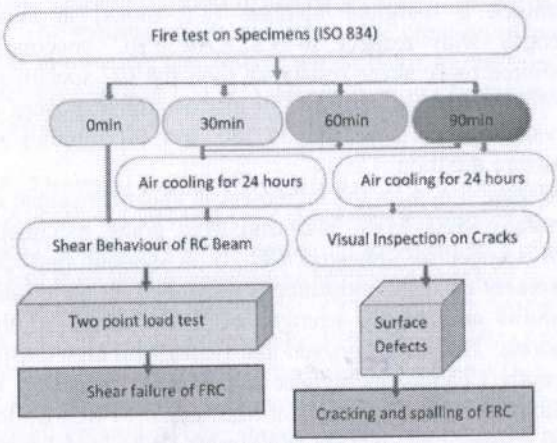


Figure 4. Methodology

3. RESULTS AND DISCUSSION

3. 1. Shear Strength During loading, shear failure was observed in the beam specimens and it is confirmed by the diagonal cracks developed near the support (Figure 5). The ultimate load was delayed according to the type of fibers added in the concrete specimens. For the RC specimens exposed to elevated temperature, the shear resistance decreased with the increase in the duration of elevated temperature.

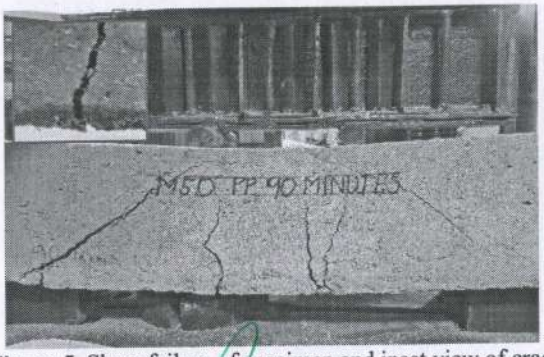


Figure 5. Shear failure of specimen and inset view of crack

3. 1. 1. Effect of Fiber Type on Unheated FRC Tables 2 to 5 summarized data for the shear failure load of different FRC specimens. It is evident from the results, that all the FRC specimens exhibited more shear capacity than the control concrete (CC). The increment of shear resistance of FRC with respect to CC were found to vary according to the fibers added in the concrete. In the case M20 grade unheated CC specimens (Table 2), carbon FRC (CFRC) exhibited 1.7 times the shear resistance of CC. This was followed by Basalt FRC (BFRC) (1.6 times) and Glass Fiber Reinforced Concrete (GFRC) (1.5 times). The significant increase in the shear strength may be due to the high tensile load carrying capacity (Table 1) of CF, BF and GF [18]. Poly Vinyl Alcohol FRC (PVAFRC) and Polypropylene FRC (PPFRC) specimens exhibited a marginal increase (1.2 times) in shear strength with respect to CC. All FRC specimens exhibited more shear resistance than the CC specimens for M20, M30, M40 and M50 grades after exposure to elevated temperature for 30, 60 and 90 minutes of exposure duration.

Figure 6 depicts the increment in shear resistance of unheated M20, M30, M40 and M50 grade specimens with respect to unheated CC. It is evident that the increment of shear resistance is depended on the elastic modulus and tensile strength of fibers added in the concrete. The results proved that fibers with high tensile strength (CF) has the highest ratio of shear resistance in an unheated condition (1.7 for M20 grade CFRC, 1.5 for M30 grade CFRC, 1.7 for M40 grade CFRC and 1.6 for M50 grade CFRC). This was followed by BFRC, GFRC, PVAFRC and PPFRC specimens that have a lower shear strength (Tables 2-5).

3. 1. 2. Contribution of Fibers in Concrete Exposure to High Temperatures Figures 7 - 10 show the comparison of the shear resistance of M20 (Figure 7), M30 (Figure 8), M40 (Figure 9) and M50 (Figure 10) grade heated FRC specimens with respect to the heated M20 grade CC, M30 grade CC, M40 grade CC and M50 grade CC specimens. This was calculated by taking the ratio of shear resistance of any specimen with the shear resistance of control concrete (CC) of a same grade exposed to same elevated temperature. It can be seen from the figures that, M20 grade CFRC, M30 grade CFRC, M40 grade CFRC and M50 grade CFRC exhibited the maximum shear resistance when exposed to elevated temperature for durations of 30, 60 and 90 minutes. These figures clearly indicate the contribution of fibers in improving the shear resistance of FRC exposed to higher temperature. The fibers in the heated M20 grade CFRC specimens exhibited almost similar contribution in the shear resistance (1.8 times) even after exposed to 30, 60 and 90 minutes. Similar phenomenon was visible on shear resistance of M30 grade CFRC, M40 grade CFRC and M50 grade CFRC specimens.

TABLE 2. Shear resistance (kN) of M20 RCC specimens

t	CC	CFRC	BFRC	GFRC	PPFRC	PVAFRC
00	70.09	116.11	110.82	105.08	84.60	85.08
30	62.57	112.60	97.67	89.92	80.87	81.53
60	51.33	92.69	78.84	71.78	62.52	62.98
90	46.04	81.52	69.91	56.06	48.88	49.10

TABLE 3. Shear resistance (kN) of M30 RCC specimens

t	CC	CFRC	BFRC	GFRC	PPFRC	PVAFRC
00	84.58	125.45	120.33	108.82	92.35	94.69
30	72.54	120.12	110.65	95.45	82.95	82.10
60	60.29	98.85	88.24	76.54	63.00	64.10
90	51.50	83.71	73.69	59.21	52.45	52.12

TABLE 4. Shear resistance (kN) of M40 RCC specimens

t	CC	CFRC	BFRC	GFRC	PPFRC	PVAFRC
0	101.5	170.52	161.60	155.68	146.25	147.55
30	86.54	152.37	138.21	120.43	109.54	109.99
60	70.54	122.16	111.05	83.58	82.37	83.02
90	55.00	94.35	85.75	61.58	57.15	57.90

TABLE 5. Shear resistance (kN) of M50 RCC specimens

t	CC	CFRC	BFRC	GFRC	PPFRC	PVAFRC
0	119.6	192.54	175.55	167.55	155.57	156.83
30	94.57	163.55	150.54	136.13	129.54	130.02
60	81.07	135.25	128.46	101.25	90.68	92.51
90	66.00	108.55	102.55	72.46	68.25	69.55

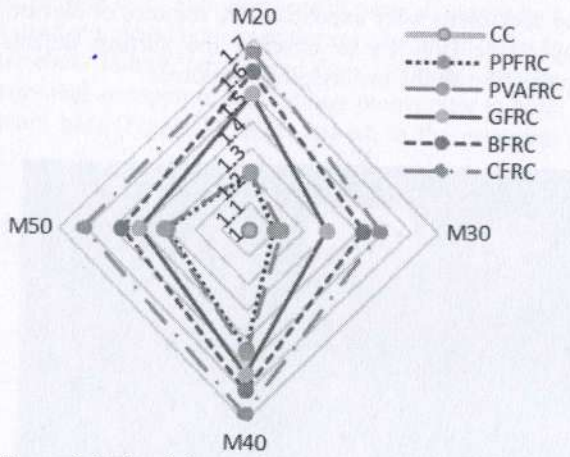


Figure 6. Ratio of shear resistance for unheated specimens

The shear resistance of M20 grade BFRC specimens were found to be 1.5 times that of the M20 grade CC specimens at elevated temperature conditions (30, 60 and 90 minutes). In addition, M30 grade BFRC (1.5 times), M40 grade BFRC (1.6 times) and M50 grade BFRC (1.6 times) exhibited similar behavior in the case of temperature exposed conditions. There was a sudden drop in the shear resistance of M20 grade GFRC specimens (1.4 times to 1.2 times) when exposed to 90 minutes of elevated temperature. M30 grade GFRC, M40 grade GFRC and M50 grade GFRC also exhibited a similar pattern. It may be due to the loss in tensile strength of glass fiber when exposed to elevated temperature [19]. With prolonged heat exposure, the shear resistance of the specimens declined but it can be strengthened by increasing the tensile strength of concrete [10].

In the case of M20 grade PPFRC and M20 grade PVAFRC specimens, a sudden drop (1.2 times to 1.06 times) was observed on the shear resistance of concrete, when exposed to 60 and 90 minutes. In the case of PPFRC and PVAFRC, the similar pattern is observed for other grades (M30, M40 and M50) of concrete. It may be because of the low melting point of these fibers which causes melting of fibers inside the specimens when exposed to elevated temperatures. This reduced the tensile strength of fibers in heated specimen compared to CC. The melting of fibers leads to the creation of pore holes in concrete specimens, which helps to reduce the crack propagation [20, 21]. Hence it shows better shear resistance capacity (1.1-1.2 times) than CC.

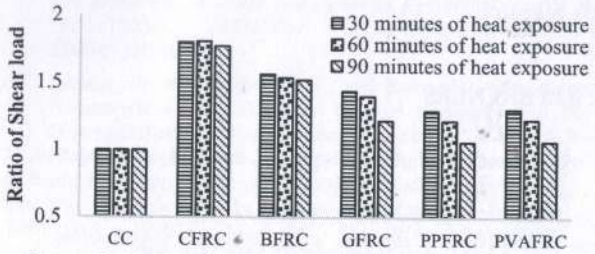


Figure 7. Shear resistance of M20 heated FRC specimens

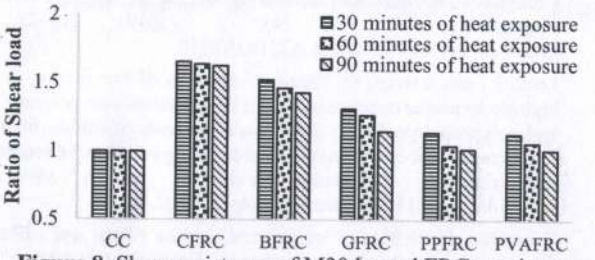


Figure 8. Shear resistance of M30 heated FRC specimens

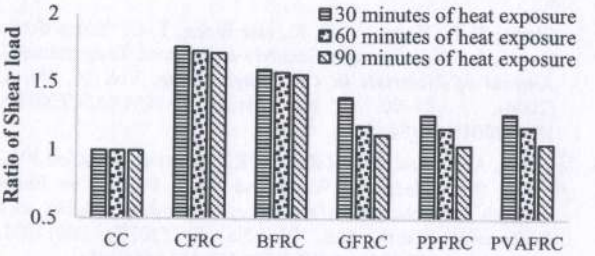


Figure 9. Shear resistance of M40 heated FRC specimens

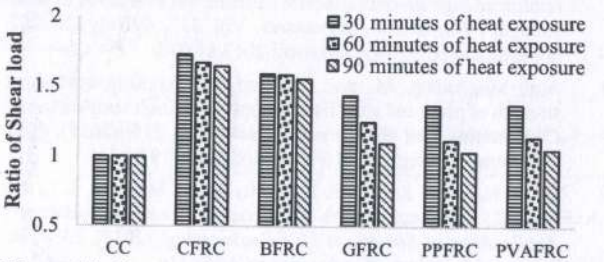


Figure 10. Shear resistance of M50 heated FRC Specimens

3. 2. Thermal Crack Formation

Figure 11 (11A, 11B, 11C, 11D, 11E, 11F) shows the surface view of M20 grade specimens heated up to 90 minutes. It is evident from the figures that the M20 grade CC had more surface pitting than the BFRC, CFRC, GFRC, PPFRC and PVAFRC specimens. For PPFRC and PVAFRC specimens, only surface pitting was observed. This is because of reduction in pore pressure through pore channel created when these specimens exposed to elevated temperature [20] GFRC, BFRC and CFRC specimens had less thermal cracks than CC. It may be due to the bridging effect of high melting point fibers (GF, BF and CF) [22]. The GFRC have small amount of progressive cracks. This is because of the reduction in the tensile capacity of GF, when it is exposed to elevated temperature [19]. Hence reduction in bridging effect between cement matrixes occurs.

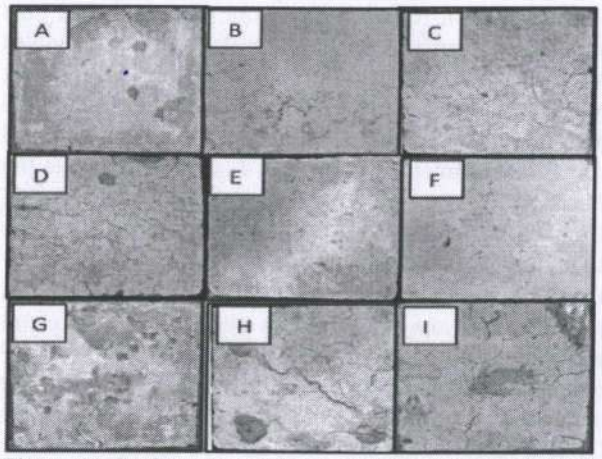


Figure 11. Surface view of specimens: A. M20 CC, B. M20 PPFRC, C. M20 PVAFRC, D. M20 GFRC, E. M20 BFRC, F. M20 CFRC, G. M30 CC, H. M40 CC and I. M50 CC

Also Figure 11 (11A, 11G, 11H, 11I) shows the surface view of the M20 grade CC, M30 grade CC, M40 grade CC and M50 grade CC specimens after being exposed to 90 minutes of heat exposure. From the visual inspection, it is identified that M50 grade CC has the maximum surface damage when compared to M20 grade CC specimens. This may be due to the high density of concrete (M50 grade CC) with less porosity [2]. When the specimens were exposed to elevated temperature, the pore pressure developed within the concrete is high in higher-grade concrete and this induced more surface cracks.

4. CONCLUSIONS

FRC specimens were exposed to elevated temperature up to 90 minutes' duration of heating following the standard fire curve. Shear resistance of FRCs were analyzed before and after heating. The higher grade concrete (M50) is found to retain high shear strength. Addition of fibers improved the shear strength of concrete. The effect of fibers on concrete in terms of shear strength and crack control after being exposed to elevated temperature are concluded below:

- The concrete specimens with CF show better residual shear strength in all grades and at different temperature levels. For 90 minutes of heat exposure, CFRC retained 116 and 91% shear strength of the unheated CC specimen for M20 grade and M50 grade, respectively.
- Concrete specimen with BF (99 - 86%) and GF (80 - 61%) also exhibited high shear strength after exposure to 90 minutes of elevated temperature but the shear strength was found to be lower than that of concrete specimens with CF.
- The residual shear strength of the PPFRC and PVAFRC specimens after exposure to 30 minutes, were found to be 115% (M20) - 108% (M50) and 116% (M20) - 109% (M50), respectively. From 60 minutes of heat exposure onwards, residual shear strength was found to be decreasing. In addition, at 90 minutes of heat exposure, PPFRC and PVAFRC specimens exhibited marginal increment in shear strength than control concrete specimen. It is proved that fibers improve the shear resistance of concrete exposed to elevated temperature. Also addition of fibers prevented the spalling of concrete specimens.
- The concrete specimens with CF and BF were found to have minimum micro cracks even after exposure to elevated temperature. Addition of PPF and PVAF reduced the spalling but the crack propagation could not be prevented at high temperatures. The specimens with GF had more cracks and more surface damage after the exposure. Concrete with higher strength grade (M50) had high rate of crack propagation.

The results of the research are applicable for RC beams exposed to standard fire following ISO 834 fire curve. In case of external fire curve, the behavior of fiber reinforced concrete may change. In addition, there is a scope to compare the performance of different FRC with the corresponding optimum volume fraction of fibers.

5. ACKNOWLEDGEMENT

The authors wish to acknowledge the Science and Engineering Research Board, Department of Science and Technology of the Indian Government for the financial support (YSS/2015/001196) provided for carrying out this research.

6. REFERENCES

1. Varghese, A., N, A., Arulraj G, P., and Johnson Alengaram, U. "Influence of fibers on bond strength of concrete exposed to elevated temperature." ***Journal of Adhesion Science and Technology***, Vol. 33, No. 14, (2019), 1521–1543. https://doi.org/10.1080/01694243.2019.1602889
2. Alwyn Varghese, M Agrima, M Balakrishnan, C Greeshma, and P S Krishnapriya. "Pure Shear Strength of PVA Fiber Reinforced Concrete." ***International Journal of Recent Technology and Engineering***, Vol. 8, No. 2, (2019), 217–221. https://doi.org/10.35940/ijrte.A2218.078219
3. Lura, P., and Terrasi, G. Pietro. "Reduction of fire spalling in high-performance concrete by means of superabsorbent polymers and polypropylene fibers: Small scale fire tests of carbon fiber reinforced plastic-prestressed self-compacting concrete." ***Cement and Concrete Composites***, Vol. 49, (2014), 36–42. https://doi.org/10.1016/j.cemconcomp.2014.02.001
4. Tanyildizi, H. "Effect of temperature, carbon fibers, and silica fume on the mechanical properties of lightweight concretes." ***Xinxing Tan Cailiao/ New Carbon Materials***, Vol. 23, No. 4, (2008), 339–344. https://doi.org/10.1016/s1872-5805(09)60005-6
5. Cheng, F.-P., Kodur, V. K. R., and Wang, T.-C. "Stress-Strain Curves for High Strength Concrete at Elevated Temperatures." ***Journal of Materials in Civil Engineering***, Vol. 16, No. 1, (2004), 84–90. https://doi.org/10.1061/(ASCE)0899-1561(2004)16:1(84)
6. Kurup, A. R., and Senthil Kumar, K. "Effect of Recycled PVC Fibers from Electronic Waste and Silica Powder on Shear Strength of Concrete." ***Journal of Hazardous, Toxic, and Radioactive Waste***, Vol. 21, No. 3, (2017), 06017001. https://doi.org/10.1061/(ASCE)HZ.2153-5515.0000354
7. Bae, B. Il, Chung, J. H., Choi, H. K., Jung, H. S., and Choi, C. S. "Experimental study on the cyclic behavior of steel fiber reinforced high strength concrete columns and evaluation of shear strength." ***Engineering Structures***, Vol. 157, (2018), 250–267. https://doi.org/10.1016/j.engstruct.2017.11.072
8. Abdi Moghadam, M., and Izadifard, R. "Evaluation of shear strength of plain and steel fibrous concrete at high temperatures." ***Construction and Building Materials***, Vol. 215, (2019), 207–216. https://doi.org/10.1016/j.conbuildmat.2019.04.136
9. Smith, H. K. M., Reid, E. R. E., Beatty, A. A., Stratford, T. J., and Bisby, L. A. "Shear strength of concrete at elevated temperature." ***Applications of Structural Fire Engineering***, (2011), 133–138. Retrieved from http://fire.fsv.cvut.cz/ASFE11/

10. Cai, B., Xu, L. F., and Fu, F. "Shear Resistance Prediction of Post-fire Reinforced Concrete Beams Using Artificial Neural Network." ***International Journal of Concrete Structures and Materials***, Vol. 13, No. 1, (2019), 1–13. https://doi.org/10.1186/s40069-019-0358-8
11. Yusuf, M. A. Shear Transfer Strength of Concrete After Exposure to Elevated Temperature, Master's Thesis, Queen's University, Canada. Retrieved from https://www.researchgate.net/publication/335795861
12. Li, H., and Liu, G. "Tensile Properties of Hybrid Fiber-Reinforced Reactive Powder Concrete After Exposure to Elevated Temperatures." ***International Journal of Concrete Structures and Materials***, Vol. 10, No. 1, (2016), 29–37. https://doi.org/10.1007/s40069-016-0125-z
13. Kalifa, P., Chéné, G., and Gallé, C. "High-temperature behaviour of HPC with polypropylene fibres - From spalling to microstructure." ***Cement and Concrete Research***, Vol. 31, No. 10, (2001), 1487–1499. https://doi.org/10.1016/S0008-8846(01)00596-8
14. Irshidat, M. R., Al-Nuaimi, N., and Rabie, M. "The Role of Polypropylene Microfibers in Thermal Properties and Post-Heating Behavior of Cementitious Composites." ***Materials***, Vol. 13, No. 2676, (2020), 1–18. https://doi.org/10.3390/ma13122676
15. Ding, Y., Zhang, Y., and Thomas, A. "The investigation on strength and flexural toughness of fibre cocktail reinforced self-compacting high performance concrete." ***Construction and Building Materials***, Vol. 23, No. 1, (2009), 448–452. https://doi.org/10.1016/j.conbuildmat.2007.11.006
16. Ding, Y., Azevedo, C., Aguiar, J. B., and Jalali, S. "Study on residual behaviour and flexural toughness of fibre cocktail reinforced self compacting high performance concrete after exposure to high temperature." ***Construction and Building Materials***, Vol. 26, No. 1, (2012), 21–31. https://doi.org/10.1016/j.conbuildmat.2011.04.058
17. Li, M., Qian, C. X., and Sun, W. "Mechanical properties of high-strength concrete after fire." ***Cement and Concrete Research***, Vol. 34, No. 6, (2004), 1001–1005. https://doi.org/10.1016/j.cemconres.2003.11.007
18. Mészöly, T., and Randl, N. "Shear behavior of fiber-reinforced ultra-high performance concrete beams." ***Engineering Structures***, Vol. 168, (2018), 119–127. https://doi.org/10.1016/j.engstruct.2018.04.075
19. Terro, M. J. "Properties of concrete made with recycled crushed glass at elevated temperatures." ***Building and Environment***, Vol. 41, No. 5, (2006), 633–639. https://doi.org/10.1016/j.buildenv.2005.02.018
20. Soleimanzadeh, S., and Mydin, M. A. O. "Influence of High Temperatures on Flexural Strength of Foamed Concrete Containing Fly Ash and Polypropylene Fiber." ***International Journal of Engineering - Transactions B: Applications***, Vol. 26, No. 2, (2013), 117–126. https://doi.org/10.5829/idosi.ije.2013.26.02b.02
21. Hafiz, T. A. "Life prediction of carbon fiber reinforced polymers using time temperature shift factor." ***International Journal of Engineering - Transactions A: Basics***, Vol. 33, No. 7, (2020), 1340–1346. https://doi.org/10.5829/ije.2020.33.07a.21
22. Li, W., and Xu, J. "Mechanical properties of basalt fiber reinforced geopolymeric concrete under impact loading." ***Materials Science and Engineering A***, Vol. 505, No. 1–2, (2009), 178–186. https://doi.org/10.1016/j.msea.2008.11.063

Persian Abstract

چکیده

سوانح آتش سوزی اجتناب ناپذیر است و یکی از مهمترین خطراتی است که باعث از بین رفتن جان و اشیاء با ارزش می شود. تحقیق حاضر به بررسی تأثیر الیاف بر استحکام برشی بتن در معرض دمای بالا طبق استاندارد ISO 834 پرداخته است. الیاف مورد استفاده در این تحقیق شامل بازالت ، کربن ، شیشه ، پلی پروپیلن و پلی وینیل الکل بودند. بتن از M20، M30، M40 و M50 استفاده شد. نتایج نشان داد که با افزایش دما مقاومت برشی کاهش یافته است. استحکام برشی با افزودن الیاف در تیرهای بتن مسلح که در معرض دمای بالا است افزایش می یابد. نمونه های بتن مسلح با فیبر کربن نسبت به سایر نمونه ها مقاومت برشی باقیمانده بهتری نشان دادند. افزودن الیاف کربن و بازالت در بتن باعث کاهش ریزگردها در نمونه های در معرض دمای بالا می شود. افزودن الیاف پلی پروپیلن و پلی وینیل الکل باعث کاهش فاصله می شود اما از انتشار ترک در نمونه هایی که در معرض دمای بالا قرار دارند ممانعت نخواهد کرد.

The Institution of Engineers (India)

Established 1920, Incorporated by Royal Charter 1935

Celebrating Centenary Year in 2020

35th Indian Engineering Congress

December 18-20, 2020

Certificate of Paper Presentation

This is to certify that

Aneesh K, Manoj G

Karunya Institute of Technology and Sciences
Coimbatore, Tamilnadu

have participated in the 35th Indian Engineering Congress held during 18-20 December 2020 and presented the paper titled **'Low Power ADC Design for Biomedical Implantable Devices'** in virtual mode.

Dr H R P Yadav, FIE
Secretary and Director General-I/C

This is an approved CPD programme of The Institution of Engineers (India)

Er Narendra Singh, FIE
President

The Institution of Engineers (India)

35th Indian Engineering Congress

President

Er Narendra Singh

Chairman, Technical Committee

Prof Swapan Bhaumik

Secretary & Director General-I/C

Dr H R P Yadav

Editorial Team

Technical Department, IEI

Dr N Sengupta, Dr S Ghosh, Mr K Sen, Mr T Chakraborty, Ms A Dutta,
Ms H Roy, Mr S Bagchi, Mr P Chakraborty, Ms P Nath, Mr P Mukhpadhyay, Mr S Misra

The Institution of Engineers (India)

35th Indian Engineering Congress

President

Er Narendra Singh

Chairman, Technical Committee

Prof Swapan Bhaumik

Secretary & Director General-I/C

Dr H R P Yadav

Editorial Team

Technical Department, IEI

Dr N Sengupta, Dr S Ghosh, Mr K Sen, Mr T Chakraborty, Ms A Dutta,
Ms H Roy, Mr S Bagchi, Mr P Chakraborty, Ms P Nath, Mr P Mukhpadhyay, Mr S Misra

Contents

Agricultural Engineering

AG/087/01	Optimization of the Growth of Microalgae Sprulina Platensis - Full Factorial Experimental Approach *Mir Shariful Islaml, Bidyut Baran Saha*	23
AG/088/02	Timer Based Automatic Family Drip System (FDS) - A Sustainable Technology for Increased Vegetable Production in Urban Sector *Chithra G, Jyothi Rachel Varghese, Dr Binu John Sam*	33
AG_105_04	Experimental Investigation of Double Collector Solar Dryer for Agricultural Products *G S Divya Laxmi1, D Sakthivadivel, P Ganesh Kumar, S Iniyan*	39
AG_106_05	Performance Study of Manually Operated Drum Seeder for Sowing of Jute *R K Naik, S K Jha, S Sarkar, A K Ghorai*	45
AG_125_06	Development of Track Width and Ground Clearance Enhancing Platform and Matching Implements for Low Horse Power Tractor *B Sanjeeva Reddy, Ashish S Dhimate, I Srinivas, R V Adake, V R Mallikarjuna, G Karthik*	51
AG_176_07	IoT Based Smart Agriculture Monitoring System *G Roja, M Ramesh*	59
AG_208_08	Design of Multipurpose Harvesting Machine for Lowland Areas for The Upliftment of Farmers *Niloy Laskar, Umar Faruk Bhuiya, Krishna Chakraborty, Dr Arindam Majumder*	65

Architectural Engineering

AR_089_01	Fractal Geometry as an Adaptive Technique for Human Capital Development: A Review based on Indian Temple Architecture *Shynu R V*	75
AR_090_02	2BHK Dignity Housing Programme in Greater Hyderabad Municipal Corporation *K Suresh Kumar, P Saroja Rani, B Venkateshwarlu, K Varalakshmi*	81
AR_181_03	Advanced Tool for Green and Energy Efficient Building Design *Ankur Mittal, Ashutosh Saxena, B N Mohapatra*	87

Aerospace Engineering

AS_014_01	Transformation of Rectangular Parallelepipeds into Fighter Jets & Airborne Missile Launching Platforms *Rajarshi Mukherjee*	95
AS_103_02	Activating Atmospheric Boundary Condition Inside the Subsonic Wind Tunnel using Passive Turbulence Grid *E Livya, S Nadaraja Pillai*	99
AS_126_03	Aerodynamic Characteristics of Grooved Rotating Circular Cylinder *Kirthika N, MadhuMadhan, Lokesh U, S Nadaraja Pillai*	105
AS_127_04	Optimum Satellite Access Techniques "TDMA / SCPC or PSMA" For Next Generation VSAT Networks *Y S Rayudu*	113
AS_229_05	Electromechanical Behavior of Graphene-based Composite Plate with Flexoelectric Effect *K B Shingare, S Naskar*	119

Contents

CP_130_14	Facial Expression based Pain Monitoring in Hospital Environment using Compact Convolutional Network *Ashish Semwal, Narendra D Londhe*	229
CP_174_19	Secured Approach for One Umbrella Management System for Improving Healthcare Services *Dr S Tamil Selvi, B Ganapathy Ram, V S Preethashree*	237
CP_218_21	Miniscule Payload Location in Least Significant Bit Stego Images using Transform based Image Denoising Cover Estimators *S Arivazhagan, E Amrutha, W Sylvia Lilly Jebarani, S T Veena, S Ananthi Roy*	245
Civil Engineering		
CV_004_01	Geopolymer Concrete: A Pathway to Sustainable Manufacturing in the Indian Concrete Industry *Jyotirmoy Mishra, Bharadwaj Nanda, Sanjay Kumar Patro*	259
CV_012_02	A Geotechnical Study on Properties and Uses of Shales of the Dharwar System, Karnataka, India *Dr Udayashankar D Hakari*	265
CV_015_03	Maintenance of PMGSY Roads in India *Sandeep K Shrivastava*	273
CV_016_04	Way Forward to Enhancing Skills for Betterment of Indian Economy through Construction Industry *Sekar Kumbeswara*	275
CV_017_05	Fibre Reinforced Geopolymer Concrete as a Repair Material for Rigid Pavements-A Review *Peter Cibi, Karthi Lathi*	281
CV_019_07	Emerging Trends in Affordable Housing – GFRG Technology for Self Reliance and Sustainable Growth *K B Agarwal*	291
CV_020_08	Managing the Risk and Uncertainty in Coastal Residential Building Codes *Gino Hosein, Indrajit Ray*	297
CV_032_09	Analysis and Affine Transformation of Skew Slab *M Ravindra*	305
CV_033_10	Prediction of Mechanical Characteristics of Concrete Containing GSA, GGBS and WF *R Murugaboopathy*	319
CV_034_11	An Experimental Study on Self Repairing Concrete to Improve Strength and Sustainability *S Ramesh Kumar, D Sakthivel, E Vellaingiri*	329
CV_043_14	Energy Efficient Building to Fight Against Covid-19 *Sushovan Sarkar, Gargi De*	337
CV_049_15	Impact of GGBS as Partial Substitution of Cement and Replacement of Robo Sand to Fine Aggrigate on M50 Grade of High Performance Concrete *L Sai Indra Sena Reddy, Dr M M Vijalakshmi Nataraj*	343
CV_054_16	Effective Quality Management for Sustainable Roads *Kishor Kumar Pahuja*	353
CV_055_17	Feasibility Study of Ferrochrome Slag as an Alternative to Natural Aggregates *P N Ojha, Abhishek Singh, Brijesh Singh, B N Mohapatra*	361

Contents

CV_059_18	Artificial Intelligence Techniques to Predict the Compressive Strength of Sustainable Eco-friendly Strain-hardening Concrete Composites *K K Yaswanth, J Revathy, P Gajalakshmi*	371
CV_068_19	Risk Assessment in an Infrastructure Project *Dr K Srinivas, Dr K R Ramana*	377
CV_075_20	Sustainable Alternative to External Curing: Use of Superabsorbent Polymer in Concrete *Jyoti P Bhusari, Akhilesh A More*	383
CV_076_21	A Case Study on Stabilized Shallow Foundation for a Large Oil Storage Steel Tank on Soft Soil *Somdev Pakrashi*	395
CV_098_23	Theoretical Calculation of Crack Width in Pile for Tension and Lateral Loading *Md Arshad Jamal, Vaishali Sharma, Deepak Singh, Ayan Khan*	403
CV_099_24	Condition Assessment of Structural Components using Internet of Things (IoT) C Harshitha, Mallika Alapati	409
CV_100_25	Comparison of GSA 2003 and 2016 Guidelines for Evaluating Progressive Collapse Potential of Steel Moment Resisting Frame Building *Parthav P Patel, Digesh D Joshi*	415
CV_101_26	PSWC-BAR for Sustainable Concrete Construction *Anil K Kar*	423
CV_102_27	Planning, Analysis and Design of G+5 Cyclone Resistant Administrative Building at Kovalam, Chennai *Amjad Latif, Shweta Devekar*	431
CV_107_28	Study on Comparative Advantages of E350 vs. E250 Grade Steel in Industrial Structures *Amresh Kumar, Saptadip Sarkar, Anurag Sinha*	447
CV_108_29	Design and Development of Floating Structure for Solar PV plant using Numerical Analysis *Harsh V Chudasama, Ashish M Vajir*	457
CV_109_30	Correlation between Ground Motion and Structural Response of Multi-storied Buildings in the Performance Based Seismic Design *Soumyan K, Deepa Balakrishnan S*	465
CV_110_31	Preliminary Results of Concrete with Shredded Disposable Face Masks *Soham Parija1, Dhanada K Mishra2, 3, Christopher Y K Leung*	473
CV_111_32	A Technical Paper on "RCC Blanket Wall" *H M Viswanatha Sastry*	479
CV_112_33	Wind Pressure Distribution over Solar PV Panels Mounted on Pitched Building Roofs *Ashish Agarwal, Hassan Irtaza, Azhar Jameel*	485
CV_113_34	Design and Construction of Irregularly Shaped Cut & Cover Box Tunnel as an Innovative Solution for Space Restriction at Site *Chiranjib Sarkar, Anant Mehendale, Harsha G M*	497
CV_114_35	1D Flood Model to Retrace the July 2018 Flood in Lower Reaches of Pampa River, Kerala *Dr T K Drissia*	505

Contents

CV_131_36	A Comprehensive Review on the usage of Waste Materials in Flexible Pavements and their Impact *Pala Gireesh Kumar, Abhirami Priyanka Pathivada*	509
CV_133_38	Developing Self-Compacting Concrete as per IS 10262: 2019 by Utilizing C and D Waste as Aggregates and Fines *Ajay N, Ashwin M Joshi, Namratha Bharadwaj, Girish S*	515
CV_134_39	Analytical Estimation of Boundary Layer Thickness for Flow Over Spillways *Suresh Kumar N, Prasanna S V S N D L*	527
CV_136_41	Application of VH Polarization Sentinel-1 Imagery for Flood Mapping of Bhagalpur, Bihar *Deepak Kumar, Kumar Yuvraj*	533
CV_137_42	Performance based Design of Shear Ductile Wall with Custom Openings *Mohammad Suhail Saifi, Dr Khalid Moin*	539
CV_138_43	Design of Framed Foundation for Absorber in Flue Gas Desulphurization System *R L Dinesh, Ranjit P Kangralkar, Sandhya Krishnamurthy, Rohit Pantoji*	551
CV_139_44	Simulation of Earthquake Forces for Equipment Supported on Structure *Papia Mandal, K Madhavilatha, Anurag Sinha*	555
CV_188_45	Review on Limestone Calcined Clay Cements (LC3) *S M Gunjal, B Kondraivendhan*	561
CV_189_46	Bolted Shear Connections: A Comparative Study on Effect of Eccentricity and Other Design Criteria as Per International Codes *Saptadip Sarkar, Papia Mandal, Anurag Sinha*	573
CV_190_47	An Analytical Study on Wind Pressure Distribution on Rectangular Tall Building with Setback and Twist using Computational Fluid Dynamics *Vigneshwaran Rajendran, Prabavathy Shanmugasundaram*	579
CV_191_48	Selection of suitable Quantity of Fly Ash and Water to Achieve Desired Workability and Strength of Geopolymer Concrete *Subhash V Patankar, Sanjay S Jamkar, Yuwaraj M Ghugal*	589
CV_192_49	A Sustainable Approach to Flood Damage Repair of Hill Roads in Tripura using Soil Filled Gabions – A Case Study *D Roychowdhury*	597
CV_193_50	Analysis of Access Control & Traffic Bottleneck on Western Express Highway using PTV Vissim *Shrivastav Laxman Sutar, Siddharth Deepak Gondhale*	605
CV_209_51	A Comparative Study of MLP and MLP-FFA Models for Flood Prediction *Sandeep Samantaray, Abinash Sahoo, Siddhartha Paul*	615

Electrical Engineering

EL_010_02	Analysis of Wireless Power Transfer Compensation Topologies for EV Battery Charging *Amarjeet S Pandey, D B Pardeshi*	625
EL_011_03	Power Electronic Interfaces on Renewable Energy System *Sanjeev Kumar Bhatnagar, Priyabrata Pradhan*	631
EL_072_06	Review on Solar Powered Hydrogen Fuel Cell: A Promising Alternative for Future Energy Sustainable Development *Rajesh Bodkhe, Rakesh Shrivastava, Vinod Kumar Soni, Kshitij Shrivastava*	637

Contents

EL_073_07	Next Generation Advanced Core Material for Reluctance Machine *K Vijayakumar, A Joseph Basanth, R Karthikeyan, S Kannan*	645
EL_086_10	Solar Energy and Hydropower Complementing Each Other – A Global Trend for Achieving SDGs *Jnan Ranjan Pal*	651
EL_123_11	Renewable Energy Sources & Smart Grids Integration *Sangeeta Deb Barman, Dr Kumari Namrata, Dr S M Ali*	657
EL_145_12	Source Side Energy Management of Hybrid Renewable Energy System by Intelligent Control *Hemlata Joshi, Ekta Mishra, Ganesh H Patil*	663
EL_147_13	Improved Adaptive Controller Based Speed Estimator at Low Speeds for Sensorless Vector Controlled Induction-Motor *Meghraj S Morey, Vasudeo B Virulkar*	669
EL_148_14	Affordable Energy for Civilization: A Global Programme to Provision Collective Clean Energy Admittance *Chilukuri Bala Venkata Subbarayudu1, Dr Katikala Premalatha, Dr Mohd Iliyas*	679
EL_178_15	Solution of Single Objective and Multi-Objective Optimal Power Flow Problem using Chicken Swarm Optimization *Saket Gupta, Narendra Kumar, Laxmi Srivastava*	685
EL_184_16	An Enhanced Power Conditioning Unit Enabling Reduction in DC Link Voltage Fluctuation for a Grid Connected Photovoltaic System during FRT *Nishij G Kulkarni, Vasudeo B Virulkar*	693
EL_200_17	Tidal Power Generation – Prospects in India and Challenges for Engineers *Kirit B Trivedi*	701
EL_201_18	Net Zero: Emission vs Employment: The Transition in Indian Power Sector *Shreya Karmakar, Joy Chakraborty*	707
EL_202_19	ANN Based Adaptive SOGI-FLL Controller for Multifunctional Grid Tied Solar Energy Conversion System *Dinanath Prasad, Narendra Kumar*	713
Environmental Engineering		
EN_037_01	Modular Air Purifier for Metropolitan Cities *Sreekala P*	727
EN_045_02	Sustainable Infrastructure Management: Recovery and Reuse of Resources and Energy in Landfills *Dr Anumita Mishra, Prof Rao Y Surampalli*	733
EN_116_03	Green Hydrogen: A Perspective *S Sakthivel, Shireesh S Swami, Atul Choudhari*	739
EN_117_04	Green Multi-Storey Society Concept for Urban Area of India *Kapil Kukreja, Manoj Kumar Soni, Bibekananda Mohapatra*	747
EN_155_05	Effluent Treatment &Wastewater Recycling-Copper Smelter Perspective *Mary Sarker*	753
EN_156_06	Conservation of Topsoil at Construction Sites *Krishna Nirmalya Sen, Gollapalli Muralidhar*	765
EN_157_07	GIS-based Well Water Monitoring of Gunjalwadi and Velhale Villages, Maharashtra, India *Navale V B, Mhaske S Y*	771

Contents

EN_166_08	Sewage Pollution of Ground Water *Mahesh Patnaik*	781
EN_168_09	Energy Audit of Waste Heat Recovery System in Indian Cement Plants - Case Studies *Prateek Sharma, M V Ramachandra Rao, Ashutosh Saxena, B N Mohapatra*	785
EN_179_11	Wealth from Waste *Bhalchandra B Bhalerao*	793
EN_204_12	Design Algorithm: Solar Powered Water Supply System for Municipalities & Rural Area *Dilip Yewalekar, Manisha Kinge*	803
EN_211_13	Master Plan for Drought Mitigation at Jhargram District of West Bengal to Ensure Sustainable and Reliant Drinking Water Supply *P RoyChowdhury*	807

Electronics and Telecommunication Engineering

ET_021_01	Design and Analysis of Converters for Hybrid Electric Vehicle *Dr K Balachander*	815
ET_023_03	IoT based Smart Energy Meter Tracking using ZigBee *Dr Belsam Jeba Ananth M, Dr Revathi KG*	823
ET_046_04	Innovative Slope Stability Monitoring Instrument for O/C *S P Singh*	829
ET_062_05	Source and Effects of Conductive Emission in the Frequency Range 2.5 to 150 kHz and Its Measurement *Y Dhayaneswaran, Dr A Amudha, Dr L Ashokkumar, Y Umamaheswri*	833
ET_063_21	Text Recognition of Embossed Metadata Obtained from Live Video of UAVs *Gagan Kumar Nigam, MGR, Sumit Srivastava, SE*	841
ET_070_06	Mitigate Challenges of Co-location Interference for SDR applications *Sandeep Singla, Sidharth Sarswat, Radheshyam Kumawat, Deepa Bajpai*	853
ET_071_07	EMI/EMC (MIL-STD) Compliant Design for 12V/28VDC Bus to Meet Ground based Military SDR Systems *Sandeep Singla, Radheshyam Kumawat, Vikas Arora, Deepa Bajpai*	861
ET_081_08	Design and Development of Forced Air Cooled Dip-brazed Chassis for Safety Critical Electronics *Prashant, A Karthikeyan*	869
ET_095_09	Low Power ADC Design for Biomedical Implantable Devices *Aneesh K, Manoj G*	877
ET_096_10	Study on Electro Magnetic Interference and Compatibility Across Various Levels and Mitigation Technique using Software *Y Uma Maheswari, Y Dhayaneswaran, Dr A Amudha, Dr L Ashokkumar*	885
ET_097_11	Comparison between Different Wavelet Transform Techniques for Indoor Optical Wireless Communication System Employing Pulse Position Modulation & On-OFF Keying *Ankita Aggarwal, Dr Gurmeet Kaur*	893
ET_121_22	Streaming Video Data from Remote Sites to Command Center under Bandwidth Constrained Environment *Anitha K M, Sampath Kumar R, Prabha Gupta, Sonu Shreshtha*	907

Contents

ET_122_12	Design of Charge Pump PLL using 180nm CMOS Technology Ashwini Desai, Uma Kulkarni	913
ET_146_18	A Brief Study of Optical Flip-flops based on Microring Resonator *Kankana Debnath, Srikanta Das, Arka Roy Bin, Bishanka Brata Bhowmik*	919
ET_149_13	Cybernation of Home Appliances using Raspberry PI *Yerramsetti Jaswanth, BathinaVenkateswara Rao, Kalagara V V R S Vishnu Thejavathu Thirumalarao*	925
ET_150_14	Data Interoperable on DVB-S /S2 "Digital Video Broadcast" Compliant Systems *Y S Rayudu*	931
ET_151_15	ML-based Constellation-rotation Correction of QPSK Signal in Optical Fiber Communication *Nitish Sinha, Satyabrata Singha, Mohua Chakraborty, Bishanka Brata Bhowmik*	937
ET_152_16	Wavelength dependent Configurable optical AND to OR Gate based on Micro Ring Resonator loaded on Mach–Zehnder Structure *Arka Roy Bin, Srikanta Das, kankana Debnath and Bishanka Brata Bhowmik*	941
ET_153_17	Soil Humidity Measurement using Microstrip Interdigital Capacitor (IDC) and Rectangular Slotted Fingers Interdigital Capacitor (RSFIDC) *Jayant Gajanan Joshi, Mandar P Joshi, Balwinder Singh Dhaliwal, Shyam S Pattnaik*	947
ET_167_20	Integrated Communication Interface with Configurable Dual Active Cellular Data Connection, Navigation and PAN Options as Generic IoT Hardware *Kiran Rawal, Harmandeep Singh, Ashish Gupta, Gurjeet Singh, Mohan Lal, Deepa Bajpai*	955

Mechanical Engineering

MC_013_01	Designing a Proper Hoe towards Zero Loading Losses to Achieve 100% Productivity with Reduced Fuel Consumption *Rajarshi Mukherjee*	963
MC_027_02	Disaster Management over Indian Railways- Reliability, Operation & Safety of 140t Gottwald Crane *Narendra Kumar Verma*	967
MC_051_03	Experimental and Prediction Analysis of the Screening Performance of Coal in Linear and Circular Vibratory Screen *Bharath Kumar Shanmugam, Harsha Vardhan, Govinda Raj M, Harish Hanumanthappa*	981
MC_058_04	Satyan King-Pin-Drive for Electric Vehicles *Dr Sathyanesan T N*	985
MC_077_05	Efficiency Improvement of Concentrated Photovoltaic Module by way of Various Active and Passive Cooling Techniques – a Review *Yogesh Nandurkar, R L Shrivastava, Vinod Kumar Soni*	991
MC_078_06	CFD Analysis of an Automotive Cabin Air Filter *Koyal V Sadaphal, Dr A S Mohite*	997
MC_079_07	Study and Analysis of Asphalt Hot Mixing Plant *Vishal K Patel, Dr A S Mohite*	1003
MC_092_08	Sustainability Adaptation by Retrofitting Volatilizer in Thermal Power Plant for Co-generation of Cement and Power *C Prabhakar Reddy, Amiya P Goswami*	1009
MC_093_09	Optimization of Cross Flow Forced Draft Air Cooled Tubular Heat Exchanger (FDAC-HE) of Fumes Extraction System in Steel Melting Plant *Vijay S Kumavat, Dr Arvind Mohite, Manish Khanna, Hemant Chaudhary*	1013

Contents

MC_094_10	Effect of Different Cooling Mediums on Friction Stir Welded AA6061 Alloy *Dinesh Chaudhary, Dr A S Mohite*	1025
MC_118_11	A Vibrational Test for Chaos using 0-1 in a Vertical Axis Wind Turbine *C B Maheswaran, R Gopal, S Nadaraja Pillai*	1033
MC_119_12	Development of Prototype of Thermal Air Sterilizer to Combat COVID-19 *Sunil Kumar Thamida1, Srikumar V R, Mohith K S, Amarendra Kumar Gupta, Vasudharani Devanatahan, Harshini Chakravarthy*	1039
MC_120_13	Design of a Centrifugal Impeller for Lean Supercharging of Motorcycle Engines *Harishankar S, Aswin A Asokan, Madhav Murali, Rejath R S, Rajesh T N*	1045
MC_203_16	Effect of Varying Surface Thickness on Wetting Delay and Rewetting Velocity through CFD Analysis *Monika Siyal, Chitranjan Agrawal, B L Salvi, S Jindal*	1051
MC_213_17	Energy Efficient Surfaces for Improved Performance of Heat Exchanger Through Enhanced Pool Boling Heat Transfer: A Review *Anil S Katarkar, Biswajit Majumder, Swapan Bhaumik*	1059
MC_214_18	Finite Element Structural Analysis of Inflatable Semicircular Air Beam *K Hans Raj1, Akash Jain, Ravi Kumar, Arun Kumar Saxena*	1067
MC_219_19	Performance Characteristics of External Gear Pump with the use of Burnt Oil *Aditya Anurag Bal, J Randhari*	1073
MC_221_20	Explosive Welding-The Need of Industry 4.0 for Atmanirbhar Bharat *Prabhat Kumar, Subrata Kumar Ghosh, John Deb Barma, S Saravanan*	1079
MC_222_21	Analysis of Latent Heat Based IC Engine Exhaust Waste Heat Recovery System *Dr S Babu1, S A Ravi Varman, R Santhosh Mugil*	1085
Materials and Metallurgical Engineering		
MM_007_01	Salvaging used Reformer Tubes for Conserving Nickel *Satish Bhagwan Kunte*	1093
MM_026_02	Spinel Magnesium Aluminate by Sol-gel Assisted Combustion Process and Its Characterization *Soumya Mukherjee*	1099
MM_050_03	Mitigating Covid-19 induced disruption to Steel use in Construction through Engineering Solutions *Manos Kumar De, Pratip Bhattacharya*	1103
MM_052_04	Effect of Vanadium on the Tensile Strength as a Function of Austenitizing Temperature on LHB Wheels *Smeeta Kujur, P P Sarkar, Asha Bajpai*	1111
MM_053_05	Challenges for using Iron-ore as Coolant in BOF Steelmaking *Sanjay Kumar Gupta*	1117
MM_162_06	Hydrothermal Synthesis and Characterization of Nanocrystalline Zinc Orthovanadate($Zn_3V_2O_8$) on Graphene Oxide Scaffolds *Lakshmana Naik R, H Seshagiri Rao, Pernapati Nagaraja, Bala Narsaiah T*	1125
MM_163_07	Study of Mechanical and Thermal Properties of ABS Reinforced with Fly Ash by using Maleic Anhydried as Coupling Agent *Bulti Kandar, Deepshikha Datta*	1131
MM_180_08	Development and Applications of Forged Microalloyed Steels in India *P K Mandal*	1139

Contents

MM_205_09	Study and Development of Graphene Oxide based Hybrid Polymer Nanocomposites *Geetha Rajamani, Jawahar Paulraj*	1147
MM_206_10	Determination of Critical Temperature for Austenite to Ferrite Transformation During Hot Rolling of Low Carbon Nb-V-Ti Steel *Santosh Kumar, B Sunita Minz, N Mondal, Dr K Mukherjee*	1155
MM_207_11	Ag@CuO Decorated Tailored Nanostructures based CO_2 Sensors: Role of n-type Semiconductors in Enhancing Heterostructured Sensor Efficiency *Shravanti Joshi*	1165

Mining Engineering

MN_158_01	Retrospection of the Longwall Mining for Mass Production of Coal from Indian Underground Mines *K Nageswara Rao, G Budi, P K Mandal, A J Das, J Vinod Kumar*	1173
MN_215_02	Innovative Methodologies of Carbon Sequestration for Sustainable Development of Unmineable Coal Seams *Singam Jayanthu, Singam Jayadarshana, Chandramohan*	1183
MN_223_03	Application of Recent Guidelines of 2020 For TARP Vis-À-Vis Design of Stable Slopes in Opencast Coal Mines-A Case Study *Singam Jayanthu, Pritiranjan Singh, K Sridhar Reddy, Rishabh Lala*	1191

Marine Engineering

MR_028_01	Design and Engineering for a Self-reliant Society in Marine Engineering *Sandeep Kumar*	1199
MR_039_02	Sustainable Shipping *N M C Nair*	1209
MR_040_03	Water Dependency Test on a Novel Method of Water Transportation at Static Conditions *Arulanantha Samy Santhiyagu, Jaikumar Mayakrishnan*	1215
MR_044_04	IoT based Oil and Gas Survey *B Kannan*	1221
MR_056_05	An Overview Study of Ocean Energy Potential and Technologies in India *Geetam Saha, Dipesh Majumdar*	1229

Production Engineering

PR_001_01	Sustainable Manufacturing: Principles, Applications and Directions *Ashok Kumar Panda*	1241
PR_036_03	Preparing for Post Covid-19 Sustainable Manufacturing Ecosystem *Dr Goutam Sengupta*	1245
PR_048_04	The Advancement of 3DBioPrinting Technology uses as Bio-Manufacturing Process *Ranjit Barua, Sudipto Datta, Pallab Datta, Amit Roy Chowdhury*	1253
PR_061_06	Challenges & Way Forward in Integration of Remote based Working Environment for a Multi-Disciplinary Engineering Design Centre *Anirban Datta, Gautam Gangopadhyay, Sushmita Choudhury*	1259
PR_091_07	Principles, Applications and Directions of Sustainable Manufacturing: A Case of Indian Micro, Small and Medium Enterprises (MSMEs) *Dr Om Parkash Mehta*	1267
PR_115_08	Unforeseen Risks in Project Execution – A Case Study *Balakrishnan Nair*	1275

Contents

PR_135_12	Engineering Solution as Sustainable Manufacturing for Protection in Pandemic Regime *A A Panja, M S Patwardhan*	1281
PR_161_11	The Sustainable Manufacturing in Chennai Plastic Sacks Cluster *Dr E Bhaskaran*	1289
PR_183_16	Application of AI based Models on 3D Printing Technology : Future Prospects for Additive Manufacturing *Shivam Raj, Sanjit Kumar Rajak, Ganta Sai Rahul, Rajat Gupta*	1303
PR_185_13	Possible Mitigation Measures for Various Hazards Associated with Cement Factories of Assam- A Discussion *Dr Sanjoy Kumar Dey, Dr Rajat Gupta*	1309
PR_186_14	Framework for Skill-Based Teaching Pedagogy for Computerized Numerical Control (CNC) Machine Programmer Course *Dr Charudatta Pathak, Rajkumar Baghel, Sumit Dubal, Yogendra Jain, Dr Hrushikesh B Kulkarni*	1315
PR_187_15	The Future of Industrial Training and Simulation *Dr Sathyanarayana A*	1321

Textile Engineering

TX_009_01	Potential of Jute & Banana Blended Engineered Fabric for Technical Application *S N Chattopadhyay, N C Pan, A N Roy, Kartick K Samanta*	1327
TX_060_02	Tensile, Impact & Dynamic Properties of Jute/E-Glass Composite by Adding Shear Thickening Fluid *Abhishek M R, Dr Suresh P M*	1337
TX_082_03	Flow Rate on the Electrospun PEG-PVA/CNF/NCG Nano-composite Fibres *Arpita Priyadarshini Samantaa, Jonathan Tersur Orasughab, Dipankar Chattopadhyay Swapan Kumar Ghosh*	1345
TX_164_04	Sustainability of Handlooms and Textiles for A Self Reliant India *Dr Sasmita Panda, Dr P L Panda*	1351
TX_165_05	Development of Portable Water Tank for Retting of Jute Ribbons and Root Cuttings *A K Thakur, V B Shambhu, A Singha*	1357

Interdisciplinary

ID_083_04	Engineering Institution for Self-reliance and Sustainable Goals *Dr S Swapna Kumar*	1365
ID_124_05	Skilling India through NSQF - A Way Forward to Atmanirbhar Bharat *Dr Anil Kumar, Suneel Grover*	1369
ID_140_06	Self Reliance and Sustainability : An Environment Perspective *Seema Garg, Navita Mahajan*	1375
ID_142_08	Self Reliance: A Context of Sustaining Indian Automobile Industry *Rohit Radhakrishnan, Vaisakh V, Dr Nidhi M B*	1381
ID_143_09	Flamingo: Labour Management Interface System *Kushal Vilas Datrange, Pankit Rajesh Rana, Dr Anil Achyut Kunte*	1387
ID_144_10	The Technical Efficiency of Unemployed Youth Employment Generation Programme in Tamil Nadu *Dr E Bhaskaran*	1391

Contents

ID_182_11	Role of Consulting Engineers in Mechanical Engineering on the way to Self-Reliant India *Anirban Datta, Tarun Kumar Ray Chaudhury*	1397
ID_194_12	Innovations, Incubation and Entrepreneurship is a Driving Force for the National Economic Development *Dr C Sendil Kumar*	1403
ID_196_14	Exploring Nexus of Socio-economic-environmental Aspects for High Speed Rail Corridors Development in India *Dheeraj Joshi, Shikha Saini, Vivek Joshi*	1407
ID_197_15	Prediction and Assessment of Environmental Impacts (Effects) on the Design and Arts Environment for Industry 3.0 Cotton Roller Ginning Process *Dr Vijayan Gurumurthy Iyer*	1413
ID_198_16	Protocol Analysis for Intrusion Detection System on IoT Based Network Communication *S Ponmaniraj, Dr Amit Kumar Goel*	1425
ID_216_17	Upliftment of Indian Economy through Sustainable Development *Vaibhav Gupta, Sudershan K Popli*	1433
ID_217_18	Education's New Normal: Some Challenges and Much Opportunity *Dr Shilpa Tripathi*	1435

Low Power ADC Design for Biomedical Implantable Devices

Aneesh K, Manoj G

Department of Electronics and Communication Engineering, Karunya Institute of Technology and Sciences, Coimbatore, Tamilnadu

✉ *aneeshk.anj@gmail.com*

ABSTRACT

Implantable biomedical devices play a vital role in acquisition and monitoring of critical biophysiological signals in the human body. Since these devices are in contact with critical organs, the reliability of the system is having great importance. The energy efficiency of the system has a direct impact on reliability. These devices are powered by non-rechargeable batteries which are also implanted in the body. It is found that, if the system draws more energy for operation, the battery drains faster. This leads to untimely failure of the system. Amongst the various blocks in a physiological signal monitoring system, ADC (Analog to digital convertor) operation contributes more to the power consumption. This paper discusses different low power techniques and methodologies to make the ADC more energy efficient.)

Keywords : Implantable devices; ADC; Capacitive DAC; Physiological signal acquisition; leakage power; comparator.

INTRODUCTION

The implantable microsystems like cardiac pacemaker, ICD (implantable cardioverter defibrillator)[1], cochlear implants, visual prosthesis systems, neural simulators have gained importance in today's world, since they all deal with the critical biophysiological signals. These devices are implanted in the body by surgical means. A constant monitoring of critical signals is being done by these devices and it should be active all the time. Each of these devices are powered by a non-rechargeable battery embedded in the system. The life of the battery directly depends on the energy efficiency of the device. A less efficient circuit draws more power and this leads to the sudden depletion of the battery. Frequent replacement of the battery is not advisable since it can only be done with surgical procedures. This is not only costly but also infectious to the patient. Recent studies show that, analog front-end design of such devices consume more power. The various blocks in a bio signal monitoring system are shown in **Fig. 1**.

Amongst these blocks, ADC (Analog to digital convertor) is found to be the major power dissipator[2]. Many types of ADC's are proposed in the past literatures like Flash type ADC, sigma- delta ADC, dual slope ADC, Pipelined ADC etc.The bio medical devices, which are discussed in this paper are dealing with electrical activities from the critical organs.

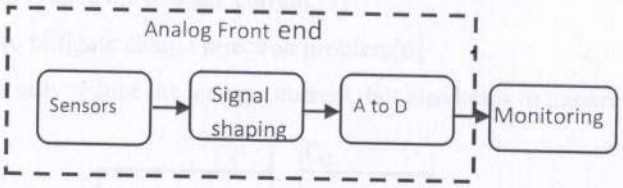


Fig. 1. Block diagram of physiological signal monitoring system

These signals are having less amplitude and they fall in low frequency spectrum (low variation). The SAR ADC with moderate speed is suitable to handle physiological information.

$$P_{dynamic} = \alpha_{act} CV^2 f \quad (1)$$

The "Equation (1)" validates the idea discussed before. Here in "(1)", α_{act} is the switching factor,C is the capacitance in the design, V is the supply voltage and f is the frequency of operation. $P_{dynamic}$ is the dynamic power consumption in the circuit. By reducing the operating frequency, the dynamic power reduction can be achieved[3]. Thus, usage of SAR ADC with a moderate

speed helps to limit the dynamic power consumption. Moreover, in SAR ADC, all the building blocks except comparator are digital in nature. This enables the designer to incorporate advanced CMOS technology in the design, and this further contributes to the low power. The basic block diagram of an SAR ADC is shown in **Fig. 2**. It is made up of capacitive DAC array, sample and Hold circuit, comparator and SAR logic. The unnecessary power dissipation of each of these blocks are to be capped to propose an efficient design. Out of these major blocks, the switching dissipation in the CADC array is mainly discussed and different methods for an energy efficient technique are analyzed in this paper. This is involved in reducing "α_{act}" (switching activity) of the CADC array. The sample and hold arrangement are used to sample the input signal to the comparator. MOS (Metal oxide semiconductor) transistors are used as switches. The size of these switches can be kept minimum by adopting new CMOS design technologies. But the sub-micron design techniques are suffered by high amount of leakage current through it. **"Fig. 3"** explains the leakage mechanisms.

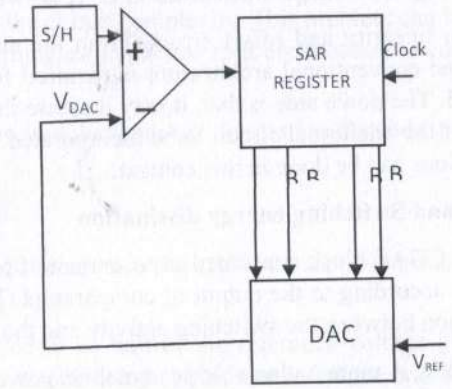


Fig. 2. Block diagram of SAR ADC

Factors to be Considered for Switch Design

Even though the switch is closed during the hold operation, output node is connected to the input side through two parameters. The first one is the drain-source leakage (modelled as R leak). This is getting worse with technology scaling. The other parameter is the drain to source capacitive coupling (modelled as CC). Due to this, output voltage of the switch is degraded even when the switch is closed.

In low speed ADC, the switch leakage is a significant factor and it degrades the system performance. Another problem that is associated with the sampling switch is the charge injection. It is a leakage mechanism due to injection of charges from the channel region to both input and output sides of the switch. In this the charge injection to the output side leads to significant changes in the output voltage. This leads to nonlinear errors[4]. These effects are shown in figure 3 and figure 4. The techniques which are used to avoid these problems are

1) Stacked transistor arrangement to reduce the leakage current [5]
2) Dummy transistor arrangement to mitigate charge injection problem[6]

The above-mentioned techniques not only reduce the leakage current, but also helps to impart linearity to the switch operation.

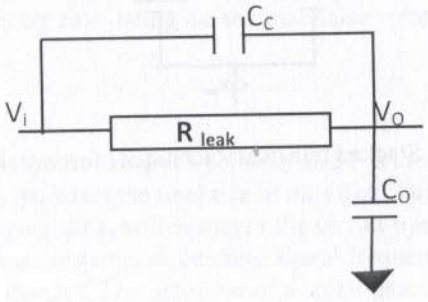


Fig. 3. Leakage mechanism in CMOS switch

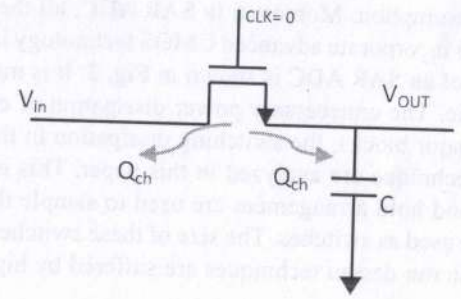


Fig. 4. Leakage mechanism in CMOS switch

This helps to avoid switch induced non linearity and offset errors. From the above discussions, it is clear that additional components or slight modifications of the conventional architecture is required for achieving power efficiency. The stacked transistor arrangement is shown in **Fig. 5**. The down side is that, it may increase the design complexity and size of the device. Hence care must be taken, in selection of the additional circuit to be incorporated. Simple and effective design is preferred in low power applications. More investigations can be done in this context.

Importance of Capacitive DAC array and Switching energy dissipation

From various literatures, it is evident that CDAC block consumes large amount of power. It consists of switches and capacitors. The values in the capacitors are updated according to the output of comparators. This involves many switching sequences to achieve the correct conversion. The relation between the switching activity and the power dissipation is given in (1).

The inevitable switching in CDAC makes it more vulnerable to dynamic power consumption. Thus, an energy efficient architecture and switching schemes are having paramount importance in DAC design. Two basic architectures available for DAC's are given below.

1): Binary weighted Capacitive array DAC: This is the conventional architecture for DAC. The capacitors in the array are controlled by the signals from the SAR logic. The values in the capacitors are updated accordingly (via charging up to supply or discharging to ground). This design is prone to high switching power dissipation[7].

2): Split Capacitor array DAC: This is a modification over the binary weighted capacitor array. Here the capacitive array is segmented in to M bit MSB (most significant bit) array and N bit LSB (least significant bit) array. The number of unit capacitors in this architecture is found to be lesser than the conventional architecture. This reduces the size and power consumption of the block. This is a more suitable architecture in low power design[8].

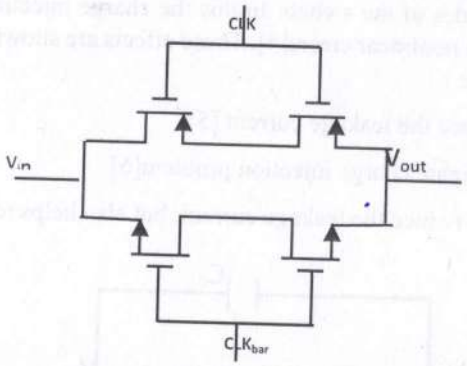


Fig. 4. Stacked transistor techniques for switches

$$E_S = CV_{ref}^2 \quad (2)$$

$$E_{stepwise} = C V_{ref}^2 / S \quad (3)$$

The various switching strategies adopted for CADC array are listed below

I) Stepwise Charging: The energy required (E_s)for updating the value of a capacitor is given in (2). The energy is directly proportional to capacitance (C) and the reference voltage (V_{ref}). The switching energy can be reduced by scaling down the voltage and the capacitance. But this may degrade the performance of the circuit. An alternate solution is enumerated in (3). In this, the capacitors are being charged in different steps[9]. This step wise charging reduces the overall switching energy dissipation by a factor (S).

II) Charge recycling: It is an effective method to mitigate the switching energy dissipation in capacitive array. In this, the discharging current from one capacitor is used to charge another capacitor[8].

III) Hybrid Techniques: In this method, more than one switching strategies are combined together to achieve better power performance[10]. But this may increase the circuit complexity. This problem can be nullified by combining energy efficient switching scheme with area efficient strategies (capacitor split architecture is combined with area efficient segmentation technique).

IV) Tri level Switching: As shown in (2), the switching energy dissipation depends on V_{ref}.

$$V_{ref} = \frac{Vcm}{2} \tag{4}$$

In this technique, V_{ref} (referenve voltage)is selected as the half of the input common voltage (V_{cm}). This leads to considerable savings in switching power dissipation[11].

V) V_{cm} based Switching: The V_{cm} is derived to be half of the reference voltage (V_{ref}). This architecture saves 97.66 % of switching energy[12]. The voltage V_{ref} is considered as positive reference and input common mode voltage V_{cm} is taken as negative reference in this case. Moreover, as per published literatures, this scheme offers better area efficiency, since it achieves 75% reduction in total number of capacitors, compared with the conventional design.

VI) Charge dumping switching scheme: This scheme is superior to the previous techniques, in terms of switching and area efficiency.

Apart from these schemes, some new ideas have been proposed in the recent literatures. The comparison of various switching scheme is given in **Table 1**. In the entries, the energy efficient scheme and the charge sharing switching methods are found to be effective in terms of switching power dissipations, since they hardly dissipate any switching power. But these two schemes exhibit logic complexity in the design level. The charge sharing switching scheme offers only a 25% reduction in area compared to the conventional architecture. The bio medical implantable devices have to exhibit higher power efficiency and area efficiency. The circuit complexity of these devices should be maintained in moderate level.

Charge dumping switching scheme[13]saves 99.86% of the switching energy. This design also achieves a 93.75% of improvement in area efficiency. The logic complexity is also less compared to the state-of-the-art design. Thus, this can be adopted for ADC architecture for bio medical devices.

Selection of Capacitance value in CADC array

The CDAC array consists of switches and unit capacitors. The selection of the value of this unit capacitor is important, when the linearity is concerned. To improve the linearity, a larger unit capacitor is preferred. Larger value of capacitor restricts the thermal noise to lower limits. The equation for calculating the thermal noise voltage is given in "(5)"

$$V_n = \frac{KT}{C} \tag{5}$$

The noise voltage is represented as V_n, K is the Boltzmann's constant and T is the temperature in Kelvin. A large unit capacitor (C_u) also introduces certain problems. This increases the total size of the CDAC array leading to additional power consumption. It necessitates more charging and discharging time, which makes the circuit operation slow. The speed of operation is not a major concern in the biophysical acquisition systems, since these signal frequencies are low. But increase in the device size is not a desirable feature for implantable devices. The selection of a small unit capacitance causes matching problems in the DAC array. One solution is to use a small unit capacitor in the design, and iron out the mismatches and offset variations using an additional calibration circuit. But this technique makes the entire design overloaded, since an additional calibration circuit

is employed in operation. Thus, a designer must evaluate the tradeoffs, and depending on the application, an optimum value of unit capacitor can be proposed. This eliminates any additional calibration techniques.

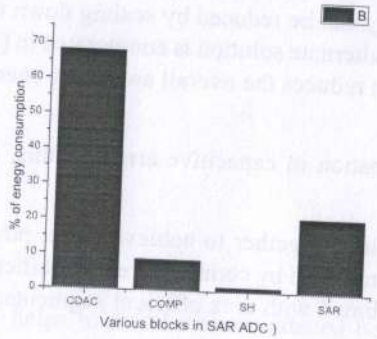


Fig. 5. Power consumed by various blocks in SAR ADC

$$C_{TDAC} \geq \frac{24KT2^{2N}}{V^2} \quad (6)$$

The minimum value of the total capacitance required for CADAC array is given in "(6)". C_{TDAC} is the total capacitance of the CADC array, N is the total number of bits involved and V is the supply voltage[16]. The selection of optimum capacitance should be done in such a way that, it should satisfy the relation given in "(6)". Hence, this is a challenging task for the designer and more studies can be done on the selection procedure. The two limiting factors to be considered for DAC design are (i) Capacitive matching (ii) Thermal noise.

Capacitive matching is more troublesome in power consumption. It is found that in-efficient capacitive matching incurs power consumption in the order of 8xper added bit. The thermal noise effect causes the power consumption in the order of 4x per added bit. The value of capacitance is an important parameter that determines the above-mentioned effects.

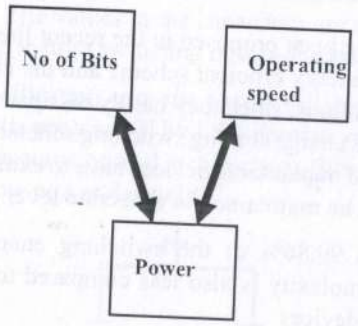


Fig. 6. Tradeoffs in ADC design [17]

Performance analysis of SAR ADC

Performance of an SAR ADC depends on the various tradeoffs associated in their design. It is shown in figure (6). The no of bits (resolution) of ADC and the power consumption is directly related. As there are a greater number of bits in the operation, the system consumes more power. Similarly, if the system operates faster, more power is being consumed. This relation is shown in "(7)". It is the responsibility of the designer to choose amongst these tradeoffs. It depends on the application that is to be realized.

In this discussion, the required device is an implantable system which handles the physiological signals. As already discussed, these signals are in low frequency spectrum. Hence, moderate speed convertor is enough for operation. The amplitude ranges of biological signals, that are being collected are also very low. To represent low amplitude ranges, moderate number of bits (8-10) are only required. This further reduces the power requirement.

Power = Energy ×Conversion rate (7)

The figure of Merit (FoM) is a number, which is used to represent the performance matrix of SAR ADC. This number reflects the design tradeoff in an efficient way. FoM's are generally higher for low speed ADC and its value decreases as the speed of ADC increases. Two types of FoM's are generally used for performance analysis in SAR ADC. They are

1): Walden figure of merit (FoM_w) : This is one of the popular figures of merit that is being used to measure the ADC performance. The formulae for calculation is given in "(8)". The low resolution and moderate speed ADC's are analyzed by this method. This is regarded as the simplest FoM calculations available. But FoM_w is not suitable for ADC's with higher resolution.

2): Schreier figure of merit(FoM_s) : To analyze the performance of a high speed and high-resolution ADC, (FoM_s) is preferred. It is shown in "(9)". In other words, for the system having SNDR (Signal to noise distortion ratio) greater than 50 dB, Schreier figure of merit is found to be more accurate than FoM_w.

Table 1. Comparison of switching schemes

SL NO	Switching method	% of Energy saving	Area efficiency	Complexity
1	Conventional[8]	Reference	Reference	Less
2	Trilevel [11]	96.89	75	Medium
3	Vcm- scheme based [12]	97.66	50	Medium
4	Hybrid method[10]	98.83	75	Low
5	Charge dumping scheme [13]	99.86	93.75	Medium
6	Energy efficient[14]	100	87	High
7	Charge sharing[15]	100	25	High

$$FoM_w = \frac{P}{f_s \times 2^{ENOB}} \tag{8}$$

$$FoM_s = SNDR + 10\log\left(\frac{f_s/2}{P}\right) \tag{9}$$

The term P represents the power consumption in the ADC, ENOB is the effective number of bits, SNDR is the signal to distortion ratio and f_s is the operating frequency of the device. From these equations it is clear that, the FoM depends on ENOB and SNDR.

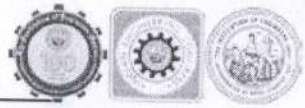
The SNDR is defined as the ratio of signal power to the noise power. To achieve a reasonably higher SNDR, the signal level must be kept high. Studies show that higher SNDR levels are achieved at the/ cost of more energy consumption. The ENOB is the measure of SNDR which is used to compute the actual ADC performance with ideal ADC. This value is calculated using the formulae given in "10"[18].

$$ENOB = \frac{SNDR - 176}{6.02} \tag{10}$$

For a low speed, ultra-low power ADC, FoM_w is preferred. In lower operating speeds, higher value of FoM is expected.

CONCLUSION

The early drainage of the battery in the implanted devices causes sudden failure of the system without warning. The ADC in the analog front end of the design draws major power for operation. In SAR ADC, the major power-hungry block is DAC. Byincorporating efficient switching methodology, the switching energy dissipation of capacitor array can be capped. Though the advancement inscaling ensures area efficiency, the leakage power dissipation becomes a concern in sub-micro meter designs. More efficient techniques can be proposed for the suppression of leakage power. Since the implantable devices deal with the critical organs, an ultra-low power, energy efficient design is to be incorporated for improving the reliability and durability of the system.



ACKNOWLEDGMENT

This work is supported by the Ministry of Electronics & Information Technology (MeitY), Government of India, through 'Visvesvaraya PhD Scheme for Electronics & IT'.

REFERENCES

1. W. Hu, T. Nguyen, Y. T. Liu, and D. Y. C. Lie, "Ultralow-power analog front-end circuits and system design for an implantable cardioverter defibrillator (ICD)," Proc. 2011 IEEE/NIH Life Sci. Syst. Appl. Work. LiSSA 2011, no. ICD, pp. 34–37, 2011.
2. D. Zhang, A. Bhide, and A. Alvandpour, "A 53-nW 9.1-ENOB 1-kS/s SAR ADC in 0.13-μm CMOS for medical implant devices," IEEE J. Solid-State Circuits, vol. 47, no. 7, pp. 1585–1593, 2012.
3. P. Zhao, J. McNeely, W. Kuang, N. Wang, and Z. Wang, "Design of sequential elements for low power clocking system," IEEE Trans. Very Large Scale Integr. Syst., vol. 19, no. 5, pp. 914–918, 2011
4. G. K. Balachandran and P. E. Allen, "Switched-current circuits in digital CMOS technology with low charge-injection errors," IEEE J. Solid-State Circuits, vol. 37, no. 10, pp. 1271–1281, 2002.
5. D. Zhang, A. K. Bhide, and A. Alvandpour, "Design of CMOS sampling switch for ultra-low power ADCs in biomedical applications," 28th Norchip Conf. NORCHIP 2010, pp. 4–7, 2010.
6. S. A. Mahmoud, H. A. Salem, and H. M. Albalooshi, "An 8-bit , 10 KS / s , 1 . 87 μ W Successive Approximation Analog to Digital Converter in 0 . 25 μ m CMOS Technology for ECG Detection Systems," Circuits, Syst. Signal Process., pp. 2419–2439, 2015.
7. J. L. Mccreary, "AII-MOS Charge Redistribution Analog-to-Digital Conversion Techniques—Part I," IEEE J. Solid-State Circuits, vol. 10, no. 6, pp. 371–379, 1975.
8. B. P. Ginsburg and A. P. Chandrakasan, "An Energy-Efficient Charge Recycling Approach for a SAR Converter With Capacitive DAC," pp. 184–187, 2005.
9. M. Van Elzakker, E. Van Tuijl, P. Geraedts, D. Schinkel, E. A. M. Klumperink, and B. Nauta, "A 10-bit charge-redistribution ADC consuming 1.9 μw at 1 MS/s," IEEE J. Solid-State Circuits, vol. 45, no. 5, pp. 1007–1015, 2010.
10. L. Xie, G. Wen, J. Liu, and Y. Wang, "Energy-efficient hybrid capacitor switching scheme for SAR ADC Liangbo Xie , Guangjun Wen , Jiaxin Liu and Yao Wang," vol. 50, no. 1, pp. 22–23, 2014.
11. C. Yuan and Y. Lam, "Low-energy and area-efficient tri-level switching scheme for SAR ADC," vol. 48, no. 9, pp. 9–10, 2012.
12. Z. Zhu, Y. Xiao, and X. Song, "VCM-based monotonic capacitor switching scheme for SAR ADC," Electron. Lett., vol. 49, no. 5, pp. 327–329, 2013.
13. S. H. W. Chiang, "Charge-dumping switching scheme for successive-approximation-register analogue-to-digital converters," Electron. Lett., vol. 52, no. 5, pp. 348–350, 2016.
14. T. Yousefi, A. Dabbaghian, and M. Yavari, "An Energy-Efficient DAC Switching Method for SAR ADCs," IEEE Trans. Circuits Syst. II Express Briefs, vol. 65, no. 1, pp. 41–45, 2017.
15. M. Akbari, O. Hashemipour, M. Nazari, and F. Moradi, "A charge sharing–based switching scheme for SAR ADCs," Int. J. Circuit Theory Appl., vol. 47, no. 7, pp. 1188–1198, 2019.
16. M. Boutemeur, "A 3,3V 12Bits rail-to-rail ADC SAR for neuronal implant," Proc. 8th IEEE Int. NEWCAS Conf. 2010, pp. 5–8, 2010.
17. B. Murmann, "The Race for the Extra Decibel: A Brief Review of Current ADC Performance Trajectories," IEEE Solid-State Circuits Mag., vol. 7, no. 3, pp. 58–66, 2015..
18. B. Murmann, "The Successive Approximation Register ADC : A Versatile Building Block for Ultra-Low- Power to Ultra-High-Speed Applications," no. April, pp. 78–83, 2016.

Journal of Critical Reviews

ISSN- 2394-5125 Vol 7, Issue 1, 2020

Review Article

QUALITY ANALYSIS OF RICE GRAINS USING ANN AND SVM

DIVYA MOHAN[1], MURUGANANTH GOPAL RAJ[2]

[1]Assistant Professor, Dept. of ECE, Ahalia School of Engineering and Technology, Palakkad, India.
[2]Prof. & Head, Dept. of EEE, Ahalia School of Engineering and Technology, Palakkad, India.

Received: 10.11.2019 *Revised: 16.12.2019* *Accepted: 18.01.2020*

ABSTRACT

Rice is the most favorable and most consuming food for all the human being in all over the world. Market for rice depends on the quality of it. Currently the type and quality of rice are assessed by visual inspection method through naked eye. This process is however tedious, time consuming, needs human expertise and depends on physical fitness of the inspector. To overcome these drawbacks, in this paper, an automated system is introduced which identifies and classifies the rice grains based on digital image processing techniques. Image processing method is most suitable as it is a non-contact technique, where in the image of the rice grains are captured. The captured images are pre-processed, segmented and features are extracted through MATLAB. From the extracted features the quality of rice is assessed based on Neural Networks (NN) and Support Vector Machine (SVM) classifier algorithms. A comparative study is made between these two methods and the results infer that SVM based classification outskirts its counterpart.

Keywords: Rice, Neural Network, Support Vector Machine, Colour Feature, Geometric Features.

© 2019 by Advance Scientific Research. This is an open-access article under the CC BY license (http://creativecommons.org/licenses/by/4.0/)
DOI: http://dx.doi.org/10.31838/jcr.07.01.79

INTRODUCTION

India is the second largest cultivator of rice through approximately 44 million hectares of land. 65% of Indian population eats rice and it accounts to 40% of the rice production. About 50 million of households rely on rice cultivation as main source of income and employment. Currently, 6000 rice varieties are being cultivated in India. Out of these the major rice variety cultivated in south India includes, polished white rice (ponni), brown rice, Palakkad matta rice, fragrant biryani rice and Kavuni (Black) rice. The quality of rice depends on moisture content, grain purity, cracks, presence of immature grains, grain dimensions, whiteness, milling degree and chalkiness. Of these parameters, grain purity, dimensions and cracks are the main features that decide the grade of the rice and cost. So, the correct assessment of quality of rice is an important task. The analysis of type of grain, grading and assessing the quality attributes are being done manually.

Manual checking process is more complex. It depends on working condition, human factors, rate of cleaning and recovery salvage. The other factors that affect rice quality include addition of impurities viz. stones, damaged seeds and broken granules. The accuracy of manual inspection through human inspectors is less, and so the possibility of mix up of impurities is more. This deteriorates the quality of rice. Also manual checking is tedious as it subjected to the operator concentration and time consuming. Sample testing method makes the testing more costly. In order to overcome these difficulties, image processing based automated classifier systems are designed to test the quality of rice grains.

RELATED WORKS

The quality of food grains play a vital role for healthy life, which is affected by increase in world population and climate change. High quality and safety standards are being entrusted by the governments to maintain healthy life. Manual inspection system is being used for the past few decades. Checking the quality of food and agriculture products through human inspection are problematic and labor concentrated. The system makes a random or sample checking from large batches. This is more time consuming and inconsistent due to lack of trained labors. These lead to huge variations during the analysis and classification of rice grains. Many researchers aimed for automated systems based on image processing techniques. Bhagyashree Mahale & Sapna Korde (2014) utilized edge detection algorithm and analyzed the quality of rice grains through grain size and shape. Morphological features have been used to train the network and their proposed system identified grain type, impurities and assessed the quality accurately.

Megha Sidhagangappa & Kulkarni (2014) developed a mobile application to grade the varieties of jowar using android emulator. This application utilizes MATLAB tool for preprocessing the image, segmentation and feature extraction. Based on the results of these processes, the established system graded the jowars. Convolution Neural Network (CNN) based approach has been presented by David Attokaren et al (2015), to classify the food grains. CNN utilizes the pixels to estimate the score function, using which the features of the images are extracted. This system resulted with an accuracy of 86%. Vidya Patil & Malemath (2015), investigated logic algorithm based model for assessing the quality of rice grains. OpenCV library has been implemented to diagnose and classify externally diseased fruits by Ashwini Awatae (2015). In order to segment the image of the fruits, the system of study used K-means clustering method. Pattern matching and disease classification are assisted by Artificial Neural Network (ANN) techniques. Aran M O et al (2016) proposed a computer based machine vision automated system to pattern and classify the types of cashew nuts. The researchers utilized the features viz. colour, texture, size and shape for grading the grains and Back Propagation Neural Networks (BPN) to classify them. Probabilistic Neural Network (PNN) based grain type identification has been addressed by Poornima Dered & Shanmukhappa Angadi (2016). Color and the geometrical features of the grains are used to classify the type of grains in this system.

In the review carried out by Abhishek Gudipalli et al (2016), machine vision based techniques have been utilized to measure the quality of grains and identifying the adulteration content in them. Rice is the food grain taken up for stud and the rice grains are detected and graded using canny edge detection method. During the year 2017, Depika Sharma & Sharad Sawant determined quality of rice grains through NN classifier. They developed an experimental setup in order to demonstrate the working of their proposed system. Digital image analysis algorithm based on color and morphological features has been developed by Mansi Kulkarni & Soni (2017). In their study, the developed algorithm has been applied to identify variety of rice seeds

planted in Zhejian Province. The aimed algorithm holds good for the application as it resulted better accuracy. In India, Agmark is a standard certification employed for agricultural products. Dipnakar Mandal (2018), estimated the quality of rice as per the present Agmark standards using image processing principles, through MATLAB. The limitations in manual rice grain quality assessment system is its relative grading, time consuming, cost and varying results. These parameters have been addressed by Kucheker & Yerigeri (2018) and they suggested that digital image processing technique will be the suitable solution for the same.

From the aforementioned literature studies, it is evident that quality of rice grains plays an important role in human health. The manual inspection method of assessing the quality of rice grains possess certain drawbacks which include tedious, time consuming, inaccuracy, eye irritation and other health problems which affect the evaluation process. In order to overcome these entire drawbacks image processing based rice grain quality assessment system has been proposed in this research work.

PROPOSED METHODOLOGY

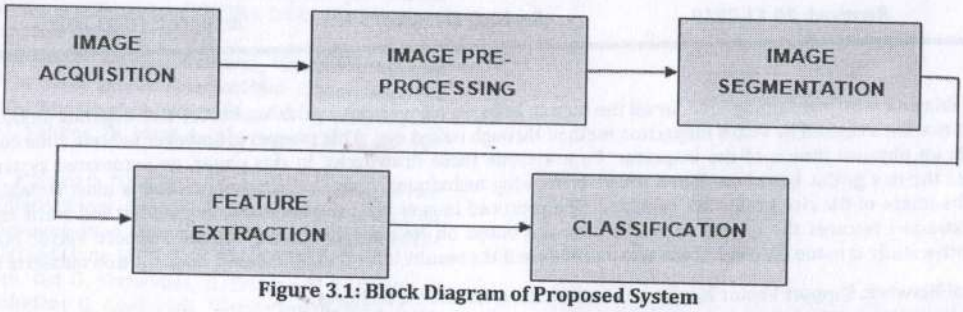


Figure 3.1: Block Diagram of Proposed System

The block diagram of the proposed automated rice quality assessment system is portrayed in Figure 3.1. The system includes image acquisition, pre-processing, segmentation, morphological feature extraction viz. geometrical structure & shape and classification process. In order to classify the rice grains ANN and SVM based algorithms have been used in this research work.

Image Acquisition

The image of the rice grains are acquired through high quality camera sensor system. The minimum prescribed pixel to be used is 8 MB, as it determines the quality of fine grains of rice and the overall efficiency of the system. Sample images of rice granules are captured and stored for training and testing purposes. Figure 3.2 (a) shows the sample rice grain image.

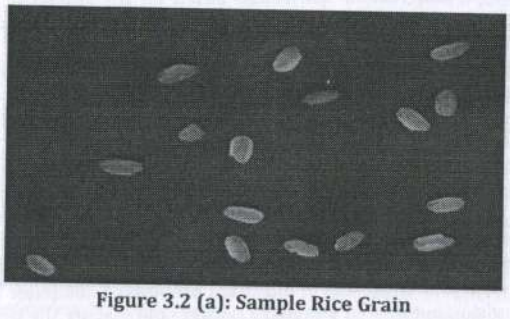
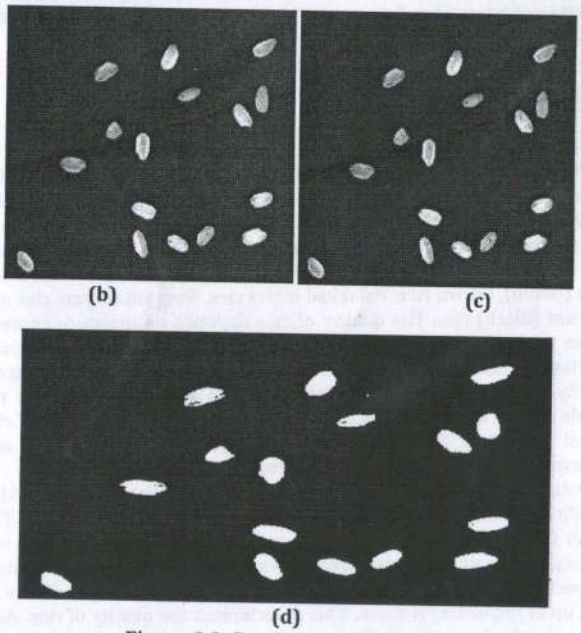


Figure 3.2 (a): Sample Rice Grain

Image Pre-Processing

Image pre-processing is the phenomenon where the images are resized, contrast of the images are adjusted as in Figure 3.2 (b) and the image is converted into gray scale, as in Figure 3.2 (c) and finally into black and white as shown in Figure 3.2 (d). These processes help to remove the unwanted distortions, noise and blur in the image, resulting in enhanced quality image, suitable for further processing.



(b) **(c)**

(d)

Figure 3.2: Pre-Processed Images

Image Segmentation

Segmenting the image into several parts assist to locate the objects and boundaries in an image. The objects and its boundaries are located by assigning labels to each pixel with similar characteristics. Once the image is pre-processed, the Region Of Interest (ROI) is segmented out from the image. Figure 3.3 depicts the segmented image.

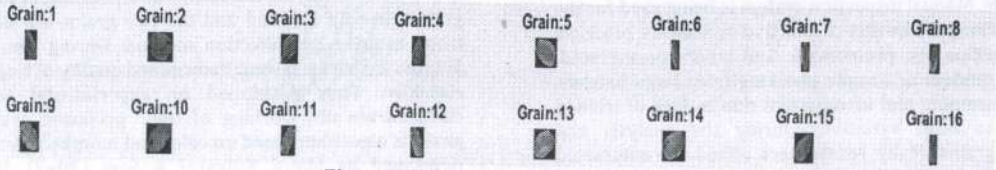


Figure 3.3: Segmented Rice Grains

3.4 Feature Extraction

Features define the behavior of an image which in turn affects the storage space occupied, classification efficiency and time consumption. The features of rice image include geometrical features viz. area, perimeter, major and minor axes and morphological features viz. mean values of Red, Green and Blue. These features are extracted and stored as knowledge base for training and testing purposes during classification process. Based on these features the rice variety and its types are identified. Figure 3.4 depicts the kernel of the rice grain showing the features.

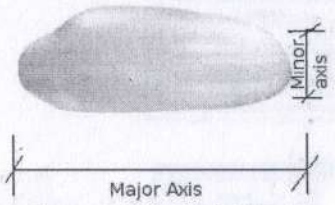


Figure 3.4 Rice Grain Kernel

Classification

Classification is the approach by which images are grouped into different classes based on the features extracted from them. In this research work, ANN and SVM classifier algorithms have been used to classify the rice grains and the results have been compared.

ANN Based Classification

ANN classification system is inspired by biological nervous system which composes of multiple nodes, emulating biological neurons of human brain. The nodes or neurons are connected and interact with each other. The nodes accept the input data, process them and transform them to other neurons as output through the link. Each link will have its own weightage, which could be modified. The output at each node is processed through the weight. The layer in between the input and output is called as hidden layer, which performs computations on weighted inputs and produce the net input. The net input is then applied with activation function to produce the actual output. The number of hidden layer is usually one or can be 2/3 of the sum of input and output nodes. During passing form input to output layer, the network randomly adds some weight and the result is passed to the successive nodes. The final output is compared with the target. If unmatched, it propagates backwards and alter the weights until the output is matched with the target. Figure 3.5 portrays the ANN architecture.

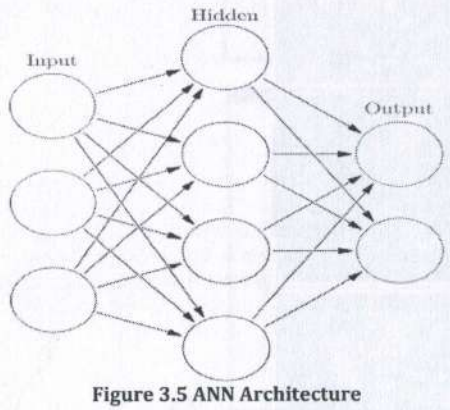


Figure 3.5 ANN Architecture

SVM Based Classification

Support Vector Machine can be employed for classification and regression purposes. It is a supervised learning method. It utilizes, support vector which are the data points of data set nearest to the hyper plane. If the data set is removed, it alters the position of the dividing hyper plan. Figure 3.6 illustrates Support Vectors and hyper plane. The distance between the hyper plane and nearest data point from either set is called as margin. The objective is to choose a hyper plane with highest margin in a training set, such that a new data is being classified correctly. Once the features are extracted from the images, the inputs are labeled as predictors and outputs as response.

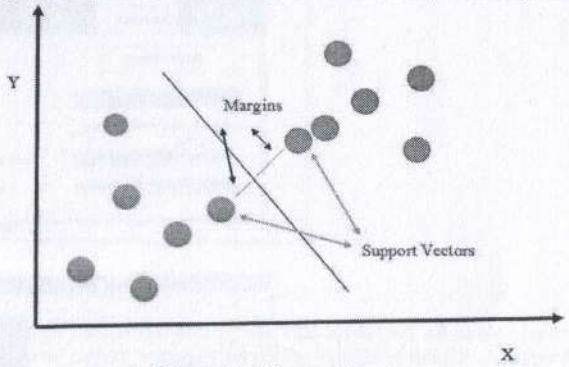


Figure 3.6: Support Vectors

EXPERIMENTAL ANALYSIS AND RESULTS

The process flow proposed automated rice grain quality assessment system based on ANN and SVM has been depicted in Figure 4.1.

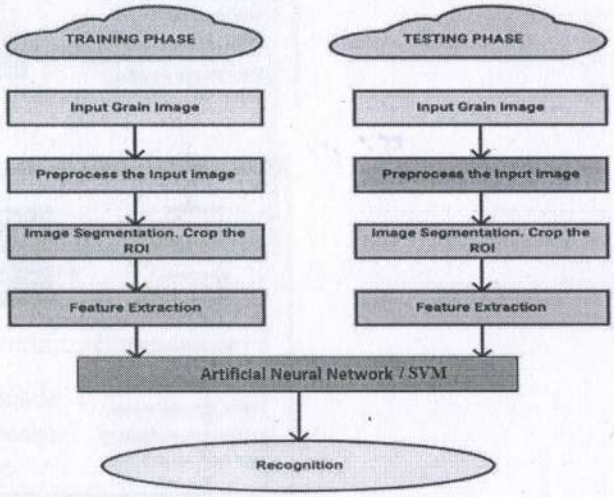
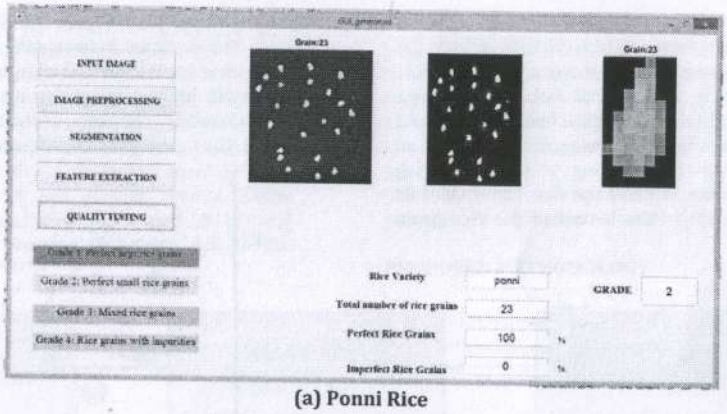


Figure 4.1: Process Flow Chart

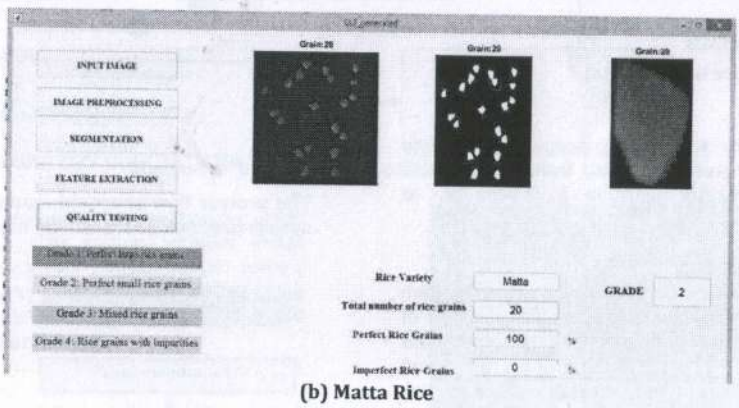
Two commonly used rice varieties are taken up for study viz. Matta and Ponni. They are classified into four grades as given in Table 1. The Mean values of RGB of different images are used to classify the rice as Ponni and Matta rice. Test results are depicted in Figure 4.2. (a) for Ponni variety and Figure 4.2 (b) for Matta rice. The geometrical features are used to grade the rice grains as grade 1, grade 2, grade 3 & grade 4. The results are shown in Figure 4.2 (c) for grade 1, 4.2 (d) for grade 2 and 4.2 (e) grade 4.

Table 1: Grade of Rice Grains

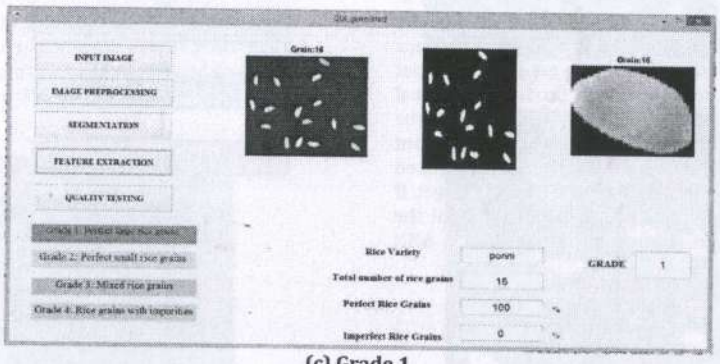
Grade	*Type*
1	*Perfect large rice grains*
2	*Perfect small rice grains*
3	*Imperfect (Mixed) rice grains*
4	*Rice grains with impurities*



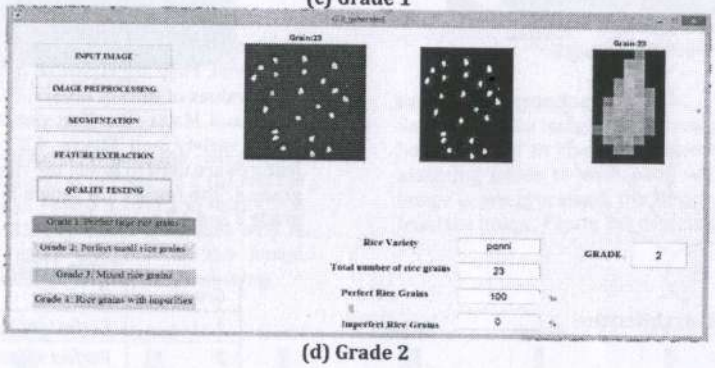
(a) Ponni Rice



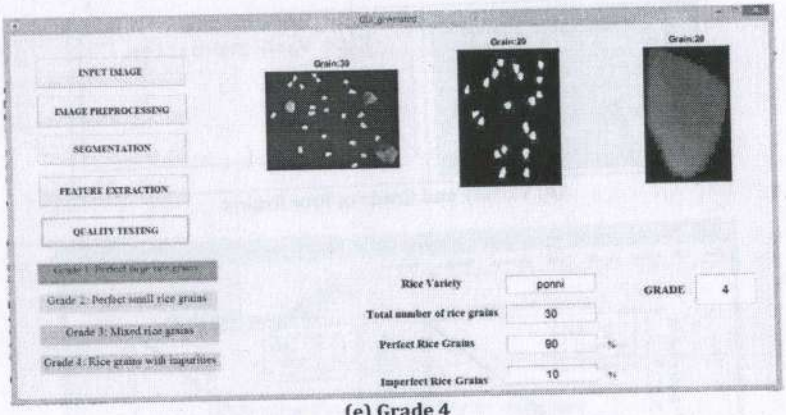
(b) Matta Rice



(c) Grade 1



(d) Grade 2



(e) Grade 4

Figure 4.2: Test Results for Rice Variety and Grades

Results of ANN Classifier

The rice grains classification system are carried out using nntool box of MATLAB. Seven data set has been used in NN classifier system. Figure 4.3 shows the ANN framework used in this research work. 7 features have been considered as inputs, whereas the rice quality and variety have been considered as outputs. This model has 48 hidden layers, as to achieve highest accuracy level. The results of the NN classifier have been depicted in Figure 4.4.

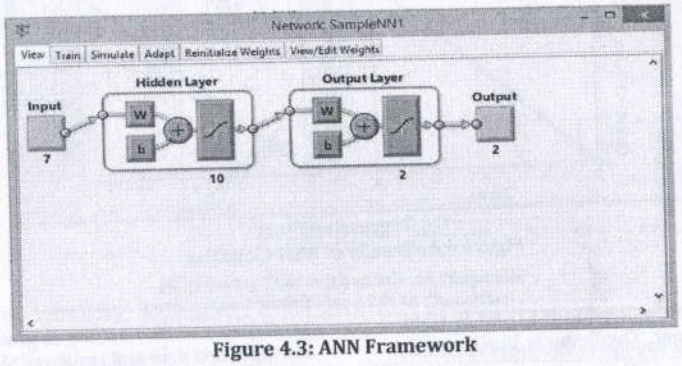
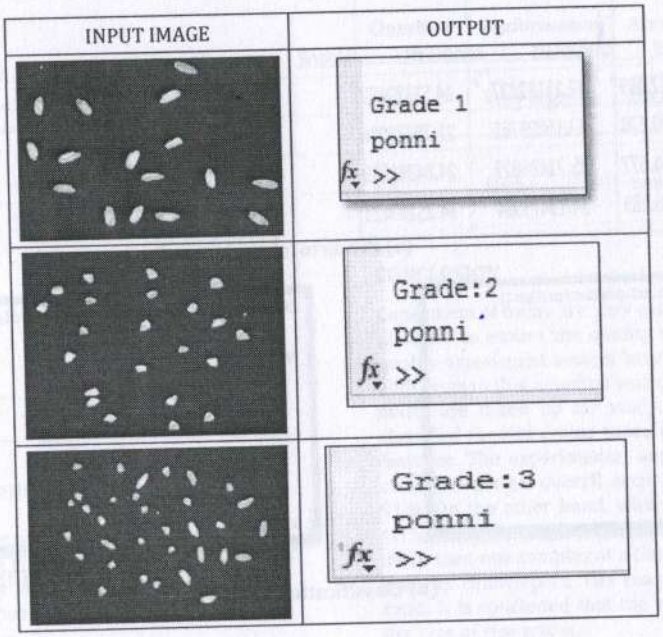
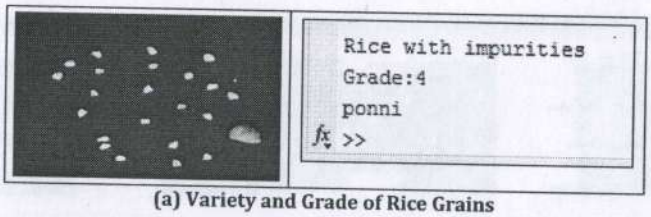
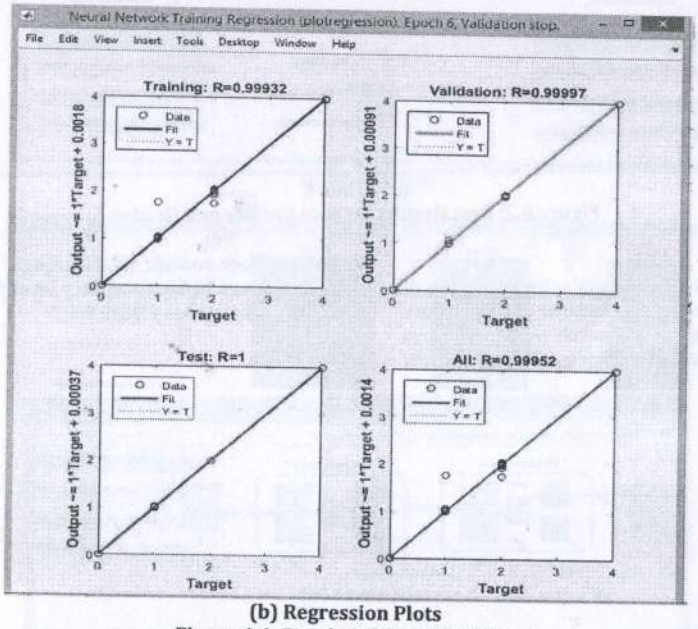


Figure 4.3: ANN Framework





(a) Variety and Grade of Rice Grains



(b) Regression Plots

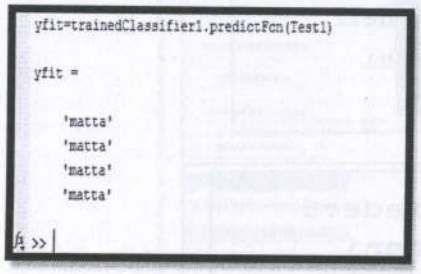
Figure 4.4: Results of ANN Classifier

Results of SVM Classifier

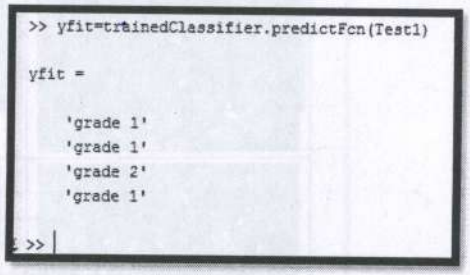
The features extracted are tabulated and utilized in MATLAB to train the classification learner and SVM trainer. The features like major & minor axes, area, perimeter and mean RGB are considered as predictors and rice variety & grade are responses. Figure 4.5 depicts the input test data and results of SVM classifier.

Area	Perimeter	MajorAxis	MinorAxis	MeanR	MeanG	MeanB
428	127.039	42.13192327	14.51272387	15.048	8.1333	12.8241
713	100.674	42.16829761	21.75631096	15.048	8.1333	12.8241
692	94.677	35.71486629	24.84381539	15.048	8.1333	12.8241
900	296.289	54.19479984	34.25243423	15.048	8.1333	12.8241

(a) Predictors

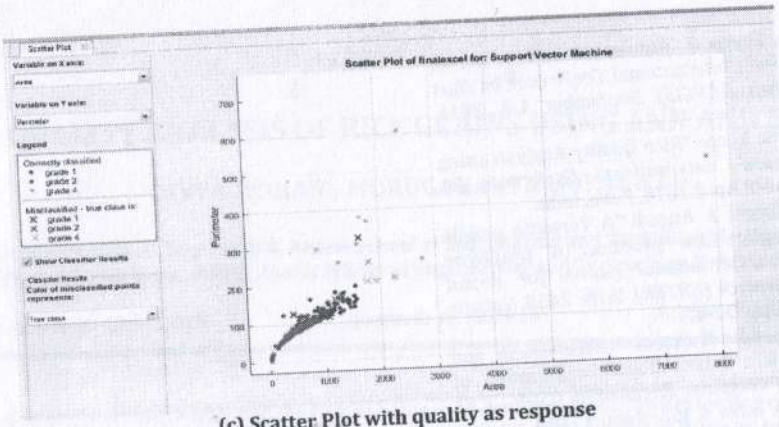


(i) Variety

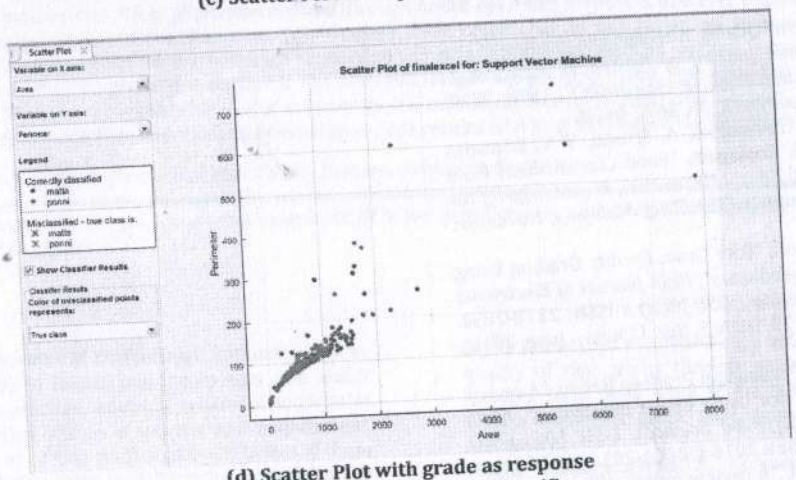


(ii) Grade

(b) Classification



(c) Scatter Plot with quality as response



(d) Scatter Plot with grade as response

Figure 4.5: Results of SVM Classifier

COMPARATIVE ANALYSIS

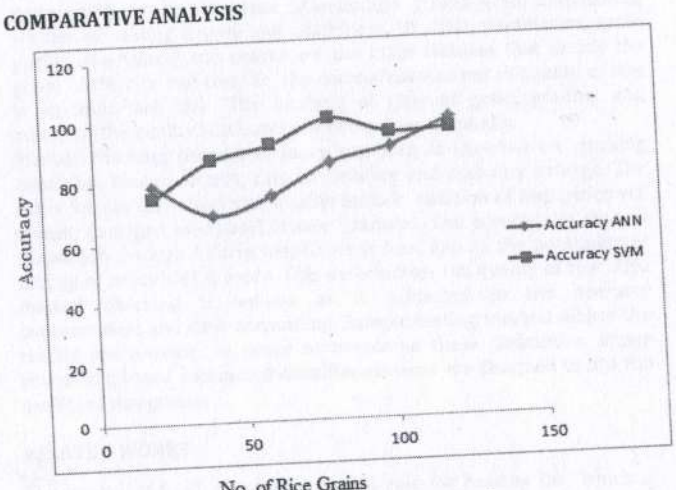


Figure 5.1: Comparative Analysis

A comparative analysis has been made between ANN and SVM Classifier algorithms on the samples of rice grains. Figure 5.1 portrays the comparative analysis of accuracy level resulted from both the classifiers and other parameters have been tabulated in Table 2.

Table 2: Comparison between Results of ANN and SVM Classifiers

Classifier	Performance	Accuracy	Classification	Time consumption for training
SVM	Very high	High	One type of classification at a time	low
NN	High	Less	More than one type of classification at a time	high

CONCLUSION

Consumers of today are very conscious about the quality of food grains. In order to ensure the quality of rice grains, an automated rice grain quality assessment system based on ANN and SVM classifiers has been addresses in this research work. Two types of rice grains viz. Ponni and Matta are taken up for study. The proposed system identified and classified the rice grains based on their morphological and geometrical features. The experimental analysis showed that the proposed ANN classifier has an overall accuracy of 83%, whereas SVM resulted in 91%. On the other hand, when the other parameters are considered, such that the computational time and parallel processing (classifying more than one samples at a time), the performance of SVM is far better than its counterpart. The reasons may be due to imbalance training ratio. It is concluded that the proposed system can effectively classify the type of rice grains.

REFERENCES

1. Aran M.O, Aneesh G Nath, Shyna A "Automated cashew kernel grading using machine vision", *International Conference on Next Generation Intelligent System (ICNGIS)*, September 1-3, 2016, Kottayam, India.
2. Bhagyashree mahale & Sapna korde "Rice Quality Analysis using image processing techniques", *International Conference for Convergence for Technology*, 6-8 April 2014, Pune, India.
3. Poornima Dered, Shanmukhappa A Angadi "A Versatile mobile application for grading agriculture produce: A prototype implementation for Jowar", *International Journal for Recent Trends in Engineering and Research (IJRTER)*, ISSN: 2455, Volume 02, Issue 09 September 2016, pp. 39-47.
4. Megha R Sidhagangappa & A.H. Kulkarni "Classification and quality analysis of food grains International Organization of Scientific Research. *Journal of Computer Engineering (ISOR - JCE)*, ISSN: 2278- 0661, Volume 16, Issue 4, July-August 2014, pp. 48–55.
5. Vidya Patil & V.S. Malemath "Quality Analysis and grading of rice grain images", *International Journal of Innovative Research in Computer and Communication Engineering (IJIRCCE)*, ISSN: 2320-9801, Volume 3, Issue 6, June 2015, pp. 5672-5678.
6. David J. Attokaren, Ian G. Fernandes, A. Sriram, Y. V. Srinivasa Murthy, and Shashidhar G. Koolagudi, "Food Classification from Images Using Convolutional Neural Networks", *Proceedings off the 2017 IEEE Region 10 Conference (TENCON)*, Malaysia, November 5-8, 2017.
7. N.A. Kuchekar & V.V. Yerigeri, "Rice Grain Quality Grading Using Digital Image Processing Techniques", *IOSR Journal of Electronics and Communication Engineering (IOSR-JECE)* e-ISSN: 2278-2834, p- ISSN: 2278-8735.Volume 13, Issue 3, Ver. I (May. – June. 2018), PP 84-88.
8. Abhishek Gudipalli, AmuthaPrabha and Pradeep Reddy, "A review on analysis and grading of rice using image processing", *ARPN Journal of Engineering and Applied Sciences*, ISSN 1819-6608, Volume 11, Issue 23, DECEMBER 2016 ©2006-2016, pp. 578-586.
9. Mansikulkarni and P. M. Soni, "A review on identification of rice grain quality using MATLAB and neural network", *International Journal of Innovations in Engineering Research and Technology (IJIERT)*, ISSN: 2394-3696, Volume 4, Issue 1, January 2017, pp. 237 – 243.
10. Dipankar Mandal, "Adaptive Neuro-Fuzzy Inference System Based Grading of Basmati Rice Grains Using Image Processing Technique", *Applied System Innovation*, ISSN: 2571-5577, DOI: 10.3390/asi1020019, 2018.
11. Ashwini Awate, Damini Deshmankar, Gayatri Amrutkar & Utkarsha Bagul, "Fruit Disease Detection Using Colour, Texture Analysis and ANN", *International Conference on Green Computing and Internet of Things (ICGCIoT)*, Noida, India, 8-10 October 2015.
12. Deepika Sharma & Sharad D Sawant, :Grain Quality Detection by using Image processing for public distribution:, *International Conference on Intelligent Computing and Control Systems (ICICCS)*, Madurai, India, 15 – 16 June 2017.

Performance Analysis of PSO Based Congestion Control Scheme in Wireless Sensor Networks

Vidhya Rathinasamy, Murugananth Gopal Raj

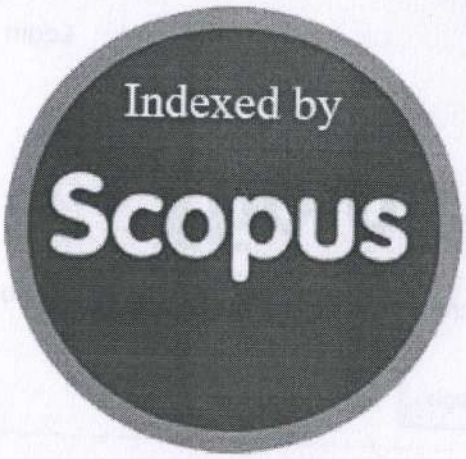
Abstract

Owing to the characteristics viz. smart sensor nodes, reduced cost and smaller size, Wireless Sensor Networks (WSN) are used for applications like environment observation and health care monitoring. The major problem identified with WSNs employing large number of sensor nodes is congestion. Congestion results in large number of packet drops, low through put and more energy consumption. In order to overcome these drawbacks, Particle Swarm Optimization based Congestion Control Scheme (PSOBCC) has been proposed in this paper. The simulation analysis of the proposed PSOBCC inferred that the aimed system effectively controlled the traffic, reduced the energy consumption and increased the packet delivery ratio.

PDF

Issue
Vol. 63 No. 5 (2020)

Section
Articles



0.3 2019 CiteScore

9th percentile

Powered by Scopus

Make a Submission

Downloads

- Copyright Transfer Form
- Paper Template

Important Links

- Home
- Aims and Scope
- Paper Topics
- Call for Papers
- Instructions for Authors
- Archive
- Download
- Ethics & Policies
- Publication Ethics and Publication Malpractice Statement
- Peer Review Policy
- Plagiarism Policy
- Copyright, Grants and Ownership Declaration
- Refund Policy
- Open Access Overview

Open Access License

Permissions

Subscription

Login to access subscriber-only resources.

World Health Organization Public Service Announcement Google



STAY HOME. SAVE LIVES.

Help stop coronavirus

1 **STAY** home as much as you can
2 **KEEP** a safe distance
3 **WASH** hands often
4 **COVER** your cough
5 **SICK?** Call ahead

General public health information

Copyright © by Solid State Technology

Antlion Optimization Algorithm Controlled Chopper Driven PMDC Motor

Murugananth Gopal Raj, Ahalia School of Engineering & Tech, Palakkad, Kerala. E-mail: gmuruganantth@gmail.com

K. Samidurai, Jaya Engineering College, Chennai, Tamilnadu.

S. Muthuksirhsnan, Sree Sathyam College of Engineering and Technology, Sankari, Tamilnadu.

A. Manickavasagam, Ahalia School of Engineering & Tech, Palakkad, Kerala.

Abstract--- Linear speed-torque characteristics feature of PMDC motor makes it to be used in orthopedic surgeries widely. The PI controller based conventional speed control schemes employed for PMDC motor has the disadvantages of poor steady and transient state characteristics. Several algorithms have been attempted to enhance the performance of this speed control system so far. This paper proposes antlion based meta heuristic algorithm embedded speed control system to improve the performance of the chopper driven PMDC motor. The proposed scheme determines the optimum pulse width required to drive the chopper circuit and controls the speed of the motor. Simulation studies of the proposed model using Matab/Simulink reveals its improved steady and transient state characteristics.

Keywords--- Antlion, Ants, ALO, Building Trap, Elitism, Random Walk, PMDC Motor, Steady State, Transient State.

I. Introduction

In orthopedic surgeries, Permanent Magnet DC (PMDC) motors are being used as it exhibits linear speed-torque characteristics. These motors find wide applications in bio-medical engineering which includes robot manipulators, surgical simulators etc. These applications need precise control of speed for some of the load conditions. Using the surgical simulators, novice surgeons practice Osteosynthesis, which is the phenomenon of joining fractured bones with metal rods and screws. They practice Osteosynthesis in cadaver bones using motorized tools. Conventional chopper driven PMDC motor are employed in these motorized tools.

Many researchers have developed various efficient training tools for Osteosynthesis. Micro-vibrated robot based controller developed by Shih-Tseng Lee et al (2001) is most popular among them. This micro-vibrated model used PMDC motor with current feedback control loop for drilling and tightening purposes. A computer assisted training simulator was proposed by Ming-Dar Tsai et al (2007). Thomas (2008) fabricated an automatic screw driver and Ann Majewicz et al (2011) designed and developed a haptic simulator. All these tool kits utilized chopper driven PMDC motor and assisted the novice surgeons to practice surgical operations easily.

In general, torque and speed are the required parameters to drill the bones and insert the screws in bones. The values of these parameters vary depending on the nature of the bones and mode of operation as well. Drilling and Screwing are the two modes of operation that require different speed and torque values. Drilling needs less torque, whereas screwing and tightening need more. Careful operation of these modes is needed; else it may lead to additional fracture in the bones. At the outset, precise control of PMDC motor is required to provide efficient training.

Several control algorithms have been suggested and developed by various researchers for the speed control of PMDC motor. The problems associated with these algorithms are undesirable overshoot and longer settling times. As the surgical operations are carried out only for a very short duration, the control system is expected to provide stable operation within a brief settling time. To have these features, this paper suggests a meta heuristic algorithm based on Antlion phenomenon for the speed control of PMDC motor. The proposed algorithm provides enhanced transient and steady state stability of the system of interest.

II. Related Works

The computer assisted orthopedic surgical simulators employed with PMDC motor consist of a chopper drive to control the motor operation. Nitai Pal et al (2012) suggested chopper driven PMDC motor for rock drilling applications. Murugananth and Vijayan (2012) analyzed the performance of chopper driven PMDC motor with

DOI: 10.5373/JARDCS/V12SP4/20201592
ISSN 1943-023X
Received: 18 Feb 2020/Accepted: 16 Mar 2020

conventional PI, PID and anti-wind up controllers. Low cost microcontroller-based speed control technique has been proposed by Pithwa and Parek (2012). Image processing assisted robotic arm has been suggested by Vipul Gohil et al (2013) for the automated surgery applications. Fuzzy logic-based drive has been recommended for the performance enhancement by Murugananth and Vijayan (2015). Experimental results of fuzzy tuned anti-wind up PI controller devised by Murugananth, Samidurai et al (2015) validate its superior operating characteristics when compared to conventional PI controller. Genetic Algorithm and Brain Emotional Logic based intelligent Controller (BELBIC) have been suggested by Vijayakumar et al (2016) and Muthukrishnan et al (2016) to improve the performance of chopper driven PMDC motor. Murugananth and Manickavasagam (2019) proposed hybrid fuzzy tuned PI controller based on raindrop algorithm.

All these controllers were developed with a focus of improving the performance of chopper driven PMDC motor in respect of its steady and transient state operations. However, the performance of these controllers under variable load conditions is not appreciable. To overcome this problem, this study proposes a controller driven by antlion optimization based algorithm. The proposed controller aids to improve the transient and steady state performance of the chopper drive system to a significant extent even under the variable load conditions.

III. Conventional Drive System

The equivalent circuit and its mathematical model of the PMDC motor have been shown in Figure 1 and Figure 2 respectively. The model has been developed using the equations (1) to (4).

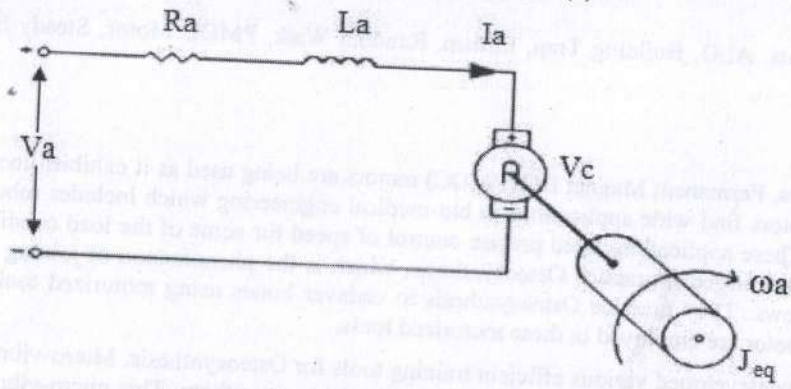


Figure 1: Equivalent Circuit of PMDC Motor

$$Va = Vc + IaRa + La\frac{dIa}{dt} \quad (1)$$

$$Vc = K_1 \omega a \quad (2)$$

$$T_E = T_L + B\omega a + J\frac{d\omega}{dt} \quad (3)$$

$$T_E = K_2 Ia \quad (4)$$

Where,

V_a - armature supply voltage in V
V_c - induced voltage in V
R_a - armature resistance in Ohms
L_a -armature inductance in H
I_a - armature current in A
K_1 -voltage constant in volts sec/rads
ω_a - angular speed in rads/sec
T_E - electromagnetic torque developed in Nm
T_L - load torque in Nm
J_{eq} - Moment of Inertia in $N.m^2/s^2$
B -damping Coefficient in Nms
K_2 - torque constant in Nm/A

DOI: 10.5373/JARDCS/V12SP4/20201592
ISSN 1943-023X
Received: 18 Feb 2020/Accepted: 16 Mar 2020

conventional PI, PID and anti-wind up controllers. Low cost microcontroller-based speed control technique has been proposed by Pithwa and Parek (2012). Image processing assisted robotic arm has been suggested by Vipul Gohil et al (2013) for the automated surgery applications. Fuzzy logic-based drive has been recommended for the performance enhancement by Murugananth and Vijayan (2015). Experimental results of fuzzy tuned anti-wind up PI controller devised by Murugananth, Samidurai et al (2015) validate its superior operating characteristics when compared to conventional PI controller. Genetic Algorithm and Brain Emotional Logic based intelligent Controller (BELBIC) have been suggested by Vijayakumar et al (2016) and Muthukrishnan et al (2016) to improve the performance of chopper driven PMDC motor. Murugananth and Manickavasagam (2019) proposed hybrid fuzzy tuned PI controller based on raindrop algorithm.

All these controllers were developed with a focus of improving the performance of chopper driven PMDC motor in respect of its steady and transient state operations. However, the performance of these controllers under variable load conditions is not appreciable. To overcome this problem, this study proposes a controller driven by antlion optimization based algorithm. The proposed controller aids to improve the transient and steady state performance of the chopper drive system to a significant extent even under the variable load conditions.

III. Conventional Drive System

The equivalent circuit and its mathematical model of the PMDC motor have been shown in Figure 1 and Figure 2 respectively. The model has been developed using the equations (1) to (4).

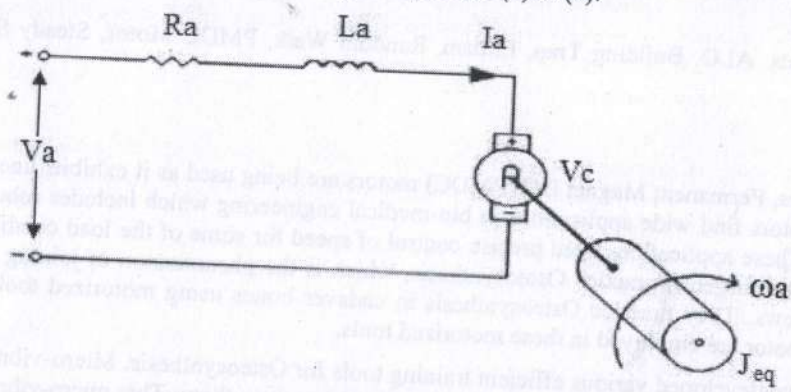


Figure 1: Equivalent Circuit of PMDC Motor

$$Va = Vc + IaRa + La\frac{dIa}{dt} \quad (1)$$

$$Vc = K_1 \omega a \quad (2)$$

$$T_E = T_L + B\omega a + J\frac{d\omega}{dt} \quad (3)$$

$$T_E = K_2 Ia \quad (4)$$

Where,

V_a - armature supply voltage in V
V_c - induced voltage in V
R_a - armature resistance in Ohms
L_a -armature inductance in H
I_a - armature current in A
K_1 -voltage constant in volts sec/rads
ω_a - angular speed in rads/sec
T_E - electromagnetic torque developed in Nm
T_L - load torque in Nm
J_{eq} - Moment of Inertia in $N.m^2/s^2$
B -damping Coefficient in Nms
K_2 - torque constant in Nm/A

DOI: 10.5373/JARDCS/V12SP4/20201592
ISSN 1943-023X
Received: 18 Feb 2020/Accepted: 16 Mar 2020

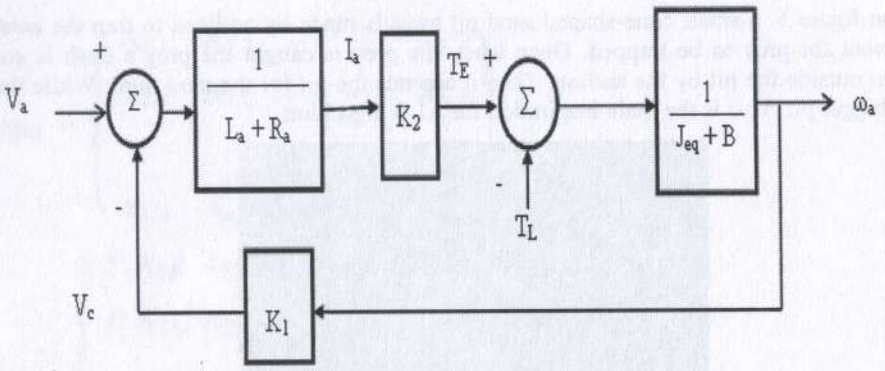


Figure 2: Mathematical Model of PMDC Motor

Figure 3 portrays the closed loop chopper drive proposed by Murugananth et. al (2012a & 2012b). This chopper drive utilizes a PI controller, whose gain values are tuned using Ziegler – Nichols method. The performance of this drive is not satisfactory in terms of peak overshoot and steady state error. Hence the antlion optimization algorithm based drive has been proposed for the significant improvement in performance.

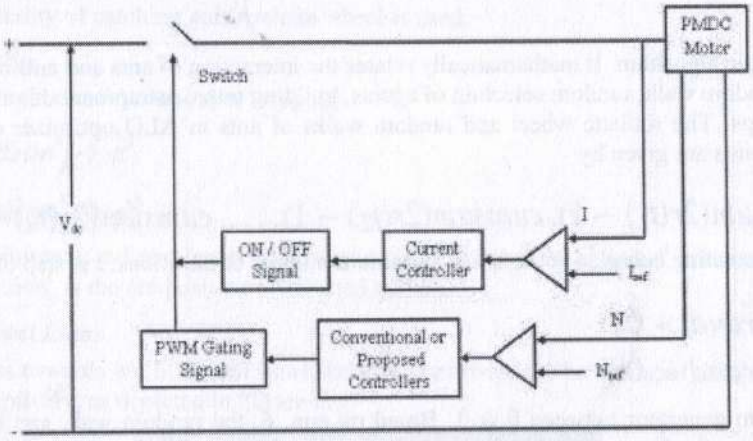


Figure 3: Chopper Driven PMDC Motor

IV. Antlion Optimization (ALO)

4.1 Background Study of ALO

Antlion Optimizer (ALO) has been proposed by Mirjalili and Seyedai (2015). Prasad and Ram (2016) proposed antlion optimization for the tuning of PID controller to achieve optimal speed control with torque ripple minimization of Synchronous Reluctance Motor (SRM) drive system. Kamaraj Premkumar et al (2017) suggested antion optimized fuzzy PID supervised on-line recurrent fuzzy neural network based controller for brushless DC motor. Dinakara Prasad Reddy et al (2018) applied ALO to fix the optimal location and size of DG sets to be integrated with distribution generation system. These studies led to the use of ALO to enhance the performance of the chopper driven PMDC motor used in orthopedic surgeries.

4.2 Life Cycle of Antlions

Antlions live in two phases: larva and adult. When they are in larva stage, their hunting mechanism is much interesting. Figure 4 (a) and 4 (b) depicts the larva and adult stages of antlions respectively.



(a) Larva (b) Adult

Figure 4: Life Cycle Stages of Antlions

DOI: 10.5373/JARDCS/V12SP4/20201592
ISSN 1943-023X
Received: 18 Feb 2020/Accepted: 16 Mar 2020

As shown in the figure 5, a small cone-shaped sand pit traps is made by antlions to trap the ants. Antlions sit under the pit and wait for prey to be trapped. Once when the prey is caught the prey's flesh is consumed. The leftovers are thrown outside the pit by the antlion. Then it amends the pit for the next hunt. While the antlions are hungry, they dig a bigger pit. This is the main inspiration for ALO algorithm.

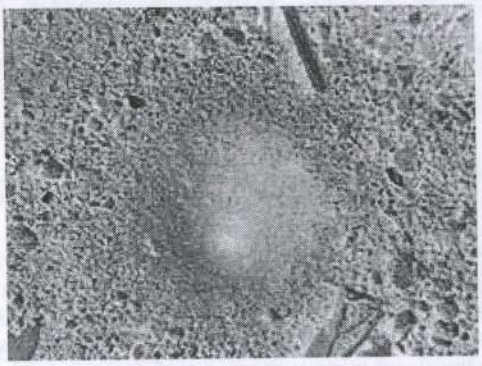


Figure 5: Sand Pit Trap

4.3 Antlion Optimization

ALO is a meta-heuristic algorithm. It mathematically relates the interaction of ants and antlions. It optimizes the problems based on the random walk, random selection of agents, building traps, entrapment of ants in traps, catching preys and re-building traps. The roulette wheel and random walks of ants in ALO optimizer can eliminate local optima. Random walk of ants are given by

$$X(t) = [0, \quad cumsum(2r(t_1) - 1), cumsum(2r(t_2) - 1), \ldots, cumsum(2r(t_n) - 1)] \tag{5}$$

Where, *cumsum* is calculating cumulative sum, n is maximum number of iterations; t is step of random walk.

$$r(t) = \begin{cases} 1 & if \quad rand > 0.5 \\ 0 & if \quad rand < 0.5 \end{cases} \tag{6}$$

Where, rand is random generator between 0 & 1. Based on eqn. 6, the random walk can be made inside the search space as given by eqn. 7.

$$X_i^t = \frac{(X_i^t - a_i) \times (d_i^t - c_i^t)}{(b_i - a_i)} + c_i^t \tag{7}$$

Where, a_i & b_i are the minimum and maximum values of random walk of i^{th} variable. c_i & d_i are the minimum and maximum of i^{th} variable in the t^{th} iteration. The location of ants and corresponding fitness function matrix are given below:

$$M_{Ant} = \begin{pmatrix} A_{1,1} & A_{1,2} & \cdots & \cdots & A_{1,d} \\ A_{2,1} & A_{2,2} & \cdots & \cdots & A_{2,d} \\ \vdots & \vdots & \vdots & \vdots & \vdots \\ A_{n,1} & A_{n,2} & \cdots & \cdots & A_{n,d} \end{pmatrix} \tag{8}$$

$$M_{OA} = \begin{bmatrix} f(A_{11}, A_{22}, \ldots, A_{1d}) \\ f(A_{21}, A_{22}, \ldots, A_{2d}) \\ \vdots \\ f(A_{n1}, A_{n2}, \ldots, A_{nd}) \end{bmatrix} \tag{9}$$

Where, M_{OA} represents fitness values of location of ants matrix M_{Ant}. If ants and antlions are hidden in search area then the corresponding location and fitness matrices of antlions are given by

DOI: 10.5373/JARDCS/V12SP4/20201592
ISSN 1943-023X
Received: 18 Feb 2020/Accepted: 16 Mar 2020

$$M_{Antlion} = \begin{pmatrix} A_{1,1} & A_{1,2} & \cdots & \cdots & A_{1,d} \\ A_{2,1} & A_{2,2} & \cdots & \cdots & A_{2,d} \\ \vdots & \vdots & \vdots & \vdots & \vdots \\ A_{n,1} & A_{n,2} & \cdots & \cdots & A_{n,d} \end{pmatrix} \quad (10)$$

$$M_{OAL} = \begin{bmatrix} f(A_{11}, A_{22}, \ldots, A_{1d}) \\ f(A_{21}, A_{22}, \ldots, A_{2d}) \\ \vdots \\ f(A_{n1}, A_{n2}, \ldots, A_{nd}) \end{bmatrix} \quad (11)$$

Where, M_{OAL} matrix represents fitness values of location of ant lions.

Building Trap

To get higher probability of catching ants roulette wheel is used.

Trapping in Ant Lion Pits

Eqn. 12 depicts the mathematical model of trapping

$$c_i^t = Antlion_j^t + c^t$$
$$d_i^t = Antlion_j^t + d^t \quad (12)$$

Where, c_i^t d_i^t are minimum and maximum of all variables at i^{th} iteration. c^t and d^t are minimum and maximum variables for i^{th} ant. $Antlion_j^t$ is the ant position of selected antlion.

Sliding Ants Towards Ant Lions

In order to slide ants towards ant lions, ant lions shoot sand outwards. The radius of ants' random walks hypersphere is decreased adaptively, as depicted in Figure 6.

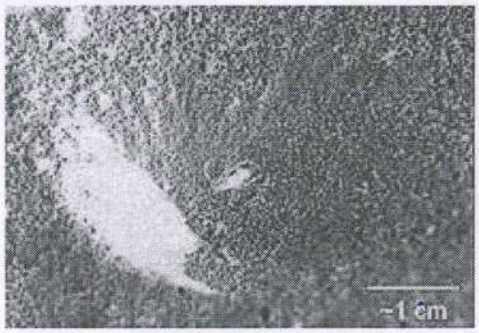


Figure 6: Sand Pit Traps with Remains of Ants

Equations 13 depict the mathematical model as

$$C^t = c^t/I$$
$$D^t = d^t/I \quad (13)$$

Where, I = 10 t/T, t is current iteration and T is maximum number of iterations.

Catching the Prey and Rebuilding the Pit

Antlion catches its prey when it becomes fitter than its associated antlion. After catching the prey the antlion update its position to the latest position of the hunted ant. This is expressed in eqn. 14.

$$Antlion_j^t = Ant_i^t \ if \ f(Ant_i^t) > f(Antlion_j^t) \quad (14)$$

DOI: 10.5373/JARDCS/V12SP4/20201592
ISSN 1943-023X
Received: 18 Feb 2020/Accepted: 16 Mar 2020

Elitism

Evolution algorithms are expected to provide best solutions. The best antlion obtained from the successive iterations is saved and considered as elite. It is the fittest antlion and should be able to affect the movement of the ants during iteration. It is assumed that every ant randomly walks around a selected antlion by the roulette wheel and the elite are given by eqn. 15.

$$Ant_i^t = \frac{R_A^t + R_E^t}{2} \tag{15}$$

Where, R^t_A and R^t_E are random walks near by the antlion by roulette wheel, elite at i^{th} iteration, Ant^t_i is the position of i^{th} ant at the end of t^{th} iteration

V. Proposed ALO Driven Chopper System

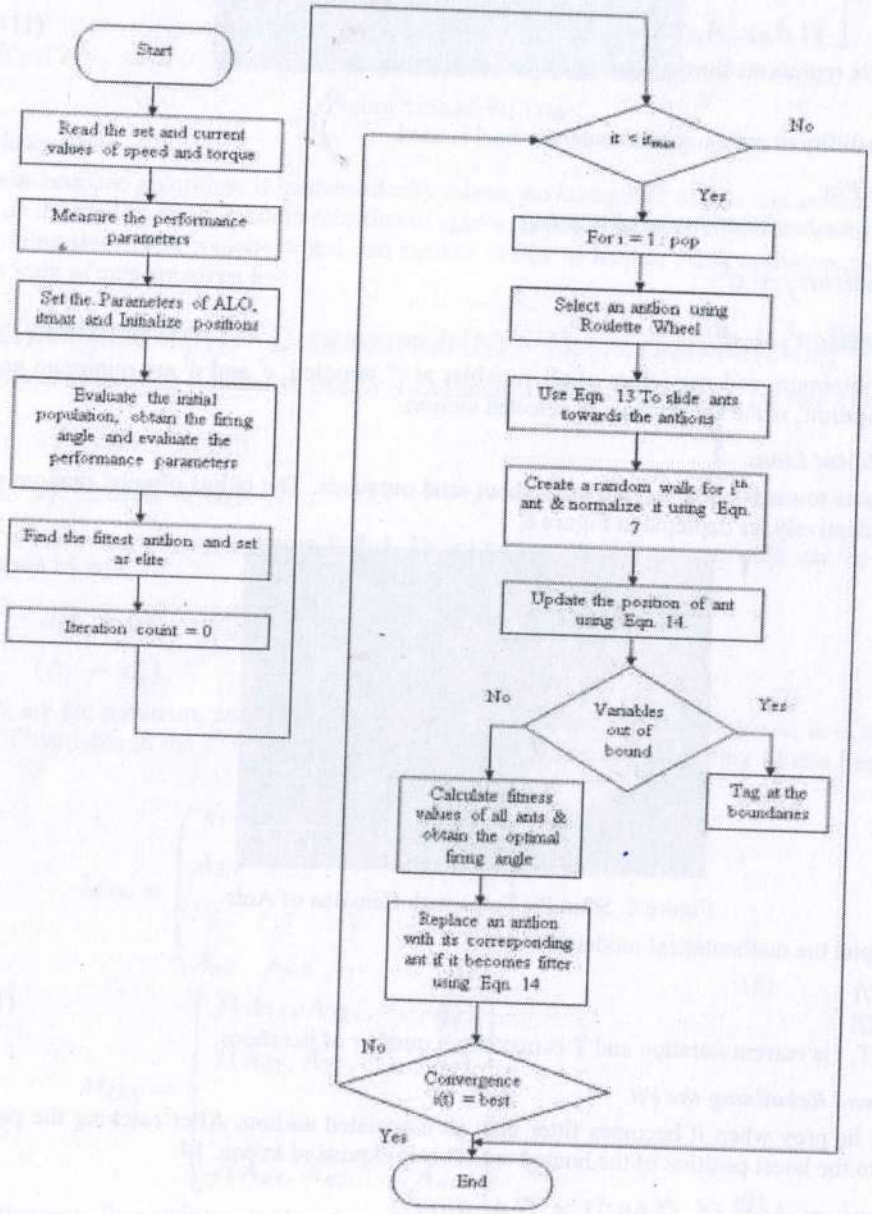


Figure 7: Flowchart of Proposed ALO Algorithm

DOI: 10.5373/JARDCS/V12SP4/20201592
ISSN 1943-023X
Received: 18 Feb 2020/Accepted: 16 Mar 2020

Figure 7 illustrates the flowchart of the proposed ALO algorithm to generate the appropriate pulse width. The pulses or control signals required for optimum speed are processed by the proposed algorithm. The current speed (rpm) and set speed (rpm) values are taken as input function to the system. The parameters for the ALO are fixed and the ant positions are fixed. The ants make random walk towards the prey. Cathces them and return backs to the pit. Once the antlion gets the prey it consumes it and throw the prey's flesh and amends the pit. By the same way, from the measured performance parameters, based on the equations 5 to 15, the control pulses are generated. The perfromance indices are peak overshoot, steady state error and integral error based on which the optimal switching pulse is obtained. When they are minimized, the optimal values are obtained. The optimum swithcing pulses offer lowest values of peak overshoot, steady state error and integral of absolute error which are the desired optimal soultions.

VI. Simulation Results

The response of the proposed system is given in Figure 8. The comparative analysis of the conventional PI and proposed ALO algorithm driven controller are depicted in Figure 9, for a set speed of 1000 rpm. It is evident from the analysis that the peak overshoot offered by the proposed system is reduced by 32.5% when compared with the conventional PI system. The peak overshoot of the proposed system is 14.7% whereas in the case of the conventional PI controller it is 21.4%.

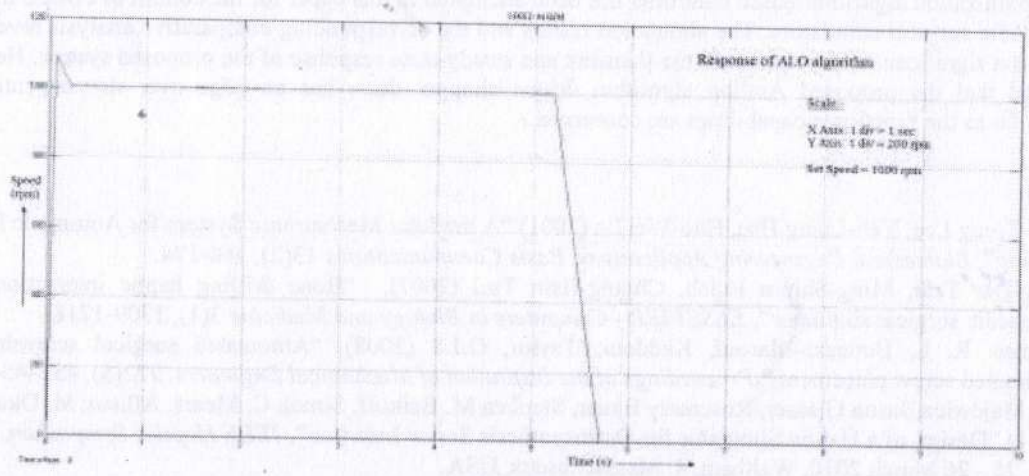


Figure 8: Response of ALO Algorithm

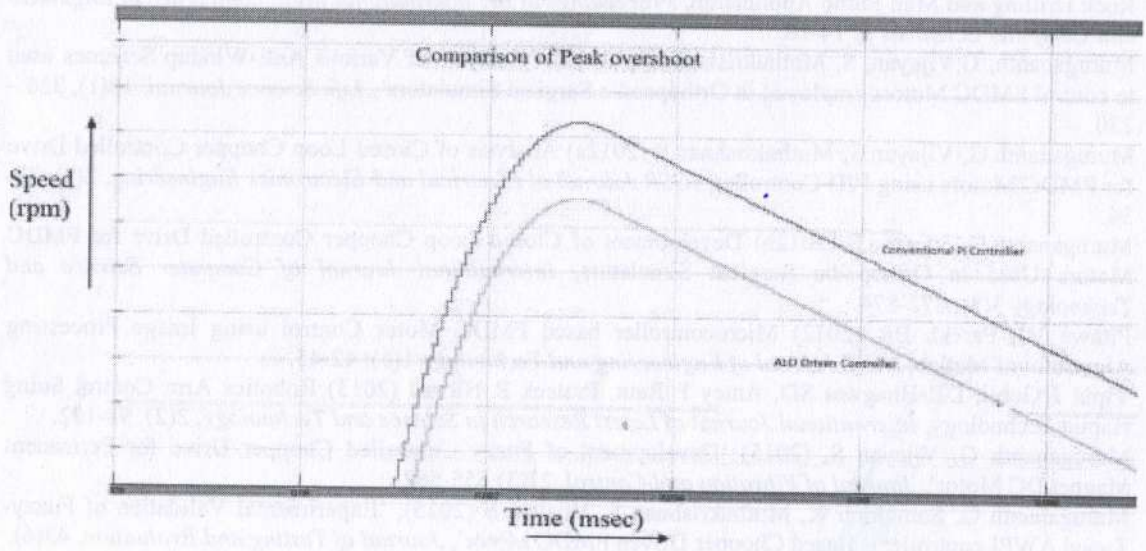


Figure 9: Peak Overshoot Comparative Analysis

DOI: 10.5373/JARDCS/V12SP4/20201592
ISSN 1943-023X
Received: 18 Feb 2020/Accepted: 16 Mar 2020

Table 1: Performance Comparison of Conventional PI and ALO Driven Controllers

Set speed rpm	Peak Overshoot %		Steady State Error		Integral Absolute Error	
	PI Controller	ALO Controller	PI Controller	ALO Controller	PI Controller	ALO Controller
750	24	16.2	11	6.3	9	4.5
1000	21.4	14.7	7.5	5.4	8.82	4.4
1200	20.2	12.6	7	4.2	8.2	3.9

The performance indices viz. peak overshoot, steady state error and the deviation in the error for various set speed values are tabulated for both the conventional PI and proposed ALO driven controller as in Table 1. It is observed that increase in set speed decreases the control parameters of interest. The proposed ALO driven controller reduces the peak overshoot offered by the conventional controller by 25% even at lower speeds. At higher speeds, it has been more than 33%. The proposed controller reduces the steady state error for about 30 to 35% at all speeds. 50% reduction of integral absolute error has been observed with the proposed controller compared to its conventional counterpart.

VII. Conclusion

Antlion Optimization algorithm-based controller has been attempted in this paper for the control of PMDC motor used in orthopedic surgical simulators. The simulation results and the corresponding comparative analysis revealed that the there is a significant improvement in the transient and steady-state response of the proposed system. Hence, it is concluded that the proposed Antlion algorithm driven chopper drive has an edge over its conventional counterpart as far as the functional capabilities are concerned.

References

[1] Shih-Tseng Lee, Yeh-Liang Hsu, Hao-Wei lin (2001) "A modular Mechatronic System for Automatic Bone Drilling", *Biomedical Engineering Applications, Basis Communications* 13(2), 168-174.

[2] Ming-Dar Tsai, Ming-Shium Hsieh, Chiung-Hsin Tsai (2007), "Bone drilling haptic interaction for orthopedic surgical simulator", *ELSEVIER - Computers in Biology and Medicine* 3(1), 1709-1718.

[3] Thomas. R. L, Bouazza-Marouf, Kaddour, Taylor, G.J.S (2008), "Automated surgical screwdriver: Automated screw placement," *Proceedings of the Institution of Mechanical Engineers,* 222(5), 451–454.

[4] Ann Majewicz, Jason Glasser, Rosemary Bauer, Stephen M. Belkoff, Simon C. Mears, Allison M. Okamur, (2011) "Design of a Haptic Simulator for Osteosynthesis Screw Insertion", *IEEE Haptics Symposium,* 497-500, 25 - 26 March 2010, Waltham, 4. Massachusetts, USA.

[5] Nitai Pal, Pradip Kumar Sadhu and Swaroop.R (2012) Closed Loop Speed Control of DC Motors used in Rock Drilling and Mud Pump Application, *Proceedings of the International Multi conference of Engineers and Computer Scientists* 2: 14-16.

[6] Murugananth, G,Vijayan, S, Muthukrishnan, S, (2012), 'Analysis of Various Anti-Windup Schemes used to control PMDC Motors employed in Orthopaedic Surgical Simulators', *Life Science Journal,* 10(1), 226 – 230.

[7] Murugananth.G, Vijayan.S, Muthukrishnan.S (2012a) Analysis of Closed Loop Chopper Controlled Drive for PMDC Motors using PID Controller, *IOSR Journal of Electrical and Electronics Engineering*, 2(3): 32-34.

[8] Murugananth.G, Vijayan.S (2012b) Development of Closed Loop Chopper Controlled Drive for PMDC Motors Used in Orthopedic Surgical Simulators, *International Journal of Computer Science and Technology* 3(3): 872-874.

[9] Pithwa VJ, Parekh BR (2012) Microcontroller based PMDC Motor Control using Image Processing Algorithm of Matlab, *NIET Journal of Engineering and Technology* 1(1): 42-45.

[10] Vipul J Gohil, DR Bhagwat SD, Amey P Raut, Prateek R Nirmal (2013) Robotics Arm Control Suing Haptic Technology, *International Journal of Latest Research in Science and Technology*, 2(2): 98-102.

[11] Murugananth G, Vijayan S, (2015) 'Development of Fuzzy Controlled Chopper Drive for Permanent Magnet DC Motor', *Journal of Vibration and Control,* 21(3) 555-562.

[12] Murugananth G, Samidurai K, Muthukrishnan S, Vijayan S (2015), 'Experimental Validation of Fuzzy-Tuned AWPI controller – Based Chopper Driven PMDC Motor', *Journal of Testing and Evaluation,* 43(6).

[13] Vijayakumar Thangavelu, Murugananth Gopalraj, Muthukrishnan S (2016) Genetic Algorithm based Speed control of PMDC motor using low cost PIC 16F877A microcontroller, *Circuits and Systems* 7: 1334-1340.

DOI: 10.5373/JARDCS/V12SP4/20201592
ISSN 1943-023X
Received: 18 Feb 2020/Accepted: 16 Mar 2020

[14] Muthukrishnan Subramainiam, Murugananth Gopalraj, Saravana Sundaram Sakthivelu (2016) BELBIC Tuned PI Controller Based Chopper Driven PMDC Motor, *Circuits and Systems* 7: 2273 – 2285.

[15] Murugananth Gopalraj, Manickavasagam Arumugam, "Fuzzy tuned Raindrop Algorithm Controlled Chopper Driven PMDC Motor:, *Journal of Engineering Technology,* ISSN No.: 0747-9964, Vol. 8, No. 1, pp. 235 – 242, January 2019.

[16] Mirjalili, Seyedali. "The ant lion optimizer." Advances in Engineering Software 83 (2015): 80-98.

[17] E. S. Prasad and B. V. S. Ram, "Ant-lion optimizer algorithm based FOPID controller for speed control and torque ripple minimization of SRM drive system," 2016 *International Conference on Signal Processing, Communication, Power and Embedded System (SCOPES), Paralakhemundi,* 2016, pp. 1550-1557.

[18] Kamaraj Premkumar, Bairavan Veerayan Manikandan & Chellappan Agees Kumar (2017) Antlion Algorithm Optimized Fuzzy PID Supervised On-line Recurrent Fuzzy Neural Network Based Controller for Brushless DC Motor, *Electric Power Components and Systems,* 45:20, 2304-2317.

[19] Dinakar Prasad Reddy, Veera Reddy, Gowri Manohar, "Ant Lion optimization algorithm for optimal sizing of renewable energy resources for loss reduction in distribution systems", *Journal of Electrical Systems and Information Technology,* vol. 5, 2018, pp. 663–680.

DOI: 10.5373/JARDCS/V12SP4/20201592
ISSN 1943-023X
Received: 18 Feb 2020/Accepted: 16 Mar 2020

Particle Swarm Optimization Algorithm Controlled Chopper Driven PMDC Motor

Murugananth Gopal Raj, Ahalia School of Engineering & Tech, Palakkad. E-mail: gmurugananth@gmail.com

C. Pradip, NSS College of Engineering, Palakkad.

N. Saju, NSS College of Engineering, Palakkad.

Abstract--- Permanent Magnet Direct Current (PMDC) motors are preferred widely in biological applications due to their linear speed torque characteristics. Conventional PI controller driven chopper drives are employed to control the speed torque characteristics of these motors. These drives suffer from poor steady state and transient state responses. To enhance their operation, this paper suggests Particle Swarm Optimization (PSO) based chopper drive system. The proposed system regulates the optimal pulse width required for the drive circuit. Simulation analysis of the proposed scheme of interest reveals the improved control system characteristics.

Keywords--- Chopper, Particle Swarm Optimization (PSO), Peak Overshoot, Steady State Error, Integral Absolute Error (IAE).

I. Introduction

Osteosynthesis is the process of joining fractured bones with the help of metal rods and screws. Motorized tools assist novice surgeons to practice it on the cadaver bones. Permanent Magnet Direct Current (PMDC) motor forms the basic component of this motorized tools system. Linear speed torque characteristics of PMDC motor makes them most suitable for these kind of applications. Their applications also include robot manipulators, surgical simulators, precise control systems etc. PMDC motor used in these tools are controlled via a conventional chopper drive system. Necessary pulses required to operate the conventional chopper are obtained through PI controllers.

Researchers focus on the development of competent chopper schemes for these motorized tools. Shih – Tseng et al (2001) developed the most popular micro-vibrated robotic controller. It utilized a feedback control approach for drilling and tightening of the screws on the bones. Ming-Dar Tsai et al (2007) designed a computer assisted trainer for Osetosynthesis. Automatic screw driver and haptic simulators have been proposed by Thomas (2008) and Ann Majewicz et al (2011) respectively. The mentioned motorized systems employ chopper driven PMDC motor to fix the fractured bones.

Torque and speed requirements govern the drilling and tightening of screws in the Osteosynthesis process. These requirements vary based on the nature of bones i.e. weak and strong and operating modes as drilling, screwing and tightening. Less torque is required for drilling, whereas more torque is required for screwing and tightening. Optimal speed and torque are essential as because, malfunctioning may lead to additional fracture in the bones. These constraints paved the path for precise control of PMDC motor in the motorized tool system.

In order to control the speed and torque requirements of the PMDC motor, numerous algorithms have been developed and suggested by researchers. The entire operation of drilling, insertion of screw and tightening takes place in a short span of time. Undesirable overshoot and larger settling times are the drawbacks offered by certain developed algorithms. Owing to these conditions, effective algorithm to provide stable operation is desired. This paper, suggests the Particle Swarm Optimization (PSO) based chopper control scheme for the PMDC motor.

II. Related Works

Chopper driven PMDC motor has been suggested by Nitai Pal et al (2012) for rock drilling applications. Analysis of PI, PID and anti-windup controllers employed for the chopper driven PMDC motor scheme has been studied by Murugananth and Vijayan (2012). Pithwa and Paerk (2012) proposed a low cost micro-controller based control technique. Vipul Gohil et al (2013) utilized image processing methods for robotic arm assisted surgical operations. Murugananth & Vijayan (2015) and Murugananth et al (2015) enhanced the performance of the fuzzy logic driven chopper drives and experimentally validated their results. Vijayakumar et al (2016) and Muthukrishnan et al (2016) improved the performance of the drive with Genetic Algorithm and Brain Emotional Logic based intelligent controllers respectively. Hybrid systems have been suggested by Murugananth and Manickavasagam

DOI: 10.5373/JARDCS/V12I7/20202033
ISSN 1943-023X
Received: 13 May 2020/Accepted: 15 June 2020

(2019). Murugananth et al (2020) optimized the chopper pulse width based on Antlion Optimization algorithm, for the chopper driven PMDC motor.

The aforementioned control systems have been developed with an aim to improve the performance of the PMDC motor drive scheme. The performance of these drives under varying load is not significant. In order to overcome this problem under both steady and transient state conditions, Particle Swarm Optimization (PSO) algorithm has been proposed in this paper. The scheme taken up for study has been simulated by subjecting it to various load conditions and the performance has been analyzed.

III. Conventional Drive System

The mathematical model of the PMDC motor has been developed based on the equations (1) to (4). Figure 1 and 2 illustrates the equivalent circuit and mathematical model of the PMDC motor system respectively.

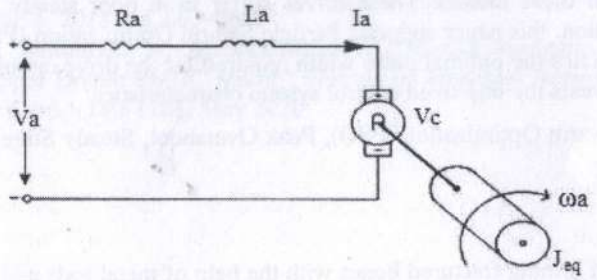


Figure 1: Equivalent Circuit of PMDC Motor

$$Va = Vc + IaRa + La\frac{dIa}{dt} \quad (1)$$

$$Vc = K_1 \omega a \quad (2)$$

$$T_E = T_L + B\omega a + J\frac{d\omega}{dt} \quad (3)$$

$$T_E = K_2 Ia \quad (4)$$

Where,

V_a - armature supply voltage in V
V_c - induced voltage in V
R_a - armature resistance in Ohms
L_a -armature inductance in H
I_a - armature current in A
K_1 -voltage constant in volts sec/rads
ω_a - angular speed in rads/sec
T_E - electromagnetic torque developed in Nm
T_L - load torque in Nm
J_{eq} - Moment of Inertia in $N.m^2/s^2$
B -damping Coefficient in Nms
K_2 - torque constant in Nm/A

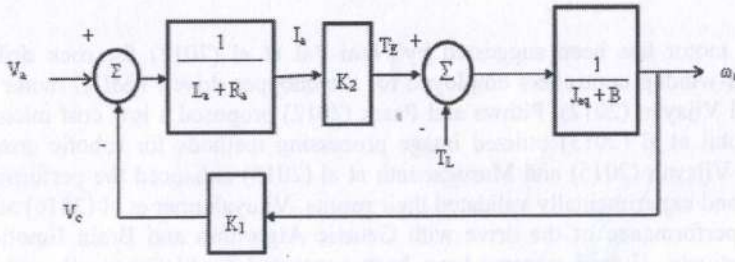


Figure 2: Mathematical Model of PMDC Motor

DOI: 10.5373/JARDCS/V12I7/20202033
ISSN 1943-023X
Received: 13 May 2020/Accepted: 15 June 2020

Murugananth et al (2012a & 2012b) proposed the closed loop chopper controlled drive based on conventional PI controller as portrayed in Figure 3. This drive scheme resulted in poor steady and transient state responses.

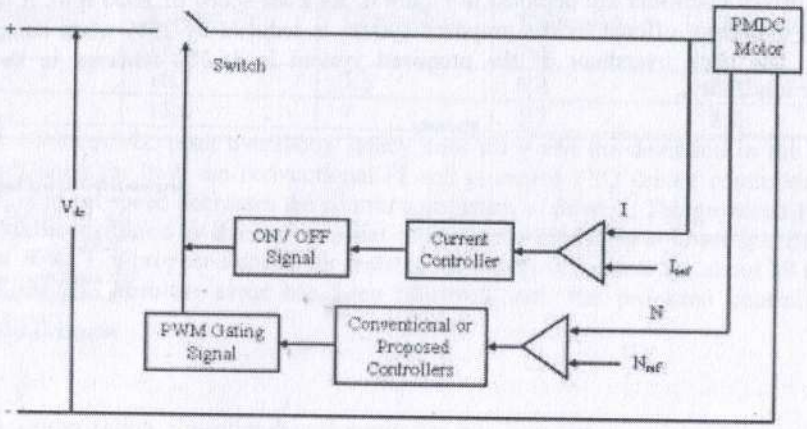


Figure 3: Chopper Driven PMDC Motor

IV. Proposed PSO Driven Chopper System

Particle Swarm Optimization was proposed by Eberhart and Keneedy in 1995. It is based on the bird flocking or fish schooling. It propels with population of random solutions and searches for optima by updating generations. It utilizes population of particles corresponding to individuals. PSO is robust in optimizing non-linear high dimensional problems through adaption. PSO has flexibility and well-balanced mechanism to enhance the global and local optimal explorations. It also converges early with too many constraints.

In the proposed PSO based chopper, the particle changes their position by flying around in a multidimensional space. The position changes ends when computational limitations are exceeded. Each particle represents a solution to the optimization problem. For each particle, current step, the record of its position, velocity and the best position found so far are needed. Each particle Xi is initialized with random velocity and position. Then the inde of best particle of the group is represented as Gbest. Then the position and velocity are changed until effective Pbest and Gbest are obtained. Figure 4 depicts the change in position and velocity to get Gbest and Pbest. In the Figure 4, X_t is the current position, X_{t+1} is the modified position. V_k is the initial velocity and V_{k+1} is the modified velocity. VPbest and GPbest are velocities based on Pbest and Gbest.

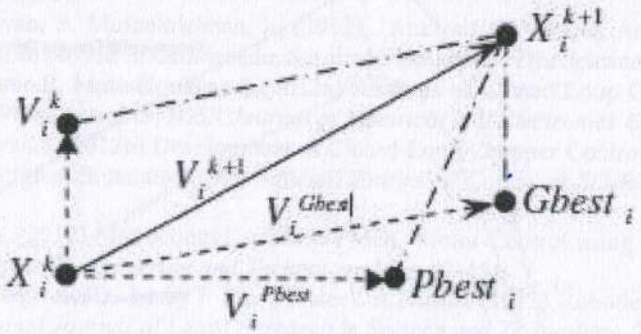


Figure 4: Parameter Search in PSO

The proposed PSO algorithm generates the appropriate pulse width. The pulses or control signals required for optimum speed are processed by the proposed algorithm. The current speed (rpm) and set speed (rpm) values are taken as input function to the system. Initially these particles are given a weightage and based on the output parameters i.e peak overshoot, steady state error and integral error the particle values are modified. The best solution is the generation of the optimal siwtching pulse. When the parameters of study are minimized, the optimal values are obtained. The optimum swithcing pulses offer lowest values of peak overshoot, steady state error and integral of absolute error which are the desired optimal soultions.

DOI: 10.5373/JARDCS/V12I7/20202033
ISSN 1943-023X
Received: 13 May 2020/Accepted: 15 June 2020

V. Simulation Results

The response of the proposed system is given in Figure 5. The comparative analysis of the conventional PI and proposed PSO algorithm driven controller are depicted in Figure 6, for a set speed of 1000 rpm. It is evident from the analysis that the peak overshoot offered by the proposed system is reduced by 25% when compared with the conventional PI system. The peak overshoot of the proposed system is 16.7% whereas in the case of the conventional PI controller it is 21.4%.

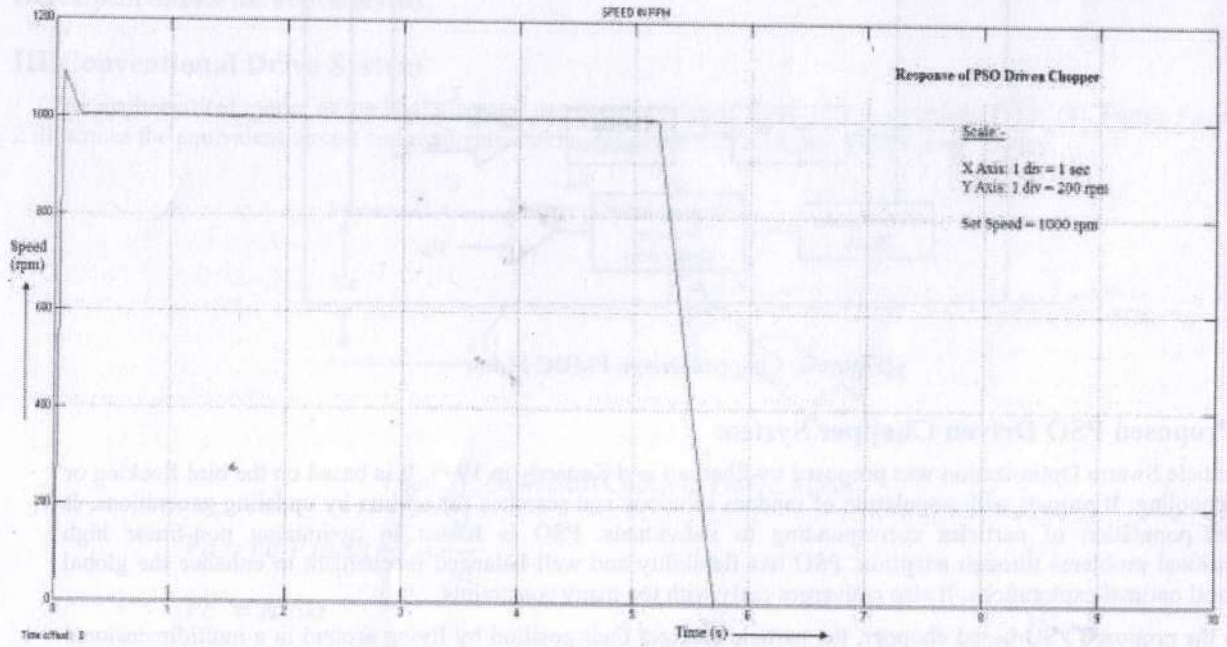


Figure 5: Response of PSO Driven Chopper

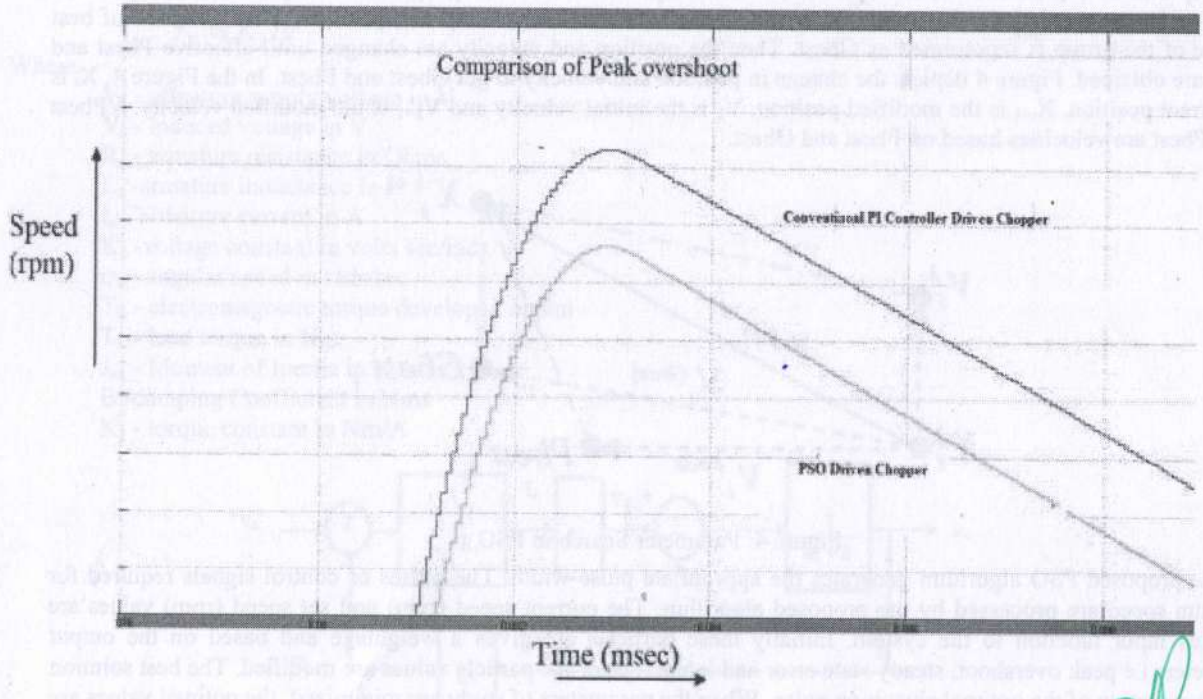


Figure 6: Peak Overshoot Comparative Analysis

DOI: 10.5373/JARDCS/V12I7/20202033
ISSN 1943-023X
Received: 13 May 2020/Accepted: 15 June 2020

Table 1: Performance Comparison of Conventional PI and ALO Driven Controllers

Set speed rpm	Peak Overshoot %		Steady State Error		Integral Absolute Error	
	PI Controller	PSO Controller	PI Controller	PSO Controller	PI Controller	PSO Controller
750	24	18.2	11	7.3	9	6.5
1000	21.4	16.7	7.5	6.4	8.82	5.6
1200	20.2	13.6	7	5.7	8.2	4.7

The performance indices viz. peak overshoot, steady state error and the deviation in the error for various set speed values are tabulated for both the conventional PI and proposed PSO driven controller as in Table 1. It is observed that increase in set speed decreases the control parameters of interest. The proposed PSO driven controller reduces the peak overshoot offered by the conventional controller by 22% even at lower speeds. At higher speeds, it has been more than 30%. The proposed controller reduces the steady state error for about 28 to 32% at all speeds. 40% reduction of integral absolute error has been observed with the proposed controller compared to its conventional counterpart.

VI. Conclusion

Particle Swarm Optimization algorithm-based controller has been attempted in this paper for the control of PMDC motor used in orthopedic surgical simulators. The simulation results and the corresponding comparative analysis revealed that the there is a significant improvement in the transient and steady-state response of the proposed system. Hence, it is concluded that the proposed PSO algorithm driven chopper drive has an edge over its conventional counterpart as far as the functional capabilities are concerned.

References

[1] Shih-Tseng Lee, Yeh-Liang Hsu, Hao-Wei lin (2001) "A modular Mechatronic System for Automatic Bone Drilling", *Biomedical Engineering Applications, Basis Communications* 13(2), 168-174.

[2] Ming-Dar Tsai, Ming-Shium Hsieh, Chiung-Hsin Tsai (2007), "Bone drilling haptic interaction for orthopedic surgical simulator", *ELSEVIER - Computers in Biology and Medicine* 3(1), 1709-1718.

[3] Thomas. R. L, Bouazza-Marouf, Kaddour, Taylor, G.J.S (2008), "Automated surgical screwdriver: Automated screw placement," *Proceedings of the Institution of Mechanical Engineers,* 222(5), 451–454.

[4] Ann Majewicz, Jason Glasser, Rosemary Bauer, Stephen M. Belkoff, Simon C. Mears, Allison M. Okamur, (2011) "Design of a Haptic Simulator for Osteosynthesis Screw Insertion", *IEEE Haptics Symposium,* 497-500, 25 - 26 March 2010, Waltham, 4. Massachusetts, USA.

[5] Nitai Pal, Pradip Kumar Sadhu and Swaroop.R (2012) Closed Loop Speed Control of DC Motors used in Rock Drilling and Mud Pump Application, *Proceedings of the International Multi conference of Engineers and Computer Scientists* 2: 14-16.

[6] Murugananth, G,Vijayan, S, Muthukrishnan, S, (2012), 'Analysis of Various Anti-Windup Schemes used to control PMDC Motors employed in Orthopaedic Surgical Simulators', *Life Science Journal,* 10(1), 226 – 230.

[7] Murugananth.G, Vijayan.S, Muthukrishnan.S (2012a) Analysis of Closed Loop Chopper Controlled Drive for PMDC Motors using PID Controller, *IOSR Journal of Electrical and Electronics Engineering,* 2(3): 32-34.

[8] Murugananth.G, Vijayan.S (2012b) Development of Closed Loop Chopper Controlled Drive for PMDC Motors Used in Orthopedic Surgical Simulators, *International Journal of Computer Science and Technology* 3(3): 872-874.

[9] Pithwa VJ, Parekh BR (2012) Microcontroller based PMDC Motor Control using Image Processing Algorithm of Matlab, *NIET Journal of Engineering and Technology* 1(1): 42-45.

[10] Vipul J Gohil, DR Bhagwat SD, Amey P Raut, Prateek R Nirmal (2013) Robotics Arm Control Suing Haptic Technology, *International Journal of Latest Research in Science and Technology,* 2(2): 98-102.

[11] Murugananth G, Vijayan S, (2015) 'Development of Fuzzy Controlled Chopper Drive for Permanent Magnet DC Motor', *Journal of Vibration and Control,* 21(3) 555-562.

[12] Murugananth G, Samidurai K, Muthukrishnan S, Vijayan S (2015), 'Experimental Validation of Fuzzy-Tuned AWPI controller – Based Chopper Driven PMDC Motor', *Journal of Testing and Evaluation,* 43(6).

[13] Vijayakumar Thangavelu, Murugananth Gopalraj, Muthukrishnan S (2016) Genetic Algorithm based Speed control of PMDC motor using low cost PIC 16F877A microcontroller, *Circuits and Systems* 7: 1334-1340.

[14] Muthukrishnan Subramainiam, Murugananth Gopalraj, Saravana Sundaram Sakthivelu (2016) BELBIC Tuned PI Controller Based Chopper Driven PMDC Motor, *Circuits and Systems* 7: 2273 – 2285.

DOI: 10.5373/JARDCS/V12I7/20202033
ISSN 1943-023X
Received: 13 May 2020/Accepted: 15 June 2020

[15] Murugananth Gopalraj, Manickavasagam Arumugam, "Fuzzy tuned Raindrop Algorithm Controlled Chopper Driven PMDC Motor. *Journal of Engineering Technology*, ISSN No.: 0747-9964, Vol. 8, No. 1, pp. 235 – 242, January 2019.

[16] Mirjalili, Seyedali. "The ant lion optimizer." *Advances in Engineering Software* 83 (2015): 80-98.

[17] E. S. Prasad and B. V. S. Ram, "Ant-lion optimizer algorithm based FOPID controller for speed control and torque ripple minimization of SRM drive system," 2016 *International Conference on Signal Processing, Communication, Power and Embedded System (SCOPES), Paralakhemundi,* 2016, pp. 1550-1557.

[18] Kamaraj Premkumar, Bairavan Veerayan Manikandan & Chellappan Agees Kumar (2017) Antlion Algorithm Optimized Fuzzy PID Supervised On-line Recurrent Fuzzy Neural Network Based Controller for Brushless DC Motor, *Electric Power Components and Systems,* 45:20, 2304-2317.

[19] Dinakar Prasad Reddy, Veera Reddy, Gowri Manohar, "Ant Lion optimization algorithm for optimal sizing of renewable energy resources for loss reduction in distribution systems", *Journal of Electrical Systems and Information Technology,* vol. 5, 2018, pp. 663–680.

[20] Murugananth Gopal Raj, Samidruai K, Muthukrishnan S, Manickavasagam A, "Antlion Optimization Algorithm Controlled Chopper Driven PMDC Motor", *Journal of Advanced Research in Dynamical & Control Systems,* Volume 12, Issue 4, pp. 1180-1188, May 2020.

DOI: 10.5373/JARDCS/V12I7/20202033
ISSN 1943-023X
Received: 13 May 2020/Accepted: 15 June 2020

International Journal of Electrical Engineering and Technology (IJEET)
Volume 11, Issue 4, June 2020, pp. 275-280, Article ID: IJEET_11_04_031
Available online at http://www.iaeme.com/ijeet/issues.asp?JType=IJEET&VType=11&IType=4
ISSN Print: 0976-6545 and ISSN Online: 0976-6553

© **IAEME** Publication **Scopus** Indexed

ANALYSIS OF ARTIFICIAL INTELLIGENCE OF THINGS

R Revathy
Assistant Professor, Department of Computer Science and Engineering,
Sathyabama Institute of Science and Technology, Chennai, India.

Murugananth Gopal Raj
Professor and Head, Department of Electrical and Electronics Engineering,
Ahalia School of Engineering and Technology, Palakkad, Kerala, India.

M Selvi
Assistant Professor, Department of Computer Science and Engineering,
Sathyabama Institute of Science and Technology, Chennai, India.

J K Periasamy
Associate Professor, Department of Computer Science and Engineering,
Sri Sairam Engineering College, Chennai, India.

ABSTRACT

Separately, the Internet of Things (IoT) and Artificial Intelligence (AI) are ground-breaking advances. At the point when we consolidate AI and IoT, we get AIoT - the artificial intelligence of things. We can consider IoT gadgets as the digital sensory method whilst AI is the brain of a framework. In this article, we are analyzing about AIoT and analyzing about the applications and real time examples of AIoT method.

Key words: Internet of Things, Artificial Intelligence, Drone, Fleet Management and Autonomous Robot.

Cite this Article: R Revathy, Murugananth Gopal Raj, M Selvi and J K Periasamy, Analysis of Artificial Intelligence of Things. *International Journal of Electrical Engineering and Technology*, 11(4), 2020, pp. 275-280.
http://www.iaeme.com/IJEET/issues.asp?JType=IJEET&VType=11&IType=4

1. INTRODUCTION

The Artificial Intelligence of Things (AIoT) is the mixture of artificial intelligence (AI) innovations with the Internet of Things (IoT) communications to realize increasingly effective IoT operations, get better human machine communications and improve information organization and analytics. AI may be utilized to convert IoT data into valuable data for enhanced result making forms, hence making a base for more up to date innovation, for example, IoT Data as a Service (IoTDaaS).

AIoT is transformational with equally favorable for the two sorts of innovation as AI adds significance to IoT by machine learning abilities as well as IoT adds significance to AI by connectivity, gesturing and information replace. Since IoT systems swell all through main enterprises, there would be gradually more value of human-situated as well as machine-created formless data. AIoT may offer help for data analytics clarifications that may generate significance out of this IoT created information [1].

With AIoT, AI is installed into communications tools, for example, courses, chipsets along with edge processing, every consistent through IoT systems. APIs are then utilized to broaden interoperability among elements at the gadget stage, software stage as well as platform stage. These elements will concentrate mainly on enhancing framework and method process with removing significance from information.

While the conception of AIoT is immobile moderately novel, a lot of prospects exist to get better trade verticals, for example, endeavor, trade and customer item and overhaul areas, and will carry on to occur by its development. AIoT can be a feasible key to take care of existing prepared issues, for example, the cost connected by compelling human capital management (HCM) or the unpredictability of flexibly chains as well as conveyance models.

To completely understand AIoT, you should start with the IoT. At this position when "things, such as, wearable gadgets, refrigerators, digital assistants, sensors as well as additional gear are connected to the internet, may be supposed through dissimilar devices with collect along with practice data, you have the IoT. AI is the stage at which a structure may conclude a set of tasks or learn from data in a way that emerges to be canny. In this way, when AI is additional to the IoT it means that those tools may analyze data with make decisions as well as act on that data with no involvement by humans.

These are "smart" tools, as well as they assist force efficiency along with adequacy. The intelligence of AIoT enables data analytics that is then utilized to enhance a structure as well as generate superior and trade experiences along with create data that helps with making enhanced decisions as well as that the structure may learn from.

2. BENEFITS OF AIOT

AIoT directs to a wide variety of advantages for corporations and customers like a practical involvement, modified understanding, and insightful mechanization [2]. Here are the absolute mainly fashionable advantages of joining these two problematic advancements to the organizations:

Enhancing Equipment Effectiveness: AI in IoT chomps the steady flow of information and identifies the outlines not beguiling on basic estimates. Additionally, machine learning combined by AI may anticipate the process states as well as identify the constraints to be altered to guarantee perfect results. Henceforth, shrewd IoT suggests an understanding into which procedures are superfluous as well as tedious, and which assignments may be tweaked to improve productivity. Google, for instance, fetches the intensity of AI into IoT to decrease its information community breezing costs.

Better Threats Supervision: Combining AI with IoT encourages organizations to realize and foresee a wide variety of dangers and computerize for the brief reaction. In this way, it permits them to all the more likely handle financial misfortune, representative security, and digital risks. Fujitsu, such as, guarantees laborer security through appealing AI for considering information sourced from linked wearable gadgets.

Activating Original and Superior Products & Services: Natural Language Processing (NLP) is showing signs of improvement at permitting individuals to converse with gadgets. Indisputably, IoT and AI jointly may straightforwardly make innovative items or improve

Electronic copy available at: https://ssrn.com/abstract=3659040

existing items and services through allowing the trade to quickly development and evaluate the data. Moves Royce, for example, maps to influence AI innovations in the execution of IoT-enabled airplane motor preservation facilities. In reality, this loom will maintain to speck guides and find equipped bits of knowledge.

Enlarge IoT Scalability: IoT gadgets range from cell phones as well as top of the line PCs to low-end sensors. Be that as it may, the mainly general IoT environment incorporates low end sensors, which proposes surges of information. AI-fueled IoT environment evaluates and reviews the information from one gadget prior to moving it to different gadgets. By itself, it diminishes huge volumes of information to useful stage and permits connecting countless IoT gadgets.

Removes Expensive Unexpected Downtime: In certain parts like seaward oil and gas as well as manufacturing industrial, hardware collapse may bring about expensive unexpected vacation. The prescient preservation by AI enabled IoT permits you to anticipate the gear breakdown in proceed and calendar systematic preservation methodology. Thus, you can shun the reactions of vacation.

3. REALISTIC MODELS OF AIOT

The combo of IoT as well as elegant frameworks creates AIoT a ground-breaking and significant instrument for numerous functions [3]. Here are some:

3.1. Drone Traffic Monitoring

In a smart city, there are numerous realistic employments of AIoT, counting traffic monitoring by drones. In the event that traffic can be screened in instantaneous as well as alterations to the traffic stream can be taken, jamming can be decreased. At the point when drones are conveyed to supervise a huge region, they can broadcast traffic information, along with AI can investigate the information as well as create results on how to finest ease traffic jamming by alterations as far as possible and time of traffic lights with no human inclusion. The ET City Brain, a result of Alibaba Cloud, streamlines the utilization of town assets through utilizing AIoT. This framework can recognize accidents, unlawful parking, as well as can alter traffic lights to assist ambulances with getting to patients who require support quicker.

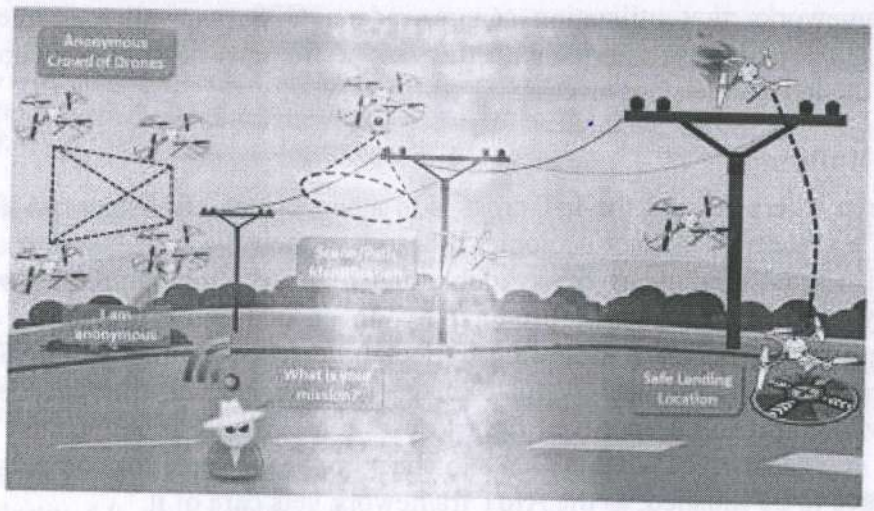


Figure 1 Traffic Monitoring using Drone

3.2. Smart Trading

In smart trade surroundings, a camera framework outfitted by PC visualization abilities can utilize facial identification to recognize clients when they amble by the entryway. The framework collects intel about clients, counting their sexual orientation, item inclinations, traffic stream and other, evaluates the information to correctly anticipate customer performance and then utilizes that data to create results about hoard process from advertising to item assignment and different results. Such as, if the framework distinguishes that the mass of clients walking into the amass are Millennials, it may promote out item posters or in-store particulars that demand to that demographic, along these lines driving up sales.

3.3. Autonomous Vehicles and Fleet Management

AIoT is utilized to in fleet management nowadays to assist supervise a fleet's motor vehicles, diminish energy costs, trail vehicle preservation, and to recognize risky driver performance. By IoT gadgets, for example, GPS as well as different sensors with an AI framework, corporations are capable to supervise their fleet superior appreciation to AIoT.

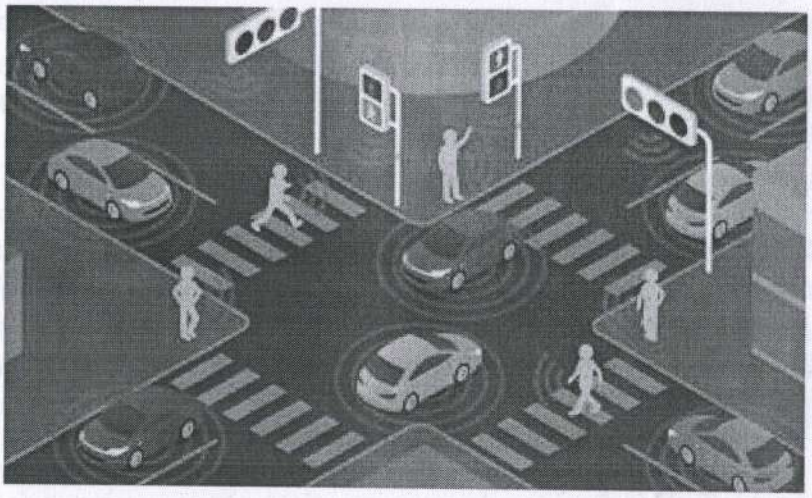


Figure 2 Fleet Management for Autonomous Vehicles

One more way AIoT is utilized nowadays is by autonomous vehicles, for example, Tesla's autopilot frameworks that utilization sonars, radars, GPS, as well as cameras to collect information about driving situations with then an AI framework to create choices about the information the IoT gadgets are meeting.

3.4. Office Buildings

One more area where AI and the IoT cross is in smart places of business. A few companies decide to fit a system of elegant ecological sensors in their place of business. These sensors may recognize what employees are available and regulate temperatures as well as lighting consequently to get better vitality productivity. In an additional utilization stage, a smart structure can manage building admission by facial identification innovation. The mixture of linked cameras with AI that can evaluate images captured in real-time beside a database to figure out who ought to be approved right to use to a structure is AIoT busy working. In a related way, representatives wouldn't have to check in, or presence for compulsory gatherings would not have to be finished, as the AIoT framework gets care of it.

3.5. Autonomous Delivery Robots

Related to how AIoT is utilized by autonomous vehicles, independent conveyance robots are a new instance of AIoT in real life. Robots have sensors that collect data about the

Electronic copy available at: https://ssrn.com/abstract=3658040

surroundings the robot is navigating along with then create second to-second choices about how to react by its onboard AI platform.



Figure 3 Autonomous Delivery Robot

4. CONCLUSION

In this article titled "Analysis of Artificial Intelligence of Things", we have discussed about the brief introduction of AIoT, how it will work, what are the benefits of AIoT with real time example and also discussed about the realistic models of AIoT. In future, we can use this AIoT technique in many equipment's implementation and also we can use this AIoT technique for bringing better performance of many appliances.

REFERENCES

[1] Gerry Christensen, (2019) "Artificial Intelligence of Things (AIoT)", Internet technologies, Verticals, February 2019, https://internetofthingsagenda.techtarget.com/definition/Artificial-Intelligence-of-Things-AIoT

[2] Bernard Marr, (2019) "What is the Artificial Intelligence of Things? When AI Meets IoT", Enterprise Tech, December 2019, https://www.forbes.com/sites/bernardmarr/2019/12/20/what-is-the-artificial-intelligence-of-things-when-ai-meets-iot/#43c09627b1fd

[3] Vinugayathri, (2020) "AI and IoT Blended - What It Is and Why It Matters?", Clarion Technologies, https://www.clariontech.com/blog/ai-and-iot-blended-what-it-is-and-why-it-matters

[4] G Ramprabu, S Sivakami, M Kanmani, (2019) "Performance Analysis of IoT based Smart Agriculture System", International Journal of Engineering and Advanced Technology, Volume 8, Issue 4, April, pp.1342-1344.

[5] Carlos M. S. Rodrigues, Bruno S. L. Castro, (2018) A Vision of Internet of Things in Industry 4.0 with ESP8266. International Journal of Electronics and Communication Engineering and Technology, 9(1), pp. 1–12

Electronic copy available at: https://ssrn.com/abstract=3658040

[6] Manan Mehta. (2015) ESP 8266: A Breakthrough in Wireless Sensor Networks and Internet of things. International Journal of Electronics and Communication Engineering and Technology, 6(8), pp. 07-11.

[7] Viswanath Naik.S, S.Pushpa Bai, Rajesh.P, Mallikarjuna Naik.B, (2015) Iot Based Green House Monitoring System, International Journal of Electronics and Communication Engineering and Technology, 6(6), pp. 45-47.

[8] Trideep Singha Roy, Soumalya Ghosh, Rimpi Datta, Arpita Santra, (2019) IoT Based Home Automation Using Raspberry PI, International Journal of Computer Engineering and Technology, 10(3), pp. 70-74.



Electronic copy available at: https://...

International Research Journal of Engineering and Technology (IRJET) e-ISSN:2395-0056
Volume: 07 Issue: 05 | May 2020 www.irjet.net p-ISSN:2395-0072

DESIGN OF LOW POWER HIGH SPEED FULL ADDER CIRCUITS USING XOR-XNOR TOPOLOGY

AKHILA KRISHNAN[1], Dr. V BALAMURUGAN[2], Anjana Krishnakumar[3], Aparna A[4], Ashna. A[5], Athira. M [6].

[1]*Professor, Dept. of Electronics and Communication Engineering, Ahalia School of Engineering and Technology, Kerala,India*

[2]*Professor, Dept. of Electronics and Communication Engineering, Ahalia School of Engineering and Technology, Kerala,India*

[3]*Student, Dept. of Electronics and Communication Engineering, Ahalia School of Engineering and Technology, Kerala,India*

[4]*Student, Dept. of Electronics and Communication Engineering, Ahalia School of Engineering and Technology, Kerala,India*

[5]*Student, Dept. of Electronics and Communication Engineering, Ahalia School of Engineering and Technology, Kerala,India*

[6]*Student, Dept. of Electronics and Communication Engineering, Ahalia School of Engineering and Technology, Kerala,India*

Abstract-*The explosive growth of battery operated portable applications such as cellular phones, smart cards, PDAs, laptops and the evolution of the shrinkage of the technology requires smaller silicon area, high throughput circuitry and most importantly low power. Power consumption of any system can be reduced by scaling the supply voltage and operating frequency. But, it increases the propagation delay of the system and degrade the driving capability of the design. Therefore, designing a full adder with improved power delay characteristics is of great interest. The greatest challenge in low power VLSI design is reduction of power dissipation. Novel circuits for XOR/XNOR and simultaneous XOR–XNOR functions are proposed. The proposed circuits are highly optimized in terms of the power consumption. The proposed circuits are investigated in terms of variations of supply and threshold voltages, output capacitance, input noise immunity, and the size of transistors. The simulations are carried out in Tanner EDA tool.*

***Words:** CMOS, Low power VLSI, Full Adder, XOR-XNOR, Tanner EDA, Virtual ground.

INTRODUCTION

TODAY, ubiquitous electronic systems are an inseparable part of everyday life. Digital circuits, e.g., microprocessors and digital communication devices, and digital signal processors, comprise a large part of electronic systems. As the scale of integration increases, the usability of circuits is restricted by the augmenting amounts of power and area consumption. Therefore, with the growing popularity and demand for the battery-operated portable devices such as mobile phones, tablets, and laptops, the designers try to reduce power consumption and area of such systems while preserving speed. Optimizing the W/L ratio of transistors is one approach to decrease the power-delay product (PDP) of the circuit while preventing the problems resulted from reducing the supply voltage. The efficiency of many digital applications appertains to the performance of the arithmetic circuits, such as adders, multipliers, and dividers. Due to the fundamental role of addition in all the arithmetic operations, many efforts have been made to explore efficient adder structures, e.g., carry select, carry skip, conditional sum, and carry look-ahead adders. Full adder (FA) as the fundamental block of these structures is at the center of attention. Based on the output voltage level, FA circuits can be divided into full-swing and non full-swing categories. Standard CMOS complementary pass transistor logic(CPL) transmission gate (TG) transmission function 14T (14 transistors),16T and hybrid pass logic with static CMOS output drive full adder (HPSC) . FAs are the most important full-swing families. Non full-swing category comprises of 10T, 9T, and8T.

In this paper, we evaluate several circuits for the XOR or XNOR (XOR/XNOR) and simultaneous XOR and XNOR (XOR–XNOR) gates and offer new circuits for each of them. Also, we try to remove the problems existing in the investigated circuits.

Afterward, with these new XOR/XNOR and XOR–XNOR circuits, we propose six new FA structures. The circuits for XOR/XNOR and simultaneous XOR–XNOR are reviewed, novel XOR/XNOR and XOR–XNOR circuits are proposed and the

simulation results of these structures are presented. In the transistor sizing methods are first investigated and the circuits are simulated for power, delay, and PDP parameters. The simulation results are analyzed and compared.

2 PROPOSED DESIGN

In this paper the circuits are designed using novel XOR-XNOR circuit. One of the important factors is that excessive power consumption is becoming the limiting factor in integrating more transistors on a single chip or on a multichip module. Unless power consumption is dramatically reduced, the resulting heat will limit the feasible packing and performance of VLSI circuits and systems. So XOR-XNOR circuit is in-cooperated in digital circuits to reduce the power consumption.

2.1 INVERTER

An inverter circuit outputs a voltage representing the opposite logic-level to its input. Inverters can be constructed using two complementary transistors in a CMOS configuration. This configuration greatly reduces power consumption since one of the transistors is always off in both logic states.

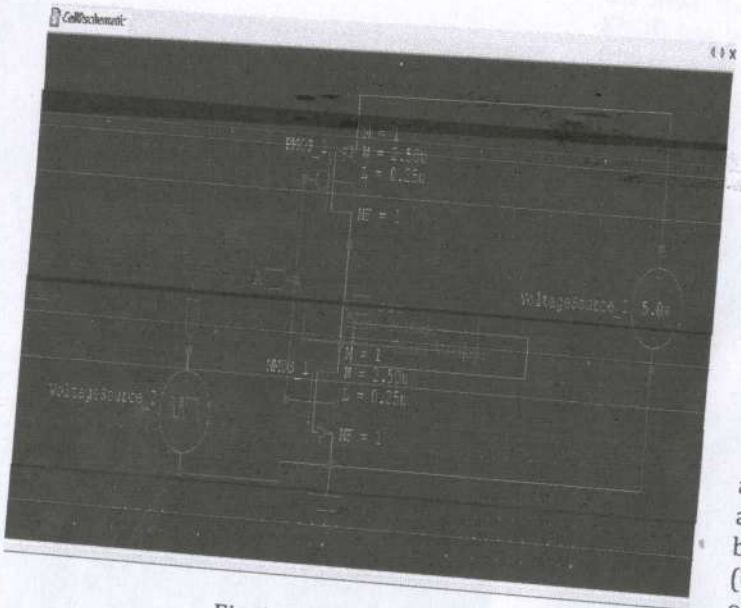


Fig-1: Inverter circuit

The proposed **XOR** and **XNOR** circuits are based on the modified version of a CMOS **inverter** and pass transistor logic. In proposed circuit-I, for **XOR** when the input B is at logic 1, the **inverter** circuit functions like a normal CMOS **inverter**. Therefore, the output is complement of input A.

2.2 CMOS HALF ADDER

Adders are used in processors in the arithmetic units, to calculate addresses, table indices, and other s operations. A fast and energy-efficient adder plays a vita in electronics industry. Adder contributes substantially t total power consumption of the system. Half Adder frequently required in VLSI from processors to applic specific integrated circuits (ASICs). Adder circuit combinational digital circuit that is used for adding numbers. A typical adder circuit produces a sum bit (den by S) and a carry bit (denoted by C) as the output. Typi adders are realized for adding binary numbers but they ca also realized for adding other formats like BCD (binary c decimal, XS-3 etc. Besides addition, adder circuits can be for a lot of other applications in digital electronics like add decoding, table index calculation etc. For more than decades, downscaling of CMOS has been the fundame strategy for improving the performance of VLSI circuits.

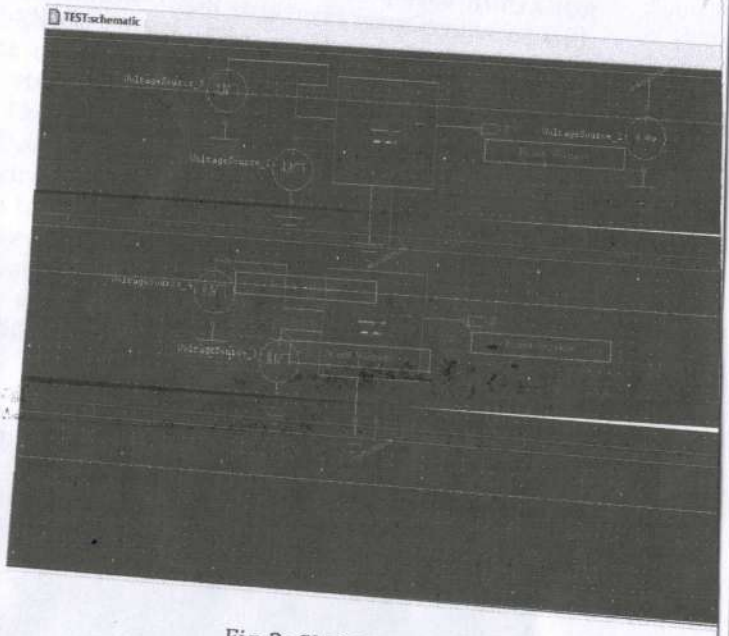


Fig-2: CMOS Half adder

In DSPs, and, versatile microprocessor, the wide-bit addition is vital in many applications such as ALUs, multiply-and accumulates (MAC) units. The half adder adds two single binary digits A and B. It has two outputs, sum (S) and carry (C). The carry signal represents an overflow into the next digit of a multi-digit addition. The value of the sum is A+B. The simplest half adder design incorporates an XOR gate for S and an AND gate for C. With the addition of an OR gate to combine their carry outputs, two half adders can be combined to make a full adder. The half adder adds two input bits and generates a carry and sum, which are the two outputs of a half adder.

2.3 XOR-XNOR CIRCUIT

Hybrid FAs are made of two modules, including 2-input XOR/XNOR (or simultaneous XOR–XNOR) gate and 2-to-1 multiplexer (2-1-MUX) gate. The XOR/XNOR gate is the major consumer of power in the FA cell. Therefore, the power consumption of the FA cell can be reduced by optimum designing of the XOR/XNOR gate. The XOR/XNOR gate has also many applications in digital circuits design. Many circuits have been proposed to implement XOR/XNOR gate which a few examples of the most efficient ones.

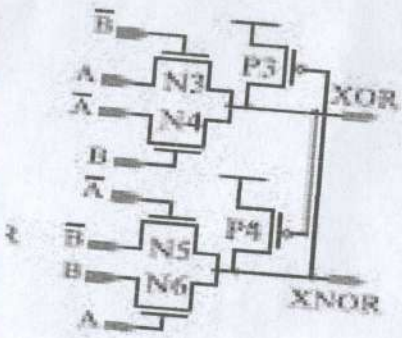


Fig-3: XOR-XNOR circuit

The main problem of this circuit is using two high power consumption NOT gates on the critical path of the circuit, because the NOT gates must drive the output capacitance. Therefore, the size of the transistors in the NOT gates should be increased to obtain lower critical path delay. Furthermore, it causes the creation of an intermediate node with a large capacitance. Of course, this means that the NOT gates drives the output of circuit through, for example, pass transistor or TG. Therefore, the short circuit power and, thus, the total power dissipation of this circuit are widely increased. Moreover, in the optimum PDP situation, the critical path delay will also be increased slightly. Therefore, to improve the XNOR circuit speed, the size of PMOS transistor (*P5*)and NOT gates should be increased.

2.4 PROPOSED XOR-XNOR CIRCUIT

The proposed structure of the simultaneous XOR–XNOR gate consisting of 12 transistors. The proposed XOR/XNOR and simultaneous XOR–XNOR structures were compared with basic XOR-XNOR circuit. The results indicate that the performance of the proposed XOR/XNOR and simultaneous XOR–XNOR structures is better than that of the compared structures. The proposed XOR and XNOR circuits have the lowest PDP and delay, respectively, compared with other XOR/XNOR circuits. Also, the delay of these proposed circuits is very close together that prevents the creation of glitch on the next stage. The proposed circuit for simultaneous XOR–XNOR has better efficiency in all three calculated parameters (delay, power dissipation, and PDP) when it is compared with other XOR–XNOR gates

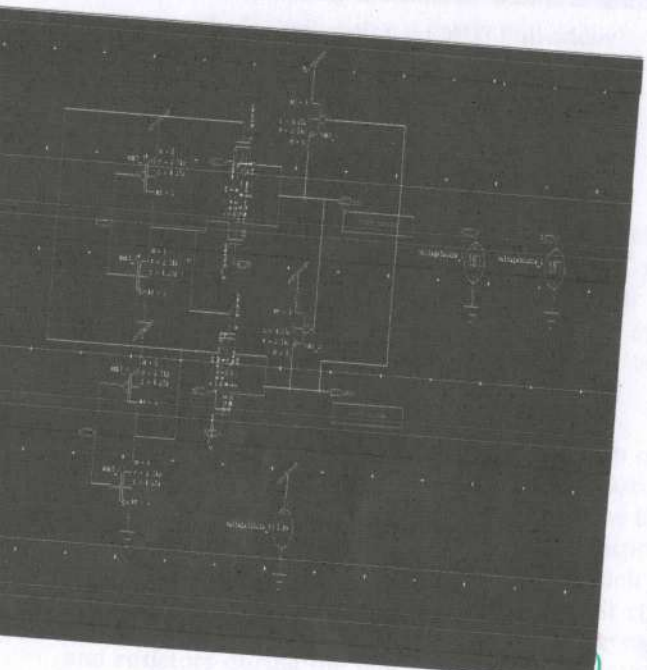


Fig-4 :XOR-XNOR circuit

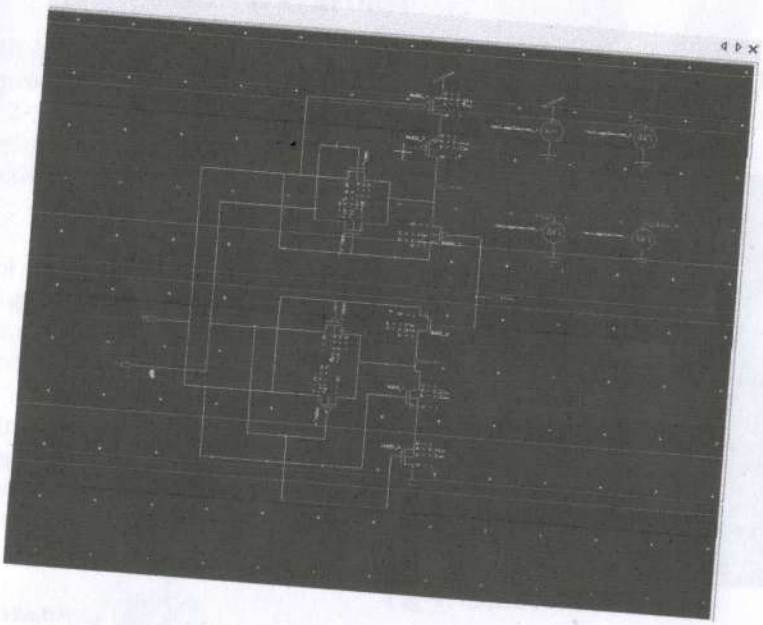


Fig-5:Proposed XOR-XNOR circuit

2.5 FULL ADDER CIRCUIT

Full adder is the adder which adds three inputs and produces two outputs. There are three types of basic structure on which full Adder is based static, dynamic and hybrid. Static full adders are less power consuming than dynamic and then more reliable. Dynamic full adder have faster switching speed, full swing voltage level and less number of transistors but suffer from charges haring, clock load, high power dissipation due to high switching activity and complexity. Hybrid full adder is basically the combination of static and dynamic full adder.

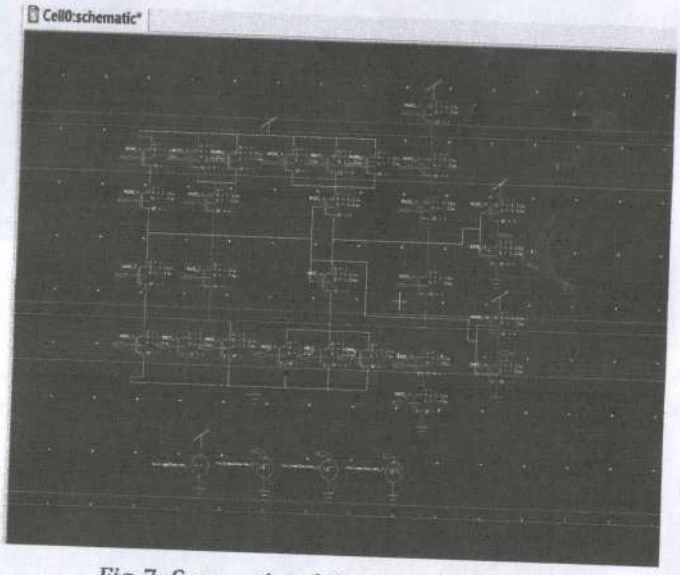


Fig-7 :Conventional CMOS Full adder

2.6 PROPOSED FULL ADDER CIRCUIT

The new FA has been employed using switch hybrid logic style, and its designed by using the proposed XOR/XNOR circuit. The well-known four-transistor 2-1-MUX structure is used to implement the proposed hybrid FA cells. This 2-1-MUX is created with TG logic style that has no static and short-circuit power dissipation.

One way to reduce the power consumption of the FA structures is to use a XOR/XNOR gate and a NOT gates to generate the other XOR or XNOR signal. using the buffer on the output of a circuit is almost mandatory, especially in applications that the output capacitance of each stage is high. In practice, the driving capability of VLSI circuits is degraded due to the creation of the parasitic capacitors and resistors during the fabrication, as well as increasing the threshold voltage of transistors over the time, but the output buffer improves this situation.

The proposed HFA-19T is made by 19 transistors. The power consumption of proposed circuit is less than that of conventional CMOS full adder due to the reduction in the number of transistors. To produce the output Sum signal C and C compliment signals are used. The XOR, XNOR signals will be connected to the data select lines of 2-1-MUX. Due to the less capacitance of XOR and XNOR nodes the power consumption and delay of HFA 19T is less.

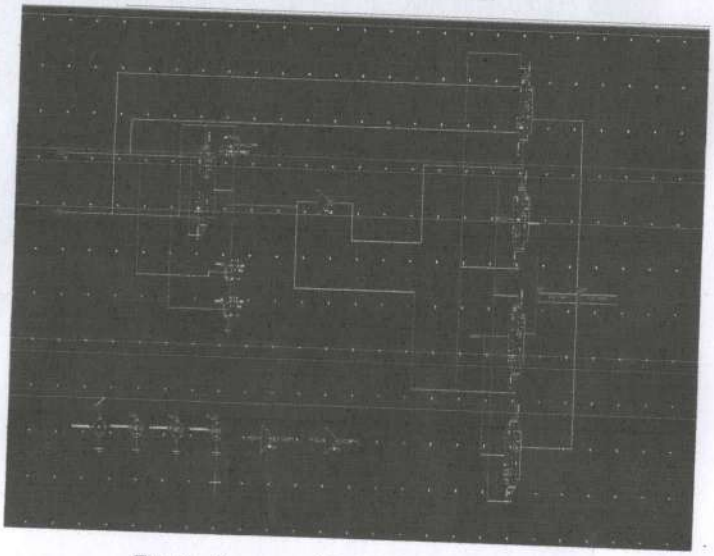


Fig-8 : Proposed Full Adder Circuit

3 RESULT AND ANALYSIS

The Tanner EDA tools were used to simulate the circuits. They offer complete design environment supporting analog/mixed-signal IC, MEMS and photonic design in highly integrated, end to end flow with an intuitive user interface for a quick learning curve and a low total cost of ownership through minimal IT support costs and competitive software license and maintenance costs.

3.1 WAVEFORM

Figure-9 depicts the obtained waveform of CMOS Inverter circuit

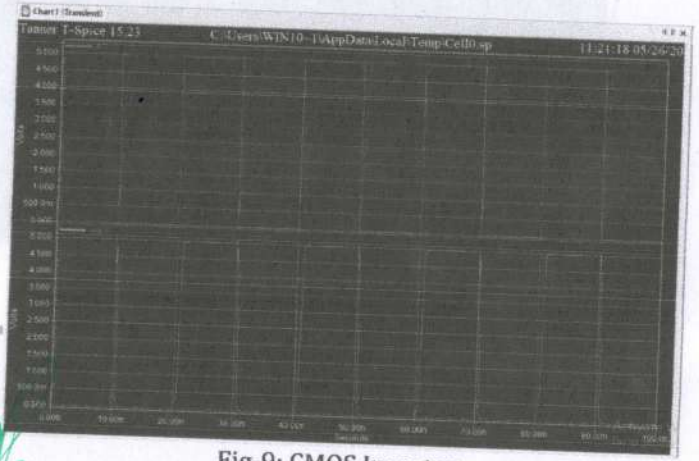


Fig-9: CMOS Inverter

Figure-10 depicts the obtained waveform of CMOS Half Adder.

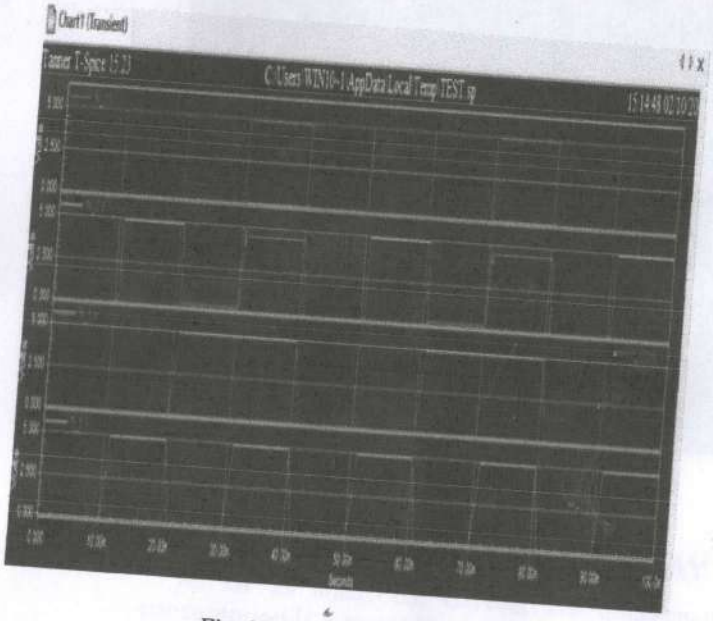


Fig-10: CMOS half adder

Figure-11 depicts the obtained waveform of XOR-XNOR Circuit.

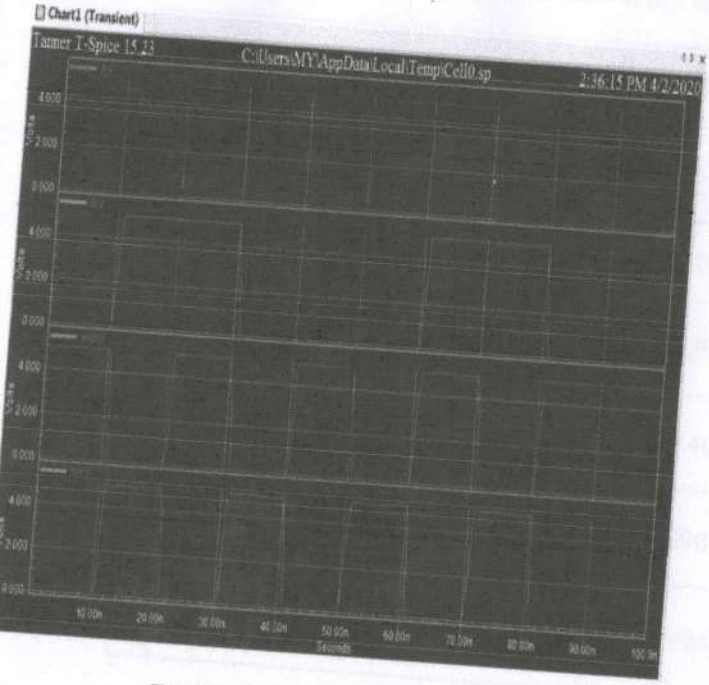


Fig-11: XOR XNOR Circuit

Figure-12 depicts the obtained waveform of proposed XOR-XNOR circuit

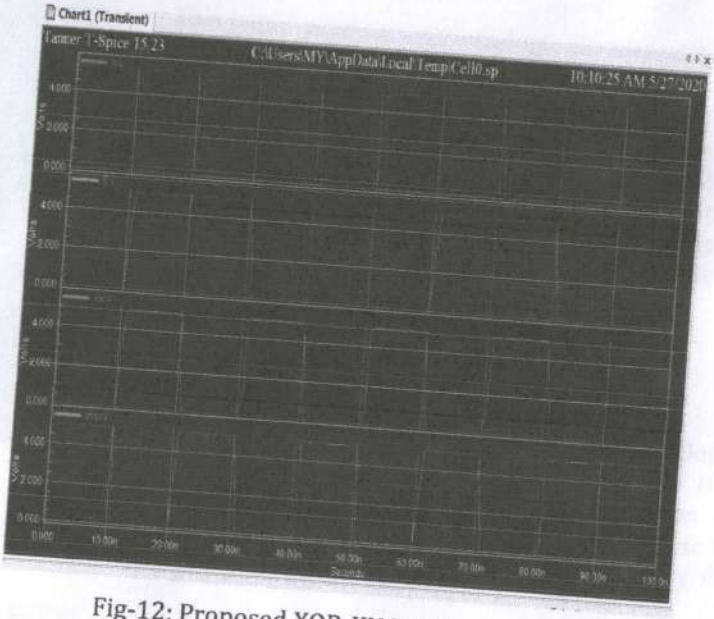


Fig-12: Proposed XOR-XNOR circuit.

Figure-13 depicts the obtained waveform of CMOS Full Adder

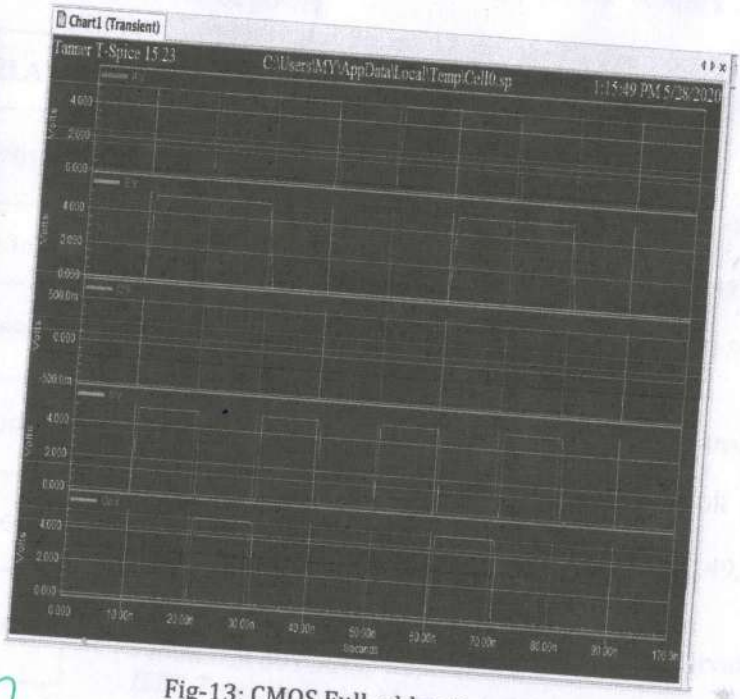


Fig-13: CMOS Full adder Circuit

Figure-14 depicts the obtained waveform of Proposed Full Adder Circuit

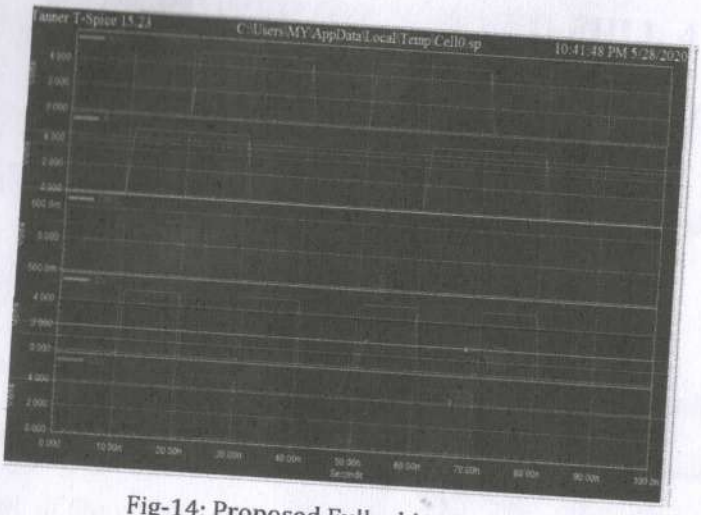


Fig-14: Proposed Full adder Circuit

3.2 COMPARISON OF POWER AND DELAY

As far as electronic circuits are concerned, power consumption is a major bottleneck of system performance. The main source is the leakage power consumption, so the power is reduced by using XOR-XNOR topologies.

Table -1: Comparison of power and delay table

CIRCUIT	POWER (W)	DELAY
Inverter	7.124e-006	9.5701n
Half Adder	5.082e-004	10.3n
XOR-XNOR Circuit	5.957e-004	39.989n
Proposed XOR-XNOR Circuit	9.364e-005	10.409n
Conventional CMOS Full Adder	4.479e-004	39.986n
Proposed Full Adder - HFA 19T	2.009e-004	9.994n

4 CONCLUSION

This paper proposes various logic circuits with XOR-XNO technique, which resulted in better terms of pow consumption. Simulations are carried out and the pow analysis has been performed. From the observation it evident that the circuit with proposed XOR-XNOR is th efficient design with minimum power consumption. Henc the proposed architecture is well suited for modern hig performance designs where power dissipation is the majo concern.

ACKNOWLEDGEMENT

We would like to acknowledge the support of Department of Electronics and Communication and our HoD who provided us an opportunity and motivation to gain knowledge through this type of work. We are also thankful to Ahalia School Of Engineering And Technology, Palakkad for providing facility for preparing this paper.

REFERENCES

[1] N. S. Kim *et al.*, "Leakage current: Moore's law meets static power,"
Computer, vol. 36, no. 12, pp. 68–75, Dec. 2003.
[2] N. H. E. Weste and D. M. Harris, *CMOS VLSI Design: A Circuits and*
Systems Perspective, 4th ed. Boston, MA, USA: Addison-Wesley, 2010.
[3] S. Goel, A. Kumar, and M. Bayoumi, "Design of robust, energy-efficient
full adders for deep-submicrometer design using hybrid-CMOS logic
style," *IEEE Trans. Very Large Scale Integr. (VLSI) Syst.*, vol. 14, no. 12,
pp. 1309–1321, Dec. 2006.
[4] H. T. Bui, Y. Wang, and Y. Jiang, "Design and analysis of low-power
10-transistor full adders using novel XOR-XNOR gates," *IEEE Trans.*
Circuits Syst. II, Analog Digit. Signal Process., vol. 49, no. 1, pp. 25–30,
Jan. 2002.
[5] S. Timarchi and K. Navi, "Arithmetic circuits of redundant SUT-RNS,"
IEEE Trans. Instrum. Meas., vol. 58, no. 9, pp. 2959–2968, Sep. 2009.
[6] J. M. Rabaey, A. P. Chandrakasan, and B. Nikolic, *Digital Integrated*
Circuits, vol. 2. Englewood Cliffs, NJ, USA: Prentice-Hall, 2002.

Investigation on Impact Strength of Fiber Reinforced Concrete Subjected To Elevated Temperature

2019

Alwyn Varghese, Anand. N, Prince Arulraj G

Abstract: ***The effect of elevated temperature on impact strength of Fiber Reinforced Concretes (FRC) is investigated in this paper. Cylinder specimens are used with different types of fibers such as Aramid, Basalt, Carbon, Glass, Polypropylene and PVA. All the specimens were exposed to elevated temperature as per standard fire curve following ISO 834. After heating the specimens are cooled by natural air prior to impact strength test. The tests are conducted as per ACI committee 544. Test result reveals that addition of fiber enhances the impact strength of concrete specimens. Concrete with Carbon fiber and Basalt fiber exhibits better performance than concrete with other fibers. In unheated condition Carbon fiber shows 5.9 times increase in impact resistance with respect to reference specimen. For 90 minutes of heat exposure, all FRCs except concrete with Aramid fiber shows 2 times better impact resistance than that of reference specimen.***

Index Terms: Fiber Reinforced Concrete, Impact Strength, Elevated Temperature, Carbon Fiber, Basalt Fiber

I. INTRODUCTION

Concrete is a brittle material due to its higher rigidity. During the past few decades, several experiments had been conducted to improve the ductility of concrete [9-13]. Presently Fiber Reinforced Concretes (FRC) is used in construction industry to overcome the deficiencies regarding the tensile strength of concrete. For better usage of fibers in cement composites, different types of fiber products are also developed [1]. Toughness is an important mechanical property, FRC exhibits higher toughness when subjected to different type of loads. Impact strength can be calculated based on the toughness of the material under impact loads. Previous researches indicates that several investigations and tests have been conducted to analysis the impact resistance of concrete specimens [2- 8]. This paper evaluates the impact resistance of different FRC specimens by impact test and the results are evaluated in terms of ultimate failure impact energy.Concrete structures are affected by a many of risks during their life span, such as earth quake, fire and impact loading etc. When concrete structures are loaded repeatedly as a function of time, severe damages may occur. Blast induced impact and fire always happen concurrently on structural members thereby encircled with a risk of impact load with fire load [14, 15].Few research works carried out on impact resistance of FRC after the heat exposure. Though some studies have considered mechanical properties of blast induced impact and fire load of concrete structures [14-16], it was not reported the impact resistance of different types of fiber reinforced concrete after exposed to heat. The objective of the investigation is to evaluate the impact resistance of plain concrete (Reference specimen) with different strength grades after exposed to elevated temperature by standard fire curve [19]

II. MATERIALS AND TEST METHODS

A. Materials and Mix Proportioning

Table 1: Properties of Fiber

Fiber	Melting Category	Density (g/cu.cm)	Melting point (^{O}C)
AF	Low	1.44	150
BF	High	2.65-2.8	1400
CF	High	1.6	1200
GF	High	2.6	1500
PPF	Low	0.90 -0.91	160 - 170
PVA	Low	1.29	220

Concrete specimen used for this investigation consists of plain concrete with fibers. Ordinary Portland Cement (OPC) of 53gradeswas used to cast all the specimens. Crushed stones of size 20mm were used as coarse aggregate. The 12mm length short fibers which are supplied in bunch are dispersed in concrete mix. Table 1 shows the properties of Aramid (AF), Basalt (BF), Carbon (CF), Glass (GF), Poly Propylene (PPF) and Polyvinyl Alcohol (PVA) fibers that were used in specimens. The volume fraction used for all fibers were 0.25%. A water reducing agent Conplast SP430 was used to improve the workability of the concrete mixtures.

B. Test specimens

Concrete specimen of 150mm diameter and 64mm height were cast. After casting the specimens were kept in the curing tank for 28 days [17, 18] (figure 1). After curing the specimens were dried for 24 hours prior to the test. Specimens were heated up to 30 minutes, 60 minutes and 90 minutes (821^{0}C, 925^{0}C and 986^{0}C) respectively as per Standard fire curve [19]. Heated specimens were cooled by natural air before testing.

Revised Manuscript Received on 8 February 2019.

Alwyn Varghese, Department of Civil Engineering, KITS, Coimbatore, India

Anand N., Department of Civil Engineering, KITS, Coimbatore, India,

Prince Arulraj G, Department of Civil Engineering, KITS, Coimbatore, India.

Published By:
Blue Eyes Intelligence Engineering

The investigation has been carried out for M20, M30, M40 and M50 grades of concrete.



Figure 1: Specimens in Curing Tank

C. Test procedure

Drop weight impact test was carried out on specimens as per the guidelines of ACI committee 544 [17]. Figure 2 shows the concrete specimen and equipment for conducting the drop weight impact resistance test. The equipment consists of a standard manually operated 4.45 kg compaction hammer with a height of 457mm drop on a hardened steel ball of 63.5mmdiameterwhich is resting on a flat base plate with positioning bracket. The test specimen is then placed on the base plate with the finished face up and positioned inside the brackets. During this testing the hammer was dropped repeatedly and the number of drops required to produce the first visible crack (N1) in the specimen and for the ultimate failure (N2) were recorded.

The impact energy of the specimens was claculated by [20]

$E = Nmgh$ (1)

Where

E - impact energy,
N - the number of drops,
m - the mass of dropped ball(4.45 kg),
g - the gravity based acceleration ($9.8 m/s^2$)
h - the height of drop (457mm).

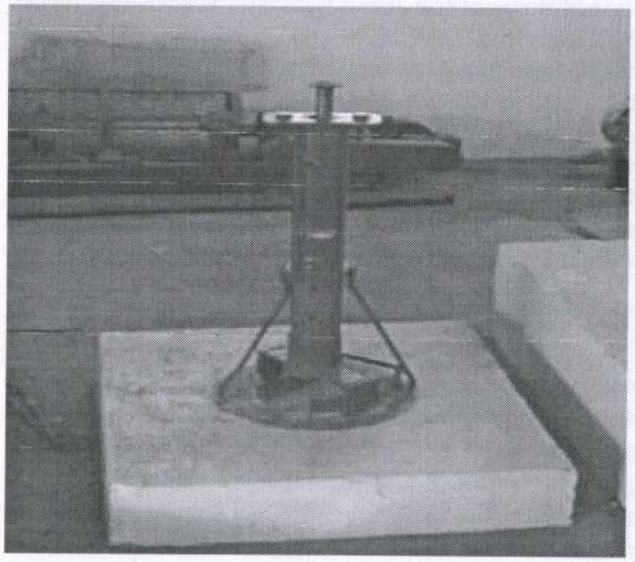


Figure 2: Impact Test Setup

III. RESULTS AND DISCUSSION

A. Impact resistance of specimens without heat exposure

It is observed that for the plain concrete specimens (without heat exposure) after the testing the pieces are fractured into separate pieces, whereas the specimens with fiber the pieces damage level was less. This phenomenon may be because of the addition of fiber leads to slow down the crack formation and final failure of the specimen [20]. From table 2 and table 3 it is understood that the impact energy of every FRC specimen increased 4-7 times with respect to the fiber properties than that of the plain concrete. This can be explained by assumption that the fiber enhanced the ductility behaviour of the concrete [20].Concrete with AF in all grades of concrete shows 5 times increase in impact energy than plain concrete. Concrete with BF and CF shows 6 times increase in impact energy. GF shows least (3 times) increment compared to other FRC's. PPF and PVA fibers shows 4 times increment in the impact energy as compared to that of plain concrete. M50 grade concrete (D series) containing CF possess highest impact energy of 2034N-m and 2733N-m for first crack and ultimate failure respectively. Similarly it was observed for the specimen with BF the impact energy was2014N-m and 2693N-m. The similar was observed for other grades (A, B and C series) of concrete. The crack bridging property of the fibers is assumed to absorb additional energy and inhibits the sudden failure of specimens. The present investigation findings support the research findings of Mohammad hosseini et al [21] and Mastali et al [22]

Published By:
Blue Eyes Intelligence Engineering

Table 2: Impact Resistance of Plain and FRC specimens (First Crack)

Mix	Characteristic compressive strength (MPa)	Type of fiber	No of blows to develop first crack				Impact Energy (N-m)			
			Duration of heating				Duration of heating			
			Reference	30 min.	60 min.	90 min.	Reference	30 min.	60 min.	90 min.
A1	20	--	9	4	2	1	179.55	79.8	39.9	19.95
A2	20	AF	40	2	1	1	798	39.9	19.95	19.95
A3	20	BF	61	5	2	1	1216.96	99.75	39.9	19.95
A4	20	CF	60	5	2	1	1197.01	99.75	39.9	19.95
A5	20	GF	26	4	1	1	518.7	79.8	19.95	19.95
A6	20	PPF	39	4	1	1	778.05	79.8	19.95	19.95
A7	20	PVA	40	4	1	1	798	79.8	19.95	19.95
B1	30	--	11	5	2	1	219.45	99.75	39.9	19.95
B2	30	AF	52	2	1	1	1037.41	39.9	19.95	19.95
B3	30	BF	73	7	2	1	1456.36	139.65	39.9	19.95
B4	30	CF	74	7	2	1	1476.31	139.65	39.9	19.95
B5	30	GF	38	6	3	1	758.1	119.7	59.85	19.95
B6	30	PPF	48	6	3	1	957.61	119.7	59.85	19.95
B7	30	PVA	47	5	3	1	937.66	99.75	59.85	19.95
C1	40	--	13	6	2	1	259.35	119.7	39.9	19.95
C2	40	AF	68	2	1	1	1356.61	39.9	19.95	19.95
C3	40	BF	89	8	3	1	1775.56	159.6	59.85	19.95
C4	40	CF	90	7	3	1	1795.51	139.65	59.85	19.95
C5	40	GF	47	6	2	1	937.66	119.7	39.9	19.95
C6	40	PPF	62	5	2	1	1236.91	99.75	39.9	19.95
C7	40	PVA	61	5	2	1	1216.96	99.75	39.9	19.95
D1	50	--	17	8	3	1	339.15	159.6	59.85	19.95
D2	50	AF	86	3	1	1	1715.71	59.85	19.95	19.95
D3	50	BF	101	10	3	1	2014.96	199.5	59.85	19.95
D4	50	CF	102	11	3	1	2034.91	219.45	59.85	19.95
D5	50	GF	61	8	3	1	1216.96	159.6	59.85	19.95
D6	50	PPF	79	7	3	1	1576.06	139.65	59.85	19.95
D7	50	PVA	80	7	3	1	1596.01	139.65	59.85	19.95

B. Impact resistance of specimens with heat exposure

For all concrete mixes, reduction in impact resistance after exposure to elevated temperature was observed. The degradation of impact strength on concrete may be due to the thermal gradient as well as different physical and chemical changes occurred in the concrete [23-26]. Table 2 and Table 3 illustrate the loss in impact strength of concrete with different mixes with reference mix. In the case of 90 minutes (986°C) of heat exposure, all the specimens broken into pieces with 1-3 number of drops and first crack was formed in the first drop itself. It may be due to the formation of voids and thermal stress formed inside the specimens during the heating process. For the temperature with higher range there were little impact energy exists for the all FRC's. Because at these temperatures bond between the fibers and matrix decreased as the mechanical properties of the fibers reduced [27-28].



Table 3: Impact Resistance of Plain and FRC specimens (ultimate failure)

Mix	Characteristic compressive strength (MPa)	Type of fiber	No of blows to develop ultimate failure				Impact Energy (N-m)			
			Duration of heating				Duration of heating			
			Reference	30 min.	60 min.	90 min.	Reference	30 min.	60 min.	90min.
A1	20	--	12	7	3	1	239.4	139.65	59.85	19.95
A2	20	AF	58	4	2	1	1157.11	79.8	39.9	19.95
A3	20	BF	70	7	3	2	1396.51	139.65	59.85	39.9
A4	20	CF	71	9	4	2	1416.46	179.55	79.8	39.9
A5	20	GF	37	7	3	2	738.15	139.65	59.85	39.9
A6	20	PPF	45	8	4	2	897.75	159.6	79.8	39.9
A7	20	PVA	43	7	4	2	857.85	139.65	79.8	39.9
B1	30	--	14	8	3	1	279.3	159.6	59.85	19.95
B2	30	AF	71	5	2	1	1416.46	99.75	39.9	19.95
B3	30	BF	86	9	4	2	1715.71	179.55	79.8	39.9
B4	30	CF	87	11	4	2	1735.66	219.45	79.8	39.9
B5	30	GF	45	9	4	2	897.75	179.55	79.8	39.9
B6	30	PPF	55	10	4	2	1097.26	199.5	79.8	39.9
B7	30	PVA	56	11	4	2	1117.21	219.45	79.8	39.9
C1	40	--	18	9	4	2	359.1	179.55	79.8	39.9
C2	40	AF	90	6	3	1	1795.51	119.7	59.85	19.95
C3	40	BF	108	11	4	3	2154.61	219.45	79.8	59.85
C4	40	CF	110	13	5	3	2194.51	259.35	99.75	59.85
C5	40	GF	56	11	4	2	1117.21	219.45	79.8	39.9
C6	40	PPF	69	12	5	3	1376.56	239.4	99.75	59.85
C7	40	PVA	70	11	6	2	1396.51	219.45	119.7	39.9
D1	50	--	22	10	4	2	438.9	199.5	79.8	39.9
D2	50	AF	112	7	3	1	2234.41	139.65	59.85	19.95
D3	50	BF	135	13	5	3	2693.26	259.35	99.75	59.85
D4	50	CF	137	16	6	3	2733.16	319.2	119.7	59.85
D5	50	GF	70	13	5	2	1396.51	259.35	99.75	39.9
D6	50	PPF	86	15	6	2	1715.71	299.25	119.7	39.9
D7	50	PVA	84	16	6	2	1675.81	319.2	119.7	39.9

Specimens heated up to 60 minutes (925^{0}C), the first crack developed with 1-3 hammer drops. But the ultimate failures of specimens were according to the type of fiber added in to it. Concrete with AF specimens suffered with severe degradation at its 3rd drop. When heated up to 30 minutes (821^{0}C) a sudden decrement in impact resistance observed for all the specimens with respect to that of plain concrete. The drastic decrease in impact strength is observed for concrete with AF and it was 64% - 67%. The least reduction (21%-27%) in impact resistance was observed for concrete with CF.

C. Impact resistance of specimens based on type of fiber

Figure 3 depicts the impact resistance of various FRC specimens exposed to heat exposure. It is clearly visible that the addition of fiber has a direct contribution on impact resistance. For unheated FRC specimens it can be seen that the impact resistance are 3 to 6 times more than that of reference specimen. A drastic drop (5.2 – 14.5 times) in impact resistance can be seen when all FRC specimens exposed to 30 minutes of heat exposure. Concrete with CF has more impact resistance (1.1 – 2.3 times) compared to other specimens in 30 minutes of heat exposure.

Published By:
Blue Eyes Intelligence Engineering

International Journal of Innovative Technology and Exploring Engineering
IJITEE
www.ijitee.org

For 60 minutes of heat exposure CF, PPF and PVA shows similar impact resistance. For 90 minutes of heat exposure, plain concrete and concrete with AF shows least impact resistance (19.95 N-m) whereas concrete with all other fibers exhibit better impact resistance (39.90 N-m).

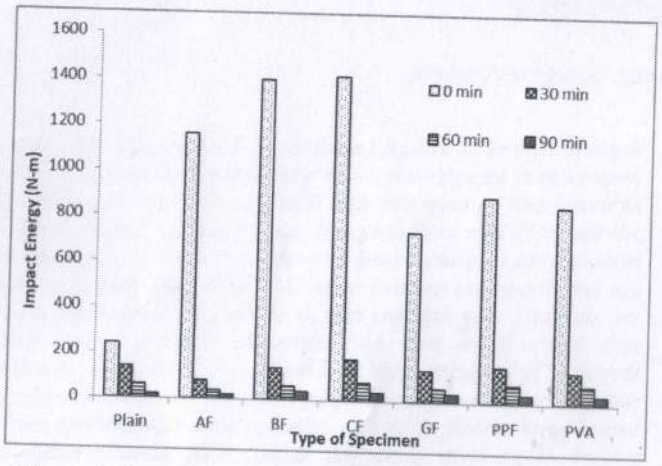


Figure 3: Impact Energy of different types of specimen

IV. CONCLUSIONS

The impact resistance of plain concrete and various fiber reinforced concretes of different grades with and without heat exposure are investigated. Based on the observations made from the investigation, the following results concluded.

- The addition of fiber enhanced the impact strength of concrete.
- The physical properties of fibers affect the impact resistance. The highest impact resistance is observed for concrete with CF.
- At elevated temperature all the specimens showed negligible variations in impact resistance due to the loss in bond with concrete, i.e. Specimen subjected to 90 minutes duration of heating.
- All the grades of concrete exhibited a similar trend in impact resistance for all the duration of heating.
- AF showed a drastic reduction in impact resistance with increase in temperature.

ACKNOWLEDGEMENTS

The authors wish to acknowledge the Science and Engineering Research Board, Department of Science and Technology of the Indian Government for the financial support (YSS/2015/001196) provided for carrying out this research

REFERENCE

1. Ramakrishna, G., & Sundararajan, T. (2005). Impact strength of a few natural fibre reinforced cement mortar slabs: a comparative study. *Cement and concrete composites*, *27*(5), 547-553.
2. Gopalaratnam, V. S. et al,. (1984). A modified instrumented Charpy test for cement-based composites. *Experimental mechanics*, *24*(2), 102-111.
3. Hibbert, A. P., & Hannant, D. J. (1978, April). The design of an instrumented impact test machine for fibre concretes. In *Testing and Test Method of Fibre Cement Composites', Proceedings of RILEM Symposium (The Construction Press, Sheffield, 1978)* (pp. 107-120).
4. Schrader, E. K. (1981, March). Impact resistance and test procedure for concrete. In *Journal Proceedings* (Vol. 78, No. 2, pp. 141-146).
5. Cantwell, W. J., & Morton, J. (1991). The impact resistance of composite materials—a review. *composites*, *22*(5), 347-362.
6. Gopalaratnam, V. S., & Shah, S. P. (1985). Strength, Deformation and Fracture Toughness of Fiber Cement Composites at Different Rates of Flexural Loading. In *Unknown Host Publication Title*. Swedish Cement & Concrete Research Inst.
7. Swamy RN, Jojagha AH. (1982 Nov) Impact resistance of steel fibre reinforced lightweight concrete. *International Journal of Cement Composites and Lightweight Concrete*. 1;4(4), 209-20.
8. Banthia, N. et al. (1998). Impact resistance of fiber reinforced concrete at subnorma temperatures. *Cement and Concrete Composites*, *20*(5), 393-404.
9. Muguruma, H., & Watanabe, F. (1990). Ductility improvement of high-strength concrete columns with lateral confinement. *Special Publication*, *121*, 47-60.
10. Ho, J. C. M., et al. (2010). Effectiveness of adding confinement for ductility improvement of high-strength concrete columns. *Engineering Structures*, *32*(3), 714-725.
11. Balendran, R. V. et al. (2002). Influence of steel fibres on strength and ductility of normal and lightweight high strength concrete. *Building and environment*, *37*(12), 1361-1367.
12. Nili, M., & Afroughsabet, V. (2010). The effects of silica fume and polypropylene fibers on the impact resistance and mechanical properties of concrete. *Construction and Building Materials*, *24*(6), 927-933.
13. Fraternali, F. et al. (2011). Experimental study of the thermo-mechanical properties of recycled PET fiber-reinforced concrete. *Composite Structures*, *93*(9), 2368-2374.
14. Ruan, Z. et al. (2015). Numerical investigation into dynamic responses of RC columns subjected for fire and blast. *Journal of Loss Prevention in the Process Industries*, *34*, 10-21.
15. Ngo, T. et al. (2007). Blast loading and blast effects on structures–an overview. *Electronic Journal of Structural Engineering*, *7*(S1), 76-91.
16. Choi, S. J., et al. (2017). Impact or blast induced fire simulation of bi-directional PSC panel considering concrete confinement and spalling effect. *Engineering Structures*, *149*, 113-130.
17. ACI Committee 544, (July 1978). Measurement of properties of fibre reinforced concrete. Journal, *American Concrete Institute*, Proc. Vol. 75, No. 7, pp. 283-90.
18. IS: 516–1959. Methods of Tests for Strength of Concrete.
19. ISO 1975 "Fire resistance tests-elements of building construction." International Standard ISO 834, Geneva.
20. Saxena, R., et al. (2018). Impact resistance and energy absorption capacity of concrete containing plastic waste. *Construction and Building Materials*, *176*, 415-421.
21. Mohammad hosseini H, et al. (2017). The impact resistance and mechanical properties of concrete reinforced with waste polypropylene carpet fibres. *Construction and Building Materials*. 143, 147-157.
22. Mastali M, et al. (2016). The impact resistance and mechanical properties of reinforced self-compacting concrete with recycled glass fibre reinforced polymers. *Journal of Cleaner Production*. 124, 312-324.
23. Guo YC, et al. (2014). Compressive behaviour of concrete structures incorporating recycled concrete aggregates, rubber crumb and reinforced with steel fibre, subjected to elevated temperatures. *Journal of Cleaner Production*. 72, 193-203.
24. Anand N and Prince Arulraj G. (2014). Effect of grade of concrete on the performance of self-compacting concrete beams subjected to elevated temperatures, *Fire Technology*. 50(5), 1269–1284.
25. Anand N, et al. (2014). Stress strain behavior of Normal compacting and Self compacting concrete under elevated temperatures, *Journal of Structural Fire Engineering*. 5 (1), 63–75.
26. Antony Godwin, et al. (2016). Influence of mineral admixtures on mechanical properties of self-compacting concrete under elevated temperature, *Fire and Materials*. 40(7), 940–958.
27. Purkiss, J. A. (1988). Toughness measurements on steel fibre concrete at elevated temperatures. *International Journal of Cement Composites and Lightweight Concrete*, *10*(1), 39-47.
28. Alwyn Varghese, et al. (2018). Studies on Behaviour of Fire Affected Fiber Reinforced Concrete, *International Journal of civil engineering and technology*. 9(10), 1668–1675.

AUTHORS PROFILE



Alwyn Varghese graduated from VLBJECT, Coimbatore in the year 2009. He completed his master degree in structural engineering from KCT, Coimbatore in the year 2013. Presently, he is pursuing Ph.D in the area of Fire resistance of fiber reinforced concrete under Department of Civil Engineering, KITS, Coimbatore. He has published more than 5 research papers in International Journals and Conferences. His areas of interest are Fire resistance of fiber reinforced concrete, Bond strength of concrete.



Dr.N.Anand graduated from Karunya Institute of Technology and Sciences, Coimbatore in the year 2003. He completed his Ph.D work in the area of Self Compacting Concrete Subjected to Elevated Temperature during the year 2014. Presently, he is working as Associate professor in Department of Civil Engineering, KITS, Coimbatore. He has published more than 55 research papers in International Journals and Conferences. His research areas are High performance concrete, Fire resistance of concrete and Lateral load behaviour of tall structures.



Dr. G. Prince Arulraj graduated from Thiagarajar College of Engineering, Madurai in the year 1982. He secured I rank in the college and II rank in Madurai Kamaraj University. He got his masters degree from IIT Madras in the year 1984. He got his Ph.D degree from IIT Madras in the year 1999. He has published 175 papers in International journals and conferences. His areas of interest are Self compacting concrete, Self curing concrete, Fire resistance of concrete and Concrete with nano materials.

IJITEE



Taylor & Francis
Taylor & Francis Group

Journal of Adhesion Science and Technology

ISSN: 0169-4243 (Print) 1568-5616 (Online) Journal homepage: https://www.tandfonline.com/loi/tast20

Influence of fibers on bond strength of concrete exposed to elevated temperature

Alwyn Varghese, Anand N, Prince Arulraj G & U. Johnson Alengaram

To cite this article: Alwyn Varghese, Anand N, Prince Arulraj G & U. Johnson Alengaram (2019) Influence of fibers on bond strength of concrete exposed to elevated temperature, Journal of Adhesion Science and Technology, 33:14, 1521-1543, DOI: 10.1080/01694243.2019.1602889

To link to this article: https://doi.org/10.1080/01694243.2019.1602889

Published online: 26 Apr 2019.

Submit your article to this journal

Article views: 45

View related articles

View Crossmark data

Full Terms & Conditions of access and use can be found at
https://www.tandfonline.com/action/journalInformation?journalCode=tast20

JOURNAL OF ADHESION SCIENCE AND TECHNOLOGY
2019, VOL. 33, NO. 14, 1521–1543
https://doi.org/10.1080/01694243.2019.1602889

Taylor & Francis
Taylor & Francis Group

ARTICLE

Check for updates

Influence of fibers on bond strength of concrete exposed to elevated temperature

Alwyn Varghese[a], Anand N.[a], Prince Arulraj G.[a] and U. Johnson Alengaram[b]

[a]Department of Civil Engineering, Karunya University, Coimbatore, India; [b]Centre for Innovative Construction Technology (CICT), Department of Civil Engineering, Faculty of Engineering, University of Malaya, Kuala Lumpur, Malaysia

ABSTRACT

Concrete is a building material having good fire resistance and the resistance depend on many factors including the properties of its constituent materials. Fiber Reinforced Concrete (FRC) apart from improving mechanical properties has better fire resistance than conventional concrete. Bond strength of concrete is one of the important properties to be considered by structural engineers while designing reinforced concrete cements. In this research, an experimental investigation has been carried out to determine the effect of fibers on the bond strength of different grades (M20, M30, M40 and M50) of concrete subjected to elevated temperature. Different types of fibers such as Aramid, Basalt, Carbon, Glass and Polypropylene were used in the concrete with a volume proportion of 0.25% to determine the bond strength by pull-out test. Prior to the pull-out test, the specimens were kept in a furnace and subjected to elevated temperatures following standard fire curve as per ISO 834. Based on the test results of the investigations, type of fiber, grade of concrete and duration of heating were found to be the key parameters that affect the bond strength of concrete. The contribution of carbon fiber in enhancing the bond strength was found to be more significant compared to other fibers. An empirical relationship has been developed to predict the bond strength of FRC at a slip of 0.25 mm. This empirical relationship is validated with experimental results.

ARTICLE HISTORY
Received 27 November 2018
Revised 10 March 2019
Accepted 28 March 2019

KEYWORDS
Bond strength; elevated temperature; fiber reinforced concrete; standard fire curve; Pull-out test

1. Introduction

The nature of failure of concrete structural elements exposed to fire shows a discrepancy due to factors such as rate of heating and magnitude of temperature. Failure of concrete may be due to loss of compressive, tensile, flexural, and bond strengths that results in spalling of concrete [1]. Significant strength loss was examined for concrete after the exposure to 600 °C [2]. There were some changes that had occurred in the pore structure due to cracking, spalling, destruction of the bond between cement paste and aggregate when the concrete was exposed to elevated heat [3,4]. In the case of

CONTACT Anand N davids1612@gmail.com Department of Civil Engineering, Karunya University, Coimbatore 641114, India

© 2019 Informa UK Limited, trading as Taylor & Francis Group

Reinforced Cement Concrete (RCC), bond strength between reinforcing steel and concrete is reduced due to fire exposure.

There is a growing interest in FRC because of its properties of the reinforcing fibers which improves the properties like fire resistance, stiffness and bond strength of concrete. Severe heat exposure can adversely affect the mechanical properties of concrete. It also leads to thermal incompatibility between concrete and steel. The high vapour pressure developed due to the inner moisture of concrete subjected to high temperature is not released by micro channels, which results in cracking and loss of strength of concrete [5].

Failure of reinforced concrete members exposed to fire may occur mainly due to the reduction in bond strength between the steel and concrete. Bond failure in concrete is due to the rapid reduction in the tensile strength of concrete as the temperature gradient rises within the concrete [6]. Reduction in bond strength depends on the duration of heating and the level of temperature to which the concrete is exposed. With the increase in temperature, bond stress decreases and the slip value increases [7]. Compressive strength of concrete, diameter of bar, concrete cover and embedded length are some of the factors that affect the bond strength of concrete. Application of fiber in concrete is one of the means to enhance the fire resistance of concrete. Recent researches indicate that the application of some types of fibers in concrete can improve the residual mechanical properties of concrete after exposure to elevated temperature [8]. When the pore pressure develops during heating, it exceeds the tensile strength of concrete and explosive spalling occurs. In this explosive spalling mechanism, thermal stress takes part in the development of strain energy [9].

Bond strength is the resistance to slipping of the steel bar, or separation of concrete around the bar which is embedded in concrete. This property is of a great significance in structural design of concrete members [10]. Moreover, the transfer of stress between concrete and steel has a great influence in controlling the width of cracks [11,12]. Effective bond creates the composite action between steel and concrete. Better performance of reinforced concrete members can be ensured only if there is an adequate bond between concrete and steel [10]. The aim of this study is to identify the suitability of fibers (Aramid, Basalt, Carbon, Glass and Polypropylene) for enhancing the bond strength of concrete exposed to elevated temperatures.

Many research works carried out on mechanical properties of FRC subjected to elevated temperature are available in literature [2,8,13–20]. Although bond strength is one of the major characteristics in reinforced concrete structures, only very limited information is available concerning the residual bond strength of different fiber reinforced concretes after exposed to high temperature. For the present study, the specimens were heated as per standard fire curve following ISO 834.

Concrete and steel maintaining a good bond by composite action so that it is used as a construction material known as reinforced concrete. It was reported [6,7,11] that there was a considerable loss in bond strength as the temperature was increased. The findings of these studies showed that the residual bond strength varies between 20% and 60% based on key factors such as the properties of concrete and rebar, diameter of rebar, embedment length of rebar, regime of heating and cooling etc.

The different studies showed a significant effect of surface characteristics of rebar, confinement of concrete, basic properties of concrete (w/c ratio, cement and aggregate

type, additives), maturity, relative humidity, and testing conditions (heating and cooling duration and rate, and testing while hot or cold) on concrete–steel bond behavior under a wide range of high temperature conditions. Earlier researches [6,7,11] explored the applications of steel fibers, polypropylene fibers or the combination of this two fibers to enhance the performance of concrete.

The present study investigates the contribution of synthetic fibers (CF,BF,AF,GF,PPF) on improving the bond strength between matured concrete and reinforcing steel at high temperatures as per standard fire. The present research explores the application of fiber with low and high melting point. The lack of information or knowledge in this area needs to be addressed so that engineers can choose the right fiber for the application. Hence the type of fiber, grade of concrete and duration of heating were considered as key factor. An empirical relationship has been developed to assess the residual bond strength of concrete with different types of fibers.

2. Materials & methods

2.1. Materials

Plain and FRC concrete were used in the study. Five types of fibers namely Aramid, Basalt, Carbon, Glass and Polypropylene fibers (Figure 1) were used to develop FRC with constant dosage 0.25% of concrete volume. The properties of constituent materials and details of mix proportion used for the investigation are given in Tables 1 and 2, respectively. Master Glenium SKY 8233 as a water reducing admixture (Super plasticizer) was used for maintaining the work ability (75 to 100 mm) during concreting. However the water cement ratio was carefully selected based on the strength point of view. So suitable optimum percentage of SP was used for maintaining the slump for developing M40 and M50 concrete. In the case of M20 and M30 the selected water cement ratio satisfied the slump.

Ribbed steel bars of 12 mm diameter and 400 mm long were used as reinforcement rod in 100 mm concrete cube specimens. Table 3 gives the properties of different fibers used for the investigation.

Aramid Fiber (AF) is in a nature of crystalline aromatic polyamides. They possess low density and high tensile strength to weight ratio. AF does not melt and it withstand against fire but starts carbonization at 427 °C. The maximum temperature suggested for continuous use for AF is 160 °C. They have very low thermal conductivity. Except

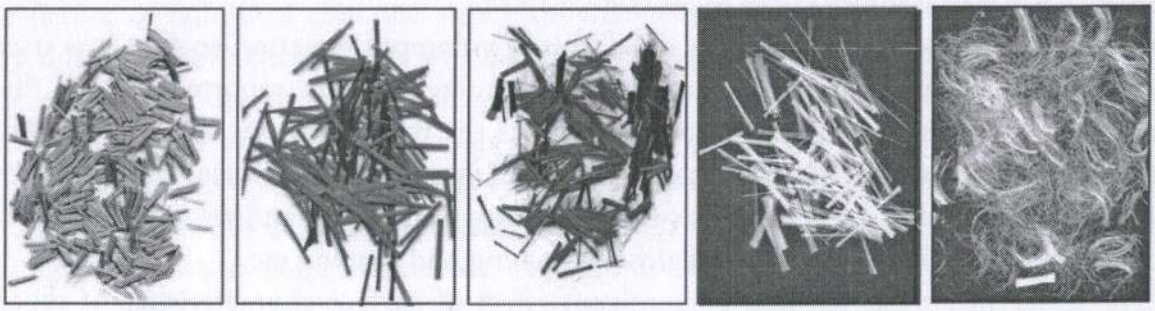


Figure 1. Types of fibers used (AF, BF, CF, GF, and PPF - from right to left).

Table 1. Properties of constituent materials.

Material	Density (kg/m^3)	Specific gravity	Surface moisture
Cement	1438	3.15	–
Fine aggregate	1620	2.74	Nil
Coarse aggregate	1800	2.90	Nil

Table 2. Concrete mix proportion.

Material	M20	M30	M40	M50
Cement (kg/m^3)	338	372	413	465
Fine aggregate (kg/m^3)	755	724	692	657
Coarse aggregate (kg/m^3)	1250	1251	1247	1237
w/c ratio	0.55	0.5	0.45	0.40

Table 3. Properties of fiber.

Fiber type	Length (mm)	Density (g/cu.cm)	Melting point (°C)	Young's modulus (GPa)	Coefficient of thermal expansion (10^{-6}/K)
AF	12	1.44	350	80	−4.0
BF	12	2.70	1450	100	8
CF	12	1.77	1200	240	−1.2
GF	12	2.55	1120	77	5.4
PPF	12	0.90	160	50	130

for a few strong acids and alkalis, their chemical resistance is good and has a negative coefficient of thermal expansion [21].

Basalt Fibers (BF) are produced by melting and processing of basalt rocks. The basalt rocks are divided into small fine particles to produce their fibers [22]. Previous researches have shown that addition of BF in concrete improves the thermal and mechanical properties of concrete [23]. Some researchers have studied the effect of BF on the mechanical properties of concrete. Heat resistance of BF can be explained in terms of natural basalt rock characteristics [24]. More over BF are not reacted with air or water and are non-flammable [25].

Carbon Fiber (CF) is a combined form of graphitic and amorphous carbon. Its high tensile modulus is a property of its graphitic form. It has negative coefficient of thermal expansion [21]. Carbon Fiber (CF) forms a bridge inside the concrete and resists crack propagation during loading. It also controls the volume change in concrete, that occurs by quick change of temperature and large temperature gradient. Due to this, it mitigates the initiation and expansion of inner micro defects of concrete. It is understood from the literature that it maintains higher residual strength of concrete after exposure to high temperature [26]. Glass Fiber (GF) is a material consisting of numerous extremely fine fibers of glass. GF are often preferred as reinforcement in a concrete due to their better impact resistance, good fatigue life and resistance against corrosion in most common environments [27]. The principal advantages of glass fibers are low cost, high tensile strength, high chemical resistance and excellent insulating properties. The disadvantages are relatively low tensile modulus, high density, sensitivity to abrasion during handling and relatively low fatigue resistance [21] which have no true melting point but softens up to 1200 °C [28]. GF are useful thermal insulators because of their high ratio of surface area to weight. However, the increased surface area makes them much more susceptible to chemical attack [29].

Polypropylene belongs to the polyolefin family of chemicals. The Polypropylene Fibers (PPF) are hydrophobic, they do not absorb water, and are not corrosive [30]. Due to this, balling is prevented in concrete with PPF during mixing. The fibers act as crack arresters. The concrete with PPF controls the propagation of cracks by holding the cement matrix together or bridging the cracks [30]. PPF melt at 160 °C and vaporize due to their lower melting point, which results in formation of micro channels in the concrete. Thus, greater vapour tension in capillaries can be alleviated and released, which may be the reason for the absence of explosive spalling in concrete with PPF [26].

2.2. Test setup

The concrete cube specimens of size 100 mm cast were cast and kept in a curing tank for 28 days. Reinforcement of diameter 12 mm and length 400 mm was inserted into fresh concrete specimen for a length of 100 mm. After curing, the specimens were surface dried for 24 hours prior to test. Then the specimens were wrapped by ceramic fiber around steel reinforcement rod to prevent the steel rod projections above concrete from heat. To determine the bond strength of concrete after exposure to elevated temperatures, a computer controlled electrical furnace with inner dimensions of $700 \times 400 \times 400$ mm and a power of 100kW was used. The maximum operating temperature of the furnace is 1200 °C, with a capability to follow the standard temperature curve, Equation 1. Type K thermocouples connected to an automatic data acquisition were used to monitor temperatures inside the furnace.

$$T - T_o = 345 \log 10(8t + 1) \quad (1)$$

Where: T - Furnace temperature at time t (degrees Celsius), T_o - Initial furnace temperature (degrees Celsius), t – Time (minutes).

Concrete specimens were exposed to heating durations of 30 min (821 °C), 60 min (925 °C), 90 min (986 °C) and 120 min (1029 °C) as per standard fire curve (Figure 2(a,b)). Heated specimens were cooled in ambient condition before the pull out test (Figure 2(c)). The investigation has been carried out for different grade of concrete such as M20, M30, M40 and M50.

2.2.1. Pull-out test

As per IS 2770:1967 Part 1, pull-out test was carried out using Universal Testing Machine (UTM) [31]. The specimen was placed in UTM in such a way that the bar could be pulled axially from the cube (Figure 3(a,b)). The pull-out loads against slippage were found and processed to obtain the relationship between bond stress and free end slip. Based on the literature [32–34], the critical bond stress is taken as the stress corresponding to a slip of the rebar considered was 0.25 mm ($BS_{0.25}$) (Figure 3(c)). The obligatory slip value of 0.25 mm is always lower than the one obtained when reaching the ultimate bond stress of unheated specimens. It may be noted that the critical bond stress ($BS_{0.25}$) is more conservative and more secure than BS_{max}. In this study, load and slip of reinforcing bar were recorded at sufficient number of intervals throughout the test, up to a slip of 0.25 mm. The bond stress was calculated for each specimen by

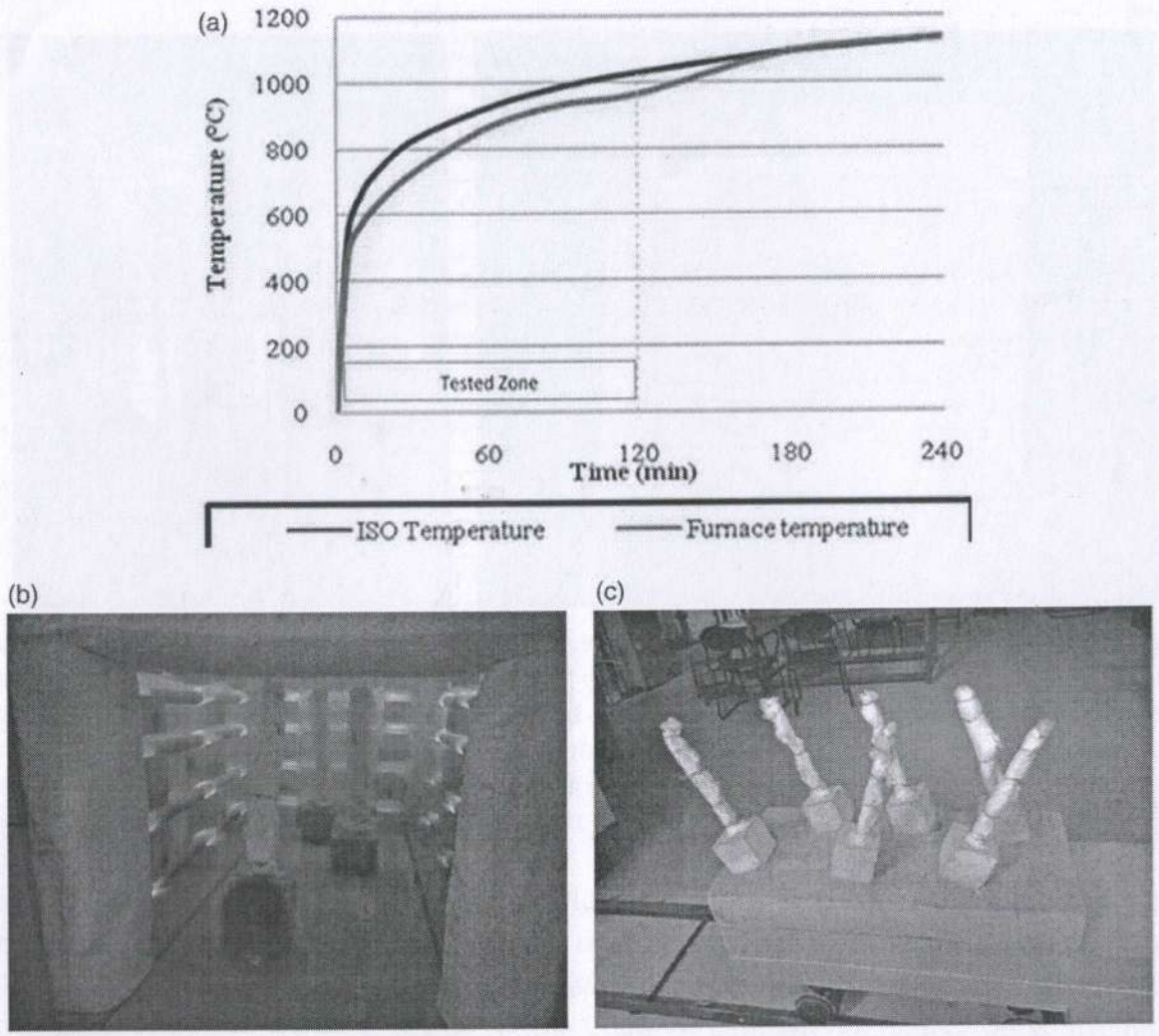


Figure 2. (a) Time temperature curve. (b) Specimens inside the furnace. (c) Specimens after exposed to elevated temperature.

dividing the applied load at the slip specified and by the surface area of the embedded length of the bar. Figure 3(d) shows the specimen after pull-out test.

2.3. Methodology

Four types of investigation were carried out to understand the influence of different fibers on bond strength of different grades of concrete.

1. Bond strength of different grades of Control Concrete (CC), i.e.; specimens without fibers and without heating.
2. Bond strength of different grades of CC specimens without fiber subjected to elevated temperature (30 min, 60 min, 90 min and 120 min).
3. Bond strength of different grades of FRC specimens without applying elevated temperature.
4. Bond strength of different grades of FRC specimens subjected to elevated temperature (30 min, 60 min, 90 min and 120 min).

The details of the experimental investigation carried out are shown in Figure 4.

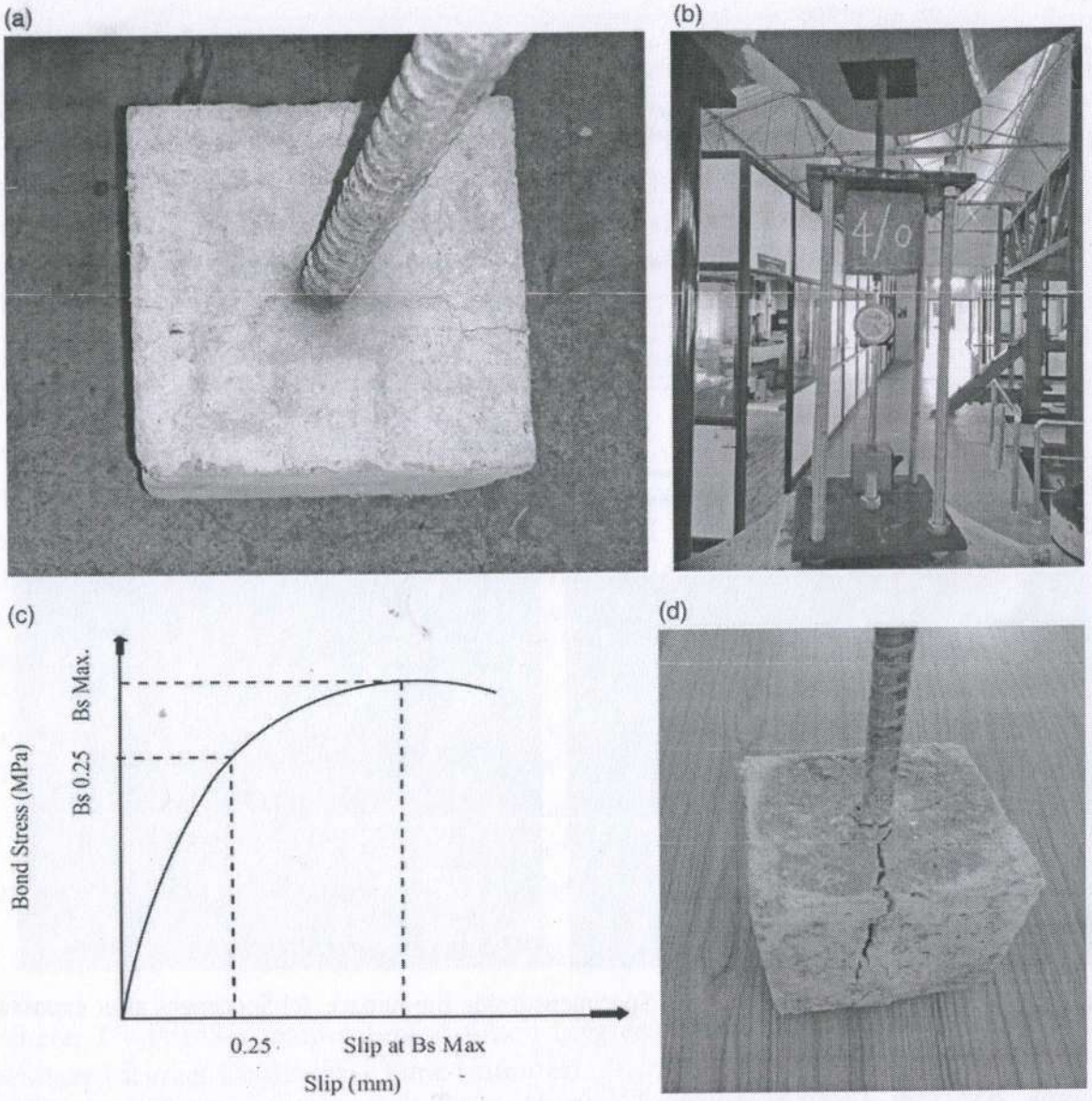


Figure 3. (a) Specimen after cooling. (b) Pull-out test. (c) Schematic bond stress and slip diagram. (d) Bond failure of specimen.

3. Results and discussion

3.1. Influence of temperature on bond strength of control concrete under elevated temperature

The ultimate failure of specimens of all grades occurred with vertical cracks. This may be due to the development of high thermal stresses inside the concrete specimens which caused the formation of micro cracks within the specimen [35]. At higher temperatures, reduction in strength of concrete is caused due to compression failure of concrete [36]. Figure 5(a–d) show the results of experimental investigation carried out to determine the pull-out bond strength of plain concrete specimens of different grades. It was found that bond strength of concrete decreased with the increase in temperature for all grades. It might be due to formation of cracks, dehydration of C-S-H gel in concrete and bond failure between aggregate and cement paste [37]. Experimental investigation also indicated that the bond strength of specimens

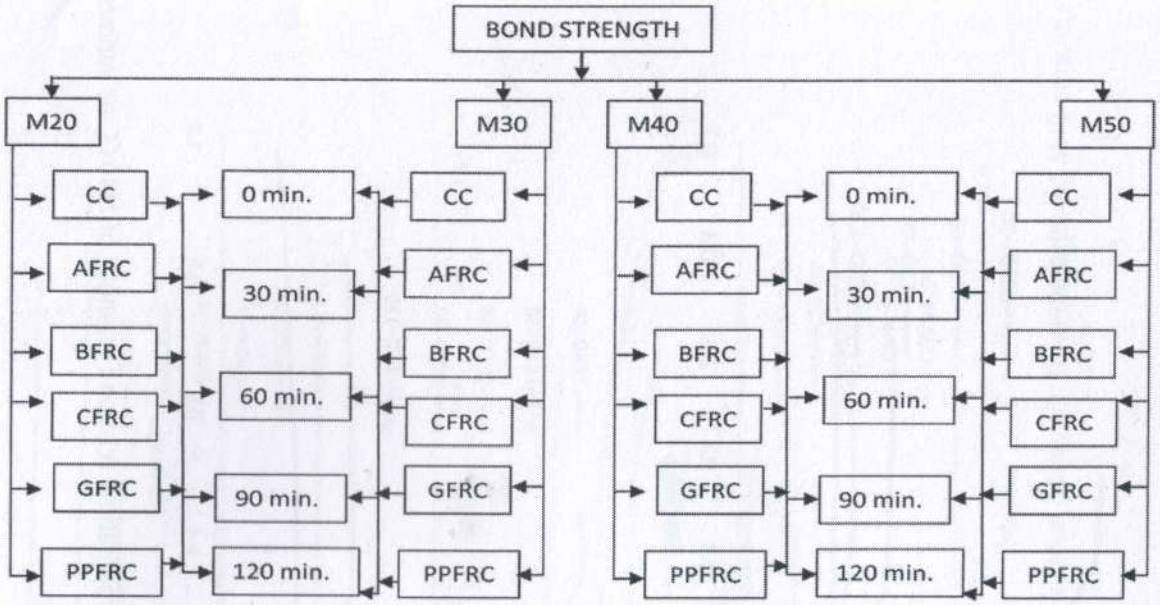


Figure 4. Details of experimental investigation. Note: CC: Control Concrete without fiber; AFRC: Aramid Fiber Reinforced Concrete; BFRC: Basalt Fiber Reinforced Concrete; CFRC: Carbon Fiber Reinforced Concrete; GFRC: Glass Fiber Reinforced Concrete; PPFRC: Polypropylene Fiber Reinforced Concrete. M20: Characteristic Compressive strength of concrete (20MPa). M30: Characteristic Compressive strength of concrete (30MPa). M40: Characteristic Compressive strength of concrete (40MPa). M50: Characteristic Compressive strength of concrete (50MPa).

subjected to heating decreased as the duration of heating increased. The slip value also was found to increase as the duration of heating increased from 30 minutes to 120 minutes. A sudden failure was observed for specimens heated up to 120 minutes (1029 °C) for all grades of concrete. As the grade of concrete increased, bond strength also increased for the specimens with and without fiber. The investigation also showed that cracks began to appear when the temperature reached around 600 °C [3]. The micro cracks were found to be more pronounced at 800 °C and extensively increased at 1000 °C. The specimen completely decomposed and lost its binding properties after exposure to 1000 °C. This was attributed to continuous crack formation [38].

The compressive strength of the specimens also decreased with respect to the loss of bond strength at elevated temperature [39]. The loss in strength of concrete was related to loss of weight of samples since reduction in compressive strength was attributed to dehydration of C-S-H gel in concrete at elevated temperatures [40]. Failure of concrete specimens might occur at elevated temperature, when heating reduced the bond strength between the steel and concrete. Bond failure was usually combined with tensile failure as the tensile strength decreases rapidly with heating [1].

3.2. Influence of addition of fiber on bond strength of concrete (without heat)

Normally synthetic fibers assist in reducing the cracks in concrete elements. For making FRC, fibers are dispersed and distributed randomly in concrete at the time of mixing and thus there could be an improvement of concrete properties in all directions. Figure 6(a–d) show the results obtained from the pull-out test to determine the bond strength of concrete specimens with and without fiber for different grades without

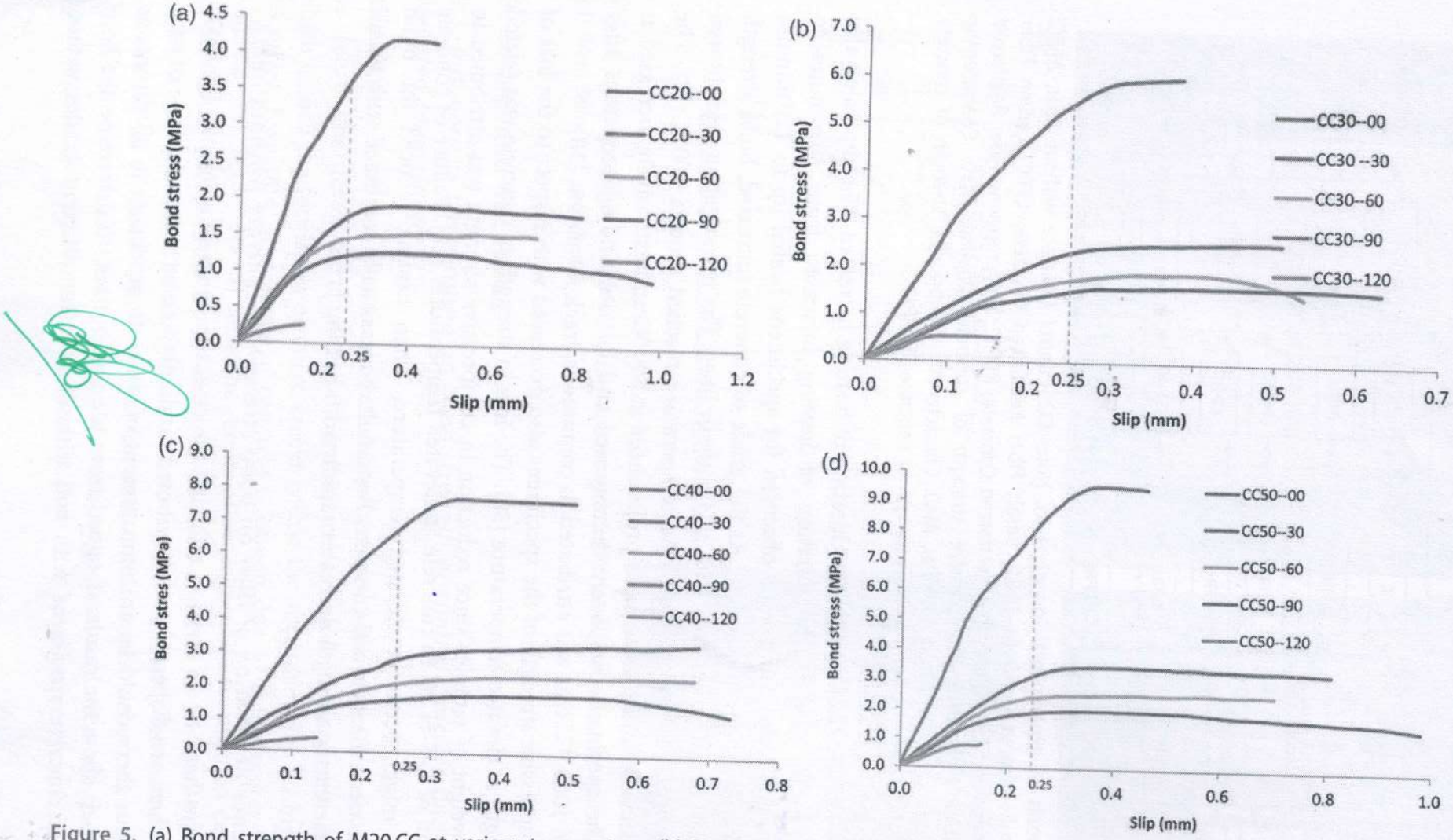


Figure 5. (a) Bond strength of M20 CC at various temperature. (b) Bond strength of M30 CC at various temperature. (c) Bond strength of M40 CC at various temperature. (d) Bond strength of M50 CC at various temperature.

exposure to heat. The bond strength of concrete was found to increase with the addition of fibers [41]. Bond strength of concrete with CF had the highest bond strength. Concrete with BF had the second highest strength and that was followed by AF and GF. The bond strength of the concrete with PPF was the least among the FRC. The bond strength was higher for specimens with fiber having higher young's modulus. Addition of fiber was found to improve the splitting tensile strength of concrete also. It was mainly due to the bridging action of the fiber across cracks, which effectively restrained the propagation of micro cracks in the primary stage. The delay in the development of macro cracks improves the splitting tensile strength [42].

The higher strength of concrete with CF may be due to its highest elastic modulus [43]. More over CF has more strength and volumetric stability than BF and GF under severe alkali condition [24]. Carbon Fiber Reinforced Concrete (CFRC) is known for higher flexural strength of concrete than any other fibers [13]. CF is very versatile, because of its extremely high strength to weight and stiffness to weight ratios. CF is highly stable and is relatively non-sensitive to chemical degradation [43].

From the investigations it is observed that bond strength of Basalt Fiber Reinforced Concrete (BFRC) is higher than that of concrete with AF, GF and PPF for all grades of concrete. It may be due to the resistance of BF to most chemicals, alkali solutions and water [44]. When BF comes in contact with other chemicals, no chemical reaction takes place [25]. The previous researchers reported that the addition of BF significantly improves the tensile and flexural strengths [42].

It is observed from the investigation that addition of AF in concrete resulted in more bond strength than GFRC, PPFRC and CC. It may be because of the higher Young's modulus of AF compared to those of GF and PPF.A previous research reported that the presence of strong alkaline aqueous solution can cause degradation of AF [45]. Concrete having a high pH value, possesses a highly alkaline environment[46]. The drop in the tensile strength and the surface degradation of AF is due to an alkaline environment [47]. Thus the bond strength of concrete with AF will decrease with ageing of concrete [1,47].

From the experiments, it is found that Glass Fiber Reinforced Concrete(GFRC) possesses more bond strength than Polypropylene Fiber Reinforced Concrete(PPFRC) and concrete without fiber (CC). It may be due to GF's more elastic modulus than PPF's.

It is found that PPFRC has more bond strength than CC. PPF can improve the flexural ductility and long-term durability of concrete [48]. It also reduces the plastic shrinkage of concrete [49]. It is reported that PPF fills the holes of mortar and thus reduces porosity and also stops the propagation of the micro cracks [50]. This improves the internal tensile, adhesion and bond strengths [51].

3.3. Influence of fibers on bond strength of concrete under elevated temperature

Figure 7(a–d) show the results of the pull-out test carried out on FRC with different grades exposed to duration of 30 minutes (821 °C). Addition of fiber can control reduction in bond strength by reducing macro cracks development on concrete [13,26]. The

reduction in bond strength is highfor CC followed by AFRC, PPFRC, GFRC, BFRC and CFRC for all grades of concrete.

It can be seen that, concrete with CF exposed to heat for a duration of 30 minutes (821 °C) exhibits higher bond strength than the concrete with other fibers. CF can resist the volume change of concrete caused by rapid change of temperature due to its negative coefficient of thermal expansion [43]. Hence in the case of CFRC cracking inside the concrete may be prevented [26]. Also CFRC has high bond strength than any other FRC at 30 minutes (821 °C) of exposure to heat. Additionally, CF has the ability to retain its tensile strength even at high temperatures [52].

Similarly BF also has higher elastic modulus, and the bond strength is higher for the specimens even after exposure to heat for duration of 30 minutes (821 °C). The tensile strength and elastic modulus are reduced when exposed to higher temperature, but they maintain their bond strength [15]. It may be due to its high melting point and its natural properties like non-combustible and explosion proof [25]. The reduction in bond strength is found to be higher for PPFRC and GFRC which may be due to low elastic modulus of PPF and GF.

It is observed from the investigation that GFRC has more bond strength than PPFRC, AFRC and CC. The reduction of bond strength of GFRC is higher at elevated temperature. It may be as a result of decrement in Young's modulus of GF with heat exposure [16].

It can be seen from the Figure 7 that the bond strength of PPFRC is higher than that of AFRC and CC. This is due to the fact that PPF turns into vapour above 340 °C [2,17] and forms vapour pressure dissipation network, which dissipates vapour within the concrete and prevents spalling [17,18,53]. This prevention of spalling helps to strengthen the bond between concrete and reinforcement. The escape channels formed by melting of the PPF impart limited improvement in bond resistance against heating because of the reduction in both splitting and compressive strengths as a result of the increase in the overall porosity [19]. Permeability of concrete with PPF is found to increase after heating due to the melting of PPF [54]. This has reduced the risk of increase in pores pressure in the PPFRC, which prevents the propagation of cracks. Thus bond strength reduction is controlled in PPFRC [55].

Observation indicates that the reduction in the bond strength of AFRC is very high at elevated temperature. Earlier researches report that AFRC subjected to more than 150 °C leads to oxidation of AF. More over degradation of AF due to the alkaline environment within the concrete is accelerated by the rise in temperature [47]. Thus AFRC, when heated, loses its bond strength between 50 and 60%.

The bond strength values of the samples heated for 60 minutes (925 °C) are shown in Figure 8(a–d). For all grades of concrete the bond strength decreased with increase in temperature. Observation indicates that at 60 minutes (925 °C) also that bond strength of CFRC is greater than that of other FRC. Bond strength of GFRC was found to decrease considerably. BFRC and PPFRC retained more bond strength (60–85%) than that of other FRC specimens. Bond strength of AFRC significantly reduced and the bond strength was found to be less than that of concrete without fiber (CC). One of the reasons behind the drop in bond strength of FRC can be partly attributed to uneven shrinkage caused by evaporation of water, dehydration and disintegration of

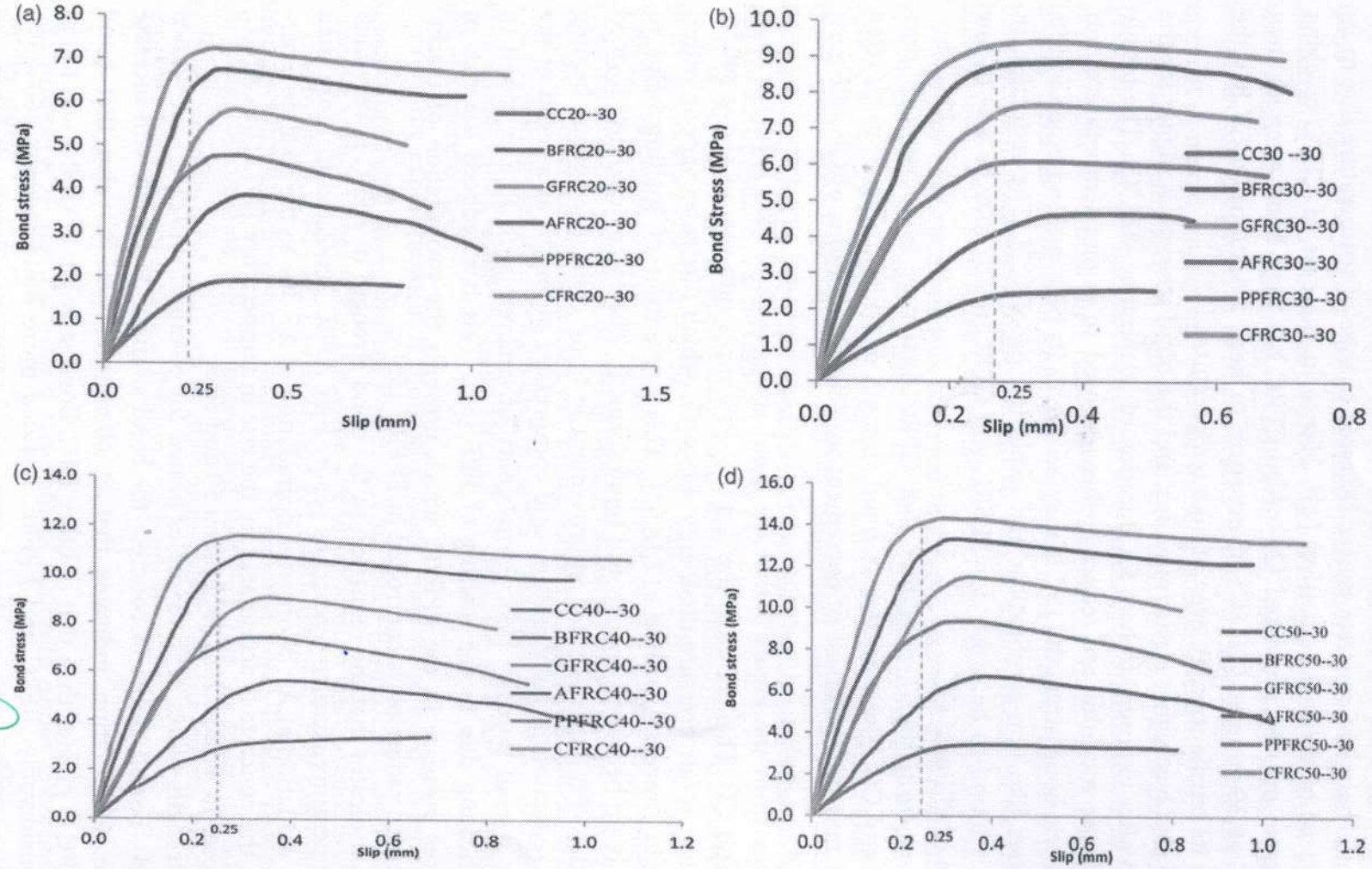


Figure 7. (a) M20 FRC specimen with 30 min heat exposure. (b) M30 FRC specimen with 30 min heat exposure. (c) M40 FRC specimen with 30 min heat exposure. (d) M50 FRC specimen with 30 min heat exposure.

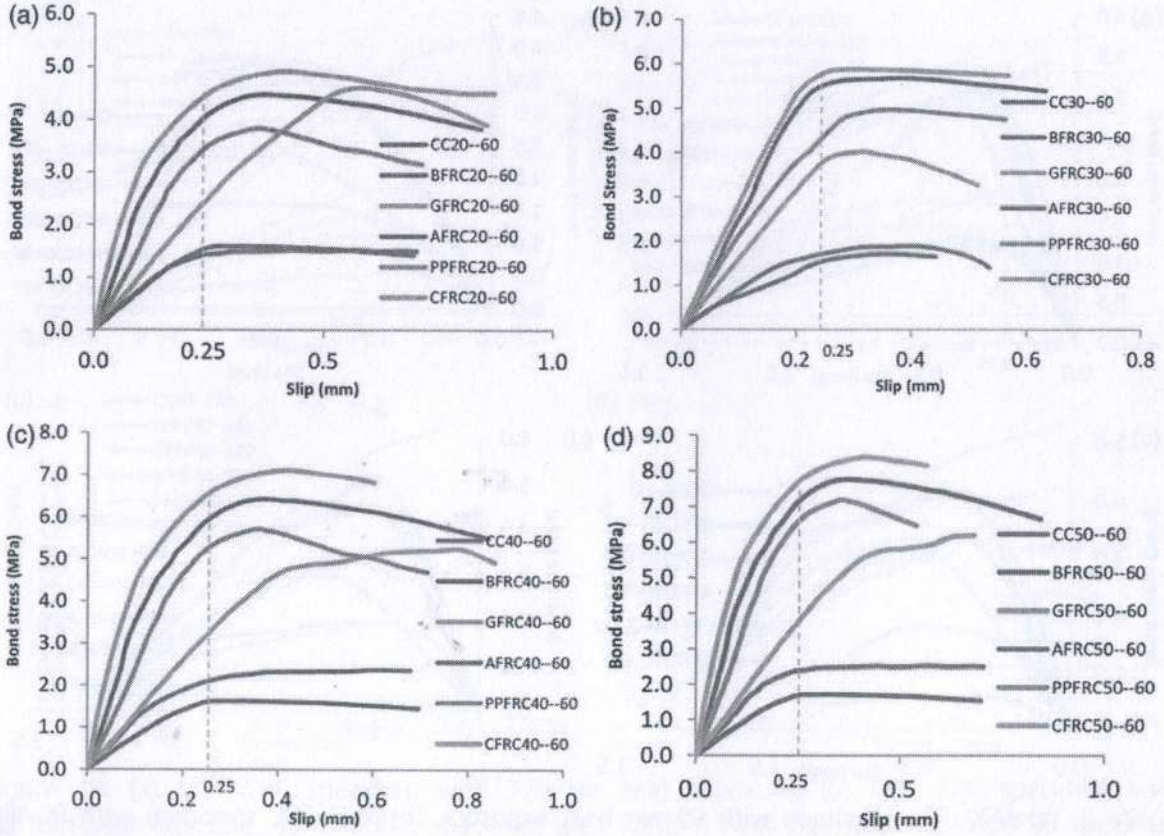


Figure 8. (a) M20 FRC specimen with 60 min heat exposure. (b) M30 FRC specimen with 60 min heat exposure. (c) M40 FRC specimen with 60 min heat exposure. (d) M50 FRC specimen with 60 min heat exposure.

ingredients of concrete at elevated temperature [54]. When the concrete surface is exposed to elevated temperature, surface cracking occurs. As a result of continuous heating, the free water existing within the concrete turns into vapour forming vapours bubbles. In the absence of pore, the vapour within the vapour bubbles induces tensile stress. When the tensile stress exceeds the tensile strength of the concrete, spalling occurs [56,57]. After 60 minutes (925 °C) of exposure, the bond strengths of CFRC and BFRC are found to be almost the same. Some research works indicate that after exposure to a very high temperature, the CF completely melts; losing volumetric stability and the GF melts partially. Concrete with BF maintains its shape even after heating and has not lost the volumetric stability. This high thermal stability is due to the material characteristics of natural basalt rocks, which nucleate at high-temperature [24].

Bond strengths of specimens after 90 minutes (986 °C) of exposure to heat are shown in Figure 9(a–d). From the observation, the bond strengths of CFRC, BFRC and PPFRC are found to be almost similar. Bond strength of GFRC is decreased lower than that of PPFRC. Bond strength of AFRC is reduced far below that of all types of FRCs.

The presence of CF and BF enhance bridging during crack growth in the concrete [2,58]. Hence it is understood from the experimental data that CFRC and BFRC have good bond strength at this temperature. Reduction in bond strength is observed for GFRC at this temperature. It may be due to reduction in elastic modulus of GF with elevated temperature [52]. Reduction in bond strength of each FRC depends on the type of fiber added to it. Exposure to higher temperature always affects the strength of

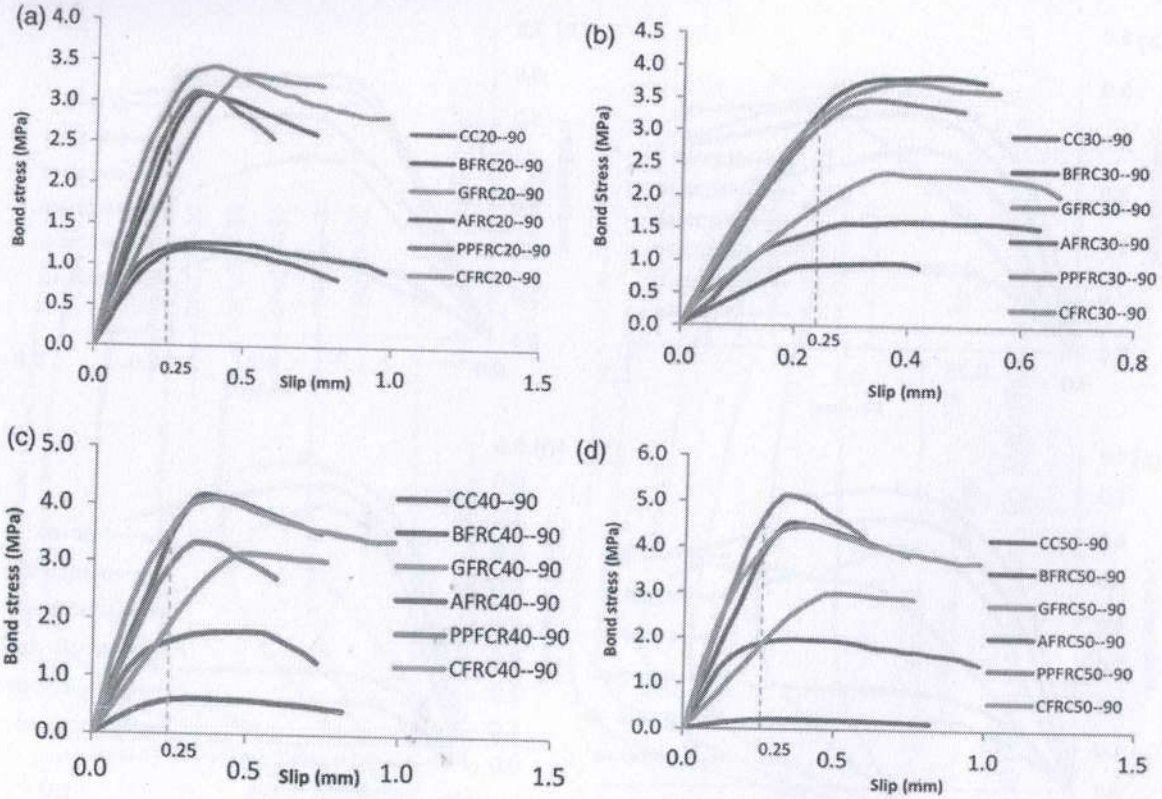


Figure 9. (a) M20 FRC specimen with 90 min heat exposure. (b) M30 FRC specimen with 90 min heat exposure. (c) M40 FRC specimen with 90 min heat exposure. (d) M50 FRC specimen with 90 min heat exposure.

concrete. Continuous heat exposure results in evaporation of water inside the concrete. This will increase the pore pressure and cause severe damage to concrete. PPF melts at high temperature and creates voids for releasing pressure inside the specimen when heated. Hence it helps control the instigation of cracks.

Figure 10(a–d) show the values of the bond strength of FRC exposure for duration of 120 minutes (1029 °C). Considerable loss of bond strength was noticed for all FRC after an exposure of 120 minutes of heat (1029 °C). When FRC was exposed for more than 120 minutes (1029 °C) of heat, the specimens were severely damaged and bond strength was found to be significantly reduced. This severe strength loss might be attributed to the decomposition of hydration products and thermal incompatibility between aggregates, fibers and cement paste [59]. The contribution of fibers at higher temperature is limited in controlling the reduction in bond strength. Concrete with PPF perform better in the case of specimens heated for 90 (986 °C) and 120 minutes (1029 °C) of exposure than the concrete with other fibers. The advantage of using PPF in high strength concrete is more pronounced from the results obtained.

3.4. Influence of grade of concrete on bond strength of concrete under elevated temperature

Figure 11(a–d) depicts the bond strength at a slip of 0.25 mm of FRC and CC for all grades exposed to different durations of heat. The bond strength of concrete is found to improve with the increase in the grade of the concrete. While heating, concrete with higher grades exhibits higher percentage of reduction with respect to its own unheated

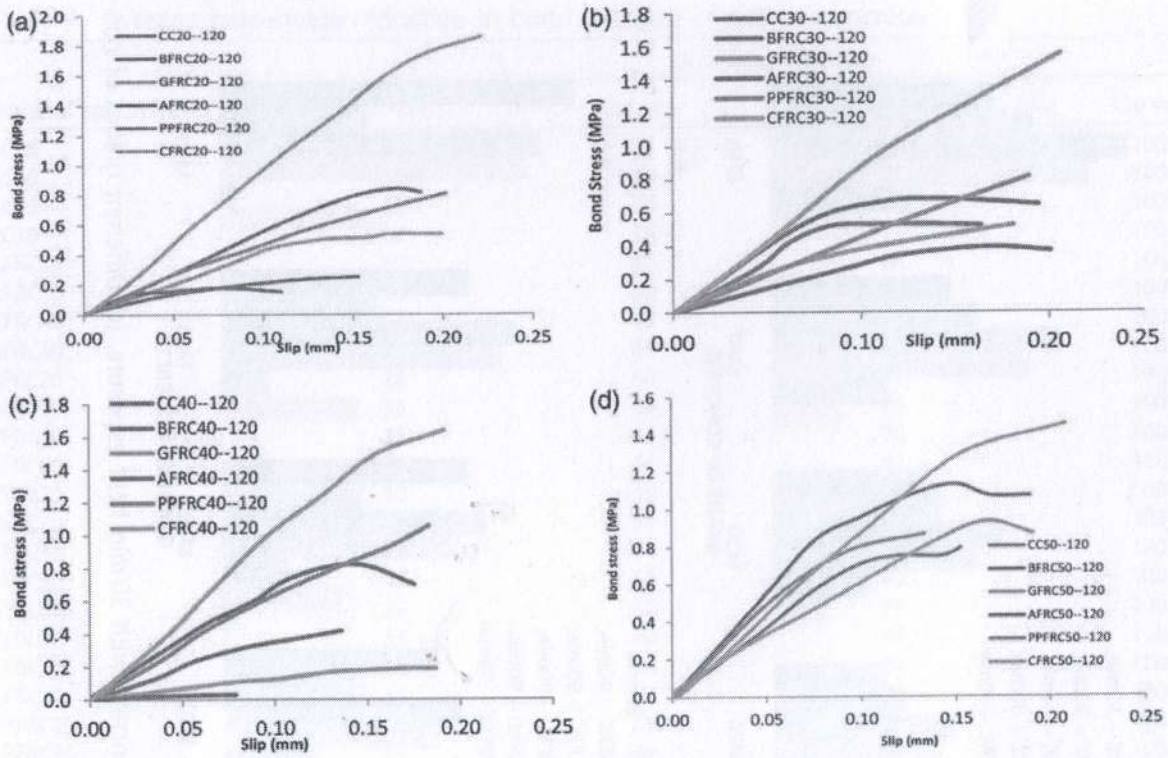


Figure 10. (a) M20 FRC specimen with 120 min heat exposure. (b) M30 FRC specimen with 120 min heat exposure. (c) M40 FRC specimen with 120 min heat exposure. (d) M50 FRC specimen with 120 min heat exposure.

specimen in bond strength (Table 4) [60,61]. Bond strength of all grades of concrete specimens fails to reach slip of 0.25 mm when exposed for duration of 120 minutes (1029 °C). The contribution of PPF begins with 60 minutes (925 °C) exposure of heating for improving bond strength of concrete. This can be visible in the case of M50 concrete specimen exposed to 90 minutes (986 °C) of heating. It may be due to the higher contribution of PPF at elevated heat by creating additional pores in high grade (M50) concrete.

3.5. Development of empirical relation to determine residual bond strength of concrete under elevated temperature

It was observed from the investigation that major reduction in bond strength occurred at a slip of 0.25 mm in most of the specimens. Hence it can be generalized that development of bond stress happens most importantly up to 0.25 mm slip for all the specimens. Table 4 gives the average percentage reduction in bond strength of heated specimens compared with its own unheated specimen. From these observations it was found that all the specimens exhibited 100% of reduction in bond strength for 120 minutes (1029 °C) of heat exposure.

Based on the experimental investigations, a statistical relation has been established to determine the residual bond strength at 0.25 mm slip. Compressive strength of concrete before heat exposure, type of fiber and duration of heating were considered as variables. The Bond Strength ($BS_{0.25}$) can be estimated using the relationship given below, the minimum value of $BS_{0.25}$ shall be considered as zero.

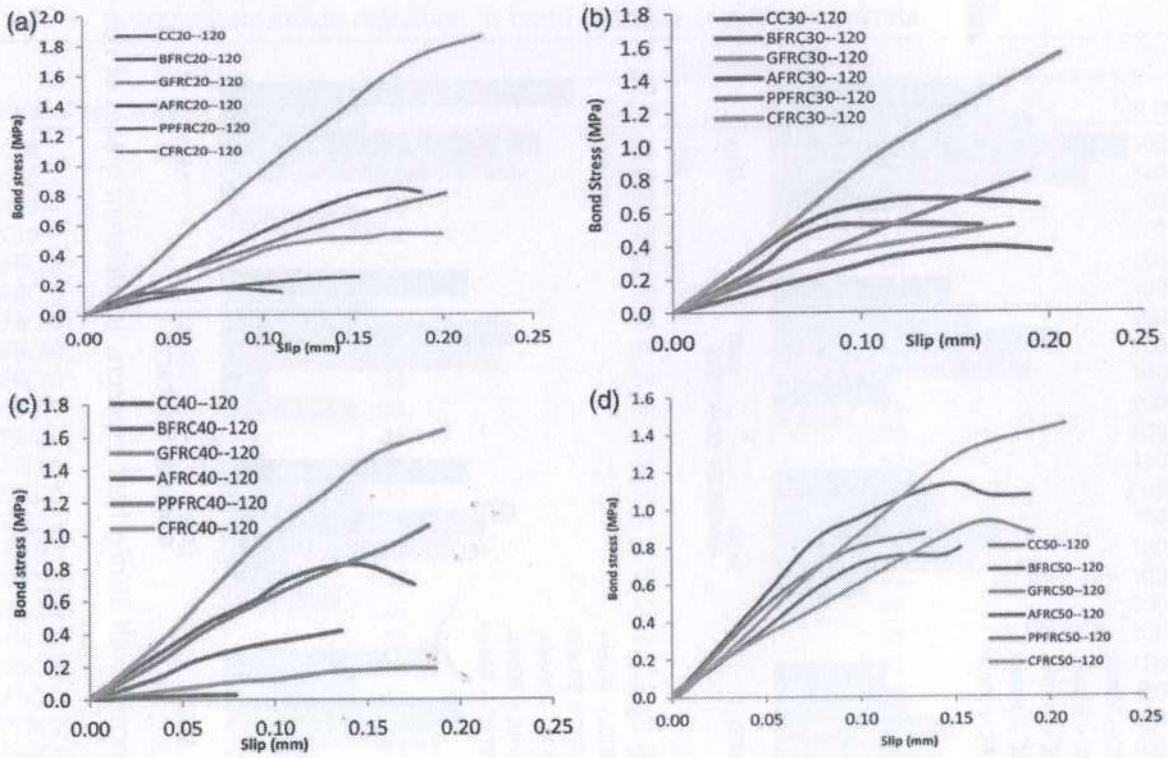


Figure 10. (a) M20 FRC specimen with 120 min heat exposure. (b) M30 FRC specimen with 120 min heat exposure. (c) M40 FRC specimen with 120 min heat exposure. (d) M50 FRC specimen with 120 min heat exposure.

specimen in bond strength (Table 4) [60,61]. Bond strength of all grades of concrete specimens fails to reach slip of 0.25 mm when exposed for duration of 120 minutes (1029 °C). The contribution of PPF begins with 60 minutes (925 °C) exposure of heating for improving bond strength of concrete. This can be visible in the case of M50 concrete specimen exposed to 90 minutes (986 °C) of heating. It may be due to the higher contribution of PPF at elevated heat by creating additional pores in high grade (M50) concrete.

3.5. Development of empirical relation to determine residual bond strength of concrete under elevated temperature

It was observed from the investigation that major reduction in bond strength occurred at a slip of 0.25 mm in most of the specimens. Hence it can be generalized that development of bond stress happens most importantly up to 0.25 mm slip for all the specimens. Table 4 gives the average percentage reduction in bond strength of heated specimens compared with its own unheated specimen. From these observations it was found that all the specimens exhibited 100% of reduction in bond strength for 120 minutes (1029 °C) of heat exposure.

Based on the experimental investigations, a statistical relation has been established to determine the residual bond strength at 0.25 mm slip. Compressive strength of concrete before heat exposure, type of fiber and duration of heating were considered as variables. The Bond Strength ($BS_{0.25}$) can be estimated using the relationship given below, the minimum value of $BS_{0.25}$ shall be considered as zero.

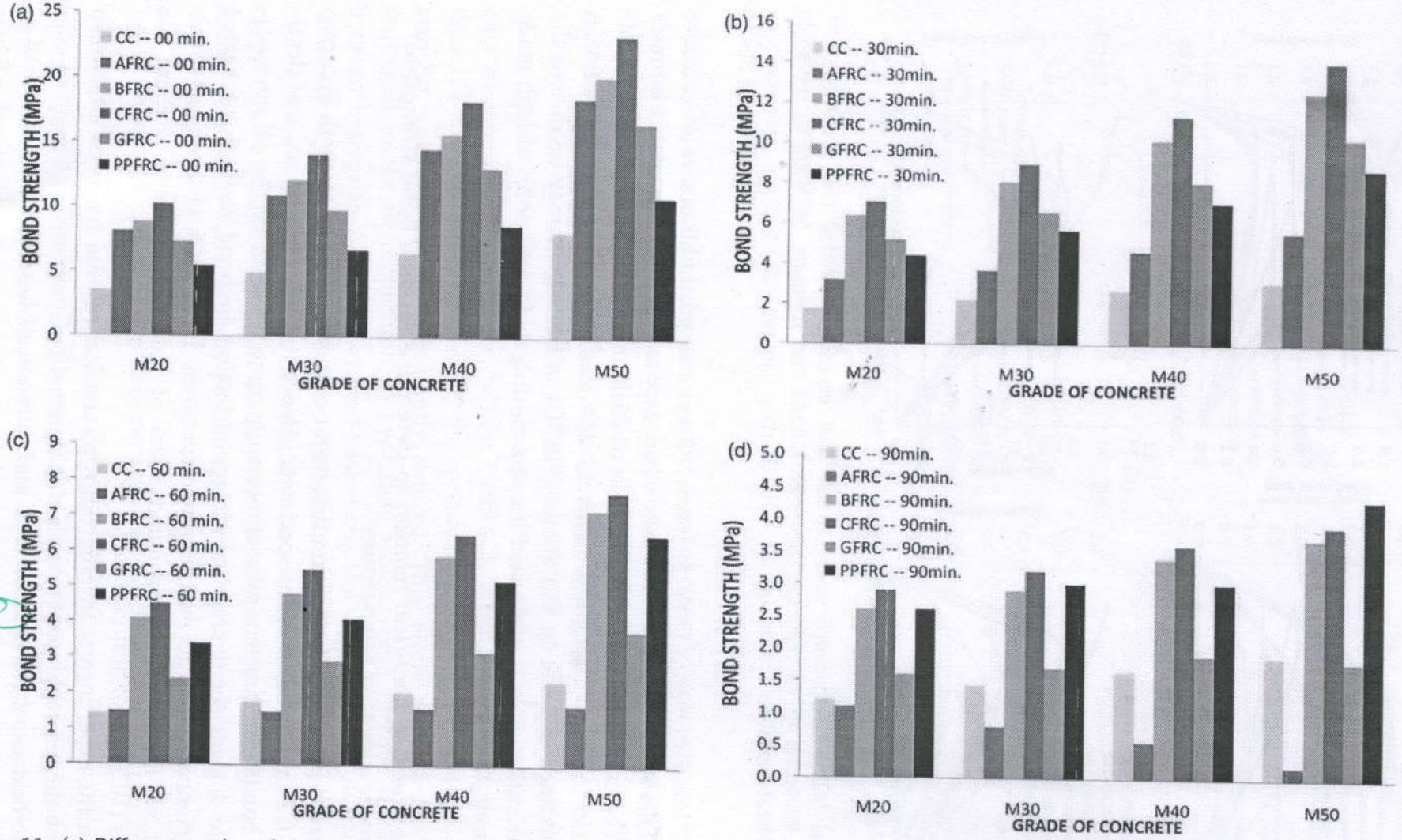


Figure 11. (a) Different grades of concrete without heat exposure. (b) Different grades of concrete with 30 min heat exposure. (c) Different grades of concrete with 60 min heat exposure. (d) Different grades of concrete with 90 min heat exposure.

Table 4. Average percentage reduction in bond strength of heated concrete.

Name of specimen	Duration of heating			
	30 min	60 min	90 min	120 min
CC20	51	59	66	100
CC30	55	64	71	100
CC40	58	68	74	100
CC50	62	71	77	100
AFRC20	60	81	86	100
AFRC30	66	86	93	100
AFRC40	68	89	96	100
AFRC50	70	91	99	100
BFRC20	28	54	71	100
BFRC30	33	60	76	100
BFRC40	35	62	78	100
BFRC50	38	64	82	100
CFRC20	30	56	72	100
CFRC30	36	61	77	100
CFRC40	38	64	80	100
CFRC50	40	67	83	100
GFRC20	29	67	78	100
GFRC30	33	70	83	100
GFRC40	38	76	85	100
GFRC50	38	77	89	100
PPFRC20	20	38	53	100
PPFRC30	15	39	55	100
PPFRC40	18	40	66	100
PPFRC50	19	40	61	100

Table 5. Bond strength at 0.25mm slip for different grades of concrete without fiber.

Grade of concrete (without fiber)	Average Bond strength at 0.25mm slip ($BS_{0.25}$) (MPa)	Standard Deviation
15	2.912	0.0775
20	3.532	0.0521
25	4.314	0.0481
30	4.913	0.0491
35	5.721	0.0512
40	6.461	0.0425
45	7.290	0.0421
50	8.122	0.0487
55	9.211	0.0473

$$BS_{0.25} = A(B + D) + A(B + D)C \quad (1)$$

Where,

A is average bond strength (at 0.25 mm slip) of plain concrete without heating (Table 5).

B is relative bond strength (at 0.25 mm slip) for different grades of concrete with different heat exposure (Table 6).

C is a constant according to type of FRC (Table 7).

D is a constant based on duration of heating based on different type of fiber (Table 8).

Thirty specimens were cast and tested in each grade to determine the bond strength of concrete with different fibers. Table 5 gives the values of constant A which is the average bond strength of specimens (without fiber) for different grade of concrete.

Table 6. Relative bond strength at 0.25mm slip for different grades of concrete with different heat exposure.

	Grade of concrete			
Temperature exposure (minutes)	M20	M30	M40	M50
0	1.00	1.00	1.00	1.00
30	0.49	0.44	0.41	0.39
60	0.41	0.36	0.32	0.30
90	0.34	0.29	0.26	0.23
120	0.00	0.00	0.00	0.00

Table 7. Constant for different type of fiber.

Fiber constant (C)				
AFRC	BFRC	CFRC	GFRC	PPFRC
1.245	1.438	1.827	1.023	0.358

Table 8. Constant based on duration of heating for different type of fiber.

	Variation of ratio of $BS_{0.25}$ of FRC from CC				
Time of exposure	AFRC	BFRC	CFRC	GFRC	PPFRC
0 min	0.00	0.00	0.00	0.00	0.00
30 min	−0.10	0.23	0.21	0.22	0.31
60 min	−0.22	0.06	0.03	−0.08	0.21
90 min	−0.21	−0.05	−0.06	−0.12	0.13
120 min	0.00	0.00	0.00	0.00	0.00

Table 9. Ratio of bond strength of frc with respect to cc at slip 0.25mm (unheated specimen).

Type of Mix	M20	M30	M40	M50
AFRC	2.295	2.220	2.254	2.278
BFRC	2.504	2.464	2.430	2.488
CFRC	2.890	2.872	2.833	2.882
GFRC	2.068	1.996	2.028	2.044
PPFRC	1.558	1.365	1.347	1.342

The concrete specimens were exposed to elevated temperature and the bond strength of specimens was found after cooling the specimens. The reduction in the bond strength was calculated. For all the concrete specimens exposed to heat for 120 minutes (1029 °C), the bond strength falls down to zero (0%). The results of thirty specimens were used to determine the relative bond strength of specimens subjected to elevated temperature for durations of 30, 60, 90 and 120 minutes (821 °C, 925 °C, 986 °C and 1029 °C). The relative bond strength is defined as the ratio between the bond strengths of heated and unheated specimen. This relative bond strength is the constant B and the values of B are given in Table 6.

When fibers added to concrete, its bond strength increases or falls depends on the type of fiber and grade of concrete. Table 9 depicts the ratio of bond strength of FRC with respect to bond strength of CC in an unheated condition. It can be seen that for different grades of concrete, the ratio of bond strength is almost same. From Table 9, it is evident that the ratio of bond strength of FRC with respect to CC in an unheated condition is independent on the grade of concrete. The constant C has been obtained based on trial and error method and the values for different fibers are given in Table 7.

Table 10. Ratio of bond strength of m20 grade concrete specimen with respect to its unheated specimen at slip 0.25mm.

Time of exposure (minutes)	CC		AFRC		BFRC		CFRC		GFRC		PPFRC	
	$BS_{0.25}$	Ratio of $BS_{0.25}$	$BS_{0.25}$	Ratio of $BS_{0.25}$	$BS_{0.25}$	Ratio of $BS_{0.25}$	$BS_{0.25}$	Ratio of $BS_{0.25}$	$BS_{0.25}$	Ratio of $BS_{0.25}$	$BS_{0.25}$	Ratio of $BS_{0.25}$
0	3.53	1.00	8.10	1.00	8.84	1.00	10.20	1.00	7.30	1.00	5.50	1.00
30	1.73	0.49	3.20	0.40	6.40	0.72	7.10	0.70	5.20	0.71	4.40	0.80
60	1.44	0.41	1.50	0.19	4.10	0.46	4.50	0.44	2.40	0.33	3.40	0.62
90	1.21	0.34	1.10	0.14	2.60	0.29	2.90	0.28	1.60	0.22	2.60	0.47
120	0.00	0.00	0.00	0.00	0.00	0.00	0.00	0.00	0.00	0.00	0.00	0.00

Table 11. Increase in $BS_{0.5}$ of M20 concrete mix with respect to CC.

Time of exposure (min)	Ratio b/w FRC and CC				
	AFRC	BFRC	CFRC	GFRC	PPFRC
0	2.3	2.5	2.9	2.1	1.6
30	1.8	3.7	4.1	3.0	2.5
60	1.0	2.8	3.1	1.7	2.4
90	0.9	2.1	2.4	1.3	2.1

For each FRC specimen, the ratio of bond strength of heated specimen varies according to the duration of heat exposure and the type of fiber. The values of bond strength and the ratio of bond strengths of heated to unheated specimen are given in Tables 10 and 11.

The constant D is defined as the algebraic difference between the ratio of bond strength of FRC and CC at the same temperature. This constant may be positive or negative according to its contribution of fibers. Also this constant is applicable for concrete with grade ranges from M20 to M50. The values of constant D are given in Table 8.

The bond strength of different specimens was estimated using the equation derived and compared with bond strength at 0.25 mm slip.

4. Conclusions

Based on the experimental studies, it was found that the increase or decrease in the bond strength depends on the physical properties of fibers added to concrete specimens. One of the major parameter which influences the bond strength of concrete is the Young's modulus of the fiber. Fiber with high Young's modulus is found to increase the bond strength of concrete. Formation ofmacro cracks is the main reason for the reduction in bond strength of concrete. Macro crack formation occurs mostly with the rise in the temperature. Addition of fibers helps to control the development and propagation of micro cracks and thus the decrease in the bond strength is controlled. At exposure duration of 120 minutes (1029 °C), the concrete specimens completely disintegrate and the bond strength becomes zero. At this temperature fibers cannot controlthe micro crack propagation and hence the bond strength of concrete decreases drastically. Some fibers like PPF melt at high temperature and are absorbed by cement matrix, which induces air voids inside the specimens. This leads to reduction in the pore pressure which helps to prevent the formation of macro cracks. Carbon and Basalt Fibers have high melting point and high Young's modulus. These fibers produce a very strong bond among cement matrixes. To break this bond, more stress is needed. Hence use of these fibers helps to reduce the cracks. The contribution

of carbon fiber on increasing the bond strength of M50 concrete is found to be 4.2 times more than that of the controlled concrete. The degradation of AF happens in alkaline environment. Moreover at elevated temperature, AF gets oxidized and disintegrated which leads to accumulation of cracks in AFRC. Young's modulus of glass fiber reduces with increase in temperature which results in the reduction of bond strength of GFRC.

Disclosure statement

No potential conflict of interest was reported by the authors.

Funding

The authors wish to acknowledge the Science and Engineering Research Board, Department of Science and Technology of the Indian Government for the financial support (YSS/2015/001196) provided for carrying out this research.

ORCID

Anand N. http://orcid.org/0000-0001-7643-9747

References

[1] Khoury GA. Effect of fire on concrete and concrete structures. Prog Struct Engng Mater. 2000;2:429–447.
[2] Behnood A, Ghandehari M. Comparison of compressive and splitting tensile strength of high-strength concrete with and without polypropylene fibers heated to high temperatures. Fire Saf J. 2009;44:1015–1022.
[3] Georgali B, Tsakiridis PE. Microstructure of fire-damaged concrete. A case study. Cem Concr Compos. 2005;27:255–259.
[4] Sukontasukkul P, Worachet P, Smith S. Post-crack (or post-peak) flexural response and toughness of fiber reinforced concrete after exposure to high temperature. Construction Build Mater. 2010;24:1967–1974.
[5] Anand N, Arulraj GP. Effect of grade of concrete on the performance of self-compacting concrete beams subjected to elevated temperatures. Fire Technol. 2014;50:1269–1284.
[6] Morley PD. "Effects of elevated temperature on bond in reinforced concrete." University of Edinburgh, 1982.
[7] Lublóy É, György BL. Temperature effects on bond between concrete and reinforcing steel. Zbornik Gfs.. 2014;30:27–35.
[8] Poon CS, Shui ZH, Lam L. Compressive behavior of fiber reinforced high-performance concrete subjected to elevated temperatures. Cem Concr Res. 2004;34:2215–2222.
[9] Suhaendi SL, Horiguchi T. Effect of short fibers on residual permeability and mechanical properties of hybrid fibre reinforced high strength concrete after heat exposition. Cem Concr Res. 2006;36:9672–1678.
[10] ACE Committee 544. State-of-the-art report on fiber reinforced concrete. ACI Concr Int. 1982;4:9–30.
[11] Morley PD, Royles R. Response of the bond in reinforced concrete to high temperatures. Mag Concr Res. 1983;35:67–74.
[12] ACI Committee 408. Bond Stress- the state of the art. ACI J. 1966;63;1161–1188.

[13] Tanyildizi H. Effect of temperature, carbon fibers, and silica fume on the mechanical properties of lightweight concretes. New Carbon Mater. 2008;23:339–344.
[14] Bhat T, Chevali V, Liu X. Fire structural resistance of basalt fiber composite. Compos Part A Appl Sci Manuf. 2015;71:107–115.
[15] Feng W, Lu Z. Effect of elevated temperature on the mechanical properties of basalt fibers and BFRP plates. Proceedings of the 6th Asia-Pacific Conference on FRP in Structures; 2017; Singpore; 156–157.
[16] Abbasi A, Hogg PJ. Temperature and environmental effects on glass fibre rebar: modulus, strength and interfacial bond strength with concrete. Compos Part B Eng. 2005;36:394–404.
[17] Kalifa P, Chene G, Galle C. High-temperature behavior of HPC with polypropylene fibres: From spalling to microstructure. Cem Concr Res. 2001;31:1487–1499.
[18] Khoury GA, Willoughby B. Polypropylene fibers in heated concrete. Part 1: molecular structure and materials behavior. Mag Concr Res. 2008;60:125–136.
[19] Haddad RH, Al-Saleh RJ, Al-Akhras NM. Effect of elevated temperature on bond between steel reinforcement and fiber reinforced concrete. Fire Saf J. 2008;43:334–343.
[20] Faiyadh FI, Al-Ausi MA. Effect of elevated temperature on splitting tensile strength of fibre concrete. Int J Cem Compos Lightweight Concr. 1989;11:175–178. Aug 1
[21] Mallick PK. Fiber-reinforced composites: materials, manufacturing, and design. USA: CRC press;2007
[22] Mingchao W, Zuoguang Z, Yubin L, et al. Chemical durability and mechanical properties of alkali-proof basalt fiber and its reinforced epoxy composites. J Reinforced Plastics Compos. 2008;27:393–407.
[23] Li XE. Study on thermal resistance of basalt filament yarn. AMR. 2011;146:666–669.
[24] Sim J, Park C, Moon DY. Characteristics of basalt fiber as a strengthening material for concrete structures. Compos Part B Eng. 2005;36:504–512.
[25] Singha K. A short review on basalt fiber. Int J Text Sci. 2012;1:19–28.
[26] Chen B, Liu J. Residual strength of hybrid-fiber-reinforced high-strength concrete after exposure to high temperatures. Cem Concr Res. 2004;34:1065–1069.
[27] Nahar S, Khan RA, Dey K. Comparative studies of mechanical and interfacial properties between jute and E-glass fiber-reinforced polypropylene composites. J Reinforced Plastics Compos. 2010;29:1078–1088.
[28] Gupta VB, Vk K. Manufactured fibre technology, 457–479. London (UK): Chapman & Hall;1997
[29] Bergman TL, Incropera FP, Lavine AS, et al. Fundamentals of heat and mass transfer. 7th ed. USA: John Wiley & Sons;2011
[30] Aulia TB. Effects of polypropylene fibers on the properties of high-strength concretes. Germany: Institutes for Massivbau and Baustoffechnologi, University Leipzig; 2002, Lacer 7.
[31] Indian Standard Methods of Testing Bond in Reinforced Concrete Part 1 Pull-Out Test (2007) Bureau of Indian Standards, Manak Bhavan, New Delhi.
[32] FIB Bulletin No. 10. Bond of Reinforcement in Concrete, State of the Art. Report prepared by Task Group Bond Models, former CEB, Task Group 5.2.CH-1015, Lausanne, 2000.
[33] Sfikas IP, Trezos KG. Effect of composition variations on bond properties of self compacting concrete specimens. Constr Build Mater. 2013;41:252–262.
[34] Foroughi A, Dilmaghani S, Famili H. Bond strength of reinforcement steel in self-compacting concrete. Int J Civ Eng. 2008;6:24–33.
[35] Noumowe AN, Clastres P, Debicki G, Costaz J-L. Transient heating effect on high strength concrete. Nucl Eng Des. 1996;166:99–108.
[36] Royles R, Morley PD. Further responses of the bond in reinforced concrete to high temperatures. Mag Concr Res. 1983;35:157–163.
[37] Morley PD, Royles R. The influence of high temperature on the bond in reinforced concrete. Fire Saf J. 1980;2:243–255.
[38] Arioz O. Effects of elevated temperatures on properties of concrete. Fire Saf J. 2007;42: 516–522.

[39] Diederichs U, Schneider U. Bond strength at high temperatures. Mag Concr Res. 1981; 33:75–84.
[40] Chan YN, Peng GF, Anson M. Residual strength and pore structure of high-strength concrete and normal strength concrete after exposure to high temperatures. Cem Concr Compos. 1999;21:23–27.
[41] Ezeldin A, Balaguru P. Bond behavior of normal and high-strength fiber reinforced concrete. Mater J. 1989;86:515–524.
[42] Jiang C, Fan K, Wu F, et al. Experimental study on the mechanical properties and microstructure of chopped basalt fibre reinforced concrete. Mater Des. 2014;58:187–193.
[43] Mallick PK. Fiber-Reinforced Composites: Materials, Manufacturing and Design. 3rd Edition. London, UK: CRC Press; 2007
[44] Wei B, Cao H, Song S. RETRACTED: environmental resistance and mechanical performance of basalt and glass fibers. Mater Sci Eng A. 2010;527:4708–4715.
[45] Yamasaki Y, Masuda Y, Tanano H, et al. Fundamental properties of continuous fiber bars. International Concrete Abstracts Portal (ACI). 1993;138:715–730.
[46] Burgoyne CJ. Aramid fibers for civil engineering applications. In: Doran DK, editor. Construction materials reference book. UK: Butterworth-Heinemann; 1992
[47] Derombise G, Schoors LVV, Messou MF, et al. Influence of finish treatment on the durability of aramid fibers aged under an alkaline environment. J Appl Polym Sci. 2010;117:888–898.
[48] Hannant DJ. Durability of polypropylene fibers in Portland cement-based composites: eighteen years of data. Cem Concr Res. 1998;28:1809–1817.
[49] Toledo Filho RD, Sanjuan MA. Effect of low modulus sisal and polypropylene fibre on the free and restrained shrinkage of mortars at early age. Cem Concr Res. 1999;29:1597–1604.
[50] Gemert DV, Czarnecki L, Lukowski P, et al. Cement concrete and concrete–polymer composites. Cem Concr Res. 2005;27:926–933.
[51] Schulze J. Influence of water-cement ratio and cement content on the properties of polymer-modified mortars. Cem Concr Res. 1999;29:909–915.
[52] Landucci G, Rossi F, Nicolella C, et al. Design and testing of innovative materials for passive fire protection. Fire Saf J. 2009;44:1103–1109.
[53] Nishida A, Yamazaki N, Inoue H, et al. Study on the Properties of High Strength Concrete with Short Polypropylene Fibres for Spalling Resistance. In Sakai K., Banthia N., Gjorv OE. editors. proceedings of the Symposium Concrete under Severe Conditions 2; 1995, Saporo, Japan; 1141–1150.
[54] Bošnjak J, Ožbolt J, Hahn R. Permeability measurement on high strength concrete without and with polypropylene fibers at elevated temperatures using a new test setup. Cem Concr Res. 2013;53:104–111.
[55] Özbay E, Türker HT, Balçıkanlı M, et al. Effect of Fiber Types and Elevated Temperatures on the Bond Characteristic of Fiber Reinforced Concretes. Wor Acad Sci. Eng. Technol. Int J Civ Environ Struct Construction Archit Eng. 2015;9:549–553.
[56] Ozawa M, Morimoto H. Effects of various fibers on high-temperature spalling in high-performance concrete. Construction Build Mater. 2014;71:83–92.
[57] Khoury GA. Polypropylene fibers in heated concrete. Part 2: pressure relief mechanisms and modelling criteria. Mag Concr Res. 2008;60:189–204.
[58] Shah SP. Do fibers increase the tensile strength of cement-based matrix? Mater J. 1992; 88:595–602.
[59] Morsy MS, Alsayed SH, Aqel M. Effect of elevated temperature on mechanical properties and microstructure of silica flour concrete. Int J Civ. Environ Eng. 2010;10:1–6.
[60] Anand N, Arulraj G, Aravindhan C. Stress strain behavior of Normal compacting and Self compacting concrete under elevated temperatures. J Struct Fire Eng. 2014;5:63–75.
[61] Godwin A, Anand N, Prince Arulraj G. Influence of mineral admixtures on mechanical properties of self-compacting concrete under elevated temperature. Fire Mater. 2016;40: 940–958.

International Journal of Scientific & Engineering Research Volume 10, Issue 5, May-2019
ISSN 2229-5518

Drip Curing Technique on Concrete For Water Conservation And Improved Compressive Strength

Alwyn Varghese, K.P. Megha, Reshma.S, Sneha chandran.V

Abstract— Concrete and its curing is an inevitable process of any construction. Curing of concrete is the process of maintaining satisfactory moisture content in concrete during its early stages in order to develop the desired properties for concrete such as developing the concrete microstructure and pore structure thereby improving its durability and performance. Water is largely used in curing process and is becoming a scarce material day by day. Even if the conventional concrete mix used has various advantages it also has disadvantages as cracking, low strength, high water consumption and brittleness. There is an urgent need to do research work pertaining to saving of water and improving strength of concrete by making modifications in curing process. The study leads to comparison of 3ways of curing techniques by means of compressive strength at 28th day. In this study the IS standard specimen tested and identified drip curing method is adaptable for different concrete need of construction. Also for curing, the drip curing method inspired from the drip irrigation system is used. This combination results in conservation of water without compromising properties of concrete.

Index Terms— Ceramic waste aggregate, Compressive strength, Concrete, Drip irrigation, Drip curing, Curing, Strength, Water conservation

1 Introduction

Concrete reduce the growth of strength gain at its early stages due to improper curing that leads the concrete not achieving the desired compressive strength.It makes the failure of total structure. The vertical member like column, in particular, is one of the most victimized RCC element-which must be carefully cured, as the entire dead and live load of super structures are supported by columns and transferred to the foundation. Unfortunately, adequate curing is not given much importance at most of the sites and traditional mathods of curing are adopted, which leads to reduction in durability of the structure [1]. The improper curing causes loss in large amount of water, evaporation of water from surface and reduction in the durability of the concrete [2]. In major cities it is banned to use domestic supply of water supplied by corporation to use [tap water] for the purpose of construction.

It is evident in form of cracks which are easily noticeable by naked eye. Unfortunately adequate curing is not given much important at most of the sites and traditional methods of curing are adopted which leads to reduction in durability of concrete and loss of large quantity water [3]. Here a comparison on 3 types of curing is done-they are immersion curing, spraying and drip curing. These types are done on normal concrete mix (M20) and also concrete containing Ceramic Waste Fine Aggregate (CWFA).

- *Alwyn varghese currentlyAsst.Prof. Civil dept. Ahalia School of engineering and technology, India, PH-91-9400661818. E-mail: alwyncv@mail.com*
- *K.P.Megha, Reshma S and Sneha chandran V currently B tech, student, civil dept, Ahalia school of engg. and technology, India, PH-91-9495706046. E-mail: megha.kpsa6@mail.com*

For the study purpose a normal concrete cube and concrete containing CWFA as per IS standards (15cm x 15cm x 15cm) are casted and tested. Studies have been done in importance of curing but no study had occurred in analyzing advantages of drip curing on concrete containing CWFA.

2 Materials and Methodology

The properties of constant materials and details of mix proportion are shown in table 1. Table 2 shows that M20 (CC) grade concrete mix propotion.

TABLE 1
PROPERTIES OF CONSTANT MATERIALS

MATERIALS	*DENSITY (Kg/m3)*	*SPECIFIC GRAVITY*	*SURFACE MOISTURE*
Cement	*1438*	*3.15*	-
Fine aggregate	*1620*	*2.74*	*Nil*
Coarse aggregate	*1800*	*2.90*	*Nil*
CWFA	*1700*	*2.78*	*Nil*

Table 1 shows that CWFA have almost same density and specific gravity as fine aggregate and coarse aggregate .Ceramic waste are higher resistant to chemical, biological and physical degradation forces and are durable and harder.The properties of these materials make them a good and suitable choice that can be used in concrete.The use of ceramic waste in concrete effects the characteristics of green and hardened concrete and make it more durable.

TABLE 2
CONCRETE MIX PROPORTION

CEMENT(Kg)	*FINE AGGREGATE(Kg)*	*COARSE AGGREGATE(Kg)*	*W/C RATIO*
339	*754*	*1290*	*0.53*

Table 2 shows that mix proportion of M20 concrete with water cement ratio of 0.53.

2.1 Preparation of CWFA

Ceramic wastes sourced from construction and demolition wastes where crushed using a quarry metal hammer. It was sieved into fine aggregate according to the standards. This aggregate was used in the preparation of rapid curing compound by replacing conventional aggregates in various Percentages (5%, 10%, 15%, 20%, 25% and 30%) and concrete was produced. Cube was casted and cured as above mentioned three types of curing methods. 28 days compressive strength of these cubes were found according to type of curing method [5].

3 TEST PROCEDURES

The 15 x 15 x 15 cm specified concrete cube casted and cured as per different curing methods as immersion, spraying and drip up to the age of 28 days. After removal of moisture content in the specimen it is tested for compressive strength of concrete as Figure 1.

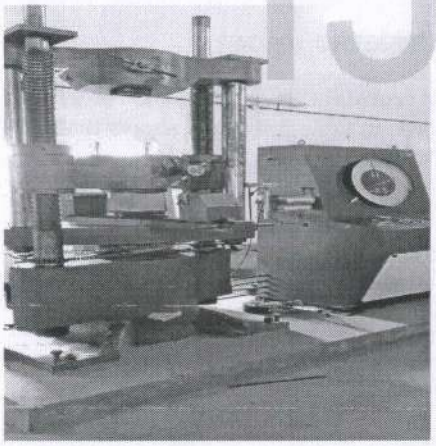


Fig. 1 Testing of cube in universal testing machine

3.1 Immersion Curing

In this concrete cubes are submerged into the water tank till the curing period gets over and every time the buckets are toped up with water to compensate the loss of water due to exothermic reaction of concrete. In this concrete gets in contact with the water for almost all the time and thus the water requirement for concrete is 100% [4].

3.2 Sprying

Sprinkling of water continuously on the concrete surface provides an efficient curing. Spraying of water is only started after the final setting period of 10 hrs. The concrete cube is kept wet continuously by sprinking water on the surface [3].

3.3 Drip curing

At site a number of pipes are used for drip curing. The network consists of mains, sub mains, secondary pipe, tertiary pipes and drip pipes. The drip pipes are the largest member of network which is kept in contact with concrete (figure 2). These pipes are connected to mains. The water is supplied to mains from an overhead water tank by gravity. The discharge is controlled by a nob attached to the main [5].

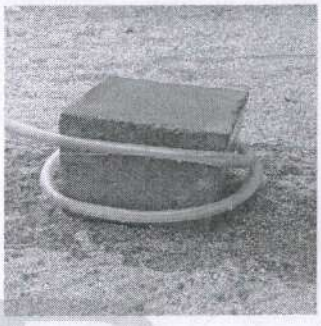


Fig. 2 The concrete cube enclosed with drip pipes.

4 METHODOLOGY

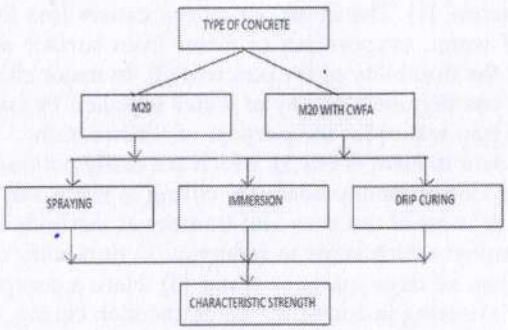


Fig. 3 methodology of reserch

Figure 3 shows that the testing procedure of research. In this three types curing method s are adopted for strength attaining for concrete at early ages (28 days)[6]. After each method of curing the specimens are tested and analysed in the terms of variation of compressive strength.

5 RESULTS AND DISCUSSION

TABLE 3

COMPRESSIVE STRENGTH OF CONCRETE

NAME OF MIX	CURING METHOD		
	SPRAYING	IMMERSION	DRIP
CC	19.51	20.1	21.33

TABLE 4

COMPRESSIVE STRENGTH OF VARIOUS MIXES UNDER DIFFERENT CURING METHODS

NAME OF MIX	% OF CWFA	CURING METHOD		
		SPRAY-ING	IMMER-SION	DRIP
CWFA-5	5	19.4	19.6	20.1
CWFA-10	10	19.6	19.9	20.2
CWFA-15	15	19.2	20.6	20.8
CWFA-20	20	19.7	21.2	21.6
CWFA-25	25	21.7	23.1	24.2
CWFA-30	30	19.8	20.1	20.8

Table 3 shows that the higher value of compressive strength of cc cube was obtained with drip curing compared to other two method of curing. Drip curing method was able to give a compressive strength of 21.33N/mm² which is the maximum out of other two methods. It may be due to countiuous moisture content at required level makes to prevent the water evaporation from the concrete when the C-S-H gel formation taken place.

Table 4 shows that the new concrete mix containing replacement of fine aggregate with CWFA was able to give higher compressive strength than that of CC cube. From the test conducted it was found that maximum percentage of CWFA as replacement of fine aggregate was 25%. Beyond this percentage of addition the compressive strength went on decreasing. It may be due to the small quantity of fine aggregate does not effect the strength of concrete. But the large quantity makes the change of zone in fine aggregate. It makes to degredation of compressive strength. Also the best result was obtained when the cube was provided with drip curing technique.

Practically drip curing is the most effective method of curing.It produced the highest level of compressive strength practically at site.This is due to non stop supply of required water to cool down the exothermic reaction of concrete,resulting from greater degree of cement hydration reaction uniformily.Since the water spreads over the area giving the concrete to absorb water and fulfill its water requirement.Without compromising with the quality and strength of concrete we can achieve the result with very less quantity of water.

6 REFERENCE

[1] N.R.Shattaf, A.M.Alshamshi and R.N.Swamy "Curing /Environment effect on pore structure of blended cement concrete,"Journel of marterials in civil engg.(ASCE)Sept.2001

[2] A.Bentur and C.Jaegermann," Effect of curing and composition on the properties of the outer skin of concrete",journals of materials in civil engg., Vol.3, no.4,nov @ASCE

[3]Neville A.M.& Brookes Concrete technology.Longman Scientific

[4] M.S.Shetty,"concrete technology ",theory and practice .s.Chand and company Pvt .Ltd.

[5] Correia J.d.,Pereira A.S. and Correria J.R.,(2004),"Mechanical behaviour of non structural concrete made with recycled ceramic aggregates".Elsevier Ltd.,cement and concrete composits 27 (2005)429-433. www.elsevier .com

[6] IS 516-1959, Method of test for strength of concrete,Bureau of Indian standards,Newdelhi

IJSER

International Research Journal of Engineering and Technology (IRJET) e-ISSN: 2395-0056
Volume: 06 Issue: 05 | May 2019 www.irjet.net p-ISSN: 2395-0072

A Novel Design of Hybrid 2 Bit Magnitude Comparator

Mahitha M. Das [1], Greshma Mohan[2], Greeshma[3], Aneesh K.[4]

[1]*Student, Dept. of Electronics and Communication Engineering, Ahalia School of Engineering and Technology, Kerala, India*
[2]*Student, Dept. of Electronics and Communication Engineering, Ahalia School of Engineering and Technology, Kerala, India*
[3]*Student, Dept. of Electronics and Communication Engineering, Ahalia School of Engineering and Technology, Kerala, India*
[4]*Professor, Dept. of Electronics and Communication Engineering, Ahalia School of Engineering and Technology, Kerala, India*

Abstract - *With the increasing demand of IoT and portable devices which are battery operated, low power designs are very essential. Comparator is the most fundamental component that performs comparison operation in circuits. In this project an efficient 2-bit magnitude comparator circuit design is proposed. This technique reduces power consumption, propagation delay, and area of digital circuits while maintaining low complexity of logic design when comparing with the traditional circuit. The performance analysis of proposed 2 bit magnitude comparator is compared with the existing technologies. The simulations are carried out in Tanner EDA tool.*

Key Words: CMOS, Gate Diffusion Input, Hybrid Designs, Low power VLSI, Magnitude Comparator, Pass transistor logic, Self Controllable Voltage Level

1.INTRODUCTION

Nowadays the semiconductor industry has been exhibiting a rapid pace of performance improvements in its products by shrinking the device geometries. The electronic devices of such products need to dissipate low power in order to conserve battery life and meet packaging reliability constraints. Consequently power consumption is a dramatic problem for all integrated circuits designed today. In the last decade, IoT devices, portable electronics such as smart phones, tablets and sensors has increased dramatically. Most of these devices are battery operated and thus power consumption has become a critical design constraint. Therefore, researchers set out to discover new methods for designing low-power electronics. Comparator is an integral part of many of the electronic circuits. When some emerging technologies are combined in the circuit, the performance and efficiency can be enhanced.

A 2 bit magnitude comparator is a hardware electronic device that takes two numbers as input in binary form and determines whether one number is greater than, less than or equal to the other number by utilizing various logic gates.

Fig 1 depicts a 2 bit magnitude comparator with inputs A1, A0, B1, B0 and outputs A<B, A=B and A>B.

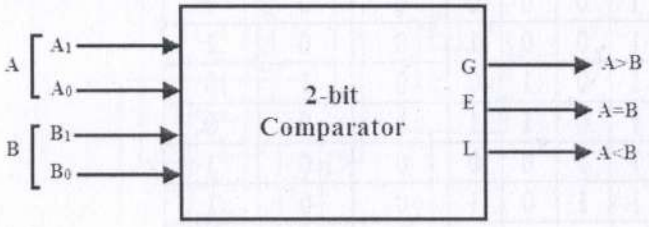


Fig -1: 2 bit magnitude comparator

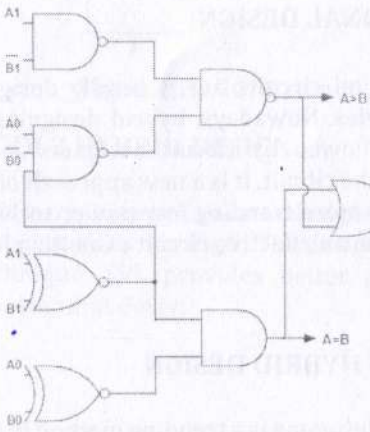


Fig -2: Gate implementation of 2 bit magnitude comparator

The gate implementation of 2 bit magnitude comparator using three NAND gates, 2 EX-NOR gates, one AND gate and one NOR gate is shown in fig 2.

The outcome of 2-Bit magnitude comparator is shown in Table 1 for different combinations of input vectors. According to different condition of inputs, appropriate outputs are generated.

International Research Journal of Engineering and Technology (IRJET) e-ISSN: 2395-0056
Volume: 06 Issue: 05 | May 2019 www.irjet.net p-ISSN: 2395-0072

A Novel Design of Hybrid 2 Bit Magnitude Comparator

Mahitha M. Das [1], Greshma Mohan[2], Greeshma[3], Aneesh K.[4]

[1]*Student, Dept. of Electronics and Communication Engineering, Ahalia School of Engineering and Technology, Kerala, India*

[2]*Student, Dept. of Electronics and Communication Engineering, Ahalia School of Engineering and Technology, Kerala, India*

[3]*Student, Dept. of Electronics and Communication Engineering, Ahalia School of Engineering and Technology, Kerala, India*

[4]*Professor, Dept. of Electronics and Communication Engineering, Ahalia School of Engineering and Technology, Kerala, India*

Abstract - *With the increasing demand of IoT and portable devices which are battery operated, low power designs are very essential. Comparator is the most fundamental component that performs comparison operation in circuits. In this project an efficient 2-bit magnitude comparator circuit design is proposed. This technique reduces power consumption, propagation delay, and area of digital circuits while maintaining low complexity of logic design when comparing with the traditional circuit. The performance analysis of proposed 2 bit magnitude comparator is compared with the existing technologies. The simulations are carried out in Tanner EDA tool.*

Key Words: CMOS, Gate Diffusion Input, Hybrid Designs, Low power VLSI, Magnitude Comparator, Pass transistor logic, Self Controllable Voltage Level

1.INTRODUCTION

Nowadays the semiconductor industry has been exhibiting a rapid pace of performance improvements in its products by shrinking the device geometries. The electronic devices of such products need to dissipate low power in order to conserve battery life and meet packaging reliability constraints. Consequently power consumption is a dramatic problem for all integrated circuits designed today. In the last decade, IoT devices, portable electronics such as smart phones, tablets and sensors has increased dramatically. Most of these devices are battery operated and thus power consumption has become a critical design constraint. Therefore, researchers set out to discover new methods for designing low-power electronics. Comparator is an integral part of many of the electronic circuits. When some emerging technologies are combined in the circuit, the performance and efficiency can be enhanced.

A 2 bit magnitude comparator is a hardware electronic device that takes two numbers as input in binary form and determines whether one number is greater than, less than or equal to the other number by utilizing various logic gates.

Fig 1 depicts a 2 bit magnitude comparator with inputs A1, A0, B1, B0 and outputs A<B, A=B and A>B.

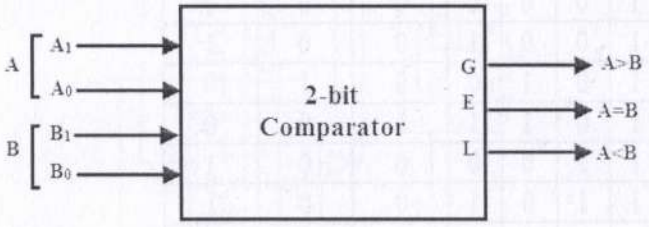


Fig -1: 2 bit magnitude comparator

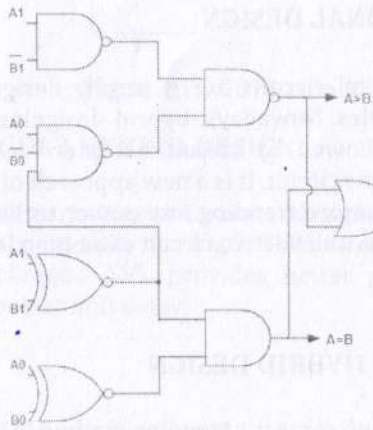


Fig -2: Gate implementation of 2 bit magnitude comparator

The gate implementation of 2 bit magnitude comparator using three NAND gates, 2 EX-NOR gates, one AND gate and one NOR gate is shown in fig 2.

The outcome of 2-Bit magnitude comparator is shown in Table 1 for different combinations of input vectors. According to different condition of inputs, appropriate outputs are generated.

Table -1: Truth table of 2 bit magnitude comparator

Inputs				Outputs		
A_1	A_0	B_1	B_0	$A<B$	$A=B$	$A>B$
0	0	0	0	0	1	0
0	0	0	1	1	0	0
0	0	1	0	1	0	0
0	0	1	1	1	0	0
0	1	0	0	0	0	1
0	1	0	1	0	1	0
0	1	1	0	1	0	0
0	1	1	1	1	0	0
1	0	0	0	0	0	1
1	0	0	1	0	0	1
1	0	1	0	0	1	0
1	0	1	1	1	0	0
1	1	0	0	0	0	1
1	1	0	1	0	0	1
1	1	1	0	0	0	1
1	1	1	1	0	1	0

2. CONVENTIONAL DESIGN

Most of the digital circuits are generally designed using various logic styles. Nowadays, hybrid designing is a new methodology followed by circuit designers for efficient performance of the circuit. It is a new approach of designing in which two or more trending low power techniques are combined to form an effective circuit exhibiting low power, area and delay.

2.1 PTL-CMOS HYBRID DESIGN

Since hybrid designing is a trending method in low power designing, PTL-CMOS hybrid 2 bit magnitude comparator is one of the existing design. The 2-bit Magnitude Comparator has a binate composition of input variables. When it is implemented by using a synthesis of Pass Transistor Logic and CMOS logic styles, very low trends in power consumption, delay, power delay product and area in terms of transistor count were obtained. Fig 3 depicts the 2 bit magnitude comparator circuit using PTL-CMOS hybrid technology. The circuit is comprised of two PTL XOR gates, six CMOS NAND gates and a CMOS AND gate. This design of magnitude comparator has achieved 50-90% reduction in power consumption. Even though the existing design is hybrid, an upswing in power consumption, delay and PDP is observed and curtailment of the design parameters can be prevailed using other hybrid designs.

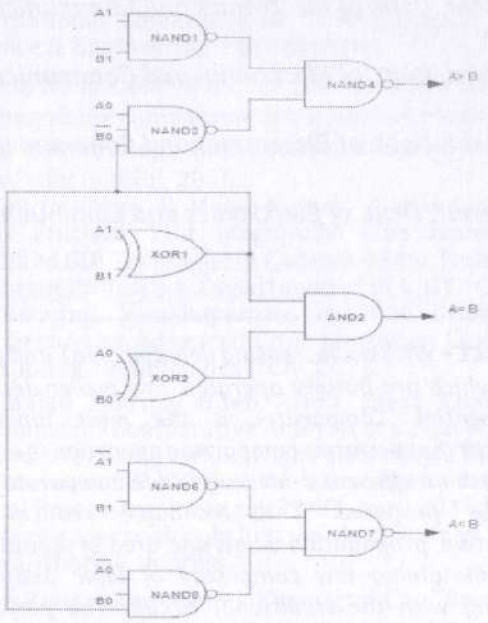


Fig -3 PTL-CMOS hybrid circuit

3. SELF CONTROLLABLE VOLTAGE LEVEL

Self- Controllable Voltage Level (SVL) circuit is a low power technique which can significantly decrease power consumption while maintaining high-speed performance of the circuit. It comprises of an upper SVL circuit and a lower SVL circuit. The SVL circuit is portrayed in fig 4.

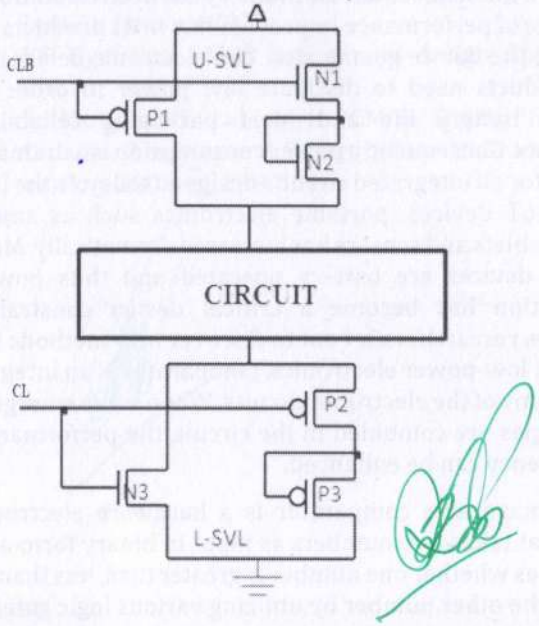


Fig -4 Self Controllable Voltage Level (SVL) circuit

The U-SVL technique is a combination of a PMOS and two NMOS transistors that are linked in parallel. Here an input clock pulse is fed to drive PMOS of U-SVL circuit and the remaining all NMOS are connected to drain terminal.

For small Power consumption applications, U-SVL technique is most accountable. The L-SVL system is an incarnation of an NMOS and two PMOS that are linked in parallel. Consequently an input clock pulse is applied to the NMOS of L-SVL circuit and the remaining all PMOS are connected to the ground. The ground terminal is allied to the L-SVL circuit.

When clock is low in U-SVL, PMOS would turn ON and maximum amount of V_{DD} is passed to load circuit. This is referred to as the active mode. In standby mode, clock is made high so that PMOS is turned OFF and NMOS is turned ON. Thus V_{DD} to the load is reduced and threshold voltage of NMOS in the load circuit is magnified. This in turn minimize subthreshold conduction and leakage current. By the utilization of this technique, sufficient amount of leakage current, PDP and average power can be considerably diminished.

4. PROPOSED DESIGNS

4.1 GDI-CMOS HYBRID DESIGN

The 2 bit magnitude comparator designed using hybrid combination of GDI and CMOS logic style is shown in Fig 5 The design comprises of different logic gates designed with GDI and CMOS. The proposed design shows good performance and power reduction with the incorporation of low power technique called SVL in the design.

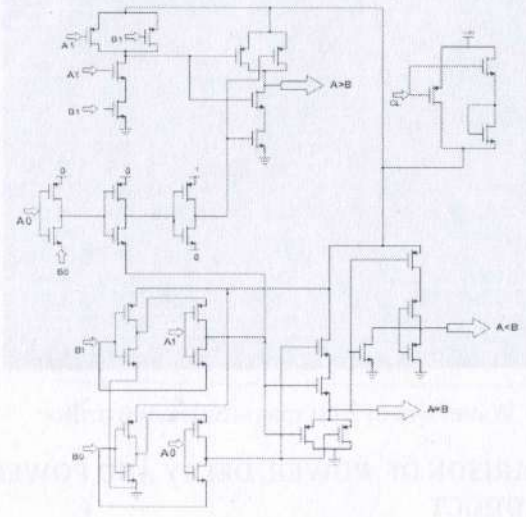


Fig -5 GDI-CMOS circuit

4.2 PTL-GDI 1 HYBRID DESIGN

The 2 bit magnitude comparator designed with a combination of PTL and GDI logic styles to form a hybrid design is shown in Fig 6. The designed circuit comprises of logic gates using PTL and GDI styles. The low power technique known as SVL is added along with the circuit to reduce the power consumption and delay to provide better performance.

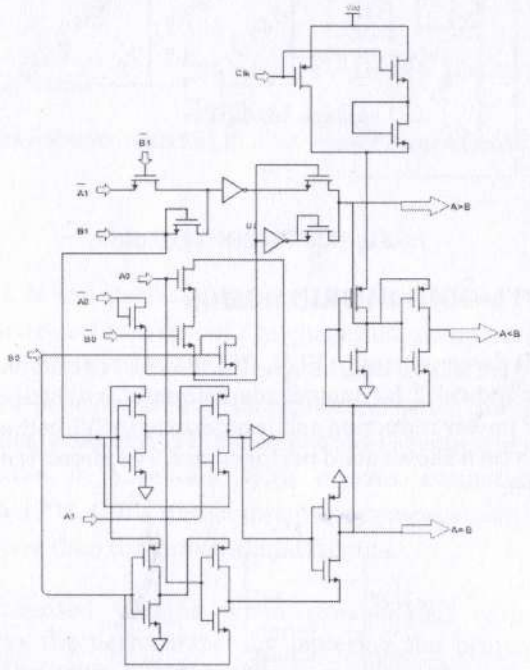


Fig -6 PTL-GDI 1 circuit

4.3 PTL-GDI 2 HYBRID DESIGN

Hybrid 2 bit magnitude comparator designed using PTL and GDI logic style is shown in Fig 7. The design along with low power technique, SVL provides better performance by reducing power and delay.

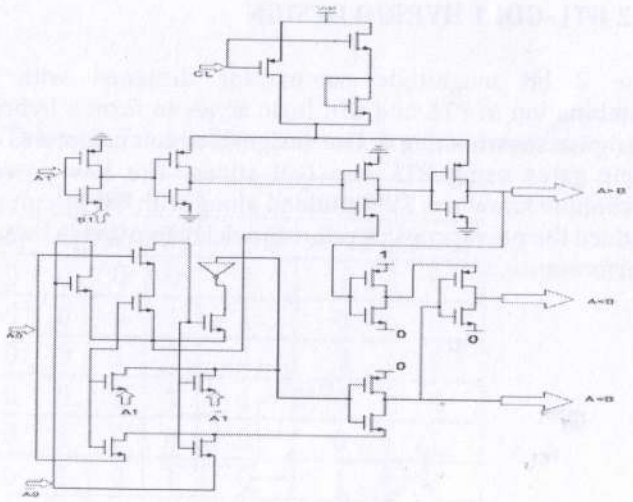


Fig -7 PTL-GDI 2 circuit

4.4 PTL-GDI 3 HYBRID DESIGN

Circuit design styles in VLSI, PTL and GDI are combined to give a hybrid 2 bit magnitude comparator which enables better power reduction and less delay with SVL in the design. This in turn shows good performance. The circuit is depicted in Fig 8.

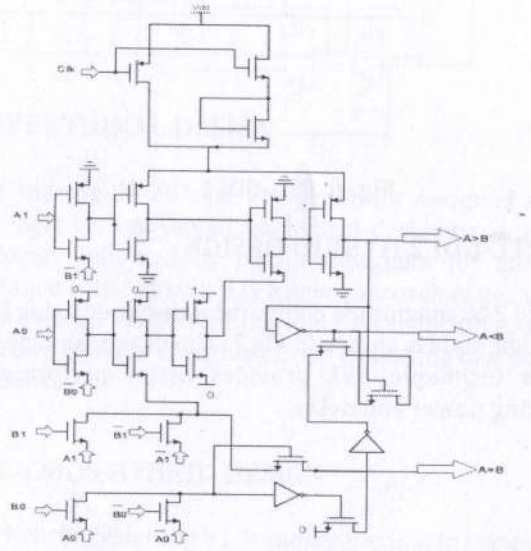


Fig -8 PTL-GDI 3 circuit

4.5 PTL-GDI 4 HYBRID DESIGN

PTL and GDI combination gives another hybrid 2 bit magnitude comparator which is shown in Fig 9. SVL technique is incorporated in the circuit design so as to reduce the power and delay to provide good performance.

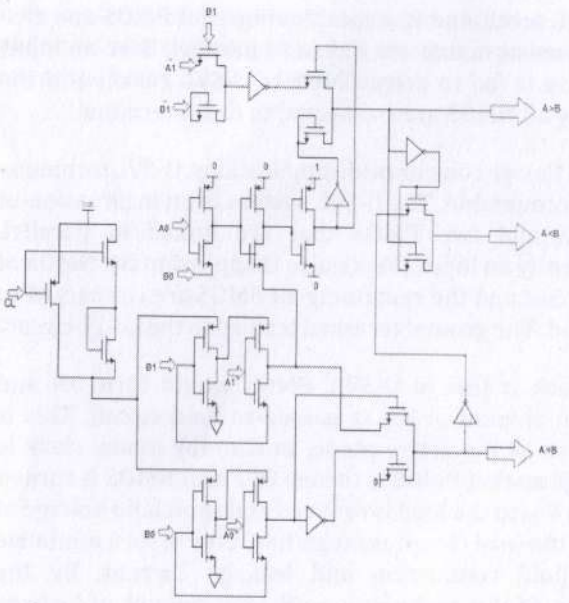


Fig -9 PTL-GDI 4 circuit

5. RESULTS AND ANALYSIS

5.1 WAVEFORM

Figure 10 depicts the obtained waveform of 2 bit magnitude comparator.

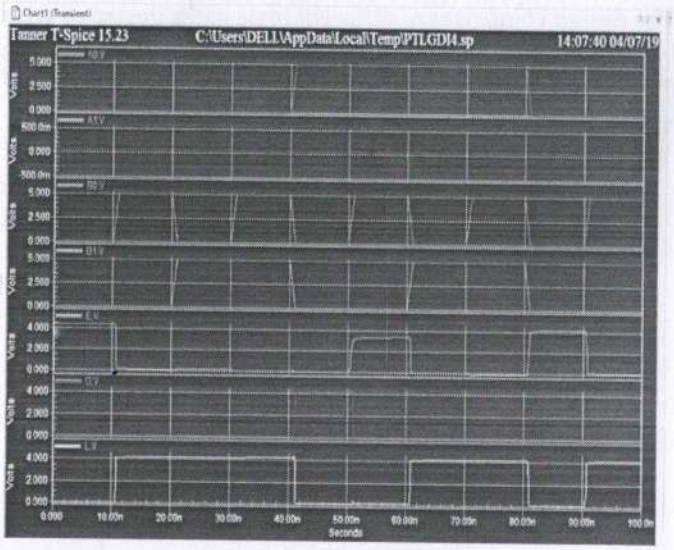


Fig -10 Waveform of 2 bit magnitude comparator

5.2 COMPARISON OF POWER, DELAY AND POWER DELAY PRODUCT

As far as electronic circuits are concerned, power consumption is a major bottleneck of system performance. The main source is the dynamic power consumption. As long as there are a number of dynamic power reduction techniques, the system performance can also be enhanced by

reducing the leakage power consumption. Along with that, the most effective leakage power reduction method i.e. SVL can be incorporated with the design. When comparing the performance and power with different hybrid designs, the design incorporating SVL shows better reduction in the total power.

Table -2: Comparison of power, delay and PDP

Magnitude Comparator	Power	Power with SVL	Delay	PDP (Wps)
GDI-CMOS	37.14e-004	14.22e-004	123.7 p	0.1759
PTL-GDI 1	6.517e-004	4.543e-004	20.14 n	9.149
PTL-GDI 2	17.82e-004	11.13e-004	25.93 p	0.0288
PTL-GDI 3	7.679e-004	5.441e-004	25.93 p	0.014
PTL-GDI 4	5.802e-004	2.61e-004	10.47 n	2.7326

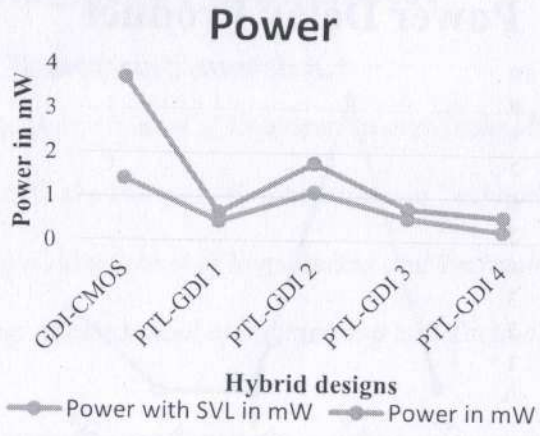


Chart -1: Power Comparison

Chart 1 is the portrayal power consumption of various proposed hybrid designs of 2 bit magnitude comparator. It is very obvious that when the designed 2 bit hybrid magnitude comparator circuits are incorporated with the power reduction technique SVL, a tremendous reduction in power dissipation is observed. With precise evaluation the proposed PTL-GDI 4 design dissipates comparatively much less power than the conventional circuits.

The proposed designs when consolidated with SVL, enhances the performance by lowering the propagation delay. The same is outlined as a graph in Chart 2 which illustrates that the proposed PTL-GDI designs exhibit better performance in terms of delay.

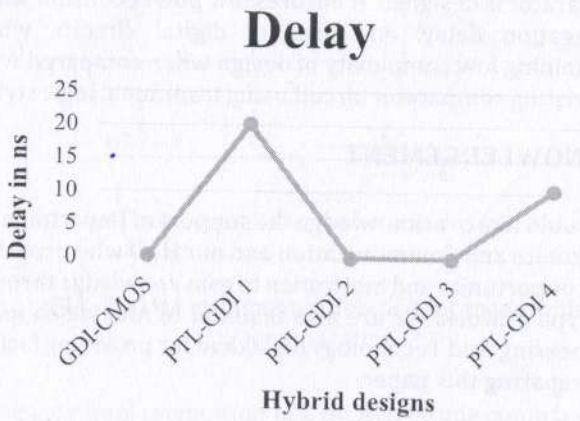


Chart -2: Delay Comparison

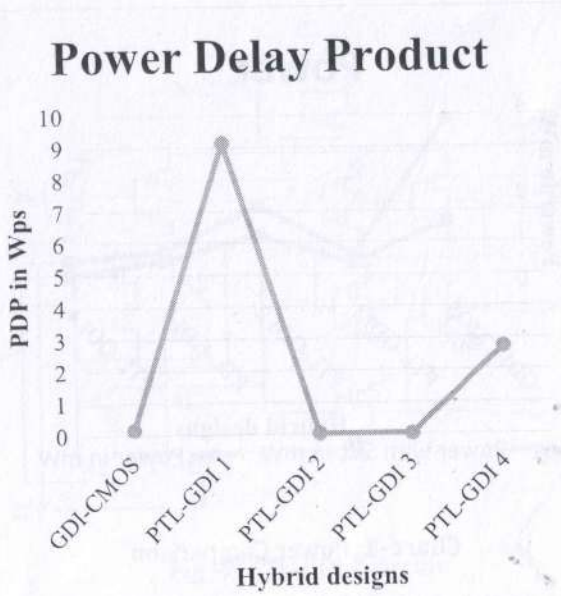


Chart-3 Power Delay Report

The Chart-3 represents the power delay product of various proposed hybrid designs. From the surveillance, PTL-GDI designs provide better performance in terms of PDP.

6. CONCLUSION

A 2-bit hybrid magnitude comparator circuit is designed using different logic styles such as GDI, PTL, CMOS and SVL. Simulations are carried out and the power analysis of the circuits have been performed. From the observations it is evident that PTL-GDI 4 is the efficient design with minimum power consumption. Thus by combining the existing technologies an efficient hybrid circuit of a 2- bit magnitude comparator is designed. It ensures low power consumption, propagation delay, and area of digital circuits while maintaining low complexity of design when compared with the existing comparator circuit using traditional logic styles.

ACKNOWLEDGEMENT

We would like to acknowledge the support of Department of Electronics and Communication and our HoD who provided us an opportunity and motivation to gain knowledge through this type of work. We are also thankful to Ahalia School Of Engineering And Technology, Palakkad for providing facility for preparing this paper.

REFERENCES

[1] Akash Gupta, Manohar khatri, Sachin Kumar Rajput, Anu Mehra, Shikha Bathla , "Design of Low Power Magnitude Comparator", 'Department of ECE ASET Amity University Uttar Pradesh, Noida in 2017 7th International Conference on Cloud Computing, Data Science & Engineering – Confluence.

[2] Dinesh Kumar, Manoj Kumar, "Design of low power two bit magnitude comparator using adiabatic logic", USICT, Guru Gobind Singh Indraprastha University, Dwarka, New Delhi in IEEE, 2016.

[3] B. Keerthi Priya , R. Manoj Kumar, "A New Low Power Area Efficient 2Bit Magnitude Comparator using Modified GDI Technique in Cadence 45nm Technology", Assistant Professors, Department of ECE, GVP College of Engineering, Visakhapatnam in 2016 International Conference on Advanced Communication Control and Computing Technologies (ICACCCT).

[4] Geetanjali Sharma, Hiten Arora, Jitesh Chawla and JuhiRamzai, "Comparative Analysis of a 2-bit Magnitude Comparator using various High Performance Techniqes" in International Conference on communication and Signal Processing, India, pp. 79-83, April 2015.R. Nicole, "Title of paper with only first word capitalized," J. Name Stand. Abbrev., in press.

[5] Sang-Yung Ahn and KyoungrokCho,"Small-swing Domino Logic Based On Twist-Connected Transistors" in IEEE, pp.1054-1056, July 2014.

[6] Vijaya Shekhawat, Tripti Sharma and Krishna Gopal Sharma, "2-Bit Magnitude Comparator using GDI Technique", ECE Department FET-MITS (Deemed University) in IEEE International Conference on Recent Advances and Innovations in Engineering (ICRAIE-2014), May 09-11, 2014, Jaipur, India.

[7] Anjuli, Satyajit Anand, "2-Bit Magnitude Comparator Design Using Different Logic Styles" in International Journal of Engineering Science Invention ISSN Volume 2, Issue 1, January 2013.

[8] J P Uyemura, CMOS logic circuit design, Springer US 2001.

[9] S. Kangand Y Leblebici, "CMOS Digital Integrated Circuits, Analysis and Design", Tata McGraw Hill, 3rd edition, 2003, pp.259-304.

International Journal of Scientific Engineering and Research (IJSER)
ISSN (Online): 2347-3878
Impact Factor (2018): 5.426

Characterization of D-Gun Coated YSZ+Mullite Mixture

Dhanesh S[1]

[1]Assistant Professor –Mechanical Engineering, Ahalia School of Engineering and Technology
dhanesh1988 [at]gmail.com

Abstract: ***This work involves study about thermal barrier coatings and the need for thermal barrier coatings in IC engines. Study was made on different materials which are in use for thermal barrier coating along with its effect on improving the performance of the engine. Based on the study about the coating materials, suitable materials were selected which can be used for thermal barrier coating in IC engines. Mullite+YSZin the ratio of 80/20 was coated using D-Gun with different set of operating parameters. The process parameters were first optimized for the coating of the chosen materials. Material characterization of the coated specimen involve the morphological analysis and hardness***

Keywords: D-Gun Coating, Mullite+YSZ, Characterization, Process Parameter, Thermal Barried Coating, hardness, morphology

1. Introduction

Thermal barrier coatings (TBC) are extensively used in areas of higher temperature like those of gas turbines and IC engines. A TBC system consists of a top coat and a bondcoat. The top coat provides thermal insulation to substrate and withstands large temperature gradients while the bond coat provides oxidation resistance along with an adhesion of the top coat to the substrate. Thermal spraying methods are used for the coating of the top coat and bond coat [1]. Plasma spraying and electron beam physical vapor deposition may be used. Even though plasma spraying can lead to a low thermal conductivity owing to the porosity and lamellar structure it does have the drawbacks of unmelted particles and defective microstructures within the coatings which may result in TBC delamination and spallation [3].

D-gun spraying is characterized by spraying of particles which are accelerated by detonation wave and impact on the substrate to be coated with high velocity of 800-1200m/s [4]. The high particle velocity produces a uniform and dense coating with a high hardness and good adhesion to substrate which gives a good coating performance.

Mullite (3Al2O3.2SiO2) is an important ceramic material which can be used for TBC applications. It do posses the advantages of low density, high thermal stability, low thermal conductivity and favorable strength and creep behavior. It has been seen that compared with YSZ, mullite do have a much lower thermal expansion coefficient and higher thermal conductivity and better oxygen resistance than YSZ. In application like in diesel engines where surface temperatures are lower than that encountered in gas turbines and where temperature variations across coatings are large, mullite is an excellent alternative to YSZ. However but at a temperature of above 1273K the thermal cycling life of mullite is found to be inferior to that of YSZ. Cystrallization too happens in mullite at 1023-1273K which is accompanied by volume contraction causing in cracking and de-bonding [2].

YSZ is found to have a higher thermal coefficient of expansion and a lower thermal conductivity than that of mullite [5]. A composite thermal barrier coating made of mullite and YSZ is found to have a better creep resistance along with the improvement in the thermal cycling life.

The objective of this work is to coat a composite mixture of mullite and YSZ in the ratio of 80:20 using D-gun and to study about the changes in the microstructure, hardness and find the optimum process parameter based on the results obtained.

2. Procedure

The Detonation gun basically consists of a long water cooled barrel with inlet valves for gases and powder. Oxygen and fuel (acetylene most common) is fed into the barrel along with a charge of powder. A spark is used to ignite the gas mixture and the resulting detonation heats and accelerates the powder to supersonic velocity down the barrel. A pulse of nitrogen is used to purge the barrel after each detonation. This process is repeated many times a second. The high kinetic energy of the hot powder particles on impact with the substrate results in a buildup of very dense and strong coatings.

The mixture of mullite and YSZ in the ratio of 80/20 is prepared by mixing the powders in ball milling machine continuously for two hours containing zirconia balls.

Before coating of the powders, the specimens are first grid blasted using sand blasting. The specimens to be coated for optimization of parameters are then fixed onto a holder and the coating is carried out.

Depending upon the powder to be coated the parameters chosen for coating varies. Oxygen is the one which controls the combustion process taking place and acetylene controls the flame velocity. Nitrogen acts as a carrier gas. The flame is that of neutralizing with oxygen to acetylene ratio remaining constant in all the parameters considered for the optimization of the parameters for coating.

The sample generated for thermal cycling test is coated on superalloyinconel. The coating consists of a bond coat of NiCrAlY which act as a adherent to the top coat. The bond

Licensed Under Creative Commons Attribution CC BY

coat thickness was in the range of 75±100μm and the top coat thickness was in the range of 100μm. The coated sample is then made to undergo thermal cycling to test for its thermal shock resistance.

3. Characterization

The coated specimens are characterized for different characteristics such as morphology, hardness and porosity [1].Based on the characterization studies being carried out on the coated specimens the optimization process parameters is made for the coating of the powders on the piston and cylinder head. The specimens to be coated are first grid blasted using sand blasting. The sand blasted specimens are then fixed on the holder. The specimens are then coated using three different set of parameter keeping the ratio of oxygen to acetylene as constant.

The coated specimens are then cut using ISOMET 1000 which is a precision sectioning saw designed for cutting various types of materials of materials with minimal deformation. The cut specimen is then hot mounted using ISOMET hot mounting press apparatus. The specimen is kept for mounting for time duration of 20minutes.

The mounted specimen is then polished using sand papers of different sizes ranging from 800 to 4000 in a systematic and sequential manner till the specimen gets mirror polish. The final polishing of the coated specimen is done using diamond polish with sizes of 3μm, 1μmm and 1/2μm. The finely polished specimens are then analyzed for morphology, hardness and porosity. Microstructural analysis of such finely polished specimens was carried out using scanning electron microscope. The hardness was tested using Viker Hardness Testing and the thermal cycling was carried out to study about the thermal resistance of the coated specimen.

4. Results and Discussion

The specimen of Mullite+YSZ was coated using the parameters shown in table 1

Table 1: List of Operating Parameters

Parameter	O2(lph)	C2H2(lph)	N2(lph)	Spraying Distance (mm)
1	4800	1720	720	200
2	5040	1920	720	200
3	5040	2240	720	200

Figure 1 shows the microstructure obtained using first set of operating parameter.

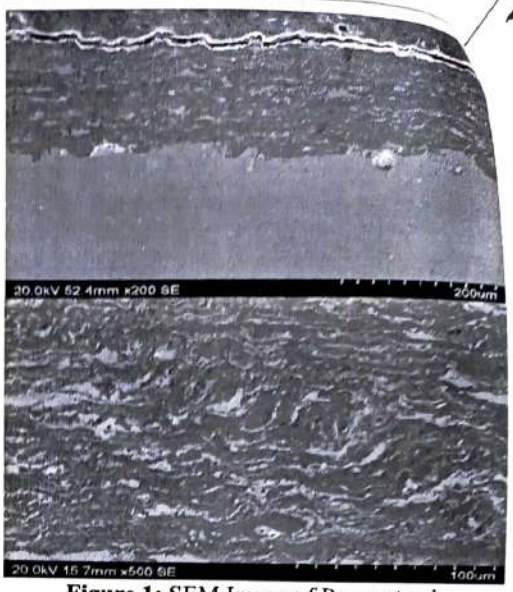


Figure 1: SEM Image of Parameter 1

The SEM analysis shows the coating using 1st parameter was uniform with proper flow if mixture of mullite and YSZ.

Figure 2 shows the EDS analysis of the specimen coated using 1st parameter of mullite + YSZ.

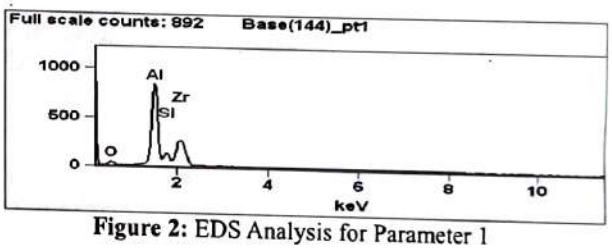


Figure 2: EDS Analysis for Parameter 1

EDS analysis shows that the percentage of mullite and YSZ was in accordance with the percentage of the materials being mixed.

Figure 3 shows the image analysis of specimen coated using 2nd parameter of mixture of mullite + YSZ

Licensed Under Creative Commons Attribution CC BY

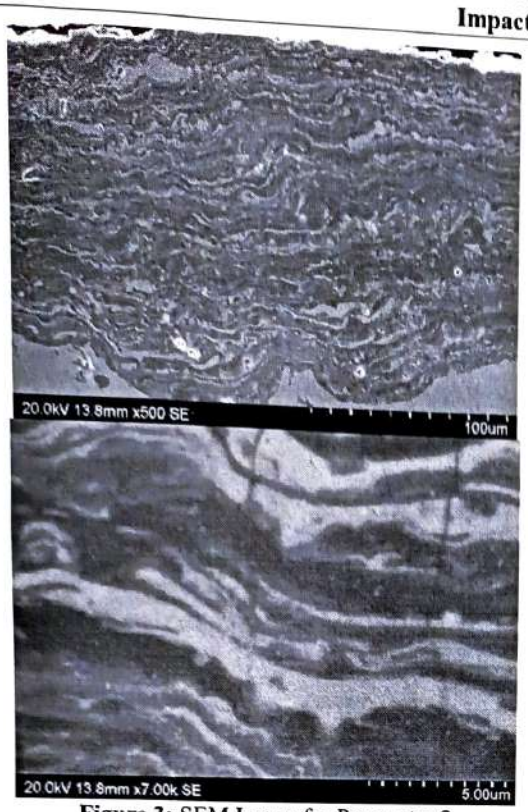


Figure 3: SEM Image for Parameter 2

The SEM image shows that the coating was uniform. But vertical cracks were found to develop in the coating which is not favored.

Figure 4.13 shows the EDS analysis of coating of specimen using 3rd parameter of mullite + YSZ

The EDS analysis shows the percentage of mullite and zirconia was found in accordance with the mixing proportion. While white flows correspond to the YSZ, the black one corresponds to that of mullite.

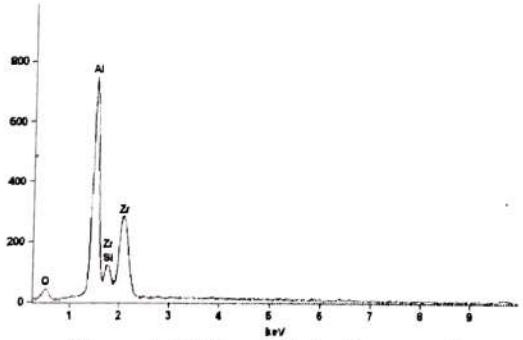


Figure 4: EDS Analysis for Parameter 2

Figure 5 shows the image analysis of specimen coating using 3rd parameter of mullite + YSZ

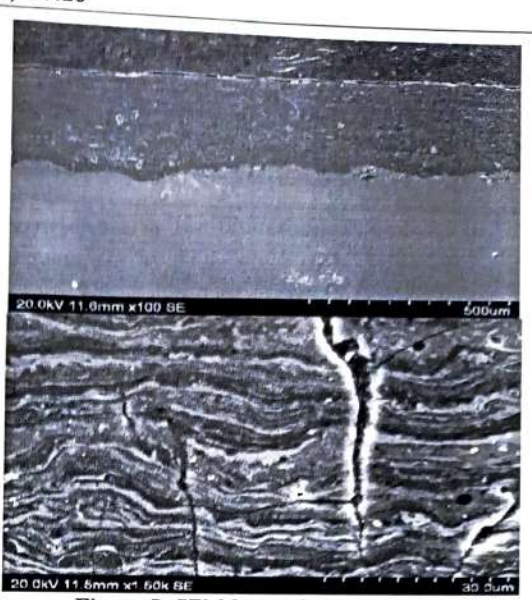


Figure 5: SEM Image for Parameter 3

The SEM analysis shows that, the coatings have developed vertical cracks as well as horizontal cracks.

Figure 6 shows the EDS analysis of the coated specimen using 3rd parameter of mullite + YSZ

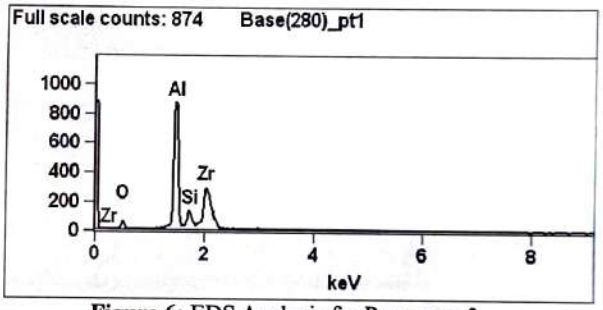


Figure 6: EDS Analysis for Parameter 3

Table 2: Hardness Value for Different Parameters

Parameter	Average	Maximum	Minimum	Std. Deviation	No. of Indentations
1	656HV 0.2	710HV 0.2	608HV 0.2	40.2	10
2	701HV 0.2	799HV 0.2	608HV 0.2	62.43	10
3	1114HV 0.2	1268HV 0.2	956HV 0.2	95.86	10

The hardness values shows that the hardness was maximum for coating using 3rd parameters but with greater deviation in the values. The hardness of coating using 1st parameter was found to be least but with lesser deviation in the hardness values.

5. Conclusion

Based on the study carried out the following observations were made.

Licensed Under Creative Commons Attribution CC BY

1. Mullite+YSZ was coated in the proportion of 20:80 using D-Gun coating using three different set of process parameters.
2. The characterization study was carried out so as to find the optimum set of process parameters for coating.
3. Microstructural analysis and hardness measurement was carried out.
4. Based on the results obtained, if was observed that first parameter for coating would result in optimum coating.

References

[1] T.M. Yonushonis, Overview of Thermal Barrier Coatings in Diesel Engines, Journal of Thermal Spray Technology, March 1997:50-56
[2] X. Q. Cao, R. Vassen, D. Stoever, Ceramic materials for thermal barrier coatings, Journal of the European Ceramic Society, June 2002:1-10
[3] Barbezat Gérard, Application of thermal spraying in Automobile Industry, Journal of Surface and Coatings Technology, June 2006:2028-2031
[4] Douglas H. Harris and Joe Lutz, Thermal Barrier Coatings-Technology For Diesel Engines, SAE Technical Paper Series, March 1988
[5] R. Soltani, H. Samadi, E. Garcia and T. W. Coyle, Development of Alternative Thermal Barrier Coatings for Diesel Engines, SAE Technical Paper Series, April 2005
[6] T. Hejwowski and A. Weronski, The Effect Of thermal barrier coatings on diesel engine performance, Jouranlof Surface Engineering, Surface Instrumentation and Vacuum Technology, 2002:427-432
[7] I. Taymaz, K.Cakir and A. Mimargolur, Experimental Study of Effective Efficiency in a ceramic coated diesel engine, March 2005:1182-1185
[8] A. Tricoire, B.Kjelman, J. Wigren, M. Vanvolsem and L. Aixala, Insulated Piston Heads for Diesel Engines, January 2009:217-222
[9] C. Cano, E. Garcia, A.L. Fernandes, M.I. Osendi, and P. Miranzo, Mullite/ZrO2 coatings Produces by Flame Spraying, Journal Of the European Ceramic Society, February 2008:2191-2197
[10] P.L. Ke, Y.N. Wu, Q.M. Wang, J. Gong, C. Sun, L.S. Wen, Study on Thermal Barrier Coatings produced by Thermal Spraying, Journal of Surface and Coatings Technology, September 2004:2271-2276

Author Profile

Dhanesh S, received his B.Tech from Government Engineering College Kozhikode and his Masters from Amrita Vishwa Vidyapeetham. He is currently working as Assistant Professor in Ahalia School of Engineering and Technology. He is also pursuing his PhD in Amrita Vishwa Vidyapeetham.



Licensed Under Creative Commons Attribution CC BY

International Journal of Civil Engineering and Technology (IJCIET)
Volume 9, Issue 10, October 2018, pp. 1668–1675, Article ID: IJCIET_09_10_166
Available online at http://www.iaeme.com/ijciet/issues.asp?JType=IJCIET&VType=9&IType=10
ISSN Print: 0976-6308 and ISSN Online: 0976-6316

© **IAEME** Publication **Scopus** Indexed

STUDIES ON BEHAVIOUR OF FIRE AFFECTED FIBER REINFORCED CONCRETE

Alwyn Varghese
(Research scholar, Department of Civil Engineering, KITS, Coimbatore, India,)

D.Jasper Selva Samuel
(M.Tech student, Department of Civil Engineering, KITS, Coimbatore, India)

Anand.N
(Associate Professor, Department of Civil Engineering, KITS, Coimbatore, India,)

Prince Arulraj G
(Dean (E &T), Department of Civil Engineering, KITS, Coimbatore, India,)

ABSTRACT

An investigation has been carried out to evaluate the influence of elevated temperature on the properties of different Fiber Reinforced Concrete (FRC) of M20 grade. Concrete specimens with Aramid fiber, Basalt fiber, Carbon fiber, Glass fiber, and Polypropylene fiber were used in the investigation. FRC specimens were exposed as per ISO standard time-temperature curve. The test temperatures were 821°C, 925°C, and 986°C with the exposure duration of 30 min, 60 min, and 90 min. The crack formation, morphological changes in the matrix, at the interface between the aggregate and mortar were examined by Scanning Electron Microscope (SEM). Surface characteristics and colour changes were also investigated for the heated specimens after the specimens were cooled to room temperature. SEM investigation has shown that, increase in temperature on the specimens increased the porosity. Elevated temperature on specimens induced formation of thermal cracks and further increase in temperature increased the density of cracks inside the specimen. Contribution of fibers in reducing the propagation of cracks has been confirmed by SEM investigation.

Keywords Elevated Temperature, Fiber Reinforced Concrete, Modulus of Elasticity, SEM, Weight Loss.

Cite this Article Alwyn Varghese, D.Jasper Selva Samuel, Anand.N and Prince Arulraj G, Studies on Behaviour of Fire Affected Fiber Reinforced Concrete, *International Journal of Civil Engineering and Technology*, **9**(10), 2018, pp. (1668)-(1675). http://www.iaeme.com/IJCIET/issues.asp?JTypeIJCIET&VType=6&IType=7

1. INTRODUCTION

Concrete is a composite material consisting of aggregates bonded together with fluid cement that hardens over time. Exposure to higher temperature during the fire is one of the most damaging environmental effects for reinforced concrete structures. Although concrete is a non-combustible material, its chemical, physical and mechanical properties changes once it is exposed to higher temperature. Cracking, spalling and colour changes occur when concrete structures are exposed to higher temperatures. The addition of fibers was found to improve the tensile strength and fracture toughness of the concrete at elevated temperature[1][2][3]. Chopped fiber has better fire endurance than Fiber Reinforced Polymer (FRP) rebar and sheets[4][5][6]. The loss of bond between the fibers and surrounding concrete was found to decrease with increase in temperature[7]. Concrete with high melting point fiber (carbon, basalt, etc) was found to have good residual bonding strength when exposed to fire. Since decomposition of fiber occurs only at very high temperature, residual bond strength is high[7][8]. Concrete with high melting point fiber had minimal internal cracks due to reduced volume changes during rapid change of temperature[9][2]. The explosive spalling can be prevented by adding low melting point fiber (polypropylene fiber) in concrete, which reduces the pore pressure by melting inside the concrete at elevated temperature[10][11]. In general, at temperatures of 300°C to 600°C, colour of concrete changes to pink or red. For temperatures ranging from 600°C to 900°C, the colour becomes whitish grey and for temperatures ranging from 900°C to 1000°C, the colour becomes buff[12].

The fibers used for the research work were Aramid, Carbon, Polypropylene, Glass, and Basalt. They were added to improve the durability and mechanical properties of concrete. It is proven that synthetic fibers helped to improve the post peak ductility performance, pre-crack tensile strength; impact strength and also they reduce the shrinkage cracks. An attempt has been made to determine the characteristics of fiber reinforced concrete specimens exposed to elevated temperature. Modulus of elasticity, weight loss and micro structure properties of FRC has been found during the present study.

2. MATERIALS AND METHODS

Table 1 gives the details of the mix proportion used to cast the FRC specimens. The water to cement ratio for all the mixtures was 0.55 and Ordinary Portland Cement (OPC) was used to prepare all the specimens. Crushed stones of 10mm size were used as coarse aggregate to prepare the specimens.

Table 1 Mix Proportion of FRC

Name of specimen	Mixture proportions*	Type of fiber	fiber vol. (%/m^3)
M1	1: 2.625: 3.198: 0.59	---	---
M2	1: 2.625: 3.198: 0.59	Basalt	0.25
M3	1: 2.625: 3.198: 0.59	Glass	0.25
M4	1: 2.625: 3.198: 0.59	Carbon	0.25
M5	1: 2.625: 3.198: 0.59	Aramid	0.25
M6	1: 2.625: 3.198: 0.59	Poly Propylene	0.25

*Cement: Fine Aggregate: Coarse Aggregate: Water

Table 2 gives the properties of the Basalt, Glass, Carbon, Aramid, and Poly Propylene fibers that were used for the experimental investigation. The volume fraction used for all fibers were 0.25%.

2.1. Test specimens

300mm long and 150mm diameter cylinders were cast using steel moulds and consolidated with on a vibrating table. Specimens were demoulded after 24 hour and cured in water for 28 days. An electric furnace was used for heating the specimen and the maximum temperature attained was 986^{0}C as per ISO rate of heating. The specimens were exposed to heat for 30 min, 60min and 90 min. Table 3 gives the details of the time and temperature of furnace set for heating. After heating, the specimens were kept in room temperature for one day to attain the room temperature. Then the specimens were tested.

Table 2 Properties of Fiber

Fiber	Length (mm)	Category	Density (g/cu.cm)	Melting point (^{o}C)	Volume fraction (%)
PP fiber	12	Low melting	0.90 -0.91	160 - 170	0.25
Basalt	12	High melting	2.65-2.8	1400	0.25
Glass	12	High melting	2.6	1500	0.25
Carbon	12	High melting	1.6	1200	0.25
Aramid	12	Low melting	1.44	150	0.25

Table 3 Time temperature details

Time, t(min)	Temperature of the furnace (^{0}C)
5	556
10	659
15	718
30	821
60	925
90	986

2.2. Experimental investigation

- Weight loss: Weight of the specimens was found before and after exposure to heat to determine the weight loss of specimen.
- Stress Strain measurement: The specimens were tested in a UTM of capacity 1000kN to determine stress-strain behaviour and modulus of elasticity of FRC exposed to elevated temperature.
- SEM analysis: The samples from the heated specimens were used to study the pores, cracks and micro cavities of fiber reinforced concrete using scanning electron microscope (SEM). Fig. 1 shows the view of SEM used for investigation.



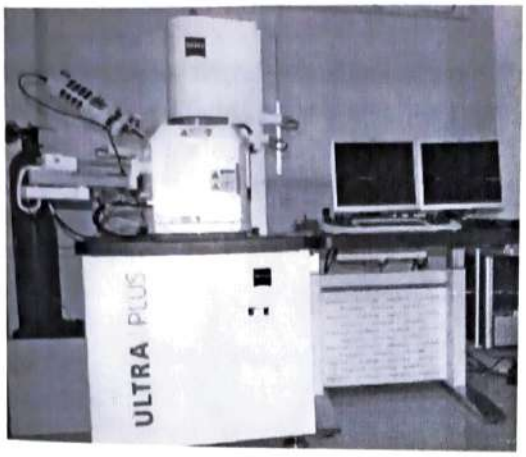


Figure 1 Scanning Electron Microscope

3. RESULTS AND DISCUSSIONS

3.1. Weight Loss

Specimens made from six concrete mixes were tested to investigate the weight loss after exposure to temperatures of 821°C, 925°C and 986°C as per ISO rate of heating. Exposure to sustained elevated temperature indicated adverse effects on the physical properties of concrete. As per Table 4 weight loss was found to be between 4.5-5.5% when heated up to 821°C, and between 5.0-6.0% when heated up to 925°C and between 6.0-7.5% when heated up to 986°C. It is understood that Glass Fiber Reinforced Concrete (GFRC) had maximum weight loss and the weight loss is minimum for Polypropylene Fiber Reinforced Concrete (PPFRC) for the specimen heated up to 30 minutes. For specimens heated for duration of 60 minutes, GFRC and Aramid Fiber reinforced concrete (AFRC) had maximum of weight loss. It may be because of the deprivation of AF in alkaline environment[13]. In the case of 90 minutes of heating, PPFRC had minimum weight loss and AFRC had maximum loss in weight. When exposed to high temperatures, minimum percentage of weight loss of PPFRC specimens attributed to the pore hole creation within the specimen and thus spalling prevented[3].

Table 4 Weight loss on FRC.

Mix	% Weight loss		
	30 min	60 min	90 min
Reference specimen (without fiber)	4.50	5.52	6.48
Aramid FRC	4.93	6.01	7.32
Basalt FRC	5.01	5.32	6.02
Carbon FRC	4.61	5.56	6.33
Glass FRC	5.34	6.00	6.87
PP FRC	4.31	5.80	5.82

3.2. Modulus of Elasticity

Modulus of elasticity of fire affected concrete was found to decrease with increase in temperature. At high temperature, disintegration of hydrated cement products and breakage of bonds in the microstructure of cement paste reduce the elastic modulus. The extent of reduction depends on moisture loss, high temperature creep and type of aggregate. Table 5 shows the

values of modulus of elasticity of specimens exposed to elevated temperature. In all conditions, the modulus of elasticity decreases with increase in temperature.

Table 5 Modulus of Elasticity of each FRC (MPa)

Mix	0 min	30 min	60 min	90 min
Reference specimen (without fiber)	1.30×10^4	1.10×10^4	6.31×10^3	2.96×10^3
AFRC	1.58×10^4	1.14×10^4	8.44×10^3	2.36×10^3
BFRC	1.46×10^4	1.35×10^4	9.65×10^3	3.71×10^3
CFRC	1.83×10^4	1.51×10^4	1.38×10^4	8.23×10^3
GFRC	2.07×10^4	1.78×10^4	9.26×10^3	3.98×10^3
PPFRC	1.42×10^4	1.36×10^4	1.03×10^4	3.40×10^3

From table 5, it can be seen that CFRC had a consistent decrease in modulus of elasticity when exposed to elevated temperature. It is because of the presence of fiber matrix within the specimen, created by high melting point fiber like CF[9]. In unheated condition GFRC had the maximum modulus of elasticity, but when exposed to elevated temperature, the values of young's modulus dropped down, because in heated condition the tensile strength of GF decreased drastically [14]. Fiber reinforced concrete had higher modulus of elasticity than the concrete without fiber in all heated conditions. Except in the cases where PPFRC and AFRC were exposed to 90 minutes of heating.

3.3. SEM Analysis

SEM images shown in Fig. 2 to Fig.ure 6 indicate significant changes in the morphology of specimens, as a result of heat exposure. Micrographs disclosed the characteristics features of damaged constituent materials after thermal exposure. A comparison between the unheated FRC and FRC specimens heated up to 90 minutes duration are shown in Figures.

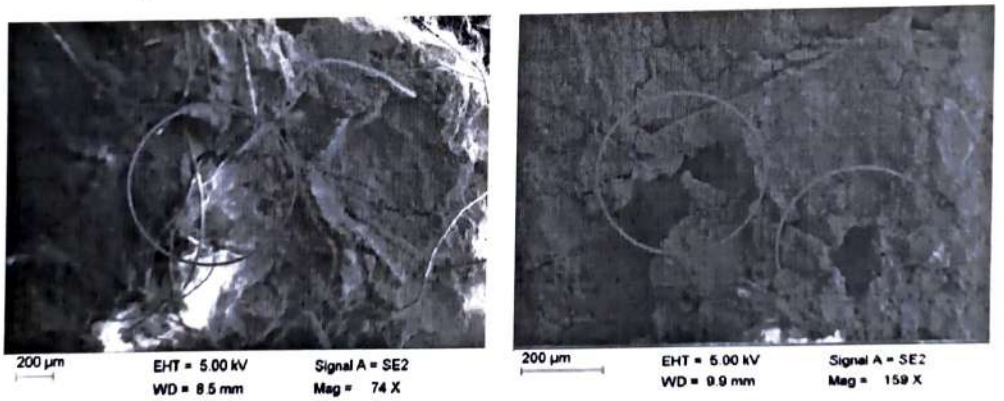


Figure 2 AFRC before and after heat

It is seen from Fig. 2 that AF disappeared after exposed to elevated temperature and several cracks with some pore holes are also developed in AFRC specimen. The fiber within the concrete melted completely and a significant change in the morphology was observed. It can be analyzed in terms of properties of AF. In an alkaline environment, degradation of AF takes place. When heated, the

degradation happens rapidly. So addition of AF creates negative impact on strength of concrete [13].

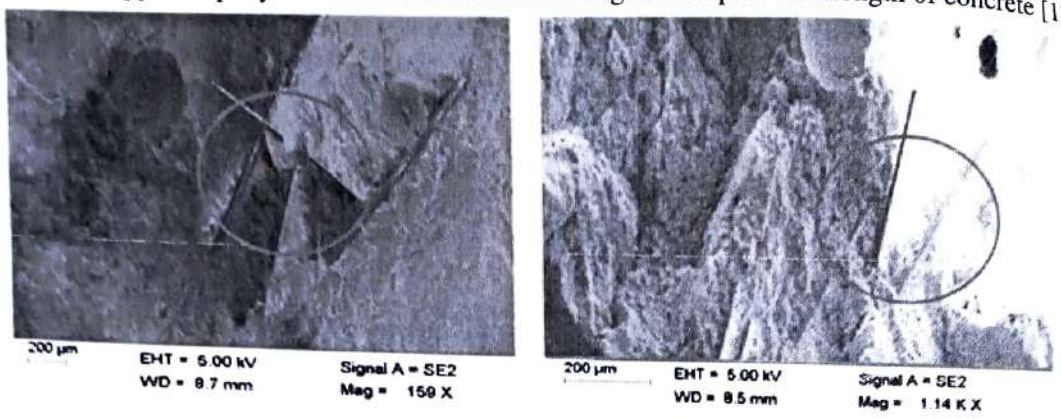


Figure 3 BFRC before and after heat exp

Fig. 3 reveals that Basalt fiber scattered in the unheated and heated specimen. In both condition, BF has shown very good bond towards cement matrix, after heat exposure no evident damage of fiber was observed. BF showed good bonding behaviour with cement paste that reduces micro cracks and bond degradation between concrete and fiber. It was understood that BF posses good cement matrix and there is no major crack formation[16][17].

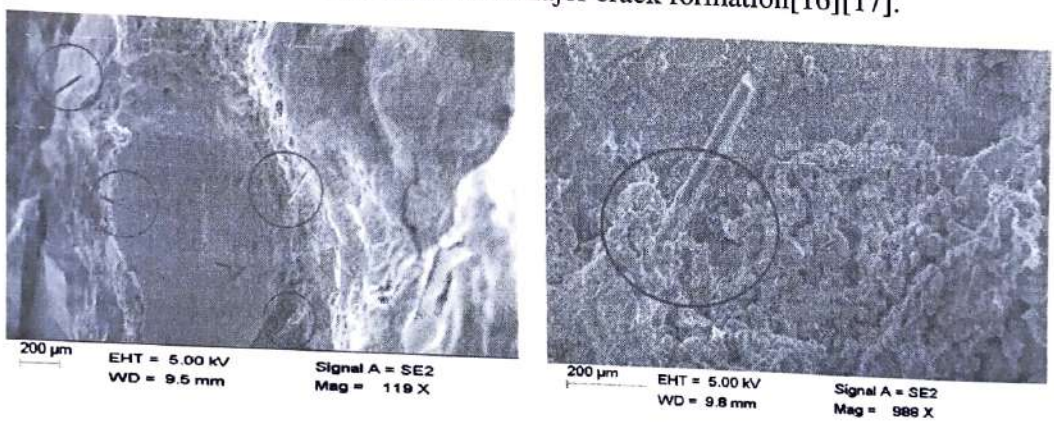


Figure 4 CFRC before and after heat exposure

As per Fig. 4, after heating the CF shows very strong bond with the concrete. Micrograph indicates less number of cracks and free from pore holes. It was observed that carbon fiber prevents micro crack propagation and thus helped to improve the performance of concrete[6][9].

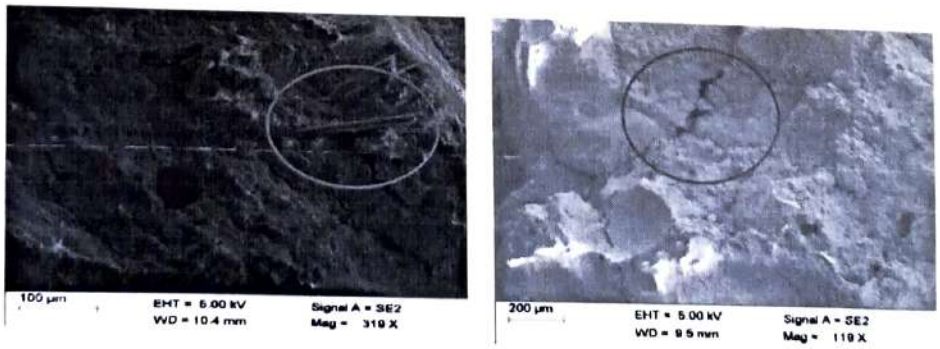


Figure 5 GFRC before and after heat exposure

GFRC samples showed in Fig. 5, after 90 minutes of heat exposure , it was found that GF's bonding to cement is not so good. GFRC possess more micro crack formations than that of BFRC and CFRC. It can be explained by the reduction of modulus of elasticity of GF at elevated temperature, thereby deprivation of bond strength happens within the specimen[15].

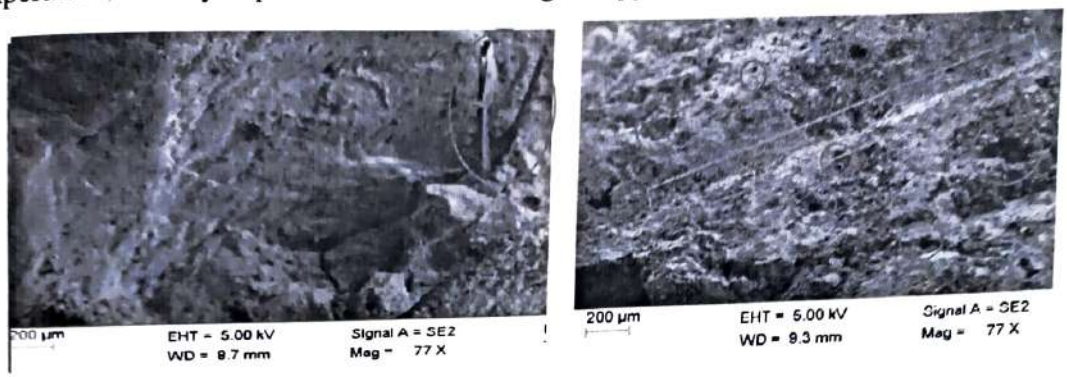


Figure 6 PPFRC before and after heat exposure

Fig. 6 shows the morphological difference between heated and unheated PPFRC. In an unheated condition, PPF were uniformly distributed within the concrete. But after exposure to elevated temperature, fiber and cracks were not visible in the figure. SEM images showed traces of melted fiber and several pore holes. The use of PPF develops additional porosity at high temperature. Some small channels were created due to melting of PPF. It may be the reason for the reduction in the internal vapor pressure within the concrete and thus spalling is reduced[11].

4. CONCLUSION

It is found that Modulus of elasticity decreased when the duration of heating increased. Addition of fiber except AF enhanced the modulus of elasticity of the specimens exposed to elevated temperature. Concrete with CF,GF and BF exhibited higher modulus of elasticity, since these fibers have high melting point. Since PPF melts at low temperature and creates pore holes, the pore pressure is reduced. This helps to prevent the propagation of internal cracks.

ACKNOWLEDGEMENT

The authors wish to acknowledge the Science and Engineering Research Board, Department of Science and Technology of the Indian Government for the financial support (YSS/2015/001196) provided for carrying out this research.

REFERENCES

1. Özbay E, Türker HT, Balçıkanlı M, Lachemi M., Effect of Fiber Types and Elevated Temperatures on the Bond Characteristic of Fiber Reinforced Concretes, World Academy of Science, Engineering and Technology, International Journal of Civil, Environmental, Structural, Construction and Architectural Engineering, 9(5), 2015 Apr 4, 549-553.
2. Mingqing S, Zhuoqiu L, Qizhao M, Darong S., A study on thermal self-monitoring of carbon fiber reinforced concrete, Cement and Concrete Research, 29(5), 1999 May 1, 769-771.
3. Kalifa P, Chene G, Galle C., High-temperature behaviour of HPC with polypropylene fibres: From spalling to microstructure, Cement and concrete research, 31(10), 2001 Oct 1, 1487-1499.

4. Williams BK, Kodur VK, Bisby LA, Green MF., The performance of FRP-strengthened concrete slabs in fire, InFourth International Conference on Advanced Composite Materials in Bridges and Structures-ACMBS-IV, July 2004, 20-23.
5. Bisby LA, Williams BK, Green MF, Kodur VK., Studies on the fire behaviour of FRP reinforced and/or strengthened concrete members, In2nd International Conference on the Durability of Fibre Reinforced Polymer Composites for Construction, 2002 May 29.
6. Rafi MM, Nadjai A., Fire Tests of Hybrid and Carbon Fiber-Reinforced Polymer Bar Reinforced Concrete Beams,ACI Materials Journal, 108(3), 2011 May 1.
7. Chen B, Liu J., Residual strength of hybrid-fiber-reinforced high-strength concrete after exposure to high temperatures, Cement and Concrete Research, 34(6) , 2004 Jun 1, 1065-1069.
8. D.A. St. John, A.B. Poole, I.S. Sims, Concrete petrography, John Wiley and Sons Editor, New York, U.S.A., 308-316.
9. Tanyildizi H., Effect of temperature, carbon fibers, and silica fume on the mechanical properties of lightweight concretes, New carbon materials, 23(4), 2008, Mar 1, 339-344.
10. Ozawa M, Morimoto H., Effects of various fibres on high-temperature spalling in high-performance concrete, Construction and Building Materials, 71, 2014 Nov 30, 83-92.
11. Behnood A, Ghandehari M., Comparison of compressive and splitting tensile strength of high-strength concrete with and without polypropylene fibers heated to high temperatures, Fire Safety Journal, 44(8), 2009 Nov 1, 1015-1022.
12. Lee J, Choi K, Hong K., Color and material property changes in concrete exposed to high temperatures, Journal of Asian Architecture and Building Engineering, 8(1), 2009 May 15, 175-782.
13. Derombise G, Vouyovitch Van Schoors L, Messou MF, Davies P., Influence of finish treatment on the durability of aramid fibers aged under an alkaline environment, Journal of Applied Polymer Science, 117(2), 2010 Jul 15, 888-898.
14. Abbasi A, Hogg PJ., Temperature and environmental effects on glass fibre rebar: modulus, strength and interfacial bond strength with concrete. Composites Part B: Engineering, 36(5), 2005 Jul 1, 394-404.
15. Chan YN, Peng GF, Anson M., Residual strength and pore structure of high-strength concrete and normal strength concrete after exposure to high temperatures, Cement and Concrete Composites, 21(1), 1999 Jan 1, 23-27.
16. Li XE., Study on thermal resistance of basalt filament yarn, in Advanced Materials Research-Vol. 146,(Switzerland: Trans Tech Publications,2011) 666-669.
17. Tumadhir M., Thermal and mechanical properties of basalt fibre reinforced concrete, World Academy of Science, Engineering and Technology, International Journal of Civil, Environmental, Structural, Construction and Architectural Engineering, 7(4), 2013 Apr 26, 334-337.



IJETSR
ISSN:2394-3386

International Journal of Engineering Technology Science and Research
IJETSR
www.ijetsr.com
ISSN 2394 – 3386
Volume 5, Issue 4
April 2018

A Study on use of Silico-Manganese Dust as Subgrade Soil Stabilizer

Vivek V S
UG Student, Dept. Of Civil Engineering, Ahalia School Of Engineering And Technology, Palakkad, Kerala, India.

Arunkumar A
UG Student, Dept. Of Civil Engineering, Ahalia School Of Engineering And Technology, Palakkad, Kerala, India.

Thirtha Jayan
UG Student, Dept. Of Civil Engineering, Ahalia School Of Engineering And Technology, Palakkad, Kerala, India.

Vivekanand S S
UG Student, Dept. Of Civil Engineering, Ahalia School Of Engineering And Technology, Palakkad, Kerala, India.

Aleeena J Augustin
UG Student, Dept. Of Civil Engineering, Ahalia School Of Engineering And Technology, Palakkad, Kerala, India.

Dr. Jino John
Professor, Dept. Of Civil Engineering, Ahalia School Of Engineering And Technology, Palakkad, Kerala, India.

ABSTRACT

This study deals with the subgrade soil stabilization in the Ambad – Chirakkal Farm Road in Palakkad district of Kerala state. Silico-manganese dust is used as the stabilizing material. Silico Manganese Dust is an industrial by-product obtained from the arc-furnace while extracting manganese from its ore. In this study, the percentage of silico manganese dust added is 5%, 10%, 15% and 20% by weight of soil for finding the optimum percentage. California bearing ratio (CBR) test and Unconfined Compression Test were performed to determine the strength properties of the Soil– silico manganese dust mixtures. Higher CBR values of soil- silico manganese dust mix extent their potential for use as a Subgrade for flexible pavement. The optimum CBR and UCC value were obtained at 10% addition of silico manganese dust.

Keywords : CBR, UCC, Soil- Silico Manganese dust mix, MDD and OMC

1 INTRODUCTION

Performance of Flexible Pavement depends on the functions of the component layers especially Subgrade. Subgrade is compacted layer of soil provide the lateral support to the pavement. Construction over soft subgrade affects the performance of pavement and results in shorter life of pavement. The typical approach of stabilization of soft subgrade is to remove the soft soil, and replace it with soil of high strength. The high cost of replacement of poor soil has caused highway agencies to assess alternative methods to construct the highway over soft subgrade. One approach is to improve the properties of soil is with addition of the waste materials. Soil stabilization is one of the most suitable alternatives which are widely used in pavement construction. Soil stabilization technique used to improve the engineering properties of soil such as strength and stability.

Traditional additives like cement, lime, fly ash can improve soil properties by themselves [12]. Non-traditional additives like rice husk ash, crumb rubber, marble dust, blast furnace slag can also improve soil properties but are less efficient[1][2][10][13][9]. But combining two or more non-traditional additive can improve their effectiveness[11][1]. RHA imparted strength combining marble dust increased the durability of soil specimen. Non-traditional additives should be used as soil stabilizer as they provide an economical alternative and also help in waste disposal[1][8][14]. In this study silico manganese dust is used as the stabilizing material.

2 OBJECTIVES OF THE STUDY

- To improve the CBR and UCC value of the subgrade soil
- To determine the MDD and OMC of the soil- silico manganese dust mix
- To design the flexible pavement as per IRC: 37 – 2012 guidelines.
- To perform the economic analysis of designed pavement with and without stabilization of subgrade soil.

3 MATERIALS USED

3.1 SUBGRADE SOIL

The soil was collected from Ambad – Chirakkal Farm Road in Palakkad district of Kerala state where it is proposed to construct a new flexible pavement. Experiments are conducted as per IS procedure to determine the properties of the subgrade soil and the test results are tabulated as follows:

Table 3.1 : Properties of soil used

PROPERTIES		RESULTS
SPECIFIC GRAVITY		2.49
SOIL CLASSIFICATION		Clayey Sand Soil
LIGHT COMPACTION	Optimum Moisture Content (OMC)	14.23 %
	Maximum Dry Density (MDD)	1.86 g/cc
HEAVY COMPACTION	Optimum Moisture Content (OMC)	6.345 %
	Maximum Dry Density (MDD)	2.38 g/cc
CALIFORNIA BEARING RATIO (CBR)		5.81%.
UNCONFINED COMPRESSION (UCC)		14.72 KN/m^2

3.2 SILICO MANGANESE DUST

Silico Manganese Dust is an industrial by-product obtained from the arc-furnace while extracting manganese from its ore. Silico Manganese Dust waste is obtained from the production of ultra low carbon silico manganese. It is a very fine pozzolonic material produced during the manufacture of manganese by electric arc furnace. The manganese dust is formed when MnO_2 gas produced in the furnace mixes with oxygen, oxidizes to MnO_2. It condenses and forms manganese which is the major part of the smoke. These dusty smokes are collected in a bag. This industrial waste can be used to stabilize the soil.



Fig. 3.1 Silico - Manganese dust

IJETSR
ISSN 2394-3386

International Journal of Engineering Technology Science and Research
IJETSR
www.ijetsr.com
ISSN 2394 – 3386
Volume 5, Issue 4
April 2018

Table 3.2: Chemical composition of Silico-Manganese dust

CHEMICALS COMPOSITION	SILICO-MANGANESE DUST
Magnesia	1484 ppm
Iron	4963 ppm
SiO_2	92670.4 ppm
Lime	134896.7 ppm

4 PROPORTIONING OF SOIL AND SILICO-MANGANESE DUST

In this study, the percentage of silico manganese dust added is 5%, 10%, 15% and 20% by weight of soil for finding the optimum percentage. The Soil - Silico-Manganese Dust mix are proportioned and designated as S1, S2, S3, S4, and S5 is shown in the table below.

Table 4.1: Proportioning of Silico manganese dust

SL No.	PROPORTIONS	DESIGNATION
1	SOIL + 0 % SILICO-MANGANESE DUST	S1
2	SOIL + 5 % SILICO-MANGANESE DUST	S2
3	SOIL + 10 % SILICO-MANGANESE DUST	S3
4	SOIL + 15 % SILICO-MANGANESE DUST	S4
5	SOIL + 20 % SILICO-MANGANESE DUST	S5

5 GEOTECHNICAL CHARACTERISATION

Detailed laboratory experiments were carried out to study geotechnical characteristics of Silico-Manganese dust and soil mix as per IS, which include: (a) Modified proctor compaction test [as per IS 2720 (part 8)] (b) Unconfined compressive strength test [as per IS 2720 (part 10)] and (c) California bearing ratio test [as per IS 2720 (part 16)]. The test was conducted and the results were obtained as tabulated in table 5.1.The detailed discussion on test results were done in the following sections.

Table 5.1 : Summary of test results

DESIGNATION	**OMC (%)**	**MDD (gm/cc)**	**UCC (kPa)**	**CBR Value (%)**
S1	6.345	2.38	14.66	5.81
S2	7.61	2.43	19.89	7.16
S3	8.482	2.52	27.48	8.86
S4	8.696	2.46	24.38	7.67
S5	9.167	2.35	16.91	5.44

International Journal of Engineering Technology Science and Research
IJETSR
www.ijetsr.com
ISSN 2394 – 3386
Volume 5, Issue 4
April 2018

5.1 MODIFIED PROCTOR TEST

The variations of MDD and OMC with addition of Silico-Manganese dust are shown in the figure. It is observed that the MDD value at 0% is 2.38 gm/cc and it increases upto 10% addition of Silico-Manganese dust with a MDD value of 2.52 gm/cc, then further increases in Silico-Manganese dust content causes decrease in MDD value of the soil. That is, at 15% addition of Silico-Manganese dust, the MDD value decreases to 2.46 gm/cc. The addition of dust causes densification initially, but later causes decrease in the density. The optimum value of MDD is 2.52 gm/cc at OMC of 8.482% by weight of soil with optimum Silico-Manganese dust content of 10% respectively.

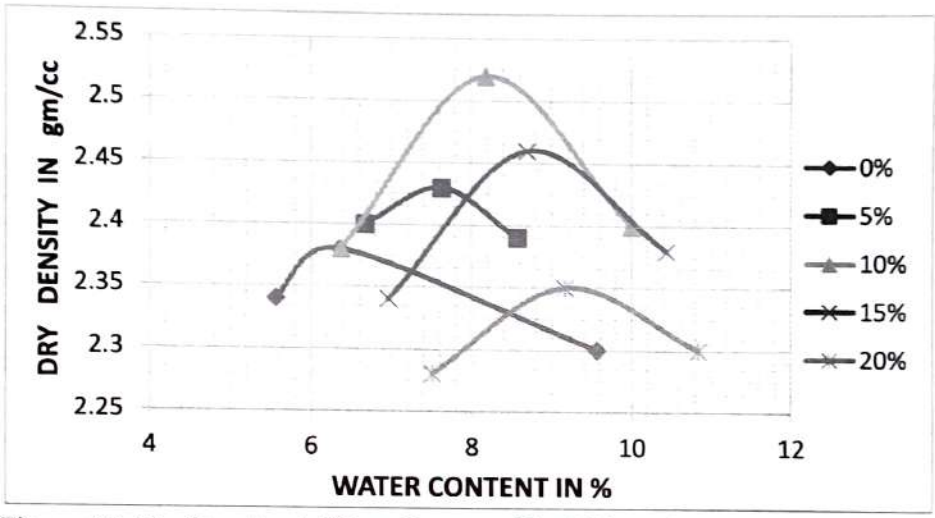


Figure. 5.2: Dry Density v/s Water Content with addition of Silico-Manganese Dust

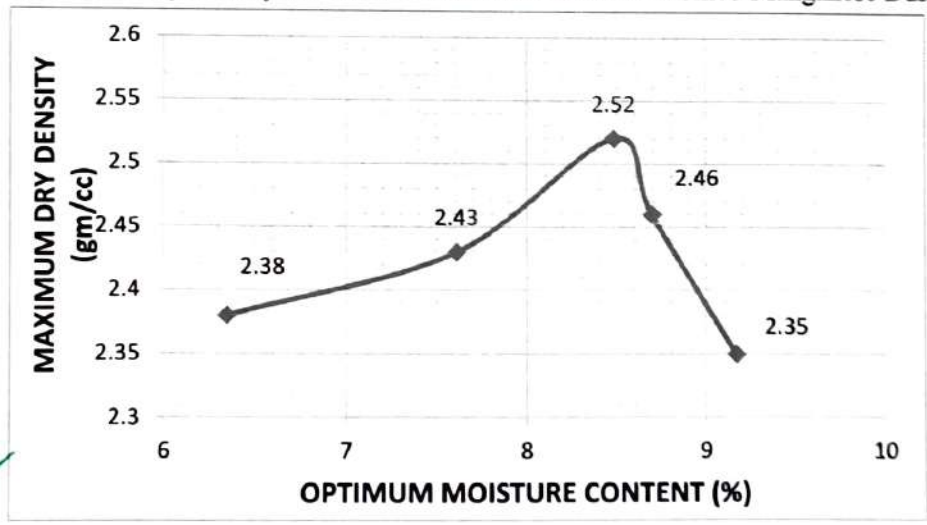


Figure 5.3 : Variation of OMC and MDD with addition of Silico-Manganese Dust

5.2 UNCONFINED COMPRESSION TEST

The variations of unconfined compressive strength with addition of Silico-Manganese dust are shown in the figure. It is observed that the UCC value at 0% is 14.66 kPa and it increases upto 10% addition of Silico-Manganese dust with a UCC value of 27.38 kPa, then further increases in Silico-Manganese dust content causes decrease in UCC value of the soil. That is, at 15% addition of Silico-Manganese dust, the UCC

International Journal of Engineering Technology Science and Research
IJETSR
www.ijetsr.com
ISSN 2394 – 3386
Volume 5, Issue 4
April 2018

value decreases to 24.38 kPa. The optimum UCC value is 27.38 kPa with optimum Silico-Manganese dust content of 10% respectively. The addition of dust causes densification initially, but later causes decrease in the density and thus the UCC value.

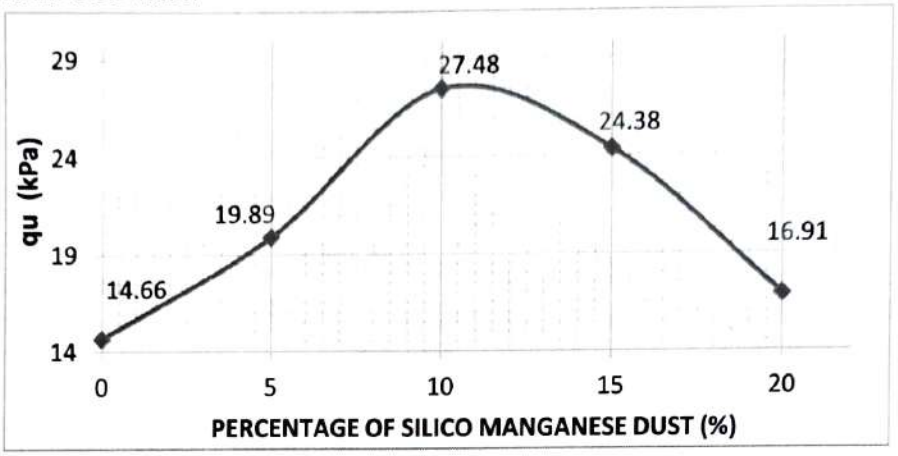


Figure. 5.4: Variation of UCS with addition of Silico-Manganese Dust

5.3 CALIFORNIA BEARING RATIO

The variations of CBR value with addition of Silico-Manganese dust are shown in the figure. It is observed that the CBR value at 0% is 5.81% and it increases upto 10% addition of Silico-Manganese dust with a CBR value of 8.86%, then a further increase in Silico-Manganese dust content causes decrease in CBR value of the soil. That is, at 15% addition of Silico-Manganese dust, the CBR value decreases to 7.67%. The optimum CBR value is 8.86% with optimum Silico-Manganese dust content of 10% respectively.

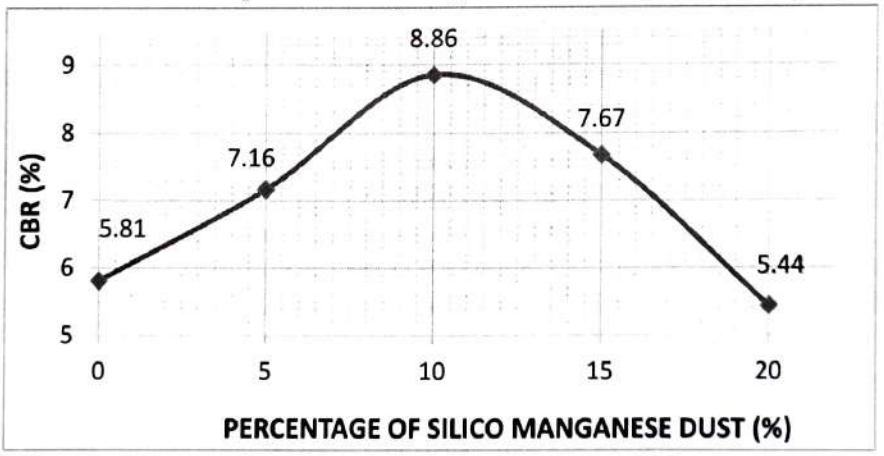


Figure. 5.5: Variation of CBR Value with addition of Silico-Manganese Dust

6 DESIGN OF FLEXIBLE PAVEMENT

The thickness of pavements and thickness for each layer is designed as per "IRC : 37 – 2012. Taking, design traffic P = 52 vehicles per day , Lane distribution factor D = 0.75, Annual growth rate r = 7.5% = 0.075, Design life n = 20 years, Vehicle Damage Factor F = 4.5.

6.1 Pavement Thickness Without Stabilization of Subgrade Soil

Total Thickness of the Pavement = 537.16 mm

Thickness of GSB Layer = 228.58 mm

Thickness of G.Base Layer = 234.7mm

IJETSR
ISSN:2394-3386
International Journal of Engineering Technology Science and Research
IJETSR
www.ijetsr.com
ISSN 2394 – 3386
Volume 5, Issue 4
April 2018

Thickness of DBM Layer = 51.94 mm

Thickness of BC Layer = 21.94 mm

6.2 Pavement Thickness With Stabilization of Subgrade Soil

Total Thickness of the Pavement = 452.76 mm

Thickness of GSB Layer = 150 mm

Thickness of G.Base Layer = 231.46mm

Thickness of DBM Layer = 50 mm

Thickness of BC Layer = 21.29 mm

Percentage Reduction in pavement thickness = $\frac{5\ .1 - 4\ .7}{5\ .1} \times 100$

= 15.71%

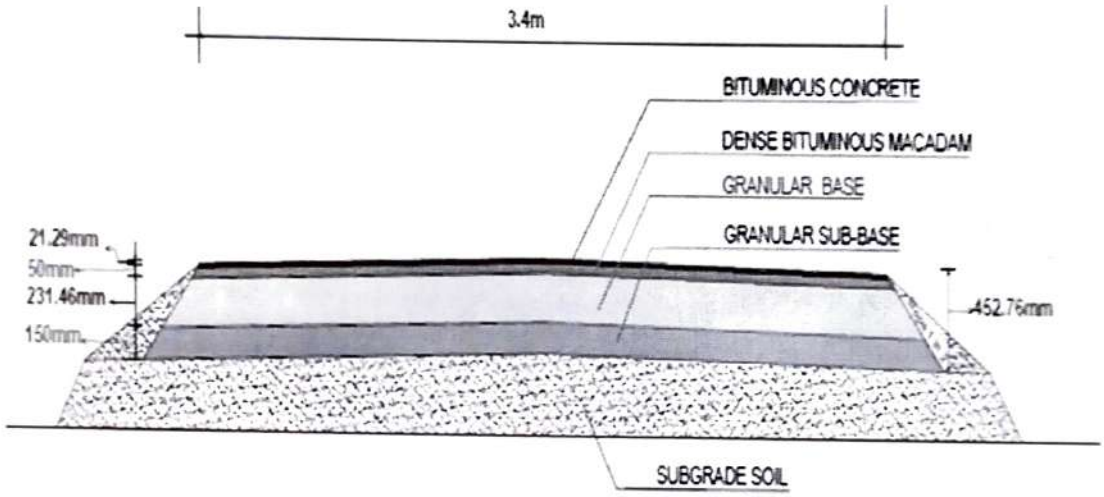


Figure 6.1 : Cross section of the designed pavement

7 COST ANALYSIS FOR PAVEMENT WITH AND WITHOUT STABILIZATION

Total cost for single lane road of 1274m long without stabilization = Rs. 11142069.92

Total cost for single lane road of 1274m long with stabilization = Rs.9545371.835

Total cost reduced = Rs.11142069.92 - Rs.9545371.835

= Rs. 1596698.085

Percentage Reduced = (Rs.1596698.085 / Rs. 11142069.92) x 100

= 14.33%

8 CONCLUSIONS

The engineering properties of the subgrade soil is also determined as per IS procedures. It is found that the CBR value of the soil is very low and thus the soil property needs to be improved by stabilization. The silico-manganese dust, a industrial waste is used as the stabilizer. After conducting several tests like Modified Proctor test CBR test, and UCC test by addition of silico-manganese dust by 5%, 10%, 15% and 20% by weight of soil and the following conclusions were made:

1. The value of OMC is 8.482% by weight of the Soil and Silico-Manganese Dust and the value of MDD is 2.52gm/cc with Optimum Silico-Manganese Dust Content of 10% by weight of soil.

2. From the results obtained from the test, it is found that the Unconfined Compressive Strength of the soil increases upto 10% of Silico-Manganese Dust and reduces with further addition of it. The highest Unconfined Compressive Strength of the soil obtained is 27.48 kPa.
3. From the results obtained from the test, it is found that the CBR value of the soil increases upto 10% of Silico-Manganese Dust and reduces with further addition of it. Thus the CBR value of the stabilized soil is 8.86%.
4. By stabilization of the subgrade soil the thickness of the pavement is reduced by 15.71% and thus, the cost is reduced by 14.33%.

9 FUTURE SCOPE

In soil stabilization using Silico-Manganese Dust on the variation CBR value and UCC value are studied. Furthermore researches can be done on effect of Silico-Manganese Dust on Atterbergs indices and limits, free swell index, direct shear test, permeability test, etc.

10 REFERENCES

[1] Adams, Joe. M., and Maria, A., Rajesh. 2015. Soil Stabilization using Industrial Waste and Lime. International Journal of Scientific Research Engineering & Technology 4(July 2015), 799-805

[2] Chandra, J. Vijaya., and Meher, Lavanya. P. 2017. Effect of Granulated Blast Furnace Slag in the Stabilization of Expansive Soil for the Pavement Sub-Grades. International Research Journal of Engineering and Technology.4 (May 2017),1735-1739

[3] IS 2720 :(Part-VII) 1980. Methods of Test for Soil, Determination of water content, dry density relation using light compaction. Published by Bureau of Indian Standards, New Delhi, India.

[4] IS 2720 :(Part-VIII) 1983. Methods of Test for Soil, Determination of water content - dry density relation using heavy compaction. Published by Bureau of Indian Standards, New Delhi, India.

[5] IS 2720 :(Part-X) 1991. Methods of Test for Soil, Determination of Unconfined compressive strength. Published by Bureau of Indian Standards, New Delhi, India.

[6] IS 2720 :(Part-XVI) 1987, Methods of Test for Soil, Laboratory determination of CBR. Published by Bureau of Indian Standards, New Delhi, India.

[7] IRC 37:2012. Guidelines for the Design of Flexible Pavements. Published by Indian Roads Congress, New Delhi, India.

[8] Kumar, U. Arun., and Kiran, B. Biradar. 2014. Soft subgrade stabilization with Quarry dust-an industrial waste. International Journal of Research in Engineering and Technology 3 (Aug 2014), 409-412.

[9] Kumarr, P. Rajendra., and Archan, P. 2017. Effect of CBR of Black Cotton Soil Reinforced With Recron Fiber. Imperial Journal of Interdisciplinary Research 3 (2017), 1093-1097

[10] Mansuree., Mohammad, Akhlak., Mohammed, Juned. Qureshi., and Mohammad, Furquan. 2017. Study on Stabilization of Black Cotton Soil Using Ferric Chloride. Imperial Journal of Interdisciplinary Research 3 (2017), 1016-1019

[11] Ramteke, N. B., Anilkumar Saxena., and Arora, T. R. 2014. Stabilization of Black Cotton Soil With Sand and Cement as a Subgrade for Pavement. International Journal of Engineering Sciences & Research Technology 3 (June 2014), 688-692

[12] Sai, K. Raga., Krishna, S., Anup, N. V., and Likitha, M. Sai. 2017. Improving CBR of Soil With Fly Ash." International Journal of Engineering Research 6 (Mar. 2017), 126-128.

[13] Ujjwal, Mishra. 2017. Enhancement in Subgrade soil strength using Glass Powder as discrete fiber: A Review. International Research Journal of Engineering and Technology 4 (Apr. 2017), 1061-1070

[14] Yadu., Laxmikant., and Tripathi, R.K. 2013. Stabilization of soft soil with granulated blast furnace slag and fly ash. International Journal of Research in Engineering and Technology 2 (Feb. 2013), 115-119.

STUDY OF BOND STRENGTH ON VARIOUS FIBRE REINFORCED CONCRETES

Alwyn Varghese[1], Sajal R K[2], Sooraj K S[3], Sanand K D[4]
[1]Assistant Professor, Dept. Of Civil Engineering, Ahalia School of Engineering and Technology, Palakkad, Kerala, India
[2,3,4]UG Student, Dept. Of Civil Engineering, Ahalia School of Engineering and Technology, Palakkad, Kerala, India

Abstract

Concrete is basically the most important material concerning with the construction and infrastructural procedures, for which it should be of good strength and durability. In conventional concrete, micro-cracks develop before structure is loaded because of drying shrinkage and other causes of volume change. When the structure is loaded, the micro cracks open up and propagate because of development of such micro-cracks, results in inelastic deformation in concrete. Fibre reinforced concrete (FRC) is cementing concrete reinforced mixture with a numbers of small fibres are dispersed and distributed randomly in the concrete at the time of mixing, and thus improve concrete properties in all directions. The fibres help to transfer load to the internal micro cracks. The behavior of reinforced concrete (RC) structures depends up on the type of bond developed between the steel reinforcement and the surrounding concrete. Maintaining composite action requires transfer of load between the concrete and steel. Proper bond between the steel reinforcement and the surrounding concrete is also crucial for the overall strength and serviceability of RC members. The failure of RC structures may be due primarily to the deterioration of the bond. Hence it is necessary to study the bond characteristics. As per IS 456:2000 the bond between steel and concrete fails during severe to extreme environmental conditions. This paper evaluates the Bond behavior of reinforcement bar of 16mm on various grades of FRC. A study on effect of steel and fibres on the bond strength of deformed steel bars embedded in fibre reinforced concrete was carried out experimentally by conducting Pull out test.

Key words: bond strength, FRC, micro cracks, pull out test, RC

1. INTRODUCTION

Nowadays large and complicated structures are being constructed and advancements are made for their construction and maintenance. Failure of building became a worst issue faced by the civil engineers. The failure of reinforced concrete (RC) structures may be due primarily to the deterioration of the bond [2] [17]. Many experiments and developments had made to maintain proper bond between steel and concrete. To improve the structural strength and reduce cracks concrete is now reinforced with fibres. Various types of fibre like Aramid Fibre (AF), Basalt Fibre (BF), Glass Fibre (GF), Polypropylene Fibre (PPF) are added to concrete. Also Fibre Reinforced Concrete (FRC) can improve the bond strength between reinforcement and concrete [17].

The behaviour of RC structures depends up on the type of bond developed between the reinforcement and the surrounding concrete [2] [17]. Bond stress is the tangential shear or friction developed between the reinforcement and the surrounding concrete that transfers the force onto the reinforcement. To ensure the integrity of various constituent or composite action of concrete and steel reinforcement, sufficient bond should be developed by the surrounding concrete with the reinforcement. It

is also crucial for the overall strength and serviceability of RC members [7] [9] [10] [11] [15] [18] [17].

The pull out tests is more popular method of testing bond strength. The Pullout behavior is a function of the reinforcement characteristics (geometry and steel type). Characteristics of the surrounding matrix and level of lateral confinement (Core thickness or the presence of stirrups). The main advantage of adding fibres to concrete is that it induces an increase in compressive and flexural strength, toughness and ductility of concrete. Also it provides a bridging of cracks on the concrete [1] [9] [19].

2. LITERATURE REVIEW

All the studies and experiments conducted on Fibre Reinforced Concrete concluded that addition of each fibre within a range of 0.3% to 1% of the total concrete mix resulted in;

- Increase in compressive strength of concrete from 20-25% [8] [12] [14] [18]
- Increase in split tensile strength of concrete from 15-20% [3] [8] [12]
- Reduction in bleeding in fresh concrete improves the surface integrity of concrete. [8] [12]
- Increase in the bond between steel and concrete. [8] [14] [19]
- Improves homogeneity and reduces micro cracks. [14] [18]
- Ductility characteristics of concrete have improved. [8] [12]

Hence we decided to adopt the fibre dosage as 0.3% of total concrete mix.

All the studies based on bond strength mainly investigated on the influence of bar diameter, embedment length, surface type of reinforcing bars, grade of concrete, age of concrete, different environmental conditions etc.

From previous researches it identified that;

- Bond strength increased with decrease in diameter and increase in compressive strength of concrete. [5] [7] [16]
- Slip decreases with increase in bond strength. [1] [11] [17]
- The predominant mode of failure is splitting mode of failure for all tested specimens. [1] [17]
- The bond strength of reinforcement bars decreases as its embedment length increases. [1] [7]

A lot of researches are conducted on the bond strength between steel and concrete. But very few researches get an open eye towards the bond strength of FRC. In this paper bond strength between steel and concrete using different fibres with various grades of concrete have to be analyzed by the experimental manner as per IS 2770 (PART 1) 1967.

3. EXPERIMENTAL PROGRAMME

3.1 GENERAL

Objective of this paper is decided to study the variations in bond strength in various grades of plain concrete and FRC. Testing of material for the purpose of calculating mix design is conducted. A mix proportions for various grades of concrete is calculated (M20, M30). Three samples of each mix is produced for the test.

3.2 MATERIALS USED

The key materials used in this study were OPC of 43 grade, fine aggregate used is artificial sand (M sand) confing to zone III is selected, coarse aggregates retaining on 4.75mm sieve and generally ranges between 9.5mm to 37.5mm in diameter are selected. Fibres used are Aramid fibre, Basalt Fibre, Glass fibre and Polypropylene fibre. 16mm reinforcement bars (as per IS 2770 (part 1) 1967) is chosen. The potable water from well is used for mixing and curing the concrete

3.3 CONCRETE MIX DETAILS

The concrete mix design is prepared as per the recommendations given in IS 10262-2009 and IS 456:2000. The grade of concrete chosen is M20 and M30. The materials were tested for the preparation of mix and various trial mixes were prepared and tested. The proportioning for the mixes are given in Table I and the average compressive test result of 30 specimens in each grade is given in Table II.

Table I Concrete mix ratio

Mix	Water cement ratio	Cement	Fine aggregate	Coarse aggregate
M 20	0.5	1	1.88	2.9
M 30	0.45	1	1.52	2.53

Table II Compressive test result

Mix	28th day avg. Strength(mPa)
M20	26.8
M30	36.65

3.4 PREPARATION OF TEST SPECIMEN

The specimen is prepared as per IS 2770 (part I) 1967. 30 specimens are prepared with 0.3% dosage of fibre on each grade of concrete and allowed curing for 28 days.

3.5 PULL OUT TEST

Test set up used for the study is shown in the Fig 1. The specimens were tested in Universal Testing Machine of capacity 1000kN. The strength at which the bond failure occurred was measured from the dial gauge of the machine. The slip values were recorded using the dial gauge attached to the UTM as shown in Fig 2.

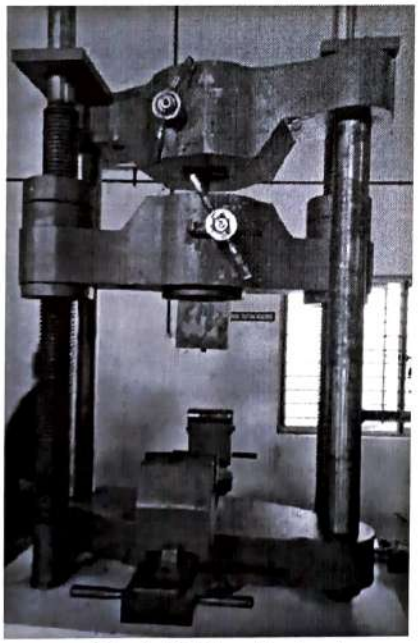
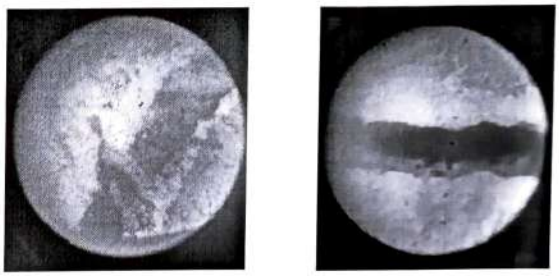


Fig 1: Pull out test setup



Fig 2 Deflection meter setup on UTM

The microscopic view of the crack occurred after pull out test were given in Fig 3.



(a) (b)

Fig 3: Microscopic view of crack (a) M20 GF (b) M20CC

3.6 DETERMINATION OF BOND STRESS

Average bond stress was obtained from the equation below

$$\tau_{bd} = \frac{P}{\pi D L}$$

where, τ_{bd} is the average bond stress in N/mm^2, P is the pullout strength in N, D is the diameter of the bar in mm and L is the embedment length in mm.

4. RESULTS AND DISCUSSIONS

The average results obtained from Pull out test is represented in graphical form as Fig 4 to Fig 17.

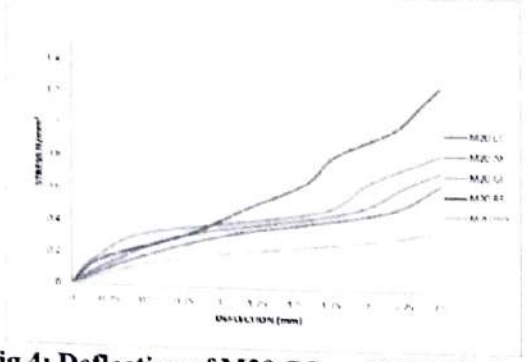


Fig 4: Deflection of M20 CC and M20 FRC up to 2.5mm

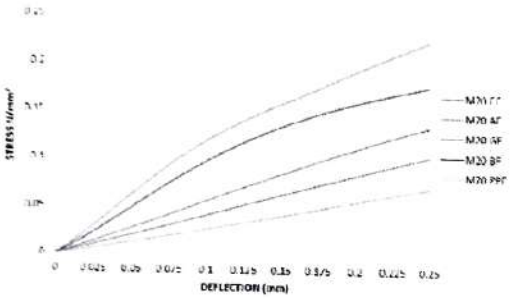


Fig 5 Deflection of M20 CC and M20 FRC up to 0.25mm

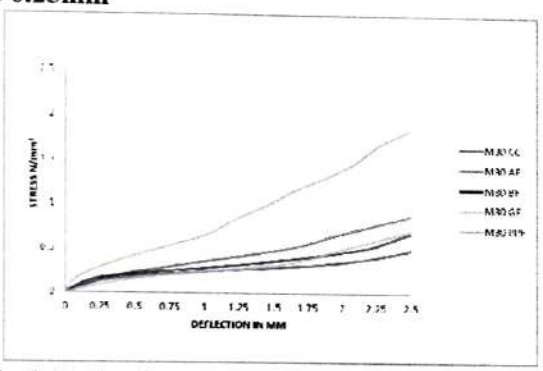


Fig 6: Deflection of M30 CC and M30 FRC up to 2.5mm

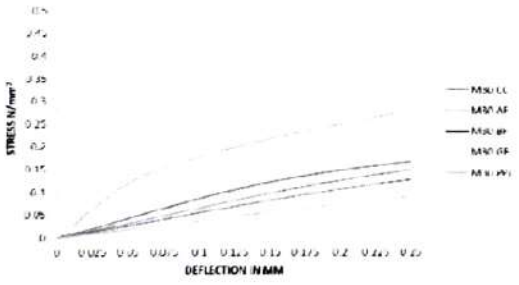


Fig 7: Deflection of M30 CC and M30 FRC up to 0.25mm

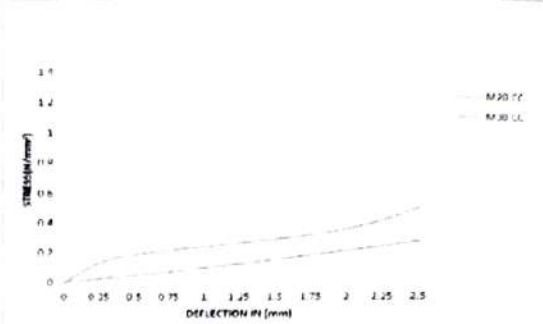


Fig 8: Deflection of M20 CC and M30 CC up to 2.5mm

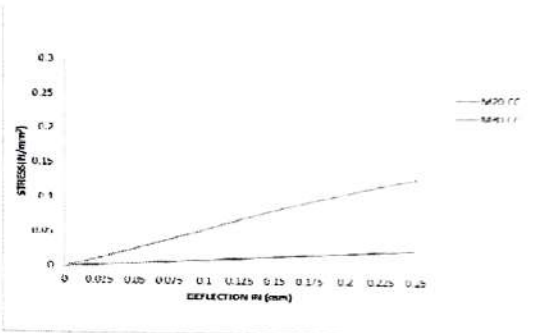


Fig 9: Deflection of M20 CC and M30 CC up to 0.25mm

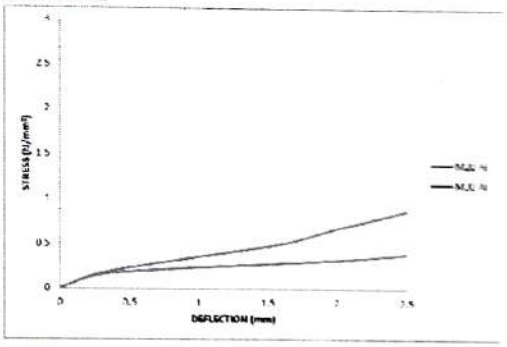


Fig 10 Deflection of M20 AF and M30 AF up to 2.5mm

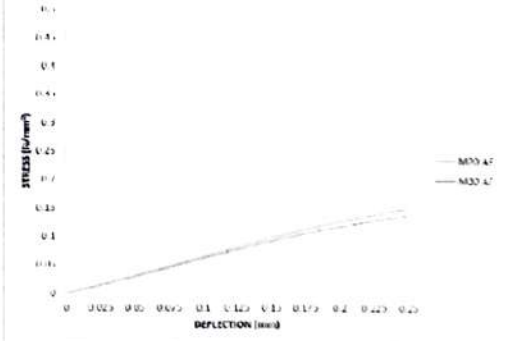


Fig 11 Deflection of M20 AF and M30 AF up to 0.25mm

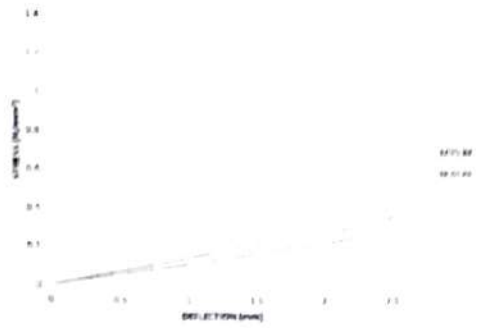


Fig 12: Deflection of M20 BF and M30 BF up to 2.5mm

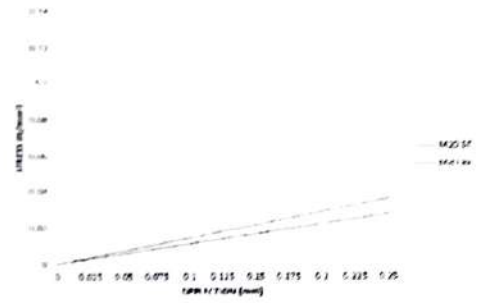


Fig 13: Deflection of M20 BF and M30 BF up to 0.25mm

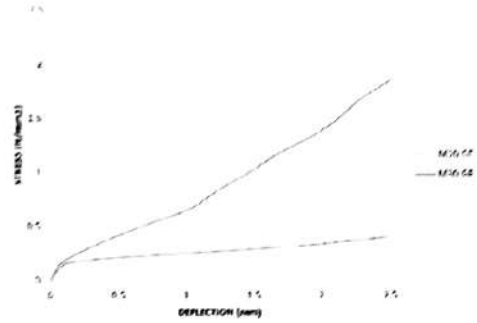


Fig 14: Deflection of M20 GF and M30 GF up to 2.5mm

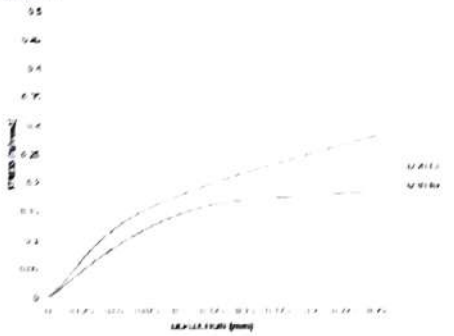


Fig 15: Deflection of M20 GF and M30 GF up to 0.25mm



Fig 16: Deflection of M20 PPF and M30 PPF up to 2.5mm

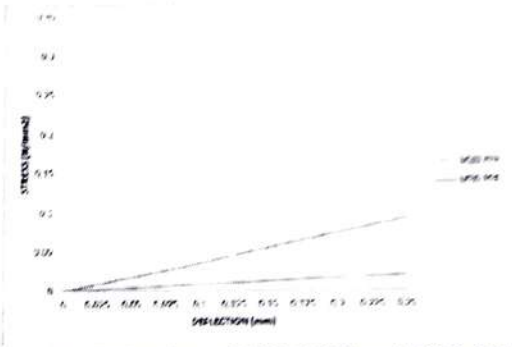


Fig 17: Deflection of M20 PPF and M30 PPF up to 0.25mm

Note:

M20 CC: M20 grade Controlled Concrete; **M20 FRC**: M20 grade Fibre Reinforced Concrete; **M20 AF**: M20 grade Aramid Fibre Reinforced Concrete; **M20 BF**: M20 grade Basalt Fibre Reinforced Concrete; **M20 GF**: M20 grade Glass Fibre Reinforced Concrete; **M20 PPF**: M20 grade Polypropylene Fibre Reinforced Concrete; **M30 CC**: M30 grade Controlled Concrete; **M30 FRC**: M30 grade Fibre Reinforced Concrete; **M30 AF**: M30 grade Aramid Fibre Reinforced Concrete; **M30 BF**: M30 grade Basalt Fibre Reinforced Concrete; **M30 GF**: M30 grade Glass Fibre Reinforced Concrete; **M30 PPF**: M30 grade Polypropylene Fibre Reinforced Concrete

From the graphs plotted using the obtained values from the pull out test conducted as per the codal provisions of IS 2770 (Part 1) 1967, the stress value at 0.025mm and 0.25mm deflection are given below.

Table III Maximum stress and stress at 0.25mm and 0.025mm slip

SL NO	SPECIMEN NAME	COMPRESSIVE STRENGTH (MPa)	AGE (DAYS)	STRESS AT SLIP (MPa)		MAXIMUM STRESS (MPa)
				0.025mm	0.25mm	
1	M20 CC	26.8	28	0.05	0.025	2.03
2	M20 AF	28.1	28	0.01	0.14	3.65
3	M20 BF	28.6	28	0.002	0.028	3.32
4	M20 GF	30.8	28	0.15	0.195	3.82
5	M20 PPF	26.5	28	0.005	0.02	3.52
6	M30 CC	36.03	28	0.015	0.13	3.14
7	M30 AF	36.5	28	0.015	0.15	2
8	M30 BF	38.5	28	0.004	0.036	3.49
9	M30 GF	41.04	28	0.06	0.28	4.15
10	M30 PPF	34.3	28	0.01	0.09	2.32

From Fig 4 the BF shows a deviation compared to other fibres may be due to its high tensile strength (4100Mpa to 4840Mpa) while the tensile strength of other fibres lies below this range [14].

From Fig 4 and Fig 5 addition of PPF had showed unsatisfactory results. It may be due to the lack of sufficient fibres i.e. addition of 0.3% of fibre will not give satisfactory result. Hence we need to increase the fibre content to 0.5% or more [3].

From Fig 6 the PPF fibre shows more satisfactory result than BF for 2.5mm deflection on M30 grade concrete as compared to M20 grade concrete. Change in grade of concrete with use of different fibres will change the matrix structure of concrete. Due to this the strength of the specimen may also vary [17] [12] [13]. Also this may be the reason that addition of GF on M30 grade concrete produced more satisfactory results compared to M20 grade concrete. Also the GF can prevent bleeding in concrete effectively than any other fibre. Reduction in bleeding increases the surface integrity of concrete [8].

From Fig 7 all the fibres follows a same trend up to deflection of 0.25mm with GF showing more satisfactory result than BF, AF and CC. PPF showed unsatisfactory result and it may be due to the lack of fibre content [3].

From Fig 8 to Fig 17 showed the variation in results of CC and FRC with the change in grade of concrete. All the graphs showed satisfactory results. All the graphs exhibited to sustain more stress for the concrete specimen with fibre content since addition of fibre increases the density of concrete and improves the surface integrity of concrete [8] [16] [17] [19]. Also M30 specimens exhibited more strength than M20 specimens.

From Table III specimens with GF exhibits more compressive strength while comparing to other specimens and the same had exhibited the capacity to withstand maximum stress.

5. CONCLUSION

Following conclusions are drawn based on the results obtained from experiment

- The pull out test on CC and FRC is conducted and the values are plotted in graphical form. Variation in strength by introduction of different fibres on different grade of concrete can be verified through the graphs.
- There is an increase in bond stress for FRC than compared to CC specimen. GF showed higher bond stress than other fibres.
- The bond strength also depends upon several factors like fibre content, compaction conditions, curing age of concrete, temperature variation, water content etc.
- An optimum value of fibre content is not advisable for all fibres since each fibre vary in its strength and other properties. Optimum value of each fibre has to be found out by trial and error method.
- There is an increase in 10-15% on 28 days compressive strength of various grades of FRC compared with CC specimens.
- FRC did not contribute much to the bond strength but prevents development of micro cracks to macro cracks formation.
- Slip decreases with increase in bond strength.
- Concrete mostly fails due to bond failure during severe to extreme weather conditions. Hence it is essential to determine the bond characteristics.

REFERENCE

[1] Harajli, M. H., M. Hout, and W. Jalkh. "Local bond stress-slip behavior of reinforcing bars embedded in plain and fiber concrete." Materials Journal 92.4 (1995): 343-353.

[2] BIS, IS. "456: 2000,—Plain and reinforced concrete code of practicel Bureau of Indian Standards." Fourth revision.

[3] Ahmed, Saeed, Imran A Bukhari, Javed Iqbal Siddiqui, Shahzad Ali Qureshi, "A study on properties of polypropylene fiber reinforced concrete." 31st Conference on Our world in Concrete and Structure. 2006.

[4] BIS, IS. "IS : 2770 (Part I) - 1967 (Reaffirmed 2007)METHODS OF TESTING BOND IN REINFORCED CONCRETEPART 1 PULL-OUT TEST." Fourth revision.

[5] Hadi, Muhammad NS. "Bond of high strength concrete with high strength reinforcing steel." (2008): 143.

[6] Proportioning-Guideline, Indian Standard Concrete Mix. "IS 10262: 2009." Bureau of Indian Standards, New Delhi (2009).

[7] Rao, G. Appa, and S. S. Injaganeri. "Evaluation of size dependent design shear strength of reinforced concrete beams without web reinforcement." Sadhana 36.3 (2011): 393-410.

[8] Avinash, G., et al. "Strength aspects of Glass Fibre Reinforced Concrete." Materials Science: An Indian Journal 8.12 (2012).

[9] Looney, Trevor J, Mahdi Arezoumandi, Jeffery S. Volz, and John J. Myers "An experimental study on bond strength of reinforcing steel in self-consolidating concrete." International journal of concrete structures and materials 6.3 (2012): 187-197.

[10]Albarwary, Ismaeel H. Musa, and James H. Haido. "Bond strength of concrete with the reinforcement bars polluted with oil." European Scientific Journal, ESJ 9.6 (2013).

[11]Al-Zuhairi, H. A., and W. D. Al-Fatlawi. "Numerical prediction of bond slip behaviour in simple pull-out concrete specimens." Journal of Engineering 19.1 (2013): 72.

[12]Borhan, Tumadhir M. "Thermal and mechanical properties of Basalt Fibre Reinforced Concrete." Proceedings of World Academy of Science, Engineering and Technology. No. 76. World Academy of Science, Engineering and Technology (WASET), 2013.

[13]Ramujee, Kolli. "Strength properties of polypropylene fiber reinforced concrete." International Journal of Innovative Research in Science, Engineering and Technology 2.8 (2013): 3409-3413.

[14]Ayub, Tehmina, Nasir Shafiq, and M. Fadhil Nuruddin. "Effect of chopped basalt fibers on the mechanical properties and microstructure of high performance fiber reinforced concrete." Advances in Materials Science and Engineering 2014 (2014).

[15]Erdem, Savaş, Tuğba Kağnıcı, and Marva Angela Blankson. "Investigation of Bond between Fibre Reinforced Polymer (FRP) Composites Rebar and Aramid Fibre-Reinforced Concrete." International Journal of Composite Materials 5.6 (2015): 148-154.

[16]Xing, Guohua, ChengZhou,TaoWu, and Boquan Liu, "Experimental study on bond behavior between plain reinforcing bars and concrete." Advances in Materials Science and Engineering 2015 (2015).

[17]Deepthi .V, Dr Sabeena M .V. "Experimental and Analytical Study on Bond Performance of Reinforced Bars Embedded in Fibre Reinforced Concrete." International Journal of Innovative Research in Science, Engineering and Technology Vol. 5, Issue 8, August 2016.

[18]Gopi N, P.Baskar, B.Dharani and P.Abinaya, "Experimental investigation of concrete with Basalt Fibre."(2016)

[19]M.narmadha, P Pandi subha , L Arun raja. "Experimental investigation on aramid fiber reinforced self-comPacting concrete. " International Conference on Recent Trends in Civil Engineering, Technology and Management April 2017.



Published by :
http://www.ijert.org

International Journal of Engineering Research & Technology (IJERT)
ISSN: 2278-0181
Vol. 6 Issue 05, May - 2017

Walayar Dam Road : A Case Study

Shadiya S
U G Student
Department of Civil Engineering
Ahalia School of Engineering and Technology
Palakkad, Kerala, India.

Shahanas P S
U G Student
Department of Civil Engineering
Ahalia School of Engineering and Technology
Palakkad, Kerala, India

Sabeera T
U G Student
Department of Civil Engineering
Ahalia School of Engineering and Technology
Palakkad, Kerala, India.

Shisina R
U G Student
Department of Civil Engineering
Ahalia School of Engineering and Technology
Palakkad, Kerala, India.

Shahabas Sahla A
U G Student
Department of Civil Engineering
Ahalia School of Engineering and Technology
Palakkad, Kerala, India.

Dr. Jino John
Professor and Head
Department of Civil Engineering
Ahalia School of Engineering and Technology
Palakkad, Kerala, India.

Abstract—**Pavement deterioration starts directly after opening of the road to traffic, this process starts very slowly so that it may not be noticeable, and over time it accelerates at faster rates. To ensure the risk of premature failure is minimized, it is necessary to use the best practice method in planning, design, construction and maintenance of the road. In this study attempts have made to improve Walayar dam road which is heavily deteriorated. And it is suggested that the existing poor condition and the problems in the Walayar dam road can be eliminated by using fly ash in the subgrade layer of the pavement and proper design.**

INTRODUCTION

A flexible pavement failure is defined by formation of pot holes, ruts, cracks, localized depressions, settlements, etc. The localized depression normally is followed with heaving in the vicinity. The sequence develops a wavy pavement surface. The failure of any one or more components of the pavement structure develops the waves and corrugations on the pavement surface or longitudinal ruts and shoving. Pavement

Unevenness may itself be considered as a failure when it is excessive. The subject of pavement failure/distress is considered to be complex as several factors contribute to its deterioration and failure Walayar Dam road is the only road which provides access to Walayar Dam, Forest training institute, Forest school and Wood depot. More than 100 families depend on this road for their daily transportation purposes. So the pavement must be of good condition and provide safe and convenient travel facilities to the road users.

I SCOPE AND OBJECTIVES

In the present study, attempt is made to study the existing road condition of Walayar dam road and to study how fly ash may be effectively utilized in combination with the soil to get an improved soil material which may be used in various soil structures. Soil collected from the site has been used in this experimental investigation. Following are the objectives of the present work:

1) To carry out survey on pavement distress in Walayar dam road.

2) To identify frequency of distress present and the causes of distresses .

3) To suggest remedies and solutions for those distresses.

II SITE INVESTIGATION

The pavement condition survey has been conducted to tails determine the various distresses of the pavement. At every 100m interval the various defects has been noted. The details given in table 1.

III SAMPLE COLLECTION

The samples of soil are collected from 3 different location such as starting point, middle and end point of the road at the depth more than 150mm. The collected samples are packed in a water tight container and transported to the laboratory.

IV ENGINEERING PROPERTIES OF SOIL

In the following table properties of the soil are given. It is determined by conducting various tests on soil as per IS code procedures. The maximum dry density of the soil is found to be low and CBR value of soil is also very less. Hence we suggest to improve the properties of soil by doing stabilization.

V MATERIALS USED FOR STABILISATION AND PROPERTIES OF MATERIALS

For the stabilization of soil we use fly ash as the admixture

1. Soil; Properties of the soil is given in the table 2
2. Fly ash

(This work is licensed under a Creative Commons Attribution 4.0 International License.)

International Journal of Engineering Research & Technology (IJ
ISSN: 2278-0
Vol. 6 Issue 05, May - 20

TABLE 1: Pavement condition survey

DISTANCE	FAILURES							
	POTHOLES		LONGITUDINAL CRACKING	TRANSVERSE CRACKING	BLOCK CRACKING	ALLIGATOR	EDGE CRACKING	BLEEDING
		NOS						
0-100m	✓	13	✓				✓	
100-200m	✓	20	✓	✓	✓		✓	
200-300m	✓	22	✓				✓	
300-360m	✓	30	✓	✓	✓	✓	✓	
360-400m	✓	34	✓	✓	✓	✓	✓	
400-430m	✓	27	✓	✓	✓	✓	✓	
430-500m	✓	20	✓				✓	
500-600m	✓	52	✓	✓	✓		✓	
600-700m	✓	33	✓				✓	
700-800m	✓	36	✓	✓	✓	✓	✓	✓
800-900m	✓	29	✓				✓	
900-1000m	✓	31	✓	✓	✓	✓	✓	✓

TABLE 2: Properties of soil

Sl No	PROPERTY	VALUE
1	Natural moisture content	18.41%
2	Specific Gravity (G)	1.418
3	Sieve analysis: Coefficient of curvature, C_c Uniformity coefficient, C_U	 0.694 4
4	Liquid Limit	40%
5	Plastic Limit (W_P)	11.11%
6	Shrinkage Limit (W_s)	16.2%
8	Maximum Dry Density (γ_d)	1.864g/cc
9	Optimum Moisture Content (OMC)	11%
10	CBR	1.88%

The maximum dry density of the soil is found to be low and CBR value of soil is also very less. Hence we suggest to improve the properties of soil by doing stabilization

VI METHOD OF TESTING

The blending operation was carried out manually and care was taken for uniform mixing as per the procedure given in IS:2720. Laboratory tests are carried out in accordance with the specification of relevant Indian Standards. To find the optimum percentage of fly ash to be added to improve the properties of soil we conducted tests on various proportions of fly ash. Following are the mixes used for testing,

Table 3: various mixes

sl.no	Mix designation	Proportions of flyash used(%)
1	M1	0
2	M2	10
3	M3	12.5
4	M4	15
5	M5	17.5
6	M6	20

VII RESULT AND ANALYSIS

A Compaction characteristics

IS heavy compaction tests were carried out on different proportions of soil and fly ash in accordance with the procedure laid in IS:2720 so as to study their moisture-density relationship. The results of Modified Procter test conducted on various proportions are shown below.

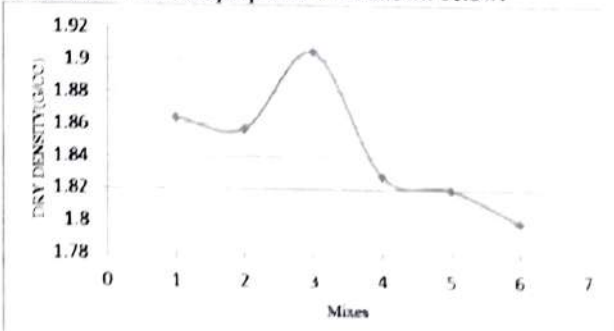


Fig 1: sample v/s dry density

(This work is licensed under a Creative Commons Attribution 4.0 International License.)

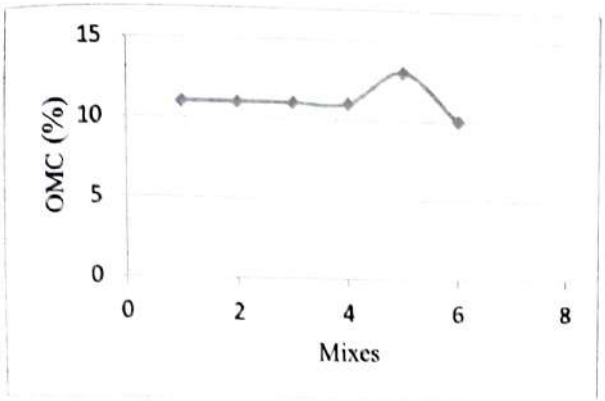


Fig 2: sample v/s OMC

The soil samples having higher maximum density mean it have greater strength and stability. Here the highest value of dry density is 1.905g/cc and is at 12.5% of fly ash and corresponding optimum moisture content is 11%.The variation of maximum dry density with various proportions of fly ash is first increasing up to 12.5% of fly ash and then it gradually decreased to 1.8g/cc. This variation of dry density is depends on the amount of fly ash and moisture content. From the obtained result, it is clear that the soil sample attain its maximum dry density and hence greater stability when the fly ash is at 12.5% with optimum moisture content of 11%.

B Strength characteristics

California Bearing Ratio(CBR) tests were carried out under soaked conditions on soil mixed with the different proportions of fly ash so as to study their load bearing capacity. The result of California Bearing tests conducted on various proportions are given in the chart below.

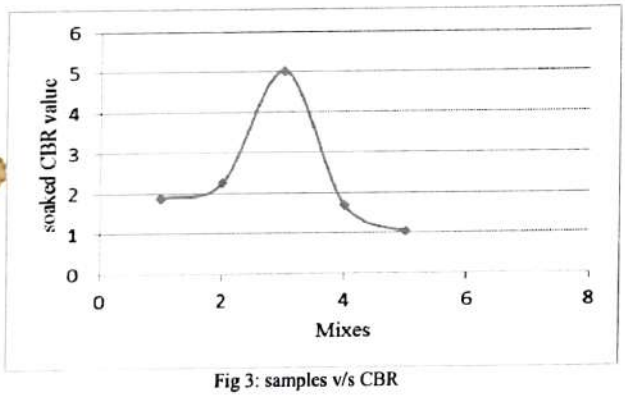


Fig 3: samples v/s CBR

Soaked CBR value represents the worst soil condition. Initially,the variation of CBR value with the addition of fly ash is increasing. For sample 3 maximum CBR value is obtained. Then the variation shows a decreasing pattern. CBR value of 12.5% increased by 3.14% when compared with the normal soil.

VIII DESIGN OF FLEXIBLE PAVEMENT

The pavement design is done for 10% and 12.5% addition of fly ash. The other values of CBR are very less than that required for the design.

Following chart shows the pavement composition of selected samples as per IRC:37-2001.

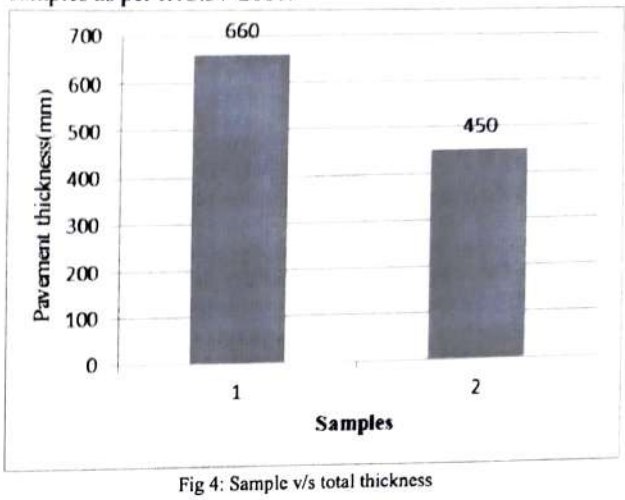


Fig 4: Sample v/s total thickness

The pavement thickness required to the corresponding CBR value of sample 1 is 660 mm while that for the sample 2 is 430mm.The thickness of pavement for further addition of fly ash has been reduced up to 230 mm. Thus stabilization saves the cost of construction of pavement and also it helps to improve the strength of the soil.

IX COST ANALYSIS

Based on PWD rates cost analysis is done for the pavement construction on soil with 10 % and 12.5% addition of fly ash for a length of 1 km.

Following table gives the construction cost of pavement,

Table 3 Cost Analysis

Sl.No	Subgrade layer	Total construction cost of the pavement
1	Soil with 10% fly ash	5130976
2	Soil with 12.5% fly ash	3753380

At 12.5% addition of fly ash the cost reduced by 27% when compared with 10% addition of fly ash.

X CONCLUSION

Based upon the above study following conclusions can be drawn:

1. Properties of soil and traffic conditions are the two main factors to be thouroughly analyzed while designing a pavement.
2. Pavement condition survey showed the worst condition of pavement. It proves that the already existing pavement is not capable of taking the wheel load that acts on the pavement.
3. The results show that the addition of fly ash improves the strength of soil. A total of 6 sample proportions were tested and we suggested sample 3(fly ash 12.5%) as the suitable proportion for the proposed pavement stabilisation. By doing stabilisation total pavement construction cost is reduced upto 27%.

(This work is licensed under a Creative Commons Attribution 4.0 International License.)

4. Transportation facility of the WALAYAR DAM ROAD can be increased by Re-construction of the road, by stabilizing sub grade soil using fly ash, it reduces the thickness of pavement thereby cost of construction.

REFERENCES

[1] Hnin Ei Ei Khaing, Dr.Tin Tin Htwe(2014), "Study on Failures and Maintenance of Flexible Pavement (Pyay-Aunglan–Koepin Portion)",Vol.03,Issue.14 June,pp 2984 to 2990.

[2] IRC : 37-2001,"Guidelines for the design of flexible pavement" (second revision), The Indian Road Congress, New Delhi.

[3] IS : 2720-Part 1 to 9, Part 16, Bureau of Indian Standards.

[4] Jayakumar.M, Lee Chee Soon(2015), "Study on Flexible Pavement Failures in Soft Soil Tropical Regions" IOP Conf. Series: Materials Science and Engineering 78,pp1 to 12.

[5] Jyothi.S.Tridevi, Sandeep Nair, Chakradhar Iyyunni(2013), "Optimum Utilization of Fly Ash for Stabilization of Subgrade Soil using Genetic Algorithm", Chemical, Civil and Mechanical Engineering Tracks of 3rd Nirma University International Conference , Procedia Engineering 51,pp 250 to 258.

[6] Kishan Khunt(2013), "Use of Additive Materials in Subgrade for Road Construction", International Journal of Engineering Trends and Technology(IJETT), Volume 4, Issue 8, September,pp 3790 to 3795.

[7] Lakshmi Keshav, Mangaiarkarasi.V(2012), "Effect of fly ash on an expansive soil for flexible pavement design" , International journal of engineering and innovative technology (IJEIT), Volume 2, Issue 3, September,pp 275 to 281.

[8] Magdi M.E. Zumrawi(2013), "Survey and Evaluation of flexible Pavement Failures", Index Copernicus Value,pp 1602 to 1607.

[9] Neero Gumsar Sorum, Thangmuansang Guite, Nungleppam Martina (2013), "Pavement Distress: A Case Study", National Conference on Recent Advances in Civil Engineering (NCRACE),pp 274 to 284.

[10] Omer G Omer, Ahmed M. Elsharief and Awad E. M. Mohamed(2014), "Failure Investigation for Recently Constructed Road in Khartoum State", Journal of Geological Resource and Engineering 2,pp 20 to 31

[11] Patil B.M and Patil K.A. (2013), "Improvement in properties of soil by using Pond ash and Chemical additive", IRC, Volume 41, August,pp 35 to 41.

[12] Praveen Kumar, Ankit Gupta(2006), "Case Studies on Failure of Bituminous Pavements". Compendium of Papers from the First International Conference on Pavement Preservation: PAPER 52,pp 505 to 518.

[13] Saladi SV Subbarao, Akhil, Tarak(2015), "Design and Analysis of Flexible Pavement: A case of Kochi Port Area", International Journal of Engineering Technology and Advanced Engineering(IJETAE), Volume 5, Issue 8 August,pp 40 to 47.

[14] Sharad.S.Adlinge, Prof.A.K.Gupta (2015), "Pavement Deterioration and its Causes", IOSR Journal of Mechanical & Civil Engineering (IOSR-JMCE),pp 9 to15.

[15] Sharma R.K (2014),"Subgrade characterestics of soil mixed with foundary sand and randomly distributed steel chips", IRC, Volume 42, April,pp 4 to 11.

[16] Vinod Kumar R, Pavithra.M.(2016), "Experimental Study on Design of Flexible Pavement using CBR Method", International Journal of Engineering Research, Volume 5, Issue special 1,pp 63 to 68.

[17] Vivek Singh Pundir and Ved Prakash(2015)," Effect of Soil Stabilizers on the Structural Design of Flexible Pavements", Pelagia Research Library, Advances in Applied Science Research,pp 134 to 147.



(This work is licensed under a Creative Commons Attribution 4.0 International License.)

International Research Journal of Engineering and Technology (IRJET) e-ISSN: 2395 -0056
Volume: 04 Issue: 05 | May -2017 www.irjet.net p-ISSN: 2395-0072

Stabilization of Black Cotton Soil Using Ayurvedic Industrial Waste

R. Aiswarya varsha[1], M. Anvar[2],G. Aswini [3], K.U. Athulya [4], R. K. Ratheesh[5], Gopika Unni[6]

[12345]*UG Student, Dept of Civil Engineering, Ahalia School of Engineering and Technology, Kerala, India*
[6]*Professor, Dept of Civil Engineering, Ahalia School of Engineering and Technology, Kerala, India*

Abstract - *In recent times, with the increase in demand for infrastructure , raw materials and fuels, soil stabilization has started to take a new shape. With the availability of better research, it is emerging as a popular and cost effective method for soil improvement. Black cotton soil are problematic in nature due to its low bearing capacity,swelling and high compressibility. Due to high plasticity, shrinkage and low strength, the soil is regarded as unsuitable for construction.Thus it is necessary to increase the strength of the soil by stabilizing it and making it more suitable for construction. The main objective of this paper is to investigate the effect of ayurvedic waste on the strength parameters of black cotton soil like compressive strength, CBR etc. These tests are conducted on virgin soil and stabilized soil samples.The results obtained are compared for the two samples and inferences are drawn. Also if the waste material proves to be an environment friendly successful stabilizing agent, it may also prove to be a suitable waste disposal method.*

***Key Words*: Black cotton soil, Ayurvedic waste, Liquid Limit, UCC, Compaction and Plastic Limit**

1.INTRODUCTION

The Black cotton soil covers about 30% of land area in India. The name "Black cotton" has an agricultural origin. Most of these soils are black in colour and are good for growing cotton. Due to it characteristics of high plasticity, excessive swelling, shrinkage and low strength when wet, soil is regarded as unsuitable for construction. Stabilization incorporates the various methods implement for modifying the properties of a soil and improves the engineering properties and performance of soil.

Soil stabilization could be applied to both sandy and clayey soil through mechanical and chemical methods. There are many common methods-mechanical or chemical –found in the literatures that were used to improve the physical properties of the soils.

The paper presents the effect of industrial waste inclusion on the strength of black cotton soil. The mixing of ayurvedic wastes may be considered same as other admixtures used to stabilize soil. The purpose of this paper is to evaluate black cotton soil behaviour induced by ayurvedic waste inclusion.

1. MATERIALS USED

The black cotton soil needed for testing was collected from Ahalia college campus. Ayurvedic waste of ksheerabala waste was used as an industrial waste. Ksheerabala is an ayurvedic drug used to treat arthritis, central nervous system disorders and insomania. The main content of Ksheerabala are kurunthotti and cow's milk.The waste which is obtained after the manufacture of medicine was collected from Ahalia Medicine Manufacturing Unit.

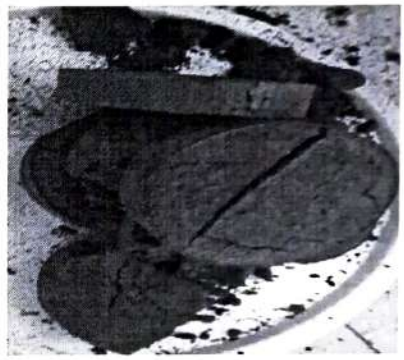


Figure 1 : Ksheerabala waste collected

3. METHODOLOGY

The soil was collected locally and was kept for air drying for 24 hours. The soil was then taken to the Geotechnical Laboratory and various properties like natural water content, free swell index, Specific gravity etc was determined. Then the fundamental properties like liquid limit, plastic limit, shrinkage limit and the particle size distribution was determined.We also conducted compaction test and unconfined compressive strength test and also classified the 0soil. The ayurvedic waste was collected and different percentages of it was added into soil. We conducted the test with soil samples containing 5%, 10% and 15% waste. The results obtained were compared and discussed.

Following tests were conducted on soil samples.

1. Unconfined compression test (as per is-2720(Part-4):1985
2. Standard proctor compaction test (as per IS-2720(Part-7):1980
3. Swell test(as per IS-2720(Part-4):1985
4. Atterberg limit test(as per IS-2720(Part-5):1985

4.RESULT AND DISCUSSION

4.1. Variation of free swell index with various percentage of waste added

The Free Swell Index test has been conducted on plain soil sample. It is observed that, the free swell index value of soil sample is 73.33%,which is very expansive. It cracks up during dry season and becomes sticky when wetted with water. The compound walls and light buildings with shallow foundation around the region having expansive soil show signs of distress like tilting, lifting, cracking etc. From the graph the degree of expansiveness is decreases with the addition of various percentage of waste content. Hence strength of soil increases.

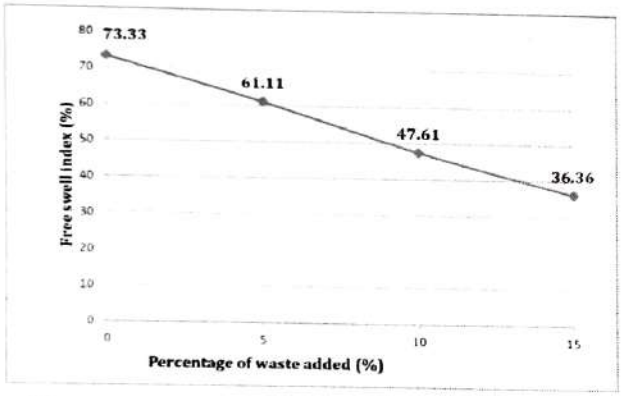


Chart -1: Variation of free swell index with various percentage of waste added

4.2. Variation of liquid limit with various percentage of waste added

The liquid limit has been conducted on soil sample with the addition of 0%, 5%, 10% and 15% of waste content. From the graph the liquid limit value increases with the addition of various percentage of waste content.

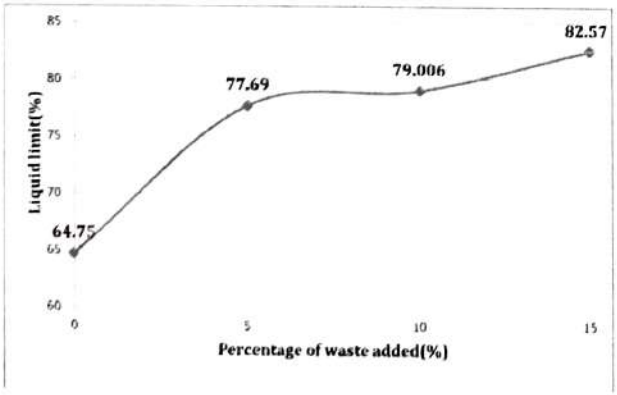


Chart -2: Variation of liquid limit with various percentage of waste added

4.3. Variation of plastic limit with various percentage of waste added

The plastic limit has been conducted on soil sample with the addition of 0%, 5%, 10% and 15% of waste content. From the graph the plastic limit value increases with the addition of various percentage of waste content.

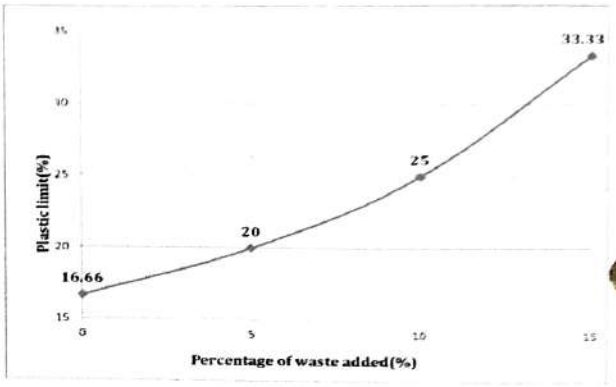


Chart -3: Variation of plastic limit with various percentage of waste added

4.4. Variation of compaction characteristics with various percentage of waste added

The compaction test has been conducted on soil sample with the addition of 0%, 5%, 10% and 15% of waste content. From the graph the maximum dry density value is decreases and optimum moisture content increases with the addition of various percentage of waste content. Weight of waste is less than that of soil at the same volume which lead to decrease MDD and increasing the surface area of mixture (soil+waste) needs more water to reach to the optimum which lead to increase in the OMC.

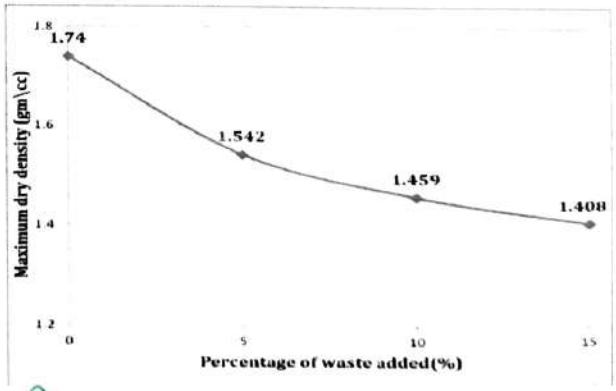


Chart -4: Variation of maximum dry density with various percentage of waste added.

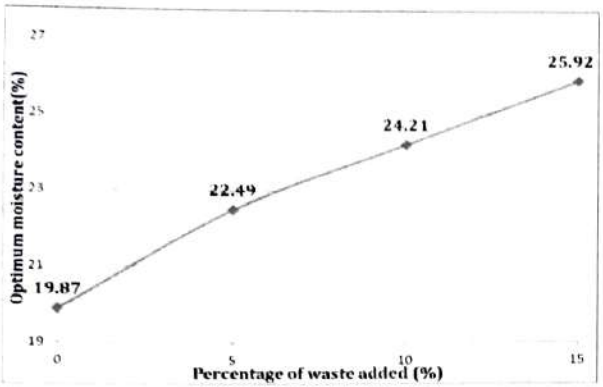


Chart -5: Variation of optimum moisture content with various percentage of waste added.

4.5. Variation of compressive strength with various percentage of waste added

The UCC test has been conducted on soil sample with the addition of 0%, 5%, 10% and 15% of waste content. From the graph the UCC value is increases with the addition of various percentage of waste content and Strength of the stabilized soil is enhanced 3.5 times the virgin soil.

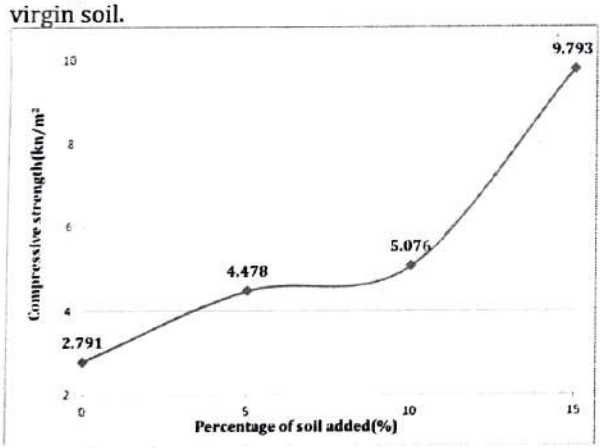


Chart -6: Variation of plastic limit with various percentage of waste added

5. CONCLUSIONS

Stabilization of weak soil using industrial wastes are gaining popularity nowadays due to the abundance in its availability and low cost involved. This study is an effort to stabilize black cotton soil using ayurvedic wastes and to evaluate benefits of stabilization. The use of ayurvedic waste has found to be suitable in behaving volume change behaviour of expansive soil.

The addition of ayurvedic waste has resulted in the improvement of strength characteristics of the black cotton soil. A total of 28 samples were used for carrying out the study. The results showed that the stabilization of black cotton soil using ayurvedic waste is an efficient and economic tool for improving the characteristics of black cotton soil.

The conclusions drawn from the experimental investigations done so as to bring out the effect of stabilization of black cotton soil using ayurvedic waste were:

- Addition of ayurvedic waste in varying percentage resulted in the decrease of maximum dry density.
- They showed a similar trend in the variation of OMC. The OMC curve represented an overall increase in the OMC.
- Addition of waste resulted in the decrease of degree of expansiveness from 73.33% to 36.36%. Hence the strength of soil increases.
- The UCC test results showed a considerable increase in the unconfined compressive strength of the soil from 2.791 kg/cm² to 9.793 kg/cm²
- The strength of the stabilized soil is enhanced 3.5 times the virgin soil.
- The liquid limit of soil is increases from 64.75% to 82.57%
- The plastic limit of soil is increases from 16.66% to 33.33%
- Thus the ayurvedic waste has proved to be a successful stabilizing agent for black cotton soil.

REFERENCES

[1] Amit Tiwari& Mahiyar, "Stabilization of Black cotton soil by Fly ash, Coconut Coir Fibre and Crushed Glass" International Journal of Emerging Technology and Advanced Engineering,(ISSN 2250-2459, ISO 9001:2008 Certified Journal, Volume 4, Issue 11, November 2014)

[2] Anas Ashraf & Arya Sunil, "Soil Stabilizaton using Raw Plastic Bottles", Proceedings of Indian Geotechnical Conference December 15-17,2011, Kochi (Paper No. H-304)

[3] Anil Kumar& Sivapullaiah, "Soil Stabilization With Waste Materials Based Binder" Proceedings of Indian Geotechnical Conference,December 15-17,2011, Kochi (Paper No. H-119)

[4] Arun Patidar & Mahiyar, "Experimental Study On Stabilization Of Black Cotton Soil Using HDPE Wastage Fibres, Stone Dust and Lime", international journal of advanced scientific and technical research issue 4 volume6,nov.

[5] Ghatge Sandeep Hambirao&P.G.Rakaraddi ," Soil Stabilization Using Waste Shredded Rubber Tyre Chips", International Journal of Scientific & Engineering Research, Volume 5, Issue 12, December-2014 977.

[6] Joydeep Sen& Jitendra Prasad,"Stabilization Of Black Cotton Soil Using Bio Enzyme", International Journal of Innovative Research in Science,Engineering and Technology,Vol. 4, Issue 12, December 2015.

[7] Keerthi.Y&Divyakanthi.P, "stabilization of clayey soil using cement kiln waste" ,International Journal of advanced structures and Geotechnical Engineering ISSN 2319-5347, Vol. 02, No. 02, April 2013

[8] Mandeep Singh& Anupam Mittal, "A Review On Soil Stabilization With Waste Materials", International Journal of Engineering Research and Applications (IJERA) ISSN: 2248-9622 National Conference on Advances in Engineering and Technology (AET- 29th March 2014) .

[9] Monica Malhotra& Sanjeev Naval, "Stabilization Of Expansive Soil Using Low Cost Materials", International Journal of Engineering and Innovative Technology (IJEIT),Volume 2, Issue 11, May 2013.

[10] Pankaj.R & Prakash.B, "Stabilization Of Black Cotton Soil Using Admixtures", International Journal of Engineering and Innovative Technology (IJEIT) Volume 1, Issue 5, May 2012.



International Research Journal of Engineering and Technology (IRJET) e-ISSN: 2395 -0056
Volume: 04 Issue: 03 | Mar -2017 www.irjet.net p-ISSN: 2395-0072

Performance Evaluation of Glass Fibre Reinforced Concrete

Prof. Anu Retnakar, Aswin.S, Shamju Kaja Hussain.S, Shilpa.T.S, Varun.V, Sandeep Kumar. M.D

Dept. of Civil Engineering, Ahalia School of Engineering and Technology, Kerala, India

Abstract - *Researchers all over the world are attempting to develop high performance concretes by using fibres and other admixtures in concrete up to certain proportions. Glass Fibre Reinforced concrete (GFRC) is a recent introduction in the field of concrete technology. GFRC is concrete that uses glass fibres for reinforcement instead of steel. The present study has been taken up for evaluating the different percentage concentration of glass fibre. Emphasis has been given to the workability, compressive strength and flexural strength properties of glass fibre concrete beams. The different dosages of glass fibre are (0%, 0.2%, 0.4% and 0.6%)*

Key Words: **Glass fibre, Concrete, compressive strength, flexural strength, durability, deformation**

1.INTRODUCTION

The application of cement concrete is limited due to the characteristics of brittle failure. This can be overcome by the inclusion of a small amount of short and randomly distributed fibres. Such concrete can be practiced where there is a weakness of concrete such as less durability, high shrinkage cracking, etc. Concrete has some deficiencies such as low tensile strength, brittleness, highly porous, susceptible to chemical and environmental attack.

The above deficiencies of plain concrete are overcome in the new materials which have unique characteristics, which make them highly susceptible to any environment. Fibre reinforced concrete is one of them and relatively a new composite material in which concrete is reinforced with short discrete (length up to 35 mm), uniformly distributed fibres so that it will improve many engineering properties such as flexural strength, shear strength and resistance to fatigue, impact and eliminate temperature and shrinkage cracks. Fibres of lengths up to 35 mm are used in spray applications and 25 mm length premix applications. Various types of glass fibres used in construction industries are glass, steel,
natural fibres, poly propylene, asbestos, carbon, basalt, etc.

Glass fibre has high tensile strength (2-4 GPa) and elastic modulus (70-80 GPa), brittle stress-strain characteristics (2.5-4.8 % elongation at break) and low creep at room temperature. Glass fibres are usually round and straight with diameters of 0.005 to 0.015 mm. They can be bundled with bundle diameter of 1.3 mm.

1.1 Advantages

- GFRC is prepared of minerals and will not easily burn. When exposed to a flame, the concrete function as a thermal regulator. It protects the materials fixed with it from the flame heat.
- These materials are comparatively lighter when compared to the conventional materials. Their installation is therefore fast, and normally simple. Concrete may be produced in thin sections.
- GFRC may be cast to almost any shape of columns, wall panels, domes, mouldings, and fireplace surrounds.
- High strength can be obtained by using GFRC, being tough and resistant to cracking. It has a high strength-to-weight ratio.
- GFRC products are durable and light. The transportation costs are reduced significantly being of less weight.
- Since GFRC is internally reinforced, other types of reinforcement are not necessary that may be complicated for complicated moulds.
- Suitable consolidation of mix is achieved for GFRC that is sprayed, without any vibrations. Use of rollers or vibrators, to attain consolidation, is simple for GFRC that is poured.

2. MATERIALS USED

The key materials used in this study were cement, sand, glass fibre and water. The cement used is Portland pozzolana cement (PPC) of 43 grade. Alkaline resistant 12mm glass fibre is used .The portable water from well is used for mixing and curing the concrete.

2.1 CEMENT

Portland cement is the most common type of cement, used as a basic ingredient of concrete, mortar. It is a fine powder produced by heating materials in a kiln to form clinker, grinding the clinker, and adding small amounts of other materials. PPC cement is manufactured by using

pozzolanic materials as one of the main ingredient. The percentage of pozzolanic material used in the preparation should be between 10 to 30. PPC cement of 43 grade is been used in our study.

Specific Gravity	2.94
Normal consistency	38
Initial setting time	3.5
Fineness of cement	6



Fig -1: PPC cement

2.2 FINE AGGREGATE

Fine aggregate are basically sands from the land or the marine environment. Fine aggregates generally consist of natural sand or crushed stone with most particles passing through a 9.5mm sieve and retaining on 75 micron IS sieve.

Specific gravity	2.6
Bulk density	1.53
Void ratio	0.37
Porosity	27.17%

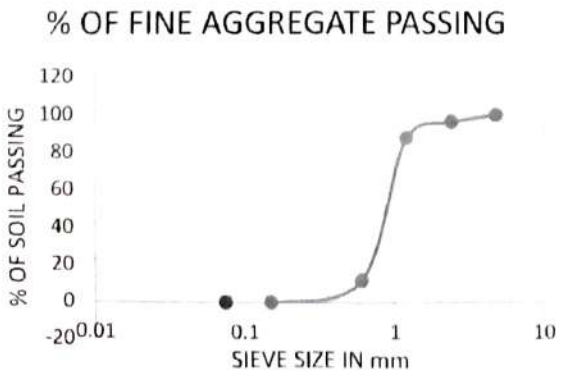


Chart -1: Sieve analysis



Fig -2: River sand

2.3 COARSE AGGREGATE

Coarse aggregates are particles greater than 4.75mm, but generally range between 9.5mm to 37.5mm in diameter.



Fig -3: Coarse aggregate

2.4 GLASS FIBRE

Glass fibre is a material consisting of numerous extremely fine fibres of glass. Glass fibre-reinforced concrete consists of high-strength, lightweight, durable, alkali-resistant glass fibre embedded in a concrete matrix. Glass fibre of 12mm length is been used.



Fig -4: 12mm Glass fibre

3. MIX PROPOTION

Table -1: Mix Proportion

Materials	Quantity (kg/m³)	Proportions
Cement	372	1
Fine Aggregate	555.33	1.49
Coarse aggregate	1270.85	3.4
Water	186	0.5

3. TEST METHODS

3.1 Workability Test

Workability tests were performed using Slump moulds as it is the quick measure of workability of concrete mixes. The slump test was done in accordance with the IS 1199-1959.

3.2 Compressive Strength Test

The wooden mould of size 100 x 100 x 100 mm is well tightened and oiled thoroughly. They were allowed for curing in a curing tank and they were tested in 200-tonnes electro hydraulic closed loop machine. The test procedures were used as per IS: 516-1979.

3.3 Flexural Strength Test

The wooden mould of size 500 x 100 x 100 mm is well tighten and oiled thoroughly. They were allowed for curing in a curing tank and they were tested in universal testing machine. The test procedures were used as per IS 516-1979.

4. RESULTS

4.1 Workability Test

Table -2: Workability

Percentage of fibre (%)	Slump value (cm)	Compaction factor
0	23	0.84
0.2	8	0.825
0.4	3	0.821
0.6	2	0.799

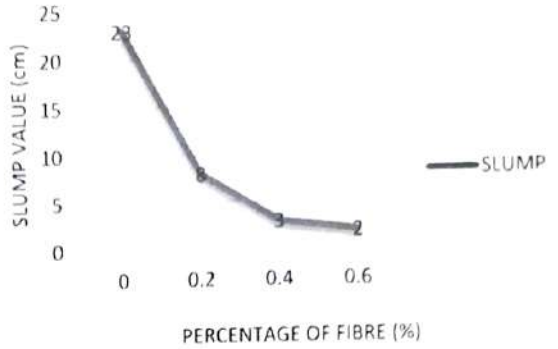


Chart -2: Slump Test

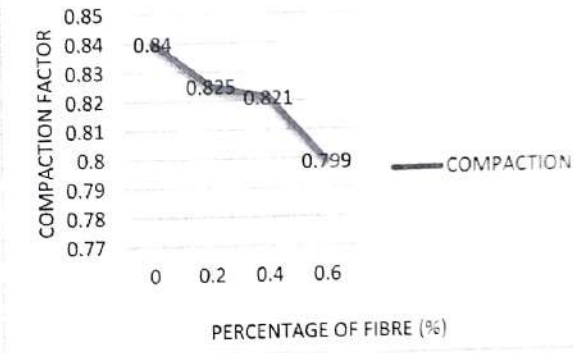


Chart -3: Compaction Factor Test

4.2 Compression Test

Table -3: Compression Test

Percentage of fibre (%)	7 Days (N/mm²)	28 Days (N/mm²)
0	12	16
0.2	13	19
0.4	18	25
0.6	15	20

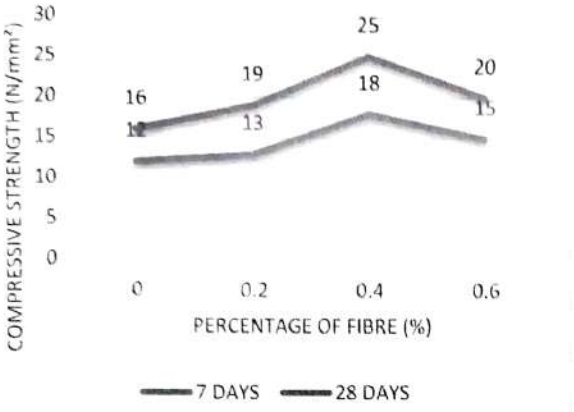


Chart -4: Compression Test

4.3 Flexural Test

Table -4: Flexural Test

Percentage of fibre (%)	7 Days (N/mm^2)	28 Days (N/mm^2)
0	2.42	3.19
0.2	2.47	3.22
0.4	2.97	3.58
0.6	2.65	3.30

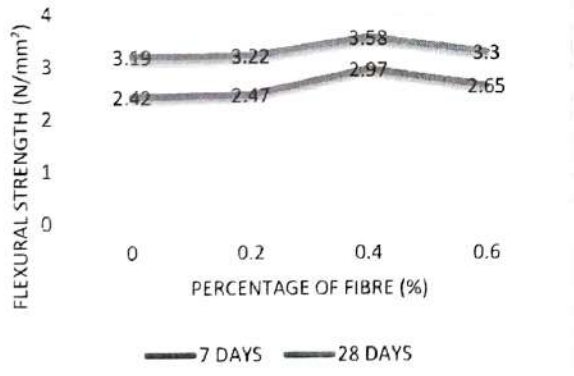


Chart -5: Flexural Test

5. CONCLUSIONS

Based on experimental investigation, addition of Glass Fibre in plain concrete increases the strength characteristics.

Maximum compressive and flexural is attaining in 0.4% addition of Glass Fibre.

Further addition of fibre showed a gradual decrease in strength aspects.

It has been observed that the workability of concrete decreases with the addition of Glass Fibres. But this difficulty can be overcome by using plasticizers or super-plasticizers.

6. REFERENCE

[1] **Hemalatha.S and Dr. Leema Rose.A** –An Experimental Study On Glass Fibre Reinforced Concrete-International Research Journal of Engineering and Technology, Vol.3, Issue 04, April 2014

[2] **Md.Abid Alam, Imran Ahmad, Fazlur Rehman** – Experimental Study on Properties of Glass Fibre Reinforced Concrete- International Journal of Engineering Trends and Technology, Vol.24, Number 6, June 2015

[3] **Saxena.A.K and Seema Singh**- Effect of Strength in Grade Concrete with Partial Replacement of Glass Fibre- International Journal for Scientific Research and Development, Vol.3, Issue 09, 2015

[4] **Praveen Kumar Goud.E and Praveen .K.S**- Optimization of Percentages of Steel and Glass Fibre Reinforced Concrete-International Journal of Research in Engineering and Technology, Vol.4, Issue, April 2015.

[5] **Adetiloye.A and Ephraim.M.E**- Structural Engineering Properties of Fibre Reinforced Concrete Based on Recycled Glass Fibre Polymer-International Journal of Engineering Researches and Application, Vol.5, Issue 04 (part 1) April 2015

[6] **Klaus Holschemacher and Philipp Lober** - Structural Glass Fibre Reinforced Concrete for Slabs on Ground-World Journal of Engineering and Technology, 2014, 2, pp 48-54

[7] **Kumar A.D and Upendre Varma.A** - Glass Fibre Reinforced Concrete-International Journal Of Engineering Reasearch and Application, Vol.3, Issue 5, Sept-Oct 2013

[8] **Adeel Ahmed and Liaqat Qureshi .A** -An investigation of Strength Properties of Glass Fibre Reinforced Concrete-International Journal of Engineering Research and Technology,Vol.2, Issue 4, April 2013.

[9] **Bharti Tekwani and Komal Chawla** - Studies of Glass Fibre Reiforced Concrete-International Journal of Structural and Civil Engineering Research,Vol.2, No.3, August 2013.

[10] **SelinRavikumar .C and Thandavamoorthy T.S.** - Glass Fibre Concrete: Investigation on Strength and Fire Resistant Properties-Journal of Mechanical and Civil Engineering, Vol.9, Issue 3, Sept-Oct 2013

[11] **Avinash Gornale, S.Ibrahim Quadri, S.Mehmood Quadri, Syed Md Akram Ali, Syed Shamsuddin Hussaini-** Strength Aspects of Glass Fibre Reinforced Concrete-International Journal of Scientific and Engineering Research, Vol.3, Issue 7, July 2012

[12] **P.Sangeetha**- Study on the Compression and Impact Strength of GFRC with combination of Admixtures-Journal of Engineering Research and Studies, Vol.2,Issue 2, Apr-June 2011

[13] **Prof.S. S. Pimplikar and Eng. Pshtiwan N. Shakor** - Glass Fibre Reinforced Concrete Use in Construction-International Journal of Technology and Engineering System, Vol.2, Jan-Mar 2011

[14] **B.L.P.Swami, A.K.Asthana and U.Masood**- Studies on Glass Fibre Reinforced Concrete Composites-Strength and Behaviour- Challenges, Opportunities and Solutions in Structural Engineering and Construction-2010

[15] **Chandramouli.K, Srinivasa Rao.P, Pannirselvam.N, Seshadri Sekhar.T and Sravana.P**- Strength Properties of Glass Fibre Concrete-APRN Journal of Engineering and Applied Sciences, Vol 5, No. 4, April 2010

ResearchGate

See discussions, stats, and author profiles for this publication at: https://www.researchgate.net/publication/316075301

MECHANICAL PROPERTIES OF GLASS POWDER AND TIN STRIPS BASED CONCRETE UNDER ACCELERATED CURING

Article · April 2017

CITATION
1

READS
423

4 authors, including:



Alwyn Varghese
Karunya University
4 PUBLICATIONS 1 CITATION
SEE PROFILE



Vivek K Viswanath
Indian Institute of Technology Madras
1 PUBLICATION 1 CITATION
SEE PROFILE

Some of the authors of this publication are also working on these related projects:

Project fiber reinforced concrete View project

Project design aspects of buiding View project



All content following this page was uploaded by Alwyn Varghese on 13 April 2017.

The user has requested enhancement of the downloaded file.

International Journal of Advanced Technology in Engineering and Science
Vol. No.5, Issue No. 04, April 2017
www.ijates.com
ijates
ISSN 2348 - 7550

MECHANICAL PROPERTIES OF GLASS POWDER AND TIN STRIPS BASED CONCRETE UNDER ACCELERATED CURING

Amritha P[1], Aparna Dandapani[2], Kezy Joy[3], Alwyn Varghese[4], Vivek K Viswanath[5]

[1,2,3]Student, [4,5]Assistant Professor, Civil Engineering,
Ahalia School of engineering and Technolog (India)

Today the construction industry is finding cost effective materials for strengthening the concrete. Waste management is becoming a major issue worldwide. One option for safe environmental and economic disposal of waste is to reuse them in building materials. Glass being non-biodegradable is not suitable for addition to landfill, and as such recycling opportunities need to be investigated. Use of metals as containers has become popular and safe now, especially to carry liquid. But its disposal is difficult. Due to high material consumption of the construction industry, the utilization of used glass as a partial replacement for fine aggregate in structural concrete is partially attractive. This paper aims to study the properties of concrete by partially replacing fine aggregate by crushed glass powder and soft drink tins strips as fibers. The study was conducted on the M25 mix with water cement ratio 0.40. The fine aggregate was partially replaced with glass powder at percentages of 10, 20, 30, 40 and 50. The addition of fibers was studied at various percentages of 0.5,1,2 and 3. Accelerated curing process was adopted. From the optimum percentage of glass powder replacement and fiber addition, the different hybrid was cast and studied its properties.

Keywords – Concrete, Fiber, Glass Powder, Replacement, Tin strips

I. INTRODUCTION

Concrete is the most used construction material. Plain concrete possesses two major drawbacks as a structural material. They behave in the brittle fashion and possess a very low tensile strength. It possesses a low modulus, limited ductility and little resistance to cracking. Micro cracks developing the material during its manufacture due to inherent volumetric and micro structural changes. Hence it is necessary to impart tensile resistance properties to concrete structural members to use it as a load bearing material. Concrete have comparatively higher compressive strength but lower tensile strength. Waste management has become a significant issue in today's growing society. Population levels around the globe are increasing rapidly, resulting in unprecedented levels of waste material. Waste utilization in cement and concrete should be maximized to achieve cost reduction, saving in energy, resource conservation, improved product quality, environmental protection and reduction in greenhouse gas emission and for improved durability. Most of the non-degradable waste materials are left as stockpiles, used as landfill material or illegally dumped in selected areas. Large quantities of this waste cannot be eliminated. However, the environmental impact can be reduced by making more sustainable use

ijates
ISSN 2348 - 7550

of this waste. Researchers into new innovative uses of waste materials are continuously advancing. These research efforts try to match societies need for safe and economic disposal of waste materials.Glass being non-biodegradable is one such material that is not suitable for addition to landfill. Fortunately, glass can be recycled indefinitely without any loss in quality, but first needs to be sorted by colour. This is an expensive process, and subsequently waste glasses is increasingly being used in application s were mixed colour is not an issue, such as an aggregate in civil construction. The construction industry presents an attractive market for the use of waste glass. One of the principal components of construction is concrete, due to its high compressive strength, durability, and ease of construction.

With natural aggregates within India being present in limited quantities, producing crushed aggregates for use in the construction industry is costly. Therefore it can be seen that incorporating recycled glass as aggregate in structural concrete has the potential to not only produce environmental benefits in the reduction of landfill and the consumption of raw materials but to also reduce costs for industry costs. The use of recycled waste glass in concrete has attracted much interest worldwide and numerous researches have been carried out, showing the possibility of use of waste glass as building materials by partially replacing concrete mixtures. The study conducted by M. Adaway et.al. [1]concluded that the compressive strength of the concrete was found to increase by the replacement of fine aggregate by glass powder. This can be attributed to the angular nature of the glass particles which facilitate better bonding with the cement paste. The research conducted by M. Iqbal Malik et.al. [2], EsraaEmaam Ali et.al. [3], S.P Gautam et.al. [4] proves glass powder as fine aggregate replacement increases the mechanical properties of concrete.

Reinforcing concrete with fibres can effectively improve the properties of concrete like mechanical strength, toughness, shrinkage, durability, etc. addition of fibres would act as a crack resistor and would substantially improve static and dynamic properties. The studies conducted by G.Muraliet. al. [5] and J. Raj Prasad et. al. [6] shows that waste materials including steel powder, lathe waster, soft drink tins can be used as fibers to improve the mechanical properties of the concrete. The study conducted by UroosaIqbalet. al [7] concludes that with the increase in size and percentage of the soft drink tin strips the workability of concrete decreases and the strength increases. From the study conducted by KampaRavinder [8], the addition of soft drink tin strips as fibers increases the mechanical properties of the concrete.

Concrete is generally weak in tensile strength and strong in compressive strength. The main aim of researches or concrete technologists is to improve the tensile strength of concrete. To overcome this serious defect partial incorporation of fibers occurs. Great quantities of steel waste fibers are generated from industries related to lathe, empty beverages, metal cans and soft drink bottles. This is an environmental issue as steel waste fibers are difficult to biodegrade and involves processes either to recycle or reuse. Hence the use of soft drink tin fibers increases tensile strength and helps to improve durability.

A hybrid concrete is the one in which more than one material is added to increase the mechanical properties of concrete. The environmental and economic concern is the biggest challenge concrete industry is facing. Today Construction industry is in search of new materials to replace natural resources. Hybrid concrete using glass powder as partial replacement of fine aggregate and soft drink tin strips as fibers increases the strength and durability of concrete and also enhance waste management. The glass, which is non-degradable waste material possess good filler property and thus can be used as a partial replacement for natural fine aggregate. The soft

drink tin waste as fiber helps to increase the strength. Hybrid concrete using glass powder and soft drink tin strips is cheaper building material than the normal concrete.

II. OBJECTIVE

- To experimentally investigate the characteristics of HYBRID CONCRETE using waste materials.
- To compare the strength of conventional concrete with hybrid concrete using waste materials.
- To study the use of waste materials in concrete and enhancing waste management in an economic way.

III. MATERIALS

Cement: Pozzolonic Portland Cement of 53 grade available in local market was used in investigation. The mechanical properties of the cement used in this investigation are given in TABLE 1.

TABLE 1.Properties of Cement

Properties of Cement	Values
Specific Gravity	2.92
Normal Consistency	34%
Initial Setting time	>30 min
Fineness Modulus	4.6

TABLE 2. Properties of fine and coarse aggregate

Particulars	Fine aggregate	Coarse aggregate
Bulk density	1.586	1.630
Void ratio	0.6746	0.641
Specific gravity	2.65	2.67
Porosity	40.2%	39.09%

Fine aggregate: Manufactured sand is a substitute of river for construction purposes sand produced from hard granite stone by crushing. The crushed sand is of cubical shape with grounded edges, washed and graded to as a construction material. The size of manufactured sand (M-Sand) is less than 4.75mm.Locally available clean, well graded M-sand was used as fine aggregate. The properties of the fine aggregate are given in the TABLE 2. Figure 1 represents the particle size distribution curve of the M- sand.

Coarse aggregate: Crushed granite angular aggregate of size 20mm nominal size from local source was used. The properties of the coarse aggregate are given in the TABLE 2

Glass powder: Glass powder is obtained by crushing the beverage bottles. The glass powder is used as partial replacement of fine aggregate. The size of particles used is 0.006-1.18mm. The specific gravity of the glass powder was found to be 2.5. Figure 2 represents particle size distribution curve of glass powder.

Fibres: Soft drink tin cut into strips of size 3mmx10mm were used as fibers. The material of tin strip is aluminum. The density of fiber was found to be 1.75g/cm^3.

ijates
ISSN 2348 - 7550

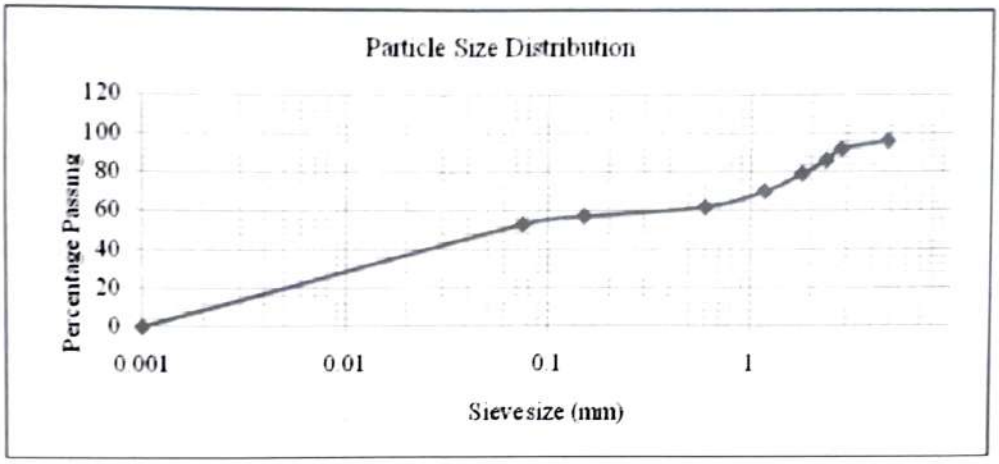


Figure 1 sieve analysis of M-sand

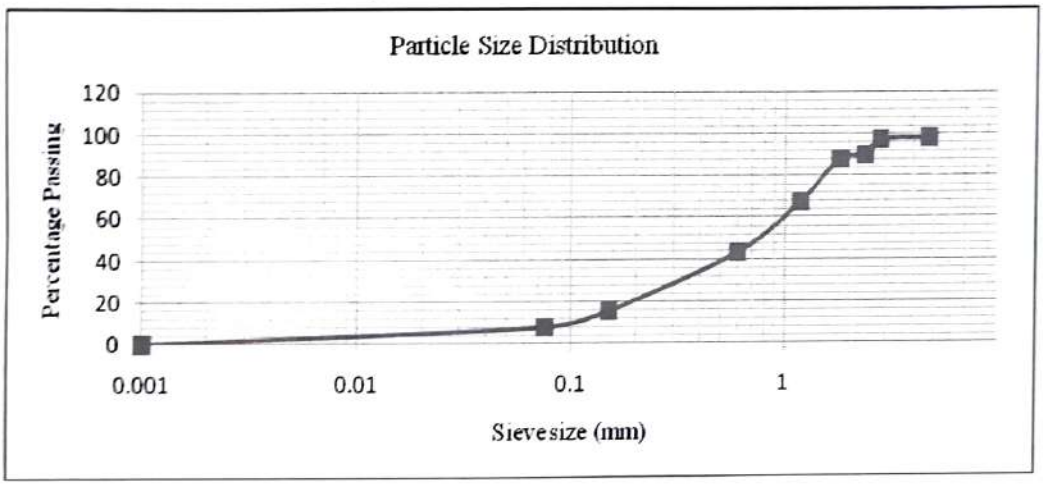


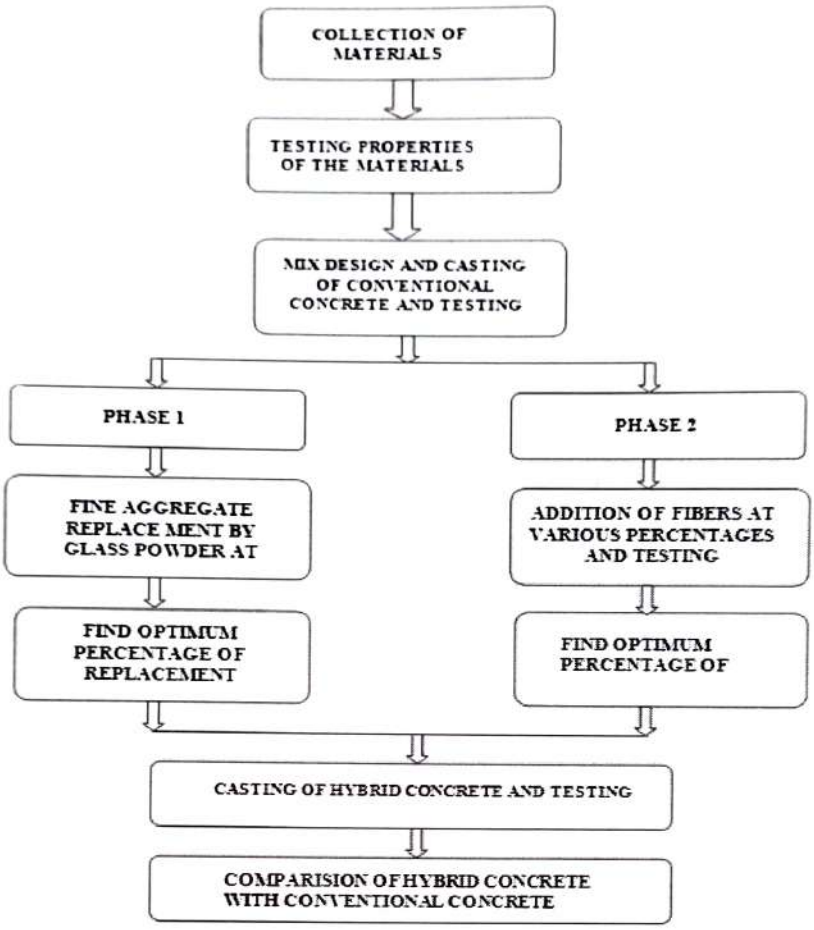
Figure 2 sieve analysis of glass powder

IV. METHODOLOGY

The beverage bottles and soft drink tins were collected. The bottles were crushed to make it into powder form. The glass powder was sieved and particles of size 4.75 to 600 micron were used for replacement. The well graded glass powder was used for partially replacing M sand. The tin was scratched to improve bonding in the concrete and was cut into strips of size 3mm X 10mm.

TABLE 3.Mix proportions

Cement	Fine aggregate	Coarse aggregate	Water
1	1.17	2.1	0.40



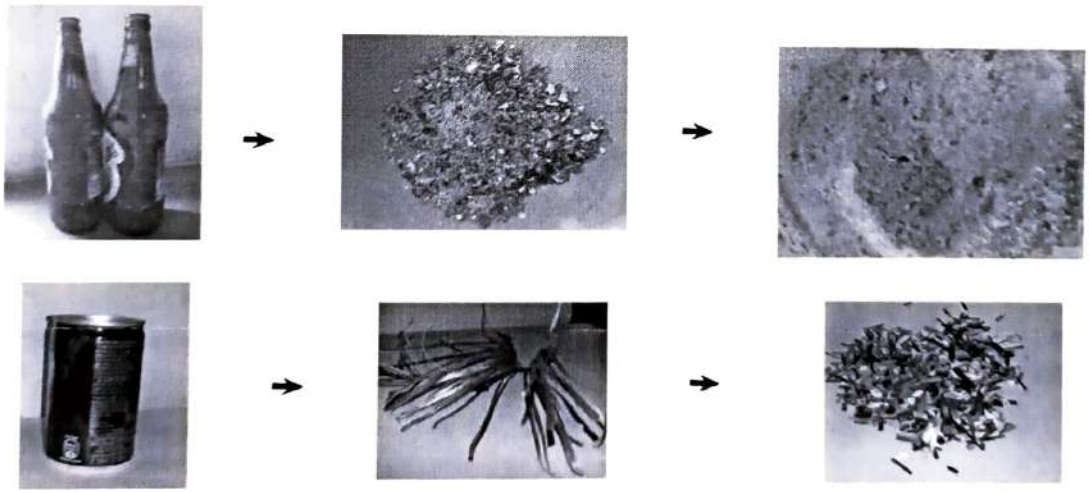


Figure 3 glass powder and tin strips

4.1 Accelerated Curing

Accelerated curing is any method by which high early age strength is achieved in concrete. The two method of accelerated curing are warm water method and boiling water method. To determine the early age strength, boiling water method of accelerated curing are adopted. The cubes of size 100mm X 100 mm X 100mm and

cylinders of 150mm diameter and 300mm length was cured in the curing tank for three and half hours and then immersed in cooling tank for two hours. According IS: 516-1959 [9] for concrete mixes with aggregate size less than or equal to 20mm the cubes with size 100mm may be used. The specimen was tested in accordance with IS: 516-1959. As per IS: 9013-1978, [10] a correlation exists between the results obtained in concrete specimens, cured by accelerated method and cured by normal method, for mixes employing different materials and mix proportions. The corresponding strength at 28 days can be found out from the following correlation. The test results obtained were correlated with the help of graph for boiling water method in the IS: 9013-1978.



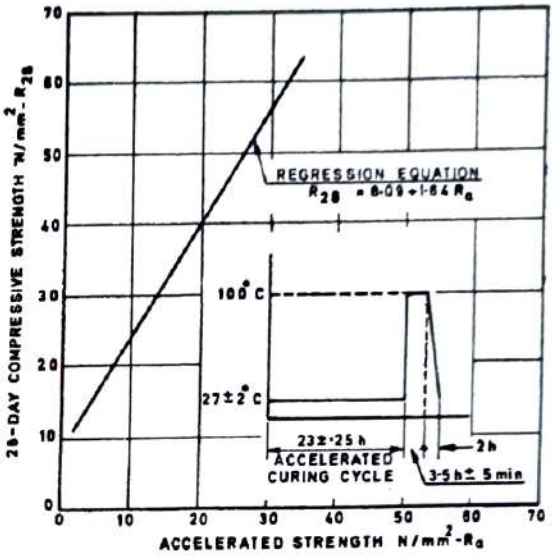


Figure 4 accelerated curing tankFigure 5 correlation chart for boiling water method

V. RESULTS

5.1 Glass powder replacements

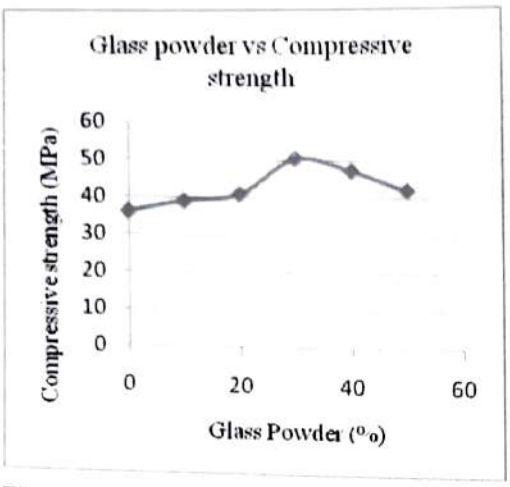
The M-sand was replaced using varying percentages of 10,20,30,40 and 50. From the test results represented in TABLE 3 the optimum percentage was found to be 30%.

5.2 Fiber addition

The tin strips as fibers were added at percentages of 0.5, 1, 2, And 3. From the test results represented in TABLE 4, the optimum percentage was found to be 0.5.

TABLE 4. Test results of Glass powder replacement

Glass powder	Slump(mm)	Compressive Strength(MPa)	Tensile strength(MPa)
0	120	36	2.76
10	90	39	2.91
20	75	40.89	2.95
30	70	50.46	3.05
40	65	47.33	2.93
50	50	42	2.89



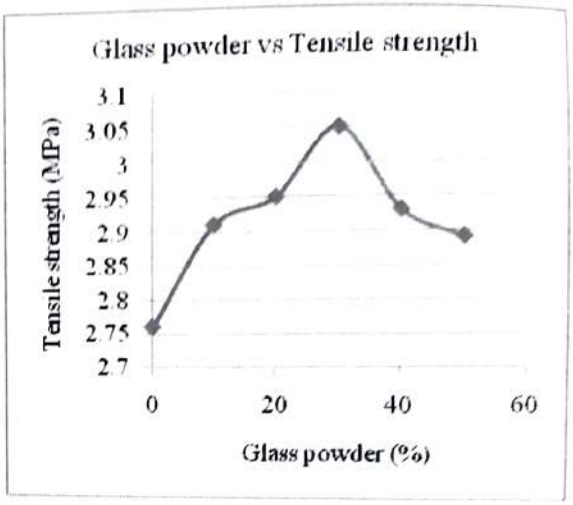


Figure 6 glass Powder vs compressive strengthFigure 7glass Powder vs tensile strength

TABLE 5. Test results of fiber addition

Fiber (%)	Slump (mm)	Compressive strength (MPa)	Tensile strength (MPa)
0	120	36	2.76
0.5	75	40.94	3.3
1	70	36.82	2.95
2	65	34.27	2.81
3	60	28.36	2.55

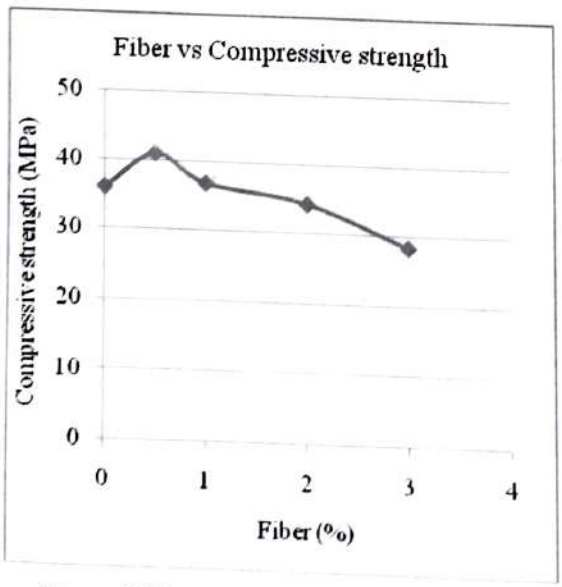


Figure 8 fiber vs compressive strength

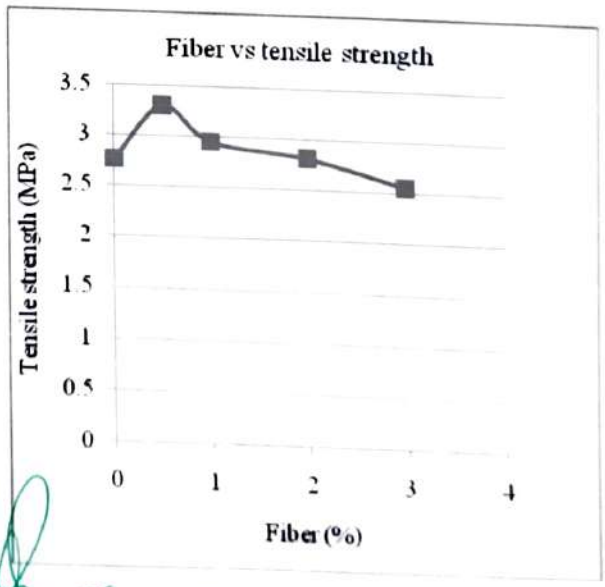


Figure 9 fiber vs tensile strength

ijates
ISSN 2348 - 7550

5.3 Hybrid mixes

In case of hybrid concrete, it is not sure about desired results. Hence, nine different hybrid concrete mixes by varying glass powder and fiber percentages were tried. From the results in TABLE 5, none of the hybrid mixes obtained the results closer to control mix. The nine hybrid mixes are:-

$G_{30}F_{0.5}$	30% Glass Powder Replacement + 0.5 % Fiber addition
$G_{30}F_{1}$	30% Glass Powder Replacement + 1 % Fiber addition
$G_{30}F_{2}$	30% Glass Powder Replacement + 2 % Fiber addition
$G_{25}F_{0.5}$	25% Glass Powder Replacement + 0.5 % Fiber addition
$G_{35}F_{0.5}$	35% Glass Powder Replacement + 0.5 % Fiber addition
$G_{40}F_{0.5}$	40% Glass Powder Replacement + 0.5 % Fiber addition
$G_{45}F_{0.5}$	45% Glass Powder Replacement + 0.5 % Fiber addition
$G_{50}F_{0.5}$	50% Glass Powder Replacement + 0.5 % Fiber addition
$G_{35}F_{1}$	35% Glass Powder Replacement + 1 % Fiber addition

TABLE 6. Test results of hybrid mixes

MIX	SLUMP (mm)	STRENGTH TESTS	
		COMPRESSION(N/mm^2)	TENSION(N/mm^2)
0 MIX	120	36	2.69
$G_{30}F_{0.5}$	90	22.65	3.075
$G_{30}F_{1}$	80	21.1	2.55
$G_{30}F_{2}$	65	16.23	2.28
$G_{25}F_{0.5}$	80	24.49	2.307
$G_{35}F_{0.5}$	75	31.05	2.602
$G_{40}F_{0.5}$	70	26.15	2.386
$G_{45}F_{0.5}$	65	17.93	1.974
$G_{50}F_{0.5}$	60	16.4	1.88
$G_{35}F_{1}$	85	23.7	2.267

ijates
ISSN 2348 - 7550

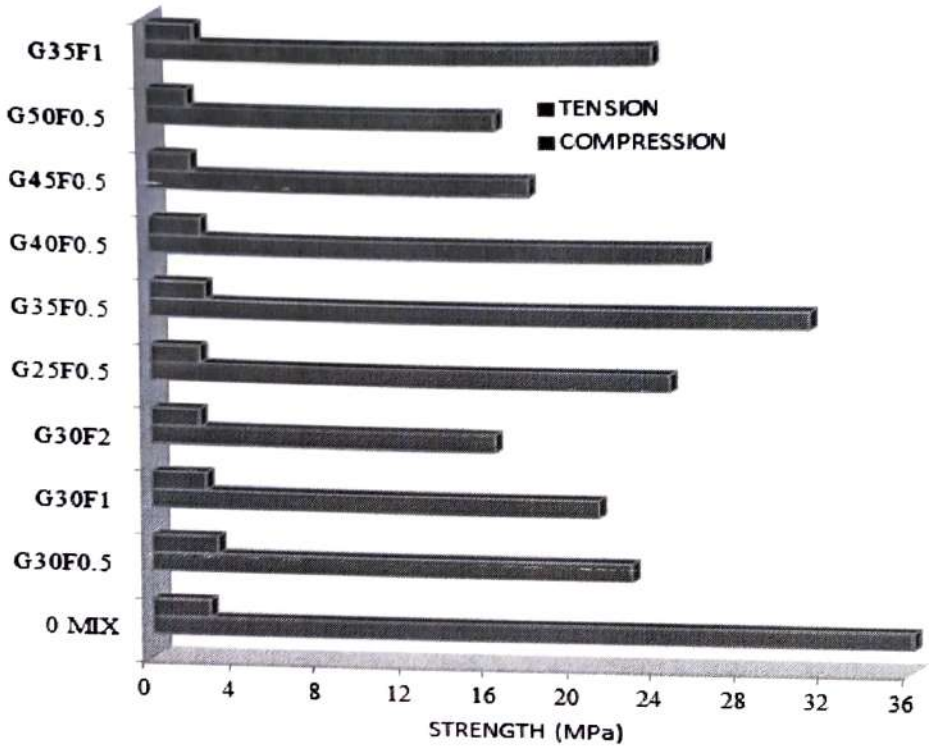


Figure 10 strength values of hybrid mixes

VI. CONCLUSION

- 30% percentage of glass powder replacement was found to be optimum. The compressive strength and tensile strength increment was found to be 40.1% and 10.5% respectively. The angular nature of the powdered glass increases the bonding in the concrete which aids to the strength increment.[1]
- 0.5% percentage of fiber addition was found to be optimum.The compressive and tensile strength increment was found to be 13% and 19.5% respectively. The addition of the tin strips as fibers reduces the micro cracks in the concrete thereby increasing the tensile strength.
- None of the hybrid mixes obtained the strength closer to that of control mix. This may be due to lack of bonding between the glass powder and tin strips.
- Both Glass powder and tin strips can be used separately in concrete to increase the mechanical properties of the concrete.

VII. SUGGESTIONS

The hybrid mixes do not have strength comparable to that of control mix. Hence glass powder as partial replacement for M- sand and tin strips as artificial fibers cannot be used together. It does not give the combined effect on concrete. But, glass powder and tin strips may be used separately in concrete for better results. The reasons for the failure of hybrid concrete using glass powder and tin strips may be:

- Lack of bond between glass particles and tin strips.
- The corrosion of the aluminum strips.

- Oxidation reaction between the constituent particles of the glass powder and tin strips.

The tin strips were scratched to improve the bonding in the concrete. So the protective coating to prevent oxidation in aluminum may get removed. Also curing in boiling water may accelerate the reaction to take place.For determining the exact reason for the failure of hybrid concrete future studies are required.

REFERENCES

[1] Ali, EsraaEmam, and Sherif H. Al-Tersawy. "Recycled glass as a partial replacement for fine aggregate in self compacting concrete." Construction and Building Materials 35 (2012): 785-791.

[2] Malik, M. Iqbal, et al. "Study of concrete involving use of waste glass as partial replacement of fine aggregates." IOSR Journal of Engineering 3.7 (2013): 08-13.

[3] Ali, EsraaEmam, and Sherif H. Al-Tersawy. "Recycled glass as a partial replacement for fine aggregate in self compacting concrete." Construction and Building Materials 35 (2012): 785-791.

[4] Gautam, S. P., VikasSrivastava, and V. C. Agarwal. "Use of glass wastes as fine aggregate in Concrete." J. Acad. Indus. Res 1.6 (2012): 320-322.

[5] Murali, G., et al. "Experimental investigation on fibre reinforced concrete using waste materials." International Journal of Engineering Research and Applications (IJERA) ISSN 2248.9622 (2012): 278-283.

[6] Iqbal, Uroosa, Muhammad Akram, and Abdullah Saand. "Soft Drink Tins as Fibre Reinforcement in Concrete."AMPE, 2015.

[7] KampaRavinder, "Strength characteristics of coca-cola tin waste as fibres in concrete,"International Journal of Advanced Research Foundation, 3(2), 2016, 9-12.

[8] IS : 516-1959 ,methods of tests for strength of concrete.

[9] IS : 9013-1978 , method of making , curing and determining compressive strength of accelarated-cured concrete test specimens.

International Research Journal of Engineering and Technology (IRJET) e-ISSN: 2395 -0056
Volume: 04 Issue: 05 | May -2017 www.irjet.net p-ISSN: 2395-0072

Design of Interlocking Block and Replacement of Msand by Concrete Roof Tile Waste

I.P.Malavika[1], Nipuna.M[2], Raina T. R[3], Sreelakshmi A.V[4], Kripa K.M[5]

[1,2,3,4] *Students Dept. of Civil Engineering, Ahalia school of Engineering and Technology, Kerala, India*
[5]*Assistant Professor, Dept. of Civil Engineering, Ahalia school of Engineering and Technology, Kerala, India*

Abstract – *Interlocking blocks are one of the alternatives for the conventional burnt clay brick. This report deals with the design of interlocking blocks and also replacement of the m-sand by concrete roof tile waste in various percentages and finding the optimum percentage of tile waste by testing the cubes casted for compressive strength of 3 days and finally casting the blocks with that optimum percentage of tile waste. The report finally gives the results of an experimental investigation in which the compressive strength, water absorption and density were investigated by using optimum percentage of tile waste, m- sand, cement and 6mm aggregate with mix proportion of 1:2:4. The experimental results are compared with that ordinary solid block. The results indicate that these blocks are slighter lighter in weight, durable in aggressive environments and have better strength for their use in building construction.*

Key Words: **Interlocking block, Roof tile waste, Replacement, Compressive strength**

1. INTRODUCTION

The interlocking blocks are different from other normal bricks as it requires less mortar or cement for masonry work. These blocks interlocked with each other by means of positives and negative frogs on the top and bottom of the blocks which disallow the horizontal compressive stress and lateral movement of blocks. The projection of one block fits into the depression of the next so that they always align perfectly. The specifications and the characteristics of this block depend on the machine used to manufacture it. The most common size of block is 300x150x120mm. The basic raw materials are cement, fine aggregate and coarse aggregate. This is usually done with mechanized compaction and vibration.

Current process of producing the interlocking block is by using a semi mechanized stationary type machine. The other production systems are - manual mould that requires hand tamping, a mobile semi-mechanized egg-laying machine and fully mechanized system that combines compression and manual concrete filling in mould. The machine also compacts and consolidates the mix so that the blocks are uniform in size and attain desired physical properties.

The blocks are cured for a minimum period of 14 days, before they are ready to use. On an average 600-800 blocks can be made in 8 hours by 1 skilled and 6-8 semi-skilled workers. There are various types of interlocking blocks. The most commonly used cement interlocking blocks are regular shaped block, half size block and u-shaped block.

1.1 Advantages of Interlocking Blocks

Interlocking blocks offer numerous advantages to other building materials. The materials required for production are widely available so they do not have to be shipped in from long distances. Since the manufacturing process is a simple one, production facilities can be easily set up at convenient geographical locations, once again reducing the cost of transporting them to the construction site. In the case of very large construction projects, an interlocking block production facility can be set up at the construction site to provide the most cost effective supply solution.

Without the need of high waged skilled masons, by saving cement and with the speed of construction, the building costs are lower than that for standard masonry construction. When compared to convention masonry block construction, interlocking blocks, which are dry assembled, save a great deal of mortar which is normally used for vertical and horizontal joints, which produces savings in terms of both cost and time. The structural stability and durability of interlocking block construction can be far greater than the normal construction.

2. DESIGN OF INTERLOCKING BLOCKS

Each blocks have two interlocks, a projection 'tongue' part and a depression 'groove' part, this helps to resist the lateral movements and horizontal compressive stresses caused due to earthquakes.

Size of the block is chosen to be 300 X 220 X150 (in mm) and width is of 220mm, it covers the total width of two normal bricks, therefore no need of plastering. It covers an area of about more than 3 normal bricks. Slopes are provided for the ease in interlocking between the blocks so that there will not be any problem in aligning the blocks. Height of the projection is about 2.5cm, therefore less amount of mortar needed. Slope is 1 in 2, therefore front view will be of pleasing nature. As well as less amount of mortar needed, if it is to be plastered. The blocks are shaped with projecting parts, which fit exactly into depressions in the blocks placed above, such that they are automatically aligned horizontally and vertically thus block laying is possible without special

masonry skills. Each block has a projection in one end of blocks side face and a depression in other end. Since the blocks can be laid dry, less mortar is required and a considerable amount of cement is saved.

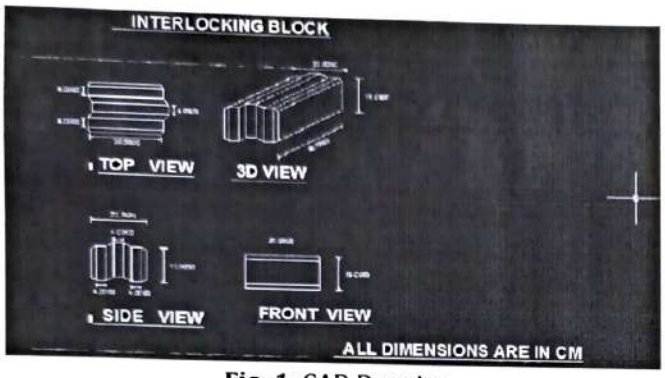


Fig -1: CAD Drawing

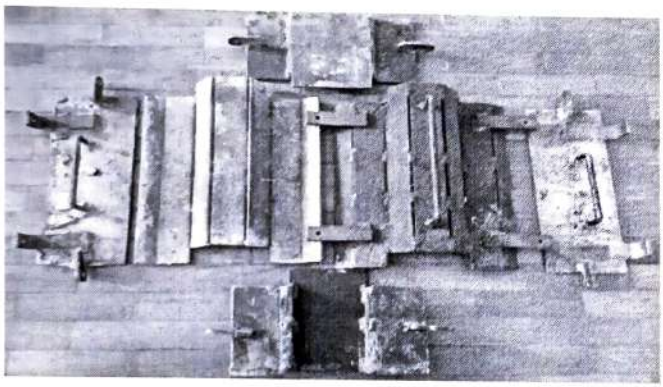


Fig -2: Parts of mould

3. METHODODLOGY

In this methodology, the materials used were:-Cement (53 grade), M-Sand, Concrete roof tile waste (collected from "PIONEEER ROOFING TILES" company), Coarse aggregate (6mm).

3.1. Trial Casting

In trial 1, mix design was done and the ratio obtained was 1:1.54:2.51.Since this ratio cannot be adopted according to clause 7.1.1 IS 2185 (Part 1):2005.Also we analyzed that the water content was not sufficient for providing workable mix. In trial 2, 4 cubes of size 15cm x 15cm were cast in the mix proportions of 1:2:4 and 1:3:6 using 53 grade cement, 6 mm coarse aggregate and M-sand. The cubes were tested for compression and the results obtained were:-
Compressive strength of M15 mix cube =15 MPa
Compressive strength of M10 mix cube =9 MPa
The ratio of M15 mix cube was adopted and decided to add Master Glenium Sky 8233 for better finishing as well as for increasing workability.



Fig -3: Cubes of M10 and M15 mix

Slump test was done in the fixed ratio of 1:2:4 for finding the water-cement ratio and thus obtained the value as 0.45. In trial 3, 14 cubes of size 10cm x 10cm were cast in the ratio of 1:2:4 with the replacement of M-sand by roof tile wastes as 0%, 5%, 10%, 15%, 20%, 25% and 30%.The cubes were tested for compressive strength test.

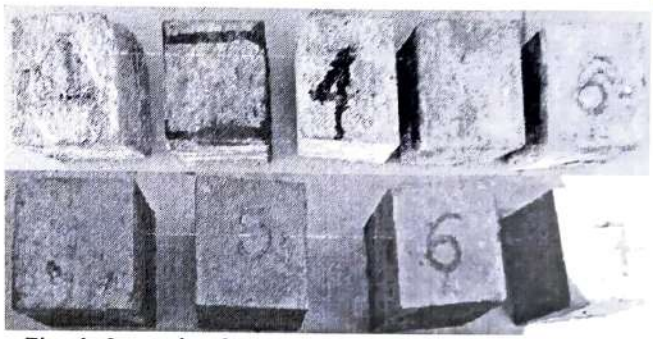


Fig -4: Cast cubes by replacement of M sand by roof tile waste in 0,5,10,15,20,25 and 30%

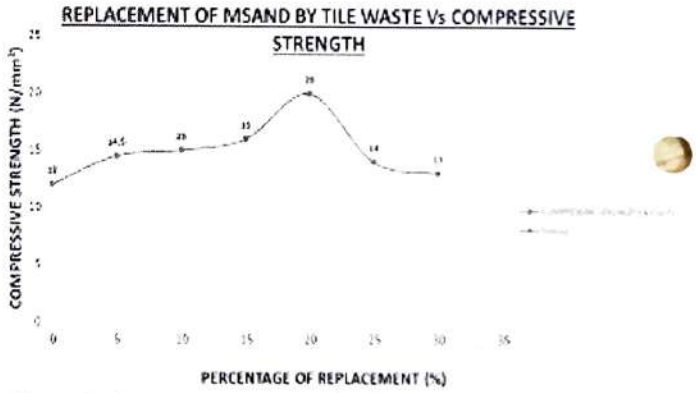


Chart 1: Compressive strength of cubes and optimum value fixation

Since 20% replacement was the optimum value, concluded to cast the interlocking block with this ratio.

3.2. Casting of interlocking blocks

The blocks were cast in the ratio 1:2:4 by using 53 grade cement, Msand replaced by 20% of roof tile waste, 6mm aggregate. All the materials were mixed in the mould and compacted using vibratory compaction machine. 11 cubes

were casted and were tested for compressive strength, water absorption, and block density.

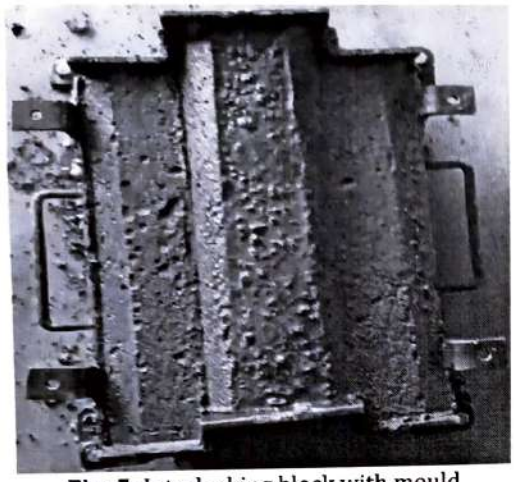


Fig -5: Interlocking block with mould



Fig -6: Interlocking blocks cast

4. TESTS AND RESULTS

4.1. Material Tests

Tests were conducted on the aggregates used and following results were obtained
Specific gravity of cement =2.92
Specific gravity of tile waste = 2.262
Specific gravity of Msand = 2.26
Normal consistency of cement = 33%
Fineness of cement = 4.6%
Sieve analysis of Msand and tile wastes were done

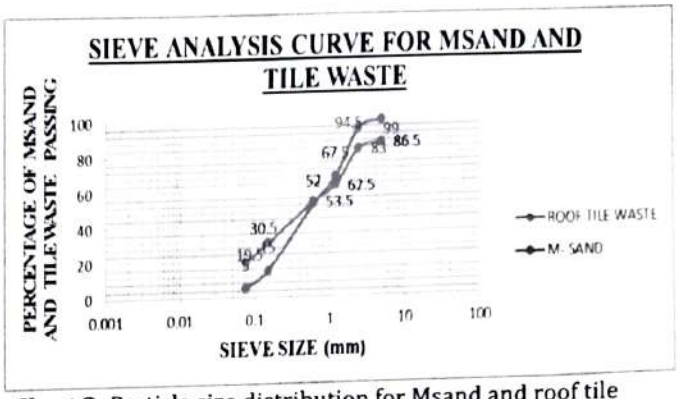


Chart 2: Particle size distribution for Msand and roof tile waste

4.2. Interlocking block tests

4.2.1. Water absorption

Table 1: Water absorption

WATER ABSORPTION		
	Wet mass (kg)	Dry mass (kg)
Specimen 1	18.820	18.500
Specimen 2	18.980	18.600
Concordant value	18.840	18.550

After 28 days continuous curing,

Water absorption = (18.84-18.55) / (18.55) x 100

=1.563.

It should not be more than 10 percent by mass.

10% by mass = 0.1 x 18.21 = 1.821; 1.563 < 1.821.

It was safe as per code IS 2185 (PART 1): 2005.

4.2.2. Compressive strength

Specimen shall be tested only after the curing period of 28 days. The bearing surface of the testing shall be wiped clean and any loose material removed from the surface. Place the specimen in the compressive testing machine and keep the steel plates on the top and bottom of the specimen. Fill the gaps the between the specimen and the steel plates using sand. The load shall be applied slowly without shock and increased continuously until the resistance of the specimen to the increased load breaks down and no greater load can be sustained. The maximum load applied to the specimen shall then be recorded.

Table 2: Compressive strength

COMPRESSIVE STERNGTH		
	Crack load (kN)	Collapse load (kN)
Specimen 1	195	350
Specimen 2	205	350
Concordant value	200	350

Crack load value=200 kN
Collapse load value=350 kN
Compressive strength of crack load =Load/Area
= $(200x10^3)/(660x10^2)$ = 3.03MPa
Compressive strength of collapse load =Load/Area
= $(350x10^3)/(660x10^2)$ = 5.30MPa

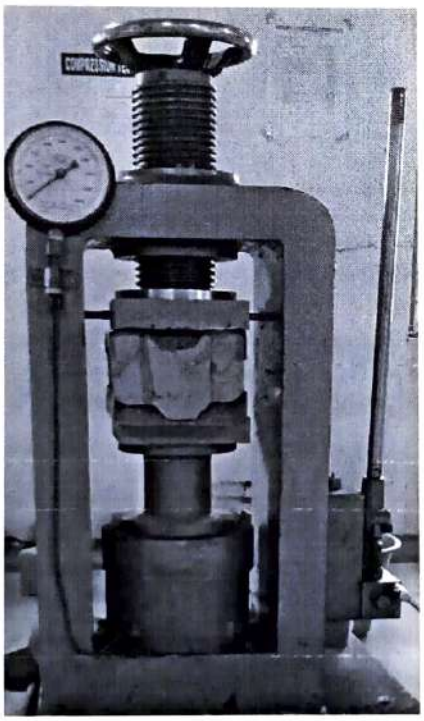


Fig-7: Compressive strength set up

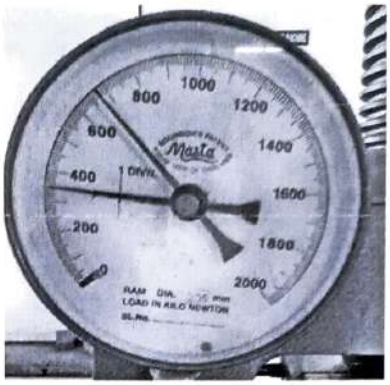


Fig-8: Compressive strength value

Compressive strength of solid block = 2.05MPa.
Therefore, when compared with solid block interlocking block is found to have greater compressive strength.

4.2.3. Block density

Table 3: Block density

BLOCK DENSITY		
	Mass (kg)	
	Before drying	After oven drying
Specimen 1	18.190	17.980
Specimen 2	18.230	17.960
Concordant value	18.210	17.980

Volume of the block=9900 cm^3
Density of block before drying = $(18.210/9900)x\ 10^6$ kg/m^3
$=1839\ kg/m^3$
Density of block after oven drying = $(17.980/9900)x\ 10^6$ kg/m^3 $=1816.1\ kg/m^3$
It was safe as per code IS 2185 (PART 1): 2005.

5. ESTIMATION

Comparison of cost estimation of Interlocking block with solid block

5.1. Cost Estimation of solid block ($1m^3$)

5.1.1. Cost of 100 blocks

Cost of cement = Rs 1788.8
Cost of Msand = Rs 536

Cost of coarse aggregate = Rs 2817.57
Total cost of solid block required for 1m³ wall = Rs 5142.434

5.1.2. Mortar

Cost of mortar = Rs 338.638 (including plastering charge of 60%)

5.1.3. Labour cost

10% of the total cost.
Therefore, Total cost = Rs 6029.22

5.2. Cost estimation of interlocking blocks (1m³)

5.2.1 .Cost of 100 blocks

Cost of cement = Rs 2400
Cost of M-Sand = Rs 384
Cost of coarse aggregate = Rs 2520
Total cost of solid block required for 1m3 wall = Rs 5304

5.2.2. Mortar

Cost of mortar = Rs 16
1.5% of the total cost for architectural works
Therefore, Total cost = Rs 5406.10

5.2.3. Labour cost

When 10% of the total cost is considered, total cost = Rs 5946.71.
Since the amount of mortar required for construction is less as well as the aligning of interlocking block requires only a fair time, it requires half of the labour cost when considered with solid block. Therefore, assuming labour cost as 5% of total cost.
Total cost = Rs 5676.405
Percentage of saving = 5.85%
Thus, it can make a large variation in the cost estimation of a building

6. CONCLUSIONS

Depending upon certain considerations, a suitable interlocking block has been designed. Interlocking blocks were cast successfully as per the code 2185:2005 (part 1) in the mould made of mild steel.
1. Optimum value of Msand by tile waste replacement was found as 20% through trials. Block density and water absorption tests were satisfactory.

2. Compressive strength of interlocking block was found greater than that of ordinary solid block of approximately same size and components. Compressive strength of interlocking block and solid block obtained were 5.45MPa and 2.05MPa respectively.

3. Comparison of cost analysis of interlocking block with solid block resulted in an economic construction. Rate of construction for 1m3 using solid block and interlocking block were obtained as Rs 6029.22 and Rs 5676.40 respectively.

4. Because of the pattern of interlock, it provides better matrix strengthening, wall stability, disallows movements and reduces mortar.

Therefore, the interlocking block masonry can be adopted as a suitable substitute for traditional masonry. And in conclusion, interlocking masonry can be recommended for housing projects as an alternative method that is cheaper than the conventional.

REFERENCES

[1] Abhinandan.R.Gupta and Deshmukh S.K, "Interlocking brick design- Paradigm for sustainable construction, IJRASET, Volume 03, Issue 01, 2015, pages 257-264.

[2] Ahmad Z, Othaman S.Z, Muhamed Yunus B, Mohamed A, "Behaviour of masonry wall constructed using interlocking soil cement bricks", International Journal for Civil, Environmental, Structural, Construction and Architectural Engineering, Volume 05, Number 02, 2011, pages 804-810. M. Young, The Technical Writer's Handbook. Mill Valley, CA: University Science, 1989.

[3] Bansal Deepak, "Sustainable dry interlocking block masonry construction", 15th International Brick and Block Masonry Conference, Brazil, 2012.

[4] Bhavani Shankar and Anusha, "Seismic analysis of interlocking block as infill wall", IRJET, Volume 03, Issue 10, 2016, pages 506-512.

[5] Chukwudi Onyeakpa and Lateef Onundi, "Improvement and the design of interlocking block sand its moulding machine", IOSR-JMCE, Volume 11, Issue 2, Version 3, 2014, pages 49-66.

[6] Edwards, M.Gayed.J, Pyra.M, Rodriguez.T, Department of Civil and Environmental Engineering, University of Alberta, 2010, pages 04-30.

[7] Praveen Kumar T and Vigneswar. R, Journal of Civil Engineering and Environmental Technology, Volume 01, Number 05, 2014, pages 114-118.

[8] Pruthvin C Shetty, Varun, Veda Kumar, Nikhil Shetty, Swetha B Poojary, "Study of strength properties using tile wastes in concrete", IJCRD, Volume 5, Issue 4, 2016, pages 659-662.

[9] Ramamurthy K and Anand.K.B, "Development and performance evaluation of interlocking block masonry", Journal of Architectural Engineering, Volume 6, 2000, pages 45-51.

[10] Sai Sarath M, Venkata Vikas.V, Sarath Chandra Kumar.B, "Sustainable construction using interlocking

bricks/blocks", IJAEM, Volume 02, Number 01, 2013, pages 06-10

[11] Sajad Ahmad, Sadam Hussain, Mohd Awais, Mohd Asif, Hakim Muzamil, Raffeq Ahmad, Shakeel Ahmad, "To study the behavior of masonry units/blocks", IOSRJEN, Volume 4, Issue 03, 2014, pages39-47.

[12] Wattle R.K.Deshmukh S.K, Gawatre D.W, "Performance of fly ash interlocking brick", IJCIET, Volume 04, Issue 04, 2013, pages 82-88.

[13] Wattle R.K, Deshmukh S.K, Mulay H.C, "Interlocking brick for sustainable housing development", IJSSBT, Volume 2, Number 02, 2014, pages 58-64.

[14] Yakubu S.O and Umar M.B, "Design, construction and testing of a multipurpose brick/block moulding machine", AJER, Volume 04, Issue 02, 2015, pages 33-43.

[15] Yomi Michael D and Adede Ji, "Sustainable housing provision: Preference for the use of interlocking masonry in housing delivery in Nigeria", Journal of Architectural Research, Volume 02, Issue 05, 2012, pages 81-86.

ResearchGate

See discussions, stats, and author profiles for this publication at: https://www.researchgate.net/publication/317258568

Ergonomic Building Design Consideration of an Earlylearning Centre

Article in International Journal of Engineering and Technology · May 2017

CITATIONS
0

READS
313

1 author:



Alwyn Varghese
Karunya University
4 PUBLICATIONS 1 CITATION

SEE PROFILE

Some of the authors of this publication are also working on these related projects:

Project fiber reinforced concrete View project

Project design aspects of buiding View project



All content following this page was uploaded by Alwyn Varghese on 31 May 2017.

International Research Journal of Engineering and Technology (IRJET) e-ISSN: 2395 -0056
Volume: 04 Issue: 05 | May -2017 www.irjet.net p-ISSN: 2395-0072

Ergonomic Building Design Consideration of an Earlylearning Centre

Prof. Alwyn Varghese, Aishwarya.N, Darsana.S, Deepthi C.P ,Nayana.N , Saranya.R

Dept. of Civil Engineering, Ahalia School of Engineering and Technology, Kerala, India

---

Abstract - *Children training through game playing are more effective than traditional academic methods. Therefore effective training can be one of the ways for improving the children's capabilities and development. The purpose of the project is to plan and design an 'Early learning centre' according to the standard parameters, which will end to more secure and safe doors, windows, playground, emergency consideration etc. are studied. This project is intended to provide a model in designing environment for kids. Various parameters such as floor area for indoor as well as outdoor activities, their shapes and position, natural and artificial lighting, door-ways and a child care following Indian standard which is functional in their design, cost effective to operate and environmentally safe and secure. Anthropometric measurements of children are also considered while planning the childcare as they are essential to ensure the safety and security and are crucial to the child's development and experience.*

***Key Words*: Early learning centre, Anthropometry, Parameters**

1. INTRODUCTION

Early education plays in improving a child's future academic performance, health and quality of life. The quality of this environment has a profound influence, especially given that many children spend close to half working hours in a childcare center. The 'Early learning center 'is a place where children experience the world and through which care givers and the community gave support.

Learning is an active process whereby the opportunity to explore and interact with the development. key components in a child's growth and sequence A child's growth follows a developmental environment are that is universal, but that within that sequence, each child proceeds at different rate and in unique ways.

Early childhood education or early learning centre is a branch of education theory which relates to the teaching of young children (formally and informally) up until the age of about eight. Infant/toddler education, a subset of early childhood education, denotes the education of children from age two to age four and half years.

Hence there is a need to provide stimulating and developmentally appropriate challenges for the individual child in a warm, secure, environment. The aim of the center is to provide consistent, high quality care to meet the needs of the active, continually developing child.

2. METHODOLOGY

When designing a space or product we must know the body dimensions of the prospective user. Reason for applying ergonomic design are that accidents, reduced productivity, ineffectiveness and user discomfort may arise from incorrect product dimension that do not match those of the user.

Anthropometric is a term used to describe the measurements of a user population for which the space is designed. Measurements are reported in terms of the range of body measurements of the particular population.

It is a well-known fact that there are serious ergonomic problem among the preschool children and toddlers of India. In fact proper design guideline for an early learning center does not exist in our country. The absence of reliable ergonomic and anthropometric data of school aged children, which measurements take in to account the application for which the children living and working spaces, furniture and equipment are designed as well as the dimensions of the children, can serve as the national in attentiveness to design principles of an ELC.

In light of these problems and in the absence of data, the following methodology was under taken to meet the urgent need for the design guideline of an ELC.

Firstly, it is need to be known who you are designing for. The group you are designing for is called user population. We consider 2.5, 3, 3.5,4 and 4.5 year old children as the user population. The anthropometric data of children of these age group were collected from Ahalia public school. The measurements of 14 anthropometric characteristics of children which constitute a set of basic data for the design of functional spaces and furniture were used. The children were made to be in sitting and standing positions to take both static as well as dynamic measurements. Next the optimum values of the furniture were calculated based on the anthropometric data previously acquired. In calculating the optimum dimensions, dynamic or static anthropometric measures, minimum and maximum values, and also the function of the furniture were taken in to considerations. All of the furniture was divided in to two groups according to reach and volumetric function based on the main criteria of anthropometric design. The different formulas for calculating the optimum values of different furniture is obtained as follows,

Maximum values were calculated for volume measurements.

Furniture dimension = X + (SD x Z)

Minimum values were calculated for reach measurements,

Furniture dimension= X - (SD x Z)

where, X is the mean and SD is the standard deviation of the anthropometric measurements of different age group children. Z is a constant value corresponding to 95 percentile confidence interval.

The next step of our project was to provide suggestions for the various parameters we identified through literature review. The parameters are

- Green building
- Space arrangements
- Openings
  - ✓ Doors
  - ✓ Windows
- Hard ware locations in doors
- Materials
  - ✓ doors and window materials
  - ✓ flooring materials
  - ✓ roofing materials
- finishes
  - ✓ ceiling finishes
  - ✓ wall finishes
  - ✓ floor finishes
  - ✓ skirting of tiles
- color
- fire protection, environmental and safety issues
- Child safety.

2.1DESIGN OF FURNITURES FOR ELC

The dimensions of the living and working space of buildings, the types of material and different riggings should be designed to conform to the user's anthropometric measures. Anthropometric measures are the most frequently used ergonomic data during the design process. In our project, anthropometric data is used in the design of children's equipment and furniture used in an Early Learning center. The anthropometric data of 2.5, 3, 3.5, 4, and 4.5 years old children were used for design.

The design features that play significant roles in the design of a final product are: aesthetics, economics, functionality and originality. The functionality of furniture is based on its comfort, safety and usefulness. And these qualities of comfort, safety, and usefulness are related to the anthropometric characteristics of the user and the suitability of materials used in furniture design.

2.2 METHOD USED

In order to calculate optimum furniture dimensions anthropometric measures were taken from a total of 55 children under age group of 2.5 years to 4.5 years were used. A total of 14 different measurements were made while the children were the in sitting and standing positions. In calculating the optimum dimensions of the furniture, dynamic or static anthropometric measures, minimum and maximum values, and also the function of the furniture were taken into consideration. All of the furniture was divided in to two groups according to reach and volumetric function based on the main criteria of anthropometric design.

The formula for calculating the optimum furniture dimension is a form of normal distribution in probability theory. The general equation for maximum and minimum is calculated.

Maximum values were calculated by: Furniture dimension = X + (SD x Z)

Minimum values were calculated by: Furniture dimension = X – (SD x Z)

Where X = Mean or Expectation of distribution

SD = Standard Deviation

Z = Constant corresponding to assumed confidence interval

Here we are taking the normal distribution with a confidence interval of 95% ,i.e., the chances of any error occurring in our design is limited to 5% and is verified too. Thus the value of Z is taken as 1.96.

Calculations of the depth, height and breadth of the furniture and equipment which are considered to be used rather frequently by children were done. Anthropometric data of children were used when calculating the measurements.

3. DESIGNS

3.1TABLE DESIGN

- Table depth (for one person) (max, value) = Forward elbow reach (X) + (SD x Z)

Table depth (for one person) (min, value) = Forward elbow reach (X) - (SD x Z)

- Table breadth/ width (max. value) = Buttock-knee depth (X) + (SD x Z)
- Table height (max. value) =0.41 x (total height (X) + (SD x Z))

NOTE: The minimum values are obtained by connecting the standard deviation by minus sign (-) instead of plus sign (+).

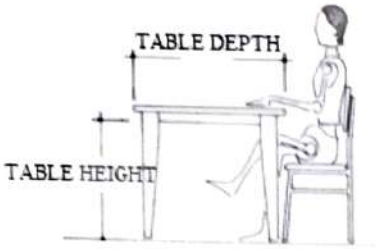


Fig 1: Table Depth and Table Height

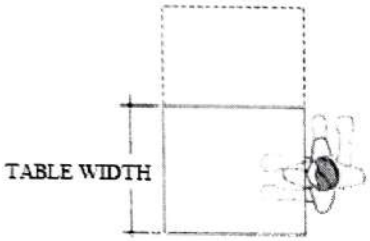


Fig 2: Table Width

Sample calculation (All dimensions are in cms)

Table height max value (age group 2.5 years) = 0.41 x (108.009 + (1.96 x 4.7)) = 48.060 cm

3.2 CHAIR DESIGN

- Chair depth (max. value) = 0.6666 x (Buttock-knee depth (X) + (SD x Z))
- Chair breadth/width (max. value) = Hip breadth (X) + (SD x Z)
- Chair height (max. value) = Sitting height (X) + SD x Z
- Seat rest height (max value) =0.75 x (upper part while sitting(X) + (SD x Z))
- Hand rest height (max value) =0.25 x (upper part while sitting(X) + (SD x Z))

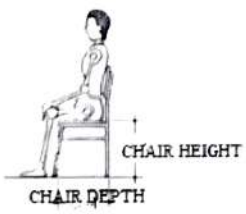


Fig 3: Chair Height and Chair Depth



Fig 4: Chair Width

Sample calculation

Chair height (max value) (age group 2.5 years) = (26.4+ (1.96 x 1.0274)) =28.413 cm

3.3 DESIGN OF BEDS AND BUNKS

- Bed breadth (max. value) = 2.5 x ((Buttock knee depth (X) + (SD x Z)) – (Hip width (X) + (SD x Z)))
- Bed length (max. value) = Stature (X) + (SD x Z) + (pillow)
- Bed height (min. value) = Sitting height (X) + (SD x Z)
- Bunk height (max. value) = (height of lower part while sitting (X) + (SD x Z)) + (height of upper part while sitting + (SD x Z))

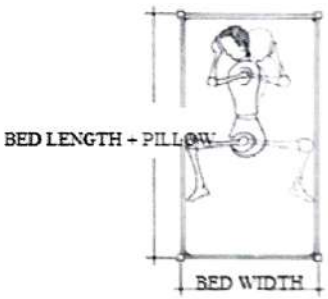


Fig 5: Bed Length and Bed Width

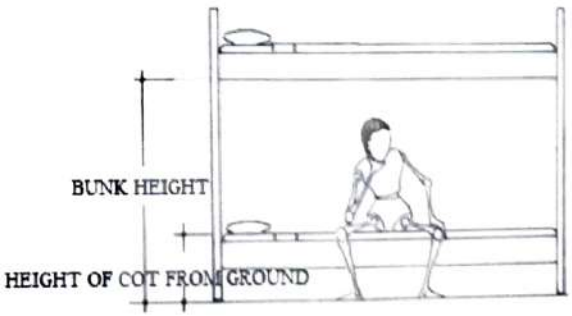


Fig 6: Height of Cot from Ground and Bunk Height

Sample calculation

Bed length (max value) for age group 2.5 years =108 + (1.96 x 4.7) = 117.2 cm

3.4 DESIGN OF TOILET ACCESSORIES

- Water Closet pan height (max. value) = Sitting height (X) + (SD x Z)
- Wash basin height (max value from ground) = height of leg while standing(X) + (SD x Z)
- Distance of person to tap(max value) = (Forward reach of arm(X) + (SD x Z))



Fig 7: Height of Water Closet

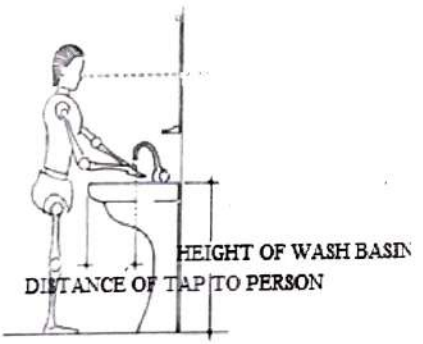


Fig 8: Wash Basin Details

Sample calculation

Water Closet pan height (max value) = 27.8727 + (1.96 x 1.89) = 31.577 cm

3.5 DESIGN OF CLASS ROOM UTILITIES

- Cupboard height/shelf height (max. value) = Eye height (X)+ (SD x Z))
- Switch height (max value from ground) = (0.75 x total height(X) + $\sqrt{2}$ forward reach of arm) + (1.96 x (1.75 x SD $_{\text{total height}}$ + $\sqrt{2}$ SD $_{\text{forward reach of arm}}$))
- Black board height (max value)= 0.44 x (Total Height (X) + (SD x Z))

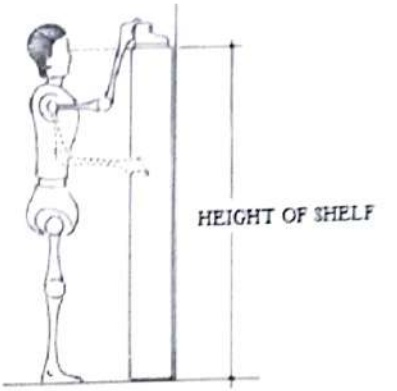


Fig 9: Height of Shelf

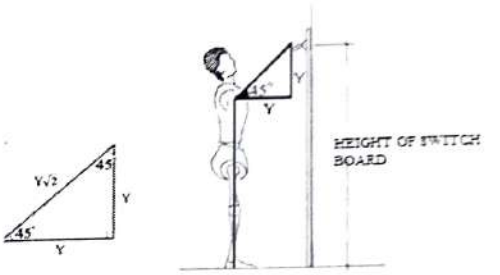


Fig 10: Height of Switch Boards

Sample calculation

Shelf Height (max value) = 93.1919 + (1.96 x 1.67) = 96.4641 cm

The measured anthropometric details along with their mean values standard deviation, error, margin of error, intervals are presented below along with all the maximum and minimum values of the design for age group.

4. RESULTS

The various furniture dimensions were calculated using the formulae mentioned earlier and a comparison between the existing range of furniture dimensions and the obtained value was made as shown in the table below.

Table 1: Comparison between Existing and Calculated Values

Parameter	Existing Value (Cm)	Calculated Value (Cm)
Table depth	20-40	23-36
Table width	25-35	28-39
Table height	40-48	34-48
Chair depth	15-20	19-26
Chair width	33-37	19-37

Chair height	24-28	24-32
Seat rest height	37-50	18-54
Hand rest height	5-20	6-18
Bed width	50-80	52-62
Bed length	80-120	83-112
Bunk height	-	49-104
Cot height from ground	20-30	24-73
Cupboard height	124-145	74-96
Switch height	75-90	95-153
Blackboard height	110-130	100-128
Water closet pan height	24-28	24-31
Wash basin height	45-52	56-62
Distance of tap from person	20-30	26-46

The minimum value of calculated furniture dimension corresponds to the age group of 2.5 and the maximum value corresponds to the age group of 4.5.

Here we see that there are variations in the existing values of furniture dimensions and the calculated values. These variations are mainly due to the fact that here, the furniture dimensions are calculated according to Indian Standards by considering the anthropometrics of the Indian children. So for the safety and comfort of the students in the Early Learning Centre, the furniture dimensions should be designed according to the calculated values.

5. CONCLUSIONS

The design guideline for an ELC has been prepared. By referring this guideline, a safe, efficient and child friendly ELC can be designed which is fully functional in design, cost effective to operate and environmentally safe and secure .

The design guidelines have been prepared based on the identified parameters from the literature studies of ELC of other countries.

The prepared guidelines are purely based on Indian Standards so that Indian children can use these living spaces, working spaces, furniture and other equipment in safe as well as comfortable manner. And hence, the center will provide consistent, high quality care to meet the needs of the active, continually developing child.

6. REFERENCES

[1] Child Care Centre Design Guide, U.S. General Services Administration, PBS-140- July 2003.

[2] Child Care Design and Technical Guideline, Prepared By: LGA Architectural Partners, 2016.

[3] Deped Educational Facilities Manual, Physical Facilities and Schools' Engineering Division Office of Planning Service Department of Education, Pasig City 2010.

[4] Design Ideas for Preschool Centres and Play Spaces, Hiroko Kishigami S. UNESCO, Bangkok, 1988.

[5] Design of Building- Green Building Concept by Ms. Anuja, Consultant, TSG.

[6] Green School, Resource Guide- Ontario, a Practical Resource for Planning and Building Green Schools in Ontario.

[7] Inclusion of Green Principles in the Design of Preschool Buildings, Aleksandra Kostic, Danica Stankovic, Milan Tanic University Of Nis, Serbia 2015.

[8] Onder Barli et al., "Anthropometric Evaluation of the Crèches Children Furniture in Turkey", Coll. Antropol.30 (2006) 4, pp. 853-865.

[9] Planning and Design Guidelines for Child Care Centres, Ministry Of Children and Youth Services, Ontario, 2006.

International Research Journal of Engineering and Technology (IRJET) e-ISSN: 2395 -0056
Volume: 04 Issue: 03 | Mar -2017 www.irjet.net p-ISSN: 2395-0072

Modified Drawer Compacted Sand Filter

Prof. Neethu John[1], Abhijith G[2], Ciji B[3], Haripriya M[4], Jivic J Panackal[5], Sijitha Sidhan[6]

[1]*Assistant Professor, Civil Engineering Dept. Ahalia School of Engineering And Technology, Palakkad, Kerala, India*
[2,3,4,5,6]*UG Student, Civil Engineering Dept. Ahalia School of Engineering And Technology, Palakkad, Kerala, India*

Abstract - *The Modified Drawer Compacted Sand Filter (MDCSF) is a modified design for a drawer compacted sand filter in which the sand layer, is broken down into several layers , each of which is 10 cm high and placed in a movable drawer separated by a 10 cm space. A lab-scale DCSF was designed and operated for 60 days fed by synthetic grey water. The response of drawer compacted sand filters and modified drawer compacted sand filter in terms of COD, BOD5, Hardness, turbidity and TDS reductions were evaluated. Each loading regime was applied for 30 days. Results showed that DCSF was able to remove > 91% of organic matter and Total Suspended Solids for all doses. Significant reduction in BOD5 (100%) and COD (95%) was noticed after water drained through the modified drawer compacted sand filter. This paper concludes that MDCSF would be appropriate for use in dense urban areas as its footprint is small and is appropriate for a wide range of users because of its convenience and low maintenance requirements.*

Key Words: Drawer compacted sand filter, grey water filter, synthetic grey water , Modified drawer compacted sand filter

1.INTRODUCTION

Water covers 70 percent of the globe's surface, but most is saltwater. Freshwater covers only 3 percent of the earth's surface and much of it lies frozen in the Antarctic and Greenland polar ice. Freshwater that is available for human consumption comes from rivers, lakes and underground sources and aquifers. Together these sources account for just one percent of all water on earth. The world's fresh water sources are threatened by climate change. Scientists around the world agree that recent climate changes occurring globally are the result of human activities. Rising global temperatures lead to heightened risk of more extreme and frequent floods and drought.

Water scarcity currently affects many region in the world. In water rich countries, urbanization and industrialization have frequently led to contaminated and deteriorated surface water and ground water such that these countries are unable to meet the ever increase water demand. The UN's climate change panel stated that the world's current population of about 6.6 billion is forecast to rise by 2.5 billion by 2050. As human population increases, the need for water also increases in domestic, agricultural, industrial and urban sectors. Consequently, water or 'blue gold' is widely predicted to be a critical resource. In 2009, the symposium on water security organized by the World Water Organization warned that two-third of the world's population will face water shortage by 2050.

2. MATERIALS

2.1Sand

In DCSF, sand was used as a major filtering medium. Sand could remove large extend of impurities from water. Each draws of DCSF was filled with different grades of sand. The purity of water increases with fineness of sand.



Fig 2.1: sand

2.2 Silver Coated Sand

Silver coated sand was obtained by treating sand with silver nitrate. It can remove micro-organisms from the impure water. The silver content present in purified water will resist the growth of unhealthy organisms. Hence it can be stored till further use.

Preparation:

1. 500gm of graded, washed and dried sand was mixed with 1gm silver nitrate and dissolved in 1lit of distilled water
2. Above ingredients are mixed thoroughly and allowed a maturing time of 1hr.
3. This mixture was then treated with 2gm of NaOH and dissolved in 50ml distilled water and mixed thoroughly

4. The sand was treated with 10ml of 1% NH_4OH solution and 15ml of reducing agent (9% of sugar solution) mixed thoroughly as before and left for 1hr.

5. The treated sand after solar drying was washed with distilled water to pH 7 and finally dried at 100-110 degree Celsius

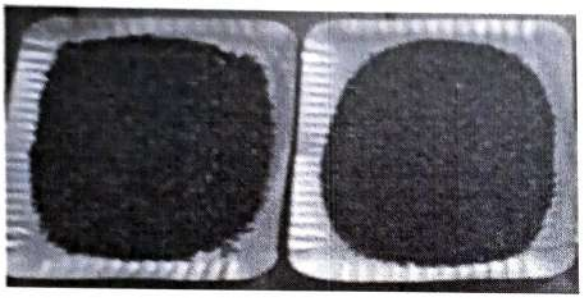


Fig 2.2: silver coated sand

2.3 Coconut Shell Activated Charcoal

Coconut shell was treated with NaCl to obtain coconut shell charcoal. It has high adsorption capacity. Hence it can purify water.

Preparation:

1. The activated carbon was produced by chemical activation of charcoal
2. NaCl was carbonized at a temperature of about 100°C
3. Then soak charcoal in NaCl.
4. After the production of charcoal, the materials were broken into smaller pieces (1-5mm in size).
5. Then the pieces were soaked in a 50% solution of NaCl for 24 hours.
6. After that it is allowed to dry in the sun or placed in an oven at 100°C



Fig 2.3: coconut shell activated charcoal

2.4 Charcoal

Charcoal is a porous material which can purify water. It is obtained by burning of wood. It is available in different grades in the market.



Fig 2.4: charcoal

3 METHODS

3.1 Synthetic waste water preparation

Synthetic grey water was prepared so that the DCSF could be tested and optimized using grey water of consistent quality. The synthetic grey water can be prepared by mixing 0.16g of dish washing solution, 0.16g hair shampoo (clinic plus brand), 0.16g washing powder, 0.1g of coconut oil, and 1 L of tap water. The synthetic grey water was prepared on daily basis and stored at room temperature.

3.2 Experimental setup

3.2.1 Drawer Compacted sand filter (DCSF) fabrication

A DCSF unit under laboratory conditions was constructed. A fabricated steel framework and six plastic drawers with dimensions of 50cm x 30cm x 10cm were obtained and placed on the frame. Each drawer except the lowest drawer (number 6) was perforated with holes. A distribution manifold was placed over the top drawer and it is connected to the storage tank which contains synthetic grey water, placed next to DCSF.

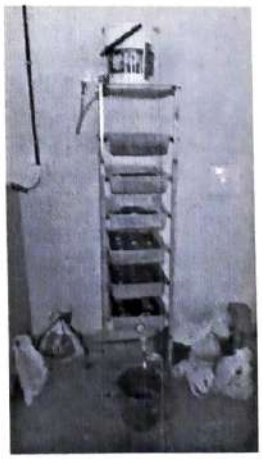


Fig 3: Model of DCSF

3.2.2 Design parameters of the laboratory DCSF

It is a Point of Use treatment unit and generally we use drawers of 1 m^2 area. For lab study here used the drawers of dimension 50 cm x 30cm x 10cm based on the availability.

Filter medium	
Drawer 1	Gravels; effective size 4.75 mm
Drawer 2	Silica; effective size 1.18 mm
Drawer 3	Silica; effective size 600micron
Drawer 4	Silica; effective size 75micron
Drawer 5	Silica; effective size 1.18mm and 600micron
Drawer 6	Granular activated carbon
Depth of media	10cm (for each drawer)
Perforation – for each drawer – except the lowest one	Orifice size=4mm Orifice spacing=10cm Number of orifices =15

Table 3.1: Design parameters

3.2.3 Operating conditions and procedures

Drawer compacted sand filter with uncoated sand were fed with synthetic grey water. They were operated under room temperature and after each treatment the effluent was tested for pH, COD, BOD, Hardness, turbidity and TDS. Same procedure is repeated by replacing 4th and 5th drawers by coconut shell activated carbon and silver coated sand.

3.2.4 Sample Collection and Storage

The synthetic waste water was prepared daily and was fed into the DCSF with and without silver coated sand. It was subjected to various operating conditions and after each treatment the effluent was collected in bottles and was tested for various parameters. The water was collected for three times at an interval of 5 days.

4. CONCLUSIONS

4.1 Results and Discussion

The performance of Drawer Compacted Sand Filter (DCSF) in the grey water treatment was studied and compared with DCSF with silver coated sand and the results of the study are reported as follows.

Parameter	Unit	Concentration
COD	mg/l	210
BOD	mg/l	18.2
pH	-	6.18
Turbidity	NTU	5
Hardness	mg/l	270
TDS	mg/l	535.73

Table 4.1: Characteristics of synthetic grey water

Parameter	Influent concentration	Effluent concentration	% Removal
COD (mg/l)	210	13.713	93.47
		13.42	93.61
		13.104	93.76
BOD_5 (mg/l)	18.2	1.08	94.065
		1.076	94.087
		1.07	94.120
Turbidity (NTU)	5	0.869	82.62
		0.411	91.78
		0.312	93.76
Hardness (mg/l)	270	164	39.25
		169	37.40
		160	40.74
TDS (mg/l)	535.73	443.76	17.16
		436.25	18.56
		435.25	18.755
pH	6.18	6.61	NA
		6.68	NA
		6.77	NA

Table 4.2: Experimental data of DCSF with uncoated sand

High removal efficiency can be seen in DCSF filter. Because, Drawer Compacted Sand Filter through dividing the sand depth into several layers and allowing air space between layers would ease the diffusion of oxygen between different layers so that the filter will function with fully aerobic conditions, thus enhancing the aerobic biological treatment of grey water and increase the treatment efficiency.

For the survival of the microorganisms within the biological zone, there needs to be a supply of oxygen. Oxygen is used in the metabolism of biodegradable components and the inactivation and consumption of pathogens. If it falls to zero during filtration anaerobic decomposition occurs, with consequent production of hydrogen sulphide, ammonia, and other taste- and odour-producing substances together with

dissolved iron and manganese, which make the treated water unsuitable for washing clothes.

Parameter	Influent concentration	Effluent concentration	% Removal
COD (mg/l)	210	10.2	95.14
		10.1	95.19
		9.8	95.23
BOD_5 (mg/l)	18.2	0	100
		0	100
		0	100
Turbidity (NTU)	5	0.513	89.74
		0.411	91.78
		0.312	93.76
Hardness (mg/l)	270	155	42.59
		150	44.44
		148	45.18
TDS (mg/l)	535.73	282.32	47.30
		276.54	48.38
		270.32	49.54
pH	6.18	6.61	NA
		6.68	NA
		6.77	NA

Table 3.2: Experimental data of the DCSF with silver coated sand

From the above analysis, it was found that MDCSF gives highest removal percentage in maximum number of parameters. The percentage removal of COD, BOD_5, turbidity, hardness and TDS are 95.18, 100, 91.76, 44.07 and 78.40 respectively.

COD removal is slightly increased in the case of silver coated sand. COD removal with uncoated sand is 93.61% and with the coated sand is 95.18%. It is due to the silver leaching in the effluent water.

BOD is one among the most important parameters for the design and operation of sewage treatment plants. BOD removal is increased in DCSF with silver coated sand. BOD removal with uncoated sand is 94.09% whereas with coated sand it is 100%. This is due to the activity of silver along with the microorganisms present in the sand. This result shows generally settable BOD may be removed by physical mechanisms of sedimentation and filtration.

Turbidity in water caused by suspended solid such as clay, finely divided organic and inorganic matter, plankton and other microscopic organism. Total suspended solids include all particles suspended in water that may pass through a filter. Higher turbidity removal efficiency is obtained for silver coated sand as some of the suspended solids are also removed as BOD. Turbidity removal with uncoated sand is 89.34% whereas with coated sand it is 91.76%

TDS removal is increased in the DCSF with silver coated sand. The increase in TDS is due to silver leaching.

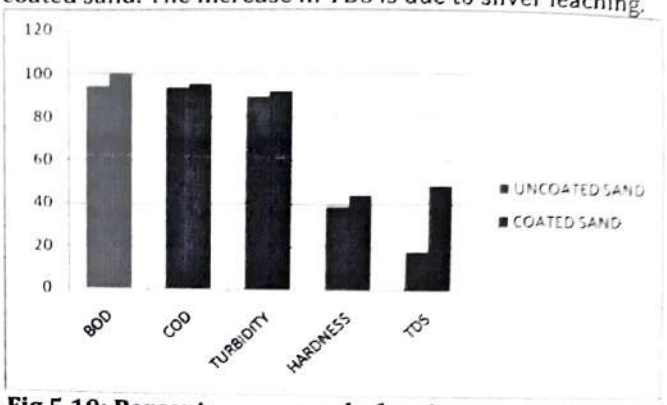


Fig 5.10: Percentage removal of various parameters in DCSF with coated and uncoated sand

Parameter	Unit	Influent concentration	Effluent concentration (uncoated sand)	Effluent concentration (coated sand)
COD	mg/l	210	13.412	10.03
BOD	mg/l	18.2	1.075	0
Turbidity	NTU	5	.530	.412
Hardness	mg/l	270	164.33	151
TDS	mg/l	535.73	438.42	276.39

Table 5.6: Comparison of effluent concentrations of different parameters in DCSF with uncoated sand and coated sand

The results revealed that MDCSF has achieved high performance in the removal of BOD_5, COD. The efficiency of BOD_5 removal ranged 100% and for COD 95-96%. The efficiency of TDS removal ranged 77-79% and for total hardness 42-45%. Finally we have concluded that, Modified drawer compacted sand filter is more efficient in removal of BOD by 6% and COD removal by 0.23%.In the case of hardness there is an improvement of 12% and an increase of 20% removal for total dissolved solids.

ACKNOWLEDGEMENT

At the foremost we would like to the almighty his blessings on us for accomplish this project work up to this. We would like to express our sincere thanks to our Principal Dr. Vishnu Ram for providing the facilities within the college our sincere thanks to our HOD Dr. Jino John for the support and suggestions to our project work we express our deepest, heartiest and sincere thanks to our coordinator Asst.Prof. Alwyn Varghese who has been spark for enlightening our knowledge, continuous support and suggestions we express our deep sense of gratitude and sincere thanks to our project

guide **Asst.Prof.Neethu** John for her support, valuable guidance and encouragement throughout the project work we convey our inmost gratitude to our staff members for their competent support in work

REFERENCES

1. Ababu T. Tirunch, Amos O. Fadiran, William N. Ndlela, Jonna Heikkila. Assessment of technical and economic feasibility of activated charcoal removal of organic matter from different streams of grey water through study of adsorption isotherms. 2016.
2. Abeer Albalawneh, Tsun-Kuo Chang. Review of the grey water and proposed grey water recycling scheme for agricultural irrigation reuses. 2015.
3. Almoayied Assayed, Jonathan Chenoweth, Steven Pedley. Assessing the efficiency of an innovative method for onsite grey water treatment: Drawer compacted sand filter –A case study in Jordan.2015.
4. Almoyied Assayed, Jonathan Chenoweth, Steven Pedley. Drawer compacted sand filter: a new and innovative method for on-site grey water treatment. 2014.
5. Ami Cobb, Mikell Warms, Dr. Edwin P Maurer, Dr. Steven Chiesa. Low-Tech Coconut Shell Activated Charcoal Production.2012.
6. Cecilia Rolence, Revocatus Lazaro Machunda, Karoli Nicholas Njau. Water hardness removal by coconut shell activated carbon. 2014.
7. Dr. Pankaj Singh, Saurabh Kumar Singh, Shilpi Singh, Pratibha Sharma. Domestic Wash Water Treatment Using Fly Ash Alone and in Combined Form. 2014.
8. Dr. Suhas V Patil, Suryakant C Nawle, Sunil J Kulkarni. Industrial Applications of Fly ash: A Review.2013.
9. Farhana M, Meera V. synthesis of nanosilver coated sand using plant extracts. 2015.
10. Fbr- Information Sheet. Greywater Recycling: planning fundamentals and operation information. 2005.
11. I. I. Nwajuaku, O. E. Ekenta, A. I. Nwajuaku. Treatment of Grey water for Non-Potable Applications. 2015.
12. K.S. Beenakumari. Removal of iron from water using modified coconut shell charcoal as adsorbent. 2009.
13. Larous S, Meniai A. The use of sawdust as by product adsorbent of organic pollutant from wastewater: adsorption of phenol. 2012
14. Mohammed Arifur Rahman, Shamim Ahsan, Satoshi Kaneco, Hideyuki Katsumata, Tohru Suzuki, Kiohisa Ohta. Waste water treatment with multi layer media of waste and natural indigenous materials. 2004.
15. Shamim Ahsan, Satoshi Kaneco, Kiyohisa Ohta, Takayuki Mizuno and Keiko Kani. Use of some natural and waste materials for waste water treatment. 2001.

Multiport Multiband Chassis-Mode Antenna Design Using Characteristic Modes

Krishna Kumar Kishor, *Student Member, IEEE*, and Sean Victor Hum, *Senior Member, IEEE*

Abstract—**Multiport antenna architectures that are well isolated, both within and across multiple frequency bands, not only support multiple technologies such as multiple-input–multiple-output and carrier aggregation, but also ease the design of the RF front end. In this letter, the theory of characteristic modes (TCM) is applied in a systematic manner to isolate the ports operating in the same frequency band and in different frequency bands, the latter of which is a new application of TCM. Moreover, by quantifying the amount of isolation between the multiple ports via the electromagnetic isolation method, the use of TCM as a decoupling tool for multiple antenna systems is verified. A four-port chassis-mode antenna is presented that features high levels of interband and intraband decoupling in three bands, two of which are below 1 GHz. The antenna is experimentally verified, and the measured port parameters and radiation patterns are found to match well with simulations.**

Index Terms—**Characteristic modes, handset antennas, multiple-input–multiple-output (MIMO) systems, mobile antennas, multiple-band antennas.**

I. Introduction

ONE of the main challenges with designing antennas for today's smartphones is the increasing number of frequency bands that the device must support. There is limited space available, and accommodating the increasing number of antennas is challenging. Utilizing multiband and wideband designs [1] can potentially alleviate this, but supporting future standards such as LTE-A which incorporate multiple-input–multiple-output (MIMO), as well as interband and intraband carrier aggregation (CA), adds additional challenges in coordinating the design of such antennas with the RF front end. The use of both multiport and multiple antennas operating at different frequencies to interface with the RF front end has been shown to offer several design benefits when compared to the use of a single wideband antenna [2]. These include the elimination of hard-wired matching between the duplexers of the different frequency bands, improved modularity of the front end for reuse in different geographical regions, simpler antenna switch control, and elimination of the frequency diplexers in the RF chain.

The use of a multiport antenna architecture requires that the feed ports be isolated from each other in the different frequency bands of operation. This prevents the radio systems that are connected to these ports from loading each other, reduces interference, and also allows each system to be tuned independently from the others. The most obvious way to achieve the isolation between the different frequency bands is to use large, high-Q microwave components with sharp filtering characteristics. On a mobile platform, this imposes stringent requirements on the front end, and hence it is desirable to introduce some additional isolation or frequency selectivity within the antenna and its feed system to reduce the burden on these components. This letter explores the design of multiport antennas designed with high interport isolation through the use of the theory of characteristic modes (TCM) [3]. TCM has been demonstrated as a powerful tool for decoupling antenna ports operating in the same frequency band for MIMO applications [4]–[6] and to design multiband antennas [7]. This letter further extends the capability of TCM by applying it for the first time to a multiport multifrequency problem, thus enabling both low intraband and interband coupling, and the operation in low-frequency bands. While three bands are considered to demonstrate the principle, the idea can be extended to include additional bands as required.

II. Design Overview and Principles

The TCM formulation for perfect electric conductors as proposed by Harrington and Mautz allows the eigencurrents on the surface of the conducting body as well as their corresponding eigenfields in the far field to be determined [3]. For this letter, the principal advantage of employing TCM is capitalizing on the orthogonal nature of the characteristic modes, which allows MIMO antennas to be designed with low correlation between the excited port patterns, with low corresponding coupling between ports at the design frequency, and a further extension of the orthogonality of the current distributions *between frequencies*, allowing for low interband coupling between the antenna ports. The latter feature is very useful in alleviating filter requirements between bands when using multiband antennas with technologies such as CA, and is a new application of TCM proposed here.

The proposed antenna is a four-port antenna supporting both *in-band decoupling* between two ports (for MIMO) and *interband decoupling* between the other two ports (for CA). Specifically, ports 1 and 2 operate in two low-frequency bands below 1 GHz and potentially support interband CA. As an example, we design port 1 for coverage in LTE band 14 (758–798 MHz) and port 2 for coverage in band 5 (824–894 MHz). High electromagnetic isolation between ports 1 and 2 is sought within each band using the proposed technique since these two bands are very close in frequency. Meanwhile, ports 3 and 4 provide MIMO

Manuscript received October 19, 2015; revised May 27, 2016 and June 30, 2016; accepted July 22, 2016. Date of publication July 27, 2016; date of current version March 20, 2017.

The authors are with the Edward S. Rogers Sr. Department of Electrical and Computer Engineering, University of Toronto, Toronto, ON M5S 3G4, Canada (e-mail: krishna.kishor@mail.utoronto.ca; sean.hum@utoronto.ca).

Color versions of one or more of the figures in this letter are available online at http://ieeexplore.ieee.org.

Digital Object Identifier 10.1109/LAWP.2016.2594093

1536-1225 © 2016 IEEE. Personal use is permitted, but republication/redistribution requires IEEE permission.
See http://www.ieee.org/publications_standards/publications/rights/index.html for more information.

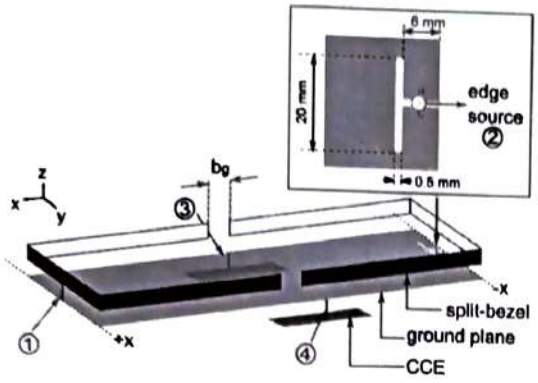


Fig. 1. Three-dimensional view of the proposed four-port antenna.

TABLE I
CHARACTERISTIC MODES UTILIZED IN THE FOUR-PORT ANTENNA

f_0 (MHz)	Mode	λ_n	f_0 (MHz)	Mode	λ_n
780	a	−0.74	1960	d	−5.27
881	b	−2.76	1960	e	−1.80
881	c	3.09	1960	f	2.83
			1960	g	3.90

operation in LTE band 2 (1850–1990 MHz). High electromagnetic isolation is sought between these two ports within this band to achieve the low envelope correlation that is essential for MIMO. Decoupling other port combinations was not deemed a requirement since they are widely spaced in frequency, and therefore isolation can be more readily facilitated using standard filter components.

The antenna design is shown in Fig. 1. The chassis used is a 110-mm × 60-mm rectangular conductor. The isolation between ports 1 and 2 is achieved by introducing a pair of split-bezels above the chassis that circumscribe the chassis footprint. The split-bezels are separated by a gap $b_y = 2$ mm. The width of the split-bezel is 3 mm, and this is placed 2 mm above the ground plane. The location of the four ports is also indicated in Fig. 1. Port 1 connects the ground plane to one of the split-bezels. It is modeled using a feeding strip of 1 mm width. Port 2 is modeled as an inductive coupling element (ICE) [8] and is located along the short edge of the chassis. It consists of a T-shaped slot in the ground plane, with an edge source between the two parts of the ground plane. Ports 3 and 4 are located on 1-mm-wide feeding strips that connect 40-mm × 6-mm capacitive coupling elements (CCEs) to the ground plane along long edges of the chassis. The CCEs are placed 6 mm below the ground plane.

The main challenge in designing chassis-based antennas below 1 GHz is the lack of availability of resonant CMs. TCM allows for the identification of new useful modes below 1 GHz when additional structures are added to the chassis [9], [10]. In this design, a pair of split-bezels (with one of the split-bezels connected to the chassis) is introduced as a new way to create an additional resonance below 1 GHz. The eigenvalues of the entire structure, including exciters, were determined using an in-house method of moments (MoM) code in a 0.7–2.1 GHz frequency range, and evaluated at the frequencies as shown in Table I. Three modes, enumerated a, b, and c, pass through resonance below 1 GHz. By utilizing these three modes, the split-bezel

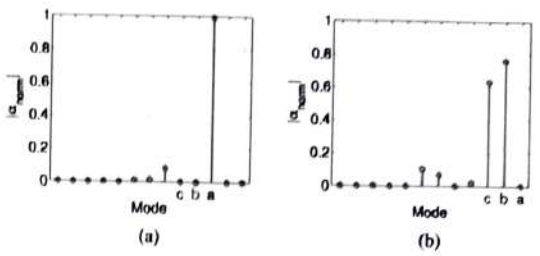


Fig. 2. Magnitude of the normalized modal weighting coefficients versus mode index: (a) port 1 at 780 MHz and (b) port 2 at 881 MHz.

is capable of operation in two frequency bands below 1 GHz. Modes d–g are close to resonance in the high band and are utilized for MIMO operation.

At 780 MHz, there is only one mode close to resonance (a). The current distribution of this mode resembles the dominant half-wave chassis-mode distribution along x. Since this mode has a current maximum at the location of the connection point between the half-bezel and the chassis, this is a good location for port 1 to excite this mode. A plot of the modal excitation coefficients $|\alpha_{\text{norm},i}|$ in Fig. 2(a) confirms the dominant excitation of mode a by port 1. Modal currents have been normalized so that the total radiated power is 1 W [3].

At 881 MHz, there are three modes close to resonance. These include modes b, c, and an unused mode not shown in Table I. Mode b is identified as the bezel mode that has a full-wave distribution along the bezel with a null at the location of the gaps, while mode c is identified as the inductive mode of the chassis that has a loop of current circulating around the edges of the chassis. Both these modes have a current maximum along the short edge of the chassis at the $-x$ boundary. Hence, the placement of an ICE here (port 2) leads to the dominant excitation of these two modes, as confirmed in Fig. 2(b). Fig. 2(a) and (b) illustrates that the set of CMs excited by each port are nonoverlapping, and hence high levels of decoupling are expected between these ports.

In the next band around 1960 MHz, ports 3 and 4 are used for two-port MIMO communication. The locations of these two ports were inspired from an earlier two-port MIMO antenna [5]. In that design, it was seen that both the ports excited the same set of two CMs with an appropriate phase difference to achieve a low correlation between the signals received at the ports. The same idea can be extended to the present design that involves four CMs, which in this case are higher-order modes of the structure. By appropriately choosing the CCE dimensions, this set of modes can approximately satisfy the following ideal conditions for zero correlation between port excitations: $\alpha'_d = \alpha_d, \alpha'_e = \alpha_e\, e^{-j\pi}, |\alpha_d| = |\alpha_e|, \alpha_f = x\angle\theta, \alpha'_f = y\angle\theta, \alpha_g = y\angle\phi, \alpha'_g = x\angle(\phi - \pi)$, where α_n and α'_n denote the modal weighting coefficients of the nth characteristic mode when ports 3 and 4 are excited, respectively, and $x, y, \theta, \phi \in \mathbb{R}$. The resulting envelope correlation coefficient (ECC) at 1960 MHz is calculated to be 0.0031, thus achieving the MIMO operation in this band.

We observed that the resonances of modes a, b, and c shift to higher frequencies with increasing bezel gaps b_y. This provides a degree of freedom that can be potentially used when designing antennas for a specific band of interest. The resonant frequencies

TABLE II
ELECTROMAGNETIC PORT ISOLATION (IN dB)

f_0 (MHz)	Excited port i	$\lvert S_{1i}\rvert$	$\lvert S_{2i}\rvert$	$\lvert S_{3i}\rvert$	$\lvert S_{4i}\rvert$
780	1	–	62.7	4.83	4.83
881	2	51.5	–	5.90	5.83
1960	3	7.87	11.1	–	18.7
	4	7.90	11.1	18.7	–

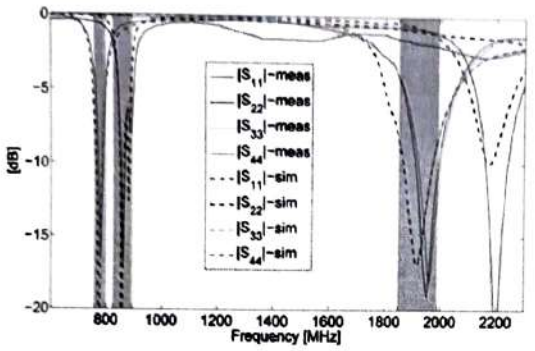


Fig. 3. Simulated and measured input reflection coefficients.

of modes b and c also get closer to each other, and in this design, this is used to increase the bandwidth associated with port 2 in the experimental prototype.

To determine the intrinsic isolation between ports across different frequency bands, the concept of electromagnetic isolation is utilized. While analytical solutions are feasible for two-port systems [11], for multiport systems this is challenging. Hence, in the proposed four-port design, the four reference impedances are solved for numerically (in MATLAB using fsolve), by setting the diagonal elements of the matrix $(Z - Z_R^*)(Z + Z_R)^{-1}$ to zero. The isolation between the different ports are then given by the S_{ij} terms of the scattering matrix, which is calculated using

$$S = F(Z - Z_R^*)(Z + Z_R)^{-1}F^{-1} \tag{1}$$

where Z is the Z-parameter matrix, Z_R is the diagonal matrix with the reference impedance ($Z_{R,i}$) on the diagonal, and F is the diagonal matrix with entries $1/(2\sqrt{\mathrm{Re}(Z_{R,i})})$.

At each design frequency (f_0), a 4×4 scattering matrix is obtained using (1). The diagonal elements of this matrix are zero, and only the coupling terms between the excited port i at f_0 and the three coupled ports are of interest. The remaining coupling terms are irrelevant from a practical point of view, as these ports do not operate at the design frequency.

Table II summarizes the electromagnetic isolation achieved between the four ports at the three design frequencies. The isolation goals set out earlier have clearly been met. At 780 and 881 MHz, it is clear that ports 1 and 2 are well isolated from each other. This is particularly useful because these two ports operate in very close frequency bands, and consequently, one does not have to rely on a high-Q match or filter to achieve the isolation between the antenna ports. At 1960 MHz, the MIMO ports 3 and 4 are also well isolated from each other, as is evident by the 18.7 dB of isolation between them. The remaining port

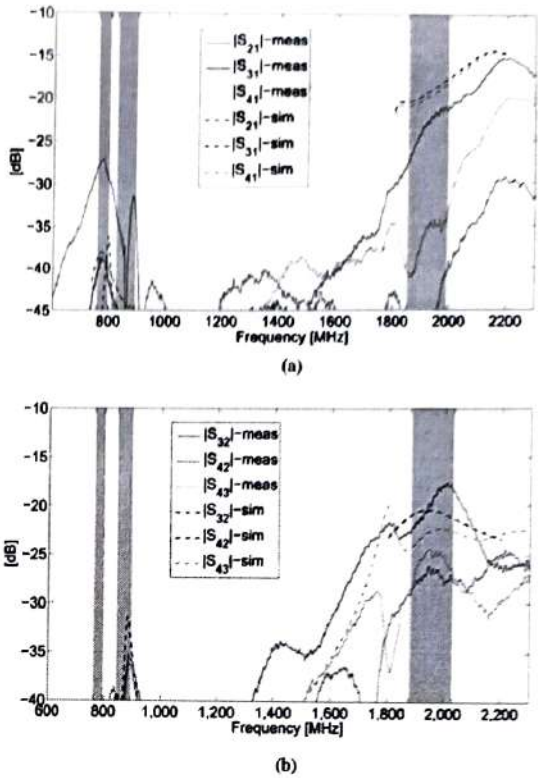


Fig. 4. Measured mutual-coupling terms associated with ports 1–4: (a) port 1 excitation and (b) ports 2 and 3 excitation.

combinations have relative low isolation, which is expected as these ports were not explicitly decoupled in the design process.

III. RESULTS

The design was first simulated in Ansoft HFSS along with a suitably designed L-match matching network at each port. An FR4 substrate with $\epsilon_r = 4.4$, loss tangent 0.02, and dimensions 110 mm × 60 mm × 0.8 mm was chosen for this design. The ground plane is located on the top part of the substrate, while the feed ports and the matching networks are located on the bottom. The gap between the two split-bezels has been changed to $b_g = 13$ mm to retune the structure to operate in the desired bands of interest. The split-bezels and the CCEs were manufactured by using 16 mil tin-plated steel to lower the cost of fabrication, and supported by 6.35-mm nylon spacers.

In Fig. 3, the measured and simulated input reflection coefficients from ports 1–4 are plotted. There is a moderate correlation between the measured and simulated data. Fig. 4 shows the unique mutual coupling terms associated with ports 1–4. For clarity, the simulation results have been plotted only near the frequency bands of interest. Overall, the measured data corresponds well with simulations. Fig. 4(a) shows the mutual coupling terms in the three frequency bands when port 1 is excited. As expected, ports 1 and 2 are very well isolated (> 20 dB) from each other in the two low bands. Fig. 4(b) plots the mutual coupling terms associated with exciting port 2 and demonstrates

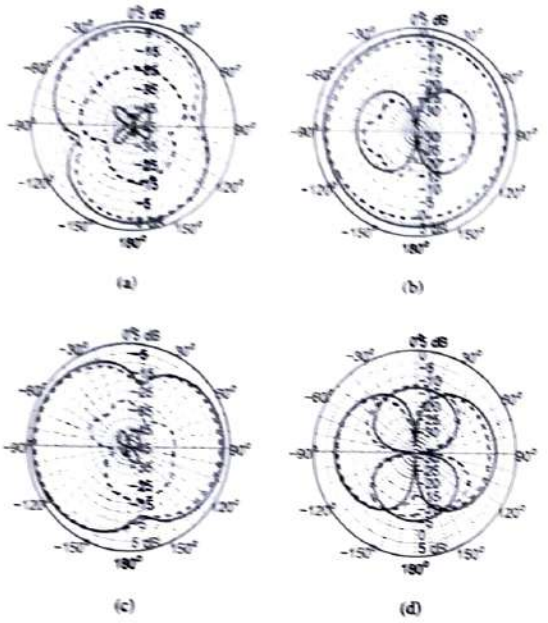


Fig. 5. Gain patterns of port 1 at 0.78 GHz and port 2 at 0.86 GHz: _ HFSS G_θ; _ HFSS G_ϕ; _ _ _ Meas G_θ; and _ _ _ Meas G_ϕ. (a) Port 1 zx-plane. (b) Port 1 yz-plane. (c) Port 2 zx-plane. (d) Port 2 yz-plane.

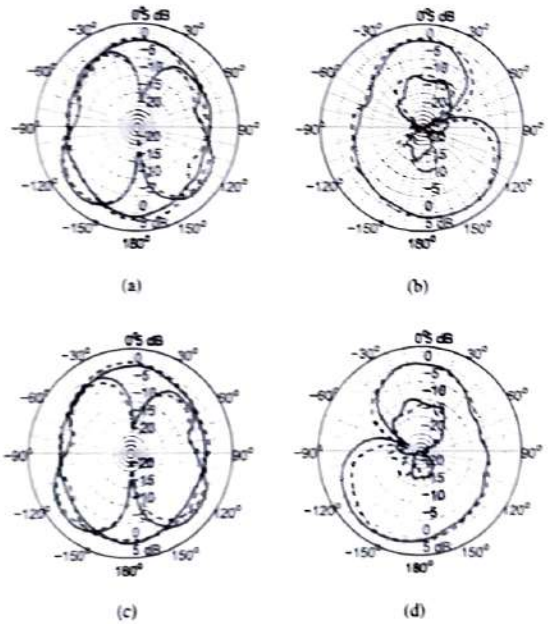


Fig. 6. Gain patterns of ports 3 and 4 at 1.95 GHz. _ HFSS G_ϕ; _ HFSS G_θ; _ _ _ Meas G_ϕ; and _ _ _ Meas G_θ. (a) Port 3 zx-plane. (b) Port 3 yz-plane. (c) Port 4 zx-plane. (d) Port 4 yz-plane.

more than 20-dB isolation is measured between ports 3 and 4 in the high band.

The radiation patterns were measured and are plotted in Figs. 5 and 6. Overall, a good match is seen between the measured and simulated radiation patterns, confirming the excitations produce the expected mixture of modes. The simulated gains from the four ports at their respective frequency of operation are 2.1, 2.2, 3.3, and 3.2 dBi. From the simulated patterns, the ECC at 1960 MHz between ports 3 and 4 is 3.54×10^{-4}, assuming a uniform angle of arrival and a cross-polarization ratio of 1. The measured ECC was 0.0889. Finally, the measured radiation efficiencies from the four ports using a Wheeler cap are 63.4% at 770 MHz, 41.8% at 858 MHz, and 80.2% and 78.6% at 1950 MHz. The simulated radiation efficiencies from the four ports are 92.6%, 71.6%, 97.3%, and 97.3%. Potential reasons for the lower-than-expected values are the ohmic losses in the steel exciters and loss in the matching networks.

IV. Conclusion

This letter has demonstrated a new application of CM theory in decoupling multiple ports of an antenna operating in three bands. A four-port antenna design was presented with high levels of intrinsic intra- and interband isolation between ports, making it useful for MIMO and CA applications. The operation below 1 GHz in two frequency bands was possible due to the introduction of the split-bezel, which allows for an additional resonant CM below 1 GHz. Using CMs to isolate ports that operate in nearby frequency bands is particularly useful, as this allows for less stringent requirements on the frequency characteristics of the microwave components in the RF front end. A future paper will consider reduction in the profile of the design by using CCEs on the same side of the bezel, and ways to increase the bandwidth and number of bands supported by the antenna.

References

[1] R. Valkonen, M. Kaltiokallio, and C. Icheln, "Capacitive coupling element antennas for multi-standard mobile handsets," *IEEE Trans. Antennas Propag.*, vol. 61, no. 5, pp. 2783–2791, May 2013.

[2] P. Ikonen, J. Ella, E. Schmidhammer, P. Tikka, P. Ramachandran, and P. Annamaa, "Multi-feed RF front-ends and cellular antennas for next generation smart phones," Pulse Electronics Corporation, Technical article, 2011.

[3] R. Harrington and J. Mautz, "Theory of characteristic modes for conducting bodies," *IEEE Trans. Antennas Propag.*, vol. AP-19, no. 5, pp. 622–628, Sep. 1971.

[4] R. Martens, J. Holopainen, E. Safin, J. Ilvonen, and D. Manteuffel, "Optimal dual-antenna design in a small terminal multiantenna system," *IEEE Antennas Wireless Propag. Lett.*, vol. 12, pp. 1700–1703, 2013.

[5] K. K. Kishor and S. V. Hum, "A two-port chassis-mode MIMO antenna," *IEEE Antennas Wireless Propag. Lett.*, vol. 12, pp. 690–693, 2013.

[6] H. Li, Z. Miers, and B. K. Lau, "Design of orthogonal MIMO handset antennas based on characteristic mode manipulation at frequency bands below 1 GHz," *IEEE Trans. Antennas Propag.*, vol. 62, no. 5, pp. 2756–2766, May 2014.

[7] Z. Miers, H. Li, and B. K. Lau, "Design of bandwidth enhanced and multiband MIMO antennas using characteristic modes," *IEEE Antennas Wireless Propag. Lett.*, vol. 12, pp. 1696–1699, 2013.

[8] R. Martens, E. Safin, and D. Manteuffel, "Selective excitation of characteristic modes on small antennas," in *Proc. Eur. Conf. Antennas Propag.*, Apr. 2011, pp. 2639–2643.

[9] J. Anguera, A. Andújar, and C. Puente, "A mechanism to electrically enlarge the ground plane of handset antennas: A bandwidth enhancement technique," *Microw. Opt. Technol. Lett.*, vol. 53, no. 7, pp. 1512–1517, Jul. 2011.

[10] H. Li, Z. Miers, and B. K. Lau, "Generating multiple characteristic modes below 1 GHz in small terminals for MIMO antenna design," in *Proc. IEEE Antennas Propag. Soc. Int. Symp.*, Jul. 2013, pp. 180–181.

[11] J. Rahola and J. Ollikainen, "Analysis of isolation of two-port antenna systems using simultaneous matching," in *Proc. Eur. Conf. Antennas Propag.*, Apr. 2007, pp. 1–5.

Scientific Research Publishing

Circuits and Systems, 2016, 7, 3448-3455
http://www.scirp.org/journal/cs
ISSN Online: 2153-1293
ISSN Print: 2153-1285

Performance Analysis of Double Boost Converter Powered FSTPI Fed Induction Motor

S. Saravanasundaram[1], S. Muthukrishnan[2], G. Murugananth[3]

[1]Department of Electrical and Electronics Engineering, Hindusthan College of Engineering and Technology, Coimbatore, India
[2]Department of Electronics and Communication Engineering, Sri Eshwar College of Engineering, Coimbatore, India
[3]Department of Electrical and Electronics Engineering, Ahalia School of Engineering and Technology, Palakkad, India
Email: ss.itdept10@gmail.com, samkumar04@rediffmail.com, gmuruganath@gmail.com

How to cite this paper: Saravanasundaram, S., Muthukrishnan, S. and Murugananth, G. (2016) Performance Analysis of Double Boost Converter Powered FSTPI Fed Induction Motor. *Circuits and Systems*, 7, 3448-3455.
http://dx.doi.org/10.4236/cs.2016.711293

Received: April 3, 2016
Accepted: May 1, 2016
Published: September 6, 2016

Copyright © 2016 by authors and Scientific Research Publishing Inc.
This work is licensed under the Creative Commons Attribution International License (CC BY 4.0).
http://creativecommons.org/licenses/by/4.0/

Open Access

Abstract

Pulse Width Modulated (PWM) inverter-fed induction motor drives are most common in industrial applications. This paper aims at development of double boost converter for PWM inverter-fed three-phase induction motor. The inverter topology is designed with four switches. The proposed drive system has been simulated using Matlab/Simulink and the performance of has been assessed in terms of output voltage, output current, power factor and THD. From the simulation results, it is evident that the three-phase voltage waveforms of the proposed system are less distorted, with their currents being more sinusoidal. A comparative analysis has been made with the conventional six-switch inverter fed drive. The proposed system offered a THD of 1.84%, whereas for the conventional system it was 13.96%. These results inferred that the proposed double boost converter with four-switch based drive scheme exhibits superior performance.

Keywords

FSTPI, Induction Motor, Harmonics, SSTPI, THD

1. Introduction

Three-phase induction motors become quite popular in industries owing to their robust construction and better speed-torque characteristics. Many researchers have focused on improving the speed control techniques of these motors. In particular, sensorless speed control techniques are becoming more popular, which are effected through Direct Torque Control (DTC). This control technique utilizes a three-phase inverted system, whose switching pulses are generated through Pulse Width Modulation (PWM) technique. Generally, the three-phase PWM inverters, used so far, consist

of a Six Switches topology. The switching sequences for these switches are obtained from a lookup table based on the inverter states [1]-[3]. In Six Switch Three Phase Inverter (SSTPI), the harmonics is generated to a greater extent, which results in over heating of the drive system.

Capacitors are meant for power factor correction, which tends to increase the total harmonic distortion. The second concern is the switching of the power factor correction capacitors. During a capacitor switching, transient over voltages are produced which contain a high frequency component. These transient over voltages, if large enough, can damage sensitive power electronic devices. The impact of the power factor correction circuit on induction motor drive system, in which the power factor correction circuit has a single power device with a forward diode in the boost configuration, has been analyzed [4]. The above approach increases the losses in diode and bridge rectifier and consequently decreases the system efficiency. A zero voltage transition isolated PWM boost converter for single stage power factor correction has been proposed [5], which suffers from the problem of existence of low ripple frequency. A canonical switching cell converter has been designed and analyzed with CMOS gate [6] [7]. The designed topology produces heat problem due to power loss and hence system performance is affected by poor efficiency. A Boost PFC converter has been analyzed in terms of input voltage and current [8]. The above converters are not suitable to relatively small size power supply due to its lower efficiency.

In most electronic power supplies, the AC input is rectified and a bulk capacitor is connected directly after the diode rectifier bridge. This type of utility interface draws excessive peak input currents and hence it produces a high level of harmonics and low input power factor. Due to low power factor the load efficiency is reduced. To overcome this drawback, a Four Switch Three Phase Inverter (FSTPI) has been addressed in this paper. In order to meet the harmonics limits, new AC-DC converter designs must employ active power factor correction at the input. Therefore boost Power Factor Corrector (PFC) converter is designed and it is implemented with FSTPI fed induction motor. By digital simulation the characteristics of the induction motor system are investigated and simulation results are presented.

2. Six-Switch Three-Phase Inverter

Figure 1 depicts the circuit of Six Switch Three Phase Inverter. The circuit consists of three legs connected in parallel across the dc source. Two switches are connected in series to form one leg. The three-phase output is taken from the midpoint of each leg. As shown in the circuit diagram, Q_1 to Q_6 are the six power switches that shape the output, which are controlled by the switching variables a, a', b, b', c and c'. When an upper switch is switched ON *i.e.*, when a, b or c is 1, the corresponding lower switches is switched OFF, *i.e.*, the corresponding a', b' or c' is zero. Therefore, the ON and OFF states of the upper switches Q_1, Q_3 and Q_5 can be used to determine the output voltage. Hence, there are eight sets of switching combinations from 0, 0, 0 to 1, 1, 1. The working principle of the conventional 6 switch 3 phase inverter is based on space vector

modulation technique.

Space Vector Modulation (SVM)

Space Vector Modulation (SVM) is quite different from the PWM methods. With PWMs, the inverter can be thought of as three separate push-pull driver stages, which create each phase waveform independently [9]. SVM, however, treats the inverter as a single unit, specifically, the inverter can be driven to eight unique states. The concept of space vector is derived from the rotating field of ac machine which is used for modulating the inverter output voltage. If three phase sinusoidal and balanced voltages are applied to a three-phase induction motor, it can be shown that the space vector $\bar{V}$ with magnitude V_m rotates in a circular orbit at angular velocity ω where the direction of rotation depends on the phase sequence of the voltages.

SVM is a digital modulating technique, where the objective is to generate PWM load line voltages that are in average equal to a given load line voltage. This is done in each sampling period by properly selecting the switch states of the inverter and the calculation of the appropriate time period for each state. The SVM for a three leg voltage source inverter is obtained by sampling the reference vector at the fixed clock frequency $2f_s$. All the eight possible switching combinations of the switching network are mapped into an orthogonal plane. The results are six non-zero vectors and two zero vectors. The six non-zero switching vectors form a hexagon as shown below in **Figure 2**.

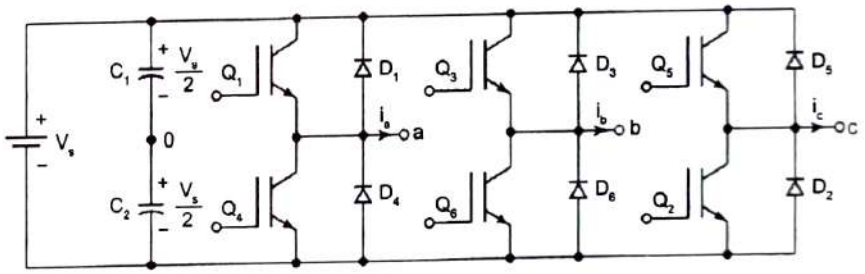


Figure 1. Six switch three phase inverter.

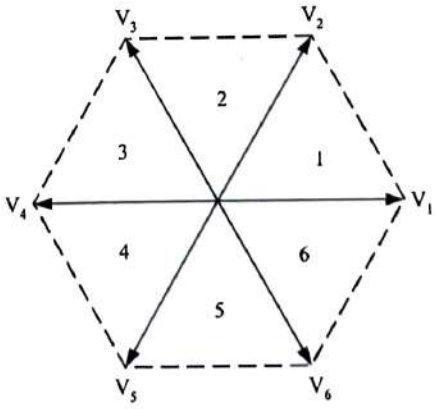


Figure 2. Vector representation.

To implement the space vector PWM, the voltage equations in the a-b-c reference frame can be transformed into the stationary d-q reference frame that consists of the horizontal (direct) and vertical (quadrature) axes. Then it involves vectorially decomposing a desired voltage space vector V into voltage vector components that can be generated using a typical three-phase inverter. There are eight possible combinations of ON and OFF patterns for the three upper power switches. The ON and OFF states of the lower power devices are opposite to the upper one and so are easily determined once the states of the upper power switches are determined.

3. Double Boost Converter: Principle of Operation

Figure 3 shows the basic circuit of Double boost converter for power factor correction. An uncontrolled diode rectifier with a boost converter is used to convert the single phase AC voltage into a constant DC link voltage, which is fed to the PWM inverter supplying an induction motor. The double boost converter is the widely used topology for achieving power factor correction. This converter draws unity power factor current from the AC mains and eliminates a harmonic current which regulates the DC link voltage even under fluctuating voltage conditions of AC mains. This circuit uses a snubber inductor which is connected in series with main switch and rectifier to control the di/dt rate of the rectifier.

The bulk energy storage capacitor sits on the output side of the converter rather than just after the diode rectifier bridge. The average inductor current which charges the bulk capacitor is proportional to the utility line voltage. For proper operation, the output voltage must be higher than the peak line voltage and current drawn from the line must be proportional to the line voltage. In circuit operation, it is assumed that the inductance of boost inductor is large so that it can be represented by constant current source and that the output ripple voltage is negligible so that the voltage across the output filter capacitor can be represented by constant voltage source. The designed values of the boost converter are tabulated in **Table 1**.

4. Simulation Studies

The conventional and proposed systems have been simulated using Matlab/Simulink. The simulation results are depicted in **Figure 4** & **Figure 5**. The input voltage, current waveforms and FFT analysis of existing converter SSTPI are shown in **Figure 4** & **Figure 5** illustrates the phase voltages, currents and FFT analysis applied to the proposed

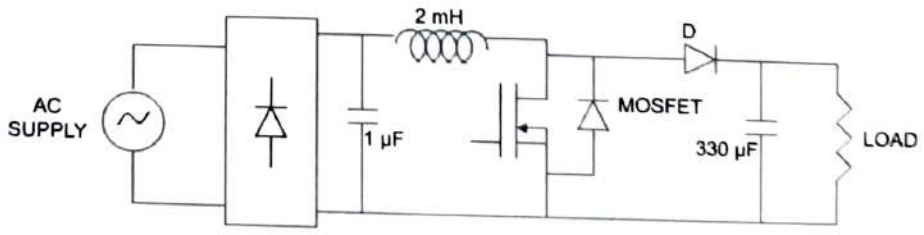
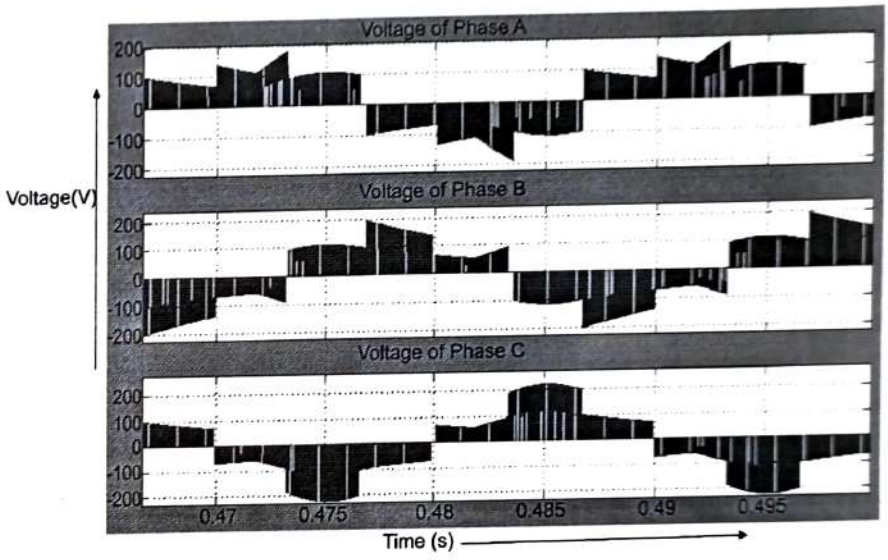


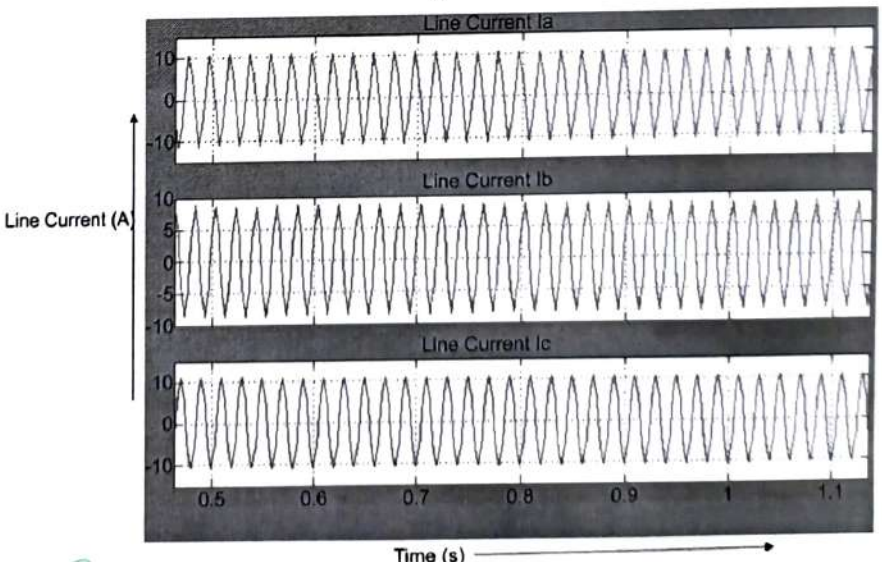
Figure 3. Double boost converter circuit.

Table 1. Parameters of double boost converter.

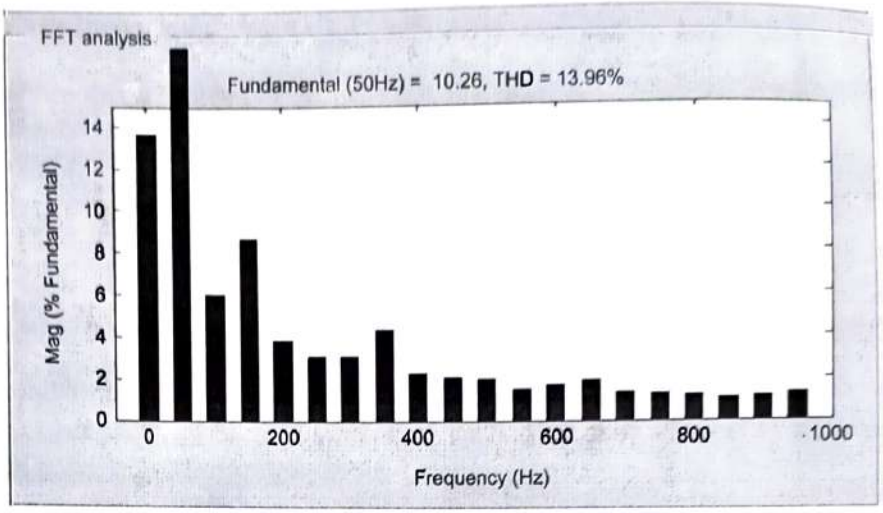
Parameter	Value
Line Voltage	200 V
Output Voltage	200 V DC
Output Power	1 kW
Boost Inductor	2 mH
Boost Capacitor	1 μF
Output Capacitor	330 μF
Switching Frequency	100 kHz



(a)

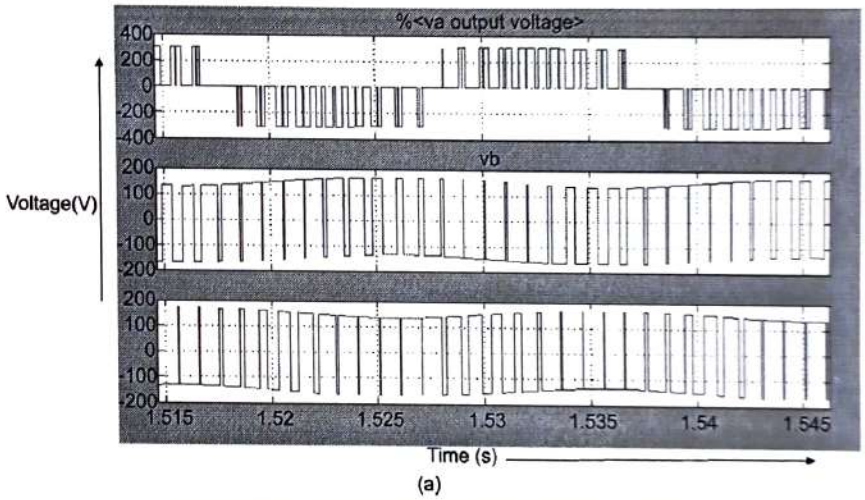


(b)

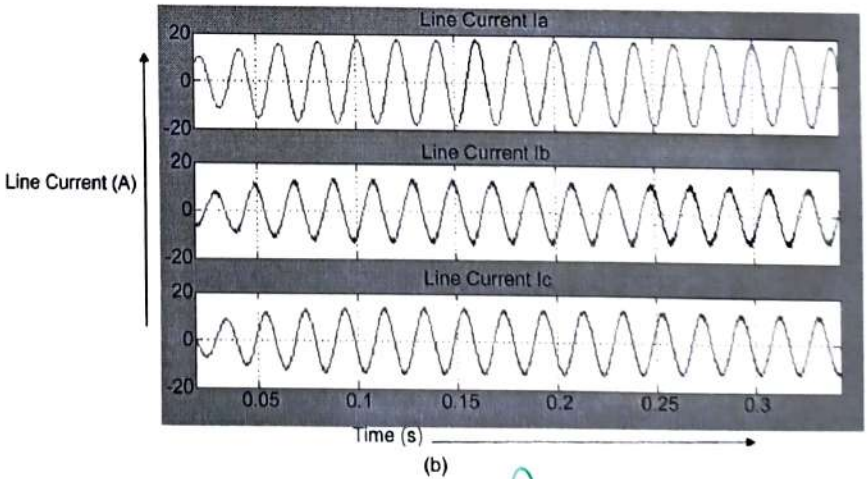


(c)

Figure 4. SSTPI simulation results. (a) Three phase voltage (Va, Vb & Vc); (b) Three current waveforms (Ia, Ib & Ic); (c) FFT analysis.



(a)



(b)

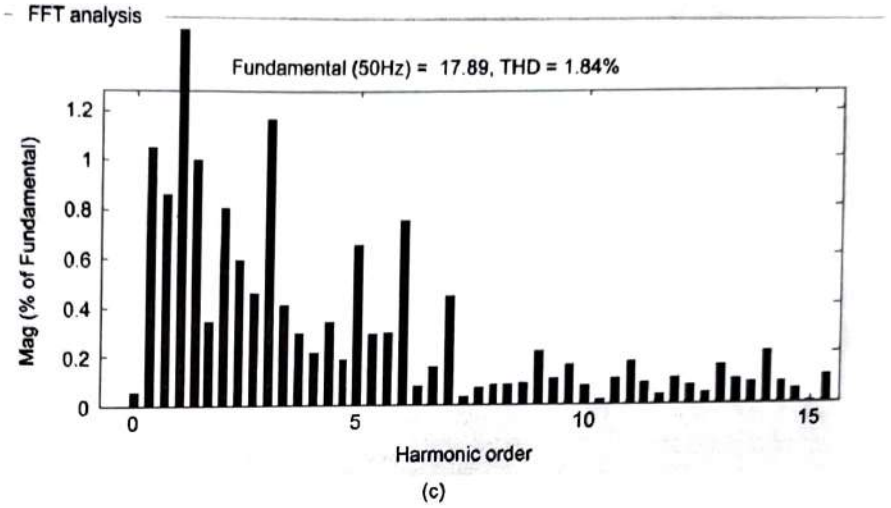


Figure 5. Simulated results of proposed system. (a) Three phase voltages (Va, Vb & Vc); (b) Three phase currents (Ia, Ib & Ic); (c) FFT analysis.

double boost converter based FSTPI fed three phase induction motor. The phase voltages observed with the conventional SSTPI is found to be more distorted and so the corresponding current waveforms. From **Figure 5**, it is obvious that the three phase voltages are resulted with less distortion and so their corresponding currents are found to be more sinusoidal.

The FFT analysis of the proposed and conventional systems illustrated the THD of the systems. The conventional system offered 13.96% of THD whereas the proposed system THD is observed as 1.84%. The inductor size and the amount of inductor current ripple will affect circuit efficiency and power factor. The designed converter increases the inductor size and hence reduces switching loss. Therefore proposed converter provides improved power factor and efficiency, which is evident from the resulted THD. The analysis indicates that the THD of the proposed system is very less compared to the conventional system.

5. Conclusion

The simulation study of implementation of boost PFC converter with FSTPI fed induction motor has been attempted. Implementation of boost PFC converter reduces the losses produced by system components and increases the system efficiency and input power factor. From the simulation study, it is established that the FSTPI fed induction motor with boost PFC converter provides reduced THD of 1.84%, whereas the THD of the conventional system is 13.96%. The simulation results also reveal that the proposed double boost FSTPI drive can be effectively used for the speed control of three-phase induction motors.

References

[1] Zhang, Y., Zhu, J., Zhao, Z., Xu, W. and Dorrell, D.G. (2012) An Improved Direct Torque

Control for Three-Level Inverter-Fed Induction Motor Sensorless Drive. *IEEE Transactions on Power Electronics*, **27**, 1502-1513. http://dx.doi.org/10.1109/TPEL.2010.2043543

[2] Zheng, L.B., Fletcher, J.E., Williams, B.W. and He, X.N. (2011) A Novel Direct Torque Control Scheme for a Sensorless Five-Phase Induction Motor Drive. *IEEE Transactions on Industrial Electronics*, **58**, 502-513. http://dx.doi.org/10.1109/TIE.2010.2047830

[3] Metwally, M.K. (2014) Direct Torque Control of Four Switch Three Phase Inverter Fed Induction Motor Sensorless Speed Drive. *International Journal of Power Electronics and Drive Systems*, **5**, 153-165.

[4] Krishnan, R., Diamantidis, D. and Lee, S. (1995) Impact of Power Factor Correction on Low Power Inverter-Fed Induction Motor Drive System. *26th Annual IEEE Power Electronics Specialists Conference*, Japan, 18-22 June 1995, 593-598. http://dx.doi.org/10.1109/pesc.1995.474869

[5] Cho, J.G., Jeong, C.Y., Baek, J.W. and Rim, G.H. (1998) Zero Voltage Transition Isolated PWM Boost Converter for Single Stage Power Factor Correction. *29th Annual IEEE Power Electronics Specialists Conference*, Taipei, 22-22 May 1998, 198-203.

[6] Yamamoto, I., Matsui, K. and Matsuo, M. (2000) A Comparison of Various DC-DC Converters and Their Application to Power Factor Correction. *26th Annual Conference of the IEEE Industrial Electronics Society*, Nagoya, 22-28 October 2000, 128-135.

[7] Chang, Y.-H. (2004) Design and Analysis of Power-CMOS-Gate Based Switched Capacitor Boost DC-AC Inverter. *IEEE Transaction on Circuits and Systems*, **51**, 1998-2016. http://dx.doi.org/10.1109/TCSI.2004.835681

[8] Ekemezie, P.N. (2007) Design of a Power Factor Correction AC-DC Converter. *AFRICON Conference*, Windhoek, 26-28 September 2007, 1-8.

[9] Elbadsi, B., Guermazi, A. and Masmoudi, A. (2005) New Space Vector PWM Strategy Intended for a Low-Cost Four-Switch Three-Phase Inverter-Fed Induction Motor Drive. *IEEE International Conference on Systems, Signals and Devices*, Sousse, 22-25 March 2011, 144-152.

Scientific Research Publishing

Submit or recommend next manuscript to SCIRP and we will provide best service for you:

Accepting pre-submission inquiries through Email, Facebook, LinkedIn, Twitter, etc.
A wide selection of journals (inclusive of 9 subjects, more than 200 journals)
Providing 24-hour high-quality service
User-friendly online submission system
Fair and swift peer-review system
Efficient typesetting and proofreading procedure
Display of the result of downloads and visits, as well as the number of cited articles
Maximum dissemination of your research work

Submit your manuscript at: http://papersubmission.scirp.org/

Pure Mathematical Sciences, Vol. 5, 2016, no. 1, 3 - 10
HIKARI Ltd, www.m-hikari.com
http://dx.doi.org/10.12988/pms.2016.51218

On πp-$\mathcal{H}$-Open Sets in Hereditary Generalized Topological Spaces

C. Janaki

Dept. of Mathematics, L.R.G. Govt. Arts College for Women
Tirupur-4, India

K. Binoy Balan

Dept. of Mathematics, Ahalia School of Engineering and Technology
Palakkad India

Copyright © 2015 C. Janaki and K. Binoy Balan. This article is distributed under the Creative Commons Attribution License, which permits unrestricted use, distribution, and reproduction in any medium, provided the original work is properly cited.

Abstract

In this paper, we define a new class of set called πp-$\mathcal{H}$-open sets and ($\pi p_{\mathcal{H}}$, λ)-continuous in hereditary generalized topological spaces. Also, we introduce the notions of πp-$\mathcal{H}$-open and πp-$\mathcal{H}$-closed functions by using πp-$\mathcal{H}$-open sets and πp-$\mathcal{H}$-closed sets, respectively and obtain new two decompositions of ($\pi p_{\mathcal{H}}$, λ)-continuous.

Mathematics Subject Classification: 54A05, 54C05
Keywords: πp-$\mathcal{H}$-open set, ($\pi p_{\mathcal{H}}$, λ)-continuous function, weakly ($\pi p_{\mathcal{H}}$, λ)-continuous, generalized topology

1. Introduction

In 2007, Á.Császár [2] defined a class of subsets of nonempty set called hereditary class and studied modification of the generalized topology with hereditary classes. A subfamily μ of $\wp(X)$ is called a generalized topology [3](briefly, GT) on X, if $\emptyset \in \mu$ and unions of elements of μ belong to μ. The pair (X, μ) is called a generalized topological space (briefly, GTS). The elements of μ are called μ-open [3] subsets of X and the complements are called μ-closed sets. The largest μ-open set contained in a subset A of X is denoted by $i_\mu(A)$) [4] and is called the μ-interior of A. The smallest μ-closed set containing A is called the μ-closure of A and is denoted by $c_\mu(A)$ [4].A generalized topology μ is said to be a quasi-topology if μ is closed under finite intersection. Let X be a nonempty set

and μ be a GT of subsets of X. A nonempty family $\mathcal{H}$ of subsets of X is said to be a hereditary class [2], if $A \in \mathcal{H}$ and $B \subset A$, then $B \in \mathcal{H}$.A generalized topological space (X, μ) with a hereditary class $\mathcal{H}$ is hereditary generalized topological space and denoted by $(X, \mu, \mathcal{H})$.
With respect to the generalized topology μ of all μ-open sets and a hereditary class $\mathcal{H}$, for each $A \subseteq X$, $A^*(\mathcal{H}, \mu) = \{x \in X: A \cap V \notin \mathcal{H}$ for every $V \in \mu$ such that $x \in V\}$[1]. $\mathcal{H}$ is said to be μ-codense if $\mu \cap \mathcal{H} = \{\emptyset\}$[2]. For $A \subset X$, define $c^*_\mu(A) = A \cup A^*(\mathcal{H}, \mu)$ for every subset A of X, with respect to μ and a hereditary class $\mathcal{H}$ of subsets of X. then $\mu^* = \{A \subset X: X - A = c^*_\mu(X - A)\}$ is a generalized topology [2], and $i^*(\mu)$ will denote the interior of A in (X, μ^*).

2. Preliminaries

By a space, we always mean a GTS (X, μ) with a hereditary class $\mathcal{H}$ with no separation properties assumed. A subset A of a GTS (X, μ) with a hereditary class $\mathcal{H}$ is said to be $\mathcal{H}$-open [2] if $A \subset i_\mu(A^*)$. The family of all $\mathcal{H}$-open sets is denoted by $\mathcal{H}O(X)$. $N(\mu)$ or simply N is the hereditary class of all nowhere dense subsets in (X, μ).

Definition 2.1 [5] Let A be a subset of hereditary generalized topological space $(X, \mu, \mathcal{H})$ and $\kappa \in \{\alpha(\mu), \sigma(\mu), \pi(\mu), \beta(\mu)\}$. Then $A^*_\kappa(\mathcal{H}, \mu) = \{x \in X: A \cap U \notin \mathcal{H}$ for every $U \in \kappa\}$. For $A \subset X$, define $c^*_\kappa(A) = A \cup A^*_\kappa$.According to [2], c^*_κ is enlarging, monotone and idempotent. Also $c^*_\kappa(A) = A \cup c_\kappa(A^*_\kappa) \subseteq c_\kappa(A)$.
Remark 2.2 [7] If A and B are subsets of hereditary generalized topological space $(X, \mu, \mathcal{H})$ and $\kappa \in \{\alpha(\mu), \sigma(\mu), \pi(\mu), \beta(\mu)\}$. Then (i) $A^*_\kappa(\mathcal{H}, \mu) = A^*(\mathcal{H}, \mu)$, if $\kappa = \mu$.
(ii)$A \subseteq B$, then $A^*_\kappa \subseteq B^*_\kappa$.
(iii)$A^*_\kappa = c_\kappa(A^*_\kappa) \subseteq c_\kappa(A)$ andA^*_κ is κ-closed set in $(X, \mu, \mathcal{H})$.
(iv) $(A^*_\kappa)^*_\kappa \subseteq A^*_\kappa$.
(v) $c^*_\kappa(A) \subset c^*_\kappa(B)$ whenever $A \subset B \subset X$.
(vi) $c^*_\kappa(c^*_\kappa(A)) = c^*_\kappa(A)$

Lemma 2.3 [8] If (X, μ) is a quasi-topology with a hereditary class $\mathcal{H}$. Then the following are hold.

(i) $\mathcal{H}$ is μ-codense if and only if $A \subset A^*$ for every $A \in \mu$.
(ii) If $A \subset A^*$, then $A^* = c_\mu(A^*) = c_\mu(A) = c^*_\mu(A)$

Lemma 2.4 [6] If (X, μ) is GTS with a hereditary class $\mathcal{H}$. For $A \subset X$,
(i) $c^*_\mu(A) = X - i^*_\mu(X - A)$.
(ii) $i_\mu(A) \subset i^*_\mu(A) \subset A$.

Definition 2.5 [1] Let (X, μ_x) be a generalized topological space and $A \subseteq X$. Then A is said to be
(i) μ- semi open if $A \subseteq c_\mu(i_\mu(A))$.
(ii) μ- preopen if $A \subseteq i_\mu(c_\mu(A))$.

(iii) μ-α-open if $A \subseteq i_\mu(c_\mu(i_\mu(A)))$.
(iv) μ-β-open if $A \subseteq c_\mu(i_\mu(c_\mu(A)))$.
(v) μ-r-open if $A = i_\mu(c_\mu(A))$
(vi) μ-rα-open if there is a μ-r-open set U such that $U \subset A \subset c_\alpha(U)$.

Definition 2.6[1] Let (X, μ_X) be a generalized topological space and $A \subseteq X$. Then A is said to be μ-$\pi r\alpha$ closed set if $c_\pi(A) \subseteq U$ whenever $A \subseteq U$ and U is μ-rα-open set. The complement of μ-$\pi r\alpha$ closed set is said to be μ-$\pi r\alpha$ open set.
The complement of μ-semi open (μ-preopen, μ-α-open, μ-β-open, μ-r-open, μ-rα-open) set is called μ- semi closed (μ- pre closed, μ-α- closed, μ-β- closed, μ-r- closed, μ-rα-closed) set.
Let us denote the class of all μ-semi open sets, μ-preopen sets, μ-α-open sets, μ-β-open sets, and μ-$\pi r\alpha$ open sets on X by $\sigma(\mu)$ (σ for short), $\pi(\mu)$ (π for short), $\alpha(\mu)$ (α for short), $\beta(\mu)$ (β for short) and $\pi p(\mu)$ (πp for short)respectively. Let μ be a generalized topology on a nonempty set X and $S \subseteq X$. The μ-α-closure (resp. μ-semi closure, μ-pre closure, μ-β-closure, μ-$\pi r\alpha$-closure) of a subset S of X denoted by $c_\alpha(S)$ (resp. $c_\sigma(S)$, $c_\pi(S)$, $c_\beta(S)$, $c_{\pi p}(S)$) is the intersection of μ-α-closed (resp. μ- semi closed, μ- pre closed, μ-β-closed, μ-$\pi r\alpha$ closed) sets including S. The μ-α-interior (resp. μ-semi interior, μ-pre interior, μ-β-interior, μ-$\pi r\alpha$-interior) of a subset S of X denoted by $i_\alpha(S)$ (resp. $i_\sigma(S)$, $i_\pi(S)$, $i_\beta(S)$, $i_{\pi p}(S)$) is the union of μ-α-open (resp. μ- semi open, μ- preopen, μ-β-open, μ-$\pi r\alpha$ open) sets contained in S.

Definition 2.7[1] A function f between the generalized topological spaces (X, μ_X) and (Y, μ_Y) is called $(\pi p, \mu_Y)$ – continuous function if $f^{-1}(A) \in \pi p(\mu_X)$ for each $A \in (Y, \mu_Y)$.

Definition 2.8 [5] Let (X, μ_X) and (Y, μ_Y) be GTS's. Then a function $f: (X, \mu_X) \to (Y, \mu_Y)$ is said to be weakly $(\pi p, \mu_Y)$- continuous function if for each $x \in X$ and each μ_Y-open set V of Y containing f(x), there exists $U \in \pi p(\mu_X)$ such that $f(U) \subseteq c_{\mu_Y}(V)$.

3. πp-$\mathcal{H}$-closed sets

In this section, first of all we introduce the notion called πp-$\mathcal{H}$-open and give some characterizations of this sets.

Definition 3.1 A subset of A of an hereditary generalized topological spaces $(X, \mu, \mathcal{H})$ is said to be
(i) π-$\mathcal{H}$-open [2] if $A \subset i_\mu(c^*_\mu(A))$.
(ii) α-$\mathcal{H}$-open [2] if $A \subset i_\mu(c^*_\mu(i_\mu(A)))$.
(iii) r-$\mathcal{H}$-open[2] if $A = i_\mu(c^*_\mu(A))$.
(iv) δ-$\mathcal{H}$-set [2] if $i_\mu(c^*_\mu(A)) \subset c^*_\mu(i_\mu(A))$
(v) t-$\mathcal{H}$-set [8] jf $i_\mu(c^*_\mu(A)) = i_\mu(A)$.

(vi) t*-$\mathcal{H}$-set [8] if $i_\mu(c^*_\mu(i_\mu(A))) = i_\mu(A)$.
(vii) $C_{\pi p}$-set if $A = G \cap F$, where G is πp-$\mathcal{H}$-open and F is t-$\mathcal{H}$-set.
(viii) $C_{\pi p^*}$-set if $A = G \cap F$, where G is πp-$\mathcal{H}$-open and F is t*-$\mathcal{H}$-set.
(ix) $r\alpha$-$\mathcal{H}$-open if there is r-$\mathcal{H}$-open set U such that $U \subseteq A \subseteq c^*_\alpha(A)$.

Definition 3.2 Let $(X, \mu, \mathcal{H})$ be a hereditary GTS in X and $A \subseteq X$, then A is said to be πp-$\mathcal{H}$-closed if $c^*_\pi(A) \subseteq U$, whenever $A \subseteq U$ and U is $r\alpha$-$\mathcal{H}$-openset.
The complement of πp-$\mathcal{H}$-closed set is said to be πp-$\mathcal{H}$-open set.

Proposition 3.3 In a hereditary generalized topological space $(X, \mu, \mathcal{H})$, the following hold.
(i) Every μ-closed set is πp-$\mathcal{H}$-closed set.
(ii) Every μ-$\pi r\alpha$ closed set is πp-$\mathcal{H}$-closed set.
Proof: (i) Obvious.
(ii) Let A be μ-$\pi r\alpha$ closed set. Then $c_\pi(A) \subseteq U$, whenever $A \subseteq U$ and U is $r\alpha$-$\mathcal{H}$-openset.Therefore $c^*_\pi(A) \subseteq c_\pi(A) \subseteq U$. Hence A is πp-$\mathcal{H}$-closed set.

Example 3.4 Let X = {a, b, c, d}, μ= {$\emptyset$, {a}, {a, b}, {b, c}, {a, b, c}} and $\mathcal{H}$= {$\emptyset$, {c}, {d}}. Then A= {b, c, d} is πp-$\mathcal{H}$-closed but not μ-closed and μ-$\pi r\alpha$ closed.

Theorem 3.5 Let $(X, \mu, \mathcal{H})$ be a hereditary generalized topological space and A, $B \subset X$.If A is πp-$\mathcal{H}$-closed set and $A \subset B \subset c^*_\pi(A)$ then B is πp-$\mathcal{H}$-closed.
Proof: Let A be a πp-$\mathcal{H}$-closed set and $B \subseteq U$, where U is $r\alpha$-$\mathcal{H}$-open set, then $A \subseteq U$ and hence $c^*_\pi(A) \subseteq U$. Now $c^*_\pi(B) \subseteq c^*_\pi(c^*_\pi(A)) = c^*_\pi(A) \subseteq U$. Hence $c^*_\pi(B) \subseteq U$. Therefore B is πp-$\mathcal{H}$-closed.

Theorem 3.6 Let $(X, \mu, \mathcal{H})$ be a hereditary generalized topological space. If A is πp-$\mathcal{H}$-closed set in X such that $A \subset Y \subset X$, then A is πp-$\mathcal{H}$-closed in Y.
Proof: Suppose that $A \subset V \cap Y$, where V is $r\alpha$-$\mathcal{H}$-open set in X. Then $A \subseteq V$. Since A is πp-$\mathcal{H}$-closed set in X then $c^*_\pi(A) \subseteq V$. So $c^*_\pi(A) \cap Y \subset V \cap Y$. Hence it follows that $c^*_{\pi Y}(A) \subset V$. This shows that A is πp-$\mathcal{H}$-closed in Y.

Remark 3.7 The following examples shows that the intersection and union of πp-$\mathcal{H}$-closed sets need not be πp-$\mathcal{H}$-closed.

Example 3.8 Let X = {a, b, c, d}, μ= {$\emptyset$, {a}, {a, b}, {b, c}, {a, b, c}} and $\mathcal{H}$= {$\emptyset$, {c}, {d}}. Then set of all πp-$\mathcal{H}$-closed sets, $\pi p(\mathcal{H}_\mu C(X))$={ X, {b, c, d}, {a, c, d}, {c, d},{b, d}, {a, d}}. Consider A= {b, d} and B = {a, d} are two πp-$\mathcal{H}$-closed sets but $A \cup B$ = {a, b, d} is not πp-$\mathcal{H}$-closed set.

Example 3.9 Let X = {a, b, c, d}, μ= {$\emptyset$, {a}, {a, b}, {b, c}, {a, b, c}} and $\mathcal{H}$= {$\emptyset$, {c}, {d}}. Then set of all πp-$\mathcal{H}$-closed sets, $\pi p(\mathcal{H}_\mu C(X))$={ X, {b, c, d},

{a, c, d}, {c, d},{b, d}, {a, d}}. Consider A= {b, d} and B = {a, d} are two πp-$\mathcal{H}$-closed sets but A ∩B = {d} is not πp-$\mathcal{H}$-closed set.

Theorem 3.10 Let (X, μ) be a GTS with hereditary class $\mathcal{H}$. If A⊂X is δ-$\mathcal{H}$-set and t-$\mathcal{H}$-set then A is t*-$\mathcal{H}$-set.
Proof: Suppose A is a δ-$\mathcal{H}$-set and t-$\mathcal{H}$-set. Then $i_\mu(c^*_\mu(A)) \subset c^*_\mu(i_\mu(A))$ and so $i_\mu(c^*_\mu(A))\subset i_\mu(c^*_\mu(i_\mu(A)))$. Since $c^*_\mu(i_\mu(A))\subset c^*_\mu(A)$, $i_\mu(c^*_\mu(i_\mu(A)))\subset i_\mu(c^*_\mu(A))$ and so $i_\mu(c^*_\mu(i_\mu(A))) = i_\mu(c^*_\mu(A)) = i_\mu(A)$. Therefore A is t*-$\mathcal{H}$-set.

Theorem 3.11 Let (X, μ) be a quasi- topology with a hereditary class $\mathcal{H}$, if A and B are t-$\mathcal{H}$-sets, then A∩B is t-$\mathcal{H}$-set.
Proof: Let A and B be t-$\mathcal{H}$-sets. Then $i_\mu(A\cap B)\subset i_\mu(c^*_\mu(A\cap B))\subset i_\mu(c^*_\mu(A)\cap c^*_\mu(B))=i_\mu(c^*_\mu(A))\cap i_\mu(c^*_\mu(B))=i_\mu(A)\cap i_\mu(B)$. This implies that A∩B is a t-$\mathcal{H}$-set.

Theorem 3.12 Let (X, μ) be a quasi-topology with a hereditary class $\mathcal{H}$, if A and B are t*-$\mathcal{H}$-sets, then A∩B is a t*-$\mathcal{H}$-set.
Proof: Let A and B be t*-$\mathcal{H}$-sets. Then $i_\mu(A\cap B)\subset i_\mu(c^*_\mu(i_\mu(A\cap B)))\subset i_\mu[c^*_\mu(i_\mu(A))\cap c^*_\mu(i_\mu(B))] = i_\mu(c^*_\mu(i_\mu(A))\cap i_\mu(c^*_\mu(i_\mu(B))=i_\mu(A)\cap i_\mu(B)$. This implies that A∩B is a t*-$\mathcal{H}$-set.

4. Decomposition of Continuity via hereditary classes

Definition 4.1 A function f: (X, μ,$\mathcal{H}$) →(Y, λ) is said to be ($\pi p_{\mathcal{H}}$, λ)-continuous if $f^{-1}(V)$ is πp- $\mathcal{H}$-open in (X, μ, $\mathcal{H}$) for every λ-open V of (Y, λ).

Definition 4.2 Let (X, μ,$\mathcal{H}$) be a hereditary generalized topological space and A⊂X and let x∈X. Then A is said to be a $\pi p_{\mathcal{H}}$-neighbourhood of x, if there exists πp-$\mathcal{H}$-open set U containing x such that U⊂A.

Theorem 4.3 Let $\pi p_{\mathcal{H}}$ is a closed under arbitrary union and f: (X, μ,$\mathcal{H}$)→(Y, λ) be a function between the hereditary generalized topological space (X, μ, $\mathcal{H}$) to the generalized topological space (Y, λ). Then the following are equivalent.
(i) f is a ($\pi p_{\mathcal{H}}$, λ)-continuous.
(ii) For each x∈X and each λ-open set V in Y with f(x) ∈V, there exists πp-$\mathcal{H}$-open set U containing x such that f(U)⊂V.
(iii) For each x∈X and each λ-open set V in Y with f(x) ∈V, $f^{-1}(U)$ is a $\pi p_{\mathcal{H}}$-neighbourhood of x.
(iv) The inverse image of each λ-closed in (Y, λ) is πp-$\mathcal{H}$-closed.
Proof. (i)⇒(ii). Let x∈X and let V be any λ-open set in Y such that f(x) ∈V. Since f is ($\pi p_{\mathcal{H}}$, λ)-continuous, $f^{-1}(V)$ is πp-$\mathcal{H}$-open set. By putting U = $f^{-1}(V)$ which is containing x, we have f(U) ∈V.
(ii)⇒(iii). Let V be any λ-open set in Y and let f(x)∈V. Then by (ii), there exists πp-$\mathcal{H}$-open set U containing x such that f(U) ⊂V. Therefore, x∈U⊂$f^{-1}(V)$. Hence $f^{-1}(V)$ is a $\pi p_{\mathcal{H}}$-neighbourhood of x.

(iii)⇒(iv).Let F be λ-closed in Y. Take V=Y\F. Then V is a λ-open in Y. Let x∈ f^{-1}(V), by (iii),f^{-1}(V) is a $\pi p_{\mathcal{H}}$-neighbourhood of x. Thus for each x∈f^{-1}(V), there exists πp-$\mathcal{H}$-open set U_x containing x such that x∈U_x⊂f^{-1}(V). Hence $f^{-1}(V) \in \bigcup_{x\in f^{-1}(V)} U_x$ and so f^{-1}(V) is πp-$\mathcal{H}$-open set in X. Hence $f^{-1}(F) = X\backslash f^{-1}(Y\backslash F) = X \backslash f^{-1}(V)$ is πp-$\mathcal{H}$-closed in X.
(iv)⇒(i).Let V be a λ-open in Y and let f(x) ∈V.Take F=Y\V. Then F is a λ-closed in Y. Let x∈ f^{-1}(F), by (iv), f^{-1}(F) is a πp-$\mathcal{H}$-closed in X. Hence $f^{-1}(V) = f^{-1}(Y\backslash F) = X \backslash f^{-1}(F)$ is πp-$\mathcal{H}$-open in X. Hence f is a ($\pi p_{\mathcal{H}}$, λ)-continuous.

Proposition 4.4 For a function f: (X, μ,$\mathcal{H}$)→(Y, λ), the following hold.
(a) Every (μ, λ)- continuous is ($\pi p_{\mathcal{H}}$,λ)- continuous.
(b) Every (πp, λ)- continuous is ($\pi p_{\mathcal{H}}$,λ)- continuous.

Theorem 4.5 Let f: (X, μ, $\mathcal{H}_1$) →(Y, λ, $\mathcal{H}_2$) and g: (Y, λ, $\mathcal{H}_2$) →(Z, η) be two functions, where $\mathcal{H}_1$ and$\mathcal{H}_2$ are hereditary classes on X, Y and Z respectively. Then g∘f is ($\pi p_{\mathcal{H}}$, λ)-continuous if f is ($\pi p_{\mathcal{H}}$, λ)-continuous and g is (λ, η)-continuous.
Proof. Let U be any η-open in (Z, η). Then g is (λ, η)-continuous, g^{-1}(U) is λ-open in (Y, λ, $\mathcal{H}_2$). Since f is ($\pi p_{\mathcal{H}}$, λ)-continuous, $f^{-1}(g^{-1}(U)) = (g\circ f)^{-1}(U)$ is πp-$\mathcal{H}$-open in (X, μ,$\mathcal{H}_1$). Hence g∘f is ($\pi p_{\mathcal{H}}$, λ)-continuous.

Definition 4.6 A function f: (X, μ) →(Y, λ, $\mathcal{H}$) is said to be weakly ($\pi p_{\mathcal{H}}$, λ)-continuous if for each x∈X and each λ-open set V of Y containing f(x), there exists πp-$\mathcal{H}$-open set U containing x such that f(U) ⊆ c^*_λ(V).
Remark 4.7 Every weakly ($\pi p_{\mathcal{H}}$, λ)-continuous function is weakly (πp, λ)-continuous but the converse is need not be true.

Example 4.8 Let X =Y= {a, b, c, d}, μx = {∅, {a}, {a, b}, {b, c}, {a, b, c}}, μ_Y={∅, {a, c},{b, c}, {a, b, c}}.Define f: (X, μx) →(Y, μ_Y) as follows f(a) = b, f(b) = f(c) = a and f(d) = c and $\mathcal{H}$= {∅, {c}, {d}}. Then the set of all πp-$\mathcal{H}$-open sets, πp ($\mathcal{H}_\mu$O(X)) ={X, {b, c, d}, {a, c, d}, {c, d},{b, d}, {a, d}} and set of all μ-πrα open sets, πp(μ)= {∅, X, {a, b, c}, {a, c}, {b, c}, {a, b}, {b},{a}, {c}} . Now f is weakly (πp, λ)-continuous but f is not weakly($\pi p_{\mathcal{H}}$, λ)-continuous.

Theorem 4.9 Let $\pi p_{\mathcal{H}}$ is a closed under arbitrary union. A function f: (X, μ)→(Y, λ, $\mathcal{H}$) is weakly($\pi p_{\mathcal{H}}$, λ)-continuous if and only if for each λ-open set V⊂Y,f^{-1}(V)⊂$i_{\pi p}$(f^{-1}(c^*_λ(V))).
Proof: Let V be any λ-open set of Y and x∈f^{-1}(V). Since f is weakly ($\pi p_{\mathcal{H}}$, λ)-continuous, there exists a μ-πrα open set U such that x∈U and f(U)⊂ c^*_λ(V).Hence x∈U⊂f^{-1}(c^*_λ(V)) and x∈$i_{\pi p}$(f^{-1}(c^*_λ(V))). Therefore, we obtain f^{-1}(V)⊂$i_{\pi p}$(f^{-1}(c^*_λ(V))).
Conversely, let x∈X and V be a λ-open set of Y containing f(x).Then x∈f^{-1}(V)⊂$i_{\pi p}$(f^{-1}(c^*_λ(V))). Let U = $i_{\pi p}$(f^{-1}(c^*_λ(V))) then f(U) = f($i_{\pi p}$(f^{-1}(c^*_λ(V)))) ⊂f(f^{-1}(c^*_λ(V)))⊂ c^*_λ(V). This shows that f is weakly ($\pi p_{\mathcal{H}}$, λ)-continuity.

Definition 4.10 A function f: $(X, \mu)\to(Y,\lambda, \mathcal{H})$ is called πp-$\mathcal{H}$-open if the image of each μ-open set of X is an πp-$\mathcal{H}$-open set of Y.

Theorem 4.11 A function $f:(X, \mu)\to(Y,\lambda, \mathcal{H})$ is πp-$\mathcal{H}$-open if and only if for each subset U of Y and each μ-closed set F of X containing $f^{-1}(U)$, there exists πp-$\mathcal{H}$-closed set V of Y containing U such that $f^{-1}(V)\subset F$.
Proof: Let $V = Y\setminus f(X\setminus F)$.Then we have $f(X\setminus F)\subset Y\setminus U$. Since f is πp-$\mathcal{H}$-open, then V is πp-$\mathcal{H}$-closed and $f^{-1}(V) = f^{-1}(Y\setminus f(X\setminus F))= X\setminus f^{-1}(f(X\setminus F))\subset X\setminus(X\setminus F)= F$. Conversely, let W be any μ-open set of X and $U = Y\setminus f(W)$. Then $f^{-1}(U) = f^{-1}(Y\setminus f(W))= X\setminus f^{-1}(f(W))\subset X\setminus W$ and $X\setminus W$ is μ-closed. By the hypothesis, there exists an πp-$\mathcal{H}$-closed set V of Y containing U such that $f^{-1}(V)\subset X\setminus W$. Then, we have $f^{-1}(V)\cap W = \emptyset$ and $V\cap f(W) = \emptyset$. Therefore, $Y\setminus f(W)\supset V\supset U= Y\setminus f(W)$ and f(W) is πp-$\mathcal{H}$-open in Y. This shows that f is πp-$\mathcal{H}$-open.

Definition 4.12 Let $f:(X, \mu,\mathcal{H})\to(Y, \lambda)$ be a function. If for each $V\in\lambda$, $f^{-1}(V)$ is a $C_{\pi p}$-$\mathcal{H}$-set (resp. $C_{\pi p^*}$-$\mathcal{H}$-set) then f is said to be a $C_{\pi p}$-$\mathcal{H}$-continuous (resp. $C_{\pi p^*}$-$\mathcal{H}$-continuous).

Theorem 4.13 For a function $f:(X, \mu,\mathcal{H})\to(Y, \lambda)$, the following properties are hold.
(i) f is $(\pi p, \lambda)$-continuous if and only if .f is $C_{\pi p}$-$\mathcal{H}$-continuous.
(ii) f is $(\pi p, \lambda)$-continuous if and only if $C_{\pi p^*}$-$\mathcal{H}$-continuous.
Proof: (i). Let V be an μ-open set in Y. Since f is $(\pi p, \lambda)$-continuous, then $f^{-1}(V)$ is a μ-$\pi r\alpha$ open set in X. Since every μ-$\pi r\alpha$ open set is πp-$\mathcal{H}$-open, then $f^{-1}(V)$ is πp-$\mathcal{H}$-open set. Since $f^{-1}(V)=A = A\cap X$, where A is πp-$\mathcal{H}$-open and X is t-$\mathcal{H}$-set.Hence $f^{-1}(V)$ is $C_{\pi p}$-$\mathcal{H}$set. Therefore f is $C_{\pi p}$-$\mathcal{H}$-continuous.
Conversely, let f be $C_{\pi p}$-$\mathcal{H}$-continuous. Then for each $V\in\lambda$, $f^{-1}(V)$ is a $C_{\pi p}$-$\mathcal{H}$-set. That is $f^{-1}(V)= A = G\cap F$, where G is πp-$\mathcal{H}$-open set and F is t-$\mathcal{H}$-set.Let U be $r\alpha$-$\mathcal{H}$-open such that $A\subseteq U$. Then $i_\pi^*(G)\cap i_\mu(F) \subseteq U$. That is $i_\pi(G)\cap i_\mu(F)\subseteq U$, $i_\pi(G\cap F)\subseteq U$.Therefore $f^{-1}(V)$ is μ-$\pi r\alpha$ open set. Hence f is $(\pi p, \lambda)$-continuous.
(ii) Similarly as that of (i).

References

[1] K. Binoy Balan and C. Janaki, μ-$\pi r\alpha$ closed sets in generalized topological space, *Int. Journal of Adv. Sci. and Tech. Research*, **2** (2012), no. 6, 352-359.

[2] Á. Császár, Modification of generalized topologies via hereditary classes, *Acta Math. Hungar.*, **115** (2007) 29-36. http://dx.doi.org/10.1007/s10474-006-0531-9

[3] Á. Császár, Generalized open sets in generalized topologies, *Acta Math. Hungar.*, **106** (2005), 53-66. http://dx.doi.org/10.1007/s10474-005-0005-5

[4] Á.Császár, Generalized open sets, *Acta Math. Hungar.*, **75** (1997), 65-87. http://dx.doi.org/10.1023/a:1006582718102

[5] C. Janaki and K. Binoy Balan, Weakly (πp, $\mu\gamma$)-continuous functions on generalized topological spaces, *Int. Journal of Computer Appli. (0975-8887)*, **85** (2014), no. 5, 15-18. http://dx.doi.org/10.5120/14836-3096

[6] Y.K. Kim and W.K. Kim, On operations induced by Hereditary classes on generalized topological spaces, *Acta. Math. Hungar.*, **137** (2012), no. 1-2, 130-138. http://dx.doi.org/10.1007/s10474-012-0212-9

[7] M. Rajamani, V. Inthumathi and R. Ramesh, Some new generalized topologies via hereditary classes, *Bol. Soc. Paran. Math.*, **30** (2012), no. 2,71-77.

[8] R. Ramesh and R. Mariappan, Generalized open sets in hereditary generalized topological spaces, *Journal of Mathematical and Comp. Sci.*, **5** (2015), no. 2, 149-159.

[9] Sheena Skaria, V. Renukadevi, *On hereditary classes in generalized topological spaces*, *Journal Adv. Res. Pure. Math.*, **3** (2011), no. 2, 21-30.

Received: December 23, 2015; Published: March 11, 2016



Asian Journal of Research in Social Sciences and Humanities
Year : 2016, Volume : 6, Issue : 11
First page : (314) Last page : (323)
Online ISSN : 2249-7315.
Article DOI : 10.5958/2249-7315.2016.01194.1 (http://dx.doi.org/10.5958/2249-7315.2016.01194.1)

Email id

Raindrop Algorithm based AWPI Controller Tuned Chopper Driven PMI Motor

Muthukrishnan S*, Sundaram S Saravana, Gopalraj Murugananth*****
*Sri Eshwar College of Engineering, Coimbatore, India

**Hindustan College of Engineering and Technology, Coimbatore, India

***Ahalia School of Engineering and Technology, Palakkad, India

Online published on 9 November, 2016.

Abstract

Permanent Magnet DC motors find wide application in precision control system applications viz. surgical equipment. Conventiona controller based chopper drive are being employed in these motor drives. To enhance the performance of the drive, this paper su an efficient Raindrop algorithm based controller Anti-Windup PI controller. The proposed drive system has been simulated using Matlab/Simulink. The simulated results have been validated using a low cost PIC microcontroller based experimental setup. The comparative studies has proven that the proposed system has an edge over the conventional drive system.

Keywords

Anti-Windup, Chopper, PI controller, Raindrop, Peak overshoot, steady state error.

Buy Now (?target=ijor:ajrssh&volume=6&issue=11&article=024&type=subscribearticle) PDF (?target=ijor:ajrssh&volume=6&issue=11&article=024&

Site map (ijor.aspx?target=site_map) | Privacy Policy (ijor.aspx?target=privacy_policy) | Copyright (ijor.aspx?target=copyright_disclaimer) | Terms & Conditions | (ijor.aspx?target=terms) Page Ra

(http://www.prchecker.info/)

621,848,174 visitor(s) since 30th May, 2005.

All rights reserved. Site designed and maintained by DIVA ENTERPRISES PVT. LTD. (http://www.divan.in).

Note: Please use Internet Explorer (6.0 or above). Some functionalities may not work in other browsers.

Design of a 3-T Half Adder

Sruthi.V[1], Akhila.Raj.K.M[2],Madhulika.A.R[3],Ajin.A.S[4]

[1,2,3]Students,Department Of Electronics and Communication Engineering,Ahalia School Of Engineering and Technology,Palakkad, Kerala,India

[4]Asst.Professor, Department Of Electronics and Communication Engineering,Ahalia School Of Engineering and Technology,Palakkad,Kerala, India

Abstract:

In this paper, we propose a new technique for implementing a half adder circuit consisting of minimum number of transistors (3-T). The W/L ratio is varied to get the required output. An adder is a digital circuit that performs addition of two numbers. In many computers and other kind of processors, adders are used not only in arithmetic logic unit but also in other parts of the processors where they are used to calculate addresses, table indices and similar operations. Simulated results indicate the performance of proposed half adder over the conventional half adders. Detailed comparison of the simulated results is presentedhere which is done in MultiSim software.

Keywords: *Pass Transistor Logic, 3-T XOR,Logical Effort and Transistor Sizing*

I. INTRODUCTION

Since the introduction of integrated circuits decades ago methods to speed up digital circuits and to reduce the area of their designs have great importance. The power dissipation per unit area grows as the number of transistors per chip increases which also increases the chip temperature. This excessive temperature reduces the reliability and lifetime of the circuit.

The CMOS technology has a great influence in the performance of microprocessors. Dynamic CMOS circuits are used in microprocessors to improve their timing performance. This method has many challenges like transistor sizing, charge sharing, noise-immunity, leakage current etc.

The growing world demands for circuits with ultra-low power dissipation. The presence of complementary transistors avoids contention. It ensures that if the inputs are not changing then there is no power dissipation. Here the output voltage level is connected to the power or ground line or both.

Various techniques have been implemented to reduce power dissipation at circuit, architectural and system level. The number of gates per chip area is constantly increasing, while the gate switching energy does not decrease at the same rate, so power dissipation rises and heat removal becomes difficult and expensive. The proposed thesis is to develop a hybrid VLSI circuit that improves the circuit performance by reducing the number of transistors. The output of the gate can be improved by changing the W/L ratio of the transistor. The points to be noted while changing the W/L ratio:

1. As W/L ratio increases the drain-to source current increases.
2. As W/L ratio increases the response time increases.
3. W/L ratio is roughly proportional to the resistance.
4. The W/L ratio of PMOS should be larger than the NMOS.
5. Make the MOSFET in the output side the largest.

Logical effort is a method to make certain decisions:

1. Uses a simple model of delay.
2. Allows back of the envelope calculations.
3. Helps make rapid comparison between comparatives.
4. Emphasises remarkable symmetries.

In electronics, an adder or summer is a digital circuit that performs addition of numbers. In modern computers adders reside in Arithmetic logic unit (ALU) where other operations are performed. Although adders can be constructed for many numerical representations, such as Binary coded decimal or Excess-3, the most common adders operate on binary numbers. In cases where two's complement or one's complement is being used to represent negative numbers, it is trivial to modify an adder into an adder-subtractor. Other signed number representations require a more complex adder.

In [2] the authors have designed a low power high speed multiplier using full adder consisting minimum no. of transistors in which the modified the blocks AND gate and the XOR gate behind this work is utilized here. Various techniques have been proposed with the aim of improving speed and power consumption [1], [3].

Paper is organized as follows. Section II describes the related work. Section III describes the proposed system. Section IV shows the simulation results.

II. RELATED WORK

An adder is a combinational arithmetic circuit. A half adder adds two one-bit binary

numbers A and B. The input variables of a half adder are called the augend and addend bits. It has two outputs, S and C which is the sum and carry respectively. Carry is the output which is carried into the next stages. The simplest half adder design pictured incorporates an XOR gate for S and an AND gate for C. If A and B are the input bits, the sum bit(S) is the X-OR of A and B and the carry bit(C) will be the AND of A and B. Half adder is the simplest of all circuit. The inputs to the XOR gates are also inputs to the AND gate. The input "wires" to the XOR gate are tied to the input wires of AND gate. Thus, when voltage is applied to the A input of the XOR gate, the A input to the AND gate receives the same voltage. The Half adder can add only two bits so if input to a half adder have a carry then it will be neglected and adds only the A and B bits which means that the binary addition process is not complete and that's why it is called a Half adder.

0+0 = Sum 0 Carry 0
0+1 = Sum 1 Carry 0
1+0 = Sum 1 Carry 0
1+1 = Sum 0 Carry 1

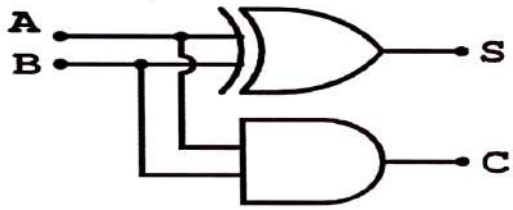


Figure 1: Block Diagram of Half Adder

Table 1: Truth Table of Half Adder

A	B	S	C
0	0	0	0
0	1	1	0
1	0	1	0
1	1	0	1

The previous work presents adder circuits using pass transistor logic based MUX & XOR gate, which contains lesser no. of transistors. The pass transistor logic reduces the count of transistors used to make different logic circuits, by eliminating redundant transistors. Transistors are used as switches to pass logic levels between nodes of a circuit voltage[4]. This reduces the number of active devices, but has the disadvantage that output levels can be no higher than the input level. Each transistor in series has a lower voltage at its output than at its input [5]. For proper operation, design [6].

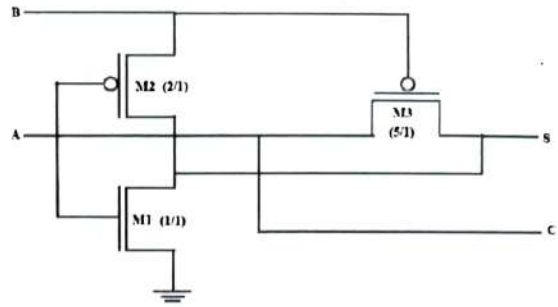


Figure 3:3-T XOR

Pass transistor logic has become important for the design of low-power high-performance digital circuits due to the smaller node capacitances and reduced transistors count it offers. The 5-T half adder was designed using this 3-T XOR and 2-T AND gate.

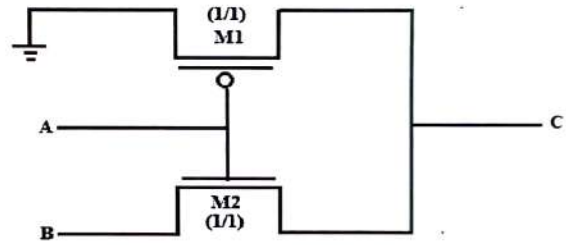


Figure 4:2-T MUX

A 2-T MUX is used as an AND gate. The input A is given to the select line. The output depends on the value given to A. When A=0 output is 0 since the MUX is off. When A=1 the value given to B is obtained as output. Hence the conditions for AND gate is satisfied.

Table 2: Truth Table of AND Gate

A	B	C
0	0	0
0	1	0
1	0	0
1	1	1

III. PROPOSED SYSTEM

The three major sources of power dissipation in a digital CMOS circuit are logic transition, short-circuit current and leakage current. The short-circuit current is the direct current passing through the supply and the ground, when both the NMOS and the PMOS transistors are simultaneously active. The proposed half adder is of 3Twhich is a variation from the existing half adder. The XOR gate itself can be used as a half adder. In the figure below the transistors M1 and M2 forms an inverter circuit.The CMOS inverter output is at high impedance when input B is at logic low and when B

is at logic high the inverter acts like a normal inverter .when input B is at logic low the pass transistor M3 is enabled and the output S gets the same logic value as input A. Now when A=1 and B=0, due to threshold drop voltage degradation occurs across transistor M3 and consequently the output S is degraded with respect to the input. The voltage degradation due to threshold drop can be considerably minimized by increasing the W/L ratio of transistor M3. The desired output is obtained by varying the W/L ratio. The sum is obtained from the M3 transistor and Carry is obtained across its drain and source.

Since the proposed circuit has only 3 transistors it reduces the chip area and thereby reduces power consumption.

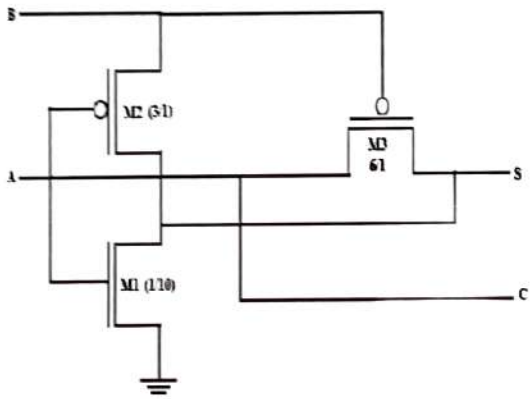
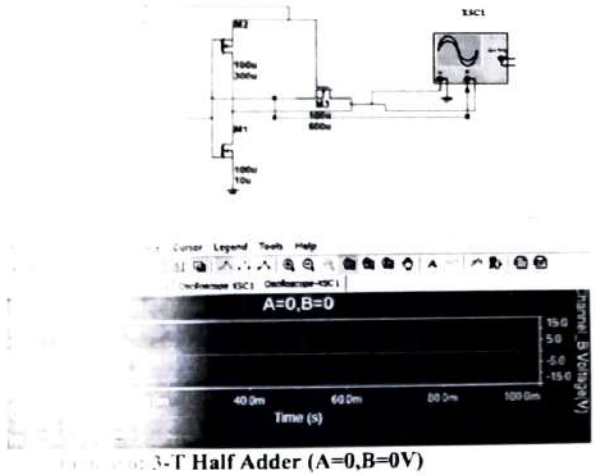


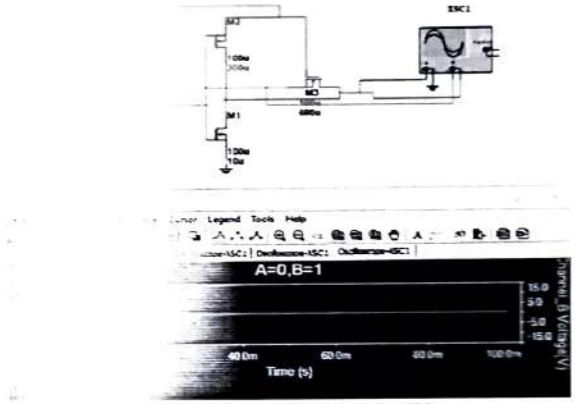
Figure 5:3-T Half Adder

IV. EXPERIMENTAL RESULTS

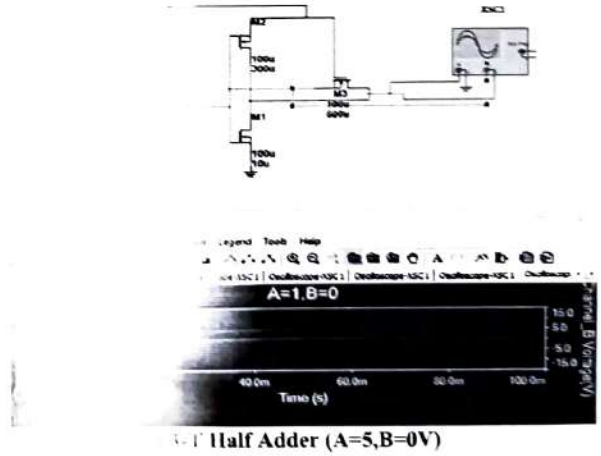
Figures show the simulation results of the proposed half adder. Simulation is done in Multisim software. The connections are made as in the circuit. A 5V represents logic 1 and a 0V represents logic 0.The two inputs are A: (S1), B:(S2).The output of the half adder the sum(S) and the carry(C) is connected to the oscilloscope. The red line represents the sum and pink line represents the carry in the graph. Figure 6, figure 7, figure 8, figure 9 shows the graph for various input combinations 00,01,10,11 respectively and Table 2 shows the output values of these input combinations. From the table it is clear that the proposed half adder shows a result which is more feasible compared to a conventional half adder.



...3-T Half Adder (A=0,B=0V)



...3-T Half Adder (A=0,B=5V)



...T Half Adder (A=5,B=0V)

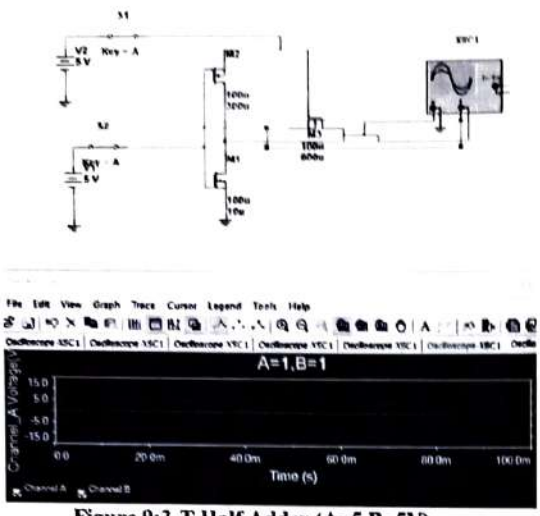


Figure 9:3-T Half Adder (A=5,B=5V)

Table 3: Output of Conventional and Proposed Half Adder

Combinations	5-T Half Adder		3-T Half Adder	
	Sum	Carry	Sum	Carry
00	0V	0 V	0 V	0 V
01	3.07 V	1.366 V	4.49 V	504.73mV
10	3.09 V	-174.82m V	4.37 V	-155.41mV
11	100 nV	4.99 V	1.0u V	4.96 V

V. CONCLUSION

A 3-T half adder by varying the W/L ratio to obtain the desired output has been implemented. The proposed circuit can be used where low power consumption is an essential requirement like in design of high-speed embedded processors. A reduction in power consumption provides several benefits. As a future scope of the work, Power of circuit can be further reduced by sizing the transistor keeping logical effort in mind.

REFERENCES

[1] Biswarup Mukherjee; Biplab Roy; ArindamBiswas; AniruddhaGhosal -"Design of a Low Power 4x4 Multiplier Based on Five Transistor (5-T) Half Adder, Eight Transistor (8-T)Full Adder & Two Transistor (2-T) AND Gate"-IEEE 20

[2] Hung Tien Bui, Yuke Wang and Ying Tao Jiang, "Design and Analysis of low Power 10 Transistor Full adders Using Novel XOR/XNOR gates", *IEEETransactions on Circuits And Systems- II, : Analog and Digital Signal Processing*, Vol.49,No.1 January 2002

[3] N. Ohkubo, et al, "A 4.4 ns CMOS 54X54 b multiplier using pass transistor multiplexer", *Proceedings of the IEEE 1994 Custom Integrated Circuit Conference*, May 1-4 1994, p599-602, San Diego, California.

[4] Jaume Segura, Charles F. Hawkins "CMOS electronics: how it works, how it fails", *Wiley-IEEE*, 2004, page 132

[5] Clive Maxfield, "Bebop to the Boolean boogie: an unconventional guide to electronics Newnes"2008, pp. 423-426

[6] Albert Raj,Latha "VLSI Design", *PHI Learning Pvt. Ltd.* pp. 150-153

ISSN (Online) 2278-1021
ISSN (Print) 2319-5940

IJARCCE
International Journal of Advanced Research in Computer and Communication Engineering
NCRICT-2017
Ahalia School of Engineering and Technology
Vol. 6, Special Issue 4, March 2017

Design and Implementation of Smart Irrigation System with Uninterrupted Power Supply

Dr. V. Balamurugan[1], Sujith P. S. [2], Meera Govind G.[3]

Head of Department, Electronics and Communication Engineering, Ahalia School of Engineering and Technology, Kerala, India [1]

Assistant Professor, Electronics and Communication Engineering, Ahalia School of Engineering and Technology, Kerala, India[2]

Student, Electronics and Communication Engineering, Ahalia School of Engineering &Technology, Kerala, India[3]

Abstract: Irrigation is need of farmer to save water resource and need to use in minimum quantity because it is not a conversational resource. Agricultural sector uses maximum water in world. Due to its immense use water is vanishing day by day. Irrigation is one solution to this problem as it saves large amount of water. In traditional irrigation method water is sometimes over supplied or less supplied to the crop. So it is hard to take a decision to save water and get maximum profit from the field. This traditional method requires manual intervention. It creates a need of more labor work and maintenance. Thus maintaining a good irrigation system is a necessity in today's water scarcity environment. Hence a new system which makes the irrigation fully automated is being proposed. In our proposed automated system the temperature of irrigation field is being measured by a temperature sensor and based on the sensed value the crops is being watered. This whole system works all the time without any interruption in the working of our proposed system using uninterruptable power supply.

I. INTRODUCTION

Agriculture is considered as the main source of income in India. This is an important factor in human society to growing demand in food production. But agricultural areas are getting reduced due to laziness in mankind. In past farmers depend on monsoon for cultivation. Thus they suffered a lot due to lack irrigation. Irrigation is defined as the science of artificial application of water to the crops. But the irrigation system which is of current technology is time consuming one and also requires high maintenance. Today farmers face the problem of unavailability of sufficient water for irrigation. Thus we can say efficient management of water resources plays a crucial role in agricultural sector. In our country most of the irrigation systems are operated manually. This unmanned system adversely affects the growth of crops.

Our system comprises some changes in usual irrigation system. The proposed automated irrigation system, contrary to a traditional irrigation method regulates supplied water automatically to the field based on the temperature in the irrigation field. We use sensors to acquire the corresponding data.

The requirement of multiple sensors spread out over the field means the presence of many wires in it. This will create a lot of problems in ploughing, harvesting etc. Wireless connectivity to the sensor is a best idea in this context. Thus the sensor data is sent through Xbee; a low cost wireless communication modules to microcontroller which then regulates the water supply. The whole system efficiently operates with UPS which protects our sophisticated devices from sudden power supply failure and supply variations.

Automating irrigation allows farmers to apply right amount of water at the right time, regardless of availability of the labors. If the plants get water at the proper time then its production can be increased up to 30%. Thus through this system we are modernizing agriculture sector, thereby conserving water resources, increasing production, save energy of the farmer.

Many features can be further be added to this like a system to identify the insects in crops and pesticides is sprayed only in that portion using a stream video camera through image processing.

II. TRADITIONAL METHODS OF IRRIGATION

The water available in wells, lakes and canals is lifted up by different methods in different regions, for taking it to the fields. Cattle and human labor is used in these methods. So these methods are cheaper, but less efficient. The various traditional ways are

Moat (Pulley system): A moat or pulley system of irrigation is one that involves pulling water up from a well

Copyright to IJARCCE

ISSN (Online) 2278-
ISSN (Print) 2319-5

IJARCCE

International Journal of Advanced Research in Computer and Communication Engineering

NCRICT-2017

Ahalia School of Engineering and Technology

Vol. 6, Special Issue 4, March 2017

or other water source in order to water plants and other crops. It is not often in use as it can be time consuming and may not always be as efficient as other methods of irrigation. On the other hand, it does not cost a lot of money to install a moat or pulley irrigation system as it does not require vast technology or machinery invested in it

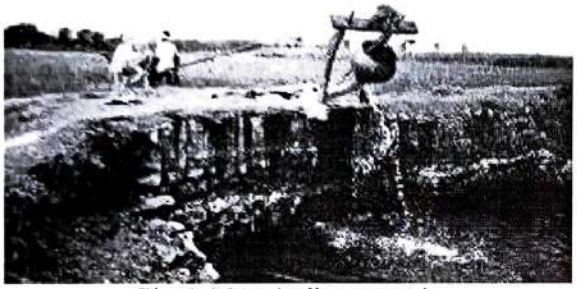


Fig. 1: Moat (pulley system)

Chain pump: These ancient Chinese irrigation systems use round metal discs and a long loop of metal chain to water soil and plants. Each metal disc runs through a pool of liquid, and each disc collects some water during this process. When the chain is pulled, the metal disc rises up to the top, and the water held inside pours out, hydrating the earth and flora. This low-cost method of traditional irrigation has been practiced for centuries.

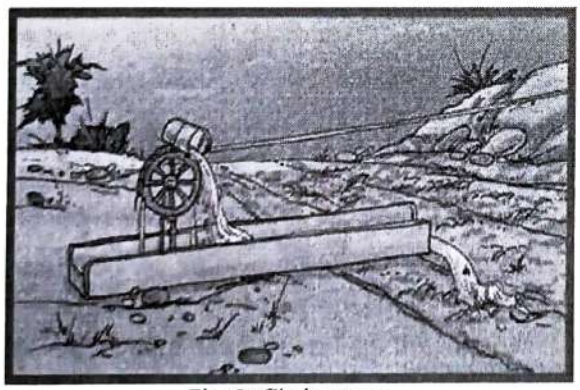


Fig. 2: Chain pump

III. MODERN METHODS OF IRRIGATION

Sprinkler System: This system is more useful on the uneven land where water is available in smaller quantity. The perpendicular pipes, having rotating nozzles on the top, are joined to the main pipeline at regular intervals. When the water is allowed to flow through the main pipe with the help of a pump, it escapes from the rotating nozzles. It is sprinkled on the crop as if it is raining. Sprinkler is very useful for the sandy soil.

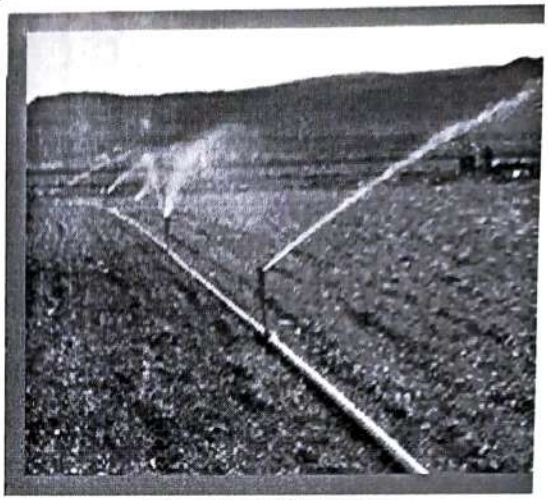


Fig. 3: Sprinkler system

Drip System: In this system, the water falls drop by drop just at the position of the roots. So it is called drip system. It is the best technique of watering fruit plants, gardens and trees. This system consists of a main pipe to which lateral pipes are joined. The specially prepared nozzles are attached to these lateral pipes to water plants drop by drop. Water is not wasted at all. So, it is a boon in regions where availability of water is poor.

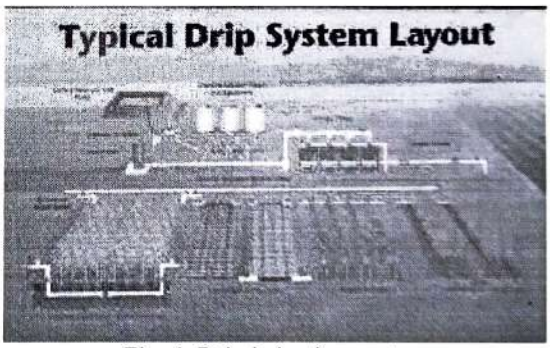


Fig. 4: Drip irrigation system

IV. METHODOLOGY

The outmoded irrigation technique has been replaced with automated technique. Many smart irrigation systems have been devised. A smart irrigation system, contrary to a traditional irrigation method, regulates supplied water according to the needs of the fields and crops. The feedback mechanism of a smart irrigation system is a temperature sensor. This temperature sensor is placed at a specific location on the irrigation field. Based on its value the water is being pumped to corresponding area up to a predetermined time. Wireless communication technology will make the communication possible between transmitter section and receiver section. This will avoid the presence of many wires in the field. Otherwise it may create a lot of problems to ploughing, harvesting, etc.

ISSN (Online) 2278-1021
ISSN (Print) 2319-5940

IJARCCE

International Journal of Advanced Research in Computer and Communication Engineering

NCRICT-2017

Ahalia School of Engineering and Technology

Vol. 6, Special Issue 4, March 2017

V.PROPOSED BLOCK DIAGRAM

The proposed block diagram of our system mainly consist of Arduino, Temperature sensor, XBEE, Relay, Valve, Pump and UPS. The temperature from the atmosphere is measured. The temperature sensor used is LM35. The LM35 is precision integrated-circuit temperature sensors, whose output voltage is linearly proportional to the Celsius temperature. The LM35 is operates at -55° to +120°

LM35 has three terminals and required Maximum of 5.5 V supply. This type of sensor consists of a material that performs the operation according to temperature to vary the resistance. This change of resistance is sensed by circuit and it calculates temperature.

Temperature sensors directly connected to microprocessor input and thus capable of direct and reliable communication with microprocessors. The sensor unit can communicate effectively with low-cost direct and reliable communication with microprocessors. The temperature sensor unit can communicate effectively with low-cost processors without the need of A/D converters.

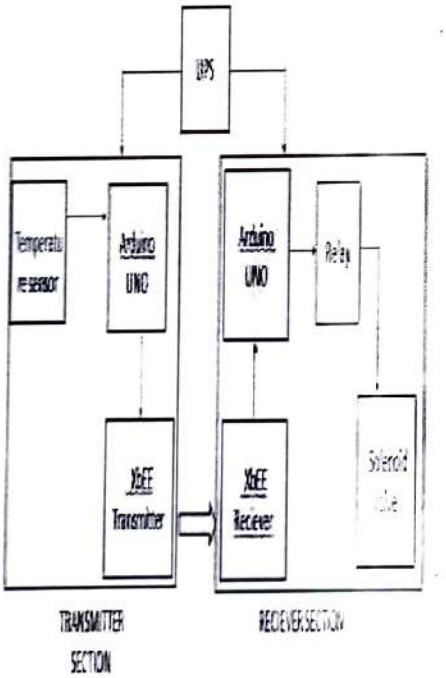


Fig. Block diagram

The output is then given to XBEE module for wireless transmission to base station. The XBEE RF modules were engineered to meet IEEE 802.15.4 standards and support the unique needs of low cost, low power wireless sensor networks, the module require minimal power and provide reliable delivery of data between devices. The module operates within 2.4MHz frequency band with a data transfer rate of 250kbps and it allows point to point, point to multipoint and mesh networking methods.

The data from XBEE router is received at the receiver side by the XBEE coordinator and this data is transferred to Arduino board.

The ARDUINO UNO is one of the most common and widely used Arduino processor boards. This is a microcontroller based on ATmega328P. It has digital input/output pins (of which 6 can be used as PWM outputs), 6 analog inputs, a 16 MHz quartz crystal, USB connection, a power jack and a reset button.

It contains everything needed to support the microcontroller; simply connect it to a battery to get started.

If the temperature is above threshold value, then the Arduino pass information to the relay for the opening of the solenoid valve and the water is pumped to the field through pump to the agriculture field.

If the temperature reaches below threshold value, then the Arduino provide information hence relay control the closing of the solenoid valve. Relays are simple switches which are operated both electrically and mechanically. Relays consist of an electromagnet and also a set of contacts. The switching mechanism is carried out with the help of the electromagnet.

The relay is used to connect and disconnect the load from the main power. An Uninterrupted Power Supply is employed along with the system to provide adequate power for the working of the entire system.

Power supply system

An UPS is the central component of any well-designed power protection architecture. A static UPS is designed to be the prime source of power to a every critical load. A UPS not only provides uninterruptible power to a critical load, but also isolation from the utility fine and the associated fine voltage variations as well as various forms of voltage transients present on the utility line. The method in which one or more UPS units are utilized will dictate the cost of the system and the degree of load protection provided by the system.

In this system, 230V supply is stepped down to 12V AC. This is then converted into 12V DC with the help of rectifiers, capacitors and regulators. This 12V DC is used to charge a battery and output of the battery is given to our smart irrigation system. Thus our system becomes independent of power supply variations and supply failures. The experimental setup of following is given below.

ISSN (Online) 2278-
ISSN (Print) 2319-59

IJARCCE

International Journal of Advanced Research in Computer and Communication Engineering

NCRICT-2017

Ahalia School of Engineering and Technology

Vol. 6, Special Issue 4, March 2017

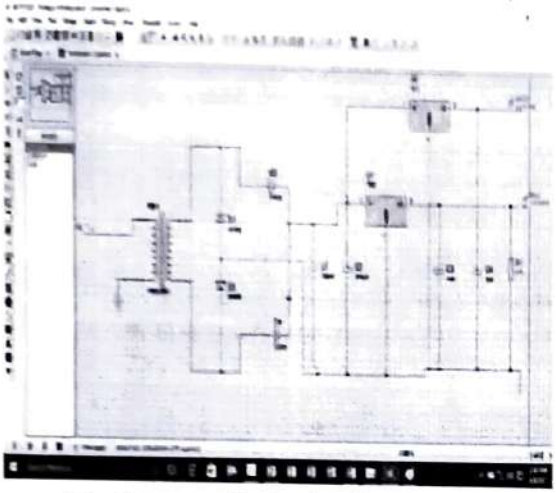


Fig. Power supply simulated in proteus 7

VI. CONCLUSION AND FUTURE SCOPE

Our proposed automated irrigation system requires less man power for operation. The water is been supplied by the field only when the soil humidity goes below the reference level. The system helps minimizing the overall watering and crops production cost. This system is considered to be cost effective and cultivation of agricultural products and plants in the area where there is water scarcity. It requires very less maintenance and is adjustable according to the changing environment. Through this system we can step in to an unmanned irrigation, which is highly efficient. Automated irrigation system has huge demand and future scope too. This system can also supply fertilizer and other agricultural chemicals like calcium, sodium, ammonium, and zinc to the field by adding new sensors and valves.

Many features can further be added to this system which definitely includes web-based communication, mobile alerts and weather adaptive systems. This type of system is a good solution for condition monitoring of agricultural setups as it is very low in cost. This idea should be implemented to large scale farms in the form of sensor grids in which each sensor will be treated as a Zig Bee node.

Additional feature to identify the insects in crops and pesticides sprayed only in that portion using the stream video camera through image processing can also be included. Proposed system can also be modified and used in such a way that it can sense the water level of the tank and whenever this water level is too low then the system can immediately provide a sound alarm, then it automatically switch on the motor. When the water level reaches 90% of the tank then the motor can be switched off through remote system. This automated system can be used in cricket stadium, golf stadium.

ACKNOWLEDGEMNT

We would like to express our sincere gratitude to **Prof. Dr. B. G. VISHNURAM**, the Honorable Principal for his timely support extended throughout the project.

We would like to express our sincere thanks to our beloved HOD **Prof. Dr. V. BALAMURUGAN** for his sincere help and guidance through the project. We would like to express our heartfelt thanks to our project guide **Mr. Sujith P. S.** for his guidance and motivation.

Any project would not be successful if it does not rely on the reference material. In this context we wish to express profound sense of gratitude to all teaching and non-teaching staff of our college for giving us a supportive environment in the college.

REFERENCES

[1] Global Humanitarian Technology Conference, 978-1-4799-7193-0/14.

[2] F. S. Zazueta and J. Xin,"Soil moisture sensor" bulletin 292: University of Florida: Gainsville, FL, USA, 2004.

[3] Jeng-NanJuangandR. Radharamanan,"Low cost soil moisture monitoring system: A Capstone design project", Mercer University, Macon, GA 31207.

[4] Ms.DeveshvreeRane, Prof. P. R Indurkar and Prof. D. M. Khatri,"Automatic irrigation system based on RF module"IJAICT Volume 1, Issue 9, ISSN 2348-9928,January 2015.

[5] S.Darsana, T. Sangavi, Sheena mohan, A. Soundarya," Smart Irrigation", IOSR Journal of Electronics and Communication Engineering (IOSR- JECE), 2278-2834,p- ISSN: 2278- 8735.Volume 10, Issue 3, Ver. II (May - Jun.2015).

[6] Gobakhlou, Sallis P, Diegel O, Zandi S and Perera A, "Wireless sensor networks for environmental data monitoring.8th annual IEEE sensor conference,Christchurch,2009.

[7] C. Bujdei and S. A. Moraru, "Wireless communication standards for intelligent buildings," in Annals of DAAAM for 2010. DAAAM International, pp. 245–246.

[8] J Arnil, Y Punsawad and Y Wongsawat,"WirelessSensor Network based Smart Room System for Healthcare Monitoring" in Int; Conf. on Robotics and Biomimeitcs, Dec, 2011.

[9] Egan. D.,"The emergence of zigBee in building automation and industrial control" computing & control engineering journal, 2005.

[10] XBee datasheet.

[11] S. P. Lim and G.H.Yeap, "Centralised Smart Home Control System via XBeeTranceivers",inIEEE Colloquium on Humanities, Science and Engineering Research(CHUSER 2011), Dec5, 2011.

[12] G. Merlin Suba, Y. M. Jagadeesh, S. Karthik and E. Raj Sampath,"Smart irrigation system through wireless sensor networks", ARPN Journal of Engineering and Applied Sciences, ISSN 1819-6608, Vol. 10, No. 17, September 2015.

[13] H. N Kamalaskar, Dr. P. H Zope," Survey of smart irrigation", IJESRT, ISSN: 2277-9655 June,2014.

[14] Arduino UNO datasheet.

[15] Pavithra D.S, M. S .Srinath, "GSM based Automatic Irrigation Control System for Efficient Use of Resources and Crop Planning by Using an Android Mobile", IOSR Journal of Mechanical and Civil Engineering (IOSR-JMCE) Vol 11, Issue I, Jul-Aug 2014, pp 49-55.

[16] LaxmiShabadi, NandiniPatil, Nikita M, Shruti. J, Smitha. P&Swati.C, "Irrigation Control System Using Android and GSM for Efficient Use of Water Power",International Journal of Advanced Research in Computer Science and Software Engineering, Volume4, Issue 7, July 2014.

[17] Shiraz Pasha B.R., Dr. B Yogesha, "Microcontroller Based Automated Irrigation System", The International Journal Of Engineering And Science (IJES), Volume3, Issue 7, pp 06-09, June.

ISSN (Online) 2278-1021
ISSN (Print) 2319-5940

IJARCCE
International Journal of Advanced Research in Computer and Communication Engineering
NCRICT-2017
Ahalia School of Engineering and Technology
Vol. 6, Special Issue 4, March 2017

BIOGRAPHIES



V. Balamurugan received B.E degree in Electrical and Electronics Engineering from Government College Technology, Coimbatore and M.E degree in Applied Electronics with distinction from Karunya Institute of Technology, Coimbatore and PhD degree in the Department of Information Technology at Madras Institute of Technology, Anna University-Chennai. India. His areas of interest include content-based image retrieval, image Processing and analysis, signal processing, wavelet theory and Application.



Sujith.P.S completed M.E in Communication Systems from EASA College of Engineering and Technology, Coimbatore in 2014. He is currently working as Assistant Professor, Dept. of Electronics and Communication Engineering, Ahalia School of Engineering and Technology, Palakkad, India. His research interests include Communication technologies.



Meera Govind G is doing B. Tech in Electronics and Communication at Ahalia School of Engineering & Technology, Palakkad, Kerala, India. Her area of interest includes circuit designing, analog electronics and communication.

ISSN: 2455-2631

Magnetic Semiconductors for the Future of VLSI

[1]Shahir Mubarak. M,[2]Greshma Mohan,[3]Ajin Surendran
[1,2]B-Tech. Student,[3]Assistant Professor
[1]Department of Electronics and Communication
[1]Ahalia School of Engineering and Technology, Palakkad,India

Abstract—**Spin as a property of electron, can be manipulated easily as its charge and is a perfect candidate for modern electronic devices. Charge of electron dissipates quickly unless an external force is constantly applied; on the other hand, spin can remain in its state for long period of time eliminating volatility. In case of magnetic semiconducting devices, materials could provide a new type of control in conduction. Traditional electronics are based on control of charge carriers; practical magnetic semiconductors would also allow control of quantum spin state. Implementation of non-volatile memory elements in logic circuits could bring several advantages such as instant on/off and run time re-configurability. Reduction of power consumption and interconnection delay are the two main targets of VLSI's. Development of such memory device has potential for exceeding the performance of traditional semiconductor-based memories, and may represent one of the major technologies for the 21st century.**

Index Terms—**Spintronics, Diluted Magnetic Semiconductors, Fluxtronics, VLSI, Spintronics in VLSI, Hybrid Circuits**

I. INTRODUCTION

An electron possesses two degrees of freedom; charge and spin. Both degrees of freedom have been individually utilized in semiconductor physics and magnetism, yielding a tremendous amount of practical applications and expansion of horizons in basic science. [1] Spintronics is a rapidly growing research field aimed at realizing new high-performance devices that takes advantage of the electron spin as well as of its charge. Spintronics is thought to be fusion domain of semiconductor physics and magnetism because both degrees of freedom in electrons are utilized simultaneously.

Semiconductor devices can display a range of useful properties such as passing current more easily in one direction than the other showing variable resistance, and sensitivity to light or heat. By doping or by application of electrical fields or light, the electrical properties of a semiconductor material can be modified and devices made from these semiconductors can be used for amplification, switching, and energy conversion. Magnetic semiconductors provide conduction by controlling both charge carriers and their quantum spin state. The main limitation of semiconductor device is it's storage of memory; also power consumption, size, and speed. The primary aim of a DMS is compatibility with existing semiconductor structures and materials. Semiconductor-DMS are based on traditional semiconductors, but are doped with transition metals instead of, or in addition to, electronically active elements. They are of interest because of their unique spintronics properties with possible technological applications.

II. SPINTRONICS

Spintronics also known as spin electronics or fluxtronics, is an emerging field of nanoelectronics which integrates the intrinsic spin of the electron and its associated magnetic moment, in addition to its fundamental electronic charge, in solid state devices.

In ferromagnetic materials there are certain domain in which the magnetic fields of the individual atoms align randomly. But this alignment is random and there exists no net magnetic field. When an external magnetic field is applied domain of the individual atoms line up in the direction of the applied field due to the nature of magnetic force. This enhances the applied magnetic field. This method of aligning the spins in the given direction is called spin polarization. This give rise to spin polarized current emerging from the ferromagnet. The photo excited electrons passing from the semiconductor into the ferromagnet have different transmission probabilities at the semiconductor/ferromagnet interface depending on their spin orientation with respect to the ferromagnet layer magnetization. In this way, a spin imbalance of the electron current can be detected and measured as a modulation of the photocurrent.

Injection of spin polarized carrier into semiconductor material is the major step in creating spin-based semiconductor devices. Spin of an electron can be controlled by the application of magnetic field [2]. The working of these devices relies on the alignment of spin in reference with the applied magnetic fields. All spintronic, or more specifically semiconductor spintronic, devices act according to the following simple scheme: (1) information is stored (written) into spins as a particular spin orientation (up or down); (2) the spins, being attached to mobile electrons, carry the information along a wire; and (3) the information is read at a terminal. Hence, the main three requirements for a spintronic device includes a source material for spin injection, a medium for transport of spin polarized electrons and an analyzer for spin detection or sensing. The long coherence time of spin makes spintronic devices attractive for memory storage and magnetic sensor applications, and potentially for quantum computing where electron spin would represent a bit of information. [15][16][17][25][27]

III. DILUTED MAGNETIC SEMICONDUCTORS (DMS)

A semiconductor is a substance, usually a solid chemical element or compound, which can conduct electricity under some conditions but not others, making it a good medium for the control of electrical current. The specific properties of a semiconductor

epend on the impurities, or dopants, added to it. Common semiconductor compounds include gallium arsenide, indium antimonide, and the oxides of most metals. Of these, gallium arsenide (GaAs) is widely used in low-noise, high-gain, and weak-signal amplifying devices. If implemented in devices, these materials could provide a new type of control of conduction. [21] [24] Semiconductors can be grouped into three classes depending on the nature of materials and their magnetic properties: (a) a magnetic semiconductor, in which a periodic array of magnetic element is present; (b) a non-magnetic semiconductor, which contains no magnetic ions; and (c) a DMS containing a very small fraction of magnetic element or ions.

Diluted magnetic semiconductors (DMS) also referred to as semi magnetic semiconductors are semiconducting alloys whose lattice is made up in part of substitutional magnetic atom. There are several naturally occurring magnetic elements, by introducing these into materials as a dopant they can introduce favorable magnetic properties in a controllable fashion. DMS are semiconductors doped with transition metal atoms. The level of doping directly affects the magnetic properties of the DMS and it affects the Curie temperature. A Curie temperature that is above room temperature is crucial in order to exploit spin polarization in electronic devices. The main disadvantage of current DMS materials is that their Curie temperatures are below room temperature and result in a loss of magnetic ordering in everyday applications. Materials design of new functional DMS is presented based on first principles calculations. If there is an insufficient hole-concentration in the magnetic semiconductor, then the Curie temperature would be very low or would exhibit only paramagnetism. However, if the holeconcentration is high, then the Curie temperature would be higher, between 100-200 K. The term DMS applies generally to semiconductors in which a fraction of its constituent ions are replaced by magnetic ions. Ion-channeling experiments reveal that these films are single crystalline and have high Mn substitutionality, while variable temperature resistivity measurements reveal the strong Mn-hole interactions characteristic of carrier-mediated ferromagnetism in homogeneous. Much of the attention on DMS materials is due to their potential applications in what is dubbed as the spintronics devices, which exploit the spin in magnetic materials along with charge of electrons in semiconductors. Transition metals, which have partially filled d states and rare-earth elements, which have partially filled f-states are used as magnetic ions in DMS. The partially filled d or f states contain unpaired electrons, in terms of their spin, which are presumably responsible for exhibiting magnetic behavior [30] [33]. Although research on DMS application is still at the stage of exploration, this field has already present its wide spread future in practice. For example, inserting DMS material into magnetic metal and semiconductor, one can realize ejection of carriers with spin polarization into non-magnetic semiconductor, and this technique can be applied to make spin polarized light-emitting diode. While for certain ferromagnetic/non- ferromagnetic multilayer structures by tuning temperature and voltage, one can control carrier concentration in semiconducting layer and magnetic coupling between magnetic layers, this property can be used to produce new magnetic-controlled and photonic-controlled devices. [38] [39] [41]

IV. SPINTRONIC DEVICES

Spintronic Memristor

A memristor is a hypothetical non-linear passive two-terminal electrical component relating electric charge and magnetic flux linkage. The memristors electrical resistance is not constant but depends on the history of current that had previously flowed through the device, i.e., its present resistance depends on how much electric charge has flowed in what direction through it in the past; the device remembers its history; the so-called non-volatility property. When the electric power supply is turned off, the memristor remembers its most recent resistance until it is turned on again.

Among all spintronic memristive structures, the spin valve memristor with spin-torque-induced domain wall motion could be the most favorable one for its simplest structure. In fact, the fabrication process of such spintronic memristors is identical to the adult technology that was used to manufacture the spin valve based GMR head in a hard disk drive. Hence, we choose it as the objective of this research work. The spintronic memristor consisting of a long spin valve strip which includes two ferromagnetic layers: reference layer and free layer. The magnetization direction of reference layer is fixed by coupling to a pinned magnetic layer. The free layer is split by a domain-wall into two segments that have opposite magnetization directions to each other. The domain wall in the free layer could be moved by the spin polarized current. The resistance per unit length of each segment is determined by the relative magnetic directions of the free layer and reference layer: when the magnetization direction of the free layer in a segment is parallel (anti-parallel) to the reference layer, the resistance per unit length of the segment is low (high). Memristor technology brings out a whole new set of possibilities. All the AI circuits and neural networks in the past have been built on digital 1's and 0's, and although they can do a great job in intelligent operations, they are still basically zombies. No one has come even close to simulating consciousness. Memory for devices, universal memory replacing hard drives, RAM, flash, etc. in all computer device, complex self-learning neural networks and hybrid transistor/memristor circuits, non-volatile memory applications, programmable logic and signal processing, crossbar latches as transistor replacements or augmenters. [18] [22]

Magnetic Tunnel Junction (MTJ)

Magnetic tunnel junctions or MTJs are nanostructured devices within the field of spintronics. The experimental observation of sizable and tunable magnetoresistance (change of materials resistance due to external magnetic fields) is intimately related to the exploitation of not only charge of the electron but also its spin. The discovery of giant magnetoresistance (GMR) in multilayered ferromagnetic films separated by thin metallic spacers has initiated an enormous research interest, particularly also for a wealth of potential applications. Since then, the impact of MTJs on the field of spintronics has hugely expanded, particularly due to the enormous magnitude of the observed magnetoresistances at room temperature and its impact on potential applications.

When electrons are tunneling between two ferromagnetic metals, the magnitude of the tunneling current depends on the relative orientation of the magnetization of both electrodes. This can be understood from a few elementary arguments: (i) the tunneling current is proportional to the product of the electrode density of states (DOS) at the Fermi level; (ii) in ferromagnetic materials, the ground-state energy bands in the vicinity of the Fermi level are shifted in energy, yielding separate majority and minority bands for

electrons with opposite spins; and (iii) assuming spin conservation for the tunneling electrons, there are two parallel current spin-up and spin-down character. As a result of these aspects, the current between electrodes with the same magnetization direct should be higher than those with opposite magnetization.In the field of spintronics, MTJs display magnetoresistance effects due the spin dependence of the tunneling current when dealing with ferromagnetic electrodes. This has dramatically increased knowledge of tunneling between ferromagnetic materials. MTJ research and development has made substantial progress over past decade, fueled by two current and important commercial applications: HDDs and MRAM. This progress has enabled ra technological advances in both applications. [36]

V. SPINTRONIC VLSI IN HYBRID CIRCUITS

Invention of transistor was the driving factor of growth in the VLSI. VLSI is basically transistors in a single chip. We can s that this is the upgraded from the embedded technology. It is the current level of computer microchip miniaturization and refers microchips containing in the hundreds of thousands of transistors. Therefore, this technique provides less area/volume. Hen compactness, less testing requirements, less power consumption, higher reliability due to improve on-chip interconnects, high speed, due to significantly reduced interconnection length, and significant cost savings. VLSI can be used in many fields which ar Defense, Navy, Air Force, etc. Using CAD tools, these modules are mapped onto the chip surface for automatic module with a goa of minimized interconnects area and signal delays. The chip is mentioned in terms of logic gates by using routing program and cell placement. The implementation of non-volatile memory elements in logic circuits could bring several major advantages such a instant on/off, built-in function programmability (in LUT, PLD or FPGA) and run time re-configurability. Moreover, the implementation of non-volatile flip-flop registers, providing an efficient way of fighting the increasing dissipation due to leakage currents within today's CMOS logic circuits. Reduction of power consumption and interconnection delay are the two other targets for very large scale integrated circuits (VLSIs). Drastic increase of static power dissipation is being anticipated due to leakage current in beyond 45 nm CMOS technology. Logic-in-memory architecture, where memory elements are distributed over a logic-circuit plane, combined with non-volatile memory is expected to realize both ultra-low-power and shorten interconnection delay.

VI. APPLICATIONS

There are many applications for diluted semiconductors in VLSI which are integrated with latest devices which have high performance and some of them are;

Threshold Logic Gates

A threshold logic gate (TLG) essentially constitutes of summation of weighted inputs, followed by a threshold operation, where INi's are multiple binary inputs, Wi's are scalar weights with which the corresponding inputs are multiplied. The same TLG circuit can implement different Boolean functions by reconfiguring the weights, threshold, or both. In previous research, TLG has been implemented in CMOS and other bulk semiconductor technologies, such as CMOS look-up-tables (LUT). Single electron transistors and resonant tunneling diode.Such hardware implements suffer from power, delay and area overhead. Recent discovery of nano-scale memristor, whose resistance can be programmed with an applied electric field, has led to proposal of energy-efficient reconfigurable memristive TLG (MTLG). Compared with CMOS LUT based TLG design, such MTLG designs can potentially provide two orders lower energy consumption and high area density. However, due to the intrinsic high energy consumption and long programming delay of memristor (Ag-Ch, TiO2), the memristor based TLG suffers from high power and long delay in reconfiguration operation, thereby eschewing the benefits of reconfigurable logic computing. Moreover, the spintronic weight device also leads to low power and fast speed in reconfiguration operation of the proposed design. Compared with reconfigurable MTLG design, the proposed STLG consumes three orders lower reconfiguration energy, opening a new door for future post-CMOS, ultra-low energy reconfigurable computing era. [8]

Non Volatile Logic in Memory towards Low Power Computing

Every 18 months, the number of transistors can be doubled, which constitutes the well-known Moore's law. And the transistor size has scaled down following this famous law for almost 40 years. However, it becomes more and more difficult to maintain this law due to power issues, such as high static power caused by the intrinsic leakage currents, and as dynamic power due to the long interconnection delay. The static power comes mainly from the cache memory between the computing chip and main memory, the dynamic power is dominated by the large data traffic. They prevent computing from reaching high frequency (~4 GHz) and limit power efficiency. Both academics and industries are looking for the solutions to tackle these bottlenecks. [5]

The magnetic tunnel junction (MTJ) is one of the most important devices of spintronics. It is the basic element of modern hard drive read heads and MRAM storage cells. Thanks to its vertical structure, which can be integrated at the back-end process of CMOS, as well as its fast and low power data access operations, a number of research groups focus on this device to build ultra - lower power logic gates. Magnetoresistive RAMis one of the newest approaches to non-volatile memory and stores data in magnetic storage elements called magnetic tunnel junctions (MTJ's). MRAM has an especially promising future as it seeks to encompass all the desirable features of the other popular types of memory (non-volatility, infinite endurance, high-speed reading/writing, low cost). [32][37]

VII. CONCLUSION

Spintronics which deals with the spin of electron has a great potential to spin this current world to digital atomic world which has a capability of manipulating at atomic level and this can even be made further smaller during the integration with "NANOTECHNOLOGY". We make use of this spin of the electron, create new devices and circuits which is beneficial for the human life. Spintronics provides architectures which allow for dramatic reduction in energy consumption which in turn allows to

proceed with miniaturization in accordance with Moore's law. Combined with the VLSI technology, MTJ makes it possible not only to realize non-volatile, high density, and fast random access memories, but also to construct nonvolatile VLSI logic circuits that have unprecedented low power capability and compactness that overcome the present limit of power and delay Spintronics related phenomena observed in ferromagnetic semiconductors are now being utilized in metal spintronic devices to realize next generation VLSI's.

VIII. ACKNOWLEDGMENT

The authors are grateful for the assistance provided by Department of ECE, Ahalia School of Engineering and Technology, Palakkad, Kerala, India.

REFERENCES

[1] A. Rossani" Electron–phonon interactions in the Fermi–Dirac spintronics", Physica A 394 publications, 2014

[2] Ahmad Bsiesy," Spin injection into semiconductors: towards a semiconductor-based spintronic device", C. R. Physique publications,2015

[3] Álvaro S. Núñez," Theory of the piezo-spintronic effect", Solid State Communications publications,2013

[4] Araghi and Ahmad NozadGolikand, "Preparation and characterization of semiconductor GNR-CNT nanocomposite and its application in F", Journal of Physical and Chemistry of Solids,2016

[5] B. Dieny, R.C. Sousa, J. He´rault, C. Papusoi, G. Prenat,U. Ebels, D. Houssameddine, B. Rodmacq, S. Auffret,I. Prejbeanu-Buda, M.C. Cyrille, B. Delaet, O. Redon,C. Ducruet, J.P. Nozieres and L. Prejbeanu," Spintronic Devices for Memory and Logic Applications", Handbook of Magnetic Materials publications,2011

[6] BekirAktaş, FaikMikailzade, BulatRameev, NumanAkdoğan," Recent advances in nanomagnetism and spintronics", Journal of Magnetism and Magnetic Materials 373 ,2015

[7] C.Gould, G.Schmidt, and L.W.Molenkamp, "Spintronic Nanodevices", Semiconductors and Semimetals publications, 2008

[8] Deliang Fan," Ultra-Low Energy Reconfigurable Spintronic Threshold Logic Gate", IEEE,2016

[9] E. Grimaldi, R. Lebrun, "Spintronic nano-oscillators: towards nanoscale and tunable frequency devices", IEEE, 2016

[10] E.I. Rashba ," Semiconductors with a loop of extrema", Journal of Electron Spectroscopy and Related Phenomena,2015

[11] Eli Rotenberg, Aaron Bostwick," Superlattice effects in graphene on SiC (0001) and Ir (111) probed by ARPES", Synthetic Metals publications,2015

[12] F. Matsukura. D Chiba, and H. Ohno," Spintronic Properties of

[13] Ferromagnetic Semiconductors", Semiconductors and Semimetals publications,2008

[14] G. Salis," Semiconductor Spintronics: Switching Spins at Low Voltage", IEEE,2013

[15] G. Schmidt, C. Gould, L.W. Molenkamp," Spintronics in semiconductor nanostructures", Physica E publications,2004

[16] Gerber," Towards Hall effect spintronics", Magnetism and Magnetic Materials publications,2007

[17] HartmutZabel," Progress in spintronics", Superlattices and Microstructures,2009

[18] Hassan Mostafa1, Senior Member, IEEE and Yehea Ismail, "Process Variation Aware Design of Multi-Valued Spintronic Memristor-Based Memory Arrays", IEEE Transactions on Semiconductor Manufacturing,2016

[19] HC Swart and OM Ntwaeaborwa," Compound Luminescent Semiconductors: Their and uses", My sciencework publications,2013

[20] IndraYudhistiraa,*, ShaffiqueAdama,," Theory for electron transport in graphene", Synthetic Metals publications,2015

[21] Jean-Marie George a,*, Marc Elsen a, V. Garcia a,b, Henri Jaffrès a, Richard Mattana," Spintronic with semiconductors", C. R. Physique publications,2015

[22] Jianlei Yang," Spintronic Memristor as Interface Between DNA and Solid State Devices", IEEE JOURNAL ON EMERGING AND SELECTED TOPICS IN CIRCUITS AND SYSTEMS,2016

[23] JoëlCibert a, Jean-François Bobo , Ulrike Lüders," Development of new materials for spintronics", C. R. Phyique publications,2013

[24] John L. Lyons, Anderson Janotti, Chris G. Van de Walle," Theory and Modeling of Oxide Semiconductors", Semiconductors and Semimetals publications,2013

[25] Kang L. Wang □, Zuoming Zhao, Alex Khitun," Spintronics for nanoelectronics and nanosystems", Thin Solid Films,2008

[26] Li-Zhong Tsai , Siao-Yin Yu , San-Yu Ting , Li-Yin Chen, Yuh Sheng Wen ,Mandy M. Lee and JiannT.Lin, "Bipolar transport materials for electroluminescence applications", Organic Electronics publications,2016

[27] Martin Jourdan," Revival of Heusler compounds for spintronics", Materials Today publications,2014

[28] Masashi Shiraishi and TadaakiIkoma," Molecular spintronics", Physica E publications,2011

[29] Minglei Sun, Wencheng Tang, QingqiangRen,Yiming Zhao, Sake Wang, JiYu, YanhuiDu,YitongHao," Low-dimensional Systems and Nanostructures", Physica E publications,2016

[30] PaataKervalishvilia and Alexander Lagutin," Nanostructures, magnetic semiconductors and spintronics", Microelectronics publications,2008

[31] Rachel Brazil, "Spintronics and superfast-computing", Engineering & Technology,2015

[32] RaminRajaei," Radiation Hardened Design of Nonvolatile MRAM-based FPGA", IEEE Transactions on Magnetics publication,2016

[33] S.J. Pearton, C.R. Abernathy, D.P. Norton, A.F.Hebard , Y.D. Park and A. Boatner, J.D. Budai , " Advances in wide bandgap materials for semiconductor Spintronics",Materiac Science and Engineering publications,2003

[34] Seba S. Varghese Sunil Lonkar K.K. Singh SundaramSwaminathan Ahmed Abdala," Recent advances in graphene based gas sensors", Sensors and Actuators B publications,2015

[35] Susan Z. HUA, Matthew R. SULLIVAN, Jason N. ARMSTRONG," Susan Z. HUA, Matthew R. SULLIVAN, Jason N. ARMSTRONG", Trans. Nonferrous Met. SOC.China,2006

[36] Swagten, Paluskar, "Magnetic Tunnel Junction", Encyclopeadia of Materials, Elsevier, 2010

[37] TaherehNematiArama,b, AsgharAsgari," Influence of Fermi velocity engineering on electronic and optical properties of graphenesuperlattices", Physics Letters A publications,2015

[38] Takahiro Hanyu, Daisuke Suzuki, NaoyaOnizawa*3), Shoun Matsunaga*4), Masanori Natsui), and Akira Mochizuki," Spintronics-Based Nonvolatile Logic-in-Memory Architecture Towards an Ultra-Low-Power and Highly Reliable VLSI Computing Paradigm", EDAA,2015

[39] Teresa Oh, "Tunneling condition at high Schottky barrier and ambipolar transfer characteristics in zinc oxide semiconductor thin film transistor", Materials Research Bulletin publications,2016

[40] Thomas Sch¨apers,1 Sebastian Heedt,1 Andreas Bringer,2 Isabel Otto,1 Kamil Sladek,1 Hilde Hardtdegen,1 Detlev Gr¨utzmacher,1 and Werner Prost," Spintronics with semiconductor nanowires", IEEE, 2016

[41] Xiang-JianMeng, Hong-Wei Zhu," Tunable transport characteristics of double-gated graphene field-effect transistors using P(VDF-TrFE) ferroelectric gating", Carbon publivations,2015

[42] Y.B. Xu, E. Ahmad, J.S. Claydon, Y.X. Lu, S.S.A. Hassan, I.G. Will, B. Cantor," Hybrid magnetic/semiconductor spintronic materials and devices", Journal of Magnetism and Magnetic Materials 304,2006

[43] Yue Zhang1, 2, Weisheng Zhao1, 2*, Jacques-Olivier Klein1, 2, Wang Kang1, 3, Damien Querlioz1, 2, Youguang Zhang3, Dafiné Ravelosona1, 2 and Claude Chappert," Spintronics for Low-Power Computing", EDAA,2014

[44] Z. V. Vardeny and T. D. Nguyen and E. Ehrenfreund, "organic spintronics", Wood head publications, 2016.